March 2023 Vol:9 Issue:1 Mart 2023 Cilt:9 Sayı:1

T.C.
ÇANAKKALE ONSEKİZ MART ÜNİVERSİTESİ
LİSANSÜSTÜ EĞİTİM ENSTİTÜSÜ

CANAKKALE ONSEKİZ MART UNIVERSITY JOURNAL OF ADVANCED RESEARCH IN NATURAL AND APPLIED SCIENCES

ISSN 2757-5195

Journal of Advanced Research in Natural and Applied Sciences

e-ISSN: 2757-5195

Volume 9 / Issue 1

Sayı 9 / Cilt 1

2023-Mart/March

Yayıncı/Publisher: Çanakkale Onsekiz Mart Üniversitesi
Rektör /Rector: Prof. Dr. Sedat MURAT

Önsöz:

Journal of Advanced Research in Natural and Applied Sciences Dergisi Fen, Mühendislik, Doğa ve Temel bilimler alanlarında daha önce yayımlanmamış orijinal araştırma makalesi, derleme yazılar, teknik not türünde araştırmaları yayınlayan ulusal ve uluslararası indekslerde taranan, hakemli ve bilimsel bir dergidir. Journal of Advanced Research in Natural and Applied Sciences Dergisi Mart, Haziran, Eylül, Aralık olmak üzere yılda dört sayı yayınlanacaktır. Tr-Dizin'de taranan Journal of Advanced Research in Natural and Applied Sciences Dergisi'nin 9.cilt 1.sayısında 19 adet araştırma makalesi ve 1 adet derleme makale yayına kabul edilmiştir.

	TÜBİTAK TR DİZİN tarafından taranmaktadır. Indexed by TR-DİZİN Database.
	TÜBİTAK-ULAKBİM DergiPark Akademik tarafından yayımlanmaktadır. Published by TÜBİTAK-ULAKBİM Turkish Journal Park Academic Database.
	CROSSREF® veri tabanı tarafından taranmakta ve makaleler DOI numarası ile yayımlanmaktadır. Indexed by CROSSREF® Database and articles are published with DOI number.
	Google Scholar'da ve SOBİAD'da taranmaktadır. Indexed by Google Scholor and SOBIAD Database.

İletişim Adresi / Publisher Address

Çanakkale Onsekiz Mart Üniversitesi Lisansüstü Eğitim Enstitüsü

Terzioğlu Yerleşkesi Çanakkale (Sağlık Hizmetleri Meslek Yüksekokulu Binası)

Tel: 0286 218 05 23

Belgegeçer / Fax: 0286 218 05 24

E-posta / E-mail: jarnas.journal@gmail.com

Dergi Web Sayfası / Journal Home Page:

http://jarna.dergi.comu.edu.tr/

https://dergipark.org.tr/tr/pub/jarnas

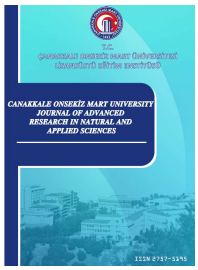

Çanakkale Onsekiz Mart University Journal of Advanced Research in Natural and Applied Sciences

Mart (March) 2023 / Cilt (Volume) 9 / Sayı (Issue) 1 / e-ISSN 2757-5195

CONTENTS / İÇİNDEKİLER
(2023, 9:1)

Çanakkale Onsekiz Mart University Journal of Advanced Research in Natural and Applied Sciences

Mart (March) 2023 / Cilt (Volume) 9 / Sayı (Issue) 1 / e-ISSN 2757-5195

Çanakkale Onsekiz Mart University Journal of Advanced Research in Natural and Applied Sciences
Mart (March) 2023 / Cilt (Volume) 9 / Sayı (Issue) 1 / e-ISSN 2757-5195

e-ISSN 2757-5195

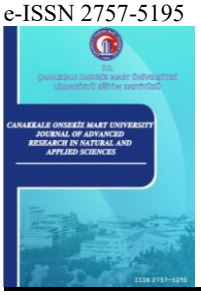

Çanakkale Onsekiz Mart University

Journal of Advanced Research in Natural and Applied Sciences

Open Access

doi.org/10.28979/jarnas.1097860 2023, Vol. 9, Issue 1, Pages: 1-14 dergipark.org.tr/tr/pub/jarnas

Evaluation of the Effect of Quince Seed Extract On Physical and Sensorial Properties of Gluten-Free Cake Batter Formulations

Ceren Cokeker[1], Sinem Argun[2], Emrah Kirtil[3,*]

[1,2,3]Department of Food Engineering, Faculty of Engineering, Yeditepe University, Istanbul, Türkiye

Article History

Received: 04.04.2022

Accepted: 26.07.2022

Published: 05.03.2023

Research Article

Abstract – Celiac disease is a serious and lifelong disorder that is associated with gluten consumption. Celiac patients should commit to a strict gluten free diet. Besides celiac patients, gluten can also cause allergenic reactions in a significant portion of population. Thus, there is a growing trend in replacing sources of gluten with alternatives. This work concentrated on improving the quality and consumer acceptance of gluten-free cakes made out of rice flour by using quince seed extract, which is a unique hydrocolloid product that exhibits emulsification properties. The cake batter and cooked cakes were characterized in terms of water activity, color, porosity, emulsion stability, textural properties, rheological behavior and sensorial attributes. Emulsion stability results indicated an excellent improvement of physical stability of batter emulsions by addition of quince seed extract (QSE) and lecithin, which was identified with no visible phase separation in samples Q0.1E and Q0.2E. All cake batters displayed a pseudoplastic flow behavior with apparent viscosities and shear thinning behavior increasing substantially with increasing QSE concentrations. Hardness values gathered from texture profile analysis, implied that best cake texture was obtained via QSE and lecithin incorporation. Sensory analysis results also supported the same result in that, samples with egg yolk and QSE both, yielded a more preferable appearance and texture. Therefore, with this study, it was possible to observe the promising effects of QSE incorporation on cake batter and baked cake properties.

Keywords *– Celiac, emulsion stability, gluten network, hydrocolloid, sensory analysis, texture*

1. Introduction

The need for gluten-free products, is advancing as a result of the growth in number of people with celiac disease (Cureton & Fasano, 2009). Trends in the market and the increasing in the numbers of celiac disease patients have provoked comprehensive research for the establishing better gluten-free products (Houben et al., 2012). Regardless, it is a big challenge to produce gluten-free bakeries at comparable qualities to gluten-containing products, as gluten is essential for an extensive dough network and absence of it is detrimental on the viscoelastic properties of the dough. Typically, gluten-free formulations involve the use of various components and additives to mimic the viscoelastic properties that gluten confers to the dough which increases final product quality (Demirkesen et al., 2014; Hager & Arendt, 2013; Sciarini et al., 2010).

For this purpose, numerous gluten-free formulations were studied, with most of them involving gluten-free flours such as rice, sorghum or maize flour (Mancebo et al., 2015; Schober et al., 2005; Sciarini et al., 2010), or pseudocereals like amaranth, quinoa, buckwheat (Hager & Arendt, 2013; Mariotti et al., 2013), legume flours such as pea, soy, chickpea (Aguilar et al., 2015), starches like cassava, corn, potato (Lazaridou et al., 2007; Mahmoud et al., 2013). These ingredients are used in combination with emulsifiers, hydrocolloids, shortenings or combinations of these as alternatives to gluten. These added ingredients give gluten-like properties to the dough, this way the sensorial and nutritional properties as well as the shelf life of the breads

[1] ceren.cokeker@std.yeditepe.edu.tr

[2] sinem.argun@yeditepe.edu.tr

[3] emrah.kirtil@yeditepe.edu.tr

[*]Corresponding Author

can be improved. However, the addition of these ingredients also leads to a higher final price (Demirkesen et al., 2014; Ronda et al., 2015).

Hydrocolloids are a type of additive that is commonly applied for this purpose (Houben et al., 2012; Matos & Rosell, 2015). Incorporation of hydrocolloid type of additive is therefore a very promising application for increasing the quality of gluten-free dough formulations. Hydrocolloids, as the name suggests, are hydrophilic compounds that are abundant in polar groups and can be observed under various chemical structures. These compounds provide a can be used for a wide range of applications one of them being the improvement of the quality of gluten-free bakery products (Li & Nie, 2016). Though different hydrocolloids all function differently, the main mechanism of action is the increase in viscosity, which enhances dough development and strengthens the dough network that is particularly essential for gluten-free formulations. The strengthened network enhances dough development by improving air retention during baking (Capriles & Arêas, 2014).

Technical parameters such as bulk volume and crumb hardness are especially critical in gluten-free products and thus, are the most studied parameters followed by sensorial attributes (Houben et al., 2012; Kittisuban et al., 2014). The positive effect of some hydrocolloids (such as xanthan gum, guar gum, pectin) on gluten-free products have been well established, are being used widely commercially in gluten-free formulations. These hydrocolloids are not only used as gluten substitutes in gluten-free formulations, they are also applied to gluten containing products to modify texture, raise moisture retention, and improve the overall consumer acceptability of the products (Rojas et al., 1999).

Hydrocolloids are seldom used alone, and are usually coupled with other similar hydrocolloids and/or emulsifiers. Dough is a unique network in that it is both an emulsion and a suspension; increased physical stability introduced by addition of emulsifiers coupled with the improved elasticity of the continuous dough network, acts synergistically and greatly enhances quality of the final gluten-free product (Demirkesen et al., 2013; Turabi et al., 2008a). Some hydrocolloids display emulsification properties and these are especially more effective in helping develop a better dough structure in gluten-free products. Gum Arabic is such a hydrocolloid and is one of the most widely studied and commercially used hydrocolloids. It is chemical structure can be summarized as being a branched polysaccharide mainly composed of L-arabinose and D-galactose. The gum contains proteins (1–2% by wt) which confers it surface activity (Vernon-Carter et al., 2008). However, the gum's general application is limited by its high price (Dickinson, 2018).

Another such hydrocolloid that also shows surface activity is quince seed extract (QSE). Quince (*Cydonia oblonga*) is a fruit that is native to the West Asian region. It's especially highly grown in the Caucasus regions, Afghanistan, Iran, Dagestan, and southern regions of Turkey (Abbastabar et al., 2015). The seeds of the fruit contain hydrocolloids that demonstrate excellent gelling capacity. The seed extract is also shown to provide viscosity enhancement and increasing shear thinning behavior to solutions (Abbastabar et al., 2015). Some recent studies have also confirmed the emulsifying effects of quince seed extract in model and real food emulsions. The extract is especially effective as an emulsifier at a pH range of 6–8 (Kirtil & Oztop, 2016; Ritzoulis et al., 2014).

Nevertheless, to the best our knowledge, there are no studies that involve the use of this novel hydrocolloid source in improving the functional properties of gluten-free cake batter. The aim of this thesis is to investigate the effect of quince seed extract used by itself or in combination with a natural emulsifier (egg lecithin) on physical quality attributes and sensorial characteristics of cake batter and cake products. For this purpose, cake formulations were produced with different quince seed extract concentrations (0.1% and 0.2%) and with or without the addition of a lecithin as an additional emulsifier. The cake batter was analyzed for its water activity, rheological behavior and emulsion stability; whereas the baked cakes were analyzed for their textural properties, porosity and sensorial properties.

2. Materials and Methods

2.1 Materials

Wheat flour (Sinangil, Tekirdağ, Turkey), gluten-free flour (Riace flour, Sinangil, Tekirdağ, Turkey), sugar (Granulated sugar, Migros, İstanbul, Turkey), margarine (Becel, İstanbul, Turkey), salt (Iodized Table Salt, Billur Tuz, İzmir, Turkey), baking powder (Dr. Oetker, İzmir, Turkey) and drinking water (Nestle, Bursa, Turkey) was purchased from a local grocery store in İstanbul. Quinces for preparation of quince seed extract

(QSE) was purchased from a local grocery store in Ankara. Egg white powder and whole egg powder was purchased from Kor Agro Organik Gıda A.Ş (İstanbul, Turkey).

2.2 Methods

2.2.1. Sample Preparation

Batter formulation was based on the amount of flour (in terms of weight). The batter consisted of sugar (%100), margarine (%25), egg white powder or whole egg powder (%9), salt (%3), baking powder (%5) and water (%36) with the given percentages. These percentages give the weight of the ingredient used with respect to the weight of the flour. For 100 g flour, 100 g sugar, 25 g margarine, 9 g egg powder, 3 g salt, 5 g baking powder and 36 g water was used.

Sugar and egg powder was first whipped on a bowl and molten margarine was added to the mixture and further sheared for 1 min. Then, the remaining dry ingredients (flour, baking powder, salt and QSE) were mixed at a separate place, to which water was incorporated and homogenized with a high speed homogenizer (Ultraturrax, WiseTis HG-15D, Wertheim, Germany) at 2000 rpm for 2 min. The two mixtures were then combined in one single bowl and mixed for 5 min with a kitchen type mixer (Philips, HR1453, Holland). After batter is prepared, they were poured into small cylindrical porcelain cupcake cups (D=70 mm, h=40 mm) and baked in a conventional home-type oven at 175ºC for 30 min.

The formulations differ in the amounts of quince seed extract (QSE) and presence of either egg white powder or whole egg powder, and the flour type (wheat flour or gluten-free rice flour). **Table 1** lists the ingredients used for each sample formulation.

Table 1 Sample formulations

Formulation	**Control**	**GF Control**	**Q0.1**	**Q0.2**	**Q0.1 E**	**Q0.2 E**
Rice Flour	-	+	+	+	+	+
Wheat Flour	+	-	-	-	-	-
Sugar	+	+	+	+	+	+
Shortening	+	+	+	+	+	+
Egg White	+	+	+	+	-	-
Egg Whole	-	-	-	-	+	+
Salt	+	+	+	+	+	+
Baking Powder	+	+	+	+	+	+
QSE	-	-	0.1 % w/v	0.2 % w/v	0.1 % w/v	0.2 % w/v

"+" sign represents the ingredients that are in the formulation of that specific sample, "-" sign represents that the formulations lacks that ingredient.

2.2.2. Rheological Characterization

For rheological characterization, shear rate ramp and amplitude and frequency sweep tests were performed. Measurements were obtained using a parallel plate (40 mm diameter and 1 mm gap) rheometer (Kinexus Dynamic Rheometer, Malvern, UK) was used. In shear rate ramp experiments, shear stress values were measured for shear rates changing from 0.1 s^{-1} to 100 s^{-1}, with a total measurement time of 2 min and 20 sample points. Shear rate ramp results were fit to a power-law model (equation 2.1)

$$\tau = K\gamma^n \tag{2.1}$$

where τ is shear stress, K is the consistency index, γ is shear rate, n is flow behavior index. Amplitude sweep tests were performed to estimate the linear viscoelastic region with strains ranging between 0.01%–1% at a set frequency of 1 Hz. Elastic (G′) and viscous (G″) moduli were recorded for strains increasing at a fixed

frequency. After amplitude sweep measurements, a strain of 0.1% was chosen to be used as a parameter for frequency sweep measurements. This strain lied within the linear viscoelastic region for all samples. Frequency sweep measurements were carried out to investigate the effect of frequency on elastic (G′) and viscous (G″) moduli. Frequency sweep tests were conducted with frequencies ranging between 0.1%–1% at a fixed strain of 0.1%. All rheological measurements were conducted at 25 ±0.1 °C within 2 h of cake batter preparation.

2.2.3. Water Activity

To investigate the water binding capability of each formulation, water activities of the cake batter samples were measured. For this purpose, a water activity device (Rotronic, HygroPalm HP23-Aw&HC2-Aw-USB, Switzerland) was used. Approximately 5 g of sample was placed into a sealed cup and placed into the device. After waiting for 30 min, for the water activity to come to equilibrium, measurements were recorded.

2.2.4. Emulsion Stability

Cake batter samples were centrifuged (Hettich Zentrifugen, EBA 20, Germany) at 4032 rcf (6000 rpm with a rotator radius of 10 cm) soon after preparation for 20 min at 25ºC. The supernatant was identified as the fat portion and the volumetric ratio of it was calculated by measuring the height of supernatant and dividing it by the total height of batter sample. This ratio was multiplied by 100 to report as percentage of emulsion stability. Percent creaming index results were calculated from equation 2.2;

$$\%CI = \frac{H_C}{H_T} \times 100 \tag{2.2}$$

Where H_C is the height of the cream later and H_T is the total height.

2.2.5. Porosity

For porosity measurements, a modified version of the displacement method from (Turabi et al., 2008b) was employed. To calculate the porosity of the cakes, first bulk and true volume of the cakes were calculated. To calculate bulk volume, cakes were cut into regular shaped rectangular prisms of which the volumes were calculated bv multiplication of the three sides. These samples were then compressed under a load of 20 N for 10 min until there was no pore left within the sample. The true volumes were calculated from the multiplication of the three sides of the final compressed samples. Porosity were then calculated from equation 2.3;

$$Porosity = 1 - \frac{True\ Volume}{Bulk\ Volume} \tag{2.3}$$

2.2.6. Color

The color of baked cakes were measured by a spectrometer (Konica Minolta, CM-5, Japan). The CIELAB color space system was utilized for the measurements. In this system, L* represents lightness, whereas a* and b* values stand for the four main colors of human vision: red, green, blue, and yellow. Color measurements were taken only from the crust and from 8 different locations (4 from the top, 4 from the bottom and 4 from the lateral section).

2.2.7. Texture Profile Analysis

Texture profile analysis of cake samples were performed with a texture analysis instrument (Stable Micro Systems, TA-XT Plus, UK) using a 35 mm diameter probe. A compression mode texture profile analysis was conducted with a pre-test speed, test speed and post-test speed of 10 mm/s, 2.0 mm/s and 2.0 mm/s, respectively. The samples were compressed with a trigger force of 5 g. until a target strain of 40% was achieved. From the TPA curves obtained, hardness of cakes were reported since these are considered to be one of the primary indicators of textural quality for cakes (Chakraborty et al., 2020).

2.2.8. Sensory Analysis

To investigate the sensorial properties of the cakes, consumer studies were performed. All cakes were freshly baked and sealed with a plastic film up until testing, and were tested within 2 h of preparation. Sensory

attributes evaluated were taste, color, texture and odour. For scoring, a five-point hedonic scale was used. The higher the rating the better that quality attribute was. Scores ranged from "Dislike very much" (score 1) to "Like very much" (score 5) (Ballesteros López et al., 2004; Thybo et al., 2004). The tests were conducted on a total of 25 untrained panelists with ages ranging between 20-45.

2.2.9. Statistical Analysis

All measurements were carried out in at least three replicates. Statistical analysis software Minitab (Version 16, State College, PA, USA) was used for the analysis of variance (ANOVA) and Tukey's multiple comparison tests. Differences were considered significant for $p \leq 0.05$.

3. Results and Discussion

3.1 Water Activity

Cake photographs are given in Figure 1 and water activity measurement results are given in Table 2. As apparent from the table, there is no difference between water activities of different cake batters. The objective of measuring water activity was to investigate the difference in water binding capability of different formulations. Control and GF Control samples contained no additives. They only contained ingredients that a standard cake formulation would contain. Wheat flour and rice flour cake batter was apparently not different in terms of their interaction with water. Flours contain high amounts of starch, where wheat flour is composed mainly of wheat starch whereas rice flour mainly consists of rice starch (Mancebo et al., 2015; Steglich et al., 2014; Wilderjans et al., 2013). Different starches differed in the relative amounts of amylose and amylopectin and granule sizes and shapes. But non-gelatanized starch is not soluble in water, thus water-starch interactions are not sufficient to have a significant effect on water activity (Tananuwong & Reid, 2004). This explains why different flours do not effect water-binding capability of cake batter.

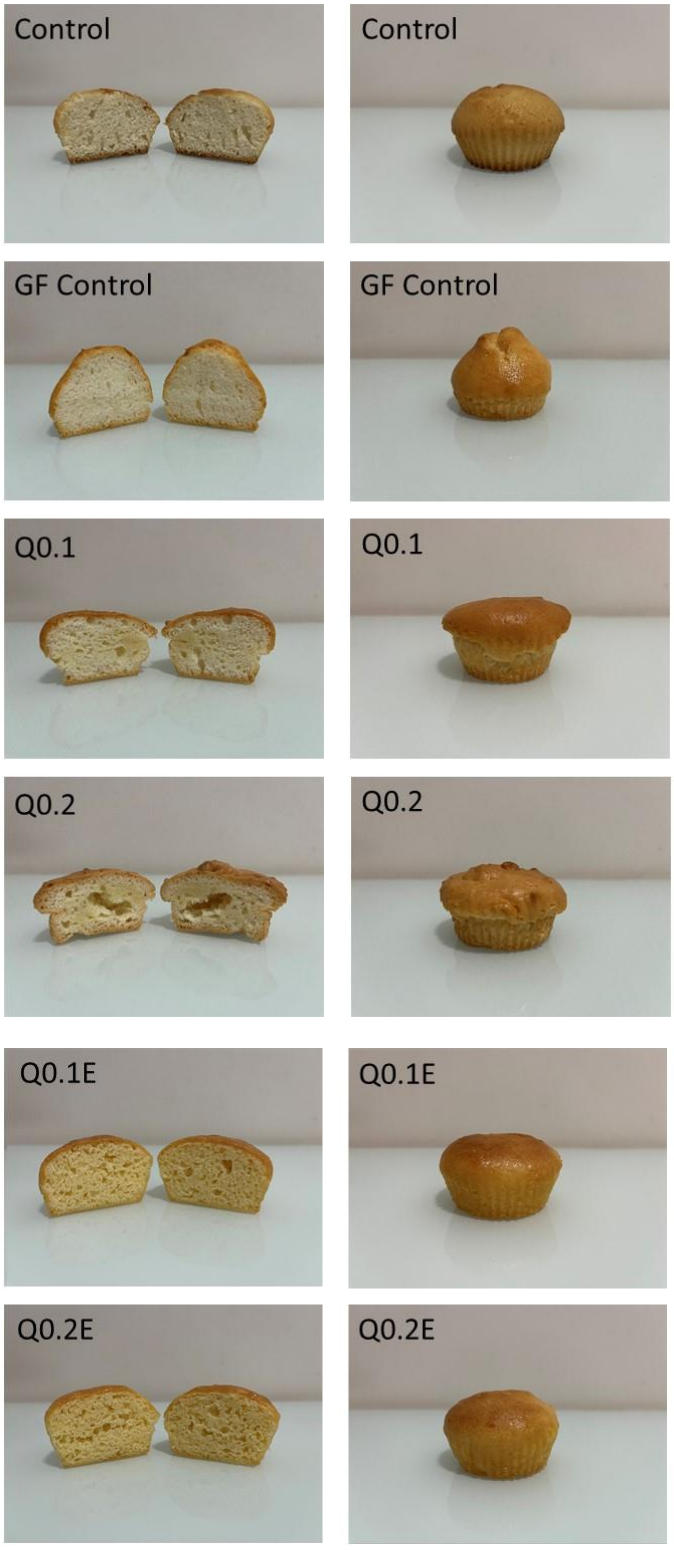

Figure 1 Photographs of cake samples

Table 2
Results of cake water activity, batter creaming index (%CI), cake porosity and cake hardness measurements

Samples	a_w	CI %	Porosity	Hardness (g)
Control	0.88±0.01^{a}	11.5±0.24^{a}	0.53±0.03^{ab}	2382±72.0^{a}
GF Control	0.88±0.01^{a}	6.73±0.34^{b}	0.59±0.03^{a}	906±56.4^{c}
Q0.1	0.87±0.01^{a}	7.21±0.38^{b}	0.46±0.04^{b}	1289±81.2^{bc}
Q0.2	0.87±0.01^{a}	7.21±0.31^{b}	0.32±0.04^{c}	1107±75.6^{bc}
Q0.1E	0.88±0.01^{a}	0	0.57±0.05^{a}	1465±92.5^{b}
Q0.2E	0.88±0.01^{a}	0	0.54±0.03^{ab}	1359±75.0^{b}

Means within the same column, followed by the different letters are significantly different ($p<0.05$).

Addition of egg yolk and quince seed extract also did not seem to effect water activities. As explained in introduction, the major portion of quince seed extract is polysaccharides, which are highly hydrophilic compounds. Thus, an increase in QSE concentration is normally expected to decrease water activities by hydrogen bonding with water molecules. However, the presence of starch-fat network dispersed in water seems to get in the way of QSE-water interactions. QSE being a surface active material, could instead position itself on the interface which decreases water-QSE interactions greatly (Kirtil et al., 2022). This coupled with the low concentrations of QSE might hinder the water binding capacity of the polymer. Hence, no difference in water activities could be observed even for samples with QSE.

3.2 Emulsion Stability

Creaming index (%CI) results can be seen in Table 2. Emulsion stability measurements involves the measurement of the height of the cream layer after a controlled destabilization procedure. Higher %CI values are associated with a lower resistance against destabilization. Control samples displayed the highest creaming index results (at 11.5%), which indicates that wheat flour was least effective in providing stability to cake batter. Rice flour was much better at providing a more stable emulsion. However, rather than the flour type, this is most likely related to the additives in GF flour used. The commercial GF flour used contained pectin and xanthan gum at unknown amounts. Both these additives are very large hydrophilic molecules. The presence of these large molecules in the aqueous phase, might have retarded the mobility of oil particles; which presumably retarded creaming rate (Kirtil & Oztop, 2016; Kontogiorgos, 2019). The same is true for samples that contain QSE. QSE has emulsification properties and is shown to be an effective emulsion stabilizer, yet in the cake batter network formed, QSE did not seem to show any emulsion stabilization properties. On the other hand, samples prepared with whole egg flour, did not show any creaming. This means lecithin in egg yolk was effective in providing thermodynamic stabilization to the cake network. Small lecithin phospholipids were much more effective than the much bulkier QSE molecules at providing stabilization at the oil-water interface. QSE molecules most likely dues to lack of water, was not hydrated enough to position itself effectively at the interface, and didn't have effective volume to take the most favorable conformation that confers it surface activity (Kirtil et al., 2022).

3.3 Porosity

Porosity results are given in Table 2. There was no significant difference between Control and GF Control samples in terms of porosities ($p>0.5$). This means cake batters prepared from rice and wheat flour were similar in terms of their air entrapment capacities. QSE containing samples had lower porosities. Moreover, with increasing QSE concentration porosities seemed to decrease. QSE is a very large biopolymer and has viscosity enhancing and gelling properties (Farahmandfar et al., 2017; Kirtil & Oztop, 2016). QSE containing batter were visibly thicker and more solid-like in terms of texture. This tougher and stiffer batter network provides a higher resistance against the rising of batter during baking. Hence, air bubble could not be formed as effectively.

For optimal porosity, an elastic network is necessary. The cake batter needs to be in optimal flexibility and toughness. Gluten is particularly essential in conferring the batter its unique properties. Gluten increases the resistance of the batter against rupturing and gives it a stronger, more flexible texture. If the batter is too tough, then batter could not rise as efficiently during baking. If it is too soft then the raised batter network could rupture and air bubble would merge, thus cake would collapse. An optimal cake batter stiffness and elasticity

would be soft enough to rise by air formation during baking and be strong enough to entrap the bubble without them merging (Milde et al., 2012; Sangpring et al., 2015).

Addition of egg yolk (samples Q0.1E and Q0.2E), increased porosities. This could be related with the softening effect of fat particles that are liquefied during cooking. The additional fat conferred softness to the batter, which decreased the stiffness of the batter network. The decreased stiffness aided with the air bubble formation and cake batter rise during cooking. This was observed as increased porosity values. Cake pictures that also give an idea of the porosity and internal structure of cakes can be seen in Figure 1.

3.4 Color

Table 3
Color measurement results

Top Surface	**Control**	**GF Control**	**Q0.1**	**Q0.2**	**Q0.1E**	**Q0.2E**
L*	88.3	88.4	88.4	88.4	88.4	88.4
a*	-0.292	-0.252	-0.257	-0.267	-0.340	-0.360
b*	0.2475	0.345	0.342	0.312	0.210	0.217
Bottom Surface						
L*	88.2	88.1	88.2	88.2	88.1	88.1
a*	-0.370	-0.380	-0.355	-0.335	-0.405	-0.400
b*	0.050	0.050	0.085	0.120	0.005	0.020
Lateral Surface						
L*	88.7	88.6	88.8	88.6	88.6	88,6
a*	-0.515	-0.555	-0.555	-0.550	-0.515	-0.515
b*	0.240	0.095	0.210	0.150	0.225	0.240

Color measurement results can be seen in Table 3. L* of the CIELAB coordinates represents lightness (total black gives L* = 0 and diffuse white gives L* = 100). For a*, the negative values represent green color and positive values represent red hues and similarly for b*, negative values represent blue color and positive values represent a yellowish hue. According to the results, regardless of formulation all cakes displayed similar lightness values (around L*=88.5). Therefore, we can say that addition of QSE or lecithin had no effect on color. The lightness of cakes is related to the Maillard reaction end products, particularly the melanoidin pigment formation (Bi et al., 2017). This shows that formulation changes had no influence on the rate and extend of Maillard reaction in cakes. The a* values of the cakes ranged between -0.25 and -0.55. Thus cakes displayed a more greenish color than a reddish color. For b* values, the measurements ranged between 0.005-0.34. This indicates that all cakes were yellowish in color. We could not observe any noteworthy trend in the change of a* and b* values with respect to formulation of position on the crust. However, the fact that L* values are identical on all points on cake crust shows that cakes were homogenously cooked, and no one surface was subjected to a higher heat transfer rate compared to others.

3.5 Rheological Characterization

Figure 2a and Figure 2b shows the change of shear viscosity (Pa.s) with shear rate (s^{-1}) in a normal and logarithmic scale, respectively. For all formulations, the apparent viscosity values decreased with increasing shear rates. This indicates that cake batter shows a pseudoplastic behavior. The pseudoplastic behavior is explained with the alignment of molecules in the mixture with the direction of flow. As the rate of shear increases more and more molecules are aligned with direction of flow and resistance against flow decreases,

which is monitored as a decrease in apparent viscosity values (Turabi et al., 2008b). Control formulation prepared with wheat flour displayed the lowest apparent viscosities. There was a considerable (almost 10 fold) difference in viscosities for the whole range of shear rates studied between control sample and GF control sample. This indicates that Control sample batter network showed the lowest resistance to flow. On the other hand, Q0.2, which is the formulation with highest amount of QSE, displayed highest apparent viscosities; which means it displayed the highest resistance against flow. This flow could be air bubble formation and rise inside the cake batter. Q0.2 should be highly resistant against the formation and rise of air bubble and this result is confirmed with the low porosity values this sample also displays as shown in Table 2.

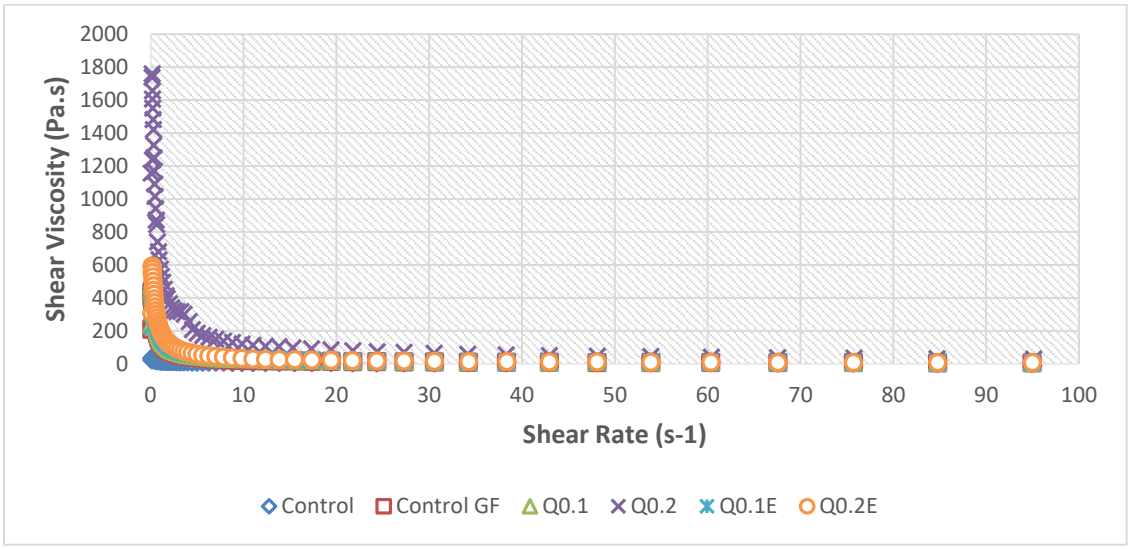

Figure 2a Change of shear viscosity with shear

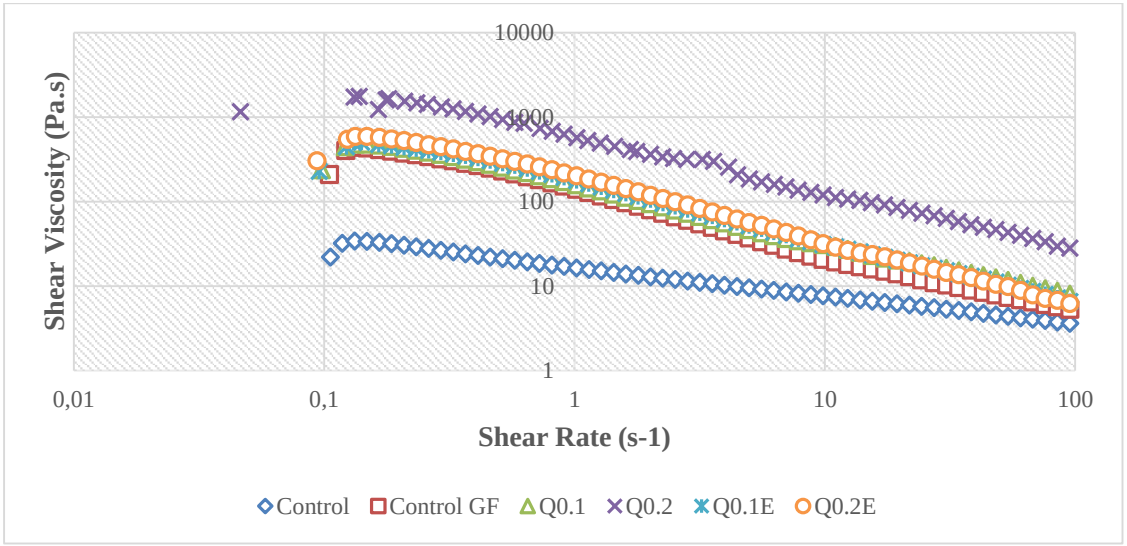

Figure 2b.Change of shear viscosity with shear rate in a logarithmic scale

As evident from the Figure 2, there is a linear trend between shear viscosities and shear rates if drawn on a logarithmic scale. This implies a shear thinning behavior. The shear rate and shear stress data were fit to a power law model and resulted in very high correlation coefficients (R^2>0.96). The results of the fittings were given in Table 4.

Table 4
Power law fitting results

	K	N	R^2
Control	16.6±0.48^{e}	0.665±0.04^{a}	0.99
Control GF	121.5±1.24^{d}	0.292±0.02^{c}	0.96
Q0.1	144.6±1.32^{c}	0.358±0.02^{b}	0.98
Q0.2	539.0±2.17^{a}	0.374±0.02^{b}	0.97
Q0.1E	153.3±1.23^{bc}	0.330±0.03^{bc}	0.96
Q0.2E	173.7±1.14^{b}	0.288±0.02^{c}	0.95

K are the consistency index value whereas n are power law index values. K can be identified as the apparent viscosities recorded at a shear rate of 1 s^{-1}, thus is a measure of the material's resistance to flow. All formulations flow behavior can be explained with a power law model and a shear thinning behavior. With increasing QSE concentration and lecithin addition, shear thinning behavior is enhanced. The batter network gets thicker and more viscous as hydrocolloid and emulsifier concentrations increase; yet it becomes easier to break this network and make it thinner with stress application. For increasing flow rates, the materials gets thinner and thinner and this effect is particularly enhanced for samples with higher QSE and lecithin content. Other studies have also reported similar flow behavior when shear thinning gums are added to gluten free flours (Turabi et al., 2008b, 2010).

3.6 Texture Profile Analysis

Hardness values are given in Table 2. Control cakes exhibited the highest hardness values. The cakes prepared from wheat flour with a standard formulation were the hardest. Gluten free cakes were significantly softer than all other formulations. This is a common problem with gluten free bakery products. Gluten is responsible for giving batter a texture that is more resistance against stretching. Without gluten, cake batters and the cakes formed from that batter, will not be strong enough to hold its own and will crumble with mild perturbation. This is not a desirable property and the hardness of control cake from wheat flour should be taken as a reference here. The closer the cake's hardness is to this value, the better the quality of the cake (Burešová et al., 2016; Sangpring et al., 2015; Schober et al., 2005). With this in mind, Q0.1E and Q0.2E samples yielded the best cakes. So addition of QSE and coupling it with an emulsifier as lecithin was successful in giving a tougher texture to the batter network. Large QSE molecules helped in formation of a more extensively bonded network, whereas egg yolk phospholipids positioned themselves on the oil-water interface and eased dispersion of fat into the batter (Burešová et al., 2016; Sangpring et al., 2015; Schober et al., 2005).

3.7 Sensory Analysis

Sensory analysis results can be seen in Table 5. The overall sensorial acceptance of the products was relatively good. Mean scores ranged between 2.8-4.1. This indicates that all formulations were acceptable in terms of taste, color, texture and odor. However, considering the data it is not possible to comment on specific differences on sensorial properties between different samples. The standard deviation of scores was too large so the differences for most attributes was not statistically significant. There are a few things to mention here. Color of whole egg containing samples (Q0.1E, Q0.2E) were found to be significantly more preferred by panelists compared to other samples. Upon visual inspection, it was possible to see a more yellowish hue in these samples, which could be reflected to the sensory analysis results as a higher preference. Again for Q0.1E and Q0.2E, texture was also more preferred. These samples were softer and mushier in texture possibly due to the higher fat content coming from egg yolk. The higher fat content was also identified by a shinier outer surface compared to other samples. Therefore, these results show that it was possible to improve the consumer acceptance of gluten free cakes in terms of texture and appearance.

Table 5
Sensory analysis results

	Taste	**Color**	**Texture**	**Odor**
Control	2.8±0.4[a]	3.6±0.4[b]	2.9±0.3[b]	3.5±0.2[a]
Control GF	3.1±0.5[a]	3.3±0.3[b]	3.5±0.5[ab]	3.3±0.2[a]
Q0.1	3.5±0.4[a]	3.3±0.3[b]	3.3±0.4[b]	3.7±0.2[a]
Q0.2	3.2±0.3[a]	3.2±0.2[b]	3.5±0.3[ab]	3.5±0.3[a]
Q0.1E	3.2±0.5[a]	4.1±0.3[a]	3.9±0.2[a]	3.4±0.2[a]
Q0.2E	3.4±0.4[a]	4.1±0.3[a]	3.8±0.2[a]	3.6±0.3[a]

4. Conclusion

This work concentrated on improving the quality and consumer acceptance of gluten-free cakes made out of rice flour by using a new hydrocolloids source, quince seed extract. Numerous researchers have used non-adsorbing hydrocolloids to increase the strength of the cake batter network and simulate the role of gluten in batter. These hydrocolloids yielded even more successful results when used in combination with emulsifiers that show surface adsorption capabilities. Quince seed extract is a unique hydrocolloid that also has emulsification properties. Hence, we wanted to see how it would function as a gluten replacement in cake batter.

The study yielded promising results. In terms of water activities, which is an indicator of water binding capacity of the batter ingredients. There was no significant difference between formulations. An increase in QSE concentration is normally expected to decrease water activities by hydrogen bonding with water molecules. However, the presence of starch-fat network dispersed in water seemed to prevent QSE-water interactions. Emulsion stability results indicated an excellent improvement of physical stability of batter emulsions by addition of QSE and lecithin, which was identified with no visible phase separation in samples Q0.1E and Q0.2E. QSE seemed to function better in presence of egg yolk lecithin and fat, this was particularly evident from porosity results that shows that the porosity of Q0.1E and Q0.2E samples were similar to porosity of control wheat flour sample.

All cake batters displayed a pseudoplastic flow behavior with apparent viscosities and shear thinning behavior increasing substantially with increasing QSE concentrations. Hardness values gathered from texture profile analysis implied that best cake texture was obtained via QSE and lecithin incorporation. Sensory analysis results also supported the same result in that, samples with egg yolk and QSE both, yielded a more preferable appearance and texture.

Therefore, with this study, it was possible to observe the effect of QSE on cake batter and baked cake properties. The results were promising in that some quality attributes of cake samples were improved with QSE addition.

Author Contributions

Ceren Cokeker: Methodology, Investigation, Writing - Original Draft

Sinem Argun: Methodology, Investigation

Emrah Kirtil: Conceptualization, Data curation, Formal analysis, Writing - Original Draft, Writing - Review & Editing, Supervision, Validation

Conflicts of Interest

The authors declare no conflict of interest.

References

Abbastabar, B., Azizi, M. H., Adnani, A., & Abbasi, S. (2015). Determining and modeling rheological characteristics of quince seed gum. *Food Hydrocolloids, 43,* 259–264.

https://doi.org/10.1016/j.foodhyd.2014.05.026

Aguilar, N., Albanell, E., Miñarro, B., & Capellas, M. (2015). Chickpea and tiger nut flours as alternatives to emulsifier and shortening in gluten-free bread. *LWT*, *62*(1), 225–232. https://doi.org/10.1016/j.lwt.2014.12.045

Ballesteros López, A. C., Guimarães Pereira, A. J., & Junqueira, R. G. (2004). Flour mixture of rice flour, corn and cassava starch in the production of gluten-free white bread. *Brazilian Archives of Biology and Technology*, *47*(1), 63–70. https://doi.org/10.1590/S1516-89132004000100009

Bi, B., Yang, H., Fang, Y., Nishinari, K., & Phillips, G. O. (2017). Characterization and emulsifying properties of β-lactoglobulin-gum Acacia Seyal conjugates prepared via the Maillard reaction. *Food Chemistry*, *214*, 614–621. https://doi.org/10.1016/j.foodchem.2016.07.112

Burešová, I., Masaříková, L., Hřivna, L., Kulhanová, S., & Bureš, D. (2016). The comparison of the effect of sodium caseinate, calcium caseinate, carboxymethyl cellulose and xanthan gum on rice-buckwheat dough rheological characteristics and textural and sensory quality of bread. *LWT - Food Science and Technology*, *68*, 659–666. https://doi.org/10.1016/J.LWT.2016.01.010

Capriles, V. D., & Arêas, J. A. G. (2014). Novel approaches in gluten-free breadmaking: Interface between food science, nutrition, and health. *Comprehensive Reviews in Food Science and Food Safety*, *13*(5), 871–890. https://doi.org/10.1111/1541-4337.12091

Chakraborty, S. K., Kotwaliwale, N., & Navale, S. A. (2020). Selection and incorporation of hydrocolloid for gluten-free leavened millet breads and optimization of the baking process thereof. *Lwt*, *119*(October 2019), 108878. https://doi.org/10.1016/j.lwt.2019.108878

Cureton, P., & Fasano, A. (2009). The Increasing Incidence of Celiac Disease and the Range of Gluten-Free Products in the Marketplace. *Gluten-Free Food Science and Technology*, 1–15. https://doi.org/10.1002/9781444316209.CH1

Demirkesen, I., Kelkar, S., Campanella, O. H., Sumnu, G., Sahin, S., & Okos, M. (2014). Characterization of structure of gluten-free breads by using X-ray microtomography. *Food Hydrocolloids*, *36*, 37–44. https://doi.org/10.1016/j.foodhyd.2013.09.002

Demirkesen, I., Sumnu, G., & Sahin, S. (2013). Image Analysis of Gluten-free Breads Prepared with Chestnut and Rice Flour and Baked in Different Ovens. *Food and Bioprocess Technology*, *6*(7), 1749–1758. https://doi.org/10.1007/S11947-012-0850-5

Dickinson, E. (2018). Hydrocolloids acting as emulsifying agents – How do they do it? *Food Hydrocolloids*, *78*, 2–14. https://doi.org/10.1016/j.foodhyd.2017.01.025

Farahmandfar, R., Asnaashari, M., Salahi, M. R., & Khosravi Rad, T. (2017). Effects of basil seed gum, Cress seed gum and Quince seed gum on the physical, textural and rheological properties of whipped cream. *International Journal of Biological Macromolecules*, *98*, 820–828. https://doi.org/10.1016/j.ijbiomac.2017.02.046

Hager, A. S., & Arendt, E. K. (2013). Influence of hydroxypropylmethylcellulose (HPMC), xanthan gum and their combination on loaf specific volume, crumb hardness and crumb grain characteristics of gluten-free breads based on rice, maize, teff and buckwheat. *Food Hydrocolloids*, *32*(1), 195–203. https://doi.org/10.1016/j.foodhyd.2012.12.021

Houben, A., Höchstötter, A., & Becker, T. (2012). Possibilities to increase the quality in gluten-free bread production: An overview. *European Food Research and Technology*, *235*(2), 195–208. https://doi.org/10.1007/S00217-012-1720-0

Kirtil, E., & Oztop, M. H. (2016). Characterization of emulsion stabilization properties of quince seed extract as a new source of hydrocolloid. *Food Research International*, *85*, 84–94. https://doi.org/10.1016/j.foodres.2016.04.019

Kirtil, E., Svitova, T., Radke, C. J., Oztop, M. H., & Sahin, S. (2022). Investigation of surface properties of quince seed extract as a novel polymeric surfactant. *Food Hydrocolloids*, *123*(September 2021), 107185. https://doi.org/10.1016/j.foodhyd.2021.107185

Kittisuban, P., Ritthiruangdej, P., & Suphantharika, M. (2014). Optimization of hydroxypropylmethylcellulose, yeast β-glucan, and whey protein levels based on physical properties of gluten-free rice bread using response surface methodology. *LWT - Food Science and Technology*, *57*(2), 738–748. https://doi.org/10.1016/j.lwt.2014.02.045

Kontogiorgos, V. (2019). Polysaccharides at fluid interfaces of food systems. *Advances in Colloid and Interface Science*, *270*, 28–37. https://doi.org/10.1016/j.cis.2019.05.008

Lazaridou, A., Duta, D., Papageorgiou, M., Belc, N., & Biliaderis, C. G. (2007). Effects of hydrocolloids on dough rheology and bread quality parameters in gluten-free formulations. *Journal of Food Engineering*,

79(3), 1033–1047. https://doi.org/10.1016/j.jfoodeng.2006.03.032

Li, J. M., & Nie, S. P. (2016). The functional and nutritional aspects of hydrocolloids in foods. *Food Hydrocolloids*, *53*, 46–61. https://doi.org/10.1016/j.foodhyd.2015.01.035

Mahmoud, R. M., Yousif, E. I., Gadallah, M. G. E., & Alawneh, A. R. (2013). Formulations and quality characterization of gluten-free Egyptian balady flat bread. *Annals of Agricultural Sciences*, *58*(1), 19–25. https://doi.org/10.1016/j.aoas.2013.01.004

Mancebo, C. M., San Miguel, M. Á., Martínez, M. M., & Gómez, M. (2015). Optimisation of rheological properties of gluten-free doughs with HPMC, psyllium and different levels of water. *Journal of Cereal Science*, *61*, 8–15. https://doi.org/10.1016/j.jcs.2014.10.005

Mariotti, M., Pagani, M. A., & Lucisano, M. (2013). The role of buckwheat and HPMC on the breadmaking properties of some commercial gluten-free bread mixtures. *Food Hydrocolloids*, *30*(1), 393–400. https://doi.org/10.1016/j.foodhyd.2012.07.005

Matos, M. E., & Rosell, C. M. (2015). Understanding gluten-free dough for reaching breads with physical quality and nutritional balance. *Journal of the Science of Food and Agriculture*, *95*(4), 653–661. https://doi.org/10.1002/JSFA.6732

Milde, L. B., Ramallo, L. A., & Puppo, M. C. (2012). Gluten-free Bread Based on Tapioca Starch: Texture and Sensory Studies. *Food and Bioprocess Technology*, *5*(3), 888–896. https://doi.org/10.1007/S11947-010-0381-X

Ritzoulis, C., Marini, E., Aslanidou, A., Georgiadis, N., Karayannakidis, P. D., Koukiotis, C., Filotheou, A., Lousinian, S., & Tzimpilis, E. (2014). Hydrocolloids from quince seed: Extraction, characterization, and study of their emulsifying/stabilizing capacity. *Food Hydrocolloids*, *42*, 178–186. https://doi.org/10.1016/j.foodhyd.2014.03.031

Rojas, J. A., Rosell, C. M., & Benedito De Barber, C. (1999). Pasting properties of different wheat flour-hydrocolloid systems. *Food Hydrocolloids*, *13*(1), 27–33. https://doi.org/10.1016/S0268-005X(98)00066-6

Ronda, F., Perez-Quirce, S., Lazaridou, A., & Biliaderis, C. G. (2015). Effect of barley and oat β-glucan concentrates on gluten-free rice-based doughs and bread characteristics. *Food Hydrocolloids*, *48*, 197–207. https://doi.org/10.1016/j.foodhyd.2015.02.031

Sangpring, Y., Fukuoka, M., & Ratanasumawong, S. (2015). The effect of sodium chloride on microstructure, water migration, and texture of rice noodle. *LWT - Food Science and Technology*, *64*(2), 1107–1113. https://doi.org/10.1016/j.lwt.2015.07.035

Schober, T. J., Messerschmidt, M., Bean, S. R., Park, S. H., & Arendt, E. K. (2005). Gluten-free bread from sorghum: Quality differences among hybrids. *Cereal Chemistry*, *82*(4), 394–404. https://doi.org/10.1094/CC-82-0394

Sciarini, L. S., Ribotta, P. D., León, A. E., & Pérez, G. T. (2010). Effect of hydrocolloids on gluten-free batter properties and bread quality. *International Journal of Food Science and Technology*, *45*(11), 2306–2312. https://doi.org/10.1111/J.1365-2621.2010.02407.X

Steglich, T., Bernin, D., Röding, M., Nydén, M., Moldin, A., Topgaard, D., & Langton, M. (2014). Microstructure and water distribution of commercial pasta studied by microscopy and 3D magnetic resonance imaging. *Food Research International*, *62*, 644–652. https://doi.org/10.1016/j.foodres.2014.04.004

Tananuwong, K., & Reid, D. S. (2004). DSC and NMR relaxation studies of starch-water interactions during gelatinization. *Carbohydrate Polymers*, *58*(3), 345–358. https://doi.org/10.1016/j.carbpol.2004.08.003

Thybo, A. K., Szczypiński, P. M., Karlsson, A. H., Dønstrup, S., Stødkilde-Jørgensen, H. S., Andersen, H. J., Szczypi??ski, P. M., Karlsson, A. H., D??nstrup, S., St??dkilde-J??rgensen, H. S., & Andersen, H. J. (2004). Prediction of sensory texture quality attributes of cooked potatoes by NMR-imaging (MRI) of raw potatoes in combination with different image analysis methods. *Journal of Food Engineering*, *61*(1 SPEC.), 91–100. https://doi.org/10.1016/S0260-8774(03)00190-0

Turabi, E., Sumnu, G., & Sahin, S. (2008a). *Optimization of Baking of Rice Cakes in Infrared – Microwave Combination Oven by Response Surface Methodology*. 64–73. https://doi.org/10.1007/s11947-007-0003-4

Turabi, E., Sumnu, G., & Sahin, S. (2008b). Rheological properties and quality of rice cakes formulated with different gums and an emulsifier blend. *Food Hydrocolloids*, *22*(2), 305–312. https://doi.org/10.1016/j.foodhyd.2006.11.016

Turabi, E., Sumnu, G., & Sahin, S. (2010). Quantitative analysis of macro and micro-structure of gluten-free rice cakes containing different types of gums baked in different ovens. *Food Hydrocolloids*, *24*(8), 755–

762. https://doi.org/10.1016/j.foodhyd.2010.04.001

Vernon-Carter, E. J., Pérez-Orozco, J. P., Jiménez-Alvarado, R., Román-Guerrero, A., Orozco-Villafuerte, J., & Cruz-Sosa, F. (2008). Application and evaluation of mesquite gum and its fractions as interfacial film formers and emulsifiers of orange peel-oil. *Food Hydrocolloids*, *23*(3), 708–713. https://doi.org/10.1016/j.foodhyd.2008.06.005

Wilderjans, E., Luyts, A., Brijs, K., & Delcour, J. A. (2013). Ingredient functionality in batter type cake making. *Trends in Food Science and Technology*, *30*(1), 6–15. https://doi.org/10.1016/j.tifs.2013.01.001

e-ISSN 2757-5195

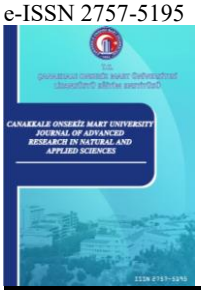

Çanakkale Onsekiz Mart University

Journal of Advanced Research in Natural and Applied Sciences

Open Access

doi.org/10.28979/jarnas.1140573 2023, Vol. 9, Issue 1, Pages: 15-27 dergipark.org.tr/tr/pub/jarnas

Kombucha Beverage: Comparative Study Based on Bioactive Properties and Antimicrobial Potentials of Different Plant Infusion

Cemhan Doğan[1], Nurcan Doğan[2*]

[1,2]Department of Food Technology, Bogazliyan Vocational School, Yozgat Bozok University, Yozgat, Türkiye

Article History

Received: 04.07.2022

Accepted: 24.08.2022

Published: 05.03.2023

Research Article

Abstract –Kombucha, a fermented beverage, is popular for its prophylactic and therapeutic properties. Kombucha is a traditionally black tea infusion fermented with a symbiotic bacteria and yeast consortium (SCOBY) under aerobic conditions for 7-21 days. However, the beneficial properties of kombucha vary according to the substrate kind, fermentation conditions, and SCOBY consortium. The present study has screened the physicochemical, bioactive, antimicrobial, and sensory properties of beverages produced by fermenting black, green, rosehip, and licorice tea infusions with kombucha starter culture for 21 days. Tea infusions before and after fermentation; pH value, titratable acidity (TA), pellicle weight, color values (L^*, a^*, b^*, ΔE), total phenolic content (TPC), antioxidant capacity against DPPH (2,2-diphenyl-1- picrylhydrazil) radicals, and antimicrobial activity was measured. Antimicrobial activity is applied to various foodborne pathogens such as *Escherichia coli* (*E. coli*), *Staphylococcus aureus* (*S. aureus*), and *C. albicans* with based disc diffusion method and spectrophotometric technique. In this study, tea type statistically affected all parameters except pH in kombucha beverages ($p<0.05$). The highest TPC and antioxidant activity were determined in the green tea kombucha sample. All kombucha beverages, especially those prepared by fermentation of licorice and green tea infusions, showed the highest antimicrobial potential against *E. coli* and *S. aureus*, respectively. Consequently, it is vital to prefer kombucha fermented with SCOBY instead of consuming beverages prepared with various plants' infusions to increase many beneficial properties and provide additional benefits.

Keywords *– Antimicrobial activity, bioactive potential, fermented beverage, Kombucha, SCOBY*

1. Introduction

The popularity of foods that provide additional health benefits beyond basic nutrition has accelerated over the past two decades (Sun-Waterhouse, 2011). Especially beverage industry is among the most dynamic food categories open to applications in the field of functional foods (Corbo et al., 2014). In addition to its thirst-quenching and refreshing/cooling, consumers expect functionality from beverages such as increasing energy, anti-aging, decreasing stress, and so on. even more so, they demand a positive effect in treating some diseases (Sethi et al., 2016). While new products are being developed to meet this demand in the beverage industry (Poveda-Castillo et al., 2018; Rojo-Poveda et al., 2019), some traditional drinks that are not valued enough are extremely striking.[1]

Kombucha is a refreshing beverage known for its added health benefits that have been traditionally consumed for thousands of years in many countries (Sun et al., 2015). The fermentation process includes sweetening the infused black tea and inoculating it with a Symbiotic Bacteria and Yeast Colony (SCOBY) and then incubating under aerobic conditions for 7-10 days (Villarreal-Soto et al., 2018). The new beverage formed after fermentation is rich in organic acids, vitamins, minerals, dietary fiber, essential amino acids, various enzymes, and secondary metabolites (Chu & Chen, 2006; Miranda et al., 2016). Its metabolites have beneficial effects such as antimicrobial (Cardoso et al., 2020), antitumor (Rasu Jayabalan et al., 2011), antihypertensive (Vitas et al., 2020), immune-modulatory (Villarreal-Soto et al., 2020), antioxidant, anticancer, antiinflammatory

[1] cemhan.dogan@bozok.edu.tr

[2] nurcan.dogan@bozok.edu.tr

[*]Corresponding Author

(Villarreal-Soto et al., 2019), and so on. The microflora of SCOBY, which is a cellulosic biofilm used as the starter culture of kombucha beverage, contains acetic acid bacteria (De Roos & De Vuyst, 2018), lactic acid bacteria (Marsh et al., 2014), and osmophilic yeasts (Coton et al., 2017). Probiotic microorganisms in the microbiota of SCOBY and the pharmacological activities of its biologically active ingredients in its liquid attracted the attention of researchers, and studies fermented using alternative substrates (raw material) other than black tea gained momentum (Oh et al., 2013; Emiljanowicz & Malinowska-Pańczyk, 2020).

Ultimately the substrate, fermentation time, sweeteners, and starter culture microflora used in kombucha production lead to the emergence of beverages with different chemical compositions and biological activities (Rasu Jayabalan et al., 2014). Especially in certain regions and cultures, plants that are traditionally consumed as cold or hot beverages and also have therapeutic potential can be preferred (Silva et al., 2021).

Rosa canina L. (Rosehip) is a wild rose in the *Rosaceae* family, known as the false fruit of its kind. Rosehip is a remarkable fruit with its high phenolic and antioxidant content (Medveckiene et al., 2020). It is used to treat infections, inflammatory diseases, chronic pain, ulcers etc., (Chrubasik et al., 2008). Therefore, rosehip is widely used in traditional medicine and is preferred in various foods (tea, jelly, jam, probiotic beverage, yoghurt, etc.) (Demir et al., 2014).

Glycyrrhiza glabra L. (Licorice) is a plant widely used, especially in the field of food. (Yang et al., 2020). Since licorice is characterized by its sweet taste and high nutritional value, it is preferred in desserts, beverages, snacks, and specialty foods (Fujii et al., 2014). In addition, the reason why licorice root is preferred in foods is associated with its antioxidant, anti-inflammatory, antimicrobial and antiviral activity originating from the triterpenoids and approximately 300 flavonoids it contains (Wang et al., 2019).

Although it varies according to society, tea is one of the most preferred beverages in the world after water. When it comes to tea, the leaves of the *Camellia sinensis* plant come to mind, and many types of tea are categorized as white, green, black and oolong tea according to the harvest time and fermentation degree of this plant (Khan & Mukhtar, 2019). Although the composition of tea changes depending on many factors, the most important active compound is polyphenols, which decrease due to fermentation. The antioxidant, anticancer, anti-hyperlipidemia, and antidiabetic effects of these compounds, which are high in green tea, are shown by studies (Kamal et al., 2021).

In this study, black tea was traditionally used in kombucha production and rosehip, licorice, and green tea were fermented separately with the kombucha liquid culture. Fermented kombucha beverages were analyzed for their physicochemical, bioactive, antimicrobial, and sensory properties.

2. Materials and Methods

Black tea (Doğuş, Turkey)/green tea leaves (Doğadan, Turkey), rosehip (Mest, Turkey)/licorice plants (Ramco, Turkey), and sugar were purchased from suppliers in Yozgat province. Kombucha liquid culture was provided from Yozgat Bozok University, Boğazlıyan Vocational School (Yozgat, Turkey). The chemicals were purchased from Merck (Darmstadt, Germany) unless otherwise stated.

2.1. Preparation and fermentation of Kombucha Beverages

Kombucha beverages were produced according to Tapias et al. (2022) with minor modifications. For this purpose, it was dissolved by adding sucrose (90 g/L) to the boiling drinking water, and then ten grams of the plant (4 g/L) were added in filtering bags for each tea sample and infused for 20 minutes, cooled to 25°C. After that, it was inoculated with 10% starter kombucha liquid culture and incubated in filtered glass jars for 21 days under dark room conditions (25±2 °C) (Figure 1). Tea samples were analyzed before fermentation (BF) and after fermentation (AF).

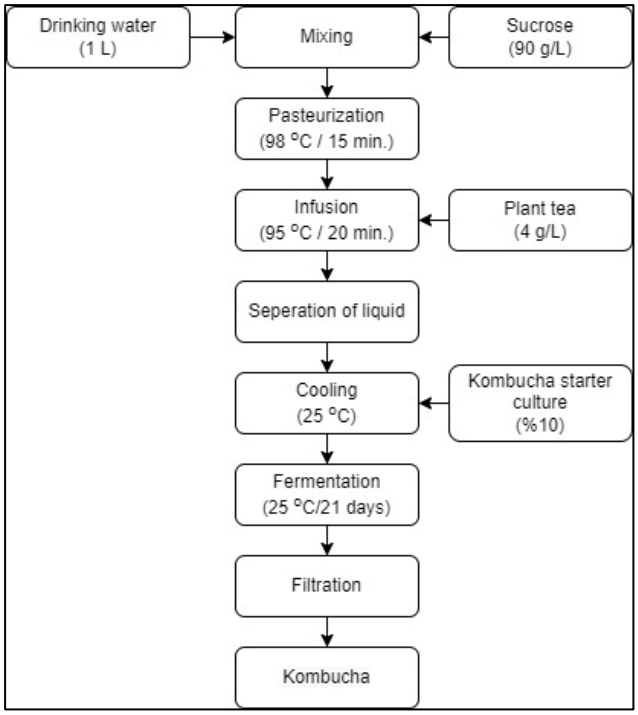

Figure 1. Kombucha production flowchart

2.2. Determination of Some Physicochemical Properties of Kombucha Beverages

Standard methods of AOAC (2002) were used pH, titratable acidity (%), and pellicle weight of the kombucha samples was determined BF and AF.

The pH value, color changes and pellicle weight of the kombucha samples were recorded using a digital pH meter (Hanna, HI 99131, U.S.A.), colorimeter (Lovibond, England), precision scale (Radwag AS 220/C/2 Poland), respectively. The titration acidity was performed by titration in the presence of 0.1 N NaOH and expressed as g/L of acetic acid. The color values (L^*, a^*, b^*) of the kombucha samples were determined according to Ramaswamy ve Richards (1980). ΔE was calculated as;

$$\Delta E = \left[\left(L_{bf} - L_{af}\right)^2 + \left(a_{bf} - a_{af}\right)^2 + \left(b_{bf} - b_{af}\right)^2\right]^{\frac{1}{2}} \quad (2.1)$$

Where *bf* and *af* express the condition of the samples before and after fermentation, respectively.

2.3. Bioactive Properties of Kombucha Beverages

2.3.1. Total Phenolic Content (TPC) Analysis

TPC was performed Folin-Ciocalteu reagent assay (AOAC, 1975). For this purpose, 0.4 mL of kombucha was vortexed in a test tube with 2 mL of Folin-Ciocalteu (10-fold diluted) and 1.6 mL of 7.5% Na_2CO_3, respectively. After 1 hour of incubation in the dark, absorbance was recorded at 765 nm (Optizen POP, Mecasys Co., Ltd, Korea). The TPC value of the samples was calculated according to a standard gallic acid curve and expressed in mg gallic acid equivalent (GAE)/mL kombucha.

2.3.2. Antioxidant Activities Analysis

The antioxidant capacity of kombucha samples was performed to the DPPH method. In context, 0.1 mL kombucha and 3.9 mL (25 mg/L) ethanolic DPPH solution were mixed in a test tube and incubated in a dark place for 30 minutes at room temperature. After incubation, the absorbance of the samples was recorded

at 515 nm using a spectrophotometer (Brand-Williams et al., 1995; Sharma & Bhat, 2009).

The antioxidant activity (DPPH inhibition (%)) was calculated according to the formula:

$$DPPH\ inhibition\ (\%) = \frac{A_B - A_S}{A_B} \times 100 \quad (2.2)$$

Where A_B is the absorbance of the blank and A_S is the absorbance of the kombucha.

2.4. *In Vitro* Antimicrobial Activity

The antimicrobial activity of kombucha was determined on several food-borne pathogens, namely gram-negative bacteria *Escherichia coli* (*E. coli*), gram-positive bacteria *Staphylococcus aureus* (*S. aureus*), and *Candida albicans* (*C. albicans*).

Antimicrobial activity was performed based on the agar-based disc diffusion method and spectrophotometric technique (Chiu et al., 2021). Stock cultures were transferred to 5 mL Mueller Hinton Broth for each microorganism and incubated at 35 °C until they reached 10^8 CFU/mL based on OD 600 absorbance. 100 µL of the diluted bacterial load was inoculated onto Mueller Hinton Agar and spread over the entire petri dish with a sterile swab. After waiting for 5 minutes for surface absorption, 6 mm diameter sterile discs were placed on the agar and 25 µL of filtered tea samples were adsorbed on the discs. After the petri dishes were incubated for 24 hours at 35 °C, the zone diameters formed around the discs were measured with a caliper and recorded.

2.5. Sensory Evaluation

Kombucha samples were evaluated at the end of 21 days of aerobic fermentation in terms of color, odor, appearance/brilliant, taste/aroma, and general acceptability. Fermented and unfermented tea samples were presented to each panelist in random order with three-digit codes, respectively.

Samples were rated on a typical 9-point hedonic scale by a consumer panel of 25 panelists. In scoring, (1) dislike extremely, (2) dislike so much, (3) dislike moderately, (4) dislike slightly, (5) neither like nor dislike, (6) like slightly, (7) like moderately, (8) like so much (9) like extremely (Maughan et al., 2012).

2.6. Statistical Analysis

IBM- SPSS 22.0 statistical package (SPSS Inc., Chicago, IL, USA) was used to determine the significance of the differences ($p<0.05$) between the data, and group means were compared with the Duncan multiple comparison test and independent samples T-test. Results were analyzed using one-way analysis of variance (ANOVA) and expressed as mean ± standard deviation. The intensity of the parameters of all samples was visualized using a color-coded heatmap. The corresponding two-dimensional plot was prepared using the software OriginPro 2021 (OriginLab Corporation, Northampton, UK).

3. Results and Discussion

The physicochemical bioactive, antimicrobial, and sensory properties of kombucha beverages are shown in Table 1.

Table 1
Physicochemical, bioactive, antimicrobial, and sensory properties of kombucha beverages

	Tea samples							
	Black tea		**Green tea**		**Rosehip tea**		**Licorice tea**	
Parameters	**BF**	**AF**	**BF**	**AF**	**BF**	**AF**	**BF**	**AF**
pH	6.58±0.02	3.20±0.01*^{a}	6.84±0.01	3.12±0,01*^{a}	4.13±0.05	3.22±0.03*^{a}	5.19±0.01	3.12±0.02*^{a}
Titratable acidity (%)	0.44±0.01	9.60±0.00*^{c}	0.51±0.01	18.60±0.02*^{a}	0.87±0.01	9.00±0.06*^{d}	0.33±0.01	18.00±0.08*^{b}
Pellicle weight (g/L)	-	19.15±0.07^{c}	-	26.88±0.11^{a}	-	23.33±0.22^{b}	-	15.1±0.05^{d}
L	50.87±2.2	49.6±1.34*^{b}	58.33±1.06	59.23±0.60*^{a}	29.60±1.10	31.30±0.80*^{c}	30.50±0.80	17.73±0.66*^{d}
a	7.17±1.01	5.83±0.85*^{c}	-3.03±0.40	-1.87±0.15*^{d}	39.03±1.53	48.87±0.35*^{a}	20.43±1.10	21.37±0.66*^{b}
b	46.3±0.90	47.97±0.55*^{a}	47.1±0.10	39.33±0.66*^{c}	27.97±1.17	37.77±0.66*^{d}	38.13±1.38	47.77±0.06*^{b}
ΔE	-	2.48±0.04^{d}	-	7.90±0.01^{c}	-	13.99±0.05^{b}	-	16.02±0.04^{a}
TPC (mg GAE/mL)	61.08±3.02	123.41±1.85*^{c}	169.41±2.63	717.08±2.89*^{a}	61.26±1.55	77.71±2.33*^{d}	50.04±1.47	225.05±3.00*^{b}
DPPH inhibition (%)	24.21±0.10	57.76±0.77*^{b}	76.29±0.11	93.24±0.63*^{a}	24.47±0.09	33.89±1.1*^{c}	15.53±0.05	27.38±1.22*^{d}
***E.coli* (mm)**	N.D	8.00±0.58^{d}	N.D	12.00±0.89^{b}	N.D	9.00±1.10^{c}	N.D	13.00±0.75^{a}
***S.aureus* (mm)**	N.D	15.00±0.22^{c}	N.D	20.00±0.30^{a}	N.D	11.00±0.35^{d}	N.D	16.00±1.00^{b}
Color	5.52±0.06	4.92±0.01*^{b}	4.72±0.07	4.04±0.3*^{c}	6.64±0.01	7.64±0.45*^{a}	5.00±0.69	3.72±0.03*^{d}
Odor	4.84±0.02	2.8±0.24*^{b}	5.72±0.34	2.8±0.22*^{b}	6.2±0.74	5.04±0.12*^{a}	4.88±0.31	2.76±0.02*^{b}
Appearance/Brightness	5.8±0.01	5.04±0.11*^{b}	5.24±0.21	4.28±0.13*^{c}	7.08±0.36	7.28±0.14*^{a}	5.76±0.47	3.64±0.01*^{d}
Taste/Aroma	6.04±0.02	3.64±0.26*^{b}	5.52±0.14	2.76±0.04*^{d}	6.76±0.57	5.92±0.03*^{a}	5.32±0.29	3.28±0.07*^{c}
Overall acceptability	6.68±0.23	4.00±0.06*^{b}	5.48±0.36	3.04±0.47*^{d}	7.12±0.06	5.88±0.05*^{a}	6.12±0.15	3.56±0.43*^{c}

BF: Before fermentation, AF: After fermentation, significant differences ($p<0.05$) between parameters after and before fermentation are expressed with *, the AF tea samples' significant differences ($p<0.05$) were expressed in lowercase letters., N.D: Non-determined.

The pH values of the tea samples before fermentation varied between 4.13 and 6.84. The pH values of the tea samples decreased dramatically after fermentation with the starter kombucha liquid culture, and this decrease was found to be statistically significant ($p<0.05$). This decrease is due to formation of organic acids associated with biological activity because of fermentation. The pH value of tea samples decreases due to the production of organic acids (acetic acid, glucuronic acid, citric acid, etc.) during fermentation. The resulting acidity has a positive effect on the activities of the yeasts, increasing the ethanol concentration and then allowing the acetic acid bacteria to dominate the environment (Dufresne & Farnworth, 2000). The rapid decrease in pH value in the first days of fermentation is important to prevent the development of microorganisms that can spoil (Sharma & Bhat, 2009). The decrease in pH values due to fermentation is similar to other studies (Battikh et al., 2013; Chakravorty et al., 2016). However, the pH change between tea samples at the end of the 21st day was statistically insignificant ($p>0.05$). Different substrate types show distinct changes in pH depending on the starting culture (yeast and acetic acid bacteria). Still, they show similar trends at the end of fermentation (final pH) (Sun et al., 2015). Differences between total acidity values for fermented and unfermented tea samples were statistically significant ($p<0.05$). Although no significant differences were observed between the tea samples at the end of the fermentation period in pH values ($p>0.05$), the total acidity values were found to be statistically significant ($p<0.05$).

There is a negative correlation between pH and total acidity in all tea samples ($r= -0.78$). It is known that the acidity value increases and the pH level decrease after fermentation in tea samples (Velićanski et al., 2014). In addition, towards the end of the fermentation, there was no significant change in the pH values of the samples, while an increase was observed in the total acidity values. On the other hand, acetic acid, one of the dominant acids of kombucha, can be broken down into water and carbon dioxide with over fermentation (R. Jayabalan et al., 2007). Therefore, pH and total acidity should be evaluated together in determining the fermentation time of kombucha samples.

SCOBY forms a film of bacterial cellulose (pellicle) on the surface during fermentation. The pellicle to be formed as a result of fermentation depends on the microorganism load/type of the kombucha starter culture,

the substrate, the metabolites produced during fermentation, the fermentation time and incubation conditions, etc. (Mukadam et al., 2016). As fermentation progresses, the pellicle forms thicker layers and protects the kombucha against contaminants (May et al., 2019). Moreover, pellicle can be evaluated as an indicator at the completion of fermentation. The suspended pellicle on the surface tends to sink to the bottom when the fermentation ends. In addition, in recent years, due to its cellulosic composition, it has been used in bio-textile and biomedical fields and as a source of food packaging materials, etc. (Azeredo et al., 2019; Cottet et al., 2020). Moreover, pellicle could be edible and used for gastronomy/culinary (Torán-Pereg et al., 2021). Pellicle; exhibits antioxidant and antimicrobial activity due to its phytochemical characterization (Ramírez Tapias et al., 2020).

Pellicle weight in kombucha teas was determined as 19.15±0.07, 26.88±0.11, 23.33±0.22, and 15.1±0.05 for black, green, rosehip, and licorice teas, respectively. The highest pellicle weight was detected in green tea kombucha (Table 1). The highest bioactivity and antimicrobial activity in fermented green tea are due to the bioactive and antimicrobial compounds provided by both the substrate source and the pellicle thickness.

Table 1 gives the color values (L^*, a^*, b^*, and ΔE). Fermented and unfermented samples of the same teas showed significance ($p<0.05$). While the L^* value increased in green tea and rosehip teas due to fermentation, it decreased in black and licorice teas. Depending on the fermentation, an increase was observed in a* values excluding black and green fermented tea, an addition was found in b* values excluding green tea. The high color change due to fermentation was observed in all tea samples. The differences in brightness in kombucha tea are due to the transformation of polyphenols as a result of the enzymatic activities of microorganisms in its natural flora (R. Jayabalan et al., 2007). Color values may vary due to phenolics, carotenoids, microbial transformation, substrate source, etc., in fermentation and storage periods (Watawana et al., 2018).

TPC and antioxidant potential of fermented tea was in the range between 77.71- 717.08 mg GAE/mL and 27.38-93.24% DPPH inhibition, respectively (Table 1). Before fermentation, black tea, green tea, rosehip, and licorice tea had high TPC and antioxidant capacity and showed statistical differences ($p<0.05$). TPC and DPPH inhibition (%) increased significantly with fermentation in four different tea samples ($p<0.05$).

The intensity of parameters such as physicochemical, bioactive, antimicrobial, and sensory properties of teas obtained from different plant infusions before and after the fermentations were visualized using a color-coded heat map in Figure 2.

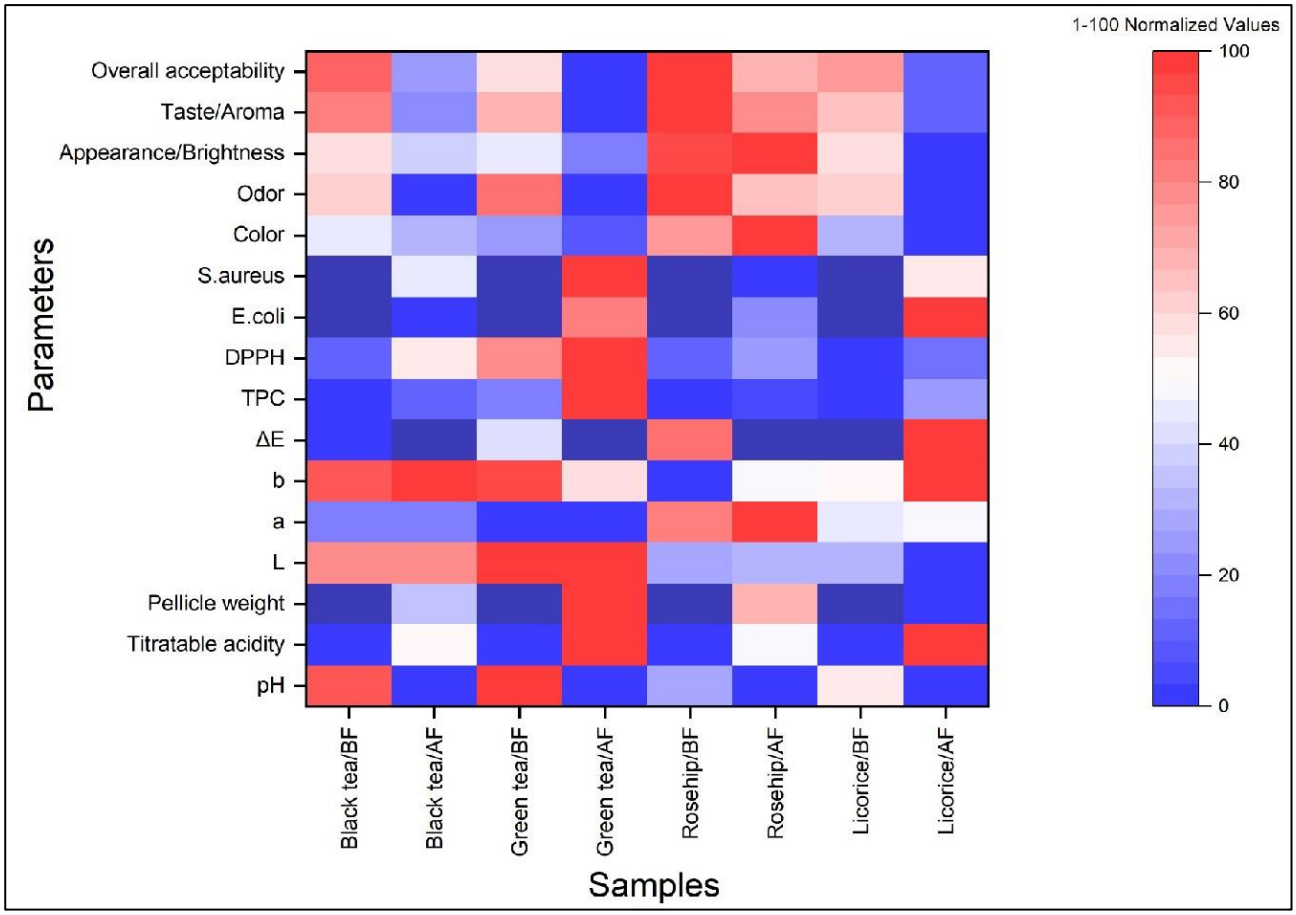

Figure 2. Heat map plot of each sample according to parameters.

In the heatmap, red tones indicate a high parameter value, while blue tones indicate visa versa. In Figure 2, when plant infusions are fermented with SCOBY, it can be observed that their bioactive properties and antimicrobial activities increase. The highest bioactive properties and antimicrobial activities were observed in kombucha samples prepared with green tea (Figure 2).

Higher TPC levels in kombucha are associated with the breakdown of complex phenolic compounds by enzymes in yeast and bacteria (Bhattacharya et al., 2013). Green tea showed the highest TPC (169.41±2.63) and antioxidant activity (76.29±0.11) before fermentation. The highest increase in TPC value (328.28%) was seen in fermented green tea. There is a positive correlation (r=0.77) between TPC and DPPH inhibition %. Kombucha exhibits high free radical scavenging activities. The potency of antioxidant activity also depends on the fermentation time, substrate, fermentation conditions, and culture microbiota. In different kombucha samples, polyphenol compounds and antioxidants activity increased in proportion to the increase in fermentation time. There is a statistical correlation between the polyphenol content of kombucha and its antioxidant capacity. In addition, the substrate used in kombucha production and the fermentation time also affects the bioactive character (Jakubczyk et al., 2020). R. Jayabalan et al. (2007) investigated kombucha phenolics such as epicatechin isomers EGCG ([-]-epigallocatechin-3-gallate), EGC ([-]-epigallocatechin), ECG (-]-epicatechin-3-gallate), and EC ([-]-epicatechin). The results showed modifiable stability of these components throughout the fermentation process. Before fermentation in green tea, EC, ECG, EGC, and EGCG polyphenols predominate, but when fermented, ECG, CG, GA, and EGCG polyphenols dominate the environment. The concentration of polyphenols (catechins and flavonols) responsible for antioxidant activity was reduced in brewed green and black teas (Record & Lane, 2001). Catechins lost in the final product, are further polymerized into high molecular weight molecules leading to the detection of higher phenolic contents in kombucha. Thus, the high phenolic component and antioxidant capacity of kombucha teas in the study can be explained by this phenomenon (Chu & Chen, 2006).

The fact that the antioxidant molecules of tea extracts have a high scavenging effect against free radicals and

that this feature increases further and probably provides protection against oxidative damage gives this beverage a functional character. In previous studies, similar results were obtained with biological activities in kombucha made with different plant extracts (Gaggìa et al., 2018; Massoud et al., 2022). Many benefits of kombucha's antioxidant activity are known, such as preventing cancer, boosting immunity, and anti-inflammatory. Beneficial effects of kombucha, it is generally associated with phenolic compounds, acids (gluconic acid, glucuronic acid, acetic acid, lactic acid), amino acids, lipids, proteins, some hydrolytic enzymes, carbon dioxide, vitamins, minerals, etc. (Rasu Jayabalan et al., 2014).

None of the unfermented tea samples showed antimicrobial activity. High antimicrobial activity was detected in fermented teas against *E. coli* and *S. aureus* (Table 1). The highest antimicrobial activity against *E. coli* was determined in licorice fermented tea with inhibition zone diameters of 13 mm. The highest activity against *S. aureus* was detected in green tea (20 mm). In addition, four different fermented tea varieties showed inhibition zone diameters against *E. coli* and *S. aureus*, and the difference between them was statistically significant ($p<0.05$). Antimicrobial activity was not detected in tea samples against *C. albicans*. It is in agreement with the literature that kombuchas did not exhibit antimicrobial activity against *C. albicans* (Greenwalt et al., 1998). In another study reported by Battikh et al. (2013), although it does not show as much inhibition zone diameter as bacteria, *C. albicans* have been shown to be effective. Based on this difference, factors such as kombucha consortium, substrate type, acidity level and type, fermentation conditions, etc., can be effective.

The antimicrobial activity of kombucha against pathogenic microorganisms has been emphasized by many researchers, and this activity has been associated with acetic acid, proteins and catechins (Greenwalt et al., 1998; Sreeramulu et al., 2001). It has been reported that the antimicrobial effect of kombucha is positively related to some organic acids (Greenwalt et al., 1998). Currently, organic acids are a common practice in food preservation against some foodborne pathogenic microorganisms. In addition, Liu et al. (1996) reported that kombucha has antimicrobial activity against pathogenic bacteria, and this is due to acetic acid. High positive correlations coefficient of 0.95 and 0.82 were determined between the antibacterial activities of fermented tea samples against *E. coli* and *S. aureus* and their titratable acidity, respectively.

The sensory parameters such as over color, odor, appearance/brightness, taste/aroma, and overall acceptability of fermented and unfermented tea samples was evaluated (Table1). Sensory score of fermented teas lower than unfermented teas, and the difference is significant ($p<0.05$). There is a statistically difference between kombucha samples prepared with different herbal infusions in terms of overall acceptability ($p<0.05$). A decrease was observed in color and appearance parameter values due to fermentation in other plant infusions except for rosehip. However, these values increased in rosehip. Color is an important criterion for consumers and is associated with appearance. It is thought that rosehip kombuchas are more appreciated in terms of color and appearance, due to the positive effect of the reddish color on the panelists. As clearly seen in Figure 2, rosehip was the most popular (in terms of general acceptability) among the kombucha samples. It was followed by samples of kombucha, in which black, licorice, and green tea infusions were prepared, respectively. However, a decrease in odor, taste, and overall acceptability was observed in all plant infusions due to fermentation. The reason for the low sensory parameters in kombucha samples is the increase in acidity and the dominant taste of acetic acid, which is one of the dominant acids, and the negative effect on consumers due to the smell of vinegar. The negative correlation ($r= -0.80$) between the titratable acidity obtained in the fermented tea samples and the overall acceptability confirms our hypothesis. Although the fermentation process negatively affects the sensory parameters, this problem can be overcome with the conscious consumers' search for healthy beverages and familiarity with long-term consumption.

Determining an optimum fermentation time to produce kombucha can significantly impact consumption acceptability. Otherwise, high acidity limits the amount of use and poses a potential risk, especially for people with stomach-related ailments. However, there are limited studies that reveal the sensory parameters of kombucha. The inclusion of gastronomic considerations in kombucha studies over the past two decades is promising (Kim & Adhikari, 2020).

4. Conclusion

The increasing consumer interest in functional foods has recently affected the soft drink industry. This interest is more in traditional fermented beverages because of their positive effects on health. Kombucha, known and consumed as fermented tea for centuries, is still consumed with or without knowing its positive effects on health, thanks to its primary and secondary components. In order to explain the health benefits of

kombucha, its antioxidant and antimicrobial capacity is emphasized. Since the beneficial properties and sensory parameters of kombucha usually depend on the fermented tea type when some other parameters remain constant (the content of SCOBY, fermentation conditions, etc.); in this study, physicochemical, bioactive, antimicrobial, and sensory properties were tested by using four different plant infusions. Kombucha samples were tested on day 21. The results showed that each fermented beverage had higher antioxidant activity than unfermented ones. DPPH inhibition activity by fermentation of teas increased by 138%, 22.22%, 38.50%, and 76.30% for black, green, rosehip, and licorice samples, respectively. Tea samples that did not show antimicrobial activity showed effective inhibition zone diameter against *E. coli* and *S. aureus* after fermentation. The most beneficial fermented beverage in terms of bioactive properties was observed in kombucha prepared from green tea. It also showed the highest antimicrobial activity against *S. aureus*. The highest antimicrobial activity against *E. coli* was detected in kombucha produced from licorice. However, kombucha prepared with rosehip infusions was most appreciated by the panelists. While fermented rosehip sample is lower than fermented green tea in terms of bioactive and antimicrobial properties, they are higher in antioxidant capacity than fermented licorice tea. In kombucha production, the kombucha starter culture, the substrate, the fermentation time, and incubation conditions affect the physicochemical, bioactive, antimicrobial, and sensory properties of the final product. Here, the final decision should be left to the consumers, depending on personal needs and demands.

Although kombucha consumption has increased rapidly in recent years, it has not come to the place it deserves. Low sensory acceptability scores can be resolved by optimizing the fermentation time and/or flavoring. Moreover, natural or artificial carbonation can positively affect consumers' purchasing.

Acknowledgement

This study was carried out without any financial support.

Author Contributions

Cemhan Doğan: Provided the concept of the study, drafting of the article and final approval of the submitted version

Nurcan Doğan: Provided the analysis and interpretation of data, drafting and revision of the article.

Conflicts of Interest

The authors declare no conflict of interest.

References

AOAC. (2002). Official Methods of Analysis of AOAC International, 17th ed. Methods 976.05, 923.03, 962.09, 920.39. USA: Association of Official Analytical Chemists. Retrieved from: https://doi.org/10.1093/jaoac/85.5.1187

AOAC. (1975). Association of Official Analytical Chemists. Official Methods of analysis. *In Methods in Enzymology* (Vol. 299, pp. 152–178). Academic Press. Retrieved from: https://doi.org/10.1016/S0076-6879(99)99017-1

Azeredo, H. M. C., Barud, H., Farinas, C. S., Vasconcellos, V. M., & Claro, A. M. (2019). Bacterial Cellulose as a Raw Material for Food and Food Packaging Applications. *Frontiers in Sustainable Food Systems*, *3*, 7. Retrieved from: https://doi.org/10.3389/FSUFS.2019.00007/BIBTEX

Battikh, H., Chaieb, K., Bakhrouf, A., & Ammar, E. (2013). Antibacterial and antifungal activities of black and green kombucha teas. *Journal of Food Biochemistry*, *37*(2), 231–236. Retrieved from: https://doi.org/10.1111/j.1745-4514.2011.00629.x

Bhattacharya, S., Gachhui, R., & Sil, P. C. (2013). Effect of Kombucha, a fermented black tea in attenuating oxidative stress mediated tissue damage in alloxan induced diabetic rats. *Food and Chemical Toxicology*, *60*, 328–340. Retrieved from: https://doi.org/10.1016/J.FCT.2013.07.051

Brand-Williams, W., Cuvelier, M. E., & Berset, C. (1995). Use of a free radical method to evaluate antioxidant activity. *LWT - Food Science and Technology*, *28*(1), 25–30. Retrieved from: https://doi.org/10.1016/S0023-6438(95)80008-5

Cardoso, R. R., Neto, R. O., dos Santos D'Almeida, C. T., do Nascimento, T. P., Pressete, C. G., Azevedo, L., Martino, H. S. D., Cameron, L. C., Ferreira, M. S. L., & Barros, F. A. R. de. (2020). Kombuchas from

green and black teas have different phenolic profile, which impacts their antioxidant capacities, antibacterial and antiproliferative activities. *Food Research International*, *128*, 108782. Retrieved from: https://doi.org/10.1016/J.FOODRES.2019.108782

Chakravorty, S., Bhattacharya, S., Chatzinotas, A., Chakraborty, W., Bhattacharya, D., & Gachhui, R. (2016). Kombucha tea fermentation: Microbial and biochemical dynamics. *International Journal of Food Microbiology*, *220*, 63–72. Retrieved from: https://doi.org/10.1016/J.IJFOODMICRO.2015.12.015

Chiu, C. T., Lai, C. H., Huang, Y. H., Yang, C. H., & Lin, J. N. (2021). Comparative analysis of gradient diffusion and disk diffusion with agar dilution for susceptibility testing of Elizabethkingia anophelis. *Antibiotics*, *10*(4), 450. Retrieved from: https://doi.org/10.3390/antibiotics10040450

Chrubasik, C., Roufogalis, B. D., Müller-Ladner, U., & Chrubasik, S. (2008). A systematic review on the Rosa canina effect and efficacy profiles. *Phytotherapy Research*, *22*(6), 725–733. Retrieved from: https://doi.org/10.1002/PTR.2400

Chu, S. C., & Chen, C. (2006). Effects of origins and fermentation time on the antioxidant activities of kombucha. *Food Chemistry*, *98*(3), 502–507. Retrieved from: https://doi.org/10.1016/J.FOODCHEM.2005.05.080

Corbo, M. R., Bevilacqua, A., Petruzzi, L., Casanova, F. P., & Sinigaglia, M. (2014). Functional Beverages: The Emerging Side of Functional Foods: Commercial Trends, Research, and Health Implications. *Comprehensive Reviews in Food Science and Food Safety*, *13*(6), 1192–1206. Retrieved from: https://doi.org/10.1111/1541-4337.12109

Coton, M., Pawtowski, A., Taminiau, B., Burgaud, G., Deniel, F., Coulloumme-Labarthe, L., Fall, A., Daube, G., & Coton, E. (2017). Unraveling microbial ecology of industrial-scale Kombucha fermentations by metabarcoding and culture-based methods. *FEMS Microbiology Ecology*, *93*(5). Retrieved from: https://doi.org/10.1093/FEMSEC/FIX048

Cottet, C., Ramirez-Tapias, Y. A., Delgado, J. F., la Osa, O. De, Salvay, A. G., & Peltzer, M. A. (2020). Biobased Materials from Microbial Biomass and Its Derivatives. *Materials 2020, Vol. 13, Page 1263*, *13*(6), 1263. Retrieved from: https://doi.org/10.3390/MA13061263

De Roos, J., & De Vuyst, L. (2018). Acetic acid bacteria in fermented foods and beverages. *Current Opinion in Biotechnology*, *49*, 115–119. Retrieved from: https://doi.org/10.1016/j.copbio.2017.08.007

Demir, N., Yildiz, O., Alpaslan, M., & Hayaloglu, A. A. (2014). Evaluation of volatiles, phenolic compounds and antioxidant activities of rose hip (Rosa L.) fruits in Turkey. *LWT - Food Science and Technology*, *57*(1), 126–133. Retrieved from: https://doi.org/10.1016/j.lwt.2013.12.038

Dufresne, C., & Farnworth, E. (2000). Tea, Kombucha, and health: A review. *Food Research International*, *33*(6), 409–421. Retrieved from: https://doi.org/10.1016/S0963-9969(00)00067-3

Emiljanowicz, K. E., & Malinowska-Pańczyk, E. (2020). Kombucha from alternative raw materials–The review. In *Critical Reviews in Food Science and Nutrition* (Vol. 60, Issue 19, pp. 3185–3194). Taylor & Francis. Retrieved from: https://doi.org/10.1080/10408398.2019.1679714

Fujii, S., Morinaga, O., Uto, T., Nomura, S., & Shoyama, Y. (2014). Development of a monoclonal antibody-based immunochemical assay for liquiritin and its application to the quality control of licorice products. *Journal of Agricultural and Food Chemistry*, *62*(15), 3377–3383. Retrieved from: https://doi.org/10.1021/JF404731Z/ASSET/IMAGES/JF404731Z.SOCIAL.JPEG_V03

Gaggìa, F., Baffoni, L., Galiano, M., Nielsen, D. S., Jakobsen, R. R., Castro-Mejía, J. L., Bosi, S., Truzzi, F., Musumeci, F., Dinelli, G., & Di Gioia, D. (2018). Kombucha Beverage from Green, Black and Rooibos Teas: A Comparative Study Looking at Microbiology, Chemistry and Antioxidant Activity. *Nutrients 2019, Vol. 11, Page 1*, *11*(1), 1. Retrieved from: https://doi.org/10.3390/NU11010001

Greenwalt, C. J., Ledford, R. A., & Steinkraus, K. H. (1998). Determination and characterization of the antimicrobial activity of the fermented tea Kombucha. *LWT - Food Science and Technology*, *31*(3), 291–296. Retrieved from: https://doi.org/10.1006/fstl.1997.0354

Jakubczyk, K., Kałduńska, J., Kochman, J., & Janda, K. (2020). Chemical Profile and Antioxidant Activity of the Kombucha Beverage Derived from White, Green, Black and Red Tea. *Antioxidants 2020, Vol. 9, Page 447*, *9*(5), 447. Retrieved from: https://doi.org/10.3390/ANTIOX9050447

Jayabalan, R., Marimuthu, S., & Swaminathan, K. (2007). Changes in content of organic acids and tea polyphenols during kombucha tea fermentation. *Food Chemistry*, *102*(1), 392–398. Retrieved from: https://doi.org/10.1016/J.FOODCHEM.2006.05.032

Jayabalan, Rasu, Chen, P.-N., Hsieh, Y.-S., Prabhakaran, K., Pitchai, P., Marimuthu, S., Thangaraj, P., Swaminathan, K., & Eok Yun, S. (2011). Effect of solvent fractions of kombucha tea on viability and

invasiveness of cancer cells-Characterization of dimethyl 2-(2-hydroxy-2-methoxypropylidine) malonate and vitexin. *Indian Journal of Biotechnology*, *10*, 75–82. Retrieved from: http://nopr.niscair.res.in/bitstream/123456789/10955/1/IJBT%2010(1)%2075-82.pdf

Jayabalan, Rasu, Malbaša, R. V., Lončar, E. S., Vitas, J. S., & Sathishkumar, M. (2014). A review on kombucha tea-microbiology, composition, fermentation, beneficial effects, toxicity, and tea fungus. In *Comprehensive Reviews in Food Science and Food Safety* (Vol. 13, Issue 4, pp. 538–550). John Wiley & Sons, Ltd. Retrieved from: https://doi.org/10.1111/1541-4337.12073

Kamal, D. A. M., Salamt, N., Zaid, S. S. M., & Mokhtar, M. H. (2021). Beneficial effects of green tea catechins on female reproductive disorders: A review. *Molecules*, *26*(9), 2675. Retrieved from: https://doi.org/10.3390/molecules26092675

Khan, N., & Mukhtar, H. (2019). Tea polyphenols in promotion of human health. In *Nutrients* (Vol. 11, Issue 1, p. 39). *Multidisciplinary Digital Publishing Institute*. Retrieved from: https://doi.org/10.3390/nu11010039

Kim, J., & Adhikari, K. (2020). Current trends in kombucha: Marketing perspectives and the need for improved sensory research. In *Beverages* (Vol. 6, Issue 1, pp. 1–19). Multidisciplinary Digital Publishing Institute. Retrieved from: https://doi.org/10.3390/beverages6010015

Liu, C. H., Hsu, W. H., Lee, F. L., & Liao, C. C. (1996). The isolation and identification of microbes from a fermented tea beverage, Haipao, and their interactions during Haipao fermentation. *Food Microbiology*, *13*(6), 407–415. Retrieved from: https://doi.org/10.1006/FMIC.1996.0047

Marsh, A. J., O'Sullivan, O., Hill, C., Ross, R. P., & Cotter, P. D. (2014). Sequence-based analysis of the bacterial and fungal compositions of multiple kombucha (tea fungus) samples. *Food Microbiology*, *38*, 171–178. Retrieved from: https://doi.org/10.1016/j.fm.2013.09.003

Massoud, R., Jafari-Dastjerdeh, R., Naghavi, N., & Khosravi-Darani, K. (2022). All aspects of antioxidant properties of kombucha drink. In *Biointerface Research in Applied Chemistry* (Vol. 12, Issue 3, pp. 4018–4027). Retrieved from: https://doi.org/10.33263/BRIAC123.40184027

Maughan, C., Tansawat, R., Cornforth, D., Ward, R., & Martini, S. (2012). Development of a beef flavor lexicon and its application to compare the flavor profile and consumer acceptance of rib steaks from grass- or grain-fed cattle. *Meat Science*, *90*(1), 116–121. Retrieved from: https://doi.org/10.1016/J.MEATSCI.2011.06.006

May, A., Narayanan, S., Alcock, J., Varsani, A., Maley, C., & Aktipis, A. (2019). Kombucha: A novel model system for cooperation and conflict in a complex multi-species microbial ecosystem. *PeerJ*, *2019*(9), e7565. Retrieved from: https://doi.org/10.7717/peerj.7565

Medveckiene, B., Kulaitiene, J., Jariene, E., Vaitkevičiene, N., & Hallman, E. (2020). Carotenoids, polyphenols, and ascorbic acid in organic rosehips (Rosa spp.) cultivated in Lithuania. *Applied Sciences (Switzerland)*, *10*(15), 5337. Retrieved from: https://doi.org/10.3390/APP10155337

Miranda, B., Lawton, N. M., Tachibana, S. R., Swartz, N. A., & Hall, W. P. (2016). Titration and HPLC Characterization of Kombucha Fermentation: A Laboratory Experiment in Food Analysis. *Journal of Chemical Education*, *93*(10), 1770–1775. Retrieved from: https://doi.org/10.1021/ACS.JCHEMED.6B00329/ASSET/IMAGES/ACS.JCHEMED.6B00329.SOCIAL.JPEG_V03

Mukadam, T. A., Punjabi, K., Deshpande, S. D., Vaidya, S. P., & Chowdhary, A. S. (2016). Isolation and Characterization of Bacteria and Yeast from Kombucha Tea. *International Journal of Current Microbiology and Applied Sciences*, *5*(6), 32–41. Retrieved from: https://doi.org/10.20546/ijcmas.2016.506.004

Oh, J., Jo, H., Cho, A. R., Kim, S. J., & Han, J. (2013). Antioxidant and antimicrobial activities of various leafy herbal teas. *Food Control*, *31*(2), 403–409. Retrieved from: https://doi.org/10.1016/J.FOODCONT.2012.10.021

Poveda-Castillo, G. D. C., Rodrigo, D., Martínez, A., & Pina-Pérez, M. C. (2018). Bioactivity of Fucoidan as an antimicrobial agent in a new functional beverage. *Beverages*, *4*(3), 64. Retrieved from: https://doi.org/10.3390/beverages4030064

Ramaswamy, H. S., & Richards, J. F. (1980). A Reflectance Method to Study the Green-Yellow Changes in Fruits and Vegetables. *Canadian Institute of Food Science and Technology Journal*, *13*(3), 107–111. Retrieved from: https://doi.org/10.1016/s0315-5463(80)73346-1

Ramírez Tapias, Y. A., Peltzer, M. A., Delgado, J. F., & Salvay, A. G. (2020). Kombucha Tea By-product as Source of Novel Materials: Formulation and Characterization of Films. *Food and Bioprocess*

Technology, *13*(7), 1166–1180. Retrieved from: https://doi.org/10.1007/S11947-020-02471-4/FIGURES/8

Record, I. R., & Lane, J. M. (2001). Simulated intestinal digestion of green and black teas. *Food Chemistry*, *73*(4), 481–486. Retrieved from: https://doi.org/10.1016/S0308-8146(01)00131-5

Rojo-Poveda, O., Barbosa-Pereira, L., Mateus-Reguengo, L., Bertolino, M., Stévigny, C., & Zeppa, G. (2019). Effects of particle size and extraction methods on cocoa bean shell functional beverage. *Nutrients*, *11*(4), 867. Retrieved from: https://doi.org/10.3390/nu11040867

Sethi, S., Tyagi, S. K., & Anurag, R. K. (2016). Plant-based milk alternatives an emerging segment of functional beverages: a review. *Journal of Food Science and Technology*, *53*(9), 3408–3423. Retrieved from: https://doi.org/10.1007/S13197-016-2328-3/FIGURES/4

Sharma, O. P., & Bhat, T. K. (2009). DPPH antioxidant assay revisited. *Food Chemistry*, *113*(4), 1202–1205. Retrieved from: https://doi.org/10.1016/j.foodchem.2008.08.008

Silva, K. A., Uekane, T. M., Miranda, J. F. de, Ruiz, L. F., Motta, J. C. B. da, Silva, C. B., Pitangui, N. de S., Gonzalez, A. G. M., Fernandes, F. F., & Lima, A. R. (2021). Kombucha beverage from non-conventional edible plant infusion and green tea: Characterization, toxicity, antioxidant activities and antimicrobial properties. *Biocatalysis and Agricultural Biotechnology*, *34*, 102032. Retrieved from: https://doi.org/10.1016/J.BCAB.2021.102032

Sreeramulu, G., Zhu, Y., & Knol, W. (2001). Characterization of antimicrobial activity in Kombucha fermentation. *Acta Biotechnologica*, *21*(1), 49–56. Retrieved from: https://doi.org/10.1002/1521-3846(200102)21:1<49::AID-ABIO49>3.0.CO;2-G

Sun-Waterhouse, D. (2011). The development of fruit-based functional foods targeting the health and wellness market: A review. *International Journal of Food Science and Technology*, *46*(5), 899–920. Retrieved from: https://doi.org/10.1111/j.1365-2621.2010.02499.x

Sun, T. Y., Li, J. S., & Chen, C. (2015). Effects of blending wheatgrass juice on enhancing phenolic compounds and antioxidant activities of traditional kombucha beverage. *Journal of Food and Drug Analysis*, *23*(4), 709–718. Retrieved from: https://doi.org/10.1016/J.JFDA.2015.01.009

Tapias, Y. A. R., Di Monte, M. V., Peltzer, M. A., & Salvay, A. G. (2022). Bacterial cellulose films production by Kombucha symbiotic community cultured on different herbal infusions. Food Chemistry, 372, 131346. Retrieved from: https://doi.org/10.1016/j.foodchem.2021.131346

Torán-Pereg, P., del Noval, B., Valenzuela, S., Martinez, J., Prado, D., Perisé, R., & Arboleya, J. C. (2021). Microbiological and sensory characterization of kombucha SCOBY for culinary applications. *International Journal of Gastronomy and Food Science*, *23*, 100314. Retrieved from: https://doi.org/10.1016/j.ijgfs.2021.100314

Velićanski, A. S., Cvetković, D. D., Markov, S. L., Tumbas Šaponjac, V. T., & Vulić, J. J. (2014). Antioxidant and Antibacterial Activity of the Beverage Obtained by Fermentation of Sweetened Lemon Balm (Melissa offi cinalis L.) Tea with Symbiotic Consortium of Bacteria and Yeasts. *Food Technology and Biotechnology*, *52*(4), 420–429. Retrieved from: https://doi.org/10.17113/FTB.52.04.14.3611

Villarreal-Soto, S. A., Beaufort, S., Bouajila, J., Souchard, J. P., Renard, T., Rollan, S., & Taillandier, P. (2019). Impact of fermentation conditions on the production of bioactive compounds with anticancer, anti-inflammatory and antioxidant properties in kombucha tea extracts. *Process Biochemistry*, *83*, 44–54. Retrieved from: https://doi.org/10.1016/J.PROCBIO.2019.05.004

Villarreal-Soto, S. A., Beaufort, S., Bouajila, J., Souchard, J. P., & Taillandier, P. (2018). Understanding Kombucha Tea Fermentation: A Review. *Journal of Food Science*, *83*(3), 580–588. Retrieved from: https://doi.org/10.1111/1750-3841.14068

Villarreal-Soto, S. A., Bouajila, J., Pace, M., Leech, J., Cotter, P. D., Souchard, J. P., Taillandier, P., & Beaufort, S. (2020). Metabolome-microbiome signatures in the fermented beverage, Kombucha. *International Journal of Food Microbiology*, *333*, 108778. Retrieved from: https://doi.org/10.1016/J.IJFOODMICRO.2020.108778

Vitas, J., Vukmanović, S., Čakarević, J., Popović, L., & Malbaša, R. (2020). Kombucha fermentation of six medicinal herbs: Chemical profile and biological activity. *Chemical Industry and Chemical Engineering Quarterly*, *26*(2), 157–170. Retrieved from: https://doi.org/10.2298/CICEQ190708034V

Wang, Z., Zhao, X., Zu, Y., Wu, W., Li, Y., Guo, Z., Wang, L., & Wang, L. (2019). Licorice flavonoids nanoparticles prepared by liquid antisolvent re-crystallization exhibit higher oral bioavailability and antioxidant activity in rat. *Journal of Functional Foods*, *57*, 190–201. Retrieved from: https://doi.org/10.1016/J.JFF.2019.04.010

Watawana, M. I., Jayawardena, N., & Waisundara, V. Y. (2018). Value-added tea (Camellia sinesis) as a functional food using the Kombucha 'tea fungus.' *Chiang Mai Journal of Science*, *45*(1), 136–146. Retrieved from: http://epg.science.cmu.ac.th/ejournal/

Yang, F., Chu, T., Zhang, Y., Liu, X., Sun, G., & Chen, Z. (2020). Quality assessment of licorice (Glycyrrhiza glabra L.) from different sources by multiple fingerprint profiles combined with quantitative analysis, antioxidant activity and chemometric methods. *Food Chemistry*, *324*, 126854. Retrieved from: https://doi.org/10.1016/j.foodchem.2020.126854

e-ISSN 2757-5195

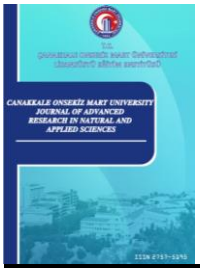

Çanakkale Onsekiz Mart University
Journal of Advanced Research in Natural and Applied Sciences
Open Access

doi.org/10.28979/jarnas.1087937 2023, Cilt 9, Sayı 1, Sayfa: 28-47 dergipark.org.tr/tr/pub/jarnas

Gökova Fay Zonu'nun Morfometrik Özellikleri ve Aktif Tektonik Açısından Önemi, Doğu Akdeniz

Aynur Dikbaş[1*]

[1] İstanbul Üniversitesi-Cerrahpaşa, Mühendislik Fakültesi, Jeoloji Mühendisliği Bölümü, İstanbul, Türkiye

Makale Tarihçesi

Gönderim: 15.03.2022
Kabul: 26.08.2022
Yayım: 05.03.2023

Araştırma Makalesi

Öz – Gökova Fay Zonu, güneybatı Anadolu'da Gökova Körfezi kuzey kıyıları boyunca, Gökova grabeninin kuzey kenarını sınırlayan aktif bir fay zonudur. Bu fay zonu, doğuda Ula ilçesinden (Muğla) batıda Kos adası güneyine kadar hem kara hem deniz alanında izlenen, güneye eğimli normal fay segmentlerinden oluşur. Gökova Fay Zonu'nun morfoloji üzerindeki etkileri hem arazi gözlemleri hem de oluşturulan sayısal yükseklik modeli temel alınarak gerçekleştirilen nitel ve nicel çalışmalar ile araştırılmıştır. Sayısal yükseklik modelinden drenaj, bakı ve yüzey eğim haritaları üretilmiş ve morfometrik indisler (hipsometrik eğri ve integral, vadi tabanı genişliğinin vadi yüksekliğine oranı, dağ önü eğriliği) hesaplanmıştır. Topoğrafik kesitler ve bakı haritası, özellikle doğu kesimde yer alan segmentlerin morfolojide süreklilik gösteren basamaklar oluşturduğunu ve bu basamakların kuzeye doğru, fay hareket yönü tersine eğimlendiğini işaret etmektedir. Mevcut drenaj ağı, litolojiden bağımsız olarak, segmentler boyunca fay doğrultusuna hem paralel hem de dik olarak gelişmiştir. Taban blok üzerinde yer alan 5 havza için hesaplanan hipsometrik integral değerleri 0.37-0.67 arasında değişir. Hipsometrik integral değerleri ve oluşturulan hipsometrik eğriler, havzaların ağırlıklı olarak genç evrede olduğunu gösterir. Taban blok üzerinde hesaplanan vadi tabanı genişliğinin vadi yüksekliğine oranı değerleri 0.12-0.78 arasındadır. Bu değerler, vadilerin V-şekilli olduğunu ve tektonik yükselmeye derine kazma meyili ile cevap verdiklerini işaret etmektedir. Gökova Fay Zonu'nun doğu ve batı kesimlerinde hesaplanan dağ önü eğriliği değerleri 1.00-1.24 arasında değişir ve dağ önlerinin gelişiminde baskın kuvvetlerin tektonik kökenli olduğunu gösterir. Gökova Fay Zonu üzerinde gerçekleştirilen kalitatif ve kantitatif morfolojik çalışmalara göre, bölgenin şekillenmesinde tektonik süreçler erozyonal süreçlere göre daha baskın rol oynamıştır.

Anahtar Kelimeler – *Aktif tektonik, Gökova fay zonu, Gökova Körfezi, morfometri, normal fay*

Morphometric Features of the Gökova Fault Zone and its' importance in Active Tectonics, Eastern Mediterranean

[1]Division of Geological Engineering, Faculty of Engineering, İstanbul University-Cerrahpaşa, İstanbul, Türkiye

Article History

Received: 15.03.2022
Accepted: 26.08.2022
Published: 05.03.2023

Research Article

Abstract – The Gökova Fault Zone is composed of south-dipping active normal fault segments that border the northern edge of Gökova graben in the Gulf of Gökova between Ula (Muğla) and Kos island. The effects of the Gökova Fault Zone on the morphology were investigated by qualitative and quantitative studies based on the derived digital elevation model and field observations. Drainage, aspect and surface slope maps were prepared and morphometric indices (hypsometric curve and integral, ratio of valley floor width to valley height, mountain front sinuosity) were calculated. According to the derived maps, the eastern segments of the fault zone form steps that express continuity in morphology and are tilted to the north in the opposite direction of fault normal slip. The drainage network mostly developed parallel or perpendicular to the fault strike, regardless of the lithology. The hypsometric integral values range between 0.37-0.67, and the hypsometric curves for the basins settled on the footwall indicate that the basins are mostly in young and moderate stages. The calculated values of the ratio of valley floor width to valley height range between 0.12-0.78 which indicates that the valleys are V-shaped and respond to tectonic uplift by rapid incision. The calculated mountain front sinuosity values range between 1.00-1.24 and express that the dominant forces in the development of the mountain front are of tectonic origin. According to the qualitative and quantitative morphological studies performed on the Gökova Fault Zone, the tectonic processes in the region is dominant rather than the erosional processes.

Keywords – *Active tectonics, Gökova Fault zone, Gulf of Gökova, morphometry, normal fault*

[1] aynur.dikbas@iuc.edu.tr
*Sorumlu Yazar

1. Giriş

Gökova Grabeni, Batı Anadolu'da Ege Açılma Sistemine bağlı gelişmiş olan doğu-batı gidişli horst ve grabenlerin en güneyinde yer alır. Gökova Körfezi boyunca izlenen graben, kuzey kenarında doğu-batı gidişli normal fay segmentlerinden oluşan aktif bir fay zonu ile sınırlanır (Şekil 1). Bu fay zonu Şaroğlu, Emre ve Boray (1987) tarafından Ula-Ören Fay Zonu olarak adlanmış, MTA tarafından güncellenen Türkiye Diri Fay haritasında (Duman, Emre, Özalp ve Elmacı, 2011) ise Gökova Fay Zonu (GFZ) adı kullanılmıştır. Gökova Fay Zonu birbirine paralel, güneye eğimli normal faylardan oluşur ve batı Toros Napları ile Ofiyolitleri içerisinde yer alır (Ersoy, 1990; 1991).

Gökova Körfezi içerisinde yapılmış olan çok disiplinli çalışmalar, Gökova Grabeni'nin kuzeyinde ve güneyinde önemli faylar ile sınırlandığını göstermektedir. Sieberg (1932), Gökova Körfezi'ni kuzeyden ve güneyden sınırlayan iki normal fay öne sürerek bu yapıyı "Kos Grabeni" olarak adlamıştır. Bu tektonik yapı Görür vd. (1995) tarafından "rift", Yılmaz vd. (2000) tarafından "graben" olarak adlandırılmıştır. Kurt, Demirbağ ve Kuşçu (1999) Gökova Körfezi içerisinde yaptığı çok kanallı sismik yansıma çalışması sonucunda körfez güneyinde Datça Yarımadası'nın kuzey kenarını sınırlayacak şekilde kuzeye eğimli bir listrik fay haritalamış ve bu fayı Datça Fayı olarak adlandırmıştır. Daha kuzeyde izlenen güneye eğimli normal fayların ise Datça Fayı'nın antitetik fayları olduğu yorumunu yapmışlardır. Çağlar ve Duvarcı (2001) Gökova Körfezi doğusunda, kara alanında yaptığı jeoelektrik çalışmalar sonucunda grabenin bu kesimdeki devamının asimetrik formda olduğunu öne sürmüşlerdir. Yazarlar körfeze doğru temelin derinleştiğini belirlemiş ve Pliyo-Kuvaterner yaşlı çökel kalınlığını 140-150 m olarak ölçmüşlerdir. Bu çalışmaya göre grabenin güneyini sınırlayan fay listrik karakterdedir. Uluğ vd. (2005) sismik yansıma profilleri ve deniz tabanı morfolojisine dayanarak, Ören köyü batısından Datça yarımadası kuzeybatı kesimlerine kadar kuzeydoğu-güneybatı doğrultusunda uzanan sol yanal atımlı bir fay zonu tanımlamış ve bu zonu Gökova Transfer Zonu olarak adlandırılmıştır. İşcan, Tur ve Gökaşan (2013) sismik yansıma ve çok ışınlı batimetri verisine dayanarak bu fay zonunun sıkışma bileşeni de bulunduğunu belirtmiştir. Tur, Yaltırak, Elitez ve Sarıkavak (2015) sismik yansıma kesitleri, çok ışınlı batimetri verisi ve güncel GPS ölçmelerine dayanarak, Gökova Grabeni'ni Nisyros-Karpathos grabeninin doğu uzantısı olarak değerlendirmişler ve bu yapıyı Helen yayına bağlı yay-ardı havza içerisinde gelişen S şekilli bir graben olarak tanımlamışlardır. Grabenin açılmasının batı kesimde Pliyosen'de başladığını ve doğuya doğru gençleştiğini ileri sürmüşlerdir. Erken Pliyosen'den itibaren, Gökova-Nisyros-Karpathos grabeninin pozisyonunda, Gökova Körfezi 'nin doğu kesiminde yer alan bir referans noktasına göre ~6° saat yönünün tersine bir dönüş meydana geldiğini hesaplamışlardır.

Batı Anadolu'da izlenen grabenleri sınırlayan fayların hareketleri bölgede yoğun bir sismik aktivite oluşturur ve bu bölgede sıklıkla hasar yapıcı depremler gözlenir (AFAD, 2022; KOERI, 2018; ISC, 2022; EMSC, 2022). Tarihsel dönemler boyunca da bu faylardan kaynaklanan pek çok hasar verici depremin meydana geldiği bilinmektedir (örn: Ergin, Güçlü ve Uz, 1967; Soysal, Sipahioğlu, Kolçak ve Altınok, 1981; Ambraseys ve Finkel, 1991; Guidoboni, Comastri ve Triana, 1994; Ambraseys ve Jackson 1998; Guidoboni ve Comastri, 2005; Ambraseys, 2009; Dikbaş, Akyüz, Basmenji ve Kırkan 2022; Mozafari et al., 2022). Aletsel dönem verilerine göre özellikle Gökova Körfezi civarında yoğun bir aktivite mevcuttur (AFAD, 2022; KOERI, 2018; ISC, 2022; EMSC, 2022) bu nedenle özellikle sismolojik anlamda her dönem araştırmacıların (örn: Taymaz, Jackson ve McKenzie, 1991; Eyidoğan, Akıncı, Gündoğdu, Polat ve Kaypak, 1996; Rontogianni, Konstantinou, Evangelidis ve Melis, 2011; Kalafat ve Horasan, 2012) ilgisini çeken bir bölgedir. Gökova Körfezi civarında yürütülen sismotektonik araştırmalar, bölgede meydana gelen depremlerin odak mekanizması çözümlerinin baskın olarak normal faylanma olduğunu işaret eder (örn: Jackson, King ve Vita-Finzi, 1982; Papazachos, Kiratzi, Hatzidimitriou ve Rocca, 1984; McKenzie, 1972; Taymaz, Tan ve Yolsal, 2004; Yolsal-Çevikbilen, Taymaz ve Helvacı, 2014; KOERI, 2018).

Aktif fay zonlarının daha iyi anlaşılmasında; sismolojik, jeolojik, sismotektonik çalışmalara ek olarak başvurulan diğer bir yöntem de morfometri çalışmalarıdır. Morfometri, morfolojik rölyefin nicel olarak ifade edilmesidir (Keller ve Pinter, 2002). Aktif tektonik araştırmalarda yürütülen morfometri çalışmaları, tektonik aktivitenin bölgedeki morfolojinin şekillenmesindeki etkilerini nicel olarak hesaplamaya imkan sağlar (ör: Bull ve McFadden, 1977; Keller ve Pinter, 2002; El-Hamdouni, R., Irigaray, C., Fernandez, T., Chacon, J. ve Keller, E.A., 2008; Peréz-Peña, J. V., Azor, A., Azañon, J. M. ve Keller, E. A. 2010; Burbank ve Anderson, 2001; Saber, R., Cağlayan, A. ve Işık, V. 2018; Saber, R., Işık, V. ve Çağlayan, A. 2020). Günümüzde sayısal yükseklik veri setlerine (SRTM, ASTER, sayısal yükseklik eğrileri vb.) ulaşabilmekteki kolaylıkla beraber birçok araştırmacı morfometrik indis hesaplamalarını da çalışmalarına dahil etmeye başlamıştır. Morfometrik indis çalışmaları ile bir bölgedeki tektonik aktivitenin sınıflandırılması ve karşılaştırılması mümkün olmaktadır (ör:

El Hamdouni vd., 2008; Burbank ve Anderson, 2001; Saber vd., 2018; Saber vd., 2020; Keller ve Pinter, 2002; Sağlam Selçuk, 2016).

Bu çalışmada, GFZ'nun karada izlenen kesiminin morfolojik özellikleri ve GFZ üzerinde gerçekleştirilen morfometri çalışmalarının sonuçları sunulmaktadır. Morfolojik çalışmalarda, fay zonu boyunca fay morfolojisini yansıtan yapılar arazi gözlemleri ve sayısal yükseklik modelleri (SYM) kullanılarak araştırılmıştır. Fay zonu ve civarını içerecek şekilde yüzey eğimi ve bakı haritası oluşturulmuş, drenaj geometrisi türetilmiş ve tektonik aktivite ile ilişkisi yorumlanmıştır. Kullanılan morfometrik indisler ise Hipsometrik Eğri ve Hipsometrik İntegral (HI), Vadi Tabanı Genişliğinin Vadi Yüksekliğine Oranı (V_f) ve Dağ Önü Eğriliği (S_{mf})'dir.

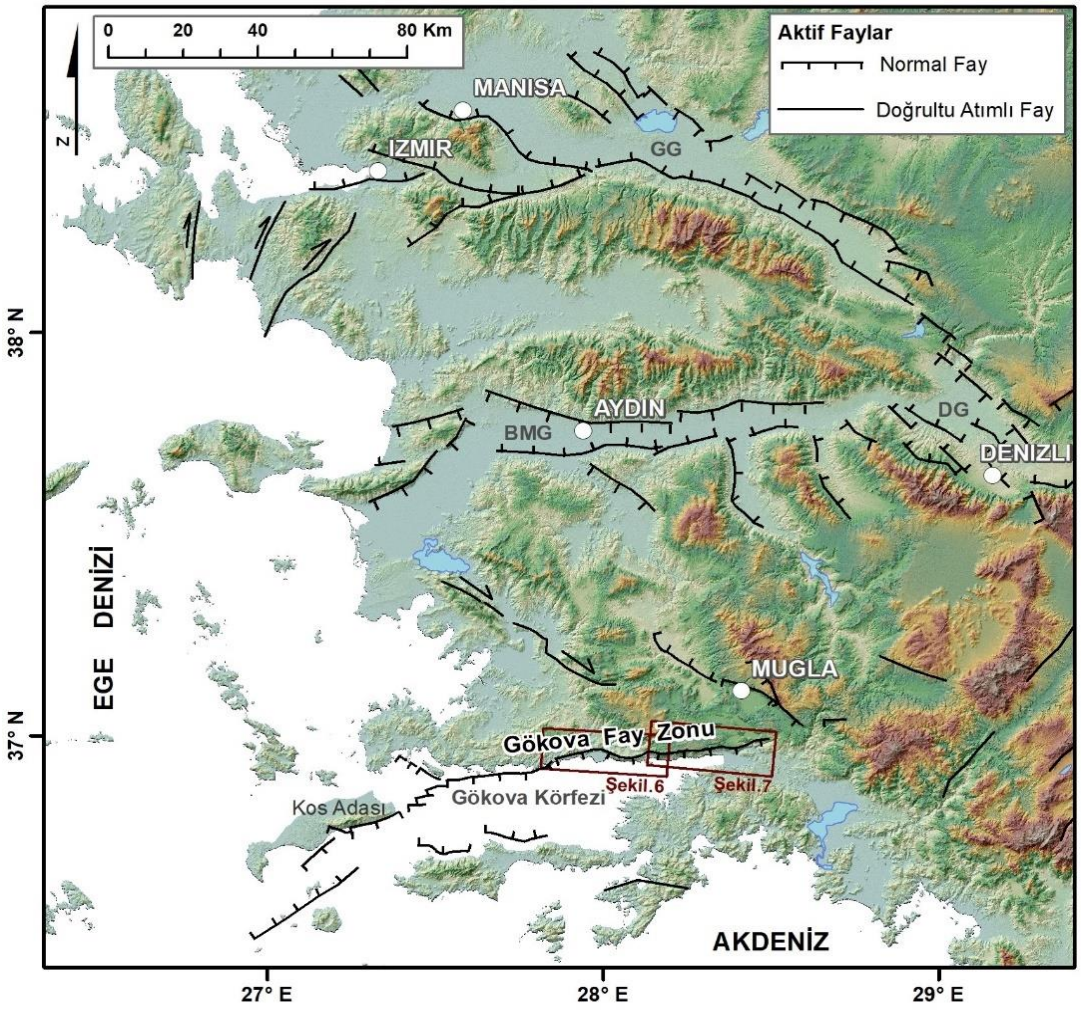

Şekil 1. Batı Anadolu'nun sadeleştirilmiş aktif tektonik haritası ve GFZ'nun konumu; Hancock ve Barka (1987); Kurt vd. (1999); Bozkurt (2003); Emre vd. (2013; 2018); Akyüz vd. (2018) ve Dikbaş vd. (2022)'den sadeleştirilmiştir. GG: Gediz Grabeni, BMG: Büyük Menderes Grabeni, DG: Denizli Grabeni.

2. Materyal ve Yöntem

GFZ'nun morfoloji üzerindeki etkisini tanımlayabilmek için 1/25.000 ölçekli sayısal yükseklik eğrileri ve ASTER yükseklik verisi kullanılarak zon boyunca SYM oluşturulmuştur. Bu model temel alınarak morfolojik analizler ve morfometrik indis hesaplamaları gerçekleştirilmiştir. Yapılan analizler aşağıda tanımlanmış ve aktif tektonik çalışmalarda kullanımları kısaca açıklanmıştır.

2.1. Hipsometrik Eğri ve Hipsometrik İntegral (HI)

Hipsometrik eğri, topoğrafik bir alanın Yükseklik/Alan (H/A) oranının tanımlamasını yapar (Strahler, 1952). Eğri, toplam havza yüksekliğinin (H/h göreli yüksekliği) oranını toplam havza alanı (a/A göreli alanı) oranına göre çizerek oluşturulur (Şekil 2). Toplam yükseklik (H) havzadaki rölyeftir. Havzanın (A) toplam yüzey alanı, her bir bitişik kontur çizgisi arasındaki alanların toplamıdır. Alan (a), belirli bir yükseklik çizgisinden (h) yukarıda havza içindeki yüzey alanıdır. Hipsometrik eğri iç bükey ise erozyon döngüsündeki (Davis,

1989; Strahler 1952; Ohmori, 1993) yaşlı evreyi, dış bükey ise genç evreyi işaret eder (Şekil 3). Eğrinin "S" şekilli olması ise morfolojinin erozyon döngüsünün olgunluk evresinde olduğunu gösterir. Elde edilen eğrinin rakamsal tanımlaması için ise Hipsometrik İntegral (HI) değeri hesaplanır (Şekil 2, Tablo 1). Bu hesaplama için aşağıdaki denklem (Denklem 2.1) kullanılır.

$$HI = \frac{\text{Ortalama yükseklik} - \text{minimum yükseklik}}{\text{Maksimum yükseklik} - \text{minimum yükseklik}} \quad (2.1)$$

HI hipsometrik eğri altında kalan alandır ve 0 ila 1 arasında bir değer alır (Şekil 2 ve 3). Hipsometrik eğri dış bükeye yaklaştıkça HI değeri yükselir, eğri içbükeye yaklaştıkça HI değeri düşer. HI değerinin 1'e yaklaşması, alandaki erozyonun nispeten düşük olduğunu veya tektonik kuvvetlerin etkisinin erozyonal süreçlere nazaran daha yüksek olduğunu ifade eder. HI değeri 0'a yaklaşması, erozyonun etkisinin daha yüksek olduğunu ve çalışma alanının morfolojik olarak yaşlı evrede olduğunu ifade eder (Şekil 3, Tablo 1) (Strahler, 1952; Ohmori, 1993; Keller ve Pinter, 1996).

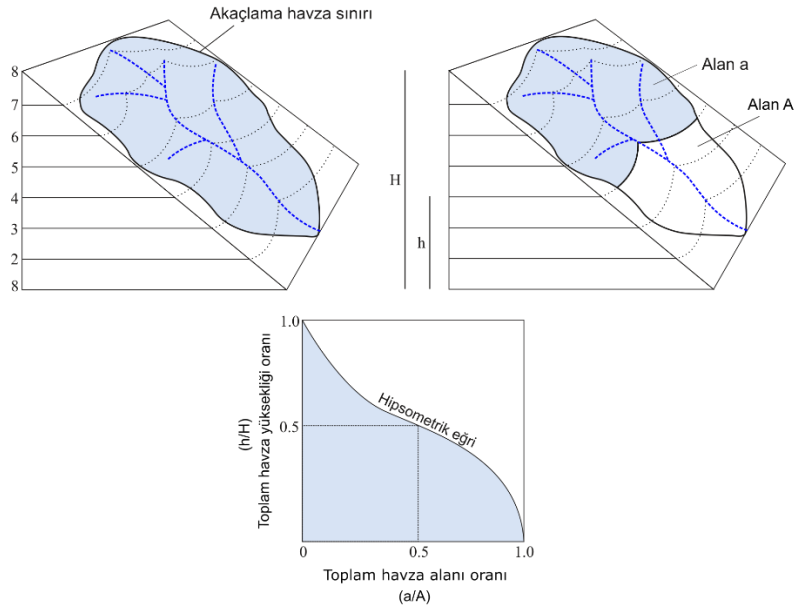

Şekil 2. Hipsometrik eğri ve hipsometik integral hesaplamasını gösteren şematik havza modeli, Strahler (1952) ile Keller ve Pinter (1996)'dan değiştirilmiştir.

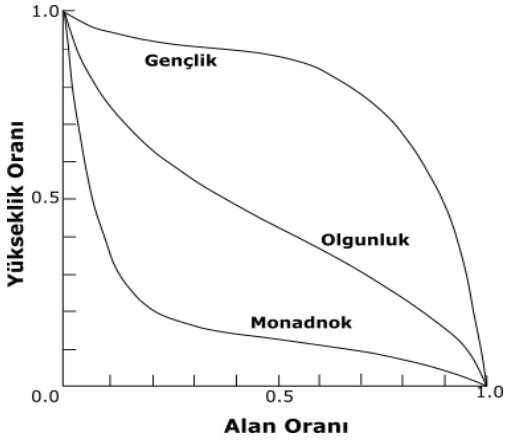

Şekil 3. Hipsometrik eğrinin temsil ettiği morfolojinin erozyon döngüsündeki konumu, Ohmori (1993)'den değiştirilmiştir.

Tablo 1
HI değerinin erozyon döngüsündeki temsil edebileceği dönem (Strahler, 1952).

Hipsometrik İntegral	**Erozyon Döngüsü**
0>HI>0.35	Yaşlı
0.35>HI>0.6	Denge (Olgunluk)
0.6>HI>1	Genç

2.2. Vadi Tabanı Genişliğinin Vadi Yüksekliğine Oranı (V_f)

V_f indisi geniş tabanlı vadiler ile dar tabanlı (V-şekilli) vadileri ayırt etmekte katkı sağlar. Geniş tabanlı vadilerde yüksek V_f değerleri hesaplanırken, dar tabanlı vadilerde düşük V_f değerleri görülür. V_f değerinin yüksek olması düşük tektonik yükselmeyi işaret eder. V_f değerinin düşük olması ise tektonik yükselmeyi ve buna paralel olarak nehir tarafından derin kazılan vadileri gösterir (Keller ve Pinter, 1996).

V_f indis değerini hesaplamak için aşağıdaki denklem (Denklem 2.2) kullanılır (Bull 1977; Bull, 1978).

$$V_f = 2V_{fw} / [(E_{ld} - E_{sc}) + (E_{rd} - E_{sc})] \quad (2.2)$$

Burada; V_f, vadi tabanı genişliğinin vadi yüksekliğine oranını; V_{fw}, vadi tabanı genişliğini; E_{ld}, akış yönüne göre vadinin sol tarafında kalan su bölümünün topoğrafik yükseklik değerini; E_{rd}, akış yönüne göre vadinin sağ tarafında kalan su bölümünün topoğrafik yükseklik değerini; E_{sc}, vadi tabanının topoğrafik yükseklik değerini ifade eder (Şekil 4).

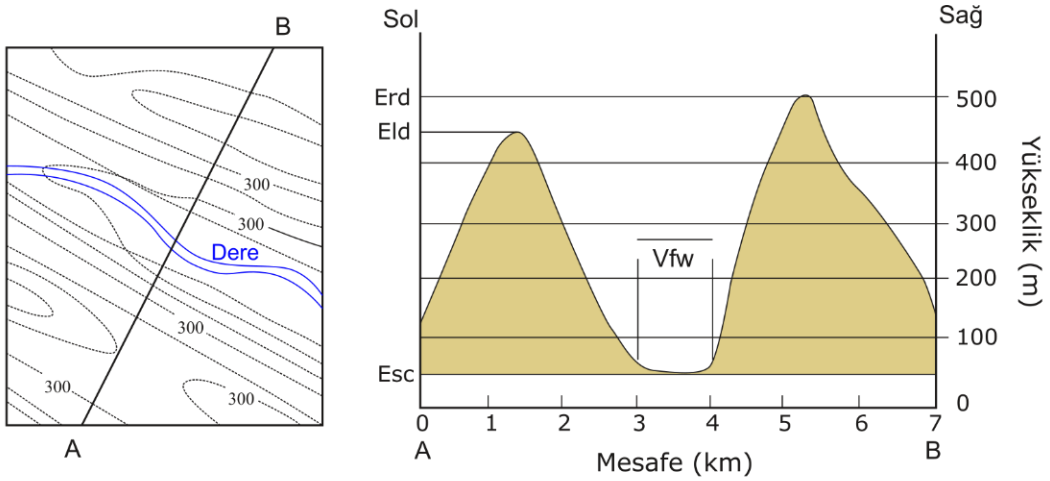

a **b**

Şekil 4. V_f indisi hesaplaması için yapılması gereken ölçümlerin **a)** harita ve **b)** en kesit üzerinde şematik gösterimi, Keller ve Pinter (1996)'dan değiştirilmiştir.

2.3. Dağ Önü Eğriliği (S_{mf})

Dağ Önü Eğriliği (S_{mf}) indeksi (Bull, 1977; 1978), dağ önünü girintili çıkıntılı bir sınır olarak şekillendirmeye meyilli erozyonal kuvvetler ile dağ önünü düz bir sınır olarak şekillendirmeye meyilli tektonik kuvvetler arasındaki dengeyi yansıtır. Aktif tektonik hareketlere maruz kalan dağ önleri göreceli olarak daha düzdür ve daha düşük S_{mf} değerleri sunarlar. Tektonik yükselme hızında bir düşüş ya da sona erme meydana gelirse erozyonal süreçler dağ önü sınır çizgisinde eğrilikler meydana getirir ve bu durumda daha yüksek S_{mf} değerleri hesaplanır (Keller ve Pinter, 1996). S_{mf} değerini hesaplamak için aşağıdaki denklem (Denklem 2.3) kullanılır:

$$S_{mf} = L_{mf} / L_s \quad (2.3)$$

Burada S_{mf}, dağ önü eğriliğini; L_{mf}, dağ önü boyunca ölçülen sınır uzunluğunu; L_s ise dağ önü boyunca ölçülen düz mesafeyi ifade eder (Şekil 5). Tektonik kuvvetlerin etkisi arttıkça S_{mf} değeri 1'e yaklaşır.

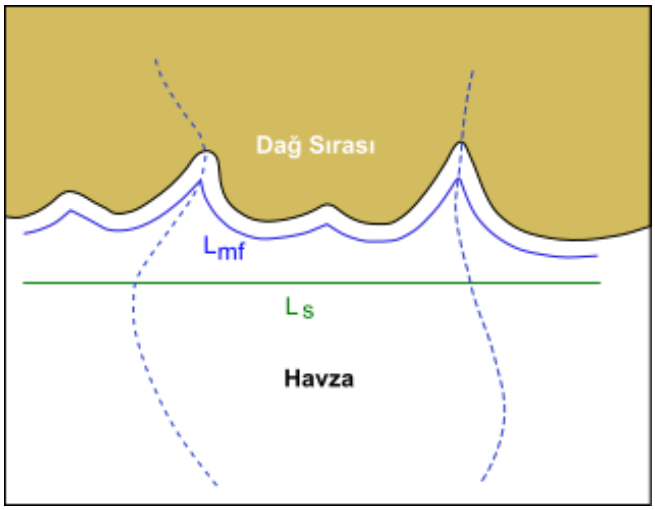

Şekil 5. Dağ önü eğriliği indisi hesaplama parametreleri, Keller ve Pinter (1996)'dan değiştirilerek.

3. Gökova Fay Zonu

3.1. Segmentasyon

Gökova Körfezi, Ege Açılma Sistemi içerisinde gelişmiş olan aktif bir graben yapısı ile şekillendirilmiştir. Körfezin kuzey kesimi sınırlayan GFZ, kıyı yakın alanı boyunca, güneye eğimli normal fay parçalarından oluşur. Karada, doğuda Ula ilçesinin güneydoğusundan başlayan fay zonu batıda Çökertme köyüne kadar ortalama K75°-80°D doğrultusu ile yaklaşık 60 km boyunca takip edilir (Şekil 1, 6 ve 7). Bu bölgeden batıya doğru deniz içine giren zon, Kos adasının güneyine kadar devam eder. Emre vd. (2018) Gökova Fay Zonu'nun, karada uzanan kesimini 4 ayrı bölümde değerlendirmiş, doğrultularının K60°D ve K80B° arasında değiştiğini, eğim değerlerinin ise 55°-65° arasında yer aldığını belirtmişlerdir. Yazarlar, odak derinliğine dayalı sismojenik kalınlığının 13 km, literatüre dayalı sismojenik kalınlığının ise 14 km olduğunu belirtmişler ve beklenen olası deprem büyüklüklerinin (Mw) 6.0-6.6 arasında olabileceğini değerlendirmişlerdir.

Çökertme ve Sarnıçköy arasında fay geometrisinin daha basit olduğu gözlenirken daha doğuya doğru kompleks ve basamaklı bir fay paterni görülür (Şekil 6 ve 7). Çökertme ve Alatepe köyleri arasında GFZ'na ait segmentler, güneyde dayanımlı litolojilerin oluşturduğu dağlık alan ile dere önlerinde gelişmiş olan fan-delta çökelleri arasında tektonik bir sınır oluşturur (Şekil 6). Çökertme köyü doğusundaki Gerin Dere önünde fan-delta çökelleri gelişmiştir. Bu çökeller ile güneydeki Mesozoyik kayalar arasındaki sınır GFZ'nun karada izlenebilen en batı segmentleri tarafından oluşturulur. Daha doğuda Türkevleri civarında Hanay Dere önünde dalga kontrollü bir delta gelişmiştir. Delta çökellerinin güney sınırında izlenen normal fay düzlemleri K60°-70°D doğrultuda uzanır. Düzlemler yaklaşık 55°-62° derecelik açılar ile güneydoğuya eğimlidir. Bu kesimde fay düzlemleri üzerinde yapılan gözlemlerde fayın kinematik davranışına dair bilgi veren oluklanma (korugasyon), fay çizikleri ve tarak yapıları izlenmiştir. Bu yapılar ve fay düzlemi arasındaki ilişki, fay düzlemi üzerinde normal bileşene sol-yanal hareketin de eşlik ettiğini göstermektedir (Şekil 8a ve 8b). Ören köyü batısından körfeze ulaşan Koca Dere önünde, dağ önünü sınırlayan faya hemen hemen dik konumda bir fan-delta gelişmiştir. Fay, Koca Dere ile kesişiminin batısında yer yer yamaç molozu ile örtülmüştür ve morfolojide bıraktığı iz oldukça düz bir çizgidir. Neredeyse doğu-batı uzanımlı izlenen fay düzleminin eğimi güneye doğru 70°-75° derece civarındadır. Ören doğusunda çoğunlukla yamaç molozu ile örtülen fay düzlemleri yer yer çok belirgin mostralar verir. Fay düzlemi doğrultusu K65°-75°B, eğimi ise 65°-75° güneybatı yönündedir. M.Ö. 2.yy'a ait Keramos (Tırpan, 1989) antik kentinin de merkezi olan bu bölge koruma altındadır. Fay düzlemi Keramos halkı tarafından yapılan birçok kral mezarı için uygun bir duvar oluşturmuştur (Şekil 8a). İyi korunmuş bu düzlemlerde yapılan gözlemlerde fay breşi, kayma çizikleri, tarak yapıları ve oluklanmalar (korugasyonlar) gözlemlenmiştir (Şekil 8a ve 8b). Kinematik göstergelere göre, Ören köyü doğusunda normal faylanma bileşenine sağ-yanal bileşen de eşlik etmiştir (Dikbaş vd., 2022).

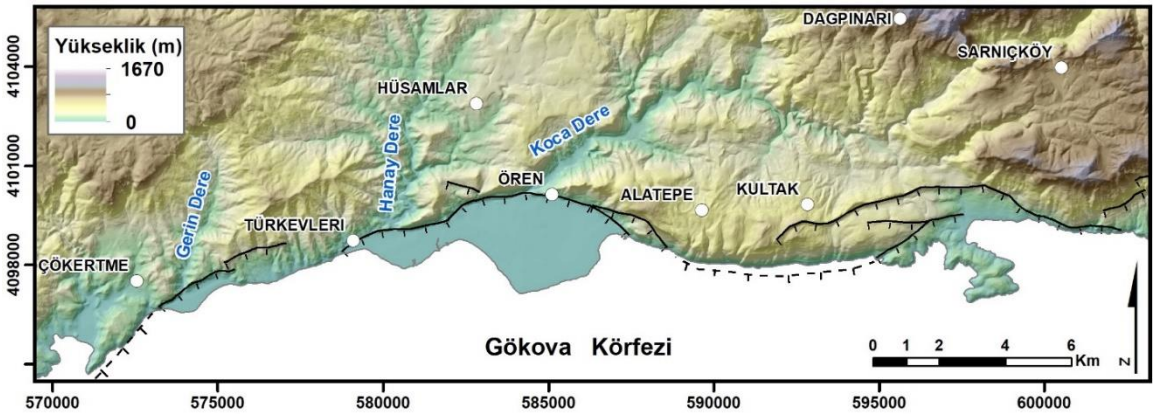

Şekil 6. Çökertme ve Sarnıçköy arasında haritalanan normal fay segmentleri, Dikbaş vd. (2022)'den değiştirilerek. Konum için Şekil.1'e bakınız.

Kultak ve Kıran köyleri arasında, fay düzlemi kıyıya az çok paralel uzanır ve eğimi genel olarak 75°-80° civarında güneye doğrudur (Şekil 6 ve 7). Bu kesimde hem saf normal faylanma hem de sağ-yanal bileşenin eşlik ettiği normal faylanma verileri gözlenmiştir.

Akyaka köyü doğusu ve batısında gözlemlenen fay düzlemleri genel olarak K70°D doğrultusunda uzanır ve eğimleri düşeye yakındır (Şekil 7). Bu bölgede, kuzeyden güneye doğru farklı normal fay segmentlerinin sıralanarak topoğrafya üzerinde geliştirdiği basamaklar çok belirgindir.

Şekil 7. Sarnıçköy ve Ula arasında haritalanan normal fay segmentleri, Dikbaş vd. (2022)'den değiştirilerek. Konum için Şekil.1'e bakınız.

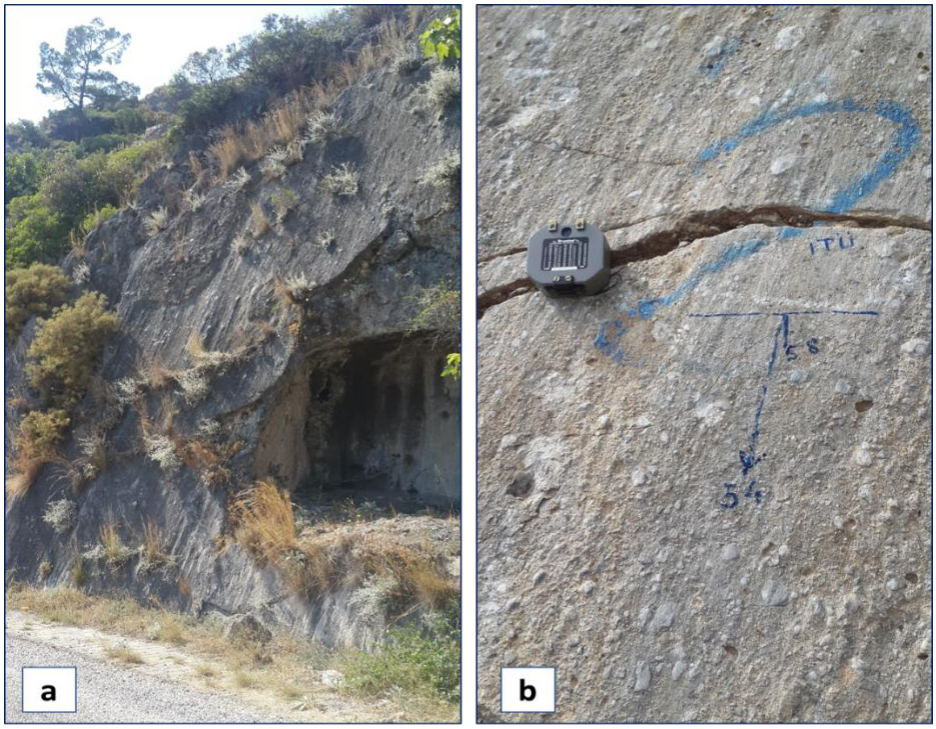

Şekil 8. Ören Fayı fay düzlemi üzerinde **a)** M.Ö. 2 yy'da bölgede yerleşmiş olan Keramos halkı tarafından yapılan kral mezarı ve **b)** düzlem üzerinde gözlenen fay breşi ve kayma çizikleri (bakış KD'ya).

3.2. Jeoloji

GFZ kara alanında Gökova Körfezi kuzey kenarı boyunca Akyaka-Çökertme arasında izlenir. Bu alanda jeolojik temel Likya Napları'na (Ersoy, 1990) ait Mesozoyik yaşlı zayıf metamorfik sedimanter kayaçlar ile temsil edilir. Mermer, dolomit ve şist litolojileri Gökova Körfezi kuzeyinde yaygın olarak gözlenen Likya Napları'na ait temel kayalardır (Şekil 9). Temel üzerinde Oligo-Miyosen yaşlı karasal ve denizel ortamda çökelmiş olan Kale-Tavas Havzası istifi yer alır (Gürer, Sanğu, Özburan, Gürbüz ve Sarıca-Filoreau, 2013). Ören–Kultak çevresinde, Likya naplarına ait Mesozoyik kireçtaşlarının üzerine, birbiriyle yanal–düşey geçişli olan Oligosen–Erken Miyosen karasal ve denizel tortullar gelmektedir (Görür vd., 1994; 1995; Sezgül-Kayseri ve Akgün, 2010). Alt Miyosen çökelleri batıda, Zeytin ve Dağpınarı köyleri güney kesimlerinden doğuda Akyaka köyü doğu kesimlerine kadar mostra verir. Alt Miyosen üzerinde uyumsuzlukla Orta-Üst Miyosen çökelleri yer alır. Gevşek tutturulmuş konglomera, kumtaşı, silttaşı, kiltaşı ve gölsel kireçtaşı ile temsil edilen bu seviyeler arasında kömür mercekleri de yer alır (Atalay, 1980; Hakyemez ve Örçen, 1982; Kaya, Tuna ve Geraads, 2001; Gürer ve Yılmaz, 2002; Gürer vd., 2013). Batıda Çökertme ve Türkevleri kuzey kesimlerinde bu birimlere ait mostralar izlenir. Daha doğuda Hüsamlar ve Pınarköy civarında geniş bir yayılım gösterir. Alatepe ve Kultak köyleri arasında bu birimler Likya Napları üzerinde bir örtü oluştururlar. Daha doğuda ise Bağyaka ve Kızılağaç köyleri civarında mostraları izlenir. Likya Napları ve Miyosen çökelleri Kuvaterner yaşlı birimlerle açısal uyumsuzluk ile örtülürler. Kuvaterner dönemi alüvyon, alüvyal fan, yamaç molozu ve delta çökelleri ile temsil edilir (Gürer vd., 2013; Gül vd., 2017; Dikbaş vd., 2022). Hem yüksek alanlardaki düzlüklerde hem de Akyaka güneyinde kıyı alanındaki düzlük alanda ve dere boylarında alüvyon çökelleri yer alır. Yamaç molozu çökelleri ise kıyı boyunca dağ önlerinde haritalanmıştır. Ören köyünden denize dökülen Koca Dere ağzında ve Türkevleri köyünden denize dökülen Hanay Dere ağzında ise fan-delta çökelleri gelişmiştir (Dikbaş vd., 2022).

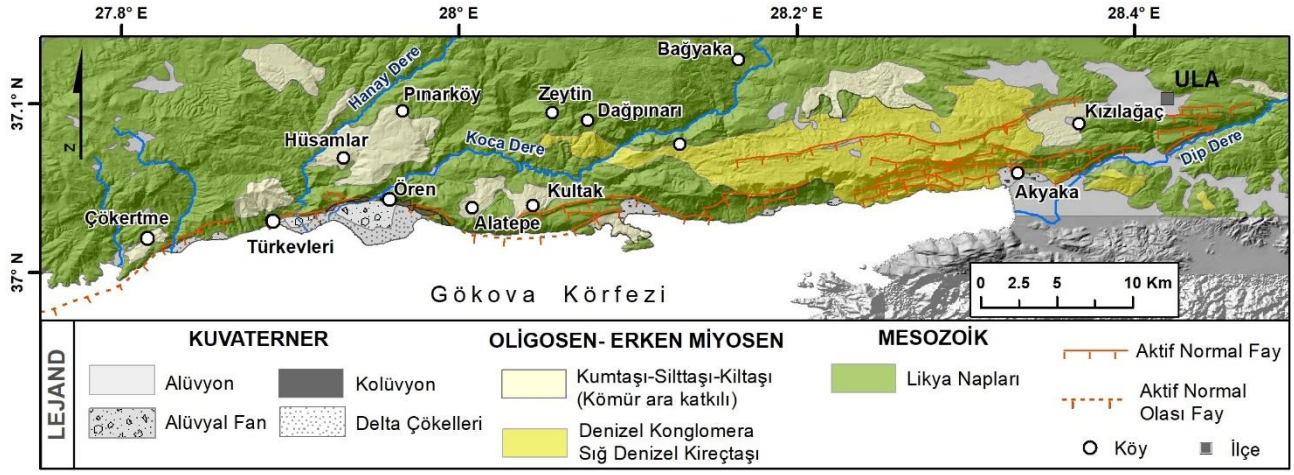

Şekil 9. GFZ civarının Ersoy (1990), Görür vd. (1995), Akbaş vd. (2011), Emre vd. (2013), Tur vd. (2015) ve Akyüz vd. (2018)'den sadeleştirilmiş jeoloji haritası; Dikbaş vd. (2022)'den değiştirilerek alınmıştır.

3.3. Morfolojik Özellikler

Gökova Körfezi kuzey kıyıları tektonik kıyı özelliğindedir (Erinç, 1996). Doğuda Ula ile batıda Çökertme arasında kalan kıyı çizgisi ardında dik falezlerde farklı segmentler tarafından oluşturulan basamaklı bir morfoloji izlenir. Bu basamaklı yapı normal faylanmanın güncel topoğrafya üzerindeki etkilerini açıkça sunar. Arazi çalışmalarında yapılan gözlemlerde faylanmanın neden olduğu topoğrafik eğim kırıklıkları net olarak takip edilmiştir.

GFZ boyunca 1/25000 ölçekli eşyükselti eğrileri kullanılarak bölgenin SYM oluşturulmuştur. Bu modele göre fay boyunca topoğrafik yükseklik değerleri deniz seviyesinden başlayıp kısa mesafede, hızlıca yaklaşık 1040 m'ye kadar yükselir (Şekil 6 ve 7). Kultak-Ula arasında GFZ, kuzeydeki yüksek alan ile güneyde neredeyse deniz seviyesinde olan yüzeyler arasında bir sınır oluşturur. Batıda, Çökertme-Kultak köyleri arasında Hanay Dere ve Koca Dere'nin aşındırması ile yüksek alanlar nispeten parçalanmış ve alçaltılmıştır. Her iki dere boyunca taşınan malzemeler Ören köyü civarında depolanmış ve burada birleşik bir fan-delta şekillenmiştir (Şekil 6 ve 9) (Dikbaş vd., 2022).

Gökova Körfezi kuzeyinde yüzey eğim açıları 0° ila 70° derece arasında değişir (Şekil 10). Yüksek eğimli yüzeyler çoğunlukla normal faylanma nedeniyle gelişmiştir. Özellikle, normal fayların hemen hemen birbirine paralel olarak haritalandığı kıyı boyunca yüzey eğiminin sıklıkla yükseldiği gözlenir. Bunun dışında, kuzeyde vadi yamacını temsil eden eğimi yüksek yüzeyler izlenir. Ören Fan-Deltası ve Akyaka düzlüğü eğimi en düşük (0°-10°) olan, neredeyse yataya yakın yüzeylerdir.

Fay zonu boyunca oluşturulan bakı haritasında zonun kuzeyinde yüzeylerin güney-güneydoğu yönüne baktıkları görülür (Şekil 11). Fay zonu kuzeyinde ise yüzeyler genel olarak kuzey-kuzeybatı yönüne bakmaktadır. Bu harita taban blokta fay üzerindeki hareketin tersi yönünde bir eğimlenme (geriye tiltlenme) göstermektedir. Bu tiltlenme fay zonuna dik alınan topoğrafik kesitlerde de izlenmektedir (Şekil 12 ve 13)

GFZ boyunca normal fay segmentlerinin oluşturduğu basamaklı morfolojiyi araştırmak amacıyla, batıdan doğuya doğru fay zonunu örnekleyecek şekilde yaklaşık kuzey-güney konumlu 3 adet topoğrafik kesit güzergahı seçilmiştir (Şekil 12 ve 13). Normal faylanmaya bağlı gelişen basamaklı morfoloji hemen hemen tüm profillerde izlenmektedir. Bu basamaklar üzerinde sıklıkla, düşen blokta faya paralel gelişen drenaj nedeniyle "V" ya da "U" şekilli dere yatakları topoğrafik profillerde görülmektedir (Şekil 13). Fay düzlemleri nedeniyle morfolojide gelişmiş basamaklar arazi çalışmalarında da takip edilebilmiştir (Şekil 14a, 14b ve 15).

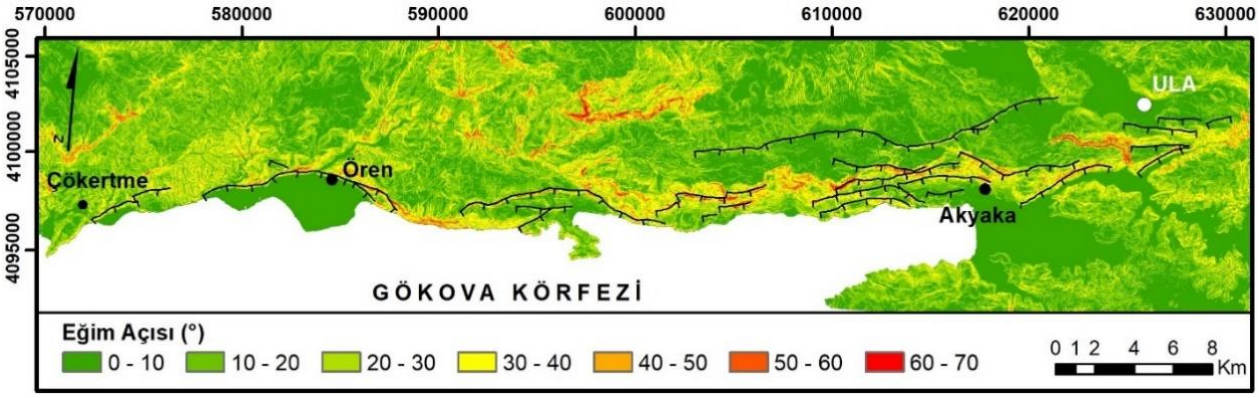

Şekil 10. Gökova Körfezi kuzeyinde GFZ boyunca üretilen topoğrafik yüzey eğim haritası.

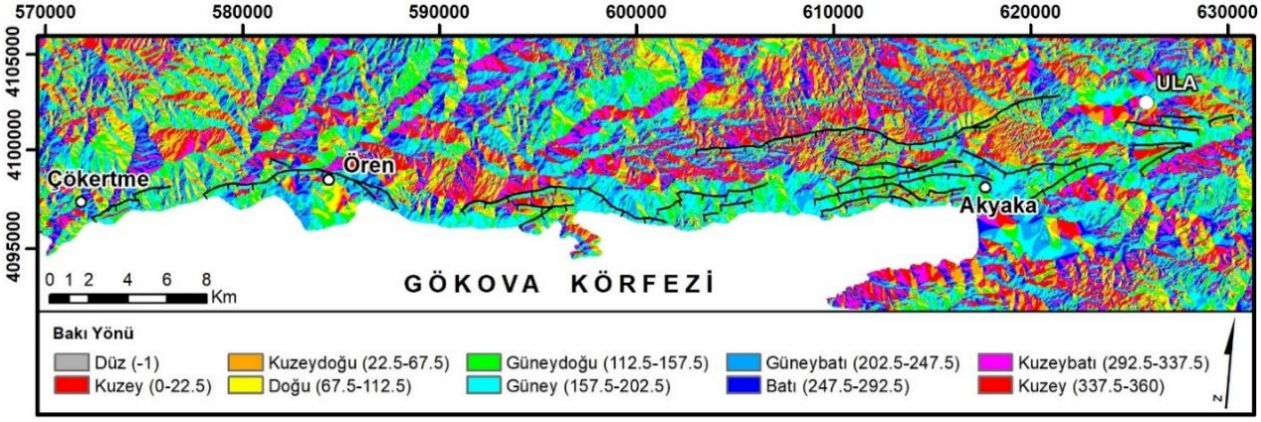

Şekil 11. Gökova Körfezi kuzeyinde GFZ boyunca üretilen bakı haritası.

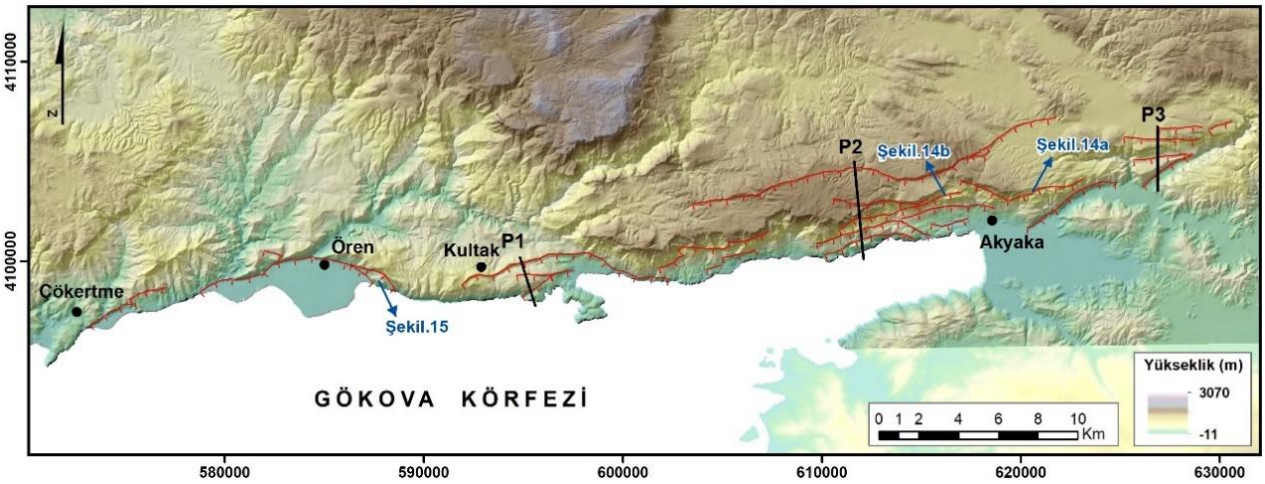

Şekil 12. GFZ üzerinde alınan topoğrafik kesit güzergâhları. Siyah çizgiler topoğrafik profil güzergahlarını ve numaralarını göstermektedir.

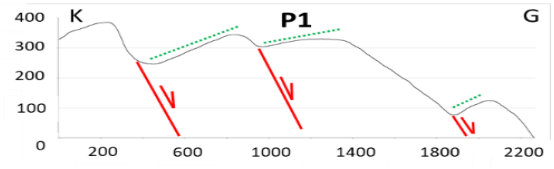

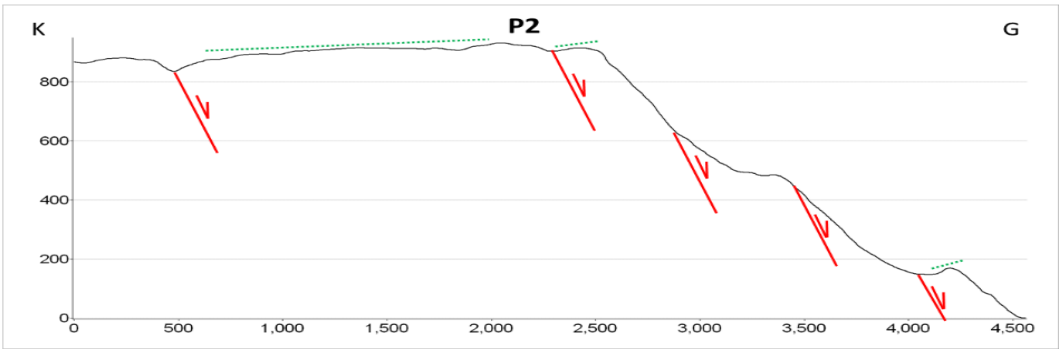

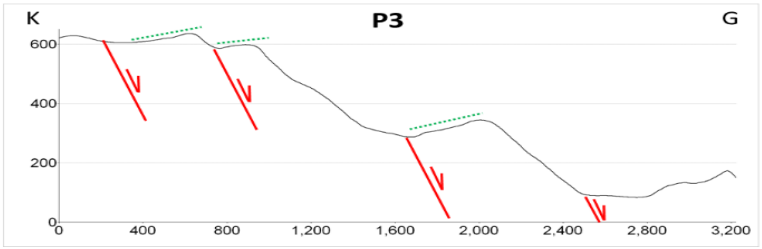

Şekil 13. GFZ boyunca SYM'den elde edilen topoğrafik profiller ve haritalanan faylarla ilişkisi. Noktalı yeşil çizgiler tiltlenen yüzeyleri temsil eder. Topoğrafik profil lokasyonları için Şekil 12'ye bakınız. Düşey ölçek x2 abartılmıştır.

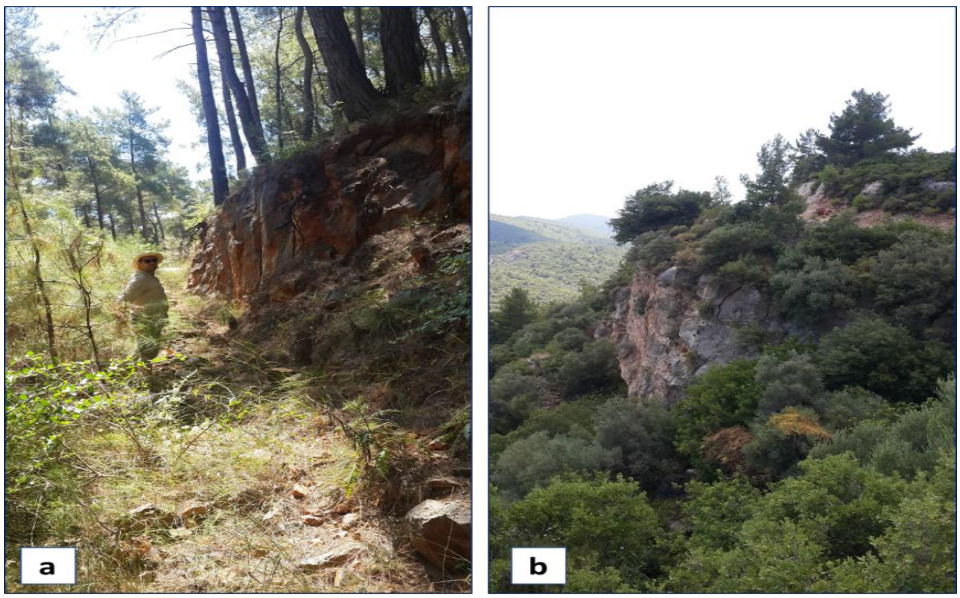

Şekil 14. Normal fay düzlemlerinin, Akyaka köyü **a)** doğusunda ve **b)** batısında oluşturduğu topoğrafik basamakların görünümü (bakış B'ya).

Bölgedeki drenaj ağı 1/25000 ölçekli sayısal yükseklik eğrileri temel alınarak ArcGIS yazılımında Hydrotools aracı kullanılarak oluşturulmuştur. Mevcut drenaj ağı gelişimi GFZ'nu oluşturan segmentlerden etkilenmiştir. Tüm segmentler boyunca, drenaj ya faylara az çok paralel ya da az çok dik bir açı ile izlenmektedir (Şekil 16a ve b). Türkevleri ve Kultak köyleri arasında faylar ile ilişkide olan tüm drenaj kolları fayları dik veya dike yakın bir açı ile keser. Kultak ve Kıran köyleri arasında faya paralel gelişen drenaj kolları gözlenmiştir. Bu kollar Şekil 16a'da elips içerisinde işaretlenmiştir. Daha doğuda Gökova köyü civarında gözlemlenen paralel gelişimler ise Şekil 16b'de elips şekli ile işaretlenmiştir. Bunların dışında kalan kolların hemen hemen hepsi

faya dik veya dike yakın açılarda gelişmiştir. Bu gözlemlere göre, drenaj ağı fay paternine göre gelişmiştir ve bölgedeki güncel tektonik kuvvetler erozyonal kuvvetlere göre daha baskındır.

Şekil 15. Ören köyü güneybatısında normal fay segmentlerinin uzanımı ve morfolojide izlenen basamaklanma (bakış D'ya).

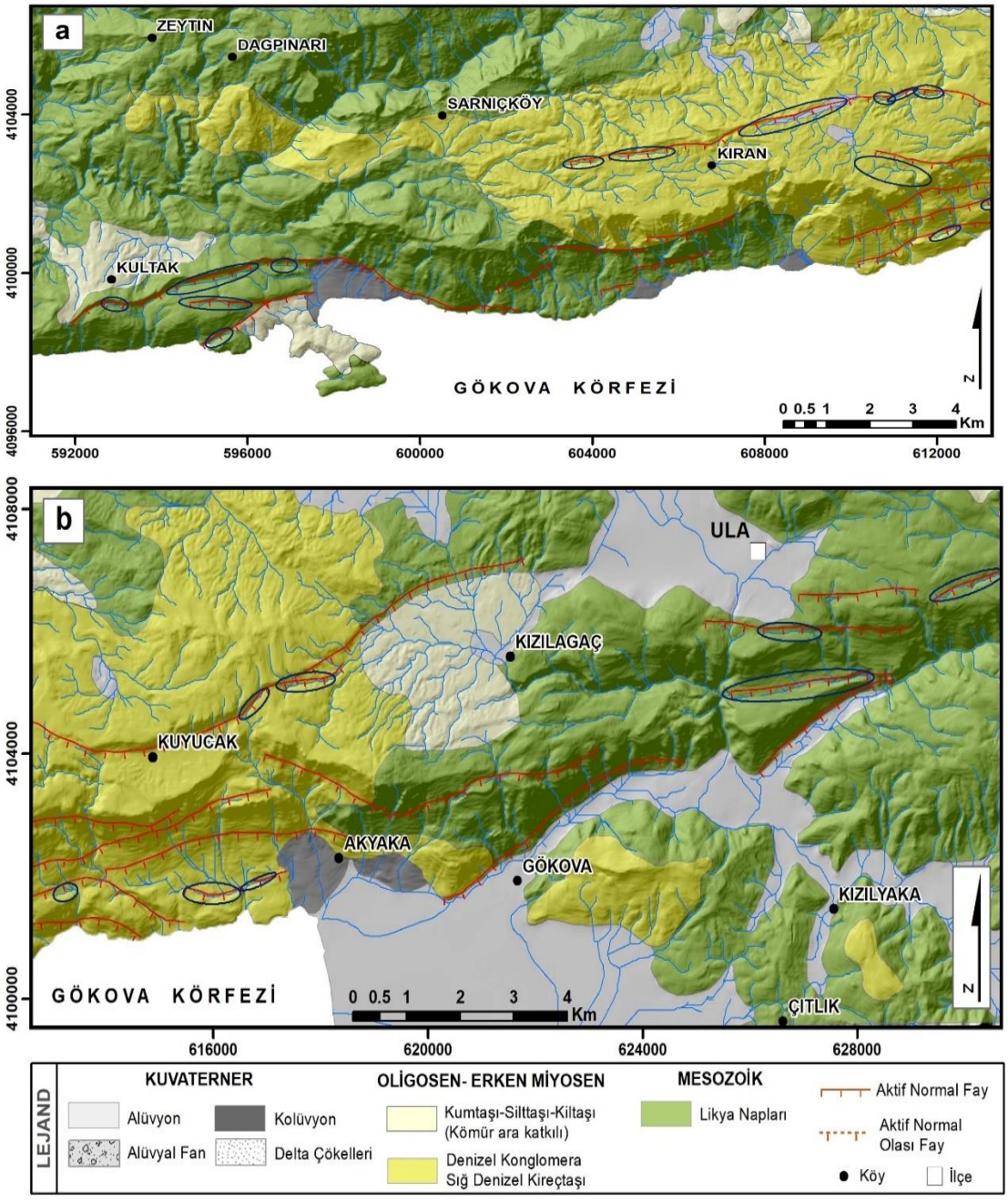

Şekil 16. a) Kultak ve Kıran köyleri arasında haritalanan faylara paralel gelişen drenaj kolları. b) Gökova köyü kuzey kesimlerinde haritalanan faylara paralel gelişen drenaj kolları.

4. Morfometri

4.1. Hipsometrik Eğri ve Hipsometrik İntegral

GFZ boyunca ArcMap yazılımında mevcut bulunan araçlar ve ek betikler (script) (Beg, 2015) kullanılarak, SYM üzerinde yapılan veri-işlem adımları ile çalışma alanında yer alan havza sınırları belirlenmiştir (Şekil 17). Buna göre GFZ kuzeyinde, taban blok üzerinde 5 adet havza ayırtlanmıştır. Bu havzaların hipsometrik eğrileri elde edilmiş ve hipsometrik integral (HI) değerleri hesaplanmıştır (Şekil 18).

Toplam 5 havza için yapılan hesaplamalara göre bu havzaların üç tanesinin (gh1, gh3, gh4) hipsometrik eğrileri dışbükeydir ve tüm havzaların HI değerleri 0.37 ila 0.67 arasında değişmektedir (Şekil 18 ve 19). Diğer iki havzanın (gh0 ve gh2) eğrileri ise hafif içbükeydir, HI değerleri sırasıyla 0.45 ve 0.37 olarak hesaplanmıştır (Şekil 18 ve 19). Bu değerler havzaların nispeten genç evrede olduklarını ve/veya tektonik kuvvetlerin havzalar üzerindeki etkisinin yüksek olduğunu göstermektedir.

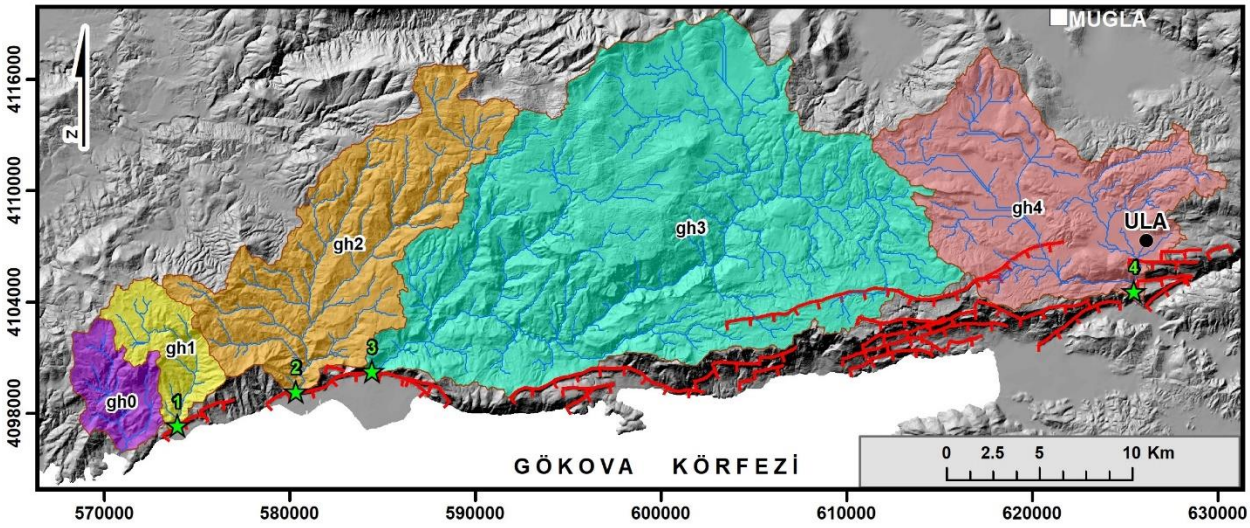

Şekil 17. GFZ taban bloğu üzerinde kalan akaçlama ağları ve havza sınırları. Yeşil yıldızlar V_f indisi hesaplanan noktaları gösterir.

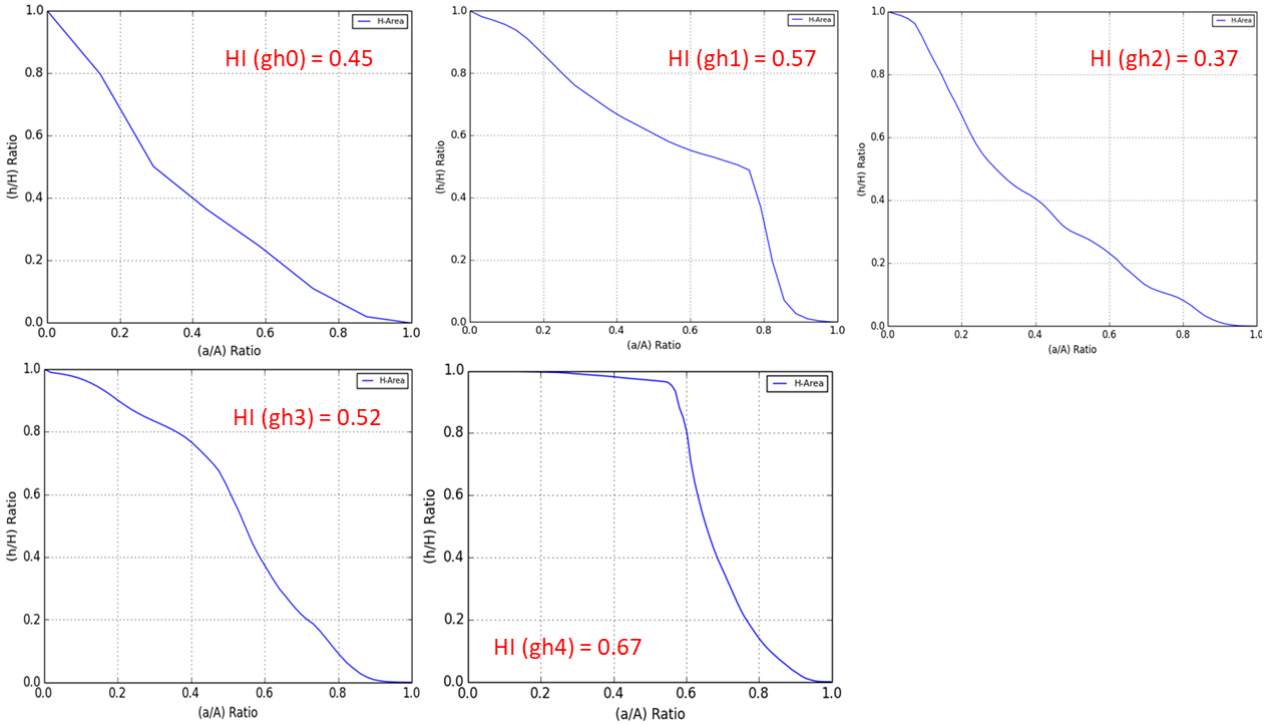

Şekil 18. GFZ taban bloku üzerinde yer alan havzaların hipsometrik eğrileri ve bu havzalara ait HI değerleri.

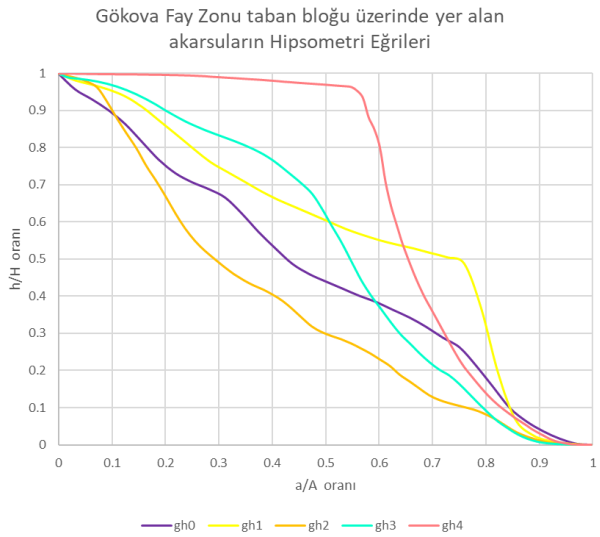

Şekil 19. GFZ taban bloku üzerinde yer alan havzaların hipsometrik eğrilerinin bir arada gösterimi.

4.2. Vadi Tabanı Genişliğinin Vadi Yüksekliğine Oranı (V_f)

GFZ Ören köyü doğusunda, körfez kuzey kenarı boyunca dik falezler oluşturmuştur. Ören köyü ve daha batıda ise, taban blok üzerinde, haritalanan faylara dik gelişmiş vadiler yer alır. GFZ boyunca V_f indis değerlerinin hesaplanabilmesi amacıyla Ören köyü ve daha batısında yer alan 3 vadide profil ölçümleri dağ önünden (aktif faydan) 200 m dere yukarısında yapılmış ve V_f indis değerleri hesaplanmıştır. GFZ doğusunda, Ula ilçesi güneyinde faya dik uzanan bir diğer vadide de profil ölçümleri yapılmış ve V_f indis değeri hesaplanmıştır (Şekil 17, Tablo 2).

Hesaplanan V_f indisi değerleri 0.12 ila 0.78 arasında değişmektedir. Bu değerler, vadilerin V şekilli olduğunu, taban bloktaki yükselmeye derine kazarak cevap verdiklerini gösterir.

Tablo 2
GFZ boyunca V_f indisi hesaplamaları için seçilen 4 adet vadide profil ölçümleri ve V_f indisi sonuçları (Vadilerin coğrafi konumları için Şekil 18'e bakınız).

No	**Litoloji**	**E_{ld}**	**E_{rd}**	**E_{sc}**	**V_{wf}**	**V_f**
1	Mermer (Mesozoik)	105	225	7	31	0.196203
2	Mermer (Mesozoik)	101	43	15	45	0.789474
3	Mermer (Mesozoik)	70	359	17	48	0.243038
4	Mermer (Mesozoik)	382	384	98	37	0.129825

4.3. Dağ Önü Eğriliği (S_{mf})

Çalışma alanında dağ önü eğriliği (S_{mf}) indeksi hesaplamaları ikisi batıda biri doğuda olmak üzere üç farklı lokasyonda, izlenen düzlük alanlar ile kuzeydeki dağlık kesim arasında yapılmıştır. Batıdaki ölçümler, Çökertme Fan-Deltası ve Ören Fan-Deltasını kuzeyden sınırlayan segmentler üzerindedir (Şekil 20). Doğudaki ölçümler ise, Gökova köyü kuzeyinde yer alan Çay Dere ve Dip Dere boyunca haritalanan segmentler üzerindedir (Şekil 21).

SYM üzerinden ölçülen L_{mf} ve L_s uzunlukları ile Çökertme ve Ören köyleri civarında hesaplanan S_{mf} değerleri 1.00 ve 1.24 arasında değişmektedir (Tablo 3). Gökova köyü kuzeydoğusunda hesaplanan S_{mf} değerleri ise 1.04 ve 1.08'dir (Tablo 3). Bu değerler, üç bölgede de dağ önlerinin fay kontrollü olduğunu göstermektedir.

Şekil 20. Çökertme köyü güneydoğusu ve Ören Fan-Deltası civarında S_{mf} indisi hesaplaması.

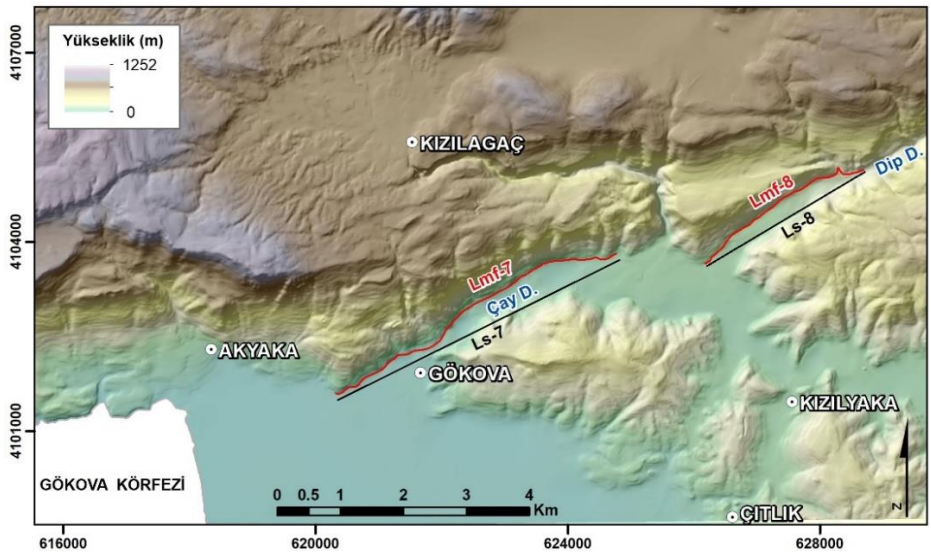

Şekil 21. Gökova köyü civarında S_{mf} indisi hesaplaması.

Tablo 3

Çalışma alanında dağ önü eğriliği (S_{mf}) indisi değerleri

Segment	**L_{mf} (m)**	**L_s (m)**	**S_{mf}**
Ls-1	3138	2522	1.244251
Ls-2	1725	1613	1.069436
Ls-3	1587	1576	1.00698
Ls-4	734	726	1.011019
Ls-5	1834	1812	1.012141
Ls-6	3429	3283	1.044472
Ls-7	5217	4998	1.043818
Ls-8	3151	2914	1.081332

5. Tartışma ve Sonuçlar

Bu çalışmada, GFZ'nun karada izlenen segmentlerinin morfolojik özellikleri araştırılmış ve GFZ boyunca morfometrik analiz çalışmaları gerçekleştirilmiştir. Gökova Körfezi'nde, bölgedeki tektonik yapıyı ortaya koymak amacıyla hem körfez içinde hem de yakın kara alanında yapılan sismik yansıma (Kurt vd., 1999; Uluğ vd., 2005), çok ışınlı batimetri (Uluğ vd., 2005, İşcan vd., 2013) ve elektrik rezistivite (Çağlar ve Duvarcı, 2001) çalışmaları; GFZ'nun karada izlenen kesimlerinde gerçekleştirilen haritalama çalışmaları (Örn: Ersoy, 1990; Şaroğlu, Emre ve Boray, 1992; Görür vd., 1994; 1995; Emre vd., 2013; 2018; Gürer vd., 2013; Dikbaş vd., 2022) körfezin bir graben yapısı içerisinde geliştiğini ortaya koymuştur. Oluşturulan SYM, körfezin kuzey kıyısında, GFZ boyunca deniz seviyesinden aniden ~1000 m yükseklikliere ulaşıldığını gösterir. Fay zonlarında topoğrafik yüzey eğim açıları 70°'ye yükselir. Fay boyunca faya dik alınan yaklaşık kuzey-güney topoğrafik profillerde fayın izi kontrol edilmiş ve doğu-batı yönlerdeki devamlılığı araştırılmıştır. Hem topoğrafik profillerde hem de bakı haritasında düşen blokların kayma yönü tersinde yani kuzey yönde bir eğimlenme gösterdiği izlenmiştir. Bölgede gelişen drenaj ağının geometrisi mevcut tektonik süreksizliklerden etkilenerek şekillenmektedir. Fay düzlemi önlerinde, drenaj geometrisi çoğu yerde faya paralel gelişmiştir. Faya dik yönde izlenen drenaj kollarının ise, yaşlarının çok genç olması ve/veya hızlarının fayın kayma hızından yüksek olması nedeniyle bu konumda gelişmiş olabileceği düşünülmüştür. Taban blok üzerinde yer alan havzalar için oluşturulan hipsometrik eğriler ve hesaplanan HI değerleri, havzaların ağırlıklı olarak genç evrede olduğunu göstermektedir (Tablo 4). Taban blok üzerinde dört vadide hesaplanan V_f indisi değerleri oldukça düşük olup, vadilerin V-şekilli olduğunu (Tablo 4) ve tektonik yükselmeye derine kazma eğilimi ile cevap verdiklerini gösterir. Dağ önü eğriliklerinin hesaplanabildiği 3 farklı alanda, sonuçlar fay kontrollü dağ önlerini işaret etmiştir (Tablo 4). GFZ boyunca yürütülmüş olan kalitatif ve kantitatif morfolojik çalışmalar bölgenin jeomorfolojik şekillenmesinde tektonik süreçlerin erozyonal süreçlere nazaran daha baskın olduğunu göstermektedir.

Tablo 4

GFZ üzerinde uygulanan morfometrik indislerin sonuçları

Morfometrik İndis	**Değer**		**Morfotektonik Yorum**
HI	gh0	0,45	Havza denge durumunda (0.35>HI>0.6) ya da genç evrede (0.6>HI>1)
	gh2	0,57	
	gh3	0,37	
	gh4	0,52	
	gh5	0,67	
V_f	V_f1	0,19	Vadi V-şekilli, genç evrede
	V_f2	0,78	
	V_f3	0,24	
	V_f4	0,12	
S_{mf}	$S_{mf}1$	1,24	Dağ önü fay kontrollü
	$S_{mf}2$	1,07	
	$S_{mf}3$	1,00	
	$S_{mf}4$	1,01	
	$S_{mf}5$	1,01	
	$S_{mf}6$	1,04	
	$S_{mf}7$	1,04	
	$S_{mf}8$	1,08	

Teşekkür

Bu çalışma TÜBİTAK 116Y179 no.lu proje çerçevesinde sürdürülen araştırmalar içerisinde yazarın sorumlu olduğu kesimlerin bir parçasıdır. Yazar; arazi çalışmalarının bir kısmına eşlik eden Mehran Basmenji ve Erdem Kırkan'a teşekkür eder.

Yazar Katkıları

Aynur Dikbaş: Morfometrik indis hesaplamaları için gerekli olan veri setini oluşturmuş, analizleri planlamış ve gerçekleştirmiş, arazi kontrollerinde bulunup makaleyi yazmıştır.

Çıkar Çatışması

Yazar çıkar çatışması bildirmemiştir.

Kaynaklar

AFAD (2022). T.C. Başbakanlık Afet ve Acil Durum Yönetimi Deprem Dairesi Başkanlığı. Erişim adresi: https://deprem.afad.gov.tr/depremkatalogu

Akbaş, B., Akdeniz, N., Aksay, A., Altun, İ., Balcı, V., Bilginer, E., Bilgiç, T., Duru, M., Ercan, T., Gedik, İ., Günay, Y., Güven, İ.H., Hakyemez, H. Y., Konak, N., Papak, İ., Pehlivan, Ş., Sevin, M., Şenel, M., Tarhan, N., Turhan, N., Türkecan, A., Ulu, Ü., Uğuz, M.F. & Yurtsever, A. (2011). *Türkiye Jeoloji Haritası*. MTA, Ankara, Türkiye.

Akyüz, H.S., Kırkan, E., Basmenji, M., Aksoy, M.E., Dikbaş, A., Zabcı, C. & Uçarkuş, G. (2018). Paleoseismological and Morphotectonical Characteristics of Active Faults in the Vicinity of Muğla Area (SW Turkey). In: Conference of the Arabian Journal of Geosciences, Tunisia, (pp. 253-256). https://doi.org/10.1007/978-3-030-01656-2

Ambraseys, N. N. (2009). *Earthquakes in the Mediterranean and Middle East: a multidisciplinary study of seismicity up to 1900*. Cambridge University Press, London. https://doi.org/10.1017/CBO9781139195430

Ambraseys, N. N. & Finkel, C.F. (1991). Long-term seismicity of Istanbul and the Marmara Sea region. *Terra Nova, 3,* 527-539. https://doi.org/10.1111/j.1365-3121.1991.tb00188.x

Ambraseys, N. N. & Jackson, J. A. (1998). Faulting associated with historical and recent earthquakes in the Eastern Mediterranean region. *Geophysical Journal International, 133,* 390-406. https://doi.org/10.1111/j.1365-3121.1991.tb00188.x

Atalay, Z. (1980). Muğla-Yatağan ve Yakın Dolayı Karasal Neojen'inin Stratigrafi Araştırması. *Türkiye Jeoloji Bülteni, 23,* 3-99.

Beg, F.A.A. (2015). Morphometric Toolbox: A New Technique in Basin Morphometric Analysis Using ArcGIS. *Global Journal of Earth Science and Engineering, 2,* 21-30. http://dx.doi.org/10.15377/2409-5710.2015.02.02.1

Bozkurt, E., (2003). Origin of NE-trending basins in western Turkey. *Geodinamica Acta, 16,* 61–81. https://doi.org/10.1016/S0985-3111(03)00002-0

Bull, W. B. (1977). Tectonic geomorphology of the Mojave Desert. U.S. Geological Survey Contact Report 14-08-001-G-394. Office of Earthquakes, Volcanoes and Engineering, Menlo Park, California.

Bull, W. B. (1978). Geomorphic tectonic classes of the south front of the San Gabriel Moun- tains, California. U.S. Geological Surfey Contact Report 14-08-001-G-394. Office of Earthquakes, Volcanoes and Engineering, Menlo Park, California.

Bull, W. B. & McFadden, L. D. (1977). Tectonic geomorphology north and South of the Garlock fault, California. In: D.O. Doehering (Ed.), Geomorphology in Arid regions. Proceedings at the Eighth Annual Geomorphology Symposium (s. 115‑138). Binghampton, State University of New York.

Burbank, D. W. & Anderson, R. S. (2001). *Tectonic geomorphology*. Blackwell Science, Malden.

Çaglar, İ. & Duvarcı, E. (2001). Geoelectric structure of inland area of the Gökova rift, southwest Anatolia and its tectonic implications. *Journal of Geodynamics, 31,* 33-48. https://doi.org/10.1016/S0264-3707(00)00014-4

Davis, W.M. (1899). The geographical cycle. *The Geographical Journal, 14,* 481-504. https://doi.org/10.2307/1774538

Dikbaş, A., Akyüz, H.S., Basmenji, M & Kırkan, E. (2022). Earthquake history of the Gökova fault zone by paleoseismologic trenching, SW Turkey. *Natural Hazards, 112,* 2695-2716. https://doi.org/10.1007/s11069-022-05284-0

Duman, T. Y., Emre, Ö., Özalp, S. & Elmacı, H. (2011). 1:250.000 Ölçekli Türkiye Diri Fay Haritası Serisi, Aydın (NJ 35-11) Paftası, Seri No:7, MTA, Ankara.

El-Hamdouni, R., Irigaray, C., Fernandez, T., Chacon, J. & Keller, E.A. (2008). Assessment of relative active tectonics, southwest border of the Sierra Nevada (southern Spain). *Geomorphology*, *96*, 150‑173. https://doi.org/10.1016/j.geomorph.2007.08.004

Emre, Ö., Duman, T.Y., Özalp, S., Elmacı, H., Olgun, Ş. & Şaroğlu, F. (2013). Açıklamalı Türkiye Diri Fay Haritası, Özel Yayın Serisi-30, MTA, Ankara.

Emre, Ö., Duman, T.Y., Özalp, S., Şaroğlu, F., Olgun, Ş., Elmacı, H. & Can, T. (2018). Active fault database of Turkey. Bulletin of Earthquake Engineering, *16* (8), 3229-3275. https://doi.org/10.1007/s10518-016-0041-2

EMSC, (2022). The European-Mediterranean Seismological Centre. Erişim adresi: https://www.emsc-csem.org/#2

Ergin, K., Güçlü, U. & Uz, Z. (1967). Türkiye ve civarının deprem kataloğu (Milattan Sonra 11 yılından 1964 sonuna kadar). İstanbul Teknik Üniversitesi, Maden Fak., Yer Fiziği Ens., Teknik Rapor No: 24, İstanbul.

Erinç, S. (1996). *Jeomorfoloji-I*. Öz-Eğitim Yayınları, İstanbul.

Ersoy, Ş. (1990). The analysis of evolution and structural items of The Western Taurus-Lycia Nappes. *Geological Engineering, 37,* 5–16.

Ersoy, Ş. (1991). Datça (Muğla) Yarımadasının Stratigrafisi ve Tektoniği. *Türkiye Jeoloji Bülteni*, *34*, 1-14.

Eyidoğan, H., Akıncı, A., Gündoğdu, O., Polat, O. & Kaypak, B. (1996). Investigation of the recent seismic activity of Gökova Basin. In: National Marine Geology and Geophysical Programme Workshop 1, Proceedings, 8-9 February, 1996, (s. 68-71).

Görür, N., Şengör, A.M.C., Sakınç, M., Tüysüz, O., Yiğitbaş, E., Oktay, F.Y., Barka, A., Sarıca, N., Ecevitoğlu, B., Demirbağ, E., Aykol, A., Algan, O., Güneysu, C. & Ersoy, Ş. (1994). Crosscutting rift systems of the Gökova region, SWAnatolia: implications for the formation of the Aegean Sea. *İTÜ Bülteni*, *47* (4), 275–292.

Görür, N., Şengör, A.M.C., Sakınç, M., Tüysüz, O., Akkök, R., Yiğitbaş, E., Oktay, F.Y., Barka, A.A., Sarıca, N., Ecevitoğlu, B., Demirbağ, E., Ersoy, Ş., Algan, O., Güneysu, C. & Akyol, A. (1995). Rift formation in the Gökova region, southwest Anatolia: implications for the opening of the Aegean Sea. *Geological Magazine, 132,* 637–650. https:/doi.org/10.1017/s0016756800018884

Guidoboni, E. & Comastri, A. (2005). *Catalogue of earthquakes and tsunamis in the Mediterranean area from. the 11th to the 15th century*. Istituto Nazionale di Geofisica e Vulcanologia, Rome

Guidoboni, E., Comastri, A. & Triana, G. (1994). *Catalogue of ancient earthquakes in the Mediterranean area up to the10th Century*. Istituto Nazionale di Geofisica e Vulcanologia, Rome.

Gül, M., Danladi, I.B. & Kore, B.M. (2017). Coastal types of graben: the Gulf of Gökova, Mugla-SW Turkey. *Journal of Coast Conservation, 21,* 127–138. https://doi.org/10.1007/s11852-016-0481-5

Gürer, F.Ö. & Yılmaz, Y. (2002). Geology of the Oren and Surrounding Areas, SW Anatolia. *Turkish Journal of Earth Sciences, 11,* 1-13.

Gürer, Ö.F., Sanğu, E., Özburan, M., Gürbüz, A. & Sarıca-Filoreau, N. (2013). Complex basin evolution in the Gökova Gulf region: implications on the Late Cenozoic tectonics of southwest Turkey. Int J Earth Sci (Geol Rundsch) *102,* 2199–2221. https://doi.org/10.1007/s00531-013-0909-1

Hakyemez, Y. & Örçen, S. (1982). Denizli-Muğla arasındaki Senozoyik yaşlı çökel kayaların sedimantolojisi ve biyostratigrafisi. Maden Tetkik ve Arama Enst. Rap. No. 7311, s.135 (yayımlanmamış), Ankara.

Hancock, P. L. & Barka, A. A. (1987). Kinematic indicators on active normal faults in western Turkey. *Journal of Structral Geology, 9* (3), 415-430. https://doi.org/10.1016/0191-8141(87)90142-8

ISC, (2022). International Seismological Centre. Erişim adresi: http://www.isc.ac.uk

İşcan, Y., Tur, H. & Gökaşan, E. (2013). Morphologic and seismic features of the Gulf of Gökova, SWAnatolia: evidence of strike-slip faulting with compression in the Aegean extensional regime. *Geo-Marine Letters, 33,* 31–48. https://doi.org/10.1007/s00367-012-0307-x

Jackson, J., A., King, G. & Vita-Finzi, C. (1982). The neotectonics of Aegean: an alternative view. *Earth and*

Planetary Sciences Letters, 61, 303-318. https://doi.org/10.1016/0012-821X(82)90062-0

Kalafat, D. & Horasan, G. (2012). A seismological view to Gökova region at southwestern Turkey. *International Journal of Physical Sciences, 7* (30), 5143–5153. https://doi.org/10.5897/IJPS12.277

Kaya, T., Tuna, V. & Geraads, D. (2001). A new late Orleanian/Early Astaracian mammalian fauna from Kultak (Milas-Mugla), southwestern Turkey. *Geobios, 34* (6), 673–680. https://doi.org/10.1016/S0016-6995(01)80028-0

Keller, E. & Pinter, N. (1996). *Active tectonics: Earthquakes, uplift, and landscape*. Prentice Hall, New Jersey.

Keller, E.A. & Pinter, N. (2002). *Active tectonic: Earthquakes, uplift, and landscape*. Prentice Hall, New Jersey.

KOERİ, (2018). Kandilli Rasathanesi ve Deprem Araştırma Enstitüsü. Erişim adresi: http://www.koeri.boun.edu.tr

Kurt, H., Demirbağ, E. & Kuşcu, İ. (1999). Investigation of submarine active tectonism in the Gulf of Gökova, southwest Anatolia - SE Aegean Sea, by multi-channel seismic reflection data. *Tectonophysics, 305*, 477–496. https://doi.org/10.1016/S0040-1951(99)00037-2

McKenzie, D.P., (1972). Active tectonics of the Mediterranean region. *Geophysical Journal of the Royal Astronomical Society, 30,* 109–185. https://doi.org/10.1111/j.1365-246X.1972.tb02351.x

Mozafari, N., Özkaymak, Ç., Sümer, Ö., Tikhomirov, D., Uzel, B., Yeşilyurt, S., Ivy-Ochs, S., Vockenhuber, C., Sözbilir, H. & Akçar, N. (2022). Seismic history of western Anatolia during the last 16 kyr determined by cosmogenic ^{36}Cl dating. *Swiss Journal of Geosciences, 115*, 5. https://doi.org/10.1186/s00015-022-00408-x

Ohmori, H. (1993). Changes in the hypsometric curve through mountain building resulting from concurrent tectonics and denudation. *Geomorphology*, *8*(4), 263–277. https://doi.org/10.1016/0169-555x(93)90023-u

Papazachos, B., Kiratzi, A., Hatzidimitriou, P. & Rocca, A.C. (1984) Seismic faults in Aegean area. *Tectonophysics, 106*, 71-85. https://doi.org/10.12681/bgsg.16865

Perez-Pena, J.V., Azor, A., Azanon, J.M. & Keller, E.A. (2010). Active tectonics in the Sierra Nevada (Betic Cordillera, SE Spain): Insights from geomorphic indexes and drainage pattern analysis. *Geomorphology*, *119*, 74‑87. https://doi.org/10.1016/j.geomorph.2010.02.020

Rontogianni, S., Konstantinou, K.I., Evangelidis, C. & Melis, N.S. (2011). Investigating Potential Seismic Hazard in the Gulf of Gökova (South Eastern Aegean Sea) Deduced From Recent Shallow Earthquake Activity. American Geophysical Union, Fall Meeting 2011, T43E-2427, San Francisco.

Saber, R., Çağlayan, A. & Işık, V. (2018). Relative Tectonic Activity Assessment and Kinematic Analysis of the North Bozgush Fault Zone, NW Iran. *Journal of Asian Earth Science*, *164*, 219-236. https://doi.org/10.1016/j.jseaes.2018.06.023

Saber, R., Işık, V. & Çağlayan, A. (2020). Tectonic Geomorphology of the Aras Drainage Basin: Implications for the recent activity of the Aras Fault Zone. *Geological Journal*, *55*, 5022–5048. https://doi.org/10.1002/gj.3724

Sağlam Selçuk, A. (2016). Evaluation of the relative tectonic activity in the eastern Lake Van basin, East Turkey, *Geomorphology, 270,* 9-21. https://doi.org/10.1016/j.geomorph.2016.07.009

Sezgül-Kayseri, M. & Akgün, F. (2010). Türkiye'de Geç Burdigaliyen–Langiyen Periyodu ve Avrupa ile Paleortamsal ve Paleoiklimsel Karşılaştırma: Muğla–Milas (Kultak) Geç Burdigaliyen-Langiyen Palinoflorası ve Paleoiklimsel Özellikleri. *Türkiye Jeoloji Bülteni, 53* (1), 1–44.

Sieberg, A. (1932). *Erdbebengeographie*. Handbuch der Geophysik, Berlin.

Soysal, H., Sipahioğlu, S., Kolçak, D. & Altınok,Y. (1981). Türkiye ve Çevresinin Tarihsel Deprem Kataloğu. TÜBİTAK Proje No: TBAG 341, Istanbul.

Strahler, A.N. (1952). Hypsometric (area-altitude) analysis of erosional topography. *Geological Society of America Bulletin, 63,* 1117-1141. https://doi.org/10.1130/0016-7606(1952)63

Şaroğlu, F., Emre, Ö. & Boray, A. (1987). Türkiye'nin diri fayları ve depremsellikleri, Rapor No: 8174 (yayınlanmamış), MTA, Ankara.

Şaroğlu, F., Emre, Ö. & Boray, A. (1992). *Türkiye Diri Fay Haritası*. MTA, Ankara.

Taymaz, T., Jackson, J. & McKenzie, D. (1991). Active Tectonics of the North and Central Aegean Sea. *Geophysical Journal International, 106* (2), 433-490. https://doi.org/10.1111/j.1365-246X.1991.tb03906.x

Taymaz, T., Tan, O. & Yolsal, S. (2004). Seismotectonics of western Turkey: a synthesis of source parameters and rupture histories of recent earthquakes. In: AGU Fall Meeting, Session T14, San Fransisco-California, *EOS Trans. Am. Geophys. Union*, 85 (47), 408.

Tırpan, A.A. (1989). Keramos. VI. Araştırma Sonuçları Toplantısı, Ankara, (s. 363-383).

Tur, H., Yaltırak, C., Elitez, İ. & Sarıkavak, K. (2015). Pliocene – Quaternary tectonic evolution of the Gulf of Gökova, southwest Turkey. *Tectonophysics, 638*, 158-176. https://doi.org/10.1016/j.tecto.2014.11.008

Uluğ, A., Duman, M., Ersoy, Ş., Özel, E. & Avcı, M. (2005). Late Quaternary sea-level change, sedimentation and neotectonics of the Gulf of Gökova: Southeastern Aegean Sea. *Marine Geology, 221*, 381–395. https://doi.org/10.1016/j.margeo.2005.03.002

Yılmaz, Y., Genç, Ş.C., Gürer, F., Bozcu,M., Yılmaz, K., Karacık, Z., Altunkaynak, Ş. & Elmas, A. (2000). When did the western Anatolia grabens begin to develop?. *Geol. Soc. Lond. Spec. Publ., 173*, 353–384. https://doi.org/10.1144/GSL.SP.2000.173.01.17

Yolsal-Çevikbilen, S., Taymaz, T. & Helvacı, C. (2014). Earthquake Mechanisms in the Gulfs of Gökova, Sığacık, Kuşadası, and the Simav Region (western Turkey): Neotectonics, seismotectonics and geodynamic implications. *Tectonophysics, 635*, 100-124. https://doi.org/10.1016/j.tecto.2014.05.001

e-ISSN 2757-5195

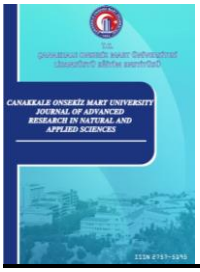

Çanakkale Onsekiz Mart University
Journal of Advanced Research in Natural and Applied Sciences
Open Access

doi.org/10.28979/jarnas.1085431 2023, Cilt 9, Sayı 1, Sayfa: 48-55 dergipark.org.tr/tr/pub/jarnas

Alyssum filiforme Bitkisinin Antimikrobiyal, Antibiyofilm, Antioksidan Aktivitesinin ve Fenolik Profilinin Belirlenmesi

İlayda Orçan[1*], Ali Savaş Bülbül[2], Yakup Kara[3]

[1] Biyoloji Bölümü, Fen Bilimleri Enstitüsü, Kahramanmaraş Sütçü İmam Üniversitesi, Kahramanmaraş, Türkiye
[2] Acil Yardım ve Afet Yönetimi, Uygulamalı Bilimler Fakültesi, Bayburt Üniversitesi, Bayburt, Türkiye
[3] Kimya Bölümü, Fen Fakültesi, Karadeniz Teknik Üniversitesi, Trabzon, Türkiye

Makale Tarihçesi

Gönderim: 17.03.2022
Kabul: 31.08.2022
Yayım: 05.03.2023

Araştırma Makalesi

Öz – Bakteriler antibiyotiklere ve türevlerine karşı günden güne direnç kazanmaktadır ve bu küresel bir sorun haline gelmektedir. Bitkilerde bulunan sekonder metabolitlerin (fenolik bileşikler, flavonoidler, alkoloidler gibi) antioksidan ve antimikrobiyal gibi çeşitli aktiviteleri sebebiyle bu küresel sorunun önüne geçilebileceği düşünülmektedir. Bu kapsamda çeşitli çalışmalar yapılmış ve halen de yapılmaktadır. Bitkisel kaynaklardan antioksidan, antimikrobiyal ve anti-biyofilm gibi etki gösteren bileşenlerin belirlenmesi ile antibiyotik ve türevlerine karşı oluşan direnç aşılabilir. B vitamini ve magnezyum açısından zengin olan Brassicacea ailesinin bir üyesi de *Alyssum filiforme* türüdür. *Alyssum filiforme* bu kapsamda değerlendirilebilecek potansiyele sahip bir endemik türdür. Bu çalışmada; endemik olarak yetişen türün antimikrobiyal, anti-biyofilm, antioksidan ve RP-HPLC-PDA ile fenolik profili belirlendi. Elde edilen ekstre antimikrobiyal aktivite için Minimum İnhibisyon Konsantrasyonu (MIC) ve Minimum Bakterisidal Konsantrasyonu (MBC) yöntemleri uygulandı, antioksidan aktiviteyi belirlemek için ise 2,2-difenil-1-pikrilhidrazil (DPPH) radikalini temizleme aktivitesi ve demir indirgeme antioksidan güç (FRAP) metodları kullanıldı. Biyofilm oluşumunu önlemedeki etkinliği gözlemleyebilmek için kristal viyole bağlama yöntemi kullanıldı. Tüm bakterilerde olumlu sonuçlar elde edildi. FRAP ve DPPH sonuçları sırasıyla 13.070 µmol $FeSO_4.7H_2O$/g ve SC_{50} 5.190 mg/ml olarak belirlendi. Elde edilen fenolik analiz sonucunda bitkinin kafeik asit ve krisin yönünden zengin olduğu bulundu. Elde edilen sonuçlar ışığında *Alyssum filiforme* türünün sağlık açısından değerli bir tür olduğu düşünülmektedir.

Anahtar Kelimeler – *Alyssum filiforme, antibakteriyel, antibiyofilm, antioksidan, fenolik bileşikler*

Determination of Antimicrobial, Antibiofilm, Antioxidant Activity and Phenolic Profile of *Alyssum filiforme*

[1] Biyoloji Bölümü, Fen Bilimleri Enstitüsü, Kahramanmaraş Sütçü İmam Üniversitesi, Kahramanmaraş, Türkiye
[2] Acil Yardım ve Afet Yönetimi, Uygulamalı Bilimler Fakültesi, Bayburt Üniversitesi, Bayburt, Türkiye
[3] Kimya Bölümü, Fen Fakültesi, Karadeniz Teknik Üniversitesi, Trabzon, Türkiye

Article History

Received: 17.03.2022
Accepted: 31.08.2022
Published: 05.03.2023

Research Article

Abstract – Bacteria are gaining resistance to antibiotics and their derivatives day by day, and this is becoming a global problem. It is thought that this global problem can be prevented due to the antioxidant and antimicrobial activities of the secondary metabolites (phenolic compounds, etc.) found in plants. In this context, various studies have been carried out. Resistance to antibiotics and their derivatives can be overcome by identifying components that act as antioxidants, antimicrobials, and anti-biofilms from plant sources. *Alyssum filiforme* is a member of the Brassicacea family, which is rich in B vitamins and magnesium. *Alyssum filiforme* is an endemic species with the potential to be evaluated in this context. In this study, the antimicrobial, anti-biofilm, antioxidant, and phenolic profile of the endemic *Alyssum filiforme* species was determined by RP-HPLC-PDA. Minimum Inhibition Concentration (MIC) and Minimum Bactericidal Concentration (MBC) methods were applied for the antimicrobial activity of the obtained extract, and 2,2-diphenyl-1-picrylhydrazil (DPPH) radical scavenging activity and iron reducing antioxidant power (FRAP) were used to determine the antioxidant activity. To observe the effectiveness in preventing biofilm formation, the crystal violet bonding method was used, and positive results were obtained in all bacteria. FRAP and DPPH results were determined as 13.070 µmol $FeSO_4.7H_2O$/g and SC_{50} 5.190 mg/ml, respectively. As a result of the obtained phenolic analysis, it was found that the plant is rich in caffeic acid and chrysin. In the light of the results obtained, *Alyssum filiforme* is thought to be a valuable species in terms of health.

Keywords – *Alyssum filiforme, antibiofilm, antibacterial, antioxidant, phenolic compounds*

[1] ilaydaa.orcan.8@gmail.com
[2] alisavasbulbul@bayburt.edu.tr
[3] yaakupkara@gmail.com
*Sorumlu Yazar

1. Giriş

Hastalıktan korunma ve tedavide bitkilerin kullanım geçmişi çok uzun yıllara dayanmaktadır. Tarihte sağlık materyalinin bilinen en eski örneklerini bitkiler, birçok hayvansal ürünler, mantarlar gibi doğal ürünler oluşturmaktadır (Altundağ ve Aslım, 2005). Önceki yıllarda çoğu uygarlıklar bu ürünleri hastalık tedavisi ve ilaç kaynağı olarak kullanmışlardır. Dünya Sağlık Örgütünün elde etmiş olduğu verilere göre dünyadaki nüfusun büyük çoğunluğu bitki kaynaklı ilaçları sağlık açısından daha güvenli bulmaktadır.

Hardalgiller (Brassicacea) ailesi dünya genelinde yaklaşık 340 cins ve 3350 türle çok geniş bir yayılım göstermektedir. Bu bitki ailesi ekonomik açıdan öneme sahip birçok yem, tohum ve çeşni bitki türünü içermektedir. Aynı zamanda *Brasscicacea* ailesi B vitaminleri ve magnezyum açısından zengin bir türdür. Bu ailenin bir üyesi olan *Alyssum filiforme* çok yıllık otsu endemik bir türdür. Türkiye'de yaklaşık 43 türe sahiptir ve genellikle *Alyssum* türleri kuraklığa dayanaklıdır. *Alyssum filiforme* Nyar. Türkiye'de Güneydoğu Anadolu ve Doğu Anadolu Bölgesinde yayılış göstermektedir. Yaygın olarak "tellikevke" adı ile bilinmektedir.

Günümüzde bakterilerin antibiyotikler üzerinde önemli güce sahip olduğu bilinmektedir ve çeşitli hastalıklara neden olan bakterilere karşı antibiyotikler artık tek başına yetememekte ve bu sebepten dolayı alternatif yollar aranmaktadır. Bitkilerin yapısındaki sekonder metabolitler sayesinde bu sorunun önüne geçilebilir (Haşimi vd., 2015). Bakteriyel biyofilmler çeşitli gıda maddelerinde, sularda, klinik yerlerde sağlık riskleri oluşturur. Biyofilmler mikroorganizmalara antimikrobiyal direnç sağladıklarından dolayı ciddi sorun oluşturmaktadır (Bazargani ve Rohloff, 2016).

Bitkisel kaynaklardaki antioksidan ve antimikrobiyal etki gösteren bileşenlerin belirlenmesine yönelik çeşitli çalışmalar mevcuttur (Kırca vd., 2007; Tomaino vd., 2005; Yetgin vd., 2017). Enfeksiyonel kaynaklı mikroorganizmalara karşı bazı bitkilerin antimikrobiyal özellik gösterdiği çeşitli çalışmalarda bildirilmiştir (Avşar vd., 2016). Bitkilerin antioksidan kapasitesinden başta fenolik bileşikler sınıfındaki sinnamik asit ve türevleri, flavonoidler, tokoferoller, kumarinler ve fenolik asitler sorumludur (Moure vd., 2001; Yıldız vd., 2017). Bu bileşenlerin oksidasyona karşı organizmayı koruduğu bilinmektedir. Günümüzde doğal antioksidan kaynaklarından biri olan bitkilerin kullanımı sentetik antioksidan kullanımından daha fazla olmaya başlamıştır (Faydaoğlu ve Sürücüoğlu, 2013).

Bu çalışmada endemik *Alyssum filiforme* bitkisinin kök üstü kısımları kullanılarak MIC, MBC, antibiyofilm ve bitkinin antioksidan aktivitesi ve fenolik profili belirlenerek literatüre katkı sağlayabileceği düşünülmektedir.

2. Materyal ve Yöntem

Çalışmada kullanılan *Alyssum filiforme* endemik bitkisi Kahramanmaraş Tevekkeli köyünden toplanmıştır. Kullanılan mikroorganizmalar ise Bartın Üniversitesi Moleküler Biyoloji ve Genetik Laboratuvarından temin edilmiştir.

2.1. Bitki Özütünün Hazırlanması

Alyssum filiforme endemik bitkisinin yaprak ve gövde kısmı sıvı azot yardımıyla havanda ezilerek öğütüldü. Öğütülen bitki örneğinden 15 g tartılıp 150 ml saf metanol kullanılarak soxhlet cihazında 4-6 saat aralığında ekstraksiyon işlemine tabii tutuldu (Tunç vd., 2014) (Şekil 1). Ardından Whatman No.1 filtre kâğıdı ile süzme işlemi yapıldı ve çözücüyü uçurmak için rotari evaporatör kullanıldı ve kuruması için 37 ^{o}C'de etüve kaldırıldı. Etüvden çıkarılan bitki örneği çalışmalarda kullanılmak üzere +4 ^{o}C'de saklandı.

Şekil 1. Bitki örneğinin ekstraksiyon işlemi ve Rotary evaporatör

2.2. Antibakteriyel Aktivite

Çalışmada antibakteriyel aktivite hastane patojeni *Entorobacter aerogenes* (ATCC 13048), *Klebsiella pneumoniae, Enterobacter durans, Bacillus subtilis* (DSMZ 1971), *Salmonella typhimurium, Staphylococcus aureus* (ATCC 25923) bakterileri üzerinde mikrodilüsyon yöntemi ile MIC değeri belirlendi. Ardından MBC değeri Müeller Hinton Agar besiyerinde belirlendi.

Minimum inhibisyon konsantrasyonu 96 kuyucuklu mikroplaka ile belirlendi. Tüm kuyucuklara ilk olarak 100 µl LB broth konulmuştur. Ardından 100 µl hazırlanan bitki ekstrelerinden sadece ilk kuyucuklara konulup pozitif ve negatif kontrol hariç diğer kuyucuklara seri dilüsyon yapılmıştır. Son olarak negatif kontrol hariç tüm kuyucuklara 10 µl bakteri konulup 37 ºC'de 18-24 saat inkübasyona bırakılmıştır. Süre sonunda 550 nm ve 600 nm de ölçüm yapılmıştır.

Minimum inhibisyon konsantrasyonu belirlendikten sonra minimum bakterisidal konsantrasyonu mikro-plaka üzerinde bulanık olmayan kuyucuklar tespit edilip MHA besiyeri üzerine öze yardımıyla ekimi yapıldı ve 18-24 saat inkübasyona bırakıldı. Süre sonunda bakterilerin %99.9'unu öldüren MBC değeri belirlendi.

2.3.Antibiyofilm Aktivite

İnkübasyona bırakılan mikroplakanın 48 saat sonunda antibiyofilm aktivitesi belirlendi. Mikroplaka tamamen boşaltılıp distile su ile 2-3 defa yıkandı ve kurumaya bırakıldı. Kuruyan mikroplakaya önce %95'lik metanol eklenip 15 dk fiksasyon yapıldı ve süre sonunda metanol boşaltılıp kurumaya bırakıldı daha sonra kuruyan mikroplakaya %0.1'lik kristal viyole eklenerek 10 dk fiksasyona bırakıldı. Fiksasyon sonrasında kristal viyole boşaltılıp 2-3 defa distile su ile yıkandı ve sonrasında kurutuldu. Kuruyan kuyucuklara tutunan bakterilerin kaldırılması için gram pozitif bakterilerin olduğu kuyucuklara glasiyel asetik asitin%33'lük çözeltisinden, gram negatif bakterilerin olduğu kuyucuklara ise %95'lik etanol eklenip 15 dk beklendi. Süre sonunda mikroplakanın OD değeri spektrofotometre de 600 nm de ölçüldü ve pozitif kontrole göre biyofilm yüzdeleri hesaplandı.

2.4. Antioksidan Aktivite

2.4.1. Toplam Fenolik Bileşen Tayini

Yöntem, örneklerin içerdiği fenolik bileşenler ile Folin Ciocalteu reaktifi arasında oluşan renkli kompleksin absorbansının ölçülmesi esasına dayanmaktadır (Singleton vd., 1999). Reaksiyon sonunda, koyu mavi renkli kompleks 760 nm'de maksimum absorbans oluşturur. Çalışmada gallik asit farklı konsantrasyon aralığında çalışılarak standart kalibrasyon eğrisi oluşturuldu ve bu eğriden faydalanılarak örnekteki fenolik madde miktarı mg gallik asit eşdeğeri (mgGAE/g) olarak ifade edildi.

2.4.2. Toplam FlavonoidBileşen Tayini

Örneğin toplam flavoid madde miktarı Fukumoto ve Mazza (2000)'ya göre yapıldı. Standart kalibrasyon eğrisi elde etmek için standart olarak kuersetin farklı konsantrasyon aralığında çalışıldı. Standart kalibrasyon eğrisinden faydalanılarak örneğin flavonoid içeriği belirlendi. Sonuç mg kuersetin eşdeğeri (mgQE/g) olarak ifade edildi.

2.4.3. Demir(III) İndirgeme-Antioksidan Güç, FRAP Tayini

FRAP metodu (Fe(III)-TPTZ- 2,4,6-tris (2-pyridly)-S-triazin)'in Fe(II)-TPTZ indirgenmesi esasına dayalı kullanılan antioksidan yöntemidir. Yöntemin esası 593 nm'de absorbans yapan mavi renkli kompleks oluşmasına dayanmaktadır (Benzeie ve Strain, 1999). Çalışmada standart olarak $FeSO_4.7H_2O$'un değişen konsantrasyonları kullanılarak standart kalibrasyon eğrisi oluşturuldu. Akabinde örnekten 50 µL ve taze olarak hazırlanmış FRAP reaktifinden 1.5 mL karıştırıldı. Dört dakika inkübe edildikten sonra 593 nm'de absorbans okuması yapıldı. Sonuç $FeSO_4.7H_2O$'la karşılaştırılmalı olarak bulundu ve µM $FeSO_4.7H_2O$ eşdeğeri antioksidan güç şeklinde ifade edildi.

2.4.4. DPPH• Radikali Temizleme Aktivitesi Tayini

2,2-difenil-1-pikrilhidrazil radikali (DPPH•) ticari olarak temin edinilebilen bir radikal olup, çalışmada metanol de hazırlanmış100 µM'lık çözeltisi kullanıldı. Molyneux (2004) tarafından belirtilen yönteme göre aktivite belirlendi. Hazırlanan ekstrakttan ve DPPH radikalinden eşit hacimde karıştırılıp 25ºC'de 50 dk inkübasyona bırakıldı. Süre sonunda örnek tüplerinin 517 nm'de absorbans ölçümleri yapıldı. Maksimum absorbansın yarıya gelen numune konsantrasyonunu ifade eden SC_{50} değerleri mg/ml cinsinden hesaplandı.

2.4.5. RP-HPLC-PAD ile Fenolik Bileşen Analizi

Fenolik bileşenlerin analizi için RP-HPLC-PDA sistemi (LC 20 AT Shimadzu) kullanıldı. Analizde ODS C18 (250 mm x 4.6 mmx 5 µm)kolonu kullanıldı (Thermo Scientific, USA). Çalışılan metod da elüsyon gradient program olarak %2'lik asetik asit-su (A) ve %70'likasetonitril-su (B) mobil fazının değişen oranları kullanılarak 1 ml/dk akış hızıyla analiz yapıldı. Analiz süresince Can ve Baltaş (2016) tarafından oluşturulan gradient metodu kullanıldı.

3. Bulgular ve Tartışma

Çalışmada kullanılan bitki ekstraktlarının antibakteriyal aktivite sonucu Tablo 1'de gösterilmiştir. Bitki ekstraktının hazırlanan konsantrasyonlar da ve çeşitli bakteriler üzerinde farklı orana sahip olduğu gözlemlenmiştir.

Tablo 1
Minimum inhibisyon konsantrasyonu ve minimum bakterisidal konsantrasyon

Mikroorganizma	MIC	MBC
E. aerogenes	20 mg/ml	-
K. pneumoniae	10 mg/ml	20 mg/ml
E. durans	20 mg/ml	-
B. subtilis	10 mg/ml	20 mg/ml
S. aereus	10 mg/ml	20 mg/ml
S.typhimurium	5 mg/ml	10 mg/ml

Özay (2015) yapmış olduğu çalışmasında, 10 adet *Alyssum* türünün biyolojik aktivitesini araştırmış ve test edilen bakterilerden *B.subtilis* bakterisine karşı etkili olduğunu tespit etmiştir. Çalışmamızın literatürde ki bu çalışma ile uyum içinde olduğu gözlenmektedir. Çalışmamızdaki MIC sonuçları literatür ile kıyaslandığında *Alyssum filiforme* türünün antibakteriyal aktivitesinin daha yüksek olduğu görülmektedir Özay (2015). Anadolu florasında bulunan *Alyssum* türleri ile yapılan antibakteriyal ve antibiyofilm aktivite sonucuna bakıldığı zaman *A. filiforme* bitkisine kıyasla daha az aktivite gösterdiği görülmüştür. (Arslan, 2019) Bu sonuçlar doğrultusunda *Alyssum filiforme* bitkisinin çeşitli hastalıklara neden olan bu bakterilere karşı bir ajan olacağı yaptığımız çalışma ile desteklenmektedir.

Tozyılmaz vd., (2020) *Alyssum* türüne ait 3 endemik bitkide yapmış olduğu bir çalışmada MIC, MBC sonuçlarına göre daha düşük konsantrasyonda *K.pneumoniae* ve *B.subtilis* bakterileri üzerinde *Alyssum filiforme* türünün daha yüksek antibakteriyal etki gösterdiğini fakat *E. aerogenes* ve *E. durans* bakterileri üzerinde herhangi bir etki göstermediğini bildirmişlerdir. Bu da *Alyssum* türlerinin hepsinin aynı sonucu vermediğini ve

farklı türlerin farklı hastalık yapan bakteriler üzerinde etkisi olduğunu göstermektedir. Aynı zamanda antibiyofilm etkisi daha düşük konsantrasyonda bile tüm bakteriler için kıyaslandığı zaman *Alyssum filiforme* bitkisinde daha yüksektir.

Bakteriyel antibiyofilm aktivite sonuçları Tablo 2' de gösterilmiştir ve çalışılan tüm bakterilerde biyofilm oluşumunu inhibe edici etkisi olduğu gözlemlenmiştir. Biyofilm oluşumu engelleyen en yüksek sonuç *S.aureus* bakterisinde görülmüştür.

Tablo 2
Antibiyofilm aktivite yüzdeleri

Mikroorganizma	**20 (mg/ml)**	**10 (mg/ml)**	**5 (mg/ml)**	**2.5 (mg/ml)**	**1.75 (mg/ml)**
E. aerogenes	26.3	19.3	16.6	---	---
K. pneumoniae	31.4	29.2	28.5	27.1	11.4
E. durans	57.7	51.81	18.8	16.9	12.3
B. subtilis	57.3	10	---	---	---
S. aureus	79.8	75.7	74.8	73.9	68.5
S.typhimurium	41.8	38.8	38.1	18.4	----

Bitki ekstraktına ait antioksidan sonuçlar Tablo 3'te verilmiştir. *Alyssum filiforme* örneğinde yüksek oranda antioksidan kapasite ve aktivite gözlenmiştir. *A.filiforme* bitkisinin toplam fenolik bileşen miktarı 1.925 mg GAE/g numune olarak, toplam flavonoid bileşen miktarı ise 0.166 mgQE/g olarak belirlendi. Antioksidan aktiviteyi belirleyebilmek adına FRAP Fe^{+3} indirgeme kapasitesi ve radikal süpürme aktivitesi olarak da DPPH testi yapıldı. Bitkinin SC_{50} değeri troloks standardına göre değerlendirildiğinde 5.190 mg/ml olarak tespit edildi. FRAP değeri de 13.070 μmol$FeSO_4.7H_2O$/g olarak tespit edildi.

Tablo 3
Alyssum filiforme örneğine ait antioksidan sonuçları

Örnek	**TP(mgGAE/g örnek)**	**TF(mgQE/g örnek)**	**FRAP(μmol$FeSO_4.7H_2O$/g)**	**DPPH SC_{50} mg/ml**
A.filiforme	1.925±0.090	0.166±0.016	13.070±0.080	5.190±0.028
Troloks				0.004±0.001

*Troloks: DPPH testinde kullanılan standart

Bitkilerin bu denli zengin etki yelpazesine sahip olması bitkisel örneklerdeki araştırmaları arttırmaktadır. Antibiyotik ve antimikrobiyal etkinin yanı sıra antioksidan etki sayesinde dokulardaki oksidatif hasarın önüne geçildiğine yönelik çalışmalar bildirilmektedir (Rakhimzhanova vd., 2018; Akarca ve Tomar, 2019; Düzgüner ve Erbil, 2020). Bu çalışmaların bazılarında kronik ve akut yaralanmalarda önemli sonuçlar elde edildiği bildirilmiştir. (Kumar vd., 2007; Khalil vd., 2007; Demirbaş, 2021). Çanakkale florası üzerinde yapılan bir çalışmada çeşitli bitkilerin sap, tohum, çiçek ve yaprakları kullanılarak hazırlanan örnekler antioksidan ve antimikrobiyal açıdan incelenmiş ve yüksek antioksidan güce sahip olduğu görülmüştür (Kırca vd., 2007).

Shan vd. (2007) yapılan bir çalışmada çeşitli bitki ve baharatların antibakteriyal ve antioksidan etkileri incelenmiş ve antioksidan değerleri ile antibakteriyal içerikleri arasında yüksek oranda ilişki olduğu bildirilmiştir. Demir vd. ve Durmaz vd. tarafından yapılan çalışmalarda ise bitki ekstraktından ki antioksidan ve antimikrobiyal etkinin örneklerdeki yoğun fenolik bileşen kompozisyonundan ileri geldiği bildirilmiştir.

Fenolik asitler son yıllarda kanser ve çeşitli hastalıkların tedavisinde kullanılabilmeleri ile üzerinde çok fazla çalışma yapılan bileşiklerdendir. Anti-alerjik, antioksidan, antitrombotik (kan pıhtılaşmasını engelleyici), antienflamatuvar (iltihap oluşumunu önleyici), antimikrobiyal ve vasodilatory (damar genişletici) gibi çeşitli etkileri olduğu bildirilmiş ve bu etkilerinin temelinde antioksidan özelliğin yattığı rapor edilmiştir (Balasundram vd., 2006). Literatürde bazı çalışmalarda, antioksidan aktivite ile fenolik bileşenler arasında ilişki olduğu belirtilmektedir (Andarwulan vd., 1999). Bu bakımdan çalışmadaantioksidan aktivitesi belirlenen bitkinin fenolik içeriği, 25 farklı fenolik standardın analizinin yapılabildiği RP-HPLC-PDA sistemi ile çalışıldı. Bitkide kafeik asit ve krisin dışında fenolik asit belirlenemedi (Tablo 4). *Brassicaceae* familyasına ait *Isatistinctoria L.* bitkisinin HPLC-PDA-ESI-MS ile fenolik bileşenleri belirlenmiş ve kafeik asit, ferulik asit veluteolin tespit edilmiştir (Taviano vd., 2018). Mevcut çalışmamızda da kafeik asit standardı belirlenmiş olup literatürdeki çalışma ile benzerlik göstermektedir. Sinnamik asit türevlerinden olan kafeik asitin antienflamatuar, antibakteriyal, antioksidan, antikanser, antidiyabetik ve antibiyofilm gibi çeşitli aktiviteye sahip olduğu çalışmalarda

gösterilmiştir (Kot vd., 2015; Matejczyk vd., 2017; Min vd., 2018). Çalışmamızda da bitkide majör bileşen olarak kafeik asit tespit edilmiş olup, bitkinin antibiyofilm aktivitesinde etkili olabileceği düşünülmektedir. Bitkide tespit edilen flavonoid grubundan krisin çoklu biyolojik özelliklere sahiptir. Yapılan çalışmalarda krisinin antikanser aktivitede etkili olduğu belirtilmiştir (Samarghandian vd., 2011). Mevcut çalışmamızda da örnek tekrisin tespit edilmiş olup bu bitkinin antikanser aktiviteye sahip olabileceği düşünülebilir.

Tablo 4
Alyssum filiforme örneğinin fenolik profili

Standart	**µg fenolik/ g ekstrak**
Kafeik asit	18.12
Krisin	0.95

4. Sonuç

Son zamanlarda bakterilerin antibiyotikler üzerindeki üstünlüğü yeni arayışlar doğurmuştur ve bu da doğal kaynaklardan elde edilen ajanların kullanımını gündeme getirmiştir. Yapılan çeşitli çalışmalarda bitkilerin antimikrobiyal ve antibakteriyal özellikleri araştırılmaktadır (Baran, 2019).Elde edilen sonuçlar doğrultusunda bitkilerin çevreci olması, doğal olması, sağlık açısından bir tehdit oluşturmaması ve ekonomik olmasından dolayı antimikrobiyal ve antibakteriyal ajan olarak kullanılması önerilebilir. Bitkisel ürünler, metabolizmada zararlı kalıntı bırakmamasının yanı sıra antimikrobiyal, antibiyotik ve antioksidan gibi pek çok yararlı etkisinin olması ile sağlıklı yaşam için önemli bir rol üstlenmektedir. Bu çalışma ile *Brassicaceae* ailesinin önemli bir üyesi olan *Alyssum filiforme* bitkisinin biyolojik aktivitesi incelenmiştir. Elde edilen bulgular ışığında *Alyssum filiforme* türünün ekonomik olduğu ve sağlık açısından geniş bir yelpazeye hitap edebileceği düşünülmektedir. Bu verilere göre yüksek antimikrobiyal ve antibakteriyal etkiye sahip olduğu görülmüştür. Düşük konsantrasyonlarda dahi antibiyofilm oluşturma kapasitesine sahip ve antioksidan açıdan da değerli bir örnek olduğu gözlemlenmiştir. Yapısında fenolik asitlerden krisin bulundurması antikanser çalışmaları için potansiyelinin araştırılabileceğini göstermektedir. Çeşitli kanser türleri üzerine yeni çalışmalar tasarlanabilir.

Teşekkür

Bu çalışma Kahramanmaraş Sütçü İmam Üniversitesi Bilimsel Araştırmalar Proje Birimi tarafından desteklenmiştir. Proje No: 2021/3-12 YLS.

Yazar Katkıları

İlayda Orçan: Veri toplamış, analizini yapmıştır ve çalışmanın istatistiksel analizlerini yapmış, makaleyi yazmıştır.

Ali Savaş Bülbül: Analizi planlamış ve tasarlamıştır.

Yakup Kara: Çalışmanın antioksidan ve fenolik bileşen analizini yapmış ve makaleyi yazmıştır.

Çıkar Çatışması

Yazarlar çıkar çatışması bildirmemişlerdir.

Kaynaklar

Akarca, G.,& Tomar, O. (2019). Afyonkarahisar ili çevresinde yetişen ve halk tarafından tüketilen bazı yabani bitkilerin antioksidan ve antimikrobiyal etkileri. *Avrupa Bilim ve Teknoloji Dergisi*, (15), 259-268. Erişim adresi: https://dergipark.org.tr/tr/download/article-file/662824

Altundağ, Ş.,& Aslım, B. (2005). Kekiğin bazı bitki patojeni bakteriler üzerine antimikrobiyal etkisi. *Orlab On-Line Mikrobiyoloji Dergisi*, *3*(7), 12-14. Erişim adresi: http://eskisite.mikrobiyoloji.org/pdfler/702050702.pdf

Andarwulan, N.,Fardiaz, D., Wattimena, G. A.,&Shetty, K., (1999). Antioxidan tactivity associated with lipid and phenolic mobilization during seed germination of Pangiumedule Reinw. *Journal of Agricultural and Food Chemistry*, 47: 3158-3163. Erişim adresi: https://pubs.acs.org/doi/10.1021/jf981287a

Arslan, A. (2019). Anadolu florasına ait bazı Alyssum L. türlerinin polen, tohum, meyve morfolojileri ve antimikrobiyal, antibiyofilm aktivitesinin incelenmesi (Master'sthesis, Bartın Üniversitesi). Erişim adresi: https://acikerisim.bartin.edu.tr/bitstream/handle/11772/1873/adnan%20arslan.pdf?sequence=1

Avşar, C., Keskin, H., & Berber, İ. (2016). Hastane infeksiyonlarından izole edilen mikroorganizmalara karşı bazı bitki ekstraktlarının antimikrobiyal aktivitesi. *Int. J. PureAppl. Sci*, *2*(1), 22-29. Erişim adresi: https://dergipark.org.tr/tr/pub/ijpas/issue/24478/259426

Balasundram, N.,Sundram, K.,&Samman, S., (2006). Phenolic compounds in plants and agri-industrialby-products: Antioxidantactivity, occurence, and potentialuses. *Food Chemistry*, 99:191-203. Erişim adresi: https://www.sciencedirect.com/science/article/abs/pii/S0308814605006242

Baran, F. M. (2019). Prunus avium kiraz yaprağı özütü ile gümüş nanopartikül (AgNP) sentezi ve antimikrobiyal etkisinin incelenmesi. *Dicle Üniversitesi Mühendislik Fakültesi Mühendislik Dergisi*, *10*(1), 221-227.Erişim adresi: https://dergipark.org.tr/en/pub/dumf/article/487255

Bazargani, M. M.,&Rohloff, J. (2016). Antibiofilm activity of essential oils and plant extracts against Staphylococcus aureus and Escherichia coli biofilms. *Foodcontrol*, *61*, 156-164.).Erişim adresi: https://www.sciencedirect.com/science/article/abs/pii/S0956713515302152?via%3Dihub

Benzeie, I.F.F.,Strain, J.J. (1996). Theferricreducingability of plasma (FRAP) as a measure of ‘‘antioxidantpower”: The FRAP assay. *Journal Analytical of Biochemistry*, 239, 70-76.Erişim adresi: https://pubmed.ncbi.nlm.nih.gov/8660627/

Can, Z.,&Baltas, N. (2016). Bioactivity and enzymeinhibitionproperties of Steviarebaudiana. CurrentEnzymeInhibition, 12(2), 188-194. Erişim adresi: https://www.ingentaconnect.com/content/ben/cei/2016/00000012/00000002/art00014

Demir, T., Akpınar, Ö., Haki, K., & Güngör, H. (2019). Nar (Punicagranatum L.) kabuğunun in vitroantidiyabetik, antienflamatuar, sitotoksik, antioksidan ve antimikrobiyal aktivitesi. *Akademik Gıda*, 17(1), 61-71. Erişim adresi: https://dergipark.org.tr/en/pub/akademik-gida/article/544647

Demirbaş, Ş. (2021). Liliumcandidum L. ekstraktları üzerinde antioksidan, histo-biyokimyasal ve içerik aydınlatma çalışmaları (Yüksek lisans tezi). Erişim adresi: https://tez.yok.gov.tr/UlusalTezMerkezi

Durmaz, H.,Hülül, M., &Celık, H. (2018). Meyan (Glycyrrhizaglabra L.) Bitkisinin Antibakteriyel ve Antioksidan Aktiviteleri. *Harran Üniversitesi Veteriner Fakültesi Dergisi*, 7, 37-41.Erişim adresi: https://dergipark.org.tr/en/pub/huvfd/issue/41493/501426

Düzgüner, V.,& Erbil, N. (2020). Ardahan Yöresinde Yetişen Kılıç Otu Bitkisinin (Hypericumperforatum) Antimikrobiyal ve Antioksidan Etkilerinin Araştırılması. *Türk Tarım ve Doğa Bilimleri Dergisi,* 7(1), 27-31.Erişim adresi: https://dergipark.org.tr/en/pub/turkjans/article/679896

Esra, U. C. A. R., Köse, E. O., ÖZYİĞİT, Y., & TURGUT, K. (2015). Bazı tıbbi ve aromatik bitkilerde esansiyel yağların antimikrobiyal aktivitelerinin belirlenmesi. *Ziraat Fakültesi Dergisi*, *10*(2), 118-124. Erişim adresi: https://dergipark.org.tr/en/download/article-file/308658

Faydaoğlu, E.,&Sürücüoğlu, M. (2013). Tıbbi Ve Aromatik Bitkilerin Antimikrobiyal, Antioksidan Aktiviteleri Ve Kullanım Olanakları. *Erzincan Üniversitesi Fen Bilimleri Enstitüsü Dergisi*, 6(2), 233-265.Erişim adresi: https://dergipark.org.tr/en/pub/erzifbed/issue/6027/80707

Fukumoto, L.R. ; Mazza G.(2000). Assessing antioxidant and prooxidant activities of phenolic compounds. *Journal of Agricultural Food Chemistry*, 48, 3597–3604.Erişim adresi: https://pubs.acs.org/doi/abs/10.1021/jf000220w

Haşimi, N., Kızıl, S., &Tolan, V. (2015). Rezene ve adaçayı uçucu yağlarının antimikrobiyal aktivitesi üzerine bir araştırma. *Batman Üniversitesi Yaşam Bilimleri Dergisi*, *5*(2), 227-235.Erişim adresi: https://dergipark.org.tr/en/download/article-file/313360

Khalil, E. A., Afifi, F. U., & Al-Hussaini, M. (2007). Evaluation of the wound healing effect of some Jordaniantraditionalmedicinalplantsformulated in Pluronic F127 using mice (Musmusculus). Journal of ethnopharmacology, 109(1), 104-112. Erişim adresi: https://doi.org/10.1016/j.jep.2006.07.010

Kırca, A.,Bilişli, A., Demirel, N. N., Turhan, H., & Arslan, E. (2007). Çanakkale florasındaki bazı tıbbi ve aromatik bitkilerin antioksidan ve antimikrobiyal aktiviteleri. *Tübitak Proje*, (104). Erişim adresi: https://dergipark.org.tr/tr/pub/erzifbed/issue/6027/80707

Kot, B.,Wicha J, Piechota M, Wolska K, Gruzewska A,(2015). Antibiofilm activity of transcinnam aldehyde, p-coumaric, and ferulicacids on uropathogenicEscherichia coli. *Turkish Journal of Medical Sciences*, 45(4), 919-924. Erişim adresi: https://journals.tubitak.gov.tr/medical/abstract.htm?id=16533

Kumar, B.,Vijayakumar, M., Govindarajan, R., &Pushpangadan, P. (2007). Ethnopharmacologicalapproachestowoundhealing—exploringmedicinalplants of *India. Journal of ethnopharmacology*, 114(2), 103-113.Erişim adresi: https://doi.org/10.1016/j.jep.2007.08.010

Matejczyk M, Świsłocka R, Golonko A, Lewandowski W, Hawrylik E, (2018). Cytotoxic, genotoxic and antimicrobialactivity of caffeic and rosmarinicacids and theirlithium, sodium and potassiumsalts as potentialanticancercompounds. *Advances in Medical Sciences*, 63(1), 14-21. Doi: https://doi.org/10.1016/j.advms.2017.07.003

Min J, Shen H, Xi W, Wang Q, Yin L, Zhang Y, Wang ZN, (2018). Synergisticanticanceractivity ofcombineduse of caffeicacidwithpaclitaxelenhancesapoptosis of non-small-celllungcancerH1299 cells in vivo and in vitro. Cellular Physiology and Biochemistry, 48(4), 1433-1442. Erişim adresi: https://www.karger.com/Article/Abstract/492253

Molyneux, P. (2004). Theuse of thestablefreeradicaldiphenylpicrylhydrazyl (DPPH) forestimatingantioxidantactivity. SongklanakarinJournal of Science and Technology, 26, 211–219. Erişim adresi: https://www.researchgate.net/publication/237620105

Moure, A.,Cruz, J. M., Franco, D., Domínguez, J. M., Sineiro, J., Domínguez, H., ... &Parajó, J. C. (2001). Natural antioxidantsfromresidualsources. Foodchemistry, 72(2), 145-171.Erişim adresi: https://doi.org/10.1016/S0308-8146(00)00223-5

Özay, C. (2015). Ege Bölgesindeki bazı Alyssum L. taksonlarının biyolojik aktivitelerinin incelenmesi ve aktif bileşenlerinin karakterizasyonu (Doktora tezi).

Rakhimzhanova, A.,Kılınçarslan, Ö., &Mammadov, R. (2018). Stellariamediaekstraktlarının antioksidan aktivitesinin belirlenmesi ve fenolik bileşenlerinin karakterizasyonu. *Ordu Üniversitesi Bilim ve Teknoloji Dergisi*, 8(2), 165-173.Erişim adresi: https://dergipark.org.tr/en/pub/ordubtd/issue/42031/505984

Samarghandian, S.,Afshari, J. T., &Davoodi, S. (2011). Chrysin reduces proliferation and inducesapoptosis in the human prostate cancer cellline pc-3. Clinics, 66(6), 1073-1079.Erişim adresi: https://www.scielo.br/j/clin/a/KKS4gNtfLkMdT9RZzbwRkJF/?format=pdf&lang=en

Shan, B.,Cai, Y., Brooks, J.D. and Corke, H. (2007). The Invitroantibacterial activity of dietary spice and medicinal herb extracts. *International Journal of Food Microbiology*. 117: 112-119.Erişim adresi: https://doi.org/10.1016/j.ijfoodmicro.2007.03.003

Singleton V.L.,Orthofer R. ve Lamuela-Raventos R.M.,(1999). Analysis of Total Phenols and Other Oxidation Substrates and Antioxidants by Means of Folin-Ciocalteu Reagent, *Methods in Enzymology*, 299, 152-178. Erişim adresi: https://www.sciencedirect.com/science/article/abs/pii/S0076687999990171

Taviano, M. F.,Filocamo, A., Ragusa, S., Cacciola, F., Dugo, P., Mondello, L., ... &Miceli, N. (2018). Phenolicprofile, antioxidant and cytotoxicproperties of polar extracts fromleaves and flowers of Isatistinctoria L.(Brassicaceae) growing in Sicily. PlantBiosystems-An International JournalDealingwithallAspects of PlantBiology, 152(4), 795-803.Erişim adresi: https://doi.org/10.1080/11263504.2017.1338629

Tomaino, A.,Cimino, F., Zimbalatti, V., Venuti, V., Sulfaro, V., De Pasquale, A. and Saija, A. (2005). Influence of heating on antioxidant activity and the chemical comparision of some spiceessential oils. *Food Chemistry*, 89, 549-554.Erişim adresi: https://doi.org/10.1016/j.foodchem.2004.03.011

Tozyılmaz, V., Bülbül, A. S., & Ceylan, Y. C. (2021). Determination of antimicrobial, antioxidant and antibiofilmactivity of some Alyssum L. species in Anatolian flora. *Kahramanmaraş Sütçü İmam Üniversitesi Tarım ve Doğa Dergisi*, 24(4), 715-724. Erişim adresi: http://dogadergi.ksu.edu.tr/en/download/article-file/1356582

Tunç,İ., Çalışkan. F., Özkan, G.,&Karacabey, E.(2014). Mikrodalga Destekli Soxhlet Cihazı ile Fındık Yağı Ekstraksiyonunun Yanıt Yüzey Yöntemi ile Optimizasyonu. Akademik Gıda , 12(1), 20-28. Erişim adresi: https://dergipark.org.tr/tr/pub/akademik-gida/issue/55791/763724

Uçar, E., Köse, E. O., Özyİğİt, Y., & Turgut, K. (2015). Determination of antimicrobial activity of essential oils in some medicinal plants. Ziraat Fakültesi Dergisi-Süleyman Demirel Üniversitesi, 10(2), 118-124.

Yetgin, A.,Şenturan, M., Benek, A., Efe, E., & Canlı, K. (2017). Pterigynandrum filiforme Hedw. türünün antimikrobiyal aktivitesinin belirlenmesi. *Anatolian Bryology*, 3(1), 43-47. Erişim adresi: https://app.trdizin.gov.tr/makale/TXpFMk1qTXpNdz09

Yıldız, S., Gürgen, A., & Can, Z. (2017). Kastamonu ilinden toplanan bazı yabani mantarların in vitro koşullar altında biyoaktif özellikleri. Kastamonu Üniversitesi Orman Fakültesi Dergisi, 17(3), 523-530.Erişim adresi: https://app.trdizin.gov.tr/publication/paper/detail/TWpVNU1EVXdNQT09

e-ISSN 2757-5195

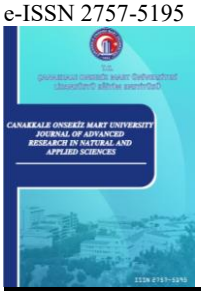

Çanakkale Onsekiz Mart University

Journal of Advanced Research in Natural and Applied Sciences

Open Access

doi.org/10.28979/jarnas.1110677 2023, Vol. 9, Issue 1, Pages: 56-64 dergipark.org.tr/tr/pub/jarnas

Azo Dye Removal from Aqueous Solution by Powder Graphite: Investigation of Parameter Effects and Optimization by Box-Behnken Design

Sertel Görücü[1], Çisil Gülümser[2*], Mesut Sezer[3], Sevil Veli[4]

[1,2,3,4]Department of Environmental Engineering, Faculty of Engineering, Kocaeli University, Kocaeli, Türkiye

Article History

Received: 29.04.2022

Accepted: 10.09.2022

Published: 05.03.2023

Research Article

Abstract − Industrial wastewaters containing dyes comprise organics that are difficult to biodegrade and when they are discharged to receiving bodies, they cause serious impacts on environment. Therefore, this wastewater requires advanced treatment besides conventional ones. Adsorption is accepted one of the favorable processes, which can be applied integrative to conventional systems during the treatment of this wastewater. In addition to the effectiveness of the materials to be utilized in the adsorption process, their cost and availability are also very important factors. In this study, the efficiency of environmentally friendly, cost-effective powdered graphite was investigated in the removal of diazo type dye (Direct Red 243) from aqueous solution by adsorption. For this purpose, Response Surface Method was applied via Box-Behnken Design and the most effective parameters were investigated in dye adsorption with graphite. Also, the morphology of the graphite before and after adsorption was scanned by Scanning Electron Microscopy. Adsorption study was carried out in batch mode and pH (2-10), adsorbent amount (0.1-1.5 g) and time (15-65 min) were designated as experimental parameters. It has been observed that the most effective parameter in color removal of dye was pH and at low values of this parameters the higher efficiencies were obtained. Additionally, it was observed that the increase in the amount of adsorbent increased the efficiency, and time had no significant effect besides two parameters. Almost complete decolorization (98%) was acquired at pH 2 with 1.5 g adsorbent for 40 min of study. As a result of the study, even it is not improved with further applications, graphite can be effective for anionic dye color removal under acidic conditions by its pristine form.

Keywords *– Anionic dye, Box-Behnken Design, decolorization, experimental design, graphite adsorption*

1. Introduction

Every year, tons of residual dye containing effluents are produced by textile industries (Choudhary et al., 2020). Especially in third world or some developing countries, the treatment plants to purify these effluents are usually insufficient to meet the discharge standards and they also lack qualified manpower (Khan & Malik, 2014). Besides, in some countries, a tendency to put economic and political concerns before the environment as is often the case, whether the legal regulations are strict or not. So, negative impacts on environment becomes inevitable and feasible solutions are required to compete these impacts. It is important to present easily applicable and cost-effective treatment methods for dye removal. The conventional treatment processes such as biological systems require pre- or post-applications to remove the color and also other pollutants in textile wastewater (Berradi et al., 2019). Among these applications, adsorption shines out as a facile and relatively cost-effective process. Since adsorption accepted as an easy to operate in plant scale, there are several types of adsorbents examined for different textile wastewaters. Especially, dye removal from synthetic aqueous solutions are hugely studied (Ahmad, Eusoff, Oladoye, Adegoke, & Bello, 2020; Lin et al., 2013; Mohebali, Bastani, & Shayesteh, 2019), and these studies are still going on. The adsorbents have great impact on the

[1] sertel72@gmail.com

[2] cisgulumser@gmail.com*

[3] mesut.sezer@kocaeli.edu.tr

[4] sevilv@kocaeli.edu.tr

*Corresponding Author

removal efficiencies and the operating expenses of the system (Adeyemo, Adeoye, & Bello, 2017). The alternative adsorbents like charcoal ash (Gengec, Ozdemir, Ozbay, Ozbay, & Veli, 2013), polypyrrole/polyaniline nanofibers (Bhaumik, McCrindle, & Maity, 2013), walnut shell (Dahri, Kooh, & Lim, 2014), pumice (Veliev, Ozturk, Veli, & Fatullayev, 2006), alumina/carbon nanotube hybrid (Malakootian, Mansoorian, Hosseini, & Khanjani, 2015) or struvite (Yetilmezsoy et al., 2020) were investigated for their performance to remove dyes from aqueous solutions. But these materials are usually need further treatment like activation, high temperature carbonization, metal doping etc. and these applications cause increasing costs during production. Pristine graphite is an alternative for its availability and low-cost for adsorption of dyes from aqueous solutions. In literature, there are very little studies for investigating the adsorptive effectiveness of pristine form of graphite, which is free from any further improvement. Usually, the studies focus on surface-enhanced graphites or its composites (Carvallho et al., 2016; Peng, Li, Liu, & Song, 2016; Travlou, Kyzas, Lazaridis, & Deliyanni, 2013).

In this study, powder graphite, which is pristine, was used in the adsorptive removal of anionic dye from aqueous solution and the process was evaluated through Box-Behnken Design to present graphite's efficiency in dye adsorption. To the best of our knowledge, pristine graphite as an adsorbent for the removal of anionic dye was not investigated through response surface methodology yet. Its effectiveness was examined as an easily accessible and economically rewarding alternative adsorbent.

2. Materials and Methods

Analytical grade chemicals were used during the experiments unless otherwise stated. Distilled water was supplied from Millipore Direct Q-UV purifier for making the solutions. The powder graphite (used as adsorbent) and diazo dye (Direct Red 243) (used as target pollutant) were obtained from local companies. The chemical structure and other properties of the dye were given in Table 1.

Table 1
General characteristics of the dye

Properties	
Generic Name	C.I. Direct Red 243 (C.I. 29315)
CAS number	86543-85-3
Maximum wavelength, λ_{max}	517
Molecular formula	$C_{38}H_{28}N_{10}Na_4O_{17}S_4$
Molecular weight	1116.91
Molecular structure	Diazo class, anionic
Chemical structure	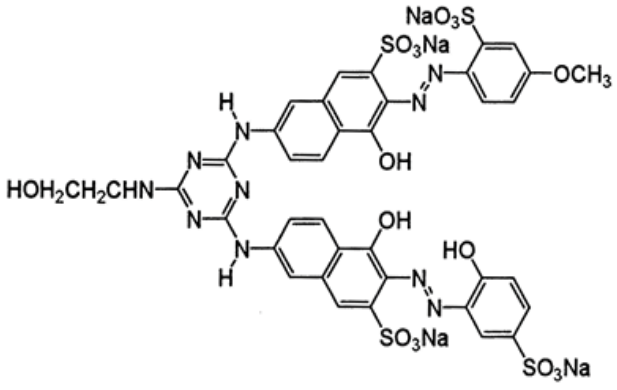

2.1. Batch Adsorption Studies

Experimental adsorption studies were carried out in batch mode. 100 mL of dye solutions including powder graphite were introduced in glass Erlenmeyer flasks (Figure 1). Initial concentration of the dye solution was 40 mg/L for all runs. To remove dye color from solution by graphite adsorption, the flasks were put into a bath shaker (NÜVE) at ambient temperature (23ºC) and mixing rate of 150 rpm.

Figure 1. Experimental setup

The dye color removal after adsorption process was determined by a spectrophotometer (HACH DR6000) at 517 nm. The removal percentage was calculated via Eq. 2.1:

$$Removal\ (\%) = \frac{(Ci - Cs)}{Ci} \times 100 \quad (2.1)$$

where; C_i and C_s were the initial and final concentrations of the dye, respectively. The adsorption experiments were repeated twice and conducted according to different levels of pH, adsorbent amount and time which were designed by Box-Behnken Design.

2.2. Batch Adsorption Studies

In this study, Box-Behnken Design, as an approach of Response Surface Methodology, was applied to investigate the effects of experimental variables on dye color removal and optimize these parameters for the highest removal. This approach of response surface methodology is comprised of a rotatable design and has one central point with three interlocking 2^3 factorials (Kumar, Prasad, & Mishra, 2007). Here, three-levels were determined for three parameters, namely, pH, adsorbent amount, and time. The design levels were shown in Table 2.

Table 2
Experimental parameters and coded/uncoded levels

Parameter		Levels		
	Coded	-1	0	+1
A: pH	Uncoded	2	6	10
B: Adsorbent Amount (g)		0.1	0.8	1.5
C: Time (min)		15	40	65

The data gained according to the design was evaluated with the statistical software, Stat-Ease® Design Expert V13. With the help of this software, ANOVA table was built up through fitting the experimental data to the linear and second-order polynomials. Also, the relations between coded and uncoded variables were presented according to the Eq. 2.2:

$$Y = \beta_0 + \sum \beta_i x_i + \sum \beta_{ii} x_{ii}^2 + \sum \beta_{ij} x_i x_j + \varepsilon \quad (2.2)$$

where β_0 is constant, β_i and β_{ij} are the effects of single parameters and two-way interactions, respectively. Also, x_i and x_j stand for the coded or uncoded single parameter levels. ε is the value of error calculated by the programme.

3. Results and Discussion

The morphological features of pristine and used graphite before/after adsorption were investigated through SEM imaging. In Fig. 2, these results were shown. For the pristine graphite (Fig. 2a-b), the surface was quite smooth and there were aggregate formation as very fine flakes. The images were in accordance with the similar studies which also presented the typical flake layered structures (Chaudhary et al., 2021; Oliveira et al., 2018). After adsorption (Fig. 2c-d), the flake layers of the graphite were preserved and any specific changes on the surface were not observed. This may be concluded to the physicochemical attachment of the dye molecules on graphite surface, which is the reason for this image.

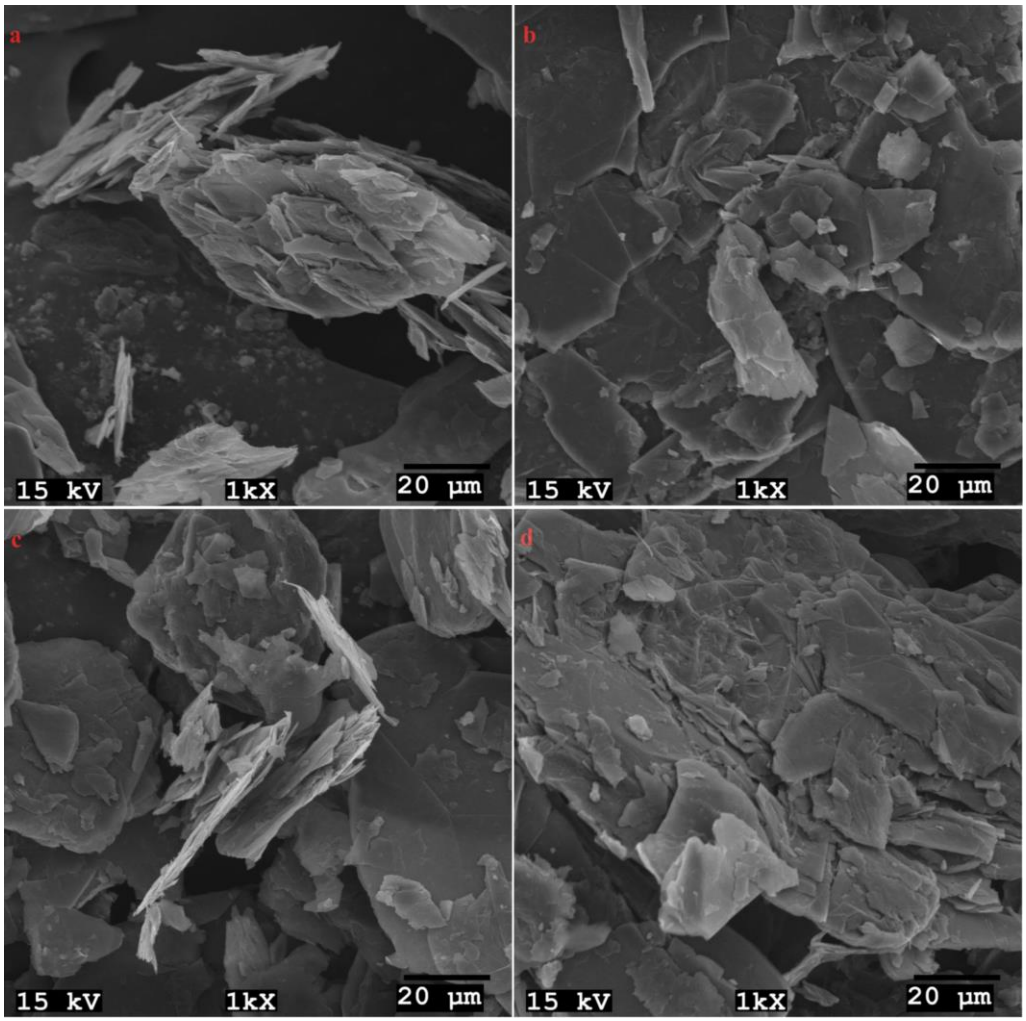

Figure 2. SEM images of graphite a-b) before and c-d) after adsorption

The design matrix and the experimental responses are listed in Table 3. All runs were repeated twice and in the table average of these results were presented. As seen from design matrix, there are three center points. The dye color removal efficiencies fluctuated between 3 and 98, which was a broader range. Despite general broadness, the efficiencies seemed to hang together around parameter groups. For example, for pH 2 and 10 or adsorbent amount 0.1 and 1.5, the difference of the effects might be perceived at first examination before the statistical analysis.

Table 3
Design matrix and dye color removal responses

Standard Order	Run	pH	Adsorbent Amount (g)	Time (min)	Dye Color Removal (%)*
1		2	0.1	40	41
2		10	0.1	40	3
3		2	1.5	40	98
4		10	1.5	40	33
5		2	0.8	15	79
6		10	0.8	15	18.5
7		2	0.8	65	86
8		10	0.8	65	31.5
9		6	0.1	15	12.5
10		6	1.5	15	49
11		6	0.1	65	14.5
12		6	1.5	65	58
13-14-15**		6	0.8	40	41

***** Average values of repeated experiments were presented.

****** The average of six experiments was presented.

ANOVA was examined to understand the statistical nature of the data, as mentioned in Section 2.2. According to the Table 4, model is statistically significant (p-value < 0.05) and the insignificance of the lack of fit p-value also supports the consistence of the residuals while fitting the model. In other words, the quadratic model was adequate to resemble the fitting of the dye color removal by graphite adsorption. Also, all linear, pH-adsorbent amount interaction and square pH and square adsorbent amount terms are statistically significant. Although, pH-time and adsorbent amount-time interactions and square time terms are insignificant, they are kept in the model to preserve the insignificancy of lack of fit.

Table 4
Statistical results of ANOVA

Source	Sum of Squares	Degree of Freedom	Mean Square	F-value	p-value	Significancy
Model	21172.76	9	2352.53	252.54	<0.0001	significant
A	11881.00	1	11881.00	1275.38	<0.0001	
B	6972.25	1	6972.25	748.45	<0.0001	
C	240.25	1	240.25	25.79	<0.0001	
AB	357.78	1	357.78	38.41	<0.0001	
AC	19.53	1	19.53	2.10	0.1631	
BC	26.28	1	26.28	2.82	0.1086	
A^2	992.60	1	992.60	106.55	<0.0001	
B^2	553.33	1	553.33	59.40	<0.0001	
C^2	8.83	1	8.83	0.95	0.3418	
Residual	186.31	20	9.32			
Lack of Fit	65.19	3	21.73	3.05	0.0570	not significant
Pure Error	121.13	17	7.13			
Total	21359.08	29				
SD: 3.05 Adeq Precision: 54.62 R^2: 0.991 adj-R^2: 0.987 pred-R^2: 0.982						

The values of R^2 statistics were higher than %98. Especially, adj-R^2 (0.987) and pred-R^2 (0.982) were agreeable due to faint difference. Additionally, the value of Adeq Precision (54.62) was higher than 4 and there were enough signal to study through the design space. In Figure 3a, experimental results are paired with predicted

responses. The coincidence also sustains high R^2 values. From Figure 3b, it is seen that the data points are sufficiently close to the line, which indicates the normal distribution of the residuals.

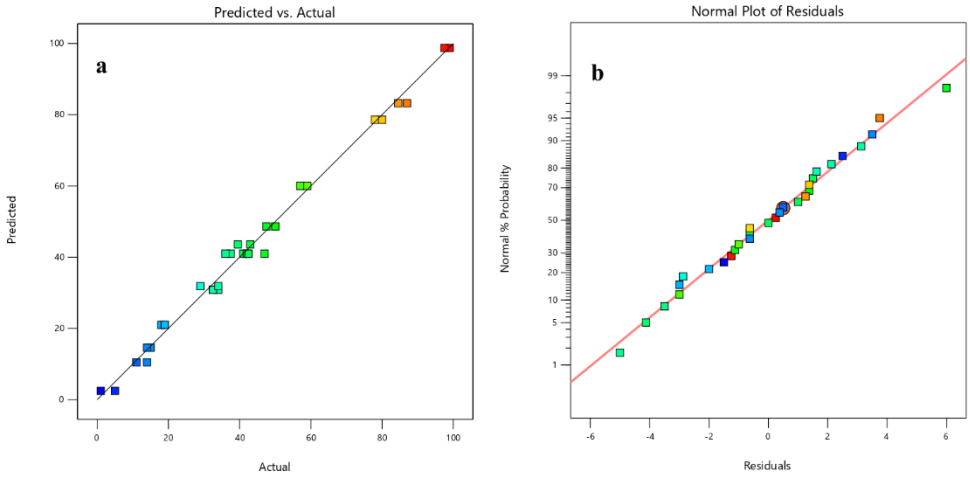

Figure 3. a) Actual vs. predicted responses b) Normal plot of residuals

The final mathematical equation of the model proposed by the software, in terms of coded and actual levels, is given in Eq. 3.1 and Eq. 3.2, respectively:

$$Dye\ Color\ Removal\ (\%) = 41.00 - 27.25xpH + 20.88xAdsorbent\ Amount + 3.88xTime - 6.69xpHxAdsorbent\ Amount + 1.56xpHxTime + 1.81xAdsorbent\ AmountxTime + 11.59xpHxpH - 8.66xAdsorbent\ AmountxAdsorbent\ Amount + 1.09xTimexTime \quad (3.1)$$

$$Dye\ Color\ Removal\ (\%) = 64.998 - 14.222xpH + 68.274xAdsorbent\ Amount - 0.162xTime - 2.388xpHxAdsorbent\ Amount + 0.016xpHxTime + 0.104xAdsorbent\ AmountxTime + 0.725xpHxpH - 17.666xAdsorbent\ AmountxAdsorbent\ Amount + 0.002xTimexTime \quad (3.2)$$

According to the Eq. 3.1, pH has the highest effect on dye color removal efficiency. The direction of the impact is in a negative way, and it can be interpreted that the efficiency may decrease in parallel to the increase in pH level. On the contrary, adsorbent amount has a positive impact that its increase supports higher removal efficiencies (Yagub, Sen, Afroze, & Ang, 2014). Here, time parameter showed no significant effect on removal compared to other two parameters, but it seems to have positive impact. Since the interaction terms of pH-time and adsorbent amount-time are statistically insignificant, only pH-adsorbent amount interaction graph is presented in Figure 4.

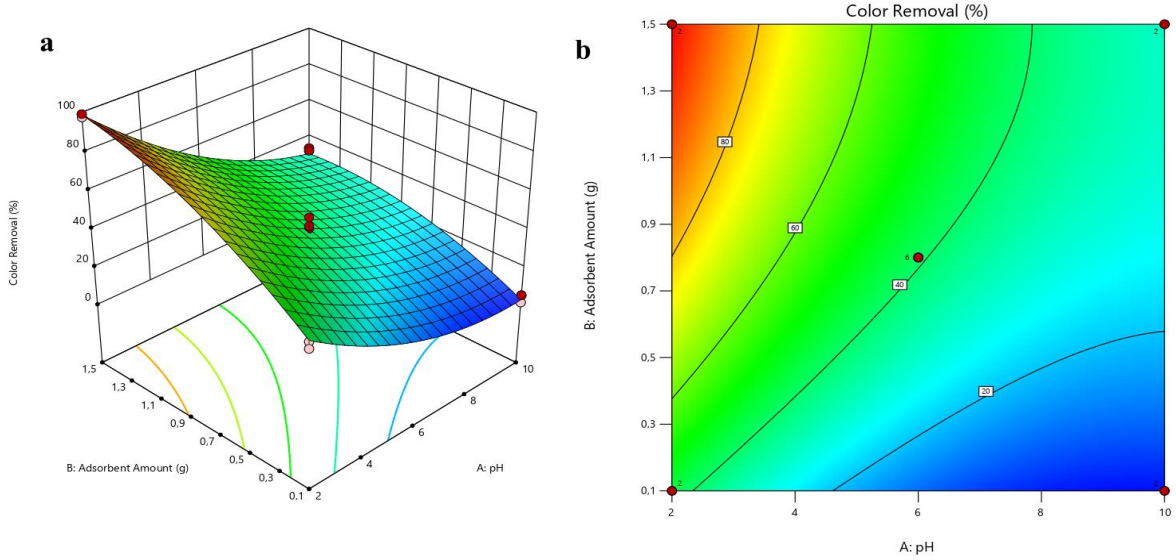

Figure 4. a) 3D surface and b) 2D contour plots of pH-adsorbent amount interaction

As seen from Figure 4a and b, the highest removal efficiencies were obtained in lowest pH levels, while the adsorbent amount is its highest. This result can be related to the nature of graphite surface under acidic conditions and to the anionic dye properties. In the acidic conditions, the graphite surface probably became positively charged and this situation led electrostatic attraction between graphite surface and anionic dye (Esmaeli et al., 2013). Also, the point of zero charge was measured in the area of pH 5.1-5.6 (Barišić et al., 2021) and it's reasonable that the surface became positively charged under this levels. Furthermore, depending on the increase in adsorbent amount, the removal efficiency was drastically improved. Probably, this was a result of increasing surface area for dye clinging as an active adsorption site (Ghaedi et al., 2015).

As seen from results, graphite shows good adsorptive efficiency for acidic dye removal, in comparison to the studies in the literature. A complex composite adsorbent showed similar efficiency (~94%) like graphite in the experimental conditions of 20 mg/L initial dye concentration, pH 4, 16 g/L adsorbent amount for 60 min (Zhang, Chen, Guo, Zhu, & Zou, 2018). Here, in this study, 98% of dye color removal was achieved in the conditions of 40 mg/L initial dye concentration, pH 2, 15 g/L adsorbent amount for 40 min.

4. Conclusion

In conclusion, graphite was found suitable alternative for the adsorption of anionic dye from aqueous solution under acidic conditions. Also, Box-Behnken Design showed good compatibility for examination of dye adsorption onto powder graphite. All the R^2 values were higher than 98%. The experimental parameters, namely, pH, adsorbent amount and time were evaluated in terms of their impacts on dye color removal. pH and adsorbent amount were concluded as the most influential but in opposite directions. Under pH 2, 98% of dye removal was achieved with 1.5 g of adsorbent for 40 min. It may be deduced that powder graphite may be a good alternative for the acidic textile effluents, which contain anionic dyes. The smooth flake structure of the pristine graphite surface was preserved after adsorption process. In comparison with other studies on graphite, the novelty of this study was its results on the efficiency of unmodified pristine graphite adsorption for dye removal to fill the gap in the literature.

Acknowledgement

This work was not supported financially by any institutions or company. The experiments were conducted in the laboratories of Environmental Engineering Department of Kocaeli University.

Author Contributions

Sertel Görücü: Data curation, running experiments, software, formal analysis, writing-original draft.

Çisil Gülümser: Conceptualization, methodology, data curation, software, visualization, formal analysis, writing-original draft.

Mesut Sezer: Data curation, investigation, software, writing-review and editing.

Sevil Veli: Project administration, supervision, resources, writing-review and editing.

Conflicts of Interest

The authors declare no conflict of interest.

References

Adeyemo, A. A., Adeoye, I. O., & Bello, O. S. (2017). Adsorption of dyes using different types of clay: a review. *Applied Water Science*, *7*(2), 543–568. https://doi.org/10.1007/s13201-015-0322-y

Ahmad, M. A., Eusoff, M. A., Oladoye, P. O., Adegoke, K. A., & Bello, O. S. (2020). Statistical optimization of Remazol Brilliant Blue R dye adsorption onto activated carbon prepared from pomegranate fruit peel. *Chemical Data Collections*, *28*, 100426. https://doi.org/10.1016/j.cdc.2020.100426

Barišić, A., Lützenkirchen, J., Bebić, N., Li, Q., Hanna, K., Shchukarev, A., & Begović, T. (2021). Experimental data contributing to the elusive surface charge of inert materials in contact with aqueous media. *Colloids and Interfaces*, *5*(1). https://doi.org/10.3390/colloids5010006

Berradi, M., Hsissou, R., Khudhair, M., Assouag, M., Cherkaoui, O., El Bachiri, A., & El Harfi, A. (2019). Textile finishing dyes and their impact on aquatic environs. *Heliyon*, *5*(11).

https://doi.org/10.1016/j.heliyon.2019.e02711

Bhaumik, M., McCrindle, R., & Maity, A. (2013). Efficient removal of Congo red from aqueous solutions by adsorption onto interconnected polypyrrole-polyaniline nanofibres. *Chemical Engineering Journal*, *228*, 506–515. https://doi.org/10.1016/j.cej.2013.05.026

Carvallho, M. N., Da Silva, K. S., Sales, D. C. S., Freire, E. M. P. L., Sobrinho, M. A. M., & Ghislandi, M. G. (2016). Dye removal from textile industrial effluents by adsorption on exfoliated graphite nanoplatelets: Kinetic and equilibrium studies. *Water Science and Technology*, *73*(9), 2189–2198. https://doi.org/10.2166/wst.2016.073

Chaudhary, J., Thakur, S., Mamba, G., Prateek, Gupta, R. K., & Thakur, V. K. (2021). Hydrogel of gelatin in the presence of graphite for the adsorption of dye: Towards the concept for water purification. *Journal of Environmental Chemical Engineering*, *9*(1). https://doi.org/10.1016/j.jece.2020.104762

Choudhary, M., Peter, C. N., Shukla, S. K., Govender, P. P., Joshi, G. M., & Wang, R. (2020). Environmental Issues: A Challenge for Wastewater Treatment. In M. Naushad & E. Lichtfouse (Eds.), *Green Materials for Wastewater Treatment* (pp. 1–12). Cham: Springer. https://doi.org/10.1007/978-3-030-17724-9_1

Dahri, M. K., Kooh, M. R. R., & Lim, L. B. L. (2014). Water remediation using low cost adsorbent walnut shell for removal of malachite green: Equilibrium, kinetics, thermodynamic and regeneration studies. *Journal of Environmental Chemical Engineering*, *2*(3), 1434–1444. https://doi.org/10.1016/j.jece.2014.07.008

Esmaeli, A., Jokar, M., Kousha, M., Daneshvar, E., Zilouei, H., & Karimi, K. (2013). Acidic dye wastewater treatment onto a marine macroalga, Nizamuddina zanardini (Phylum: Ochrophyta). *Chemical Engineering Journal*, *217*, 329–336. https://doi.org/10.1016/j.cej.2012.11.038

Gengec, E., Ozdemir, U., Ozbay, B., Ozbay, I., & Veli, S. (2013). Optimizing dye adsorption onto a waste-derived (modified charcoal ash) adsorbent using box-behnken and central composite design procedures. *Water, Air, and Soil Pollution*, *224*(10). https://doi.org/10.1007/s11270-013-1751-6

Ghaedi, A. M., Ghaedi, M., Vafaei, A., Iravani, N., Keshavarz, M., Rad, M., … Gupta, V. K. (2015). Adsorption of copper (II) using modified activated carbon prepared from Pomegranate wood: Optimization by bee algorithm and response surface methodology. *Journal of Molecular Liquids*, *206*, 195–206. https://doi.org/10.1016/j.molliq.2015.02.029

Khan, S., & Malik, A. (2014). Environmental and health effects of textile industry wastewater. In *Environmental Deterioration and Human Health: Natural and Anthropogenic Determinants* (Vol. 9789400778, pp. 55–71). https://doi.org/10.1007/978-94-007-7890-0_4

Kumar, A., Prasad, B., & Mishra, I. M. (2007). Process parametric study for ethene carboxylic acid removal onto powder activated carbon using Box-Behnken design. *Chemical Engineering and Technology*, *30*(7), 932–937. https://doi.org/10.1002/ceat.200700084

Lin, L., Zhai, S. R., Xiao, Z. Y., Song, Y., An, Q. Da, & Song, X. W. (2013). Dye adsorption of mesoporous activated carbons produced from NaOH-pretreated rice husks. *Bioresource Technology*, *136*, 437–443. https://doi.org/10.1016/j.biortech.2013.03.048

Malakootian, M., Mansoorian, H. J., Hosseini, A., & Khanjani, N. (2015). Evaluating the efficacy of alumina/carbon nanotube hybrid adsorbents in removing Azo Reactive Red 198 and Blue 19 dyes from aqueous solutions. *Process Safety and Environmental Protection*, *96*, 125–137. https://doi.org/10.1016/j.psep.2015.05.002

Mohebali, S., Bastani, D., & Shayesteh, H. (2019). Equilibrium, kinetic and thermodynamic studies of a low-cost biosorbent for the removal of Congo red dye: Acid and CTAB-acid modified celery (Apium graveolens). *Journal of Molecular Structure*, *1176*, 181–193. https://doi.org/10.1016/j.molstruc.2018.08.068

Oliveira, L. S., Alba, J. F. G., Silva, V. L., Ribeiro, R. T., Falcão, E. H. L., & Navarro, M. (2018). The effect of surface functional groups on the performance of graphite powders used as electrodes. *Journal of Electroanalytical Chemistry*, *818*, 106–113. https://doi.org/10.1016/j.jelechem.2018.04.022

Peng, W., Li, H., Liu, Y., & Song, S. (2016). Adsorption of methylene blue on graphene oxide prepared from amorphous graphite: Effects of pH and foreign ions. *Journal of Molecular Liquids*, *221*, 82–87. https://doi.org/10.1016/j.molliq.2016.05.074

Travlou, N. A., Kyzas, G. Z., Lazaridis, N. K., & Deliyanni, E. A. (2013). Graphite oxide/chitosan composite for reactive dye removal. *Chemical Engineering Journal*, *217*, 256–265. https://doi.org/10.1016/j.cej.2012.12.008

Veliev, E. V, Ozturk, T., Veli, S., & Fatullayev, A. G. (2006). Application of diffusion model for adsorption

of azo reactive dye on pumice. *Polish Journal of Environmental Studies*, *15*(2), 347–353.

Yagub, M. T., Sen, T. K., Afroze, S., & Ang, H. M. (2014). Dye and its removal from aqueous solution by adsorption: A review. *Advances in Colloid and Interface Science*, *209*, 172–184. https://doi.org/10.1016/j.cis.2014.04.002

Yetilmezsoy, K., Özçimen, D., Koçer, A. T., Bahramian, M., Kıyan, E., Akbin, H. M., & Goncaloğlu, B. İ. (2020). Removal of Anthraquinone Dye via Struvite: Equilibria, Kinetics, Thermodynamics, Fuzzy Logic Modeling. *International Journal of Environmental Research*, *14*(5), 541–566. https://doi.org/10.1007/s41742-020-00275-0

Zhang, C., Chen, Z., Guo, W., Zhu, C., & Zou, Y. (2018). Simple fabrication of Chitosan/Graphene nanoplates composite spheres for efficient adsorption of acid dyes from aqueous solution. *International Journal of Biological Macromolecules*, *112*, 1048–1054. https://doi.org/10.1016/j.ijbiomac.2018.02.074

e-ISSN 2757-5195

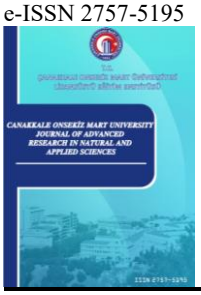

Çanakkale Onsekiz Mart University

Journal of Advanced Research in Natural and Applied Sciences

Open Access

doi.org/10.28979/jarnas.1121842 2023, Vol. 9, Issue 1, Pages: 65-77 dergipark.org.tr/tr/pub/jarnas

Safety Assessment of Speed Governing Systems in Hydroelectric Power Plants: A Functional Safety Perspective

Özgür Turay Kaymakçı[1,*], Nezihe Merve Balcı[2]

[1]Department of Electrics & Electronics Engineering, Faculty of Engineering, Çanakkale Onsekiz Mart University, Çanakkale, Türkiye
[2]BRK Energy Investment Comp., Istanbul, Türkiye

Article History

Received: 26.05.2022

Accepted: 12.09.2022

Published: 05.03.2023

Research Article

Abstract − In line with the advancing technology, reliability has become one of the critical factors to be taken into consideration by the operators in the energy sector to minimize losses regarding cost and time. This issue is directly related to the reliability of the elements, namely the subsystems that make up the system. This study examines the control architecture of speed governing system within the turbine control system of hydroelectric power plants, which has to be regarded as a critical system and provides an indispensable source of guidance and knowledge to researchers and also implementation engineers as well. For this perspective, a reliability analysis has been performed for the speed governing system and the risks with the control system have been revealed. Taking IEC 61508 and IEC 61511 standards as reference within this scope, the safety concepts and the related parameters have been explained and the corresponding methods for risk analysis have been mentioned. As a result, a new safety-related control system configuration overcoming the unacceptable risks with the speed governing system has also been proposed. It has been proved that safety integrity level of the proposed safety-related control system is at the desired level that can make the related safety related functions verify the identified safety level.

Keywords *– Functional Safety, hydraulic power plants, reliability, safety critical systems, speed governing systems*

1. Introduction

Need for energy in the world has been rising as a result of numerous socioeconomic factors which are increasing population, social and economic growth, as well as other factors, such as urbanization and technological development. Energy projection of EIA (US Energy Information Administration) forecasts that demand for energy will grow nearly %50 between 2021 and 2050 especially driven by non OECD Asia countries. 25% of this energy demand is foreseen to be generated from renewable resources. So hydroelectric power plants must have high-level safety systems to fulfil this high level of energy demand in due time and an uninterrupted manner. This would also enhance the useful life of the plant while keeping production, efficiency, reliability, and availability at the highest level possible (Nalley & LaRose, 2021). The 1950s mark the start of studies on reliability regarding electricity distribution. In the 1960s, the development of new methods for system reliability analyses became the focus of studies. The implication of failures occurring in components on the system and environment was also examined by time. New methods were developed during that period and firstly adapted to nuclear power plants, the most critical process of today's world. The possible consequences of a series of failure scenarios developed were also studied (Brennan, 2001).

As the application of reliability analyses in industrial systems become more widespread; IEC 61508 identifying the references of safety applications for electrical, electronic and programmable electronic systems were formed (IEC, 2010). In time, more detailed standards were developed for different sectors, using IEC 61508

[1] okaymakci@comu.edu.tr
[2] merve.balci@yahoo.com
[*]Corresponding Author

as reference. IEC 61513 is one of those which provides requirements and recommendations for the instrumentation and control of nuclear power plants (IEC, 2011).

Numerous studies, in which reliability analyses of plants are available in literature, such as different electrical energy generation resources (i.e. nuclear, thermal and wind) were examined according to the dynamic characteristics of the power systems. By identifying dynamics through methods such as Monte Carlo simulation, reliability analyses were realized by using Markov model and fault tree method in these studies (Billinton & Wang, 1999; Brown, Gupta, Christie, Venkata, & Fletcher, 1996; Chowdhury, Bertling, Glover, & Haringa, 2006; Gubbala & Singh, 1995; Tripathi, Singh, Singh, & Singh, 2021; Zio, 2013). The authors used the reliability index approach in all the parts of the power plants (Khosravi, Azli, & Babaei, 2010; Perman, Senegacnik, & Tuma, 1997; Yu, Tong, Zhao, & Zhang, 2009). Besides, different stochastic characteristics regarding the integration of the wind energy power plant into the grid were studied. Particularly, the reliability effects of the energy power plants' interconnected system connection on the grid have also recently been addressed (Kilic & Basa Arsoy, 2013; Zhang, Chowdhury, & Koval, 2010). Besides, there exist certain studies in the literature that deal with the frequency control in hydro power plants by the help of governing systems. In these studies, working characteristics and frequency control modes of governing systems were analysed (C. Wang, Wang, & Zhang, 2021). Since the critical position of the speed governing system in energy production is well known by the sector representatives, even a standard has been revealed in this context (IEEE, 2007, 2011). Also, simulation of the speed controller and valve correlation were realized (Zhu et al., 2021).

There are also articles in which improvement of frequency control is aimed at, assessing factors that identify the limits of stability and reliable working (Naghizadeh, Jazebi, & Vahidi, 2012). Also Wang et. al. have worked over speed protection of speed governing systems related to nuclear power plants (L. Wang, Sun, Zhao, & Liu, 2019). Pan et. al. worked on transient performance improvement of speed governing systems by regulating the control strategy in order to improve the safety (Pan, Zhu, Liu, Liu, & Tian, 2021). The studies in the literature conducted mainly dwelled on the frequency control function of the speed governing system, placing emphasis on modelling of the systems and stability thereof.

The risks of the governing system were not analysed from a functional safety perspective. Neither has a theoretical nor a practical work been carried out, concerning the necessity of using the governing system along with a safety related system that is capable of realizing safety functions that will eliminate unacceptable risks. The disaster that occurred in the Sayano Shushenskaya dam in Russia, on August 17, 2009, proved the accuracy of this idea. The disaster occurred as a result of an incorrect start-up process of the turbine and the governing system malfunctioning of the Sayano Shushenskaya dam unit. This failure was not detected by the control system. As a result of this, the system could not respond to the change required by the grid, which led to the over-speeding of the unit having de-loaded. 75 people died as a result of the incident and the entire power plant with 6400 MW was almost totally destroyed (Kuznetsov, Yuldashev, & Yuldashev, 2021; Leonov, Kuznetsov, & Solovyeva, 2015; Naymushin, 2009). This recent incident reveals the necessity of considering governing systems in hydroelectric plants as a safety critical system. It also shows that the reliability analysis of the interaction of speed governing system with the turbine generator system has critical importance and this analysis has to be included in the system design phase (Bulut & Özcan, 2021; Danciu, Popescu, & Rasvan, 2020). It is also a good example that shows the importance of doing reliability analysis by taking the interaction of speed governing system with the turbine generator system into account.

In a power system with high quality, frequency is required to be within an acceptable range. That is why speed control is conducted. Speed governing is a system where both the speed of the turbine generator system and that of electrical energy to be generated is controlled. As one can see from the Sayano Shushenskaya incident, any critical failure occurring in the speed governing system bears many crucial risks such as failure system being unable to stop the system in a safe way, over-speeding of the unit or not being able to synchronize with the grid. At least some part of the speed governing system, which plays a critical role in operating the hydroelectric power plants, should be evaluated from the perspective of safety related system. It should also be ensured that the relevant safety integrity level is at an acceptable level. This approach is of great importance for the sustainability of the system (Glavitsch, Reichert, Peneder, & Singh, 2003). Within this scope, this study was carried out the reliability analyses based on IEC 61362 and IEC 60308 standards so as to ensure the maintenance of operating hydroelectric power plants safely and efficiently by taking the digital speed regulator providing the speed, power and frequency control of the turbine generator system (IEC, 2005a, 2012). For this purpose, medium scale river type Midilli hydroelectric power plant (HEPP) has been examined such that

the Midilli HEPP has 32.548 MWe install capacity provided by 3 big units and 1 small unit. Here the big units have 10.485 MWe and the small one has 1.093 MWe install capacity. The Midilli HEPP has Francis type turbines and its annual power generation is 124 GWh.

The failure records of similar hydroelectric power plants have systematically been reviewed in order to analyse all possible failures and define the risk scores correctly. Besides, the failures that are likely to occur in the system, their possible causes, such as material losses in the event of failure occurrences, damage on the environment and personnel health have been also studied.

At this point, long meetings were held with the experts in the energy sector. The possible effects and frequencies of these determined failures were revealed and the safety functions that can eliminate these relevant risks have been proposed. Also, a safety related system that can realize the identified safety functions has been offered. Finally, the safety integrity level of the overall system has been calculated according to IEC 61511.

2. Materials And Methods Methodology

2.1. Safety Related Systems And Functional Safety

IEC 61508 expresses a safety related system as a "designated system used to implement the required safety related functions necessary to achieve or maintain a safe state for the equipment under control". According to this expression, safety related system is planned to accomplish the required safety functions which are dedicated to take the process to a safe state when outlined conditions are contravened. The safety related systems are composed of special design sensors, logic solver, and final elements. Here reducing risk to the tolerable level is the common aim of implemented safety related functions. On the other hand, to maintain a certain quality in the relevant sectors, independent organizations developed some standards. IEC 61508 is the international and leading standard that defines the functional safety for electrical, electronic and programmable electronic devices. It is also an umbrella document including various industries such that specific standards like IEC 62061 and IEC 61511 were introduced from this perspective (IEC, 2003, 2005b).

IEC 61508 put forth some safety parameters for the sake of reliability. The safety related systems were classified and compared over these defined parameters.

Failure rate: It is the frequency with which the system fails and denoted with λ. It is the rate of the failure density function (f(t)) that denotes the probability of the system's failure to the reliability function (R(t)) which means that the system can perform the identified functions. The failure rate is denoted by λ and modelled as provided in 2.1. It is usually expressed as failures per million hour (FPMH). Failure rate consists of two different types of failure such that these are safe failure and dangerous failure respectively. The ratio of the safe failure is defined with safety ratio (S). These can be seen in Equation 2.1 and 2.2. (IEC, 2010).

$$\lambda(t) = \frac{f(t)}{R(t)} \tag{2.1}$$

$$\lambda = \lambda_S + \lambda_D \tag{2.1}$$

$$\lambda_S = S\ x\ \lambda \tag{2.2}$$

As provided in- Equation 2.3, a dangerous failure consists of two, which are dangerous detected failure (DD) and dangerous undetected failure (DU). In safety-related studies, it is accepted that the failure rate is constant within the use period of the system (Rausand, 2014).

$$\lambda_D = \lambda_{DD} + \lambda_{DD} \tag{2.3}$$

Safe failure fraction (SFF): Safe failure fraction is the percentage of the safe failures such that IEC 61508 expresses the calculation of it in IEC 61508-6 Annex C as Equation 2.4

$$SFF = \frac{\sum \lambda_S + \sum \lambda_{DD}}{\sum \lambda_S + \sum \lambda_{DD} + \sum \lambda_{DU}} \quad (2.4)$$

Diagnostic coverage: Diagnostic coverage (DC) is a measurement as to what extent dangerous failures might occur in failure related systems. DC is defined as given in Equation 2.5 according to IEC 61508-4 section 3.8.6.

$$DC = \frac{\sum \lambda_{DD}}{\sum \lambda_{DD} + \sum \lambda_{DU}} \quad (2.5)$$

The values of this parameter differ a great deal in safety related systems such that while DC is 99% for fail-safe programmable logic controllers, the percentage varies for sensors and actuators. The DC level of the unit can be identified taking IEC 61508-6 Annex C table C.2 as the reference.

Probability of failure on demand: IEC 61608 expresses the system's likelihood of a failure during a time when safety related system is supposed to be working with probability of failure on demand (PFD). It is obvious that, the lower this value is, the safer the system is considered. Then average probability of failure on demand is defined as Equation 2.6

$$PFD_{avg} = \frac{1}{T}\int_0^T P(t)dt \quad (2.6)$$

Mean time to failure (MTTF): This is one of the common parameters used by the industry which is the statistical mean length of time a system or any other product last in operation till the first failure incidence. Products in safety related systems sector are generally compared based on their MTTF values given in Equation 2.7. For example, if a component's failure rate is equal to λ then its MTTF value is equal to 1/λ. The greater the MTBF value of a component, the less likely that component will fail per unit time.

$$MTTF = \int_0^T R(t)dt \quad (2.7)$$

Mean time to repair (MTTR): Another commonly used parameter in the industry is MTTR. This parameter expresses the required average time to repair a failed component or subsystem. If it is not mentioned by the vendor, the IEC 61508 recommends to take 8 hours as MTTR value.

Proof test interval (TI): It is the time that passes in between the main repairs to check whether the system or equipment accurately fulfil all its functionality or not (Rausand, 2014).

Common cause failures: This kind of failures are the interconnected failures of multiple subsystems that arise as a result of single specific event or cause. Although multiple methods are introduced in the literature, the β factor method, which was proposed by Fleming, is still commonly used (Fleming, 1975). It proposes a quantitative method to determine the corresponding values of β and β_D. Here β and β_D parameters define the overall common cause failure factor for undetected failures and the overall common cause failure factor for detected failures respectively.

Hardware fault tolerance (HFT): Hardware fault tolerance is the maximum number of failures that the subsystem or component can still continue to operate its intended function. The HFT is calculated according to Equation 2.8 (Rausand, 2014).

$$HFT_{sys} = \min_i HFT_i \quad (2.8)$$

2.2. Risk Analysis

Risk analysis is a process that occurs in analysis phase of the project management that includes gathering data and synthesizing information to develop an understanding of the risk of a particular system or subsystem. Within this scope, risk (R) is the combination of the frequency of the damage (F) and consequences of the damage (C). It is denoted as given in Equation 2.9 (IEC, 2006).

$$R = F\ x\ C \tag{2.9}$$

It would be possible to identify the risks in a realistic manner only when one can have thorough knowledge regarding the process. Failure records of many hydroelectric power plants with similar scale have been analysed in depth in this study so that the risks are analysed accurately. All the detected failures have been evaluated together with the experts in relevant sector. Besides, relevant standards have been taken as reference, results obtained have been compared with updated data numerous times and consistency of the results have been ensured accordingly.

2.3. Fault Tree Analysis

Fault tree analysis method is one of the most widely used reliability analysis methods. It is based on Boolean algebra, probability calculations and reliability theory such that the logical combination of unwanted situations are depicted graphically. IEC 61508-3 table B.4 and also IEC 61508-2 section 7.4.5.2 define that the method can be used both in software and hardware related failure analysis (IEC, 2006).

2.4. Safety Integrity Level Verification

The designed safety related functions must be verified according to the safety requirements. For this purpose, the standard takes into account Probability of Failure on Demand average (PFD_{avg}), probability of dangerous failure per hour, SFF and HFT measures in order to identify the safety performance of the safety related system. When the safety related function is active at low demand mode, PFD_{avg} is selected. On the other hand, probability of dangerous failure per hour is selected for high demand and continuous mode operations. IEC 61508-1 section 7.6.2.9 table 2 indicates a bounded probability interval for every safety integrity level (SIL) in case of low demand mode. Maximum allowable safety level that a system could achieve based on SFF and HFT is presented in IEC 61508-2 section 7.4.4.2.2 table 3 as well (IEC, 2010). In long discussions with experts in the sector and with reference to IEC 61508 Part 5 Annex B, it has been determined that the minimum safety integrity level of a governing system should be SIL 2.

3. Results and Discussion

3.1. Reliability Analysis Of Speed Governing System

Speed governing system functions in the synchronization of the turbine generator unit in the plant into the interconnected system. Thus, it ensures the transfer of the generated energy into the system and integrity of the grid system. Identifying the risks that could impact the performance of the governing system which plays a critical role within electrical energy generation process, and reducing the intolerable detected risks will significantly contribute to the correct functioning of the process.

For this study, the failure records of Suat Ugurlu, Hasan Ugurlu, Gezende, Berke, Midilli and Yavuz hydroelectric power plants located in Turkey have been examined. The risks that could delay the sustainability of frequency control cycle releasing at the digital speed governing system are determined in accordance with these detailed investigations. In this perspective, the frequency of failure occurrences, damages to be caused and technical analysis were evaluated with expert technical personnel. As a result of this intense collaborative work, the risk matrix has been formed concerning failures. In the matrix, the likehood of hazard is given under the frequency tab such that it is classified in five intervals as *very likely*, *likely, possible, unlikely and very unlikely*. Similarly, severity of the accident that will occur if the relevant danger is revealed is described under the consequence tab and it is classified in five levels, starting from *insignificant* to *catastrophic*. In addition, the risk scores are calculated according to Equation 2.9 such that these scores are classified in four main groups. The risks with a score in the range of 1..4 are considered *Low*, on the other hand the risks with a score in the range of 5..8 are considered *Moderate*, those with a score in the range of 9..15 are considered as *High*, and finally those with a score of 16 and above are classified as *Extreme*. While making this classification, the opinions of the sector experts were taken into consideration and a conservative approach was adopted during the classification phase. The corresponding risk matrix is given in Table 1.

Table 1.
Risk matrix

Frequency	**Consequence**				
	Insignificant (1)	*Minor (2)*	*Moderate (3)*	*Major (4)*	*Catastrophic (5)*
Very likely (5)	Moderate (5)	High (10)	High (15)	Extreme (20)	Extreme (25)
Likely (4)	Low (4)	Moderate (8)	High (12)	Extreme (16)	Extreme (20)
Possible (3)	Low (3)	Moderate (6)	High (9)	High (12)	High (15)
Unlikely (2)	Low (2)	Low (4)	Moderate (6)	Moderate (8)	High (10)
Very Unlikely (1)	Low (1)	Low (2)	Low (3)	Low (4)	Moderate (5)

As mentioned before, the obtained technical data have been analysed by operation maintenance engineers, power generation process operators, experts and specialists who have been working in energy sector for many years. As a result of in-depth examinations, 26 major hazard scenarios have been identified but ten of them with a *high* and above risk score are listed in Table 2. Here the relevant hazards are enumerated and each hazard is briefly described. In addition, the frequency value and consequence of each hazard are also expressed. These values were intuitively generated as a result of field studies and were submitted to the approval of industry experts. In addition, the risk scores are calculated according to Equation 2.9

Table 2
The hazard scenarios and their risk scores

No	Hazard	Frequency		Consequence		Risk score	Risk
Hzd.01	Over speed	Likely	4	Catastrophic	5	20	Extreme
Hzd.02	Frequency cannot be balanced	Likely	4	Major	4	16	High
Hzd.03	Programmable logic controller failure	Possible	3	Major	4	12	High
Hzd.04	Main distribution valve failure	Possible	3	Major	4	12	High
Hzd.05	Step motor failure	Likely	4	Moderate	3	12	High
Hzd.06	Power supply failure	Possible	3	Major	4	12	High
Hzd.07	Disruption in grid frequency	Unlikely	2	Catastrophic	5	10	High
Hzd.08	Required water level can't be supplied	Possible	3	Moderate	3	9	High
Hzd.09	Servo motor failure	Possible	3	Moderate	3	9	High
Hzd.10	Pump works too loudly	Possible	3	Moderate	3	9	High

It is also be noted that risk analyses and evaluation may vary depending on time, working conditions and opinion of the experts who assess the subject matter. As some of the failures that are likely to emerge in the governing system could be due to hydraulic oil impact based on expert view, pressurized oil system has been accepted as the auxiliary system within the speed governing system, and included in the risk evaluation accordingly (Başeşme, 2003; Boardman, 1994; Cebeci, 2008; Naghizadeh et al., 2012).

Because of the scores given in Table 2, the safety function should be actuated against risks with extreme and high significance so that system can work in a safe mode in actual setting and practice. This study, however, presents the solution for the most critical ones. Besides, PFDavg, SFF and HFT values of safety related system are calculated and safety integrity level are identified.

The suggested speed governing safety system consists of fail-safe programmable logic controller, different type of sensors and actuators. It is clear that the exact failure rates of the subsystems are needed in order to calculate the SIL of the safety related functions precisely. For this reason, the corresponding reliability parameters of the fail-safe programmable logic controller have been acquired from its supplier. Also the failure rates of the other components are obtained from the suppliers and the OREDA handbook (OREDA, 2002). The failure rate values of these components are provided in Table 3.

Table 3.
The failure rate values of system components

Devices	λ (FPMH)	MTTF (h)	DC (%)	S (%)	MTTR (h)
Speed sensor	6.64	150517	75	50	8
Proximity sensor	5.24	190682	90	50	8
Pressure sensor	4,456	224405	75	50	8
Emergency Shutdown Valve	5.48	182287	70	50	8
Control valve	37,38	26747	75	50	8
Safety Relief Valve	7,01	142654	90	50	8
Fail-safe CPU	2,439	446627	99,63	50	8
Fail-safe Input Module	1,517	659195	99,31	50	8
Fail-safe Output Module	2,592	385802	99,24	36	8

Safety related function suggestion has been made for 3 critical situations that have the highest risk potential for speed governor. Relevant safety related function is as follows. The proposed safety related function is designed in order to realize imbalance at the frequency, over pressure and over speed protection functionalities. The proposed block diagram for the safety-related system suggested for safety related function is illustrated in Figure 1. The safety architectures of the components are also given. The safety function consists of inputs with 1oo2 and 2003 safety architectures, outputs with 1oo2 safety architecture and a fail-safe controller with 1oo2D safety architecture. Here all sensors, actuators and controller are designed with redundant architectures so that the system does not crash due to single failures. Three different types of sensors are used as inputs, including speed sensor (SS), proximity sensor (PRS) and pressure sensor (PS). The turbine speed and frequency data are measured by speed sensors. On the other hand, if the turbine speed exceeds the critical speed limit, the proximity sensors generate fail-safe outputs by opening normally closed contacts. The oil pressure in the pistons are measured pressure sensors.

The fail-safe controller consists of CPU module, input modules and output modules. CPU, input modules and output modules used in the system are equipment, which embody advanced technology, have diagnostic capabilities of 99.99% and work in accordance with the inherent 1oo2D architecture.

Emergency shutdown valve, safety relief valve and control valve have been integrated to the safety related system in order to safely stop the system in different risk scenarios. Each actuator is designed into the system in a redundant architecture, ensuring that the system is still safe in case of a single failure.

Over speeding of the turbine that is targeted to be prevented within safety related function scope is an undesirable critical scenario. For this purpose, an electronic proximity sensor system with a high level of safety obtained with 2oo3 safety architecture is used in order to be able to identify the over speeding of the unit. In the event of over speed, it is aimed that emergency shutdown valve is activated and deactivates the governing system safely. Also the high oil pressure in pistons that move main control valve cause a treat for speed governing system availability. Another aim of the safety related system is to deactivate the system safely in case of high oil pressure. The safety related function activates the safety relief valve in this situation. Finally, the imbalanced frequency poses serious risk over the governing system. Here the proposed safety related function cope within this risk and in the event of imbalanced frequency, the control valve is activated by safety related system.

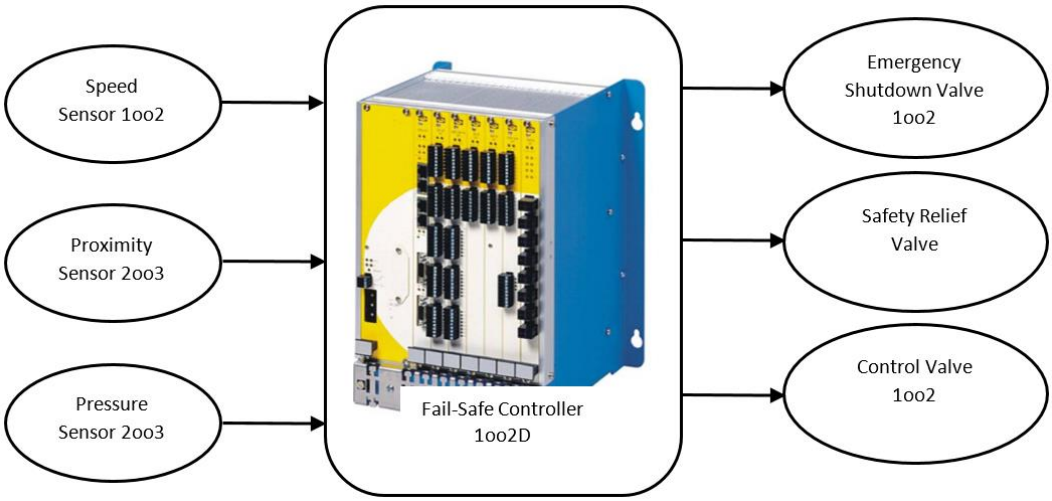

Figure 1 - The block diagram of the system

In order to calculate the safety integrity of the system, some non-conservative assumptions are made. There ones are as follows. The most of the components' periodic maintenance interval is 1 year. It is assumed that the proof test interval is 1 year and the testing is perfect. Failures regarding instalment and commissioning have been ignored. Similarly, it has been acknowledged that all the equipment, which has completed their useful life cycle, will be replaced by their equivalent counterpart. For this reason, failures that emerge during worn out phase have not been taken into account. The electrical connection and cabling failures have been ignored. The beta factor for common cause failure is calculated as 2% according to the IEC61508-6 annex D. The failure rates of all redundant components are assumed to be equal. It is supposed that the mean time to repair is 8 hours and the repair is perfect.

Some parts of possible failures can be easily detected by the help of relevant feedback obtained from speed sensor, pressure sensor, proximity sensor, safety relief valve, control valve and emergency shutdown valve elements. Diagnostic capability has been included in such elements through the control system used. In light of information obtained from the supplier, PFDavg calculation of the fail-safe controller has been made based on IEC 61508 annex B.3.2.2.4 as the reference. The fault tree analysis of the safety related function is given in Figure 2 .

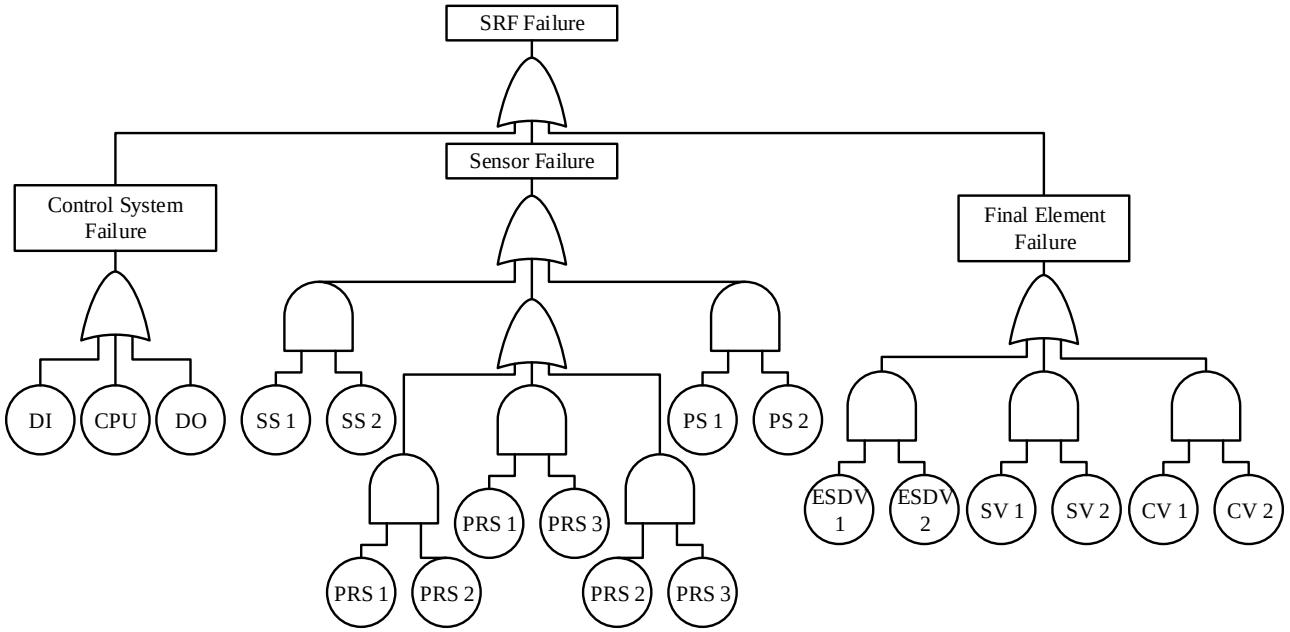

Figure 2. The FTA Analysis of the safety related function

Safety related function is assumed to fall into error upon demand when conditions defined below occur:

- Turbine speed and frequency data are perceived through speed and proximity sensors in the system. In case of a failure in sensors, speed data cannot be perceived, thus the frequency cannot be balanced. This leads the system to fall into error upon demand.
- The system has two ESDVs with 1oo2 architecture. Both of the ESDVs should fall into error so that the system gets into error.
- The system has two SRVs with 1oo2 architecture. If both of the SRVs should fall into error, the system gets into error.
- The system has two control valves with 1oo2 architecture. Both of the control valves should fall into error so that the system gets into error.
- If a common cause failure occurs at the subsystems with 1oo2 architecture, the system gets into error.

The corresponding failure rates of the devices and PFD_{avg} values calculated according to IEC 61508-6 annex B3.2.2 are given at Table 4. Considering the safety architectures, hardware fault tolerances are also listed separately.

Table 4.
PFDavg and HFT values of the subsystems

Devices	λ (FPMH)	PFD_{avg}	Architecture	HFT
Speed sensor	6.64	$9{,}06.10^{-5}$	1oo2	1
Proximity sensor	5.24	$2{,}86.10^{-5}$	2oo3	1
Pressure sensor	4,456	$5{,}69.10^{-5}$	1oo2	1
ESV	5.48	$8{,}95.10^{-5}$	1oo2	1
Control valve	37,38	$9.66.10^{-4}$	1oo2	1
SRV	7,01	$1{,}85.10^{-5}$	1oo2	1
Fail-safe CPU	2,439	$1{,}96.10^{-5}$	1oo2D	1
Fail-safe DI	1,517	$2{,}09.10^{-7}$	1oo2D	1
Fail-safe DO	2,592	$3{,}86.10^{-7}$	1oo2D	1

Based on Equation 2.8 and 2.4, it is obtained that a SFF of 98.60%. According to IEC 61508-2 section 7.4.4.2.2 Table 3, for 99% > SFF > 90% and HFT=1 the maximum allowable SIL that the system could have is 3. Given that PFD_{avg}=1,27.10^{-3} for the relevant safety related function 1, within 10^{-3} and 10^{-2} range, the safety level of safety related function is SIL 2 according to IEC 61508-1 section 7.6.2.9 Table 2.

This value is the minimum required safety level that should be possessed by the safety side of the governing system. Accordingly, it is seen that the proposed safety system ensures the required minimum safety level.

It must be stated that the risk reduction factor (RRF) is the inverse of PFD_{avg} according to IEC 61508 and IEC 61511. Then if a system is SIL 2 then its PFD_{avg} have to be between within 10^{-3} and 10^{-2} range so the risk reduction factor varies between 100 and 1000. For the proposed safety related system, as the PFD_{avg} value is equal to 1,27.10^{-3} then the risk reduction value is approximately 787. In other words, the risk was reduced by an average of 787 times.

In a qualified and reliable power system, it is desirable that the output frequency of the system be constant in an acceptable range. For this purpose, speed control is performed in hydroelectric power plants. Both the speed of the turbine generator system and the power of the electrical energy to be produced are controlled with the speed governor system. On the other hand, any malfunction in the speed governor system may cause the unit to go over speed or break down. As a result, it can cause many accidents, from not being able to synchronize with the network, to serious damage to the power plant.

At this point, the reliability of this critical system, which plays a role in the operation of hydroelectric power plants, is of great importance for the sustainability of the overall system.

With this motivation, in this study, the reliability of digital speed governor systems in river-type hydroelectric power plants was examined according to IEC 61511 and IEC 61508 standards. The "Over Speed" failure, which can be considered as the most critical hazard for speed governor systems, has been examined and a safety function that increases the safety integrity level is proposed. Different safety architectures such as 1oo2, 1oo2D and 2oo3 were used for the sensors, actuators and controller side, as a result, a fail-safe solution was proposed. With this solution, the hardware fault tolerance of the system was increased to 1, and the average probability of failure on demand was reduced by an average of 79 times. As a result, it is calculated that the solution has SIL 2 safety integrity level.

In this study, a safety function that increases the safety reliability level is proposed for the "Over Speed" error, which can be considered as the most critical error for regulator systems. As can be observed from Table 4, a safe solution to the fault has been proposed by using different safety architectures such as 1oo2, 1oo2D and 2oo3. With this solution, the tolerance of the system to error was increased to 1, and the average error probability during the demand was reduced by an average of 787 times. As a result, the solution was calculated to have a SIL 2 safety integrity level.

Thus, as a result of possible risks, the possibility of a safe stop of the system increases significantly and the useful life of the facility is guaranteed to be longer.

4. Conclusion

In this study, the incidents leading to the failure of turbine speed governing system has been examined and a new safety related system architecture has been proposed for the critical scenarios based on IEC 61508 perspective. For this purpose, the failure records of Suat Ugurlu, Hasan Ugurlu, Gezende, Berke, Midilli and Yavuz hydroelectric power plants located in Turkey have been examined and the obtained data have been evaluated by experts and specialists who have been working in energy sector for many years and risk scores were determined with the support of relevant experts. It is revealed that the governing system incorporates unacceptable risks and the safety integrity level of the currently used control systems does not cover the desired safety level. Neither the corresponding international standards nor the local technical specifications express the safety of the speed governing systems within the scope of functional safety. So in order to overcome these unacceptable risks and define a new perspective for the safety of the governing systems, an innovative safety related system suggestion has been made based on IEC 61508. The proposed speed governing safety system has been designed with reference to the Midilli hydroelectric power plant in Amasya. It should also be stated that the proposed can be used in other hydroelectric power plants with minor modifications if the technical specifications meet the plant requirements.

It is also proofed that the safety integrity level of the proposed system is SIL 2, which is the minimum level of safety demanded by the sectorial experts. As a result, the risk reduction factor of the prosed speed governing system reduces the risk at least 100 times.

Acknowledgement

The author received no specific funding for this study.

Author Contributions

Özgür Turay Kaymakçı: Validated the analysis, wrote the manuscript

Nezihe Merve Balcı: Collected data, performed reliability analysis, wrote the manuscript

Conflicts of Interest

The authors declare no conflict of interest.

References

Başeşme, H. (2003). *Hidroelektrik Santraller ve Hidroelektrik Santral Tesisleri* (2. Baskı ed.). Ankara: Hidrolik Santraller Daire Başkanlığı Yayınları. https://divit.library.itu.edu.tr/record=b1147743

Billinton, R., & Wang, P. (1999). Teaching distribution system reliability evaluation using Monte Carlo simulation. *IEEE Transactions on Power Systems, 14*(2), 397-403. doi: https://doi.org/10.1109/59.761856

Boardman, J. R. (1994). Operating experience feedback report - reliability of safety-related steam turbine-driven standby pumps: US Nuclear Regulatory Commission. 27005885.pdf (iaea.org)

Brennan, R. L. (2001). An Essay on the History and Future of Reliability from the Perspective of Replications. *Journal of Educational Measurement, 38*(4), 295-317. doi: https://doi.org/10.1111/j.1745-3984.2001.tb01129.x

Brown, R. E., Gupta, S., Christie, R. D., Venkata, S. S., & Fletcher, R. (1996). Distribution system reliability assessment using hierarchical Markov modeling. *IEEE Transactions on Power Delivery, 11*(4), 1929-1934. doi: https://doi.org/10.1109/61.544278

Bulut, M., & Özcan, E. (2021). A new approach to determine maintenance periods of the most critical hydroelectric power plant equipment. *Reliability Engineering & System Safety, 205*, 107238. doi: https://doi.org/10.1016/j.ress.2020.107238

Cebeci, M. E. (2008). *The effects of hydro power plants' governor settings on the turkish power system frequency.* (M.S. - Master of Science), Middle East Technical University, Ankara. Ulusal Tez Merkezi | Anasayfa (yok.gov.tr)

Chowdhury, A. A., Bertling, L., Glover, B. P., & Haringa, G. E. (2006). *A Monte Carlo Simulation Model for Multi-Area Generation Reliability Evaluation.* Paper presented at the 2006 International Conference on Probabilistic Methods Applied to Power Systems. doi: 10.1109/PMAPS.2006.360430

Danciu, D., Popescu, D., & Rasvan, V. (2020, 2020-10-27). *Stability and Control Problems in Hydropower Plants.* Paper presented at the 2020 21th International Carpathian Control Conference (ICCC). doi: https://doi.org/10.1109/ICCC49264.2020.9257294.

Fleming, K. N. (1975). A reliability model for common mode failures in redundant safety systems. San Diego, California, USA: General Atomic Co. https://inis.iaea.org/search/search.aspx?search-option=everywhere&orig_q=RN%3A6204768

Glavitsch, H., Reichert, K., Peneder, F., & Singh, N. (2003). Power System Operation and Control *Electrical Engineer's Reference Book* (pp. 40-41-40-50): Elsevier. doi: 10.1016/B978-075064637-6/50040-X:

Gubbala, N., & Singh, C. (1995). Models and considerations for parallel implementation of Monte Carlo simulation methods for power system reliability evaluation. *IEEE Transactions on Power Systems, 10*(2), 779-787. doi: https://doi.org/10.1109/59.387917

IEC. (2003). IEC 61511 - Functional Safety - Instrumented Systems for the Process Industry Sector, Parts 1-3. Genoa, Switzerland: International Electrical Commission. https://webstore.iec.ch/publication/5527

IEC. (2005a). IEC 60308 - Hydraulic turbines testing of control systems. Genoa, Switzerland: International Electrical Commission. https://webstore.iec.ch/publication/1312

IEC. (2005b). IEC 62061 - Safety of machinery - Functional safety of safety-related electrical, electronic and programmable electronic control systems. Genoa, Switzerland: International Electrical Commission. https://webstore.iec.ch/publication/59927

IEC. (2006). IEC 61025 - Fault tree analysis (Second Edition ed.). Genoa, Switzerland: International Electrical Commission. https://webstore.iec.ch/publication/4311

IEC. (2010). IEC 61508 - Functional Safety of Electrical/Electronic/Programmable Electronic Safety-related Systems. Genoa, Switzerland: International Electrical Commission. https://webstore.iec.ch/publication/5515

IEC. (2011). IEC 61513 - Nuclear power plants-Instrumentation and control important to safety-general requirements for systems. Genoa, Switzerland: International Electrical Commission. https://webstore.iec.ch/publication/5532

IEC. (2012). IEC 61362 - Guide to specification of hydraulic turbine control systems. Genoa, Switzerland: International Electrical Commission. https://webstore.iec.ch/publication/5383

IEEE. (2007). Recommended practice for preparation of equipment specifications for speed-governing of hydraulic turbines, intended to drive electric generators. New York, USA: Institute of Electrical and Electronics Engineer. https://standards.ieee.org/ieee/125/3394/

IEEE. (2011). Guide for the application of turbine governing systems for hydroelectric generating units. New York, USA: American National Standards Institute. https://ieeexplore.ieee.org/document/6042284

Khosravi, F., Azli, N. A., & Babaei, E. (2010, 11/2010). *A new modeling method for reliability evaluation of Thermal Power Plants.* Paper presented at the 2010 IEEE International Conference on Power and Energy (PECon). doi: 10.1109/PECON.2010.5697644

Kilic, L., & Basa Arsoy, A. (2013, 10/2013). *A reliability study of medium voltage grid with private sector power plants.* Paper presented at the 2013 3rd International Conference on Electric Power and Energy Conversion Systems (EPECS). doi: 10.1109/EPECS.2013.6713045

Kuznetsov, N. V., Yuldashev, M. V., & Yuldashev, R. V. (2021). Analytical-numerical analysis of closed-form dynamic model of Sayano-Shushenskaya hydropower plant: stability, oscillations, and accident. *Communications in Nonlinear Science and Numerical Simulation, 93*, 105530. doi: https://doi.org/10.1016/j.cnsns.2020.105530

Leonov, G. A., Kuznetsov, N. V., & Solovyeva, E. P. (2015). A simple dynamical model of hydropower plant: stability and oscillations. *IFAC-PapersOnLine, 48*(11), 656-661. doi: https://doi.org/10.1016/j.ifacol.2015.09.262

Naghizadeh, R. A., Jazebi, S., & Vahidi, B. (2012). Modeling hydro power plants and tuning hydro governors as an educational guideline. *International Review on Modelling and Simulations (I.RE.MO.S.), 5*(4), 1780-1790. https://www.researchgate.net/publication/235675537_Modeling_Hydro_Power_Plants_and_Tuning_Hydro_Governors_as_an_Educational_Guideline

Nalley, S., & LaRose, A. (2021). International Energy Outlook. In S. Nalley & A. LaRose (Eds.): U.S. Energy Information Administration. International Energy Outlook 2021 - U.S. Energy Information Administration (EIA)

Naymushin, I. (2009, 17 August 2009). Russian dam disaster kills 10, scores missing, https://www.reuters.com/article/worldNews/idUSTRE57G0M120090817?sp=true

OREDA. (2002). *OREDA: Offshore Reliability Data Handbook*. Norway: OREDA Participants : Distributed by Der Norske Veritas. https://www.oreda.com/

Pan, W., Zhu, Z., Liu, T., Liu, M., & Tian, W. (2021). Optimal Control for Speed Governing System of On-Grid Adjustable-Speed Pumped Storage Unit Aimed at Transient Performance Improvement. *IEEE Access, 9*, 40445-40457. doi: https://doi.org/10.1109/ACCESS.2021.3063434

Perman, M., Senegacnik, A., & Tuma, M. (1997). Semi-Markov models with an application to power-plant reliability analysis. *IEEE Transactions on Reliability, 46*(4), 526-532. doi: https://doi.org/10.1109/24.693787

Rausand, M. (2014). *Reliability of Safety-Critical Systems: Theory and Applications*. Hoboken, NJ, USA: John Wiley & Sons, Inc. Reliability of Safety-Critical Systems: Theory and Applications | Wiley

Tripathi, M., Singh, L. K., Singh, S., & Singh, P. (2021). A Comparative Study on Reliability Analysis Methods for Safety Critical Systems Using Petri-Nets and Dynamic Flowgraph Methodology: A Case Study of Nuclear Power Plant. *IEEE Transactions on Reliability*, 1-15. doi: https://doi.org/10.1109/TR.2021.3109059

Wang, C., Wang, D., & Zhang, J. (2021). Experimental study on isolated operation of hydro-turbine governing system of Lunzua hydropower station in Zambia. *Renewable Energy, 180*, 1237-1247. doi: https://doi.org/10.1016/j.renene.2021.09.014

Wang, L., Sun, W., Zhao, J., & Liu, D. (2019). A Speed-Governing System Model with Over-Frequency Protection for Nuclear Power Generating Units. *Energies, 13*(1), 173. doi: https://doi.org/10.3390/en13010173

Yu, Y., Tong, J., Zhao, R., & Zhang, A. (2009, 07/2009). *Reliability analysis for continuous operation system in nuclear power plant.* Paper presented at the 2009 8th International Conference on Reliability, Maintainability and Safety (ICRMS 2009). doi: 10.1109/ICRMS.2009.5270214

Zhang, Y., Chowdhury, A. A., & Koval, D. O. (2010, 05/2010). *Probabilistic wind energy modeling in electric generation system reliability assessment.* Paper presented at the 2010 IEEE Industrial and Commercial Power Systems Technical Conference - Conference Record. doi: 10.1109/IREP.2010.5563301

Zhu, L., Si, P., Liu, S., Xie, C., Zhang, T., Hu, Y., & Qiu, X. (2021). The Design of Parameter Modeling Software Applicable for Turbine Control Systems of Power Units Operated at Deep Shaving States. *Journal of Physics: Conference Series, 2076*(1), 012106. doi: https://doi.org/10.1088/1742-6596/2076/1/012106

Zio, E. (2013). *The Monte Carlo Simulation Method for System Reliability and Risk Analysis*. London: Springer London. The Monte Carlo Simulation Method for System Reliability and Risk Analysis | SpringerLink

e-ISSN 2757-5195

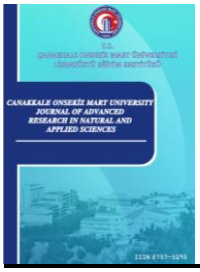

Çanakkale Onsekiz Mart University
Journal of Advanced Research in Natural and Applied Sciences
Open Access

doi.org/10.28979/jarnas.1072471 2023, Cilt 9, Sayı 1, Sayfa: 78-88 dergipark.org.tr/tr/pub/jarnas

Yüksek Mukavemetli DP1200 Çeliği Fiber Lazer Bindirme Kaynağında Lazer Açısı Parametresinin Etkisi

Meryem Altay[1,*], Hakan Aydın[2]

[1,2] Makine Mühendisliği Bölümü, Mühendislik Fakültesi, Bursa Uludağ Üniversitesi, Bursa, Türkiye

Makale Tarihçesi

Gönderim: 12.02.2022
Kabul: 22.09.2022
Yayım: 05.03.2023

Araştırma Makalesi

Öz – Çalışma kapsamında yüksek mukavemete sahip DP 1200 çelik malzemenin, fiber lazer kaynak işlemiyle birleştirilmesi bindirme formunda yapılmıştır. Lazer gücü (2500 W) ve ilerleme hızı (55 mm/s) sabit tutularak lazer açısı (70°, 80°, 90°) değişiminin kaynaklı bağlantıların kaynak dikiş yüzeyi, kaynak geometrisi, kırılma yüzeyleri ve mekanik özelliklere etkisi incelenmiştir. Lazer kaynaklı numunelerin arka yüzeylerinde, ön yüzeylerine göre sıçrama etkilerinin (spatter effect) daha fazla olduğu tespit edilmiştir. Eşit ısı girdisinde lazer açısının, ara seviyede kullanılmasındansa düşük (70°) ya da yüksek seviye (90°) kullanılmasının kaynak geometrisinde optimum sonuçlar vereceği tespit edilmiştir. Çekme testinde yüksek kuvvet ve yüzde uzama değerleri elde edilmiştir: 70° lazer açısına sahip numunede maksimum kesme kuvveti 5.8266 kN olarak elde edilmiştir. Ayrıca kesme kuvveti ile kaynak geometrisindeki erime bölgesinde ölçülen tam birleşme mesafesi (bonding) arasında ilişki kurulmuştur. Düşük lazer açısı parametresi (70°) ile üretilen numunelerde yüksek gevrekliğin göstergesi klivaj kırılmalar gözlenmiştir; yüksek lazer açısı (90°) ile üretilen numunelerde ise kırılma yüzeyleri sünektir, oluşan çukurlar küçük boyutludur. Lazer açısının yüksek dereceye sahip olması (90°), kırılmanın gerçekleştiği bölgenin Isı Tesiri Altındaki Bölge içerisinde yer almasına neden olmuştur.

Anahtar Kelimeler – *Lazer kaynak, kaynak işlem parametreleri, kırılma yüzeyi, mekanik özellikler, DP1200 çeliği*

Effect of Laser Angle Parameter in High Strength DP1200 Steel Fiber Laser Overlap Welding

[1] Department of Mechanical Engineering, Faculty of Engineering, Bursa Uludağ University, Bursa, Türkiye

Article History

Received: 12.02.2022
Accepted: 22.09.2022
Published: 05.03.2023

Research Article

Abstract – In this study, high-strength DP 1200 steel plates were welded with fiber laser welding method in the form of overlapping without gaps. The effects of the laser angle (70°, 80°, 90°) changed on the weld bead surface, weld geometry, fracture surfaces and mechanical properties were investigated by keeping the laser power (2500 W), and the scanning speed (55 mm/s) was constant. It has been determined that the rear surfaces of the laser-welded specimens have more spatter effects than the front surfaces. Low level (70°) or high level (90°) laser angle was achieved a good result in terms of weld geometry rather than an intermediate level. High strength and relatively high percent elongation values were obtained in the tensile test: the highest shear force was achieved as 5.8266 kN in the sample with a laser angle of 70°. In addition, the shear force and the fusion zone bonding distance were correlated. Cleavage fractures in specimens produced with a low laser angle (70°), demonstrated high embrittlement; the fracture surfaces were ductile and the voids formed were small in size in specimens manufactured with a high laser angle (90°). The high laser angle parameter (90°) was caused the fraction region to moved away from the weld center and stayed within the Heat Affected Zone (HAZ) region.

Keywords – *Laser welding, welding parameters, fracture surface, mechanical properties, DP1200 steel,*

[1] meryemaltay@uludag.edu.tr
[2] hakanay@gmail.com
*Sorumlu Yazar

1. Giriş

Lazer ışını yüksek genliğe sahip, aynı frekanslı ve birbirine paralel dalgalardan oluşur. Lazer kaynak metodu, lazer ışınının kaynak yapılacak yüzeye aktarılması, malzemelerin ergitilerek birleştirilmesi prensibine dayanır (Şekil 1). Yüksek penetrasyon, yüksek mekanik dayanım, korozyona dayanım, düşük distorsiyon, yüksek kalitede ve hızlı üretim avantajları sayesinde tercih edilmektedir. Kaynak alanına yeterli ısı girdisi sağlandığı için ergime dar bir bölgede gerçekleşir ve deformasyondan korunur. Ancak, kullanılan temel malzemenin yansıtma özelliği olması nedeniyle verimliliğin düşmesi ve ilk yatırım maliyetinin fazla olması dezavantajlarıdır.

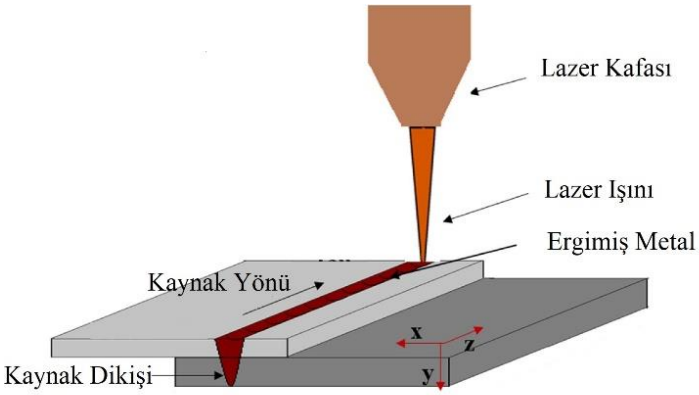

Şekil 1. Lazer kaynak metodu şematik gösterim (Indhu vd., 2018)

Lazer kaynak işleminde proses parametreleri: lazer gücü, ilerleme hızı, odak mesafesi, lazer açısı, koruyucu gazdır. İstenilen kaynak kalitesini elde edebilmek ve kaynak hatalarının önüne geçebilmek adına optimum proses parametrelerinin seçilmesi gereklidir (Altay, 2021). Alves ve ark. (2018) ferritik martenzitik özellikteki DP1000 çeliğinin birleştirmelerinde lazer kaynak yönteminin uygunluğunu araştırmışlardır. Lazer gücü (0.4 kW, 2 kW) ve kaynak hızı (20 mm/s, 150 mm/s) parametre değişimlerinin mikroyapıdaki etkilerini taramalı elektron mikroskobunda incelemişler; optimum kaynak koşulunun 2.0 kW lazer gücü ve 150 mm/sn kaynak hızı olduğunu tespit etmişlerdir (Alves vd., 2018). DP800 malzemesinin lazer kaynak işlemine yönelik çalışmalar da bulunmaktadır. Özgültekin ve ark. alın kaynak konfigürasyonunda mikroyapı ve mekanik özellikler için incelemeler gerçekleştirmişlerdir. Mikroyapıda ince tanelerin gevrek kırılmayı tetiklediğini tespit etmişlerdir (Özgültekin vd., 2022). Li ve ark. DP800 galvanizli çeliklerin birleştirilmesinde çift ışınlı lazer kaynağını kullanmışlardır. Lazer gücü (7-8-9-10 kW) ve ilerleme hızı (100 mm/s) parametre değişimlerinin ergiyik havuz ve anahtar deliği davranışı üzerindeki etkilerini bir termal kamera yardımıyla izlemişlerdir.Tandem ışın ile lazer kaynak işleminde öncü ışın gücünün azalması ile sıçrama etkisinin azaldığını tespit etmişlerdir. Ayrıca Erime Bölgesinde uzamış martenzit yapısı oluşurken, Isı Tesiri Altındaki Bölgede ise temperlenmiş martenzit ve ferrit içeren kalın martenzitlerin bulunduğunu gözlemlemişlerdir (Li vd., 2022). Kim ve ark. (2012) alüminyum alaşımlarının (5J32) bindirme kaynağında lazer gücü, kaynak hızı ve lazer geliş açısı değişkenlerinin kaynak dikişi şekli ve kopma mukavemetine etkilerini incelemişlerdir. Lazer gücü arttıkça ve kaynak hızı azaldıkça çekme mukavemeti artmıştır. Proses parametrelerinin kaynak özellikleri üzerindeki etkisini belirlemek için yapılan varyans analizi sonucunda lazer gücü parametresinin en büyük etkiye sahip olduğu tespit edilmiştir (Kim & Park, 2012).

Otomotiv sektöründe son yıllarda güvenlik açısından kritik komponentlerde DP (dual phase) çelikleri tercih edilmektedir, kaynaklı birleştirmeleri kritik öneme sahiptir. Bu çalışma kapsamında, yüksek mukavemete sahip DP 1200 çelik malzeme seçilerek, bindirme kaynağı fiber lazer kaynak yöntemi için araştırılmıştır. Lazer gücü, ilerleme hızı, lazer açısı için uygun parametre değerleri belirlenerek deneyler gerçekleştirilmiş; kaynaklı bağlantılar kaynak dikiş yüzeyleri, kaynak geometrisi, kırılma yüzeyleri ve mekanik özellikler açısından incelenmiştir. Elde edilen çıktılarının hem literatüre hem de sektöre katkı sağlaması hedeflenmektedir.

2. Materyal ve Yöntem

Çalışmada kullanılan DP1200 (dual phase) çelik malzeme: akma mukavemeti 900-1100 MPa, çekme mukavemeti 1180-1350 MPa ve minimum uzama %6 değerlerine sahiptir. Tablo 1'de kimyasal kompozisyonu gösterilmiştir.

Tablo 1
DP1200 malzemesinin kimyasal kompozisyonu

Element	C	Si	Mn	Al	P	S	Cr+Mo	Nb+Ti
% ağırlık	0.23	1	2.9	0.15-1	0.05	0.01	1	0.15

Kaynak işlemleri 1070 nm dalga boyu, 100 µm lazer ışın çapı, maksimum 6 kW lazer gücüne sahip fiber lazer kaynak teknolojisi ile üretilen lazer ışını ile gerçekleştirilmiştir. Kullanılan fiberi 0.2 mm, odak lensi 200 mm, kolimatör lensi 100 mm, lazer ışını odak çapı 0.4 mm, odaklamada kullanılan mesafe 190 mm değerlerindedir. Fiber optik kablolar ve altı eksende çalışabilen KUKA marka robot sayesinde lazer ışını hareket ettirilmektedir (Şekil 2). Koruyucu gaz olarak 12 lt/dk akış hızında Argon kullanılmıştır.

Şekil 2. Lazer kaynak işlemlerinde kullanılan cihaz

Birleştirilecek sac malzemeler bindirme kaynağı formunda konumlandırılmıştır, plakaların boyutları (Şekil 3)'de gösterilmiştir. Lazer ışını, bindirme mesafesinin ortasına konumlandırılarak kaynak işlemi uygulanmıştır

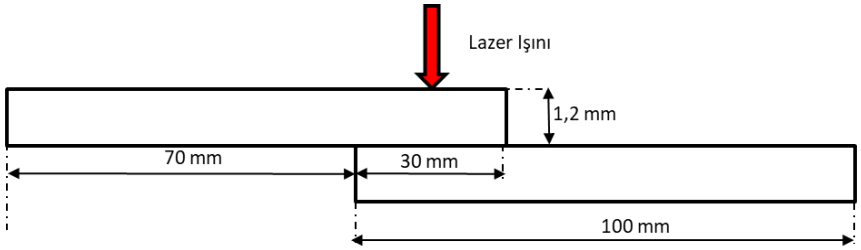

Şekil 3. Fiber lazer bindirme kaynak formu

Lazer kaynak işleminde yüksek etkinliğe sahip lazer gücü, ilerleme hızı, lazer açısı parametreleri incelenmek üzere belirlenmiştir. Otomotiv sektöründeki uygulamalarda kullanılmakta olan parametre değerleri tespit edilmiştir, belirlenen değerler (Tablo 2)'de gösterilmiştir. Lazer açısı değişiminin kaynak dikiş yüzeyleri, kaynak geometrisi, kesme kuvveti, kırılma yüzeyine etkileri incelenmiştir. Isı girdisi, lazer gücü ve ilerleme hızı parametrelerinin birbirine oranlanması ile hesaplanmaktadır (Eşitlik 2.1), kaynak işlemleri sırasında ısı girdisi 45.45 J/mm'dir.

$$Isı\ Girdisi\left(\frac{J}{mm}\right) = \frac{Lazer\ Gücü\ (W)}{İlerleme\ Hızı\ (\frac{mm}{s})} \quad (2.1)$$

Tablo 2
Çalışmada kullanılan işlem parametreleri

Deney No	Lazer Gücü (W)	İlerleme Hızı (mm/s)	Lazer Açısı (°)	Isı Girdisi (J/mm)
1	2500	55	70	45.45
2	2500	55	80	45.45
3	2500	55	90	45.45

Metalografik inceleme ve çekme deneyleri için, lazer kesim yapılarak kaynak işlemi uygulanmış plakalardan numuneler üretilmiştir. Numuneler metalografik kesme cihazı ile kesilerek bakalite alınmış, zımparalama ve parlatma işlemleri yapılmıştır. Mikroyapının ortaya çıkarılması için uygulanan dağlama işleminde %3 Nital kullanılmıştır. Nikon Eclipse MA100 mikroskobu ve Clemex programı ile numunelerin 50 büyütmede fotoğrafları alınmıştır.

Çekme deneyinde kullanılacak numuneler lazer kesim yöntemiyle elde edilmiştir (Şekil 4) (Liu vd., 2020). Çekme deneyleri 3 mm/dk çekme hızında UTEST-7014 çekme test cihazında yapılmıştır. Çekme deneyleri üç adet numune ile gerçekleştirilerek sonuçların ortalaması hesaplanmıştır. Deneyler gerçekleştirildikten sonra maksimum kesme kuvveti ve yüzde uzama değerleri belirlenmiştir; numunelerin kırılma yüzeyi Scanning Electron Microscope (SEM) ile incelenmiştir.

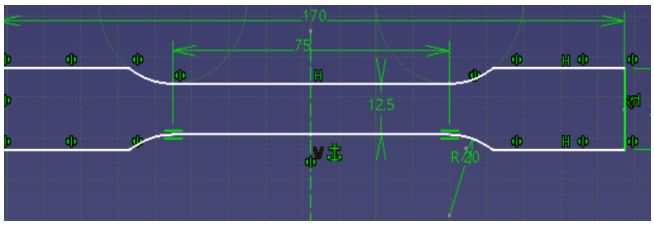

Şekil 4. Çekme deneyi numune boyutları

3. Bulgular ve Tartışma

3.1. Kaynak Dikişi İncelemeleri

Numunelerin kaynak dikiş yüzeyi ilerleme yönüne zıt doğrultuda olacak şekilde, dışbükey bir yapıdadır (Şekil 5). Numunelerin tamamında tam penetrasyon gerçekleşmiştir: bu durum ısı girdisinin yeterli düzeyde olduğunun göstergesidir. Kaynak dikişinde sıçrama problemleri gözlenmiştir (spatter effect). Ergiyik haldeki metal üzerinde geri tepme basıncı, yüzey gerilimi ve viskozite etkileri bulunmaktadır, sıvı hareketi bu etkiler ile birlikte metal kaynak havuzunun arka tarafına doğru gerçekleşir. Geri tepme basıncı etkisiyle anahtar deliği dinamik dengesi değişir ve ergimiş metal damlacıklar şeklinde kaynak dikişi ve çevresine sıçramaktadır. Numunelerin kaynak dilişi ön ve arka yüzey görüntüleri çekilmiştir ve sıçrama (spatter) etkisi ortaya konulmuştur, Şekil 6 ve Şekil 7'de gösterilmektedir. Sıçrama etkisi numunelerin arka yüzeyinde daha fazla görülmüştür.

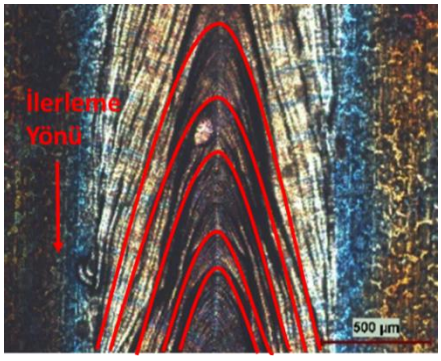

Şekil 5. Lazer kaynak dikişi görüntüsü (50 büyütme)

Ergiyik metal, ilerleme yönünün tersinde ve aşağı yönde hareket etme eğilimindedir:bu hareketlerinde geri tepme basıncı etkisi ve yer çekimi etkilidir, yukarıya hareket yüzey gerilimi nedeniyle daha zordur. Alt yüzeyde sıçrama etkisinin daha fazla gözlemlenmesinin nedeni geri tepme basıncı, yüzey gerilimi ve yer çekimi etkisi ile ergimiş metalin hareketinin aşağı yönde olmasındandır. Metal ergiyiğin geriye doğru hareketi olsa da yüzeyin üst kısmına sıçrama etkisinin meydana gelmesi zordur; aşağıya akış, geriye akış hareketinden hızlı gerçekleşmektedir. Ek olarak, kaynak sırasında bir buhar bulutu oluşmaktadır. Buhar bulutunun yarattığı geri tepme basıncı etkisiyle sıvı metal aşağı yönde hareket eğilimindedir. Anahtar deliği çıkışının yüzey gerilimi sebebiyle dar olmasıyla buhar bulutu ile birlikte dışarıya çıkan metal, damlacık olarak anahtar deliğinden sıçrama gerçekleştirmektedir (M. J. Zhang vd., 2013).

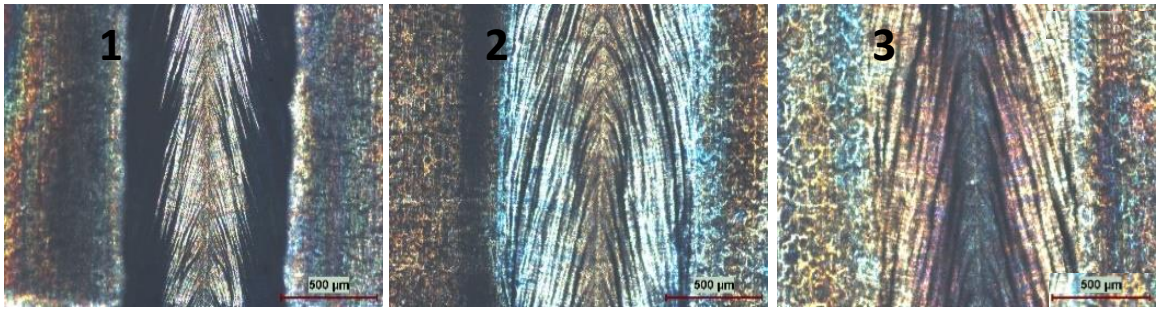

Şekil 6. Numunelerin ön yüzey kaynak dikişi görüntüleri

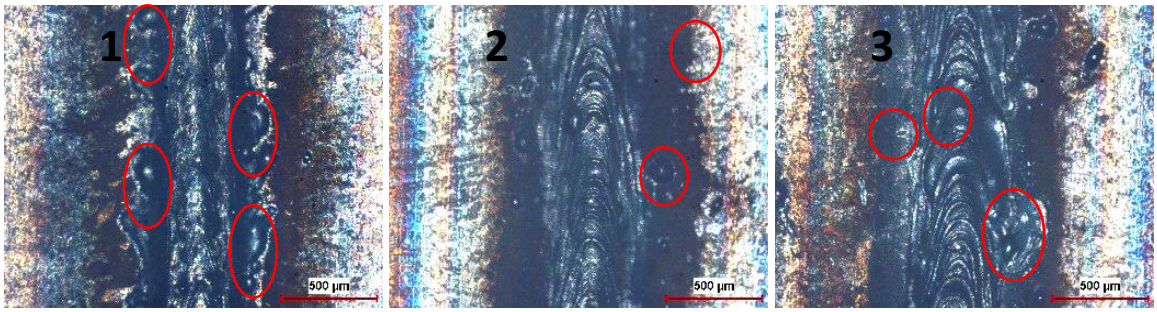

Şekil 7. Numunelerin arka yüzey kaynak dikişi görüntüleri

3.2. Kaynak Geometrisi İncelemeleri

Numunelerin enine kesiti incelendiğinde, tüm numunelerde tam penetrasyon gerçekleştiği görülmüştür (Şekil 8). Kaynak şekli ısı girdisine göre değişkenlik göstermektedir: ısı girdisi yeterli ise kum saati biçiminde, ısı girdisi az ise yetersiz penetrasyon nedeniyle koni biçimini almaktadır.

Kaynak bölgesinde mikro yapı erime bölgesi (EB), Isı Tesiri Altındaki Bölge (ITAB) ve temel malzeme (TM) bölgelerinden oluşmaktadır (Elitaş, 2021). Numunelerin optik mikroskopta çekilen genel mikro yapı görüntüleri Şekil 9'da verilmiştir. Çift fazlı DP1200 çeliği ferrit ve martenzitten oluşmaktadır. EB sıcaklığı, malzemenin erime noktasını geçtiğinden füzyon bölgesinde iç yapı soğuma sırası katı hal dönüşümlerine göre değişkenlik göstermektedir. ITAB'da, tamamen erime gerçekleşmemesine rağmen oldukça yüksek sıcaklıklara ulaşılır. ITAB mikro yapısı maksimum sıcaklığın etkisinde gerçekleşen faz dönüşümlerine bağlıdır. EB ve ITAB geometrik uzunlukları proses parametreleri değişimi ile farklılık göstermektedir. Deney numunelerinin maksimum ve minimum kaynak genişlikleri, ITAB genişlikleri üst ve alt plaka için ölçülmüştür, kaynak geometrileri Tablo 3'de verilmiştir.

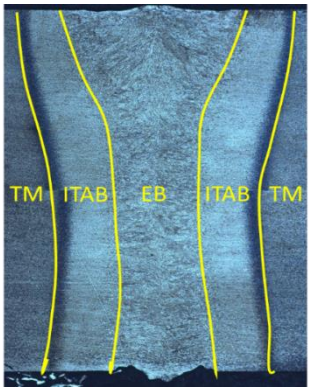

Şekil 8. Kaynak alanında oluşan mikro yapı bölgeleri

Kaynaklı bağlantıda EB'nde tam birleşmenin gerçekleşmediği, plakalar arasında boşluk bulunduğu tespit edilmiştir; kaynak sırasında üst ve alt plakalar arasında bir miktar boş mesafe kaldığı için bu durum gerçekleşmiştir. EB tam birleşme bölgelerinin görüntüleri Şekil 10'da, ölçülen kaynak geometrileri Tablo 3'te verilmiştir.

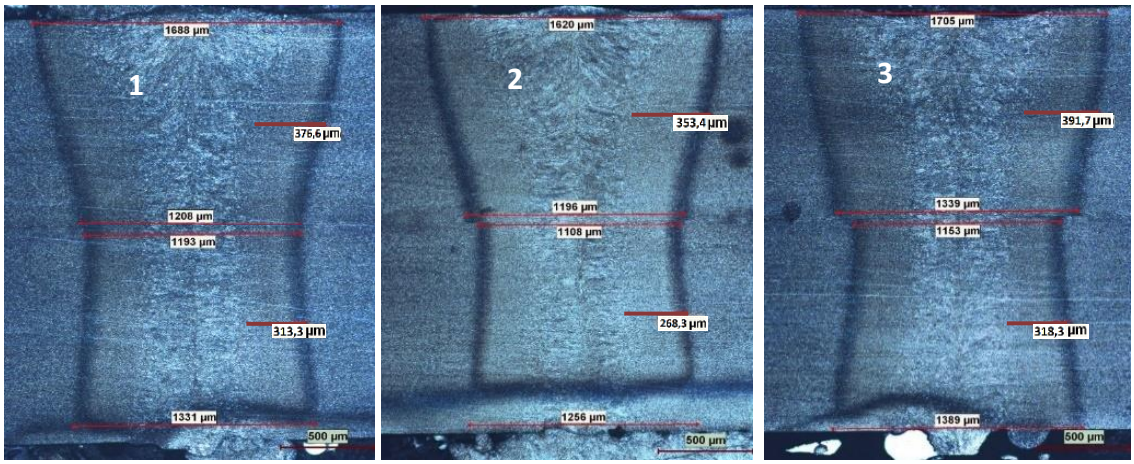

Şekil 9. Numunelerin mikro yapı görüntüleri

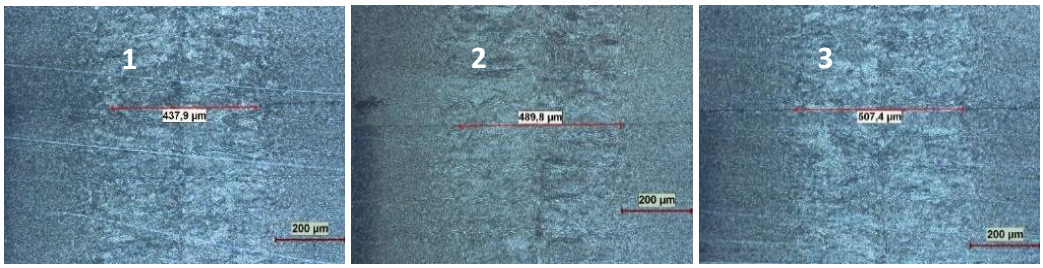

Şekil 10. Numunelerin EB tam birleşme mesafeleri

Tablo 3
Numunelerin ölçülen kaynak geometrileri

Deney No	Üst Plaka Maksimum Genişlik (µm)	Üst Plaka Minimum Genişlik (µm)	Alt Plaka Minimum Genişlik (µm)	Alt Plaka Maksimum Genişlik (µm)	Üst Plaka ITAB Genişliği (µm)	Alt Plaka ITAB Genişliği (µm)	Bonding Mesafesi (µm)
1	1688	1208	1193	1331	376.6	313.3	437.9
2	1620	1196	1108	1256	353.4	268.3	489.8
3	1705	1339	1153	1389	391.7	318.3	507.4

70° ve 80° lazer açısı parametresi ile kaynak işlemi gerçekleştirilen "1" ve "2" numaralı numuneler kıyaslandığında, "1" numaralı numunede daha yüksek geometrik uzunluk değerleri ölçülmüştür. 90° lazer açısına sahip "3" numaralı numunede elde edilen değerler ise, 70° lazer açısına sahip "1" numunesi ile yakın olmakla birlikte daha yüksektir. Lazer açısı parametresi değiştirildiğinde farklılaşan kaynak geometrisi Şekil 11'de gösterilmektedir, ısı girdisi 45.45 J/mm olarak sabittir. Parametre değerleri aynı ısı girdisi için incelendiğinde lazer açısının düşük ya da yüksek seviyede (70° ya da 90°) kullanılmasının kaynak geometrisi için iyi sonuçlar getireceği söylenebilir.

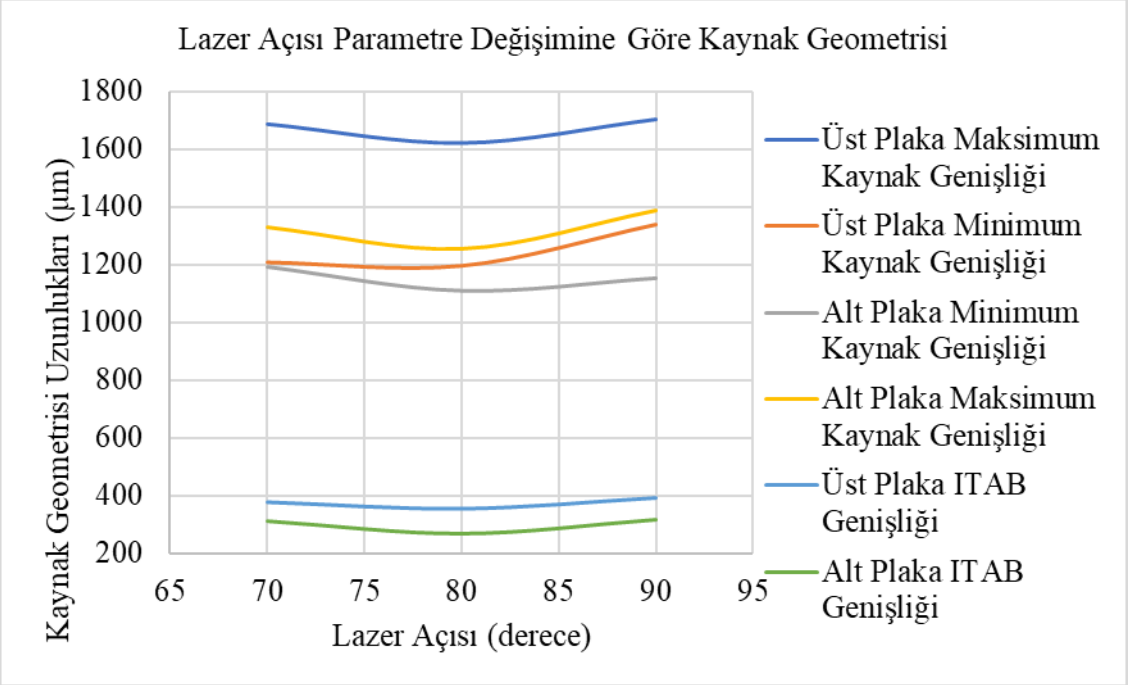

Şekil 11. Lazer açısı parametresinin ölçülen kaynak geometrik uzunluklarına etkisi

3.3. Mekanik Dayanım İncelemeleri

Mekanik özelliklerinin belirlenmesi için çekme testi uygulanmıştır: kesme kuvveti ve yüzde uzama değerleri alınmış; kaynaklı bağlantının bir birime (mm) karşılık gelen taşıyabileceği yük hesaplanmıştır (Tablo 4).

Gerçekleştirilen deneyler sonucunda genel olarak yüksek kesme kuvveti ve yüzde uzama değerlerine ulaşılmıştır. En yüksek kesme kuvveti 70° lazer açısına sahip numunede 5.8266 kN olarak elde edilmiştir, birim başına taşıyabileceği yük 46.6125 kg ve yüzde uzama miktarı %0.3891'dir. En düşük kesme kuvveti ise 80° lazer açısına sahip numunede 4.9672 olarak elde edilmiştir, birim başına taşıyabileceği yük 39.7375 kg ve yüzde uzama miktarı %0.3273'dır.

Lazer açısının düşük seviyede (70°) olması, maksimum kesme kuvveti ve uzama değerlerinin elde edilmesinde etkilidir. Yüksek seviye lazer açısı parametresinde (90°) de nispeten yüksek mekanik özellikler elde edilmiştir,

en düşük mekanik özellikler ise lazer açısının 80° olduğu numunede elde edilmiştir. Mekanik özelliklerin üretim parametreleri ile doğrudan ilişkili olduğu yorumu yapılabilir. Kumar ve ark. AISI 304 paslanmaz çeliklerin Nd:YAG lazer kaynağında lazer açısı parametre değişimini 83°, 85.5° ve 89.7° değerleri için incelemişlerdir. Lazer açısı 85.5° için maksimum kesme mukavemeti 579.26 MPa olarak elde edilmiştir (Kumar,2017).

Tablo 4
Çekme testi sonucunda elde edilen değerler

Deney No	Maksimum Kesme Kuvveti (kN)	Birim (mm) başına taşınan yük (kg)	Uzama (%)
1	5.8266	46.6125	0.3891
2	4.9672	39.7375	0.3273
3	5.1443	41.1542	0.2820

Çekme testinde elde edilen maksimum kesme kuvveti, kaynak geometrisinde EB tam birleşme mesafesi değerleri ile ilişkilendirilmiştir. İngilizce "bonding" olarak adlandırılan bu geometrik uzunluğun kaynak kalitesinde etkinliği vardır (Kouadri-Henni, 2017). Maksimum kesme kuvveti ile "bonding" uzunlukları arasındaki ilişki Şekil 12'de gösterilmiştir; grafikler genel anlamda örtüşmektedir, artma ve azalma eğilimi doğru orantılıdır.

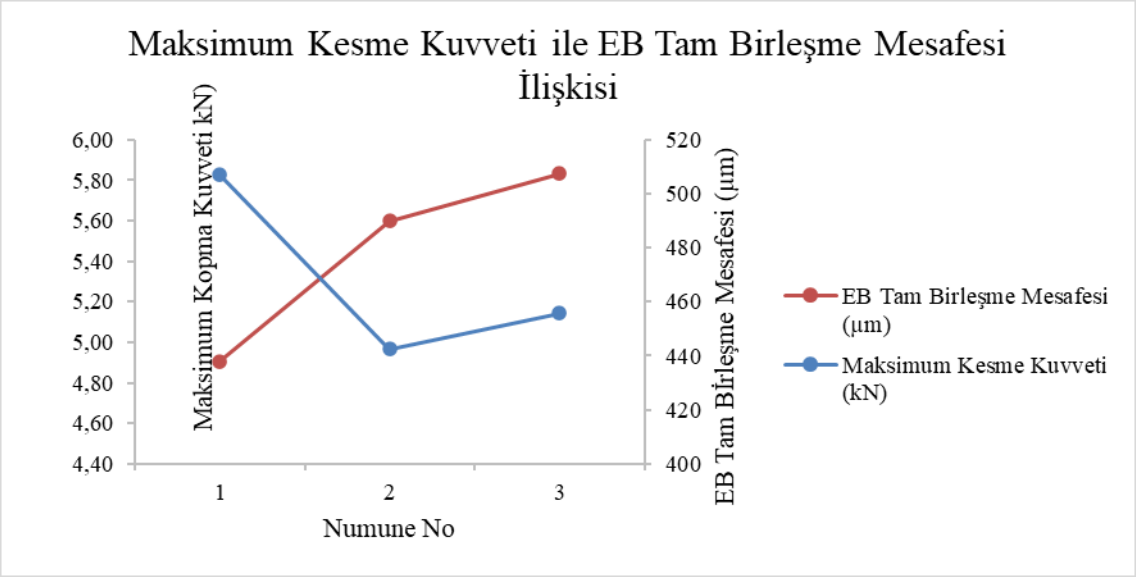

Şekil 12. Maksimum kesme kuvveti ile EB tam birleşme mesafesi değerlerinin ilişkisi

3.4. Kırılma Yüzeyi SEM İncelemeleri

Kırılma morfolojilerinde "dimples" olarak açıklanan büyük ve sığ çukurlar sünek kırılmayı işaret eder; gevrek bölgeler ise "klivaj" kavramıyla açıklanır, tokluğun zayıf olduğunun göstergesidir.

DP1200 çeliklerde sünek ve gevrek yapı birlikte bulunur: sünek özellikteki ferrit sayesinde plastik deformasyon oluşabilir, martenzit ise yüksek sertliğe sahip olduğundan deformasyon daha az oluşacaktır. İncelenen numunelerin kırılma yüzeyleri farklı büyütmeler altında (250, 500, 750, 1000, 2000, 4000) SEM cihazında alınmıştır.

"1" numaralı numunenin kırılma yüzeyi incelendiğinde klivaj kırılmalarının yoğun olduğu gözlenmektedir, klivaj kırılmalar gevrek bir yapının göstergesidir, sünekliği ifade eden boşluk ve çukurlar bulunmamaktadır (Şekil 13). Kırılma bölgesinde düz bir yüzey oluşmuştur ve bölünme sırtları bulunmaktadır. Düşük lazer açısı parametre kullanımı ile, gerçekleşen klivaj kırılmaları yüksek gevreklik ve yüksek sertlik ile ilişkilendirilebilir. Ayrıca düşük lazer açısı (70°) parametresi ile üretim sonucunda numunede kırılma, erime bölgesinden meydana gelmiştir.

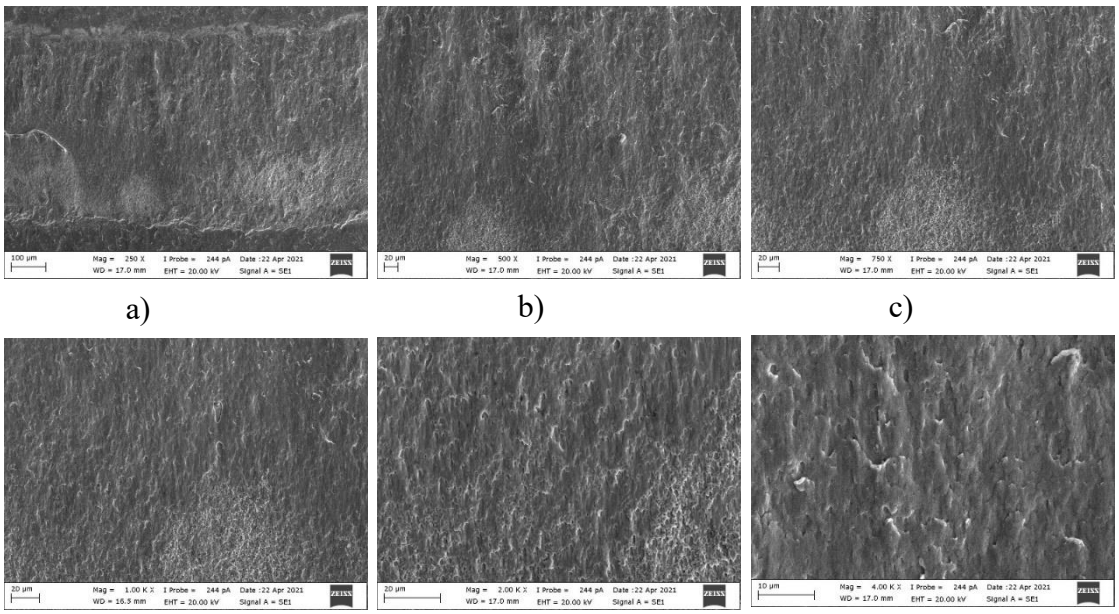

a) b) c)

d) e) f)

Şekil 13. "1" numaralı numune kırılma yüzeyi incelemeleri

Numune "2" kırılma yüzeyindeki çukurlar sünekliğin göstergesidir, oluşan çukur boyutları küçülmüştür (Şekil 14). Büyük çukur oluşumlarındansa, ince ve küçük boyutlu çukur oluşumları tokluğun daha fazla olduğunun kanıtıdır. Kırılma, ITAB bölgesi içerisinden gerçekleşmiştir; çukurların çok küçük boyutlu olması ile sünekliğin yüksek ve kırılmanın intergranüler olduğu söylenebilir. Şekil 14.a-b'deki elips şeklinde siyah renkli oluşumların gözenek olduğu yorumu yapılabilir.

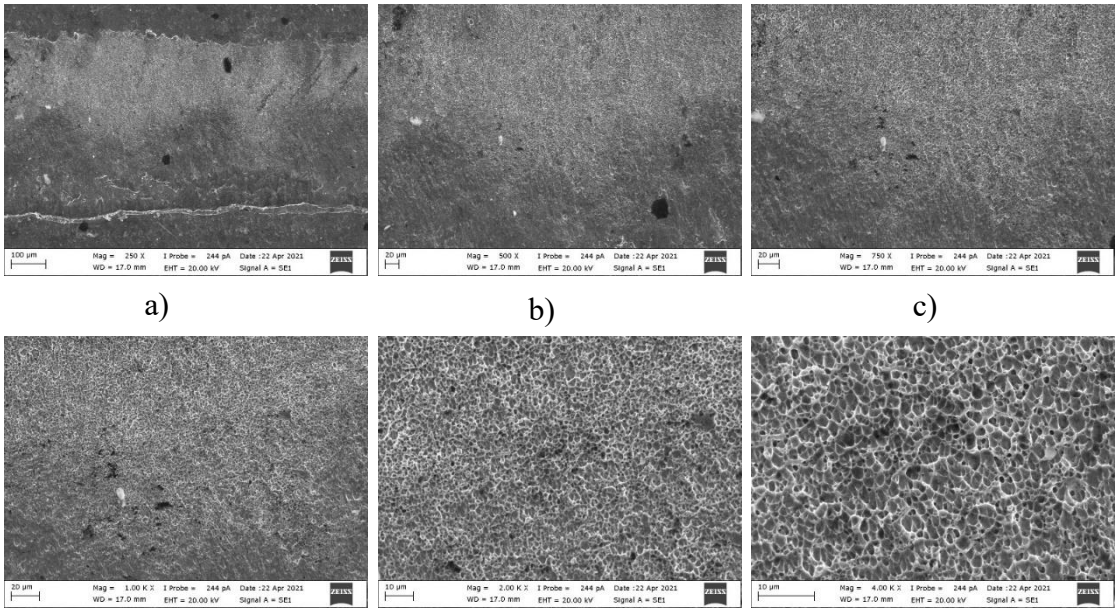

a) b) c)

d) e) f)

Şekil 14. "2" numaralı numune kırılma yüzeyi incelemeleri

Numune "3" için incelenen kırılma yüzeyi görüntüleri Şekil 15'dedir. Kırılma yüzeyinde gözlemlenen ufak yapılı dimple oluşumları sünek morfolojinin göstergesidir. Tane sınırlarında gerçekleşen gerilme yığılmaları düşük uzama elde edilmesinde etkili olmuştur. Mikro yapı ince taneli olduğu için kırılmanın ITAB bölgesinden gerçekleştiği söylenebilir. Lazer açısının yüksek seviye (90^{o}) kullanılması ile kırılma, erime bölgesinden ITAB

bölgesine kaymıştır. Lazer açısı parametresinin düşük olması ise gevrekliği artırarak kırılmanın EB'den gerçekleşmesini sağlamıştır. Şekil 15.a'da gözlemlenen siyah renkli nokta benzeri yapıların ise gözenek olduğu yorumu yapılabilir.

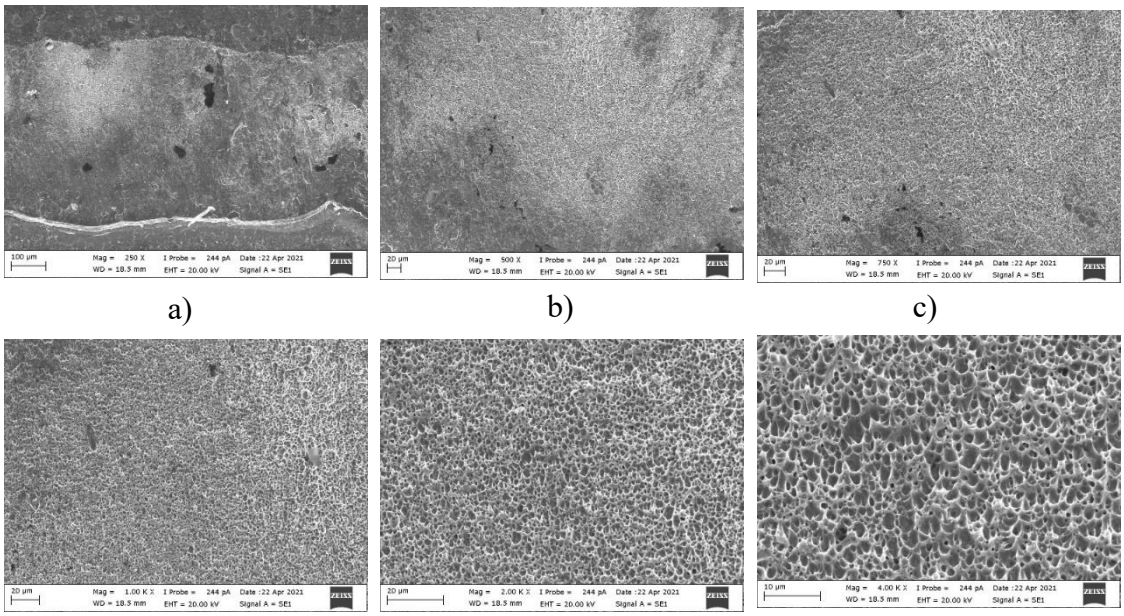

a) b) c)

d) e) f)

Şekil 15. "3" numaralı numune kırılma yüzeyi incelemeleri

4. Sonuçlar

Bu çalışmada DP 1200 çift fazlı çelik malzeme, fiber lazer kaynak metodu ile bindirme formunda birleştirilmiştir. Lazer gücü ve ilerleme hızı sabit tutularak lazer açısı parametresinin değişiminin kaynaklı bağlantıların kaynak dikiş yüzeyi, kaynak geometrisi, kırılma yüzeyleri ve mekanik özelliklere etkisi incelenmiştir. Lazer kaynaklı numunelerin arka kaynak dikiş yüzeylerinde, ön yüzeylerine göre sıçrama etkileri daha fazladır: Ergiyen metal, geri tepme basıncı ve yer çekimi etkisi ile ilerleme yönünün tersinde aşağıya doğru hareket etmektedir. Lazer kaynak sonrası tüm numunelerde tam penetrasyon elde edilmiştir. Kaynak geometrileri proses parametreleri ile değişkenlik göstermektedir. Eşit ısı girdisi için inceleme yapıldığında lazer açısının, düşük (70^o) ya da yüksek seviyede (90^o) kullanılmasının kaynak geometrisi açısından optimum sonuçlar vereceği söylenebilir. Çekme testinde yüksek kuvvet ve uzama değerleri elde edilmiştir. En yüksek kesme kuvveti 70^o lazer açısına sahip numunede 5.8266 kN olarak elde edilmiştir, birim başına taşıyabileceği yük 46.6125 kg ve yüzde uzama miktarı %0.3891'dir. Maksimum kesme kuvveti ve uzama değerlerinin elde edilmesinde lazer açısının düşük seviyede (70^o) kullanılması etkili olmuştur. Kesme kuvvetinin, tam birleşme mesafesi (bonding) ile bağlantılı olduğu ortaya konulmuştur. Düşük lazer açısı numunelerinde yüksek gevrekliğin göstergesi klivaj kırılmalar elde edilmiştir, kırılma kaynak merkezinden (EB) gerçekleşmiştir. Yüksek lazer açısı ile üretilen numunelerde ise kırılma yüzeyleri sünektir ve oluşan çukurlar küçük boyutludur. Lazer açısı parametresinin yüksek olması (90^o) kırılmanın ITAB içerisinde kalmasını sağlamaktadır.

Teşekkür

Bu çalışma Bursa Uludağ Üniversitesi Bilimsel Araştırmalar Proje Birimi tarafından desteklenen OUAP (MH)-2019-6 numaralı proje kapsamında gerçekleştirilmiştir. Yazarlar, fiber lazer kaynak işlemlerinin gerçekleştirilmesinde sağladığı imkanlar dolayısıyla LASER ISSE firmasına teşekkür eder.

Yazar Katkıları

Meryem Altay: Verilerin toplanması, analizi ve makale yazımı konularında katkıda bulunmuştur.

Hakan Aydın: Çalışmanın tasarlanması, verilerin analizi ve yorumlanması konularında katkıda bulunmuştur.

Çıkar Çatışması

Yazarlar çıkar çatışması bildirmemişlerdir.

Kaynaklar

Altay, M. (2021). *Otomotiv Endüstrisinde Kullanılan Yüksek Mukavemetli DP1200 Çeliğinde Lazer Kaynak Parametrelerinin Optimizasyonu* (Yüksek Lisans tezi). Erişim adresi: https://tez.yok.gov.tr/UlusalTez-Merkezi

Alves, P. H. O. M., Lima, M. S. F., Raabe, D., & Sandim, H. R. Z. (2018). Laser beam welding of dual-phase DP1000 steel. *Journal of Materials Processing Technology*, *252*, 498–510. https://doi.org/10.1016/j.jmatprotec.2017.10.008

Elitaş, M. (2021). Effects of welding parameters on tensile properties and fracture modes of resistance spot welded DP1200 steel. *Materials Testing for Welding and Additive Manufacturing Applications, 63 (2), 124-130.* https://doi.org/10.1515/mt-2020-0019

Indhu, S., Saundarapandian, S. ve Vijayaraghavan, L. (2018). Yb: YAG laser welding of dual phase steel to aluminium alloy. *Journal of Materials Processing Technology*, 262, 411-421. 10.1016/j.jmatprotec.2018.05.022

Kim, D. Y., & Park, Y. W. (2012). Weldability evaluation and tensile strength estimation model for aluminum alloy lap joint welding using hybrid system with laser and scanner head. *Transactions of Nonferrous Metals Society of China*, *22*(3), 596–604. https://doi.org/10.1016/S1003-6326(12)61771-3

Kouadri-Henni, A. (2017). Effect of welding laser process on macrostructures and the mechanical properties of coating steel DP600: Influence of vaporization zinc. *Journal of Manufacturing Processes*, *30*, 83–96. https://doi.org/10.1016/j.jmapro.2017.07.025

Kumar, N., Mukherjee, M., Bandyopadhyay, A. (2017). Study on laser welding of austenitic stainless steel by varying incident angle of pulsed laser beam. *Optics and Laser Technology*, 94, 296-309. http://dx.doi.org/10.1016/j.optlastec.2017.04.008

Li, Y., Zhu, Z., Tang, X., Han, S., Zhang, R. Cui, H. (2022). Improvement of welding stability and mechanical properties of galvanized DP800 steel lap joint by high-speed tandem beam laser. *Optics and Laser Technology, 150*(107958). https://doi.org/10.1016/j.optlastec.2022.107958

Liu, G., Gao, X. D., Peng, C., Liu, X. H., Huang, Y. J., Zhang, Y. ve You, D. Y. (2020). Tensile resistance, microstructures of intermetallic compounds, and fracture modes of welded steel/aluminum joints produced using laser lap welding. *Transactions of Nonferrous Metals Society of China*, *30*(10), 2639–2649. https://doi.org/10.1016/S1003-6326(20)65408-5

Özgültekin, A. G., Başer, T., Tekelioğlu, O., Tamer, E., Aydın, B., Alpay, B. (2022). Effects of different laser welding parameters on the microstructural and mechanical properties of an advance dual phase steel grade. *Journal of the Faculty of Engineering and Architecture of Gazi University, 37* (1), 455-468. 10.17341/gazimmfd.846628

Zhang, M. J., Chen, G. Y., Zhou, Y., Li, S. C. ve Deng, H. (2013). Observation of spatter formation mechanisms in high-power fiber laser welding of thick plate. *Applied Surface Science*, *280*, 868–875. https://doi.org/10.1016/j.apsusc.2013.05.081

e-ISSN 2757-5195

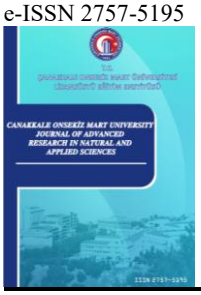

Çanakkale Onsekiz Mart University

Journal of Advanced Research in Natural and Applied Sciences

Open Access

doi.org/10.28979/jarnas.1172336 2023, Vol. 9, Issue 1, Pages:89-106 dergipark.org.tr/tr/pub/jarnas

Effect of Turntable Rotation Rate on Drying Kinetics and Functional Properties of Lemon Peel during Microwave Drying

Işıl Barutçu Mazı[1,*], Sevilay San[2]

[1,2] Department of Food Engineering, Faculty of Agriculture, Ordu University, Ordu, Türkiye

Article History

Received: 08.09.2022

Accepted: 12.10.2022

Published: 05.03.2023

Research Article

Abstract – The aim of this study is to investigate the effect of the rotational rate of the turntable on drying kinetics of lemon peels and some functional and flow properties of lemon peel powders. Lemon peels were dried by microwave drying using different rates of rotation (0, 6.5, 9.5, and 12.5 rpm) at different microwave power levels (180W, 300W, 450W and 600W), and dried by oven drying and freeze-drying methods. Drying time was shortened by 72-95% by microwave drying compared to oven drying. Microwave drying with rotation provided 5.6-23.8% reduction in drying time of peels compared to drying without rotation. Effect of rotation rate on drying time of lemon peels depended on the microwave power level. Page model provided lower SSE, RMSE, and higher R^2 values within 5 different thin layer models. The effective moisture diffusivity value, ranging between $1.7x10^{-8}$ m^2s^{-1}-$7.6x10^{-8}$ m^2s^{-1}, was higher during microwave drying with rotation. The activation energy ranged between 21.3-22.7 W/g. Microwave drying provided higher bulk density, similar or lower water holding capacity and oil retention capacity values compared to freeze drying and oven drying. Freeze dried lemon peel powder had the lowest bulk density due to its porous structure. Microwave drying without rotation and the highest power level caused lower bulk density. At higher power levels, influence of turntable rotation on water holding capacity was more notable. Microwave drying technique can be used as alternative drying techniques to obtain high quality dried lemon peel powder if appropriate processing conditions are selected.

Keywords – *Drying kinetics, functional properties, lemon peel, microwave drying, turntable,*

1. Introduction

Nowadays, there has been a growing interest in utilization of agro-industrial by-products (Trigo et al., 2020). Citrus fruits are one of the most cultivated crops worldwide. Citrus family includes economically important fruits such as orange, lemon, grapefruit, mandarin. World citrus fruit production was nearly 143.8 million tons in 2019 (FAO, 2021). During fruit juice processing, approximately 50-70% of the citrus fruits are discarded as waste (Zema et al., 2018). Globally, 110–120 million tons of citrus waste are produced from citrus processing industries yearly (Mahato et al., 2020). Citrus waste includes peel (flavedo+albedo), pulp (vesicular membranes), rag (core, carpellary membranes) and seeds. Citrus peel is a rich source of valuable phytochemicals, and dietary fibers and thereby may be utilized in preparation of new food products. However, it is prone to quick spoilage due to its high moisture content and thereby requires preservation for later use. Citrus peel powders obtained by drying can be used as an ingredient for innovative food formulations (Trigo et al., 2020).

Various drying techniques have been employed for drying citrus peels with the aim of achieving improved product quality in a shorter time. Among the artificial drying methods, hot-air drying is the most widely used

[1] ibarutcu@odu.edu.tr

[2] sevilaysan1993@gmail.com

[*]Corresponding Author

method for drying of citrus peels. Microwave drying is known to offer opportunity of high drying rate, especially in the falling rate period. Some researchers studied on the effects of microwave drying on drying kinetics and various quality properties of citrus peels (Ozcan et al., 2020; Farahmandfar et al., 2019, 2020; Abou Arab, Mahmoud, & Abu-Salem, 2017; Ghanem et al., 2012, 2020; Bejar, Kechaou, & Mihoubi, 2011b; Tekgül & Baysal, 2018; Tuncer, Güler, & Usta, 2020; Kirbas et al., 2019) and noted that microwave drying may be used as a convenient and effective drying method for drying of citrus peels.

Drying kinetics is used to express the water removal process. The rate of water removal depends on many factors and changes with time during drying. The understanding of drying kinetics helps the control and optimization of drying processes. For fruits and vegetables, thin layer drying models have been found in wide application (Onwude et al., 2016). Some semi-theoretical and empirical models have been used to describe the relationship between the moisture content and the drying time of citrus peels. Bejar et al. (2011b) indicated that microwave drying kinetics of Maltaise orange peel was well described by Page model. 9 different thin layer models were used to describe the dehydration behavior of lemon peel during microwave drying by Ghanem et al. (2020). These studies indicated that dehydration rate and some quality characteristics of citrus peels were influenced by microwave power level.

In the microwave drying process, the homogeneity of the temperature distribution in the product is extremely important in terms of drying efficiency and product quality. Turntables used in microwave ovens are one of the frequently used methods to create a homogeneous temperature distribution. To the best of the author's knowledge, no study has been conducted to investigate the effects of rotational rate of turntable on drying kinetics or quality characteristics of foods during microwave drying. In this study, it was aimed to investigate the effect of the rotational rate of turntable (0, 6.5, 9.5, and 12.5 rpm) on drying kinetics of lemon peels during microwave drying at different microwave power levels (180W, 300W, 450W and 600W). In addition, SEM images, flow properties, and some functional properties of lemon peel powders dried under different microwave drying conditions were obtained and the results were compared with the powders prepared using freeze drying and oven drying methods.

2. Materials and Methods

Fresh *Citrus limon* fruits were purchased from a local market in Giresun, Turkey and stored at 4±0.5°C until further use.

2.1 Drying Process

Lemon fruits were taken out of the refrigerator and left for 2 hours to come to ambient temperature before the experiments. The fruits without blemishes or damage were chosen, washed, and dried with tissue paper. Peels (containing flavedo and albedo) of the cleaned fruits were manually separated and cut into slices (1x1 cm).

The lemon peel samples were dried by 3 methods, which were oven drying (OD), freeze drying (FD), and microwave drying (MWD). Oven drying was performed in a fan oven (Ordel OC770) at 60°C which was selected based on the data from literature surveys about the drying of citrus peels (Garau et al., 2007; Ozcan et al., 2020). A domestic microwave oven (MC32F604TCT, Samsung) was used for microwave drying. The oven was modified so that the speed of the microwave's turntable can be adjusted. Lemon peel samples were spread in a single layer on a petri dish 115 mm in diameter. The petri dish was positioned at the center of the turntable. The drying process was carried out using 4 different microwave powers (180W, 300W, 450W, and 600W) as provided on the control panel of the microwave oven (Ghanem et al., 2020). Some preliminary tests exhibited that the samples were burned at the microwave power level higher than 600W. At each power level, the lemon peels were subjected to three different rotational rates of turntable (6.5, 9.5, and 12.5 rpm). Lemon peels were also dried using the same microwave oven without rotating the turntable at 180W, 300W, 450W, and 600W power levels. Dried lemon peels were ground into powder using a grinder for 30s (Sinbo, SCM-2934) and then sieved (40 mesh sieve). Sieved powder samples were used in the further analysis. Functional

and flow properties of microwave dried, and oven dried samples were compared with that of lemon peels dried by freeze drying in a lab-scale freeze dryer (FreeZone 2.5L 7670530, Labconco) at -50°C and 0.1 mbar vacuum pressure.

2.2 Determination of Moisture Content

The determination of moisture content of lemon peel was done by drying in an oven at 105 °C to constant weight (AOAC, 1995).

2.3 Drying Characteristics

2.3.1. Moisture Ratio (MR)

Lemon peel samples were dried until the moisture content of samples dropped to 0.11 g/g on dry basis. During microwave and oven drying processes, lemon peels were weighted at specified time intervals to obtain moisture content of samples. MR values were calculated from the experimental moisture content (kg water kg^{-1} dry matter) data. Each drying treatment was carried out two times. The arithmetic average of data was taken for the calculation of MR values by Equation (2.1).

$$MR = \frac{X(t)-X_e}{X_0-X_e} \tag{2.1}$$

$X(t)$, X_e and X_0 represent the moisture content obtained at any drying time, equilibrium moisture content, and the initial moisture content, respectively.

2.3.2. Drying Rate

The drying rates (DR) of lemon peels during the microwave and oven drying processes were determined using Equation 2.2. (Deng et al., 2019):

$$DR = \frac{X_{t1}-X_{t2}}{t_2-t_1} \tag{2.2}$$

DR is the drying rate (kg water kg^{-1} dry matter min^{-1}), X_{t1} and X_{t2} are the moisture contents (kg water kg^{-1} dry matter) at time $t_1$and t_2(min), respectively.

2.3.3. Kinetic Modelling

Experimental MR data were fitted to five widely used single-layer drying models given in Table 1 (Ertekin & Firat, 2017). The model parameters were estimated by nonlinear least-squares procedure using MATLAB software (R2021b, Mathwork, Inc., MA, US). For evaluation of accuracy of fit, the statistical parameters, the determination coefficient (R^2), the sum of square error (SSE), the root mean square error (RMSE) values were calculated using Eq. 2.3., 2.4, and 2.5, respectively.

$$R^2 = 1 - \left[\frac{\sum_{i=1}^{N}\left(MR_{exp,i}\text{-}MR_{pred,i}\right)^2}{\sum_{i=1}^{N}\left(MR_{exp,i}\text{-}MR_{mean}\right)^2}\right] \tag{2.3}$$

$$SSE = \sum_{i=1}^{N}\left(MR_{exp,i}\text{-}MR_{pred,i}\right)^2 \tag{2.4}$$

$$\text{RMSE}=\left[\frac{\text{SSE}}{\nu}\right]^{\frac{1}{2}} \quad \text{where } \nu = N - m \tag{2.5}$$

$MR_{exp,i}$ and $MR_{pred,i}$ are the ith experimental and predicted MR values, respectively; MR_{mean} is the mean of experimental MR values;. N is the number of experimental data points; m is the number of constants in drying model.

Table 1
Single-layer drying models

Model	**Equation**
Newton	MR= exp (-kt)
Page	MR= exp (-kt^n)
Henderson & Pabis	MR= a exp (-kt)
Logarithmic	MR= a exp (-kt)+ c
Two-term	MR= a exp (-k_0 t)+ b exp (-k_1 t)

2.3.4. Effective Moisture Diffusivity (D_{eff})

For most food materials, the internal diffusion occurring during the falling rate period is described by Fick's second law of diffusion. For a slab geometry, Crank (1979) provided the solution of diffusion equation (Equation 2.6) with the application of several boundary conditions (Onwude et al., 2016).

$$MR = \frac{8}{\pi^2}\sum_{n=1}^{\infty}\frac{1}{(2n-1)^2}\exp[-(2n-1)^2\pi^2\frac{D_{eff}}{4L^2}t] \tag{2.6}$$

For long drying times, only the first term (setting n = 1) of Equation 3.6 is used to estimate D_{eff} in many cases. Thus, the simplified equation (Equation 2.7) can be written in logarithmic form as follows:

$$\ln MR = \ln(\frac{8}{\pi^2}) - \frac{\pi^2 D_{eff}}{4L^2}t \tag{2.7}$$

D_{eff} (m^2/s) is the effective moisture diffusivity, and L is the half thickness of the slab (m). The D_{eff} can be determined from the slope of the plot of ln MR versus t.

2.3.5. Activation Energy (E_a)

For microwave drying, the activation energy may be estimated by using an Arrhenius-type relationship given as below (Onwude et al., 2016).

$$D_{eff} = D_0 \exp(-\frac{E_a m}{P}) \tag{2.8}$$

E_a (Wg^{-1}) is the activation energy, D_0 (m^2s^{-1}) is the preexponential factor of the Arrhenius equation, P (W) is the microwave output power and m (g) is the mass of the sample.

2.4 Bulk Densities

2 gr of lemon peel powder was weighted into 10 mL graduated cylinder without touching the interior wall. The volume occupied by the peel powder was noted and used to calculate poured bulk density (ρ_p). Then, the same cylinder containing powder was manually tapped until no further volumes change occurs, and the new volume was used to calculate tapped bulk density(ρ_t) (Farahmandfar et al., 2020). Bulk densities were expressed as grams per milliliter (g/ml).

2.5 The Hausner's ratio (HR) and Carr index (CI)

Carr Index (Carr, 1965) and Hausner ratio (Hausner, 1967) values were calculated from the following equations using the obtained poured bulk density (ρ_p) and tapped bulk density(ρ_t) values (Seerangurayar et al., 2017).

$$CI = \frac{\rho_t - \rho_p}{\rho_t} \, x \, 100 \tag{2.9}$$

$$HR = \frac{\rho_t}{\rho_p} \tag{2.10}$$

2.6 Water Holding Capacity (WHC)

0.5 g of powder sample was hydrated (24 h) in 30 ml of distilled water. Then, it was centrifuged at 2000g for 25 min. After decanting the supernatant, sample was weighted and the water holding capacity was calculated as g water/g dry sample (Romdhane et al., 2015).

2.7 Oil Retention Capacity (ORC)

0.5 g of powder sample was mixed with 10 ml of sunflower oil. Then, it was centrifuged at 2000g for 20 min. The supernatant was decanted, and the oil retention capacity was calculated as g oil/g dry sample (Romdhane et al., 2015).

2.8 Microstructure

The lemon powder samples were fixed with carbon tape on the sample holder plate and then coated with gold and the microstructure of powder samples were evaluated with scanning electron microscope (SEM) (SU1510; Hitachi, Tokyo, Japan) at 10kV.

2.9 Statistical Analysis

Data were presented as means ± standard deviations. Mean comparisons were performed by Analysis of variance (ANOVA) at a 5% significance level. (Minitab 17). Multiple comparisons were carried out using Tukey test.

3. Results and Discussion

3.1 Drying Process

Drying curves of lemon peels obtained during oven drying, during microwave drying were presented in Figures 1 and 2, respectively. Drying processes were continued until the moisture content of samples was reduced to about 10% (w.b.). It took nearly 130 min to reduce the moisture content of lemon peel to 9.3% moisture content by oven drying at 60 °C. During freeze drying, the time required to drop the moisture content of lemon peel to 9.23% was 8 h. Freeze drying (FD) of lemon peel took a longer time compared to oven drying. Despite of many advantages, freeze drying has been known to require long processing time. In studies on drying of citrus peels, similar findings have been recorded by different authors (Mello et al., 2020; Kirbas et al., 2019; Xu et al., 2017). Abd Rahman et al. (2016) showed that the moisture content of flavedo and albedo parts of pomelo peels reduced to 5.15 and 5.88% after drying in a convection oven at 60 °C for 24 h and reduced to 9.33 and 8.63 % after freeze drying for 96 h, respectively.

For each microwave drying condition, the time required for the moisture content of lemon peel samples to decrease from its initial moisture content of 78.4% (w.b.) to below 10.0% (w.b.) were given in Table 2. Compared to oven drying, the drying time shortened by 72.3-75.4%, 83.8-87.7%, 91.3-93.1%, and 93.5-94.6%

at 180, 300, 450, and 600W power levels, respectively by the application of microwave drying. This is an expected result since microwave drying is known to offer opportunity of high drying rate, especially in the falling rate period. In a study, Ghanem et al. (2020) reported that microwave drying is more effective in shortening drying time of lemon peel compared to infrared drying and hot air drying. Similarly, Kirbas et al. (2019) dried albedo parts of pomelo peel by microwave, forced convection and freeze drying and indicated that microwave drying provided the shortest drying time. In a different study, Talens, Castro-Giraldez, & Fito, (2016) observed that the application of microwave during hot air drying (55 °C) increased the mass reduction rate of orange peels. The result about the decrease in drying time of lemon peel with increasing power level was in accordance with the literature (Bejar et al., 2011b; Ghanem et al. 2012, 2020; Shu et al. 2020). Increasing power level from 180W to 600W provided 76.4-90.6 % shorter drying times. This is an expected result since higher power level causes increased level of energy absorption by the sample. This yields higher volumetric heat generation and consequent higher levels of moisture vapor generation creating significant pressure inside the food material.

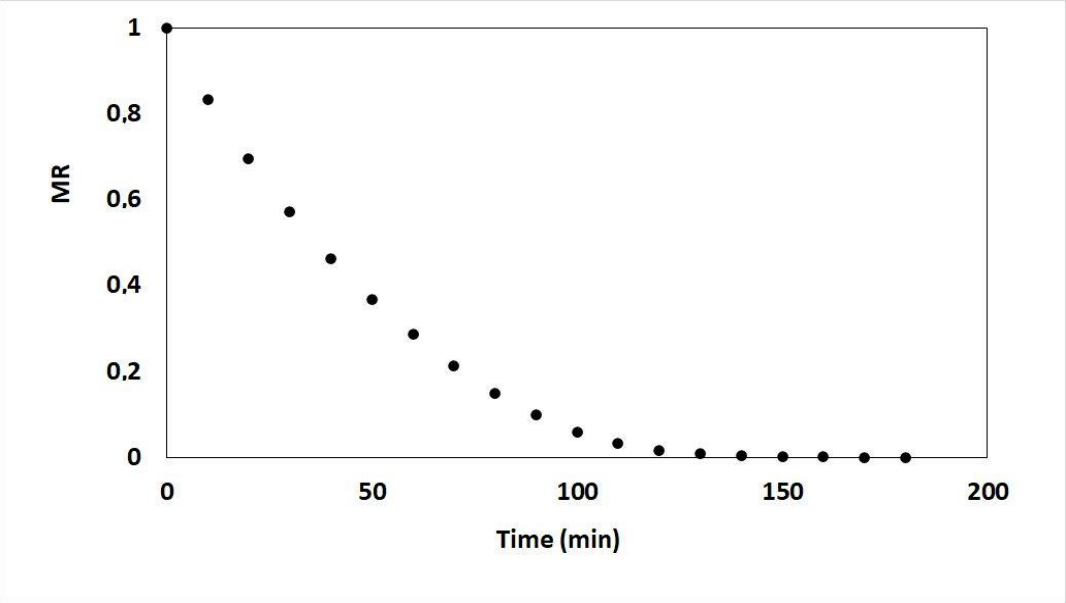

Figure 1. Drying curve of lemon peel during oven drying

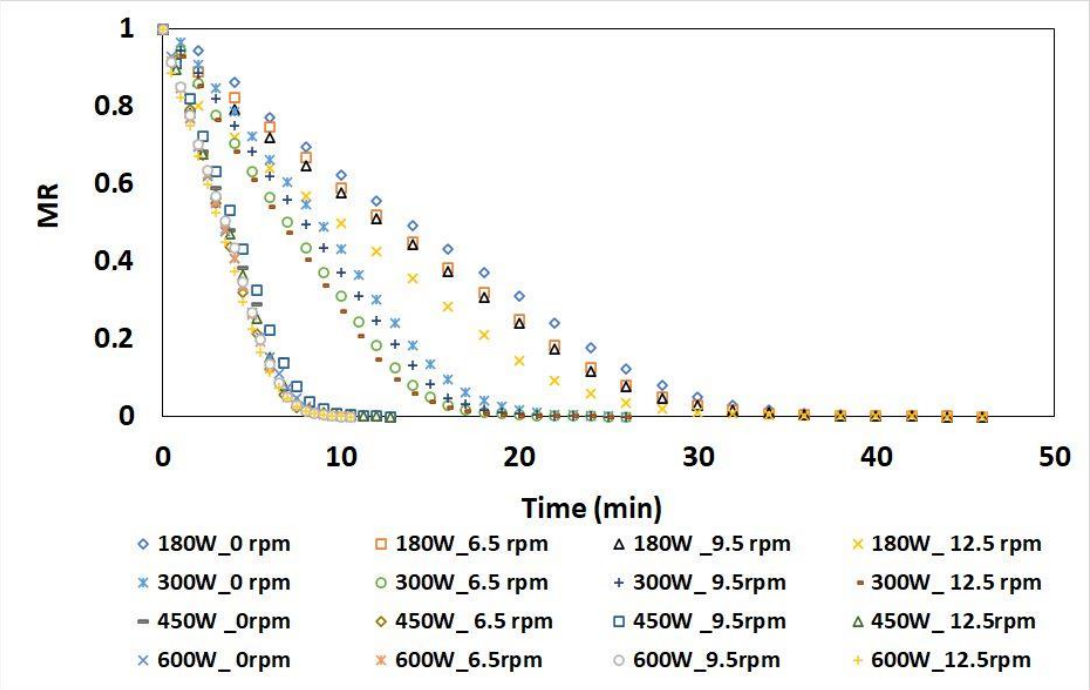

Figure 2. Drying curves of lemon peel during microwave drying

Rotation of turntable at different rates yielded 5.6-23.8% reduction in drying time of peels compared to drying without rotating the turntable. This reduction was the lowest at 180W (5.6-11.1%). For different power levels, the effect of rate of rotation on drying time did not follow a clear trend. At lower power levels (180, 300W), the highest rate of rotation (12.5 rpm) provided lower drying times. However, this is not valid for higher power levels. At higher power levels (450 W, 600W), 9.5 and 12.5 rpm gave similar drying times. Compared to 9.5 and 12.5 rpm, 6.5 rpm provided lower drying time at 450W, while higher drying time at 600W. These findings show that effect of rotation rate on drying time of lemon peels depended on the microwave power level.

Table 2
Microwave drying times of lemon peels

Rate of rotation	180W		300W		450W		600W	
	Time (min)	M.C.*	Time (min)	M.C.	Time (min)	M.C.	Time (min)	M.C.
0 rpm	36	8.88	21	9.50	11.3	8.17	8.5	8.94
6.5 rpm	34	8.94	18	9.13	9.0	8.53	7.5	9.41
9.5 rpm	34	9.06	19	9.57	9.8	8.58	7.0	9.31
12.5 rpm	32	8.86	16	9.38	9.8	8.08	7.0	9.48

*M.C.: Moisture content (%wet base)

3.2 Drying Rate

Drying curve includes three major stages which are transient period, constant rate period, and one or more falling rate periods. For lemon peels, a constant rate period was not observed during oven drying (Figure 3). The rate fell steadily with the decrease in water content. Similar to this finding, some researchers could not detect constant drying rate period during hot air drying of citrus peels (Deng et al., 2019; Mello et al., 2020; Garau et al., 2006; Romdhane et al., 2015; Xu et al., 2017). The absence of a constant drying rate suggests that diffusion was the dominant mechanism for removing of water from lemon peels during oven drying.

Microwave drying significantly enhanced the drying rate of lemon peels. During microwave drying of lemon peels, after the initial unsteady state warming-up period, both constant and falling rate periods were detected

(Figure 4). After 20-24, 11-12, 5-6, and 4.5-5 minutes of drying at power levels of 180, 300, 450, and 600W, a rapid decrease in drying rate was seen. In literature, constant drying rate period have also been observed during microwave drying of mint leaves by Soysal, (2005), tomato slices by Abano et al., (2013) and amaranth leaves by Mujaffar & Loy (2016). Our results are also in agreement with the drying rate curves obtained for convective and microwave drying of onion slices (Demiray, Seker, & Tulek, 2017). In a study, Tasirin et al. (2014) observed both constant and falling rate periods during fluidized bed drying of orange peel.

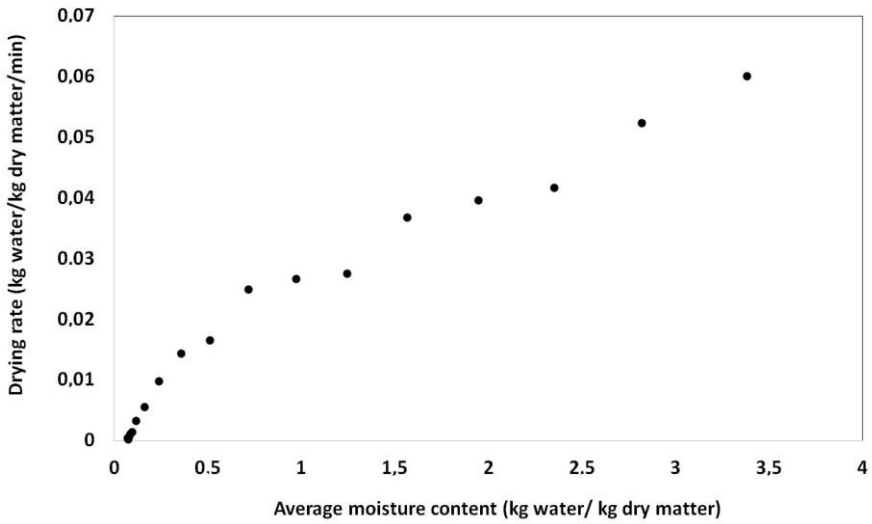

Figure 3. Variation of drying rate with moisture content during oven drying

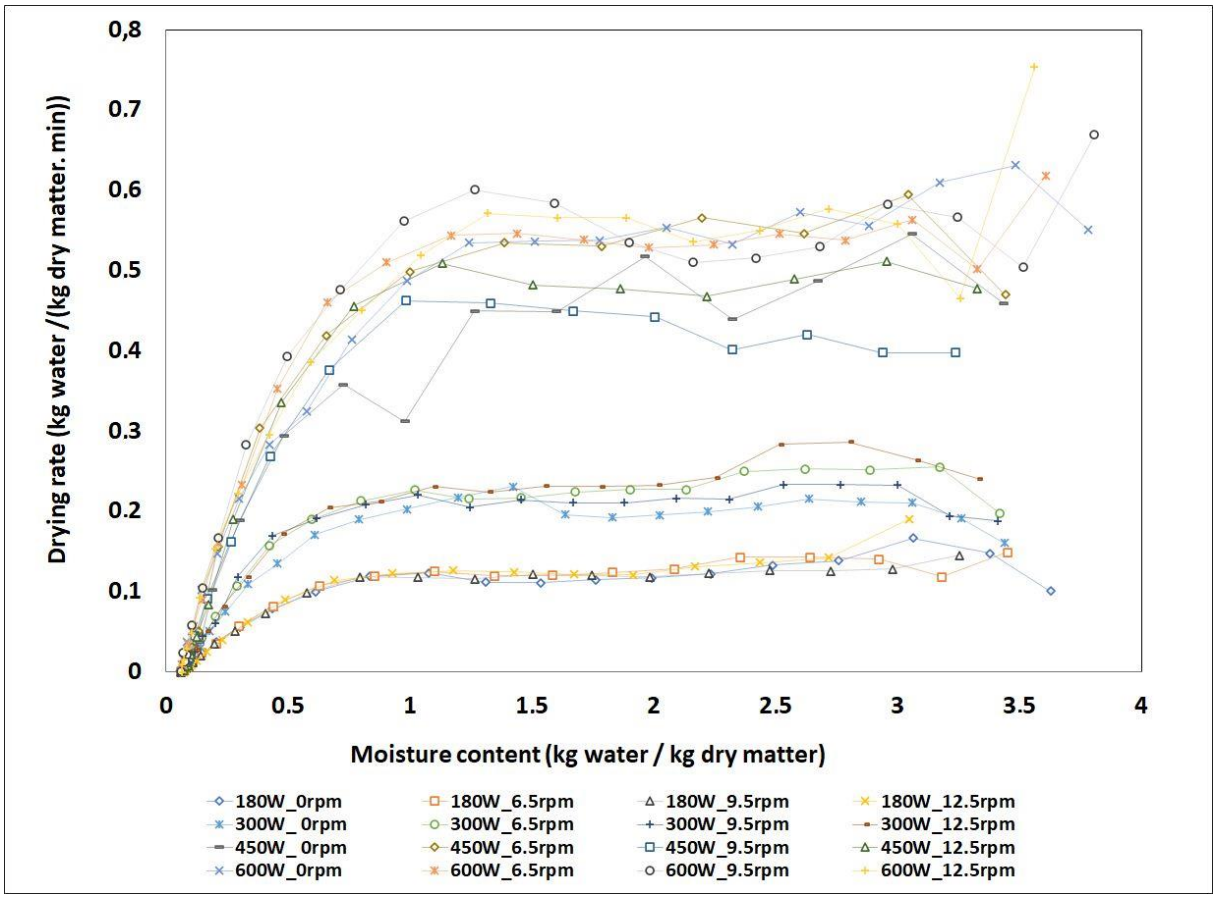

Figure 4 Variation of drying rate with moisture content during microwave drying

The rate of rotation did not create a clear effect on drying rate at the highest (600W) power level. At 600W power level, higher rate of heat generation within sample creates significant internal pressure which increases rate of moisture loss. Rapid rate of moisture removal at this power level may be a reason for not observing the effect of the rate of rotation on drying rate. At power levels of 180, 300, and 450 W, 9.5 rpm yielded lower drying rates compared to 6.5 and 12.5 rpm until reaching moisture contents of nearly 2.0, 1.0, and 0.4 kg water kg^{-1} dry matter, respectively. When the moisture contents fell below these values, drying rates obtained at different rotational rates were quite similar. At 300W and 450W, 12.5 and 6.5 rpm rotational rates gave the highest initial drying rates, respectively.

In general, drying rate was higher at higher power levels during drying. When 450 and 600W powers were compared, this general trend showed some variations depending on the rate of rotation. At 6.5 rpm, both 450W and 600W power levels indicated similar drying rates during whole drying period. At 0 rpm and 12.5 rpm, 600W power level enhanced the drying rate of peels during initial period of drying compared to 450W, however, the drying rate curves almost overlapped under the moisture contents of 0.58 kg water kg^{-1} dry matter (at 450 W) and 1.05 kg water kg^{-1} dry matter (at 600W).

3.3 Mathematical modelling of the drying curves

In literature, some semitheoretical and empirical models have been used to describe the relationship between the moisture content and the drying time of citrus peels. In this study Page, Newton, Logarithmic, Henderson & Pabis and Two-term models were fitted to experimental microwave and oven drying data of lemon peels. The R^2, SSE and RMSE values ranged between 0.984-0.997, 0.0058-0.0286, and 0.0184-0.0422, respectively for oven drying and between 0.928-0.997, 0.0064-0.2291, and 0.0199-0.0939, respectively for microwave drying (results not shown). Results of nonlinear regression analysis indicated that all the applied models were notable in description of the thin layer drying characteristics of lemon peel. Page model provided lower SSE, RMSE, and higher R^2 values over the other models for all drying treatments. In a study, Shu et al., (2020) reported that Page model showed the best fit to experimental data within 9 different thin layer models during microwave vacuum drying (600W) of tangerine peels. It has been reported that the change of moisture ratios of lemon (Ghanem et al. 2020), orange (Bejar et al., 2011b), and pomelo (Tuncer et al., 2020). peels with microwave drying time were successfully described by the Page model. However, the most appropriate model for lemon and pomelo peels was found as the Midilli & Küçük and Logarithmic models, respectively. The statistical parameters and model coefficients (k and n) obtained from the fit of the Page model were reported in Table 3.

Some authors reported relations between the k value of Page model and the drying process variables like temperature, air velocity, microwave power density, sample thickness (Onwude et al., 2016). In this study, drying rate constant (k) values increased with increasing power level. It ranged between 0.014-0.0436 min^{-1} and 0.1143-0.1306 min^{-1} at power levels of 180W and 600W, respectively. During microwave drying of various foods, some authors similarly reported an increase in k value of Page model with increasing power level (Darvishi et al., 2014; Demiray et al., 2017). For microwave drying of orange slices, Alibas & Yilmaz (2021) noted an increase in k value (obtained from Modified Henderson model) with an increase in power density. A lower k value (0.00752 min^{-1}) was estimated during oven drying compared to microwave drying. This was an expected result since microwave drying enhanced the drying rate of lemon peel as stated before. The change of k value with rate of rotation showed variance depending on the power level. In general, higher k values were obtained at 12.5 rpm compared to 6.5 and 9.5 rpm at all power levels.

Table 3
Fitting parameters of the Page model.

Power level	Rate of rotation (rpm)	Parameters		SSE	R^2	RMSE
		k (1/min)	n			
Oven drying		0.00752	1.270	0.0058	0.9968	0.0184
180W	0	0.0124	1.556	0.0176	0.9934	0.0283
	6.5	0.0170	1.494	0.0205	0.9919	0.0305
	9.5	0.0214	1.423	0.0275	0.9887	0.0353
	12.5	0.0436	1.253	0.0311	0.9856	0.0376
300W	0	0.0174	1.735	0.0170	0.9947	0.0261
	6.5	0.0349	1.571	0.0173	0.9941	0.0263
	9.5	0.0234	1.674	0.0203	0.9935	0.0285
	12.5	0.0395	1.553	0.0149	0.9949	0.0244
450W	0	0.1022	1.533	0.0081	0.9960	0.0224
	6.5	0.0946	1.704	0.0064	0.9970	0.0199
	9.5	0.0700	1.723	0.0123	0.9943	0.0278
	12.5	0.0961	1.637	0.0119	0.9942	0.0273
600W	0	0.1143	1.552	0.0134	0.9945	0.0259
	6.5	0.1058	1.618	0.0182	0.9927	0.0301
	9.5	0.0975	1.653	0.0234	0.9907	0.0342
	12.5	0.1306	1.529	0.0188	0.9921	0.0307

3.4 Effective moisture diffusivity (D_{eff}) for microwave drying

The D_{eff} values at different microwave drying conditions were calculated by using Equation 2.7. The citrus peel was considered as homogeneous by neglecting the thickness of flavedo compared to albedo. The water loss through flavedo was assumed to be prevented due to waxy layer (cuticle) covering it (Garau et al., 2006; Garcia-Perez et al., 2009, 2012). Some researchers have observed that after hot air drying, the characteristic distribution of waxy components over the cuticular surface of orange peel disappeared and the stomatal pores become clogged (Garcia-Perez et al., 2012; Tamer et al., 2016). Garcia-Perez et al. (2012) stated that spread of waxy components over surface makes the moisture removal from this surface more difficult.

The D_{eff} values were listed in Table 4. The D_{eff} value was found to be 0.454×10^{-8} m^2s^{-1} for oven drying while it ranged between 1.688×10^{-8} m^2s^{-1} - 7.595×10^{-8} m^2s^{-1} for microwave drying. These results are comparable with literature. For citrus peels subjected to various drying methods, D_{eff} values ranging between 0.0495×10^{-8} -7.295×10^{-8} m^2s^{-1} have been reported in literature (Garcia-Perez et al. 2009; Deng et al. 2019; Tuncer et al. 2020). At similar rates of rotation, D_{eff} values increased with increasing power level. This result agrees with the results presented by other authors (Darvishi et al., 2014; Alibas & Yilmaz, 2021; Demiray et al., 2017). Microwave drying performed without rotating the turntable caused lower D_{eff} values at all power levels. No significant effect of rate of rotation on D_{eff} values was observed.

Table 4
Effective diffusivity (D_{eff}) and activation energy (Ea) values obtained during microwave drying

	$D_{eff} \times 10^8$ (m^2s^{-1})							
Power level	**0 rpm**		**6.5 rpm**		**9.5 rpm**		**12.5 rpm**	
180W	1.688	(R^2=0.895)	1.882	(R^2=0.912)	2.012	(R^2=0.868)	2.077	(R^2=0.941)
300W	2.856	(R^2=0.882)	3.700	(R^2=0.899)	3.375	(R^2=0.895)	3.635	(R^2=0.938)
450W	5.777	(R^2=0.921)	6.945	(R^2=0.956)	6.037	(R^2=0.922)	6.686	(R^2=0.933)
600W	6.556	(R^2=0.870)	7.010	(R^2=0.890)	7.595	(R^2=0.833)	7.530	(R^2=0.878)
Activation Energy (W/g)								
	22.541	(R^2=0.953)	22.650	(R^2=0.973)	21.327	(R^2=0.963)	21.886	(R^2=0.971)

3.5 Activation Energy

For microwave drying, activation energy values calculated using Eq. 2.8. were reported in Table 4. The high values of R^2 (>0.96) are indicative of good fitness of empirical relationship to represent the relationship between D_{eff} and the ratio of sample mass to microwave power level (m/P). Ea values estimated from D_{eff} values ranged between 21.33 and 22.65 W/g. The values of D_{eff} obtained for lemon peel are consistent with the D_{eff} values for different types of fruits and vegetables (ranging between 5.54-24.22 W/g) reported in literature (Murthy & Manohar, 2012; Darvishi et al., 2014; Demiray et al., 2017). However, D_{eff} values obtained in this study were lower than that presented by Tuncer et al. (2020) for the pomelo peel (124.36 and 115.03 W g^{-1} for 0.5 and 1 cm thick peels, respectively) subjected to microwave drying at 7 W.g^{-1} power density.

3.6 Bulk Density

Citrus peels are rich source of dietary fibers (DFs). DFs are commonly classified as soluble dietary fibers (SDFs) including non-cellulosic polysaccharides, oligosaccharides, pectin, β-glucans, gums, and insoluble dietary fibers (IDFs) including cellulose, hemicellulose, lignin. Drying process may lead to the modification of the microstructures of the dietary fibers of citrus peel powders and consequently their physical properties (Abou-Arab et al., 2017, Romdhane et al., 2015, Ghanem et al., 2020). Bulk density is an important physical property which is related with the interparticle voids in the sample. Lower proportion of air volume in sample give higher bulk density (Barbosa-Canovas et al., 2005). Greater bulk density is desirable for reducing packaging and transportation costs. Bulk density values of the powder samples were given in Table 5.

Table 5
Poured bulk density (ρ_p), Tapped bulk density (ρ_t) , Hausner ratio (HR) and Carr index (CI) of lemon peel powders

Drying Treatment	Rate of rotation	ρ_p (g/ml)	ρ_t (g/ml)	HR	Cohesiveness **	CI (%)	Flowability ***
Freeze drying		0.212±0.029 d*	0.335±0.055 c	1.576±0.117 a	High	36.184±4.975 a	Bad
Oven drying		0.374±0.018 c	0.495±0.020 b	1.327±0.068 b	Intermediate	24.448±3.852 b	Fair
180W	0	0.468±0.016 ab	0.603±0.029 a	1.290±0.071 b	Intermediate	22.276±4.073 b	Fair
	6.5	0.468±0.020 ab	0.615±0.042 a	1.313±0.070 b	Intermediate	23.623±4.042 b	Fair
	9.5	0.466±0.026 ab	0.615±0.040 a	1.322±0.085 b	Intermediate	24.076±4.878 b	Fair
	12.5	0.460±0.022 ab	0.617±0.041 a	1.340±0.075 b	Intermediate	25.193±4.105 b	Fair
300W	0	0.452±0.040 ab	0.594±0.048 a	1.318±0.093 b	Intermediate	23.808±5.419 b	Fair
	6.5	0.472±0.025 a	0.616±0.041 a	1.308±0.093 b	Intermediate	23.198±5.541 b	Fair
	9.5	0.468±0.031 ab	0.617±0.038 a	1.321±0.099 b	Intermediate	23.884±5.546 b	Fair
	12.5	0.467±0.030 ab	0.621±0.042 a	1.332±0.090 b	Intermediate	24.659±4.913 b	Fair
450W	0	0.463±0.025 ab	0.608±0.028 a	1.317±0.051 b	Intermediate	23.958±2.920 b	Fair
	6.5	0.470±0.032 a	0.614±0.031 a	1.311±0.072 b	Intermediate	23.515±4.167 b	Fair
	9.5	0.465±0.019 ab	0.622±0.029 a	1.338±0.084 b	Intermediate	25.009±4.840 b	Fair
	12.5	0.471±0.022 a	0.618±0.036 a	1.315±0.075 b	Intermediate	23.753±4.309 b	Fair
600W	0	0.428±0.013 b	0.571±0.030 ab	1.334±0.074 b	Intermediate	24.851±4.193 b	Fair
	6.5	0.444±0.028 ab	0.603±0.031 a	1.363±0.091 b	Intermediate	26.326±4.688 b	Fair
	9.5	0.448±0.024 ab	0.614±0.035 a	1.373±0.072 b	Intermediate	27.016±3.745 b	Fair
	12.5	0.455±0.018 ab	0.611±0.044 a	1.344±0.079 b	Intermediate	25.343±4.285 b	Fair

*Values represent mean ± standard deviation. Different small letters in the same column shows significant difference ($p < .05$).
** The cohesiveness is low (HR<1.2), intermediate (1.2<HR<1.4) and high (HR>1.4) (Hausner, 1967)
***The flowability is very good (CR<15), good (15<CR<20), fair (20<CR<35), bad (35<CR<45%) and very bad (CR>45) (Carr, 1965)

The poured and tapped bulk densities of the freeze dried and oven dried powder samples was lower than the microwave dried ones. Microwave dried peel powders had tapped bulk densities ranging between 0.571 and 0.622 g/ml. Freeze drying yielded the lowest poured and tapped bulk densities. This was thought to be due to the more porous structure of the freeze-dried powders. This result is in line with those reported by different authors (Farahmandfar et al. 2019, 2020; Tekgül & Baysal, 2018, Liu et al., 2017; Lee et al., 2012). Liu et al., (2017) obtained the scanning electron micrographs of orange peel dietary fiber powders and reported that the

three-dimensional structures of soluble and insoluble dietary fiber particles were affected by the drying method. They noted that the increase of the porosity and surface area of the fibers during freeze drying lead to lower bulk density compared to hot air drying. Tekgül & Baysal (2018) obtained lower bulk density for freeze dried (0.17 g/ml) lemon peel powder compared to open-air, hot air and microwave dried samples (0.24-0.25 g/ml). Farahmandfar et al. (2019, 2020) obtained bulk density values ranging between 1.32-and 3.20 g/ml for powder of orange peels dried by various drying methods (shade, sun, oven, vacuum oven, microwave, and freeze-drying) and similarly indicated that the freeze-dried samples had the lowest bulk density. This was attributed by the authors to the protection of structure of freeze-dried sample with minimal shrinkage.

For microwave drying, the data were analyzed using general linear model and Tukey's pairwise comparison test. The mean of the bulk densities obtained at 600W was found to be lower compared to those obtained at lower power levels. However, this difference was not statistically significant for tapped bulk density. The other power levels provided similar bulk density values. Microwave drying without rotation caused lower mean value of tapped density compared to microwave drying with rotation. Bulk densities of lemon peels dried at rotational rates of 6.5, 9.5 and 12.5 rpm were similar. Microwave drying without rotation (0 rpm) causes non uniform heating. This may create variation in the degree of peel matrix destruction during drying which could affect the grinding performance resulting in relatively non uniform particle size distribution in powder. This may be one of the reasons for the lower density of the samples dried at 0 rpm. When the SEM images were examined, no clear difference was observed between the samples dried at 600W and the ones dried at 180W. However, during drying at 600W, local burns occurred due to the high temperatures reached in the sample. This may be a reason for the observation of the lower bulk density obtained at 600W as explained above. Non uniform heating was not observed at 180W.

3.7 Hausner ratio (HR) and Carr index (CI)

Hausner ratio (HR) and Carr index (CI) are generally used to assess flowing properties of powders. Higher HR value means that this sample was relatively more cohesive resulting in decreased flowability of the powder. Freeze drying caused the highest HR (1.576) and CI (36.184) values which means freeze dried peel powder had bad flowability (Seerangurayar et al., 2017). Oven dried and microwave dried samples had similar HR and CI values. HR and CI of the microwave dried lemon peel powders ranged from 1.29 to 1.37 and 22.28 to 27.02, respectively. According to the reference values given in Table 5, oven dried, and microwave dried powders had fair flowability. Lee et al. (2012) showed that the Hausner ratio values of powders from pressed cake of citrus “Hallabong” ranged between 1.105 and 1.150 depending on frying method and particle size. In their study, for the samples having similar particle size, freeze drying yielded higher HR values. These results are in good agreement with the results of this study. Power level and the rotational rate of turntable were not significant factors effecting HR and CI of the samples.

3.8 Functional Properties of Powder

Drying may have positive or negative effects on some functional properties of citrus peels depending on citrus variety and drying treatment. Water holding capacity (WHC) and oil retention capacity (ORC) are the functional properties of powders that have been widely studied. The effect of various drying treatments on WRC and OAC of citrus peels are presented in Table 6. In literature, the WHC and ORC of the dried citrus peel powders ranged between 2.7-13 g water/ g DM and 0.52-5.1 g oil/g DM, respectively.

In this study, dried lemon peel powder had the WHC and ORC values ranging between 6.34-9.32 g water/ g DM and 0.96-3.03 g oil/g DM, respectively (Table 7). Microwave drying at 180W irrespective of rate of rotation and at 450 and 600 W without rotation yielded significantly lower WHC values compared to oven drying. Except those samples, microwave drying yielded lower WHC values compared to freeze drying and oven drying, however the difference was not statistically significant. This is at least in part may be due to the higher temperatures reached in samples during microwave drying. Drying temperature is known to influence the functional properties of powders. The functional properties of citrus peel powders have been shown to be negatively affected by the higher drying temperatures (≥60 °C) (Garau et al., 2007; Romdhane et al., 2015;

Ghanem et al., 2020; Deng et al., 2019). Deng et al. (2019) reported no significant change in WHC of orange peel dried at 50 and 60 °C, however, further increase in temperature exhibited a reduction in WHC. Ghanem et al. (2020) noted that formation of more rigid structure resulting from higher temperature may lead to a lower WHC in lemon peel. Similar finding was reported by Bejar et al. (2011a) for orange peel undergoing infrared drying. Garau et al. (2007) recorded that high (90 °C) and low (30 °C) drying temperatures caused significant losses of pectic polymers during air-drying of orange peels. Degradation of pectic substances during processing is known to influence the functional properties. Higher temperature and the internal pressure created within material during microwave drying may cause deformation of cellular tissue resulting loss in WRC (Bejar et al., 2011a; Romdhane et al., 2015). However, our result differed from the results presented by Abou-Arab et al. (2017) who showed that microwave (900W) dried citrus (orange, tangerine, and lemon) peels had better functional properties compared to solar (40 °C) and oven (40 °C) dried ones.

Table 6
Effect of drying treatments on some functional properties of citrus peels

Peel Material	Drying Method	WHC (g water/g DM)	OAC (g oil /g DM)	References
C. sinensis (Newhall navel orange)	Hot air impingement dry-ing(50-70°C)	7.9- 8.8 ; T↑ WRC ↓	-	Deng et al. (2019)
C. limon (L.) (Lamas lemon)	Hot air drying (HAD); Open air drying (AD); Freeze drying (FD); Microwave drying (MD)	HAD:5.6; AD: 5.3; FD:5.8 MD:5.5	-	Tekgül & Baysal (2018)
C. sinensis (Washington navel orange)	Hot air drying (HAD) (55°C) Microwave assisted HAD (MW-HAD) (2-6 W/g. 55°C)	HAD: around 11.3 MW-HAD: between 11.5-13 Power level↑ WRC↑	-	Talens et al. (2018)
-*C. Valencia* -*C. Balady* -*C. Limon* -*C. reticulate*	Microwave drying (MD) (900W) Solar-drying (SLD) (40°C) Oven drying (OD) (40°C)	dried > raw MD: 3.6-5.5 SLD: 3.0-5.0 OD:2.7-4.9	dried > raw (except solar dried *C.retucula*) MD:1.16-1.95; SLD:0.52-1.42; OD:0.89-1.37	Abou Arab et al. (2017)
C. limon cv. Lunari	Convective air drying (40-60°C)	dried< raw Dried at 40 °C: 7.7 Dried at 60 °C: 6.6 T↑ WRC ↓	dried< raw Dried at 40 °C: 1.6 Dried at 60 °C: 1.5 T↑ OAC ↓	Romdhane et al. (2015)
C. sinensis (Thompson orange) *C. limon* (lemon) *C. reticulata* (mandarin)	Microwave drying (100-600W)	dried > raw; Max. values: Orange dried at 180W: 8.3 Lemon dried at 450 W:8.2 Mandarin dried at 100 W:6.1	dried< raw Raw: Orange (4.8); lemon (4.5); mandarin (5.1)	Ghanem et al. (2012)
C. sinensis (Maltaise orange)	Infrared drying (40-70°C)	dried > raw Dried at 40 °C: 9.5; at 70 °C: 5.5	dried< raw; not affected by T Dried: around 2.5	Bejar et al. (2011a)
C. sinensis (Maltaise orange)	Microwave drying (100-850W)	dried > raw Max: dried at 180W:10.3	dried < raw Max: dried at 700W:3.8	Bejar et al. (2011b)

WHC: Water holding capacity; OAC: Oil absorption capacity; T: Temperature

The power level did not exert a clear effect on WHC of citrus peels during microwave drying. For the microwave drying with rotation, 600W provided slightly higher WHC values (7.6-7.9 g water/ g DM). The maximum WHC (7.9 g water/ g DM) obtained in this study was similar to that presented by Ghanem et al., (2012) for lemon peels (8.15 g water/ g DM) dried by microwave drying at 450W power level. In their study, the change of WHC did not follow a clear trend with increasing power level (100-600W) and the citrus peels from different citrus varieties had the maximum WHC values at different power levels (100-600W). At higher power levels, influence of turntable rotation on WHC was more notable. At 600W, microwave drying with rotation provided 20-25% higher WHC values compared to microwave drying without rotation. The level of increase was 9-14%

at 450W. In the case of microwave drying with rotation, 9.5 rpm provided slightly higher WHC values compared to 6.5 and 12.5 rpm at all power levels. However, differences were not significant. Variation of rotational rate yielded 1-5.5 % change in WHC values.

Table 7
Water holding capacity (WHC) and oil retention capacity (ORC) of lemon peel powders

Drying Treatment	**Rate of rotation**	**WHC (g water/g DM)**	**ORC (g oil/g DM)**
Freeze drying		8.464±0.404 ab*	3.034±0.134 a
Oven drying		9.316±0.128 a	1.687±0.024 b
180W	0	6.717±0.670 b	1.359±0.006 bc
	6.5	6.458±0.467 b	1.410±0.013 bc
	9.5	6.812±0.173 b	1.418±0.013 bc
	12.5	6.736±0.407 b	1.444±0.000 c
300W	0	7.502±0.996 ab	1.580±0.090 bc
	6.5	7.442±0.658 ab	1.407±0.026 bc
	9.5	7.456±0.628 ab	1.447±0.028 bc
	12.5	7.383±0.644 ab	1.494±0.080 bc
450W	0	6.393±0.818 b	1.441±0.002 bc
	6.5	7.080±1.228 ab	1.488±0.012 bc
	9.5	7.267±1.041 ab	1.442±0.070 bc
	12.5	7.001±1.040 ab	1.534±0.158 bc
600W	0	6.340±0.494 b	1.692±0.090 b
	6.5	7.625±1.002 ab	1.496±0.025 bc
	9.5	7.841±1.272 ab	1.453±0.068 bc
	12.5	7.924±1.061 ab	1.575±0.134 bc

*Values represent mean ± standard deviation. Different small letters in the same column shows significant difference ($p < .05$).

Microwave dried lemon peels had ORC values ranging between 1.359 and 1.692 g oil/ g DM. These values were similar to ORC of microwave dried citrus peels (1.16-1.95 g oil/ g DM) (Abou Arab et al., 2017) and lemon peels (around 1.8 g oil/ g DM) (Ghanem et al., 2012) but lower than ORC of microwave dried orange peel measured by Bejar et al. (2011b). Freeze drying provided the highest ORC. Microwave dried samples except the one dried at 180W (12.5rpm) had similar ORC values compared to oven dried ones. Some authors noted the opposite direction of the changes in WHC and ORC which was explained by the alteration in water affinity of components due to modification of the structural characteristics and change in the composition of fiber after microwave drying process (Ghanem et al., 2012; Bejar et al., 2011b). No such effect was observed in the results obtained in this study. The highest power level (600W) provided relatively higher ORC values. Influence of turntable rotation on ORC did not follow a clear trend. In general, 12.5 rpm provided slightly higher ORC values compared to 6.5 and 9.5 rpm at all power levels.

3.9 Microstructure

SEM images of the lemon peel powders dried by different drying treatments were obtained to examine the microstructures (Figure 5). It is clear that the freeze-dried powder had large pores. It is widely known that freeze drying protects the structure and shape of the materials with minimal shrinkage. Dehydration via sublimation creates pores within material during freeze drying. The larger size and more porous particle structure of freeze-dried peel powders explains why the bulk densities of the freeze-dried samples was lower than the others. This result is consistent with the results of Lee et al. (2012) who obtained larger pore size for the freeze-dried powders obtained from pressed cake of citrus “Hallabong” compared to hot air-dried ones.

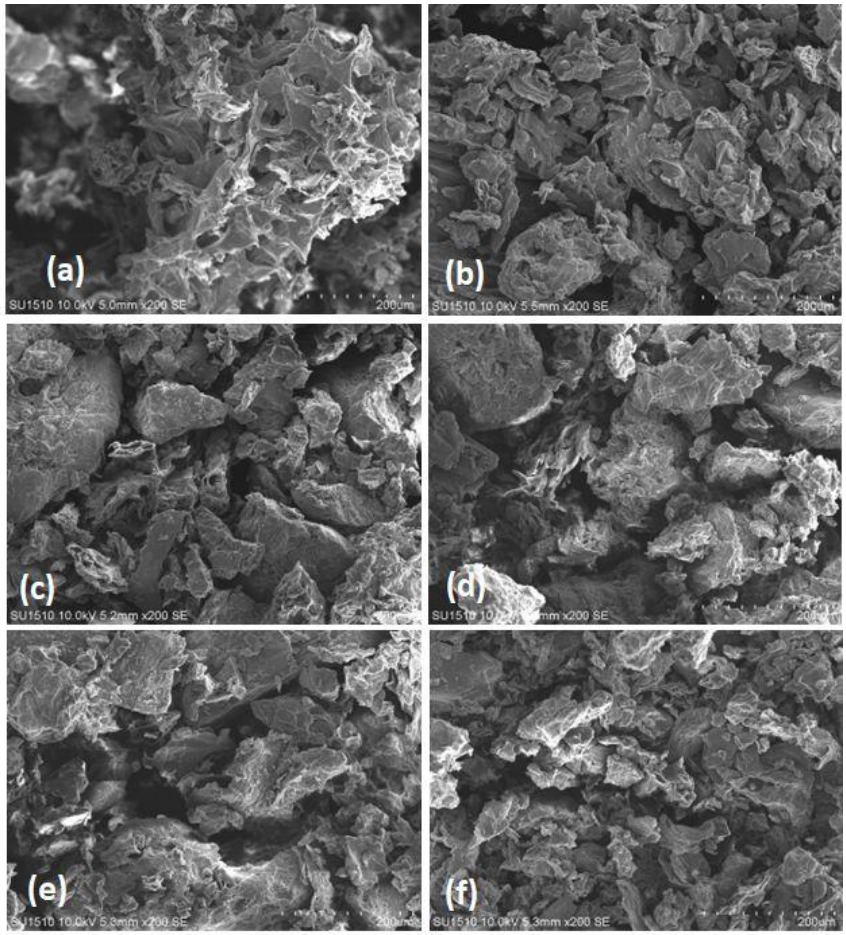

Figure 5. SEM images of lemon peel powder subjected to (a)freeze drying, b) oven drying, and microwave drying at c) 180W-0rpm, d)180W-12.5rpm, e)600W-0rpm, f)600W-12.5 rpm.

Oven dried and microwave dried samples had irregular shapes and rough surface. It can be seen that the particle size distribution differs between the samples. However, it is not possible to talk about a clear effect created by the higher microwave power level or rotation of turntable.

4. Conclusion

Lemon peels with high moisture content were dried with microwave drying to obtain a powder product. Microwave drying with rotation provided lower drying time compared to drying without rotation. Rate of rotation did not exert a clear effect on drying time of lemon peel at 300 and 450W power levels. Rate of rotation influenced initial drying rate of peels at 300 and 450 W power levels. Page model best described the drying characteristics of lemon peels at all drying conditions. Microwave drying at 600W gave higher D_{eff} values. Microwave dried lemon peels had higher bulk density values and similar or lower water holding and oil retention capacities compared to freeze dried and oven dried ones. Variation of rotational rate from 6.5 to 12.5 rpm did not yield a significant change in WHC and ORC values. The findings showed that, when the appropriate parameters are selected, microwave drying may be an alternative method that can be used for drying of lemon peels. Higher power levels gave better results regarding drying time and the investigated quality parameters. Microwave dried lemon peel powder has the potential to serve as a functional component in the food processing industry in terms of its flow properties and functional features. However, apart from the functional properties, the physical properties and the chemical composition of the lemon peel powder need to be evaluated to determine the most suitable microwave drying parameters in respect of preserving the desired quality attributes.

Acknowledgement

This study was funded by Ordu University (B 2127).

Author Contributions

Sevilay San: Performed the analyzes

Işıl Barutçu Mazı: Planned the study, performed statistical analysis, and wrote the paper.

Conflicts of Interest

The authors declare no conflict of interest.

References

Abano, E. E., Haile, M. A. Owusu, J., & Engmann, F. N. (2013). Microwave-vacuum drying effect on drying kinetics, lycopene and ascorbic acid content of tomato slices. *Journal of Stored Products and Postharvest Research, 4*, 11-22. DOI: https://doi.org/10.5897/JSPPR12.030

Abd Rahman, N. F., Shamsudin, R., Ismail, A., & Shah, N. N. A. K. (2016). Effects of post-drying methods on pomelo fruit peels. *Food Science and Biotechnology, 25*, 85-90. DOI: https://doi.org/10.1007/s10068-016-0102-y

Abou-Arab, E. A., Mahmoud, M. H., & Abu-Salem, F. M. (2017). Functional properties of citrus peel as affected by drying methods. *American Journal of Food Technology, 12*, 193-200. DOI: https://doi.org/10.3923/ajft.2017.193.200

Alibas, I., & Yilmaz, A. (2021). Microwave and convective drying kinetics and thermal properties of orange slices and effect of drying on some phytochemical parameters. *Journal of Thermal Analysis and Calorimetry*, 1-21. DOI: https://doi.org/10.1007/s10973-021-11108-3

Barbosa-Canovas, G. V., Ortega-Rivas, E., Juliano, P., & Yan, H. (2005). *Food powders: physical properties, processing, and functionality*. Springer, New York.

Bejar, A. K., Ghanem, N., Mihoubi, D., Kechaou, N., & Mihoubi, N. B. (2011a). Effect of infrared drying on drying kinetics, color, total phenols and water and oil holding capacities of orange (*Citrus sinensis*) peel and leaves. *International Journal of Food Engineering, 7*, 5. DOI: https://doi.org/10.2202/1556-3758.2222

Bejar, A. K., Kechaou, N., & Mihoubi, N. B. (2011b). Effect of microwave treatment on physical and functional properties of orange (*Citrus sinensis*) peel and leaves. *Journal of Food Processing and Technology, 2*, 109. DOI: https://doi.org/10.4172/2157-7110.1000109

Carr, R. L. (1965). Evaluating flow properties of solids. *Chemical Engineering, 72*, 163-168.

Crank, J. (1979). *The mathematics of diffusion*. Oxford, Great Britain: Clarendon Press.

Darvishi, H., Asl, A. R., Asghari, A., Azadbakht, M., Najafi, G., & Khodaei, J. (2014). Study of the drying kinetics of pepper. *Journal of the Saudi Society of Agricultural Sciences, 13*, 130-8. DOI: https://doi.org/10.1016/j.jssas.2013.03.002

Deng, L. Z., Mujumdar, A. S., Yang, W. X., Zhang, Q., Zheng, Z. A., Wu, M., & Xiao, H. W. (2019). Hot air impingement drying kinetics and quality attributes of orange peel. *Journal of Food Processing and Preservation, 44*, e14294. DOI: https://doi.org/10.1111/jfpp.14294

Demiray, E., Seker, A., & Tulek, Y. (2017). Drying kinetics of onion (*Allium cepa* L.) slices with convective and microwave drying. *Heat Mass Transfer, 53*, 1817-27. DOI: https://doi.org/10.1007/s00231-016-1943-x

Ertekin, C., & Firat, M. Z. (2017). A comprehensive review of thin layer drying models used in agricultural products. *Critical Reviews in Food Science and Nutrition, 57*, 701-717. DOI: http://dx.doi.org/10.1080/10408398.2014.910493.

FAO (Food and Agriculture Organization of the United Nations) (2021). Citrus Fruit Statistical Compendium 2020. Rome.

Farahmandfar, R., Tirgarian, B., Dehghan, B., & Nemati, A. (2019). Comparison of different drying methods on bitter orange (*Citrus aurantium* L.) peel waste: Changes in physical (density and color) and essential oil (yield, composition, antioxidant and antibacterial) properties of powders. *Journal of Food Measurement and Characterization, 14*, 862-75. DOI: https://doi.org/10.1007/s11694-019-00334-x

Farahmandfar, R., Tirgarian, B., Dehghan, B., & Nemati, A. (2020). Changes in chemical composition and biological activity of essential oil from Thomson Navel orange (*Citrus sinensis* L. Osbeck) peel under freezing, convective, vacuum, and microwave drying methods. *Food Science and Nutrition, 8*, 124-138. DOI: https://doi.org/10.1002/fsn3.1279

Garau, M. C., Simal, S., Femenia, A., & Rossello, C. (2006). Drying of orange skin: drying kinetics modelling and functional properties. *Journal of Food Engineering, 75*, 288-95. DOI: https://doi.org/10.1016/j.jfoodeng.2005.04.017

Garau, M. C., Simal, S., Rossello, C., & Femenia, A. (2007). Effect of air-drying temperature on physico-chemical properties of dietary fibre and antioxidant capacity of orange (*Citrus aurantium* v. Canoneta) by-products. *Food Chemistry, 104*, 1014-24. DOI: https://doi.org/10.1016/j.foodchem.2007.01.009

Garcia-Perez, J. V., Carcel, J. A., Riera, E., & Mulet, A. (2009). Influence of the applied acoustic energy on the drying of carrots and lemon peel. *Drying Technology, 27*, 281-87. DOI: https://doi.org/10.1080/07373930802606428

Garcia-Perez, J. V., Ortuno, C., Puig, A., Carcel, J. A., & Perez-Munuera, I. (2012). Enhancement of water transport and microstructural changes induced by high-intensity ultrasound application on orange peel drying. *Food and Bioprocess Technology, 5*, 2256-65. DOI: https://doi.org/10.1007/s11947-011-0645-0

Ghanem, N., Mihoubi, D., Bonazzi, C., Kechaou, N., & Boudhrioua, N. (2020). Drying characteristics of lemon by-product (*Citrus limon*. v. lunari): Effects of drying modes on quality attributes kinetics. *Waste Biomass Valorization, 11,* 303-22. DOI: https://doi.org/10.1007/s12649-018-0381-z

Ghanem, N., Mihoubi, D., Kechaou, N., & Mihoubi, N. B. (2012). Microwave dehydration of three citrus peel cultivars: Effect on water and oil retention capacities, color, shrinkage, and total phenols content. *Industrial Crops and Products, 40,* 167-77. DOI: https://doi.org/10.1016/j.indcrop.2012.03.009,

Hausner, H. H. (1967). Friction conditions in a mass of metal powder. *International Journal of Powder Metallurgy, 3*, 7-13.

Kirbas, I., Tuncer, A. D., Sirin, C., & Usta, H. (2019). Modeling and developing a smart interface for various drying methods of pomelo fruit (*Citrus maxima*) peel using machine learning approaches. *Computers and Electronics in Agriculture, 165,* 104928. DOI: https://doi.org/10.1016/j.compag.2019.104928

Lee, C., Oh, H., Han, S., & Lim, S. (2012). Effects of hot air and freeze drying methods on physicochemical properties of citrus 'hallabong' powders. *Food Science and Biotechnology, 21*, 1633-9.

Liu, Y., Fan, C., Tian, M., Yang, Z., Liu, F., & Pan, S. (2017). Effect of drying methods on physicochemical properties and in vitro hypoglycemic effects of orange peel dietary fiber. *Journal of Food Processing and Preserv*ation, *41*, e13292. DOI: https://doi.org/10.1111/jfpp.13292

Mahato, N., Sharma, K., Sinha, M., Baral, E. R., Koteswararao, R. Dhyani, A., Cho, M. H., & Cho, S. (2020). Bio-sorbents, industrially important chemicals and novel materials from citrus processing waste as a sustainable and renewable bioresource: A review. *Journal of Advanced Research, 23*, 61-82. DOI: https://doi.org/10.1016/j.jare.2020.01.007.

Mello, R. E., Fontana, A., Mulet, A., Luiz, J., Correa, G., & Carcel, J. A. (2020). Ultrasound-assisted drying of orange peel in atmospheric freeze-dryer and convective dryer operated at moderate temperature. *Drying Technology, 38*, 259-67. DOI: https://doi.org/10.1080/07373937.2019.1645685

Mujaffar, S., & Loy, A. L. (2016). Drying kinetics of microwave-dried vegetable amaranth (*Amaranthus dubius*) leaves. *Journal of Food Research, 5*, 33-44. DOI: https://doi.org/10.5539/jfr.v5n6p33

Murthy T. P. K., Manohar, B. (2012). Microwave-drying of mango ginger (*Curcuma amada Roxb*): prediction of drying kinetics by mathematical modeling and artificial neural network. *International Journal of Food Science and Technology, 47,* 1229-36. DOI: https://doi.org/10.1111/j.1365-2621.2012.02963.x

Onwude, D. I., Hashim, N., Janius, R., Nawi, N. M., & Abdan, K. (2016). Modeling the thin-layer drying of fruits and vegetables: A review. *Comprehensive Reviews in Food Science and Food Safety, 15*, 599-618. DOI: https://doi.org/10.1111/1541-4337.12196

Ozcan, M. M., Ghafoor, K., Al Juhaimi, F., Uslu, N., Babiker, E. E., Ahmed, I. A. M., & Almusallam, I. A. (2020). Influence of drying techniques on bioactive properties, phenolic compounds and fatty acid compositions of dried lemon and orange peel powders. *Journal of Food Science and Technology, 58*, 147-58. DOI: https://doi.org/10.1007/s13197-020-04524-0

Romdhane, N. G., Bonazzi, C., Kechaou, N., & Mihoubi, N. B. (2015). Effect of air-drying temperature on kinetics of quality attributes of lemon (*Citrus limon* cv. lunari) peels. *Drying Technology, 33*, 1581-89. DOI: https://doi.org/10.1080/07373937.2015.1012266

Seerangurayar, T., Manickavasagan, A., Al-Ismaili, A. M., & Al-Mulla, Y. A. (2017). Effect of carrier agents on flowability and microstructural properties of foam-mat freeze dried date powder. *Journal of Food Engineering, 215*, 33-43. DOI: https://doi.org/ 10.1016/j.jfoodeng.2017.07.016

Shu, B., Wu, G. X., Wang, Z. N., Wang, J. N., Huang, F., Dong, L. H., Zhang, R. F., Wang, Y., & Su, D. X. (2020). The effect of microwave vacuum drying process on citrus: drying kinetics, physicochemical composition, and antioxidant activity of dried citrus (*Citrus reticulata* Blanco) peel. *Journal of Food Measurement and Characterization, 14*, 2443-52. DOI: https://doi.org/10.1007/s11694-020-00492-3

Soysal, Y. (2005). Mathematical modeling and evaluation of microwave drying kinetics of mint. *Journal of Applied Sciences, 5*,1266-1274. DOI: https://doi.org/10.3923/jas.2005.1266.1274

Talens, C., Castro-Giraldez, M., & Fito, P. J. (2016). Study of the effect of microwave power coupled with hot air drying on orange peel by dielectric spectroscopy. *LWT - Food Science and Technology, 66*, 622-628. DOI: https://doi.org/10.1016/j.lwt.2015.11.015

Talens, C., M. Castro-Giraldez, & P. J. Fito. (2018). Effect of microwave power coupled with hot air drying on sorption isotherms and microstructure of orange peel. *Food and Bioprocess Technology, 11*(4), 723-734. DOI: https://doi.org/10.1007/s11947-017-2041-x.

Tamer, C., Isci, A., Kutlu, N., Sakiyan, O., Sahin, S., & Sumnu, G. (2016). Effect of drying on porous characteristics of orange peel. *International Journal of Food Engineering, 12*, 921-928. DOI: https://doi.org/10.1515/ijfe-2016-0075

Tasirin, S. M., Puspasari, I., Sahalan, A. Z., Mokhtar, M., Ghani, M. K. A., & Yaakob, Z. (2014). Drying of citrus sinensis peels in an inert fluidized bed: Kinetics, microbiological activity, vitamin C, and limonene determination. *Drying Technology, 32*, 497-508. DOI: https://doi.org/10.1080/07373937.2013.838782

Tekgül, Y., & Baysal, T. (2018). Comparative evaluation of quality properties and volatile profiles of lemon peels subjected to different drying techniques. *Journal of Food Process Engineering, 41*, e12902. DOI: https://doi.org/10.1111/jfpe.12902

Trigo, J. P., Alexandre, E. M. C., Saraiva, J. A., & Pintado, M. E. (2020). High value-added compounds from fruit and vegetable by-products - Characterization, bioactivities, and application in the development of novel food products. *Critical Reviews in Food Science and Nutrition, 60*, 1388-1416. DOI: https://doi.org/10.1080/10408398.2019.1572588

Tuncer, A. D., Güler, H. Ö., & Usta, H. (2020). Modeling of drying characteristics of pomelo (*Citrus maxima*) peel. *El-Cezeri Journal of Science and Engineering, 7*, 198-210. DOI: https://doi.org/10.31202/ecjse.616497

Xu, M. Y., Tian, G. F., Zhao, C. Y., Ahmad, A., Zhang, H. J., Bi, J. F., Xiao, H., & Zheng, J. K. (2017). Infrared drying as a quick preparation method for dried tangerine peel. *International Journal of Analytical Chemistry,* 6254793. DOI: https://doi.org/10.1155/2017/6254793

Zema, D. A., Calabro, P. S., Folino, A., Tamburino, V., Zappia, G., & Zimbone, S. M. (2018). Valorisation of citrus processing waste: A review. *Waste Management, 80*, 252-73. DOI: https://doi.org/10.1016/j.wasman.2018.09.024.

e-ISSN 2757-5195

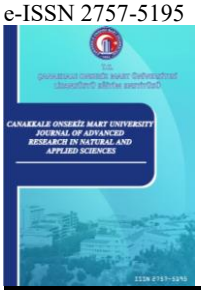

Çanakkale Onsekiz Mart University

Journal of Advanced Research in Natural and Applied Sciences

Open Access

doi.org/10.28979/jarnas.1087772 2023, Vol. 9, Issue 1, Pages: 107-126 dergipark.org.tr/tr/pub/jarnas

Which Emotions of Social Media Users Lead to Dissemination of Fake News: Sentiment Analysis Towards Covid-19 Vaccine

Maide Feyza Er[1], Yonca Bayrakdar Yılmaz[2,*]

[1]Department of Software Engineering, Faculty of Engineering and Natural Sciences, Bandırma Onyedi Eylül University, Bandırma, Türkiye

[2]Department of Computer Engineering, Faculty of Engineering, Çanakkale Onsekiz Mart University, Çanakkale, Türkiye

Article History

Received: 15.03.2022

Accepted: 10.10.2022

Published: 05.03.2023

Research Article

Abstract − The use of social media as a news source is quite common today. However, the fact that the news encountered on social media are accepted as true without questioning or checking their validity is one of the main reasons for the dissemination of fake news. For the social media ecosystem, the question arises as to which emotion is more effective in spreading fake news, as the accuracy and validity of the news are under the control of opinions and emotions rather than evidence-based data. From this point of view, our study investigates whether there is a relationship between users' reaction to the news and the prevalence of the news. In our study, sentiment analysis was conducted on the reactions of Twitter users to fake news about the COVID-19 vaccine between December 31, 2019 and July 30, 2022. To fully assess whether there is a relationship between the reactions and the prevalence of the news, the spread of real news published in the same period in addition to fake news is also taken into consideration. Fake and real news comments, which were selected in different degrees of prevalence from the most to the least, were examined comparatively. In the study, where text mining techniques were used for text pre-processing, analysis was carried out with NLP techniques. In 83% of the fake news datasets and 91% of the overall news datasets considered in the study, negative emotion was more dominant than other emotions, and it was observed that as negative comments increased, fake news spread more as well as real news. While neutral comments have no effect on prevalence, users who comment on fake news for fun significantly increase the prevalence. Finally, to reveal bot activity NLP techniques were applied.

Keywords − *Bot detection, fake news, nlp, sentiment analysis, text mining*

1. Introduction

Today, it is very common that society uses social media as a news source. In 2021, while the rate of getting news from social media is over 40% in European countries, it is 42% in America and above 50% in Asian countries (Newman et al., 2021). This situation has various negative effects such as accepting the news that encountered as true without questioning or checking the validity of them. While distorting existing news or producing non-existent news, supporting it with elements such as text, audio, images or video, and the fact that the news is extremely difficult to confirm, turns social media into an ecosystem that rapidly spreads fake news, users also play a major role in the spread of fake news by liking and re-sharing the news. In order to see how serious the effects of fake news have reached, it is enough to look at the effects of fake news and conspiracy theories on people, about the so-called harms and side effects of the COVID-19 vaccine in the past period. The decrease in the rate of vaccination with vaccine opposition and vaccine indecision is attributed to exposure to misinformation about the COVID-19 vaccine on social media (Islam et al., 2021).

[1] mer@bandirma.edu.tr

[2] yonca@comu.edu.tr

[*]Corresponding Author

For the social media ecosystem, the question arises as to which emotion is more effective in spreading fake news, as the accuracy and validity of the news are under the control of opinions and emotions rather than evidence-based data. With this viewpoint, our study investigates whether there is a relationship between users' reaction to the news and the prevalence of the news. "When users encounter fake news, what type of emotion drives them to spread that fake news?" or in other words, "Is there a relationship between the reaction to fake news and the prevalence of the news?" are the research questions of our study. To fully reveal whether there is a relationship between users' reactions to the news and the prevalence of the news, the spread of real news is also discussed in addition to fake news. The emotional impact of real news, as well as fake news, on people has been examined and it has been evaluated whether there is a similarity between fake news and the emotion that spreads the real news. In this study, which is unique in its own right with its research questions and content, the comments on the Twitter platform, which is known as the first source of the news and the first place to go to learn the agenda, were used. A sentiment analysis was conducted on the reactions of Twitter users to fake news about the COVID-19 vaccine between December 31, 2019, and July 30, 2022. Fake and real news comments selected in different degrees of prevalence from very common to less common were examined comparatively.

Sentiment analysis is considered as a classification problem in the literature. Go, Bhayani & Huang (2009), who applied sentiment analysis to tweets for the first time, used sentiment expressions in tweets to classify sentiment, and classified tweets as positive or negative. Pak & Paroubek (2010), similar to the study of Go et al. (2009), by looking at the emotion expressions at the end of the tweets, handled the problem as a multi-class classification task and classified the tweets into three classes as positive, negative and neutral. It is important to determine which features are more effective in revealing the emotion in the text. To this end, a number of researchers (Agarwal et al., 2011; Hamdan, Bechet & Bellot, 2013; Kouloumpis, Wilson & Moore, 2011; Saif, He & Alani, 2012) examined the effect of different features on the Twitter sentiment analysis problem. Saif, He & Alani (2012) presented a novel approach to add semantic features in addition to the features in the training set. Neethu & Rajasree (2013) suggested feature extraction after applying two-step pre-processing to the text to process typos and slang words in their study. Another important study belongs to Hutto & Gilbert (2014). In their study, they recommended VADER as a lexicon and rule-based sentiment analysis tool. Thanks to the ability of easily accessing the thoughts of many users from all over the world on Twitter, sentiment analysis on Twitter has recently become a subject of study in the social and psychological fields. Dzogang, Lightman & Cristianini (2018), who conducted one of such studies, measured the daily variation of 73 psychometric variables in Tweets they analyzed from the UK, and found two main factors, "Categorical Thinking" and "Existential Thinking", which peaked at opposite time points throughout the 24-hour day. Another study was conducted by Snefjella, Schmidtke & Kuperman, (2018). They measured the emotional variation of tweets between Canada and the United States, with the aim of measuring the use of certain types of language across different cultures.

The increase in the spread and social impact of fake news as a result of the popularization of social networks has led to a growing interest in examining fake news on social networks. One of the key tricks that fake news producers use to support the success of fake news is to excite the emotions of the readers. Therefore, sentiment analysis turned out to be a very useful method for examining fake news when applied to both news items and related information such as user comments (Alonso et al., 2021). In this context, Del Vicario et al. (2019) provided a framework for early warning of potential misinformation targets in social media. In their study, they fed several classic machine learning classifiers with text features and emotion-based features of user behavior to detect fake news. The best performance was obtained with a logistic regression classifier. In another study, the authors investigated whether the hidden sentiments found in user comments on social media help distinguish fake news from credible content. Experimental results have shown that the component that contributes the most to the performance of the system is sentiment analysis (Cui, Wang & Lee, 2019). Anoop, Deepak & Lajish (2020) worked on the detection of fake news in the field of health. In their study, they looked at different types of emotional traits displayed in fake and real health news to detect fake news. They extracted emotion features from a lexicon to feed classical and deep learning classifiers and stated that the performance of all classifiers increased with emotion information.

Zhang et al. (2021) noted that most of the existing studies on fake news, even for fake news that go viral, focus on the emotional signals of the content conveyed by publishers rather than the emotions the news evokes in the crowd. Therefore, in their study, they investigated whether the emotions and content in news comments are useful for fake news detection. They stated that their proposed feature set could be well compatible with

existing fake news detectors and effectively improve fake news detection performance. Iwendi et al. (2022) proposed a model in which they use 39 features from multimedia texts to detect fake news about COVID-19. They used information fusion in their work to extract social media data, where they applied cutting-edge deep learning models such as Long Short-Term Memory (LSTM), Gated Recurrent Units (GRU), and Recurrent Neural Network (RNN). RNN achieved a high precision of 85% for the model they used, while using GRU model for fake news, the best F1-Measure and recall were 83%. Another study examining the spread of fake news is by Bodaghi & Oliveira (2022). In their study, which examined users in different roles during the spread of fake news, they analyzed the real and fake news spread on Twitter. For this purpose, they analyzed 5 fake news collected from Twitter, which includes 8 million nodes and 28 million links in total, using graphs. With their work, they aimed to provide a better understanding of the nature of fake news spread on social media (Bodaghi & Oliveira, 2022). Studies in the literature used sentiment analysis to detect fake news and suggested different methods to examine its spread. There is no study we came across which deals with the spread of fake news using sentiment analysis.

In addition to being a research topic that has not been studied before in the literature, our study, which will shed light on the nature of fake news that causes its rapid spread, will provide a deeper understanding of human psychology and behavior, and raise awareness of individuals on how they can recognize when they come across a piece of news, whether it is fake news or not, before they spread it. The rest of the study organizes as follows. In Section 2 data collection, normalization of the text and analysis processes are explained. In Section 3, the findings are given and the results are discussed.

2. Materials and Methods

In this section, the steps performed in the study are given. The data and analysis methods of the study, which was carried out with three basic processes, namely data collection, text normalization and text analysis, are explained in this section. The system architecture proposed in our study is given in Figure 1.

2.1. Data Collecting

Fake and real news about the COVID-19 vaccine used in our study were selected from news verification sites such as Snopes (2018), FactCheck.org (2008) and Check Your Fact (2019), which are independent confirmatory. The fake and real news headlines we collected in our study and the number of comments made on these news are given in Table 1 and Table 2, respectively. The prevalence was determined by the number of comments made on fake/real news.

It is known in the literature that most of the researchers use Twitter APIs to collect tweets (Giachanou & Crestani, 2016). However, since Twitter's free access policy, prices, and different access options change over time, there are limitations on the number of requests per minute, tweets per request, and access to historical data in Twitter API (Antonakaki, Fragopoulou & Ioannidis, 2021). To overcome these limitations, Twint was used as a tweet collection tool in our study. Although Twint is open-source software, it does not rely on Twitter's API and allows unlimited tweet downloads (Zacharias & Poldi, 2018).

Table 1
Fake news circulated on social media about the COVID-19 vaccine between December 31, 2019 and July 30, 2022.

Fake news headlines	Number of comments
COVID-19 vaccine impairs fertility	62722
COVID-19 vaccine can monitor the human	56052
COVID-19 vaccine will reduce the planet's population	30792
COVID-19 vaccine can change human DNA	21073
COVID-19 vaccine contains aborted fetal cells	13164
COVID-19 vaccine makes our body magnetic	11206
Thousands of Americans died after receiving their COVID-19 vaccine	5435
Bill Gates admits that a COVID-19 vaccine could kill up to 700K people	3145

Table 2
Real news circulated on social media about the COVID-19 and COVID-19 vaccine between December 31, 2019 and July 30, 2022

Real news headlines	Number of comments
US Deaths from COVID Hit 1 Million, Less Than 2 1/2 Years in	51783
Biden Say "You Won't Get COVID if You're Vaccinated"	31673
US Opens COVID-19 Vaccine to Little Kids; Shots Begin This Week	17732
COVID-19 Shots Might Be Tweaked if Variants Get Worse	14888
FDA Advisers Recommend Updating COVID Booster Shots for Fall	14579
Pfizer to Discuss COVID-19 Vaccine Booster with US Officials	8717
Dr. Anthony Fauci Said US Is 'Out of the Pandemic Phase'	2565
Masks Could Return As COVID Surges Nationwide	2053

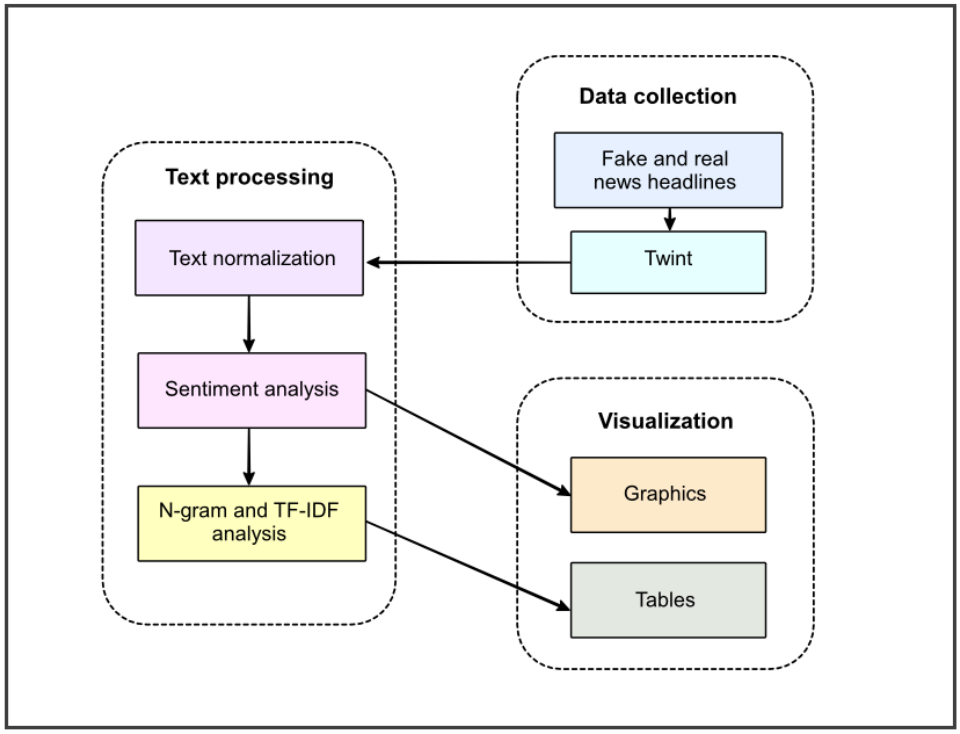

Figure 1. The proposed system architecture.

Comments were collected by giving parameters, such as search keywords, the display of replies to tweets and the first time the fake news was seen to CLI (Command Line Interface) commands specific to Twint. For example, a false news title such as “COVID-19 Vaccine Impairs Fertility” was questioned with the keywords “covid vaccine impact fertility”, “covid vaccine cause infertility” and “covid vaccine cause miscarriage”.

2.2. Text Normalizing

Tweets collected with Twint; along with the body of the tweet, contain the username, mentions, tweet ID, the date and time of the tweet, and the UTC (Coordinated Universal Time) time difference identifier. In addition to the noise brought by the data collection tool, the informal language and style used in social media also necessitate the text normalization process. The aggregated data, which appears extremely complex even with human reading, are given in the “Raw Text” column of Table 3. In this context, in our study, the data were subjected to a detailed text cleaning and normalization process. For this, text mining techniques and NLP tools were used for text normalizing. The workflow followed for text cleaning is shown in Figure 2.

Examples of raw data and the text after normalization are given in Table 3. Since the characters, numbers, date and time information belonging to Twitter are not related to the analysis we applied to the text, it was appropriate to delete them from the data set. Since the sentiment analysis tool we applied to the data is lexicon-based, "happy😀" and "happy😀" are perceived as two separate words. To overcome this challenge, emoticons, emojis and other characters are separated from the words they are attached to. Since emojis are the most contributing component in revealing the emotion in the text, emojis have been replaced with their textual counterparts in the data set. For example, the "😀" emoji has been replaced by the phrase "smiling_face_with_smiling_eyes". This transformation was achieved by using the open-source emoji module (Kim & Wurster, 2015).

It is very common to use abbreviations because of the character limit of Twitter. In order to capture the emotion that abbreviations add to the text, the data sets were subjected to a three-stage process for the full forms of abbreviations. Respectively, the full forms of official abbreviations used in English, unofficial abbreviations used in daily speech, and internet slang abbreviations were carried out. Abbreviations are created manually and kept in dictionary data structure type. Examples of abbreviation dictionaries are given in Table 3.

Table 3
Three randomly selected tweets from the "COVID-19 Vaccine Contains Aborted Fetal Cells" dataset. The first version after being collected from Twitter with Twint is given in the "Raw Text" column, the text after applying normalization is given under the "Normalized Text" column. Usernames and mentions have been replaced with "username" in accordance with the personal data protection law

Raw Text	Normalized Text
1389044057830273027 2021-05-03 05:28:05 +0300 <username> @username Covid vaccine contains chimpanzee bodyparts and aborted fetuses to steralise and kill society. https://t.co/tf1SgL4Rg5	covid vaccine contains chimpanzee bodyparts and aborted fetuses to steralise and kill society
1387590968019353600 2021-04-29 05:14:01 +0300 <username> A colleague at my school—a teacher-actually said today aborted fetuses are in the Covid vaccine...I'm done... 🤦‍♀️🤦‍♀️	a colleague at my school a teacher actually said today aborted fetuses are in the covid vaccine i am done person facepalming light skin tone female sign person facepalming light skin tone female sign
1377049899787825152 2021-03-31 03:07:35 +0300 <username> My mother won't get the Covid vaccine because she says it contains aborted fetuses. Can some of you medically knowledgeable people please help set her straight? I'm so tired of the bullshit and she might listen if it comes from someone else. She's vulnerable! 🥺 #CovidVaccine	my mother will not get the covid vaccine because she says it contains aborted fetuses can some of you medically knowledgeable people please help set her straight i am so tired of the bullshit and she might listen if it comes from someone else she is vulnerable pleading face covid vaccine

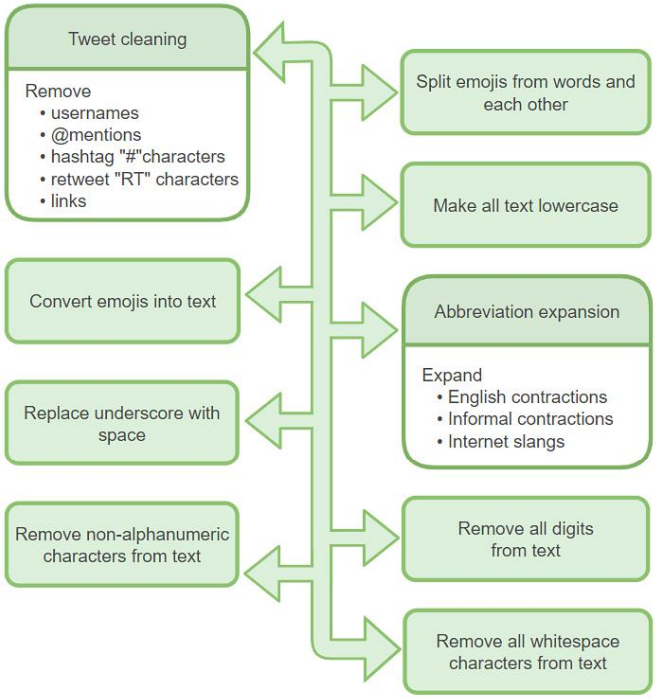

Figure 2. Workflow for text normalization

Table 4
Respectively; Sample abbreviations from English Contractions (2022), Informal Contractions List in English (2020), and Internet Slang Terms (2021) dictionaries.

English Contractions		Informal Abbreviations		Internet Slang	
Abbreviation	Full form	Abbreviation	Full form	Abbreviation	Full form
‘m	am	c’mon	come on	csl	can’t stop laughing
‘r	are	dija	did you	lol	laughing out loud
‘s	is	sorta	sort of	jk	just kidding
‘ve	have	dunno	don’t know	smh	shaking my head
‘ll	will	lemme	let me	qq	crying
‘d	had	innit	isn’t it	w8	wait

After replacing the underscores between words with a space character, deleting all characters except numbers and alphanumeric characters, and removing the white space character, the text normalization process was completed. Checking if the text contains the specified search pattern and replacing it with the desired character was performed using Python’s re module.

2.3. Analyzing the Text

In our study, dictionary and rule-based open-source VADER sentiment analysis tool was used to classify the emotional polarity of the texts (Hutto & Gilbert, 2014). VADER includes a dictionary of emotions labelled by multiple independent human reviewers, which considers the average of these labels as the word’s “valence” score. While calculating the perceived emotional intensity in the text at sentence level, it applies the grammatical and syntactic rules explained in their study. VADER, which is sensitive to both the polarity and the intensity of the expressed emotions, can be applied for sentiment analysis in all areas in general, as well as adapting to the emotions expressed in social media (Hutto & Gilbert, 2014).

When sentiment analysis is applied to a sentence, the composite score, referred to as "compound", is calculated by summing the valence scores of each word in the dictionary, adjusting them according to the rules, and then normalizing them from -1 (most negative) to +1 (most positive). The "pos", "neu" and "neg" scores indicate the proportions of texts falling into each category and therefore their sum should be 1 (Hutto & Gilbert, 2014). Based on this context, in our study, standard thresholds were used, and the sentences were classified as positive, negative or neutral according to the composite score.

After applying the sentiment analysis separately for each data set, the rate of positive, negative, and neutral polarity in the comments emerged. N-grams are used to count how often consecutive word strings occur in the datasets. N-gram is basically a string of N words that occur together in a particular document. The n-gram analysis was performed using the N-grams module of the NLTK (Natural Language Toolkit) library in two different ways (Bird, Klein & Loper, 2009). In the first process, n-grams were produced without deleting the stop words. Stop words (such as the, and, but, if, as in English) do not have a meaning on their own and are the most commonly used words such as adverbs, prepositions and conjunctions in a language. English stop words corpus of the NLTK library was used in our study. In the second process, n-grams were produced after the stop words were deleted. This enabled us to catch important abstract word groups.

Finally, in our study, TF-IDF (term frequency-inverse document frequency) analysis of the data sets was made under their own news headlines. TF- IDF is obtained by multiplying TF and IDF values, and TF, that is, "term frequency", refers to the frequency of occurrence of the term in the document. It is obtained by dividing the number of occurrences of the term in the document by the total number of words in the document. IDF is the inverse document frequency and is the logarithm of the ratio of the total number of documents to the number of documents containing the relevant word. The equation of IDF is given in 2.1.

$$idf_t = \log \frac{N}{df_t} \tag{2.1}$$

In 2.1, N represents the number of documents, and df_t represents the number of documents containing the t term. From this point of view, if a word occurs frequently in other documents, the IDF value will decrease. In other words, the higher the IDF value, the more unique the word is. The equation for the TF-IDF obtained by combining the term frequency and the inverse document frequency to produce a combined weight for each term in each document is given in 2.2.

$$tf - idf_{t,d} = tf_{t,d} \times idf_t \tag{2.2}$$

In 2.2, $tf_{t,d}$ shows the frequency of the term t in the document d; idf_t is the inverse document frequency calculated in 2.1. The TF-IDF value will take the lowest value when the term occurs in almost all documents (Manning, Raghavan & Schutze, 2008). To measure the diversity and uniqueness of the comments in the data set, TF-IDF analysis was performed at the last stage. In Section 3, the sentiment classification and polarity rates of fake news were compared in ascending order, and the diversity and uniqueness of the comments in the data set were interpreted in the light of the most common n-grams and TF-IDF values.

3. Results and Discussion

After the comments on the fake and real news headlines given in Table 1 and Table 2 were collected, they were converted into a dataset under separate headings and sentiment analysis was applied by isolating them from each other. The titles of the data sets, the number of data they contain, the rates of negative, neutral and positive comments are given in Figure 3 and Figure 4 for fake news, and Figure 5 and Figure 6 for real news, in ascending order. Data sets from Set 1 to Set 8 represent fake news datasets, while those from Set 9 to Set 16 represent real news datasets.

In Figure 3 and Figure 4 in which the emotional polarity rates and data numbers of the datasets are given, it is seen that the rate of negative comments is always higher in all fake news datasets than the other emotional polarities (positive and neutral). For the fake news datasets, all of the eight datasets had a higher rate of negative

polarity than the others. That is, the predominant rate of negative polarity is 100% for fake news. This shows that fake news - whether its prevalence is more or less - is largely fed by negative mood. However, when Figure 5 and Figure 6 are examined, we see that the same is not valid for real news data sets. Four of the eight datasets had a higher rate of positive polarity than the others. Thus, the predominant rate of positive polarity is 50%. This shows that there are more positive comments on real news than fake news. However, for real news, negative polarity is predominantly found at 50%, while neutral polarity is dominant at 0%. That is, neutral polarity is not dominant in any data set. In this respect, real news and fake news are similar to each other.

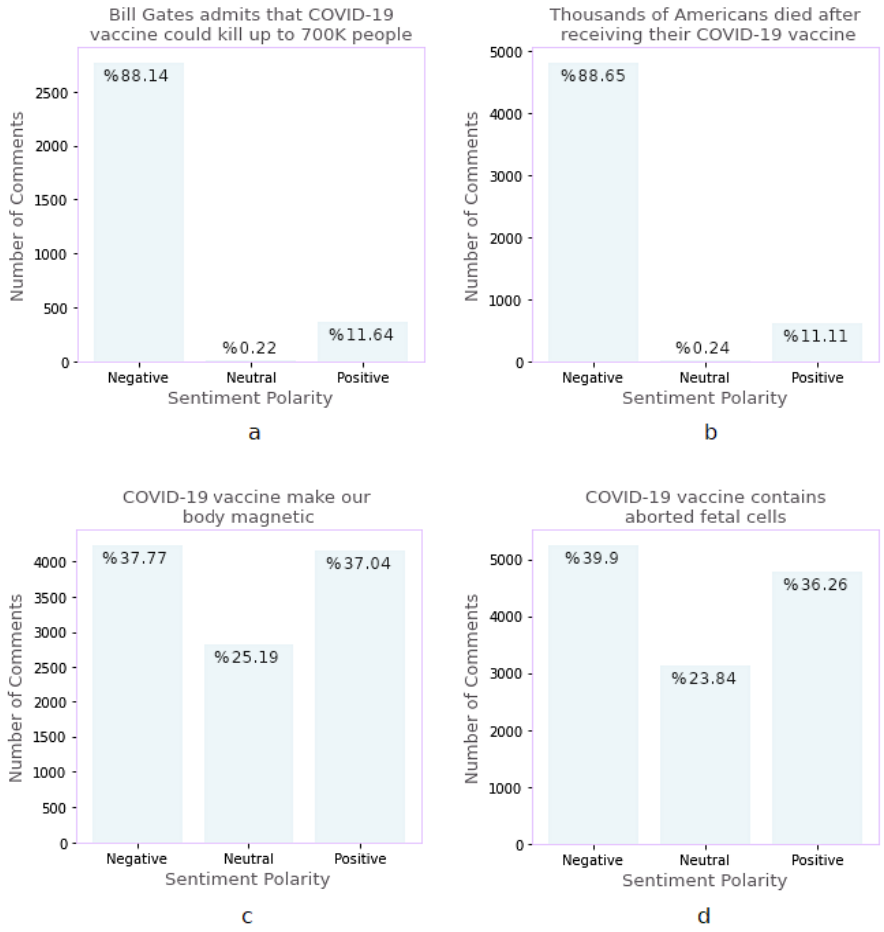

Figure 3. Polarity analysis of fake news datasets 1-4 (a) Set 1 “Bill Gates admits that a COVID-19 vaccine could kill up to 700K people”, number of data is 3145. (b) Set 2 “Thousands of Americans died after receiving their COVID-19 vaccine”, number of data is 5435. (c) Set 3 “COVID-19 vaccine makes our body magnetic”, number of data is 11206. (d) Set 4 “COVID-19 vaccine contains aborted fetal cells”, number of data is 13164.

However, except for Set 1 and Set 2, which had the lowest number of data, the interpretation rates in the other sets showed consistent changes. For this reason, it was appropriate that Set 1 and Set 2 were not included in the interpretation rate change graphs in Figure 7 in order not to prevent generalization, considering that they are insufficient to reflect the characteristics of the data due to the small number of data. However, while Set1 and Set2 are very similar to each other, displaying a completely different characteristic from the others is a situation that should be examined in particular. To understand the reason, the specific analyzes applied to Set 1 and Set 2 are explained later in the article.

When Set 1 and Set 2 are not included in the comment rate change graphs in Figure 7, the data set with the lowest data number of the fake news data sets is Set 3 with 11206 comments. Since the dataset with the least spread among fake news contains 11206 comments, it is necessary to provide equal conditions for real news. Therefore, datasets with less than 11206 comments (Set9, Set10, and Set11) from real news datasets are not included in the comment rate change graphs in Figure 7. Thus, the datasets with the lowest spread for fake and real news were brought to the same level.

When Figure 7 (a) and (b) are examined together, while the number of data increases in both, an increase in the rate of negative comments is observed. From this point of view, it can be said very clearly that as negative comments increase, the prevalence of news, whether it is fake news or real news, increases. In Figure 7(c), though not as much as the rate of change in Figure 7(a) a decrease in the rate of positive comments is observed. It is interesting, however, that the rates of positive comments range from 40% to 30% for all datasets given in the graph. In Figure 7(d), the decrease in the rate of positive comments is clearly seen. It is not possible to make any generalizations for Figure 7(e) and Figure 7(f) where the change in the neutral interpretation rate is given. Therefore, it turns out that neutral comments have no effect on prevalence. In 83% of the fake news datasets and 91% of the overall news datasets considered in the study, it is observed that the prevalence of the news increases as the negative emotional comments increase.

Another common element seen in Figure 7(a) and Figure 7(c) is that Set 7 behaves contrary to the general data set characteristic. The rate of negative comments decreases when it should increase, and the rate of positive comments increases when it should decrease. To understand the reason for this behavior, n-gram analysis was applied to Set 7. The most frequent words and word groups in the data set are given in Table 5.

When Table 5 is examined, the most common words in the data set are “vaccine” and “microchip”. The first two 5-gram structures that are most common in the document appear as emojis that are converted into words to add emotion to the text in the text normalization step. These two emojis corresponding to 5-grams are given in parentheses. When the other 5-grams are examined, it is seen that the word groups “a microchip in the vaccine” are encountered again and at higher frequency when going from specific to general, that is, from 5-grams to 1-grams. Especially when 2-grams are examined, the words “microchip” and “vaccine” are frequently used in the document with different conjunctions and prepositions. This indicates that the comments are diverse and unique. The words “5g”, “5g chip” and “laughing” are also among the most common words that appear singularly in the document. When this document, which has a high positive polarity rate, is examined in the light of n-grams; it can be clearly stated that the rumor of “There is a microchip in the vaccine” is dominant and therefore fake news is not taken seriously, and users tweet under this title for fun. However, the “mark of the beast” word group, which is common in 4-gram and 5-gram, is not found among other common n-grams. This word, which is linked to the fake news “COVID-19 Vaccine Is Linked to the Mark of the Beast” (Conversation, 2021), which emerged at about the same time as the other news headlines used in the study, indicates that this word group was not accepted among Twitter users, and therefore this word group was put into circulation as a result of a bot activity.

A detailed analysis was needed as the polarity ratios of Set 1 and Set 2, given in Figure 3 (a) and (b), were very different from the general trend. Even if it is a small dataset, it is not necessary to read all the comments in the dataset one by one to understand why it is so different from the general trend. Instead, the most frequently occurring word groups in the data set can be identified using n-grams. Therefore, an n-gram analysis was performed to count how frequently consecutive word strings in the data set were seen. After the most common word groups and the number of their use together were noted, it was manually examined whether there were potential sentences starting with the same word groups. These potential sentences were tabulated manually, and a visual representation of the word groups most frequently found together in the data set is given in Table 6 and Table 7. In Tables 6 and 7, a sentence is obtained by taking one word from each column from left to right. In this way, it is possible to see the frequently encountered sentences and the number of their occurrences in a summarized way, without the need to read all the comments in the relevant data set. For example, looking at Table 7, we see that the phrase "Americans have died from the vaccine" is used 105 times in Set 2. The word group summary for sentences starting with the “Bill Gates” in Set 1 is given in Table 6. This group of words was chosen because the 2-gram number has the highest value for “Bill Gates”. A similar analysis is given in Table 7 for Set 2. The word "Americans" was chosen to start n-grams because it is at the highest frequency in Set 2. The most common sentences in the data set are given in each row from the first column to the other columns, and the numbers of frequent word groups up to 6-grams are summarized. In the 3rd and 5th rows where the n-gram representation of the sentences starting with “Bill Gates vaccine” and “Bill Gates said”, the 4-gram and 5-gram columns were left blank because the same word groups could not be found that repeat often enough to aggregate. The sequence in the continuation of these word groups is seen in the 6-gram+ column. The first column is 2-grams, which means that the ‘Bill’ ‘Gates’ pair is found side by side 2635 times.

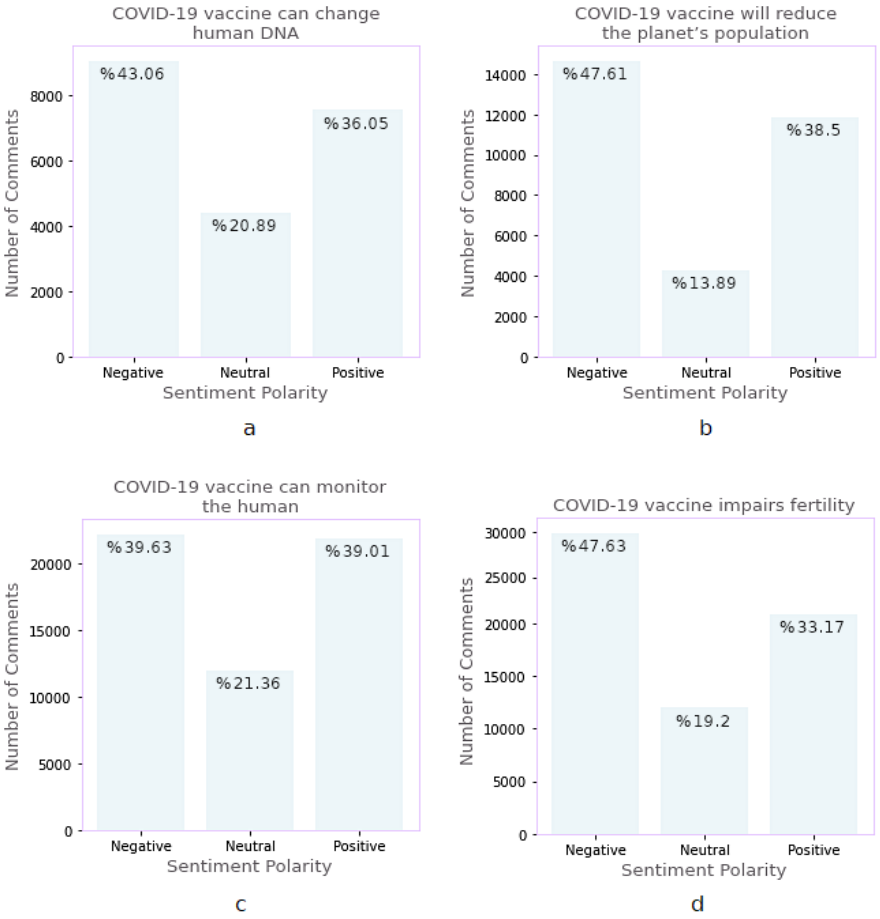

Figure 4. Polarity analysis of fake news datasets 5-8 (a) Set 5 "COVID-19 vaccine can change human DNA", number of data is 21073. (b) Set 6 "COVID-19 vaccine will reduce the planet's population", number of data is 30792. (c) Set 7 "COVID-19 vaccine can monitor the human", number of data is 56052. (d) Set 8 "COVID-19 vaccine impairs fertility", number of data is 62722

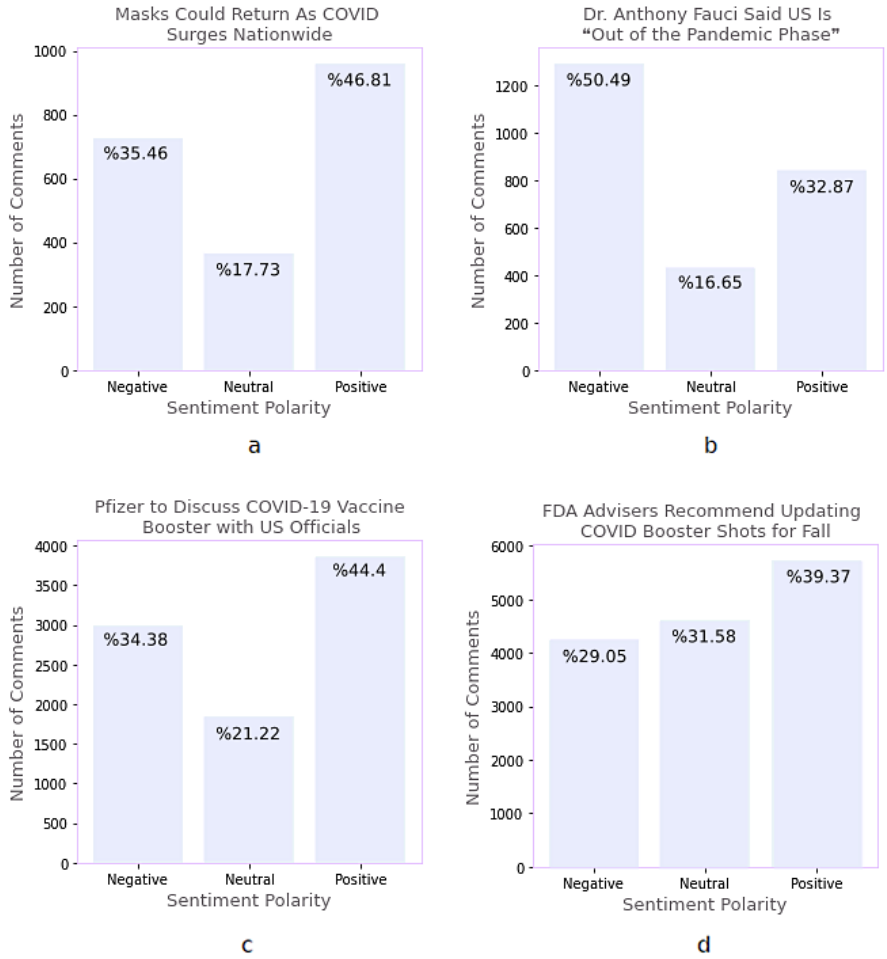

Figure 5. Polarity analysis of real news datasets 9-12 (a) Set 9 "Masks Could Return As COVID Surges Nationwide", number of data is 2053. (b) Set 10 "Dr. Anthony Fauci Said US Is 'Out of the Pandemic Phase'", number of data is 2565. (c) Set 11 "Pfizer to Discuss COVID-19 Vaccine Booster with US Officials", number of data is 8717. (d) Set 12 "FDA Advisers Recommend Updating COVID Booster Shots for Fall", number of data is 14579.

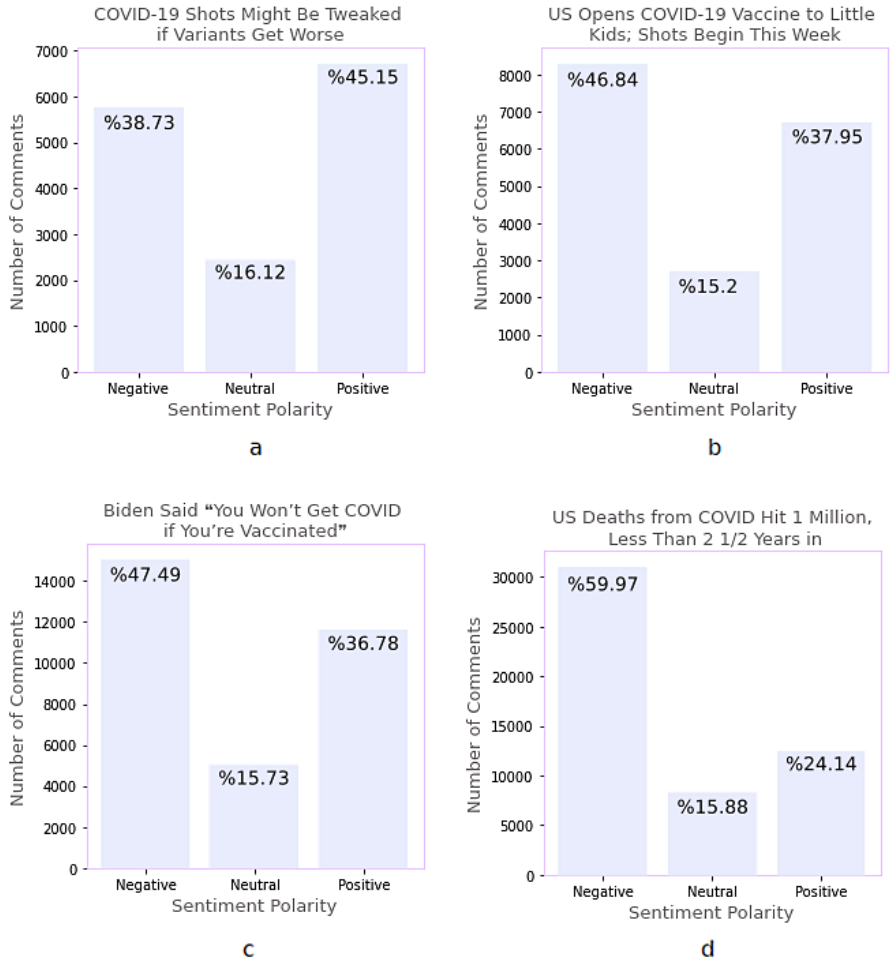

Figure 6. Polarity analysis of real news datasets 13-16 (a) Set 13 "COVID-19 Shots Might Be Tweaked if Variants Get Worse", number of data is 14888. (b) Set 14 "US Opens COVID-19 Vaccine to Little Kids; Shots Begin This Week", number of data is 17732. (c) Set 15 "Biden Say 'You Won't Get COVID if You're Vaccinated'", number of data is 31673. (d) Set 16 "US Deaths from COVID Hit 1 Million, Less Than 2 1/2 Years in", number of data is 51783.

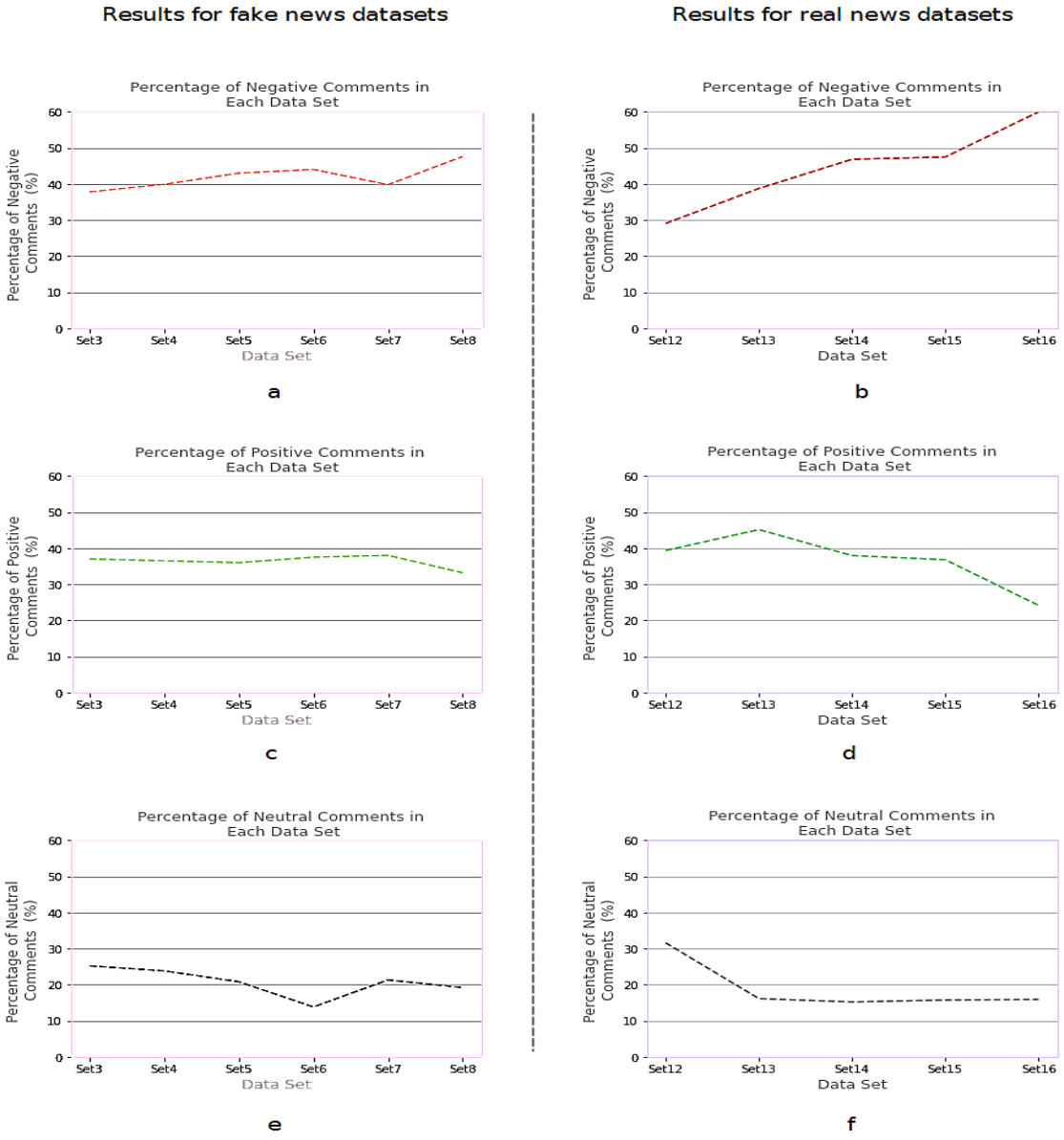

Figure 7. (a) The change in the rate of negative comments in the fake news data set according to the increasing number of data from Set 3 to Set 8. (b) Change in the rate of negative comments in the real news dataset with increasing data number from Set 12 to Set 16. (c) The change in the rate of positive comments in the fake news dataset according to the increasing number of data from Set 3 to Set 8. (d) Change in the rate of positive comments in the real news dataset with increasing data number from Set 12 to Set 16. (e) Neutral comment rate change in fake news dataset with increasing data number from Set 3 to Set 8. (f) Neutral comment rate change in real news dataset with increasing number of data from Set 12 to Set 16.

For example, if we read the table up to the 4th column of the 2nd row, which is 5-grams, the phrases “Bill Gates wants to kill” are found 87 times in the Set 1 data set, or if we read up to the 3rd column of the 4th row (4-gram) the phrases “Bill Gates will kill” appear side by side 54 times. The words in the last column of the table are the aggregated representation of the sentences in the data set from top to bottom such as “Bill Gates is tryingto kill people”, “Bill Gates is tryingto kill more people”, “Bill Gates is tryingto kill poor people”.

When we examine the n-gram analysis for Set 1, it is interesting to see that, comments can be so aggregated and have so many common word groups. From the last column showing 6-grams and more, it is understood that new phrases are derived using the adjectives of the same word (people, poor people, white people, old people, millions of people) and certain word groups (us all, them) are used in many of the sentences. These results suggest that the sentences are automatized and derived, and bots are used. In addition, the presence of

the “Bill Gates” word group in 2635 of a dataset with 3145 comments is another important result that shows that the comments are not diverse and unique.

A similar situation applies to Set 2. It is interesting that prepositions come especially after the “Americans, have, died” group; like “from, of, due, and, in” or after “Americans, who, died”; like “from, without, of, because”. It appears that all possible sentences that can be written with a given set of words are produced. This situation regards that there are artificial sentence experiments produced to spread the existing word group.

In Table 8 and Table 9, the TF, IDF and TF-IDF scores of the six most frequent words in Set 1 and Set 2 are given, respectively. In Table 8, it is seen that the TF-IDF values of the words “vaccine”, “people” and “kill” with the lowest IDF values are also very low. For Table 9, the TF-IDF values of the words "americans" and "dead" are zero. This indicates that these words appear in most of the comments, and their uniqueness is extremely low. In the aggregated word group summary in Table 6 and Table 7, we see that these words are found in almost every comment. The frequent use of the word “kill” and “dead”, which has a high negative emotion intensity, explains the negative polarity rate of Set 1 to 88.14% and Set 2 to 88.65%. The fact that the IDF, which is the uniqueness score of words with high term frequency, is very low – or even zero for Set 2 – shows that similar sentences containing the same words are constantly tweeted.

Table 5
The most common words and phrases of Set 7

n-gram	Most frequent n-grams	Numbers
5-gram	'face', 'with', 'tears', 'of', 'joy' (😂)	2736
	'rolling', 'on', 'the', 'floor', 'laughing' (🤣)	1675
	'a', 'microchip', 'in', 'the', 'vaccine'	1355
	'the', 'mark', 'of', 'the', 'beast'	1241
4-gram	'microchip', 'in', 'the', 'vaccine'	2725
	'mark', 'of', 'the', 'beast'	2356
3-gram	'a', 'microchip', 'in'	5969
	'the', 'covid', 'vaccine'	3675
	'in', 'the', 'vaccine'	3637
	'there', 'is', 'a'	1608
2-gram	'a', 'microchip'	35055
	'the', 'vaccine'	26723
	'microchip', 'in'	20994
	'a', 'vaccine'	14293
	'to', 'microchip'	12810
	'the', 'microchip'	11508
	'microchip', 'vaccine'	4910
	'microchip', 'and'	3575
	'microchip', 'that'	3512
	'and', 'microchip'	3183
	'5g ', 'chip'	1713
1-gram	Vaccine	62572
	Microchip	54270
	5g	7763
	Laughing	2459

This result indicates that there is an effort to deliberately spread fake news and the use of bots. Since it is fake news that has not been spread, organic users' comments are in the data set, but since they are in the minority, the derived comments of bot accounts are especially evident as a result of such an analysis, and the low number of data in Set 1 turns into an advantage. The use of bots in the comments of this fake news, which could not reach Twitter users, is an intervention to the natural flow. Therefore, the interpretation rates of Set 1 and Set 2 were not considered within the scope of the analysis in the study. Thus, the results obtained in these data sets do not affect the fact that the increase in negative comments increases the prevalence of fake news.

When the data sets were examined, it was observed that negative emotions were intense in fake news comments, and positive and negative polarity were found to be balanced in real news. In our study, positive polarity is dominant at the rate of 50% in real news datasets, while negative polarity is dominant at 100% in fake news datasets. This observation is consistent with some previous studies (Dey et al., 2018; Dai, Sun & Wang, 2020). Dey et al. (2018) showed that credible tweets mostly have positive or neutral poles, while tweets with fake content have a strong tendency towards negative emotions. Dai, Sun & Wang (2020) made sentiment analysis on health news, and they found that responses to real news were more positive than fake news. The rise of negative comments as the prevalence of the news increases is common to both fake and real news reactions. This situation shows that the emotion that activates the desire to spread the news is negative emotions. This result is in parallel with the result obtained in the study of Bodaghi & Goliaei (2018). Bodaghi & Goliaei (2018), stated that an individual will feel a cognitive dissonance when they see that their belief is not known by others, or when they encounter an opposing view (true for those who believe in fake news, or fake news for those who believe in real news), and will tend to spread fake or true news by acting according to the backlash effect. In their study, where they provide a general framework for describing bots, Dickerson, Kagan & Subrahmanian (2014) stated that people tend to disagree more with the entire Twitter population than bots. This supports our analysis of bots in our study. While the rate of negative comments is over 88% in datasets inflated only by bots (Set 1 and Set 2), negative, positive and neutral comment rates in other datasets show a balanced distribution, which indicates differences of opinion in accordance with human nature.

Table 6
Word group summary of Set 1

2-gram	3-gram	4-gram	5-gram	6-gram+
Bill Gates (2635)	is (350)	tryingto (70)	kill (69)	people more people poor people black people us all them
	wants (159)	to (139)	kill (87)	people poor people millions of people white people old people us all them
	vaccine (103)			could kill more people kills enough people kill people will kill us all will kill millions will change our dna actually does kill did kill people
	will (80)	kill (54)	people (49)	
	said (77)			that the vaccine will kill people a vaccine would kill people the vaccine will kill million people a vaccine will kill almost a million people he was going to kill billion people
	admits (54)	his (21)	covid (19)	vaccine will kill people vaccine will kill millions of people vaccine might kill nearly people

Table 7
Word group summary of Set 2. (The number of words is less than 20 and the parts that cannot be divided further are given as N/A in order not to increase the complexity.)

1-gram	2-gram	3-gram	4-gram	5-gram	6-gram
Ameri-cans (6180)	have (2194)	died (1917)	from (946)	covid (870)	as (77)
					and (67)
					with (50)
				the (423)	vaccine (105)
					flu (89)
					covid (29)
					virus (20)
				it (100)	N/A
			of (300)	covid (396)	N/A
				the (108)	N/A
			due (160)	to (159)	the (100)
			and (143)	N/A	N/A
			in (103)		
		already (115)	died (100)	N/A	N/A
	died (1739)	from (385)	covid (152)	N/A	N/A
			the (114)		
		because (259)	of (144)	N/A	N/A
		of (195)	covid (98)	N/A	N/A
	who (531)	died (278)	from (62)	covid (24)	N/A
			without (55)	getting (55)	
			of (30)	covid (28)	
			because (26)	N/A	
		have (196)	died (167)	from (62)	covid (31)
				of (21)	covid (16)

Table 8
tf, idf and tf-idf values for the six words of Set 1 with the highest term frequency.

words	tf	idf	tf-ifd
vaccine	11.0	0.000318	0.003498
admits	9.0	3.749504	33.745535
gate	9.0	0.137126	1.234137
bill	9.0	0.137126	1.2345137
people	9.0	0.000636	0.005725
kill	9.0	0.000318	0.002862

Table 9
tf, idf and tf-idf values for the six words of Set 2 with the highest term frequency.

words	tf	idf	tf-ifd
americans	10.0	0.000000	0.000000
died	10.0	0.000000	0.000000
vaccine	9.0	1.340795	8.044771
another	9.0	3.804824	11.414473
virus	9.0	1.908531	5.725593
covid	9.0	0.684902	2.054705

4. Conclusion

In this study, sentiment analysis was applied on the reactions to fake and real news at different prevalence rates. Although there are minor differences, the changes in the emotional states of the comments made on real news and fake news show parallelism with each other. Fake news is successful as long as it resembles real news. Therefore, the success of fake news depends on how good it presents itself as real news. The better the fake news copies the real news and the more it makes an impression that it is real, the more attention it receives as if it were real news. However, it has been revealed that negative emotion is a very effective and key emotion in spreading the news, whether for fake news or real news. However, especially for fake news, negative polarity was seen to predominate in all datasets without exception. This clearly reveals that the strongest emotion in spreading fake news is negative emotions.

When it comes to real news, we can say that people take a much more serious approach by looking at the obvious decrease in the positive comment rates of real news as the prevalence increases. However, it is found that users who comment on fake news for fun significantly increase the prevalence. Even if there is a widespread fake news with the highest rate of positive comments among all data sets, the fact that the rate of negative comments is higher than the rate of positive comments shows that negative emotion is extremely effective in spreading fake news.

Another factor that we come across about fake news is bot activities. It is seen that bot activities come into play to spread the fake news after it is revealed. To reveal bot activity NLP techniques were applied in the study. The presence of word groups pointing to a different fake news headline in the comments made on a fake news headline makes us think that the fake news came out deliberately from a single source.

Author Contributions

Maide Feyza Er: Collected data and performed the analysis.

Yonca Bayrakdar Yılmaz: Performed statistical analysis and wrote the paper.

Conflicts of Interest

The authors declare no conflict of interest.

References

Agarwal, A., Xie, B., Vovsha, I., Rambow, O., & Passonneau, R. J. (2011, June). Sentiment analysis of twitter data. In Proceedings of the workshop on language in social media (LSM 2011) (pp. 30-38). Retrieved from: https://aclanthology.org/W11-0705

Alonso, M. A., Vilares, D., Gómez-Rodríguez, C., & Vilares, J. (2021). Sentiment analysis for fake news detection. Electronics, 10(11), 1348. DOI: https://doi.org/10.3390/electronics10111348

Anoop, K., Deepak, P., & Lajish, V. L. (2020). Emotion cognizance improves health fake news identification. In IDEAS (p. 24). DOI: https://doi.org/10.48550/arXiv.1906.10365

Antonakaki, D., Fragopoulou, P., & Ioannidis, S. (2021). A survey of Twitter research: Data model, graph structure, sentiment analysis and attacks. Expert Systems with Applications, 164, 114006. DOI: https://doi.org/10.1016/j.eswa.2020.114006

Bird, S., Klein, E., & Loper, E. (2009). Natural language processing with Python: analyzing text with the natural language toolkit. O'Reilly Media, Inc.. Retrieved from: https://www.jstor.org/stable/40925581

Bodaghi, A., & Goliaei, S. (2018). A novel model for rumor spreading on social networks with considering the influence of dissenting opinions. Advances in Complex Systems, 21(06n07), 1850011. DOI: https://doi.org/10.1142/S021952591850011X

Bodaghi, A., & Oliveira, J. (2022). The theater of fake news spreading, who plays which role? A study on real graphs of spreading on Twitter. Expert Systems with Applications, 189, 116110. DOI: https://doi.org/10.1016/j.eswa.2021.116110

Check Your Fact. (2019). Retrieved from checkyourfact website: https://checkyourfact.com/

Contractions. (2022). Retrieved July 26, 2022, from https://dictionary.cambridge.org/de/grammatik/britisch-grammatik/contractions

Conversation, T. (2021, April 8). COVID-19 vaccine is not linked to the mark of the beast. Retrieved June 12, 2021, from https://www.snopes.com/news/2021/04/08/no-the-covid-19-vaccine-is-not-linked-to-the-mark-of-the-beast

Cui, L., Wang, S., & Lee, D. (2019). Same: sentiment-aware multi-modal embedding for detecting fake news. In Proceedings of the 2019 IEEE/ACM international conference on advances in social networks analysis and mining (pp. 41-48). DOI: https://doi.org/10.1145/3341161.3342894

Dai, E., Sun, Y., & Wang, S. (2020, May). Ginger cannot cure cancer: Battling fake health news with a comprehensive data repository. In Proceedings of the International AAAI Conference on Web and Social Media (Vol. 14, pp. 853-862). DOI: https://doi.org/10.1609/icwsm.v14i1.7350

Dey, A., Rafi, R. Z., Parash, S. H., Arko, S. K., & Chakrabarty, A. (2018, June). Fake news pattern recognition using linguistic analysis. In 2018 Joint 7th International Conference on Informatics, Electronics & Vision (ICIEV) and 2018 2nd International Conference on Imaging, Vision & Pattern Recognition. (pp. 305-309). IEEE. DOI: 10.1109/ICIEV.2018.8641018

Dickerson, J. P., Kagan, V., & Subrahmanian, V. S. (2014, August). Using sentiment to detect bots on twitter: Are humans more opinionated than bots?. In 2014 IEEE/ACM International Conference on Advances in Social Networks Analysis and Mining (ASONAM 2014) (pp. 620-627). IEEE. DOI: 10.1109/ASONAM.2014.6921650

Dzogang, F., Lightman, S., & Cristianini, N. (2018). Diurnal variations of psychometric indicators in Twitter content. PloS one, 13(6), e0197002. DOI: https://doi.org/10.1371/journal.pone.0197002

FactCheck.org. (2008). Retrieved from FactCheck.org website: https://www.factcheck.org/

Giachanou, A., & Crestani, F. (2016). Like it or not: A survey of twitter sentiment analysis methods. ACM Computing Surveys (CSUR), 49(2), 1-41. DOI: https://doi.org/10.1145/2938640

Go, A., Bhayani, R., & Huang, L. (2009). Twitter sentiment classification using distant supervision. CS224N project report, Stanford, 1(12), 2009. Retrieved June 22, 2021, from https://www-cs.stanford.edu/people/alecmgo/papers/TwitterDistantSupervision09.pdf

Hamdan, H., Béchet, F., & Bellot, P. (2013, June). Experiments with DBpedia, WordNet and SentiWordNet as resources for sentiment analysis in micro-blogging. In Second Joint Conference on Lexical and Computational Semantics (* SEM), Volume 2: Proceedings of the Seventh International Workshop on Semantic Evaluation (SemEval 2013) (pp. 455-459). Retrieved from: https://aclanthology.org/S13-2075

Hutto, C., & Gilbert, E. (2014, May). Vader: A parsimonious rule-based model for sentiment analysis of social media text. In Proceedings of the international AAAI conference on web and social media (Vol. 8 No. 1, pp. 216-225). DOI: https://doi.org/10.1609/icwsm.v8i1.14550

Informal contractions list in English. (2020, December 25). Retrieved July 26, 2021, from https://7esl.com/informal-contractions-list

Internet Slang Terms. (2021, March 21). Retrieved July 28, 2021, from https://7esl.com/internet-slang

Islam, M. S., Kamal, A. H. M., Kabir, A., Southern, D. L., Khan, S. H., Hasan, S. M., ... and Seale, H., "COVID-19 vaccine rumors and conspiracy theories: The need for cognitive inoculation against misinformation to improve vaccine adherence." PloS ONE, 16 (5): e0251605, (2021). DOI: https://doi.org/10.1371/journal.pone.0251605

Iwendi, C., Mohan, S., Ibeke, E., Ahmadian, A., & Ciano, T. (2022). Covid-19 fake news sentiment analysis. Computers and electrical engineering, 101, 107967. DOI: https://doi.org/10.1016/j.compeleceng.2022.107967

Kim, T. & Wurster K. (2015). emoji (Version v1.7.0) [Computer software]. https://github.com/carpedm20/emoji

Kouloumpis, E., Wilson, T., & Moore, J. (2011). Twitter sentiment analysis: The good the bad and the omg!. In Proceedings of the international AAAI conference on web and social media (Vol. 5, No. 1, pp. 538-541). DOI: https://doi.org/10.1609/icwsm.v5i1.14185

Manning, C. D., Raghavan, P., Schutze, H., & Cambridge University Press. (2008). Introduction to information retrieval. Cambridge: Cambridge University Press.

Neethu, M. S., & Rajasree, R. (2013, July). Sentiment analysis in twitter using machine learning techniques. In 2013 fourth international conference on computing, communications and networking technologies (ICCCNT) (pp. 1-5). IEEE. DOI: 10.1109/ICCCNT.2013.6726818

Newman, N., Fletcher, R., Schulz, A., Andi, S., Robertson, C. T., & Nielsen, R. K. (2021). Reuters institute digital news report 2021. Reuters Institute for the Study of Journalism. Retrieved from: https://papers.ssrn.com/sol3/papers.cfm?abstract_id=3873260

Pak, A., & Paroubek, P. (2010, May). Twitter as a corpus for sentiment analysis and opinion mining. In Proceedings of the Seventh International Conference on Language Resources and Evaluation (LREC'10). Retrieved from: http://www.lrec-conf.org/proceedings/lrec2010/pdf/385_Paper.pdf

Saif, H., He, Y., & Alani, H. (2012, November). Semantic sentiment analysis of twitter. In International semantic web conference (pp. 508-524). Springer, Berlin, Heidelberg. DOI: https://doi.org/10.1007/978-3-642-35176-1_32

Snefjella, B., Schmidtke, D., & Kuperman, V. (2018). National character stereotypes mirror language use: A study of Canadian and American tweets. PloS one, 13(11), e0206188. DOI: https://doi.org/10.1371/journal.pone.0206188

Snopes. (2018). Retrieved from Snopes.com website: https://www.snopes.com/

Vicario, M. D., Quattrociocchi, W., Scala, A., & Zollo, F. (2019). Polarization and fake news: Early warning of potential misinformation targets. *ACM Transactions* on the Web (TWEB), 13(2), 1-22. DOI: https://doi.org/10.1145/3316809

Zacharias, C. & Poldi, F. (2018). Twint (Version 2.1.4) [Computer software]. https://github.com/twintproject/twint

Zhang, X., Cao, J., Li, X., Sheng, Q., Zhong, L., & Shu, K. (2021). Mining dual emotion for fake news detection. *In Proceedings of the Web Conference 2021* (pp. 3465-3476). DOI: https://doi.org/10.1145/3442381.3450004

e-ISSN 2757-5195

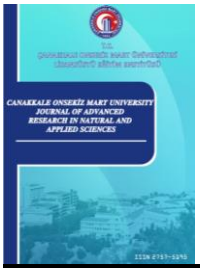

Çanakkale Onsekiz Mart University
Journal of Advanced Research in Natural and Applied Sciences
Open Access

doi.org/10.28979/jarnas.1162578 2023, Cilt 9, Sayı 1, Sayfa: 127-144 dergipark.org.tr/tr/pub/jarnas

Covid-19 Verileri için Bayes Ağlari ile Makine Öğrenmesi

Hüseyin Can Yılmaz[1], Serpil Aktaş Altunay[2*]

[1]Gelir İdaresi Başkanlığı, Ankara, Türkiye
[2]Hacettepe Üniversitesi, Fen Fakültesi, ,İstatistik Bölümü, Ankara, Türkiye

Makale Tarihçesi

Gönderim: 16.08.2022
Kabul: 13.10.2022
Yayım: 05.03.2023

Araştırma Makalesi

Öz − Covid-19 pandemisi, 17 Kasım 2019 tarihinde Çin'in Vuhan Eyaleti'nde ilk defa görülmüştür. Küresel pandemi ilk başta Vuhan'daki deniz mahsülleri ve hayvan satışı yapılan yerlerde görülmüştür. Sonra insanlar arasında da yayılışını devam ettirerek ilk olarak Vuhan ve Çin'in diğer eyaletindeki bölgelere ve dünya üzerinde diğer ülkelere de yayılmıştır. 14 Ağustos 2022 tarihi itibariyle dünyada 590.624.000 vaka meydana gelmiştir ve 6.431.291 hasta ölmüştür. Ülkemizde ve dünya genelinde Covid-19 pandemisinin etkilerini gösteren birçok araştırma ve analiz çalışmaları yapılmıştır. Bu çalışmada dünya genelinde 104 ülkeden oluşan 215.968 adet dünya çapında meydana gelen vaka analiz edilmiştir ve Bayes Ağları (Bayesian Networks) ile makine öğrenimi tekniği kullanılarak hastalar sınıflandırılmaya çalışılmış ve dokuz adet değişkenle Covid-19 virüsüne yakalanan hastaların hayatta kalıp kalmayacağını araştırılmıştır. Böylelikle hangi hastaya öncelik verip tedavi edilmesi gerektiği veya gözlem altında tutulması gerektiği belirlenecektir. Sonuç olarak bu çalışmayla dünya genelindeki Covid-19 pandemisinden kaynaklı ölüm oranlarının düşürülmesi hedeflenmektedir.

Anahtar Kelimeler − *Bayes ağları, Covid-19, makine öğrenmesi, pandemi*

Machine Learning with Bayesian Networks for Covid-19 Data

[1]Revenue Administration, Ankara, Turkey
[2]Hacettepe University, Faculty of Science, Department of Statistics, Ankara, Turkey

Article History

Received: 16.08.2022
Accepted: 13.10.2022
Published: 05.03.2023

Research Article

Abstract − The Covid-19 pandemic emerged on November 17, 2019, in Wuhan Province of China. The outbreak was initially detected in those found in the seafood and animal market in this region. Later, it spread from person to person and spread to other cities in Hubei province, especially in Wuhan, other provinces of China, and other world countries. Until Aug 14, 2022, 590.624.000 cases occurred globally and 6.266.278 patients died from Covid-19. Many research and analysis studies have been conducted in our country and around the world showing the effects of the Covid-19 pandemic. In this study, 215,968 worldwide cases from 104 countries around the world were analysed and the patients were tried to be classified using Bayesian Networks and machine learning techniques. It was investigated whether the patients who caught the Covid-19 virus would survive using nine variables. In this way, it will be determined which patient should be given priority and treated or kept under observation. Thus, this study aims to reduce the death rates due to the Covid-19 pandemic worldwide.

Keywords − *Bayesian networks, Covid-19, machine learning, pandemic*

[1] canyilmaz.hun@gmail.com
[2] spxl@hacettepe.edu.tr
*Sorumlu Yazar

1. Giriş

İlk defa 15 Aralık 2019'da Çin'in Hubei bölgesindeki Wuhan şehrinde, canlı hayvan ticareti olarak adlandırılan Huanan Deniz Ürünleri ve Canlı Hayvan Toptan Satış Pazar'ında ortaya çıktığı düşünülen bir hastalık kısa sürede salgına dönüşmüştür. Bu pazarda vahşi hayvanların satıldığı bilinmektedir. Virüse rastlandıktan kısa süre içinde bilim insanları ve epidemiyolojistlerden oluşan uzman bir ekip; bulaşıcı patojenlerle oluşan (Severe Acute Respiratory Syndrome) SARS-CoV; 2002, (Middle East Respiratory Syndrome) MERS-CoV; 2012, influenza kuş (H5N1 Avian Influenza) gribi adı verilen binlerce insanı öldüren solunum yolları hastalıklarına etken olan virüsleri, gelişen bu yeni tablodan dışarda tutarak farklı bir hastalığın meydana geldiğini ve bununda yeni Coronavirüs, Covid-19 şeklinde tanımlandığını duyurmuşlardır. Bu virüsler soğuk algınlığına sebep olan virüslerdir. Ayrıca hayvanlarda görülen birçok koronavirüs çeşidi vardır ve bazılarının hayvanlardan insanlara geçerek insanlarda ciddi hastalıklara neden olabilmektedir. SARS-CoV, 21. Yüzyılda, ilk milletler arasındaki acil sağlık durumu 2003 yılında ortaya çıkmıştır. Önceden hiç duyulmamış bir virüs olarak meydana gelen ve binlerce kişinin hayatını yitirmesine sebep olan SARS-CoV yaklaşık on sene sonra koronavirüs ailesinden, öncesinde hiç insan ya da hayvanlarda ortaya çıkmamış olan MERS-CoV ortaya çıkmıştır, Eylül 2012'de ilk defa Suudi Arabistan'daki kişilerde görüldüğü sanılmıştır ancak daha sonradan yapılan araştırmalarda ilk vakaların Nisan 2012'de Ürdün Zarqa'daki bir hastanede görüldüğü kayıtlara geçirilmiştir. Tek zincirli, zarflı ve pozitif polariteli virüslere RNA virüsleri denir. Pozitif polariteli bu virüsler RNA'ya bağımlı RNA polimeraz enzimi içermezler fakat RNA polimeraz enzimini genomlarında kodlarlar. Üst katmanlarında çubuksu çıkıntıları vardır. Bu uzantılara latince "corona", yani "taç" denilmektedir. Bu tanımdan yola çıkılarak bu virüslere Coronavirus (taçlı virüs) denilmiştir (Zhou, 2019). Dünya Sağlık Örgütü (DSÖ) 31 Aralık 2019'da, Çin'in Hubei bölgesindeki Wuhan kentinde etiyolojisi bilinmeyen pnömoni vakalarını kayıt altına almıştır. 7 Ocak 2020'de vaka öncesinde insanlarda gözlemlenmemiş olan yeni bir koronavirüs (2019- nCoV) olarak kayıt altına alınmıştır. Sonrasında 2019-nCoV salgının adı Covid-19 olarak kabul görmüş ve virüs SARS CoV'e çok benzerlik gösterdiğinden SARS-CoV-2 olarak nitelendirilmiştir. DSÖ, Covid-19 kürsel pandemisini 30 Ocak 2020'de "uluslararası boyutta halk sağlığı acil durumu" ile sınıflandırmış ve salgının başladığı Çin'in Hubei bölgesi dışında 113 ülkede Covid-19 hastalığının görülmesi, virüsün salgını ve ağır geçirilmesi nedeniyle 11 Mart'ta küresel salgın (pandemi) olarak tanımlamıştır. Aynı zamanda bu virüstün halk sağlığı üzerinde yaratacağı etkilerde tartışılmıştır (Hui, 2020). Türkiye'de Covid-19 ile ilgili araştırmalar 10 Ocak'ta başlamış ve 22 Ocak'ta T.C. Sağlık Bakanlığı Bilimsel Danışma Kurulu ilk toplanmasını yapmıştır, Covid-19'a yönelik almış olduğumuz önlemlere rağmen ilk Covid-19 vakası 11 Mart'ta görülmüştür. DSÖ 13 Mart 2020'de hastalığın seyrini değiştirebilecek ve insanların kafasındaki soru işaretlerini gidermekte yardımcı olacak basın açıklamasında "Nerede olduğunu bilmediğiniz bir virüsle savaşamazsınız. Covid-19 yayılım zincirini kırmak için tespit edin, izole edin, test edin ve tedavi edin! Bulduğumuz ve tedavi ettiğimiz her olgu hastalığın yayılımını kısıtlayacak." açıklamalarında bulundu. Covid-19 verileri ile ilgili çok sayıda araştırma yapılmıştır (Şencan, 2020).

Bu çalışmada, Türkiye'de 11 Mart 2020 – 19 Mayıs 2020 tarihleri arasında ortaya çıkmış olan toplam Covid-19 vaka sayıları için Lojistik Büyüme ve Üstel Büyüme modellerini kullanarak ileriki dönemler için vaka sayılarını tahmin etmişlerdir. Covid-19 teşhisinde Yapay Sinir Ağları yöntemleri kullanılarak sınıflama yapan çalışmalar da vardır (Tang, 2021; Karacan & Eryılmaz, 2021). Yaptıkları çalışmada bazı matematiksel modeller kullanarak salgının gidişatı hakkında tahminler yapmışlardır (Adiga, 2020). Bu modellerden en çok bilineni SIR modelidir. ARIMA modelini kullanarak İtalya Covid-19 verilerini analiz etmiştir (Perone, 2020). Covid-19 verileri için matematiksel modeller, istatistiksel modeller ve derin öğrenme yöntemlerini karşılaştıran bir çalışma yapmışlardır (Masum, 2022). Derin öğrenme yöntemleri ile Covid-19 verilerini analiz etmişlerdir (Zeroual, 2020). Zaman serisi modelleri ile Covid-19 verilerini analiz etmişlerdir (Maleki, 2020).

Diğer çalışmalardan farklı olarak bu çalışmadaki amaç, Bayes Ağları ile COVID-19 hastalarının yaşama ve ölüm tahminlerini yapmaktır. Bayes ağları son zamanlarda psikoloji, biyoloji, sosyal bilimler tıp vb. birçok alanda kullanılmaktadır (Gemela, 2001). En yaygın kullanım alanlarından biride risk tahminleridir.

2. Materyal ve Yöntem

Veri madenciliğinin önemli sınıflandırma modellerinden biri Bayes ağlarıdır. Bayes Ağları, olasılığı belirsizliğin bir ölçüsü olarak kullanan olasılıksal uzman sistemlerin (probabilistic expert systems) bir türüdür (Spiegelhalter et.al, 1993). Bayes Ağları aynı zamanda Bayesçi İnanç Ağları (Bayesian Belief Networks), Nedensel Olasılık Ağları (Causal Probabilistic Networks), Olasılıksal Sebep - Sonuç Modelleri (Probablilistic Cause - Effect Models), Olasılıksal Etki Diyagramları (Probabilistic Influence Diagrams) olarak da isimlendirilmektedir (Spiegelhalter et.al., 1993). Yapay zekâ ve makine öğrenmesi konularındaki birçok çalışmada Bayes Ağları sıklıkla kullanılmaktadır. Özellikle karmaşık koşullu ilişki yapılarının ortaya çıkarılmasında Bayes Ağları tercih edilmektedir.

2.1. Bayes Ağları

Veri madenciliğinin önemli sınıflandırma modellerinden biri Bayes ağlarıdır. Bayes Ağları, olasılığı belirsizliğin bir ölçüsü olarak kullanan olasılıksal uzman sistemlerin (probabilistic expert systems) bir türüdür (Spiegelhalter et.al, 1993). Bayes Ağları aynı zamanda Bayesçi İnanç Ağları (Bayesian Belief Networks), Nedensel Olasılık Ağları (Causal Probabilistic Networks), Olasılıksal Sebep - Sonuç Modelleri (Probablilistic Cause - Effect Models), Olasılıksal Etki Diyagramları (Probabilistic Influence Diagrams) olarak da isimlendirilmektedir (Spiegelhalter et.al., 1993). Yapay zekâ ve makine öğrenmesi konularındaki birçok çalışmada Bayes Ağları sıklıkla kullanılmaktadır. Özellikle karmaşık koşullu ilişki yapılarının ortaya çıkarılmasında Bayes Ağları tercih edilmektedir.

Bu teknikler değişkenlerin koşullu olasılıkları ile temsil edilen anlaşılması zor ilişkilerin matematiksel modelini yönlendirilmiş döngüsüz diyagram (DAG =Directed Acyclic Graph) ile görselleştirir. Bayes Ağlarının yapısı "Grafiksel Kısım" ile gösterilirken ilişkili değişkenler arasındaki koşullu olasılıklar "Koşullu Olasılıklar Tablosu" nda gösterilmektedir. Bayes Ağları tablodaki rastgele değişkenler arasındaki bağımlılık ilişkilerinin anlaşılmasını ve görselleştirilmesini sağlayan grafiksel olasılık yapısı ortaya çıkaran istatistiksel bir yöntemdir (Jensen & Nielsen, 2007). Aynı zamanda bu ağ koşullu olasılıklar için çıkarsama yapılmasını sağlar. Bayes Teoremi yardımıyla araştırmacıların eldeki verilerin yanında uzman bilgisini de ağa katmasını sağlar (Atılgan & Ersel, 2017). TAN (Tree augmented naive) Bayes ağı son zamanlarda, şu andaki makine öğrenmesi ve veri madenciliği yöntemlerinden daha çok ilgi görmektedir. TAN modelleri bir ağaç oluşumuna katkı sağlayan Naive Bayes ağlarına kadar uzanır.

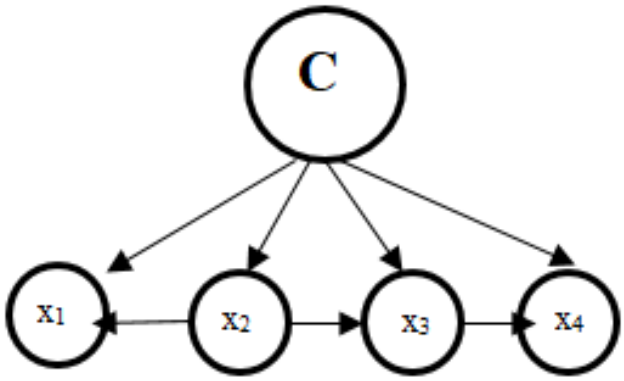

Şekil 1. Tipik bir TAN yapısı ağı

Şekil 1'deki TAN yapısındaki "C" bir düğümü, X1, X2, X3, X4 ise çocukları temsil etmektedir. G=(V,A) grafiği ve P bileşik olasılık dağılımı verilen bir Bayes Ağı verildiğinde grafikte yer alan herhangi bir X düğümünün ebeveynleri verildiğinde X düğümü ebeveyni ya da torunu olmayan herhangi bir düğümden yönsel ayrılmıştır. Yani ağda bulunan tüm v ∈ V düğümleri için v⊥Nondesc(v)\Pa(v) ise, Bayes Ağı Markov koşulunu sağlamaktadır. Markov koşulu dikkate alındığında yönsel ayrılma ve koşullu bağımsızlık arasında güçlü bir ilişki vardır (Heckerman, 2008).

G=(V,A) yönlü döngüsel olmayan grafikte herhangi X,Y,Z düğümleri ve P olasılık fonksiyonları için:

$\boldsymbol{G}$: düğüm, P: olasılık

1) G ve P her zaman tutarlı ise (X⊥Y\Z) ⇒ (X⊥Y\Z)P

2) (X⊥Y\Z)P G ile tutarlı tüm dağılımları sağlıyorsa (X⊥Y\Z)$\boldsymbol{G}$ olacaktır (Jensen, 2007; Nielsen, 2007).

Bayes Ağları oluşturdukları koşullu olasılıklarla, olasılığa dayalı çıkarım yapabilen bir sistem gibi düşünülebilir. Olasılığı kullanan çıkarımsal sistemlerde, düğümler bütünü için bazı düğümlere ilişkin bilgiler sunulduğunda, olasılıkların çıkarılması öğrenen sistemlerde ana görevini oluşturmaktadır. Olasılık çıkarma süreci ağ güncellemesi diye de nitelendirilmektedir. Bayes Ağları'nda bir düğüm için bilgi girdisi olduğunda diğer bütün düğümlerin yeniden revize edilmesinden dolayı çıkarımlar geniş bir yelpazeye aittir (Korb & Nicholson, 2011). X değişkenler vektöründe tanımlı olan Bayes Ağları, X vektöründeki değişkenlere ait bileşik olasılık dağılımlarını ortaya koyduğu için Bayes Ağları'ndan faydalanarak bu vektörler kümesindeki tüm olasılıklar hesaplanır (Heckerman, 2008; Laurìa, 2006; Duchessi, 2006).

Bayes Ağları'nın yapısal özelliklerini meydana getiren olmazsa olmazlarından biri de öğrenme kısmıdır. Pratikte çoğunlukla araştırılan konu veya soruna ait Bayes Ağı yapısının çok iyi bilinmemesinden kaynaklı mevcut veriler üzerinden modelin öğrenilmesi gerekir (Olmuş ve Erbaş, 2012). "Bayes Ağları Öğrenme" (Bayesian Network Learning) ile tanımlanan bu öğrenme süreci, Bayes Ağı'ndaki DAG ve bileşik olasılık dağılımlarının parametrelerinin tahmin edilmesi olarak nitelendirilebilmektedir . Bayes Ağları'nda yapısal öğrenme ve parametre öğrenme olmak üzere iki çeşit öğrenme tanımı olduğu söylenebilir. Bu öğrenme modelleri oluşturulacak olan modelin yapısını, modelin düğümlerini ve ilişkilerini belirleme amacıyla etkin bir şekilde kullanılmaktadır. Yapısal öğrenme algoritmaları, Bayes Ağı'nın diyagramsal yapısını kendi kendine oluşturmak için uygulanan metotlardır. Yapısal öğrenme algoritmaları hakkındaki ilk araştırma (Pearl & Verma, 1990) neden sonuç araştırması üzerinde olmuştur. Yapısal öğrenme algoritmaları koşullu bağımsızlık testlerini uygulayarak Bayes Ağları'nın yapısını öğrenmek adına bir temel oluşturmaktadır (Scutari, 2011).

Bir Bayes Ağı bir dizi ayrık değişkenler üzerinde ortak bir olasılık dağılımı sunar. Bayes Ağları sınıflandırıcıları, sınıflama problemi için tasarlanan Bayes Ağları'nın özel bir çeşididir. Denetimli sınıflandırma, bir dizi değişken veya özellikleri tahmin etmek için etiketleme veya kategorilere ayırmayı amaçlamaktadır. Pratikte basit bir Bayes ağ sınıflandırıcısı olan Navie Bayes sınıflandırıcıları genellikle şaşırtıcı derecede iyi performans gösterir. Bu sınıflandırıcılar temel olarak her bir Xi değişkenin koşullu olasılıklarından öğrenir.

Naive Bayes ve TAN birbirine bağlı çeşitli türler arasında birçok belirsizlik içeren büyük veri kümelerini modellemek için kullanılan olasılığa dayalı grafiksel modellerdir. Bu modellerin, resim parçalama, tıbbi teşhis, diğer çeşitli veri sınıflandırmaları gibi yaygın uygulamaları mevcuttur. Bir sınıflandırma problemi, bu tür çeşitli örneklerin analiziyle elde edilen önceki bilgilere dayanarak belirli bir örneğin hangi kategoriye ait olduğunun belirlenmesiyle ilgilenir.

Naive Bayes modeli, bir örneğin tüm niteliklerinin, o örneğin sınıfı verildiğinde birbirinden bağımsız olduğunu varsayar fakat bu modelde yapılan bağımsızlık varsayımı doğru ve gerçekçi değildir.

TAN modeli, sistemin öznitelikleri arasına bir etkileşim düzeyi daha ekleyerek Naive Bayes modelini geliştirir. Tan modelinde her nitelik sınıflara ve diğer niteliklere bağlıdır. Bu model, nitelikler arasındaki bağımlılıkları içerdiğinden, Naive Bayes modelinden daha gerçekçidir. TAN süreci Chow and Liu tarafından önerilen eski bir algoritmanın temeline dayanır. Kısıtlı olmayan Bayes Ağı sınıflandırıcı ise Navie Bayes ve TAN Ağlarından farklıdır. Kısıtlı olmayan Bayes Ağı modelinin DAG'ı değişkenler arasında (marjinal ve koşullu) bağımsız ilişkiler kurar. Sınırsız bir olasılıksal ağın yapısını öğrenmek için birkaç farklı yaklaşım mevcuttur. Bu çalışma için Bayes yapısal öğrenme yaklaşımından yararlanılmıştır.

2.1.1. Veriler

Bu çalışmanın amacı, Covid-19 geçiren kişiler için bazı değişkenleri kullanarak bir risk tahmini yapmak ve bu kişilerin hayatta kalma olasılıklarını hesaplamaktır. Bu nedenle github kaynağında 104 ülke için verilmiş olan yaklaşık 10 milyon Covid-19 hastası içeren veriye her değişken için bir değer olacak şekilde temizleme

işlemleri yapılarak yaklaşık 215 bin veri elde edilmiştir. Bu veriye Bayes Ağları ile çözümlenmesi yapılarak hayatta kalıp kalmayacaklarına dair olasılık hesaplamaları ve sınıflama sonuçları verilmiştir.

Veriler github üzerinden "https://github.com/beoutbreakprepared/nCoV2019/blob/master/latest_data/latestdata.tar.gz" linkinden çekilmiştir.

Analiz Sonuçları

Bu çalışma sayesinde koronavirüse yakalanan kişilerin, Bayes Ağları yöntemi kullanılarak hayatta kalıp kalamayacağı sınıflandırılıp tahmin edilecektir. Öte yandan hastalığa yakalanan kişiler ya da diğer ilgili kişiler yapılan modele o hastanın verilerini girerek ölüm riskini hesaplayabileceklerdir. Sonuç olarak dünya genelinde oluşacak olan farkındalık sayesinde ölüm riski yüksek olan kişiler tespit edilecek ve ölüm oranları en aza indirilmesi sağlanacaktır.

Bu çalışmanın amacı, Covid-19 geçiren kişiler için bazı değişkenleri kullanarak bir risk tahmini yapmak ve bu kişilerin hayatta kalma olasılıklarını hesaplamaktır kullanılmamalıdır.

Tablo 1
Veri kümesine genel bakış

YAS	CINSIYET	ULKE	KRONIK	SONUC	SEYAHAT	HASTALIK TARIHI	SEMPTOM	HASTALIK AYI
35	Erkek	Afganistan	Yok	Hayatta	Var	24.02.2020	Yok	Şubat
35	Erkek	Afganistan	Yok	Hayatta	Var	24.02.2020	Yok	Şubat
53	Kadın	Cezayir	Yok	Hayatta	Var	2.03.2020	Yok	Mart
24	Kadın	Cezayir	Yok	Hayatta	Var	2.03.2020	Yok	Mart
53	Kadın	Cezayir	Yok	Hayatta	Yok	2.03.2020	Yok	Mart
24	Kadın	Cezayir	Yok	Hayatta	Yok	2.03.2020	Yok	Mart
78	Kadın	Cezayir	Yok	Hayatta	Yok	5.03.2020	Yok	Mart
62	Erkek	Cezayir	Yok	Öldü	Yok	5.03.2020	Yok	Mart
54	Kadın	Cezayir	Yok	Hayatta	Yok	5.03.2020	Yok	Mart
84	Kadın	Cezayir	Yok	Öldü	Yok	15.03.2020	Yok	Mart
77	Kadın	Cezayir	Yok	Öldü	Yok	16.03.2020	Yok	Mart
50	Erkek	Cezayir	Yok	Hayatta	Yok	17.03.2020	Yok	Mart
42	Erkek	Cezayir	Yok	Öldü	Yok	17.03.2020	Yok	Mart
83	Erkek	Cezayir	Yok	Hayatta	Var	19.03.2020	Yok	Mart
75	Erkek	Cezayir	Yok	Hayatta	Var	19.03.2020	Yok	Mart
78	Erkek	Cezayir	Yok	Hayatta	Var	20.03.2020	Yok	Mart
49	Erkek	Cezayir	Yok	Hayatta	Var	20.03.2020	Yok	Mart
21	Erkek	Cezayir	Yok	Hayatta	Yok	20.03.2020	Yok	Mart
85	Erkek	Cezayir	Yok	Öldü	Yok	21.03.2020	Yok	Mart
64	Erkek	Cezayir	Yok	Hayatta	Yok	25.03.2020	Yok	Mart

Tablo 1'de görüldüğü üzere tüm verinin 20 satırlık bir kesiti verilmiştir. Veriler 10.309.980 hastanın içinden seçilen 215.968 hastadan oluşan ve dokuz değişken içeren 104 ülkeye ait bir veri kümesidir. Seçilen hastaların yaşları 1'den 105'e kadar değişmektedir. Ek olarak hastaların kronik rahatsızlığı olup olmaması, son üç ay içinde yurtdışı seyahatinde bulunup bulunmadığı, cinsiyeti ve hangi ayda hastalığa yakalandığı bilgileri mevcuttur. Bağımlı değişken ise hastanın koronavirüs sonucunda hayatta kalıp kalamadığıdır.

Tablo 2
Verinin içerdiği değişkenler ve tanımları

Değişken Adı	**Tanımı**
YAS	Hastaların hastalığa yakalandığı tarihteki yaşları
CINSIYET	Hastanın cinsiyeti
ULKE	Hastanın hangi ülkede yaşadığı
KRONIK	Hastanın kronik rahatsızlığı olup olmadığı
SONUC	Hastanın koranavirüs sonucu hayati durumu
SEYAHAT	Hastanın son 3 ay içinde yurtdışı seyahati durumu
HASTALIKTARIHI	Hastanın hastalığa yakalandığı tarih
SEMPTOM	Hastalığa yakalandığında semptom gösterme durumu
HASTALIKAYI	Hastanın hastalığa yakalandığı ay

Tablo 2'de veri kümesindeki dokuz değişkenin tanımları tanımları verilmiştir.Verilerin analizi IBM SPSS Modeler 18.0 programı ile yapılmıştır (IBM Corp., 2016) IBM SPSS Modeler uygulaması ile "Makine Öğreniminin Bayes Ağları" modeli kullanılmıştır (Wendler & Sören, 2016). Tan ve Markov modelleri denenmiş ve birbirleri ile karşılaştırılmıştır. Test modülü çalıştırılarak gözelerin %20'si tahmin edilmiştir.

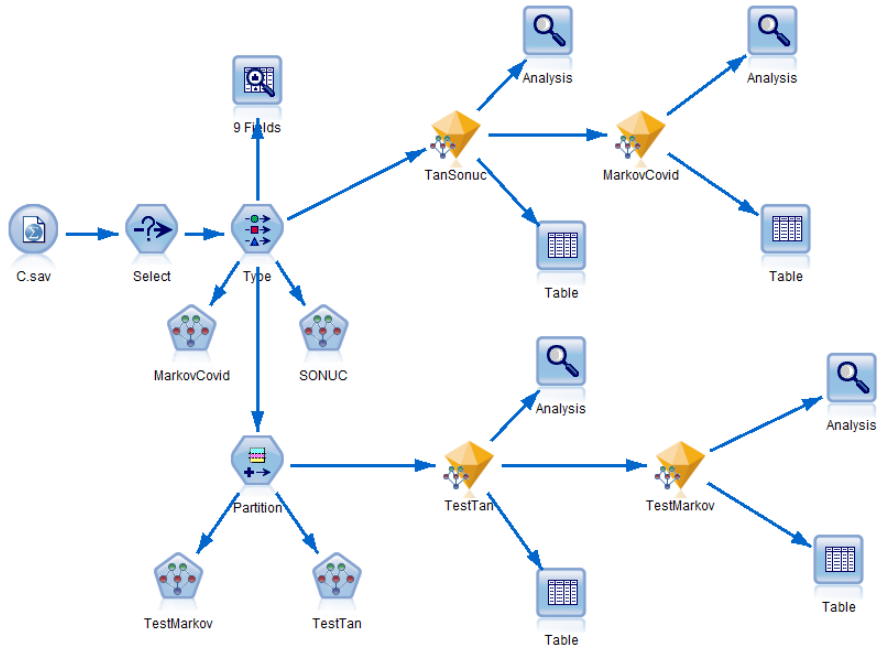

Şekil 2. IBM SPSS Modeler programı ile Bayes Ağları kesiti

Şekil 2'de (IBM Corp., 2016) IBM SPSS Modeler uygulaması ile "Makine Öğreniminin Bayes Ağları" modeli kullanılarak yapılan analizin görsel bir şeması verilmiştir.

Tablo 3
Tan modeli ve olasılıkları

YAŞ	CINSIYET	ULKE	KRONIK	SONUC	SEYAHAT	HASTALIK TARIHI	SEMPTOM	HASTALIK AYI	TAN-SONUC	TAN-P-SONUC
39	Kadın	Avustralya	Yok	Hayatta	Var	27.01.2020	Yok	Ocak	Hayatta	0,87
29	Kadın	Avustralya	Yok	Hayatta	Var	27.01.2020	Yok	Ocak	Hayatta	0,87
21	Kadın	Avustralya	Yok	Hayatta	Var	27.01.2020	Yok	Ocak	Hayatta	1,00
21	Kadın	Avustralya	Yok	Hayatta	Var	27.01.2020	Yok	Ocak	Hayatta	1,00
79	Erkek	Avustralya	Yok	Hayatta	Var	27.01.2020	Yok	Ocak	Hayatta	0,85
79	Erkek	Avustralya	Yok	Hayatta	Yok	27.01.2020	Yok	Ocak	Hayatta	0,99
29	Kadın	Avustralya	Yok	Hayatta	Yok	27.01.2020	Yok	Ocak	Hayatta	1,00
44	Erkek	Avustralya	Yok	Hayatta	Var	29.01.2020	Yok	Ocak	Hayatta	0,84
44	Erkek	Avustralya	Yok	Hayatta	Var	29.01.2020	Yok	Ocak	Hayatta	0,84
42	Kadın	Avustralya	Yok	Öldü	Var	30.01.2020	Yok	Ocak	Hayatta	0,87

Yapılan analiz sonucunda Tablo 3'e bakıldığında Tan Modeli için 10 kişiye ait tahminler ve hastanın hayatta kalıp kalamayacağı görülmektedir. Örneğin 29 yaşındaki bir kadın hasta için gerçekleşen sonuç "Hayatta" iken Tan Modeli tarafından "Hayatta" şeklinde %87 olasılıkla doğru tahmin edilmiştir. 42 yaşındaki kadın hasta için gerçekleşen sonuç "Öldü" iken Tan Modeli tarafından "Hayatta" şeklinde %87 olasılıkla yanlış tahmin edilmiştir.

Tablo 4
Markov modeli ve olasılıkları

YAŞ	CINSIYET	ULKE	KRONIK	SONUC	SEYAHAT	HASTALIK-TARIHI	SEMPTOM	HASTALIK AYI	MARKOV-SONUC	MARKOV-P-SONUC
20	Erkek	Avustralya	Yok	Öldü	Var	25.02.2020	Yok	Şubat	Öldü	0,52
20	Erkek	Avustralya	Yok	Öldü	Var	25.02.2020	Yok	Şubat	Öldü	0,52
79	Erkek	Avustralya	Yok	Hayatta	Var	27.02.2020	Yok	Şubat	Öldü	0,59
79	Erkek	Avustralya	Yok	Hayatta	Var	27.02.2020	Yok	Şubat	Öldü	0,59
69	Kadın	Avustralya	Yok	Hayatta	Var	28.02.2020	Yok	Şubat	Hayatta	0,57
59	Erkek	Avustralya	Yok	Hayatta	Var	28.02.2020	Yok	Şubat	Hayatta	1,00
69	Kadın	Avustralya	Yok	Hayatta	Yok	28.02.2020	Yok	Şubat	Hayatta	0,94
59	Erkek	Avustralya	Yok	Hayatta	Yok	28.02.2020	Yok	Şubat	Hayatta	1,00
59	Kadın	Avustralya	Yok	Hayatta	Var	29.02.2020	Yok	Şubat	Hayatta	1,00
59	Kadın	Avustralya	Yok	Hayatta	Var	29.02.2020	Yok	Şubat	Hayatta	1,00

Yapılan analiz sonucunda Tablo 4'e bakıldığında Markov modeli için 10 örnek için tahmin oranları ve hastanın hayatta kalıp kalamayacağı görülmektedir. 69 yaşındaki kadın hasta için gerçekleşen sonuç "Hayatta" iken Markov modeli tarafından "Hayatta" şeklinde %94 olasılıkla doğru tahmin edilmiştir. 79 yaşındaki erkek hasta için gerçekleşen sonuç "Hayatta" iken Markov modeli tarafından "Öldü" şeklinde %59 olasılıkla yanlış tahmin edilmiştir.

Tablo 5
Tan ve Markov modelleri için karşılaştırma oranları

Modelleri Oransal Karşılaştırma	Doğru Sayısı	Oran	Yanlış Sayısı	Oran
Tan Modeli	213.768	%98,98	2.200	%1,02
Toplam		**215.968**		
Markov Modeli	214.149	%99,16	1.819	%0,84
Toplam		**215.968**		
Tan-Markov Modeli Birlikte	215.253	%99,67	715	%0,33
Toplam		**215.968**		
Modelin Aynı Tahmin Ettiği	213.601	%99,23	1.652	%0,77
Toplam		**215.253**		

Yapılan analiz sonucunda Tablo 5'te görüldüğü üzere Tan modeli verinin %98,98'ini doğru sınıflarken, %1,02'sini yanlış sınıflamıştır. Markov modeli verinin %99,16 doğru sınıflarken, %0,84'ünü yanlış sınıflamıştır. Her iki modelin aynı sonucu verdiği oran %99,67'dir. İki model de birbiri ile uyumludur denilebilir. Her iki modelin aynı sonucu verdiği 215.253 hastadan 213.601 tanesi ham verideki sonuçla aynı iken 1.652 tanesi farklı sonuç vermiştir. Bu olasılıklar dikkate alındığında Markov modeli seçilmiş ve analizlere Markov modeli üzerinden devam edilmiştir.

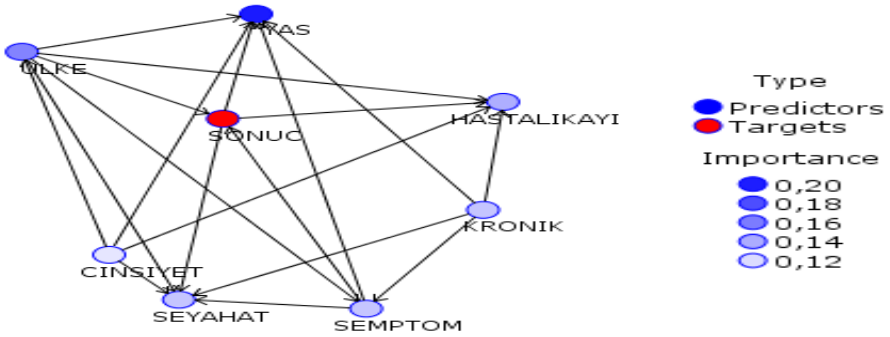

Şekil 3. Markov modeli için değişkenlerin anlamlılık düzeyleri

Seçilen Markov modeli üzerinden değişkenlerin anlamlılık düzeyi Şekil 3'te görüldüğü gibi, hastanın koronavirüsten sonra yaşayıp yaşayamayacağını etkileyen en önemli değişken, %20'lik bir oranla "Yaş" faktörüdür. İkinci önemli değişken yaklaşık %16 ile hastanın hastalığa yakalandığı ülkedir. Üçüncü ve dördüncü önemli değişkenler ise sırası ile %14'lük bir oranla hastanın hastalığa yakalandığı ay ile %13'lük bir oranla hastanın kronik rahatsızlığı olup olmadığı gelmektedir. Yapılan araştırmada; hastanın cinsiyeti ve son üç ay içinde yurt dışına çıkıp çıkmaması değişkenleri bilinen algının aksine hastanın hayatta kalıp kalamayacağına en az etkili değişkenlerdir.

Tablo 6
Hastalığa hangi ayda yakalandığına ait koşullu olasılık tablosu

Aile						Olasılık		
Sıra	**Cinsi-yet**	**Ülke**	**Kronik**	**Sonuç**	**Semptom**	**Mart**	**Nisan**	**Mayıs**
1	Erkek	Ekvator Ginesi	Yok	Hayatta	Var	0	0,333	0,666
2	Erkek	Ekvator Ginesi	Yok	Hayatta	Yok	0	0	1
3	Erkek	Ermenistan	Yok	Hayatta	Yok	0	0	1
4	Erkek	Estonya	Yok	Hayatta	Yok	0,717	0,281	0,001
5	Erkek	Esvatini	Yok	Hayatta	Yok	0	0,333	0,666
6	Erkek	Etiyopya	Yok	Hayatta	Yok	0	0,116	0,848
7	Erkek	Etiyopya	Yok	Öldü	Yok	0	0.5	0,5
8	Erkek	Fildişi Sahili	Yok	Hayatta	Yok	0	0,333	0.666
9	Erkek	Filipinler	Var	Hayatta	Var	0	1	0
10	Erkek	Filipinler	Var	Hayatta	Yok	0	0,833	0,166
11	Erkek	Filipinler	Var	Öldü	Var	0	0,938	0,061
12	Erkek	Filipinler	Var	Öldü	Yok	0	1	0
13	Erkek	Filipinler	Yok	Hayatta	Var	0	0,4	0,6
14	Erkek	Filipinler	Yok	Hayatta	Yok	0	0,304	0,646
15	Erkek	Filipinler	Yok	Öldü	Var	0	0,714	0,285

Hastalığa hangi ayda yakalandığına ait koşullu olasılık tablosuna (Tablo 6) bakıldığında, hastanın cinsiyeti "Erkek, ülkesinin "Etiyopya", kronik rahatsızlığının olmadığı, semptomunun olmadığı ve hastalık sonucu öldüğü bilindiğinde bu hasta %50 ihtimalle ya Mayıs ayında ya da Nisan ayında hastalığa yakalanmıştır. Hastanın cinsiyetinin "Erkek", ülkesinin "Filipinler", kronik rahatsızlığının olduğu, semptomunun olmadığı ve hastalık sonucu öldüğü bilindiğinde bu hastanın nisan ayında hastalığa yakalanma olasılığı yaklaşık %94'tür.

Tablo 7
Yaşa ait koşullu olasılık tablosu

Aile				Olasılık				
Sıra	**Cinsiyet**	**Ülke**	**Sonuç**	**<=21.8**	**21.8-42.6**	**42.6-63.4**	**63.4-84.2**	**>84.2**
1	Erkek	Afganistan	Hayatta	0	1	0	0	0
2	Erkek	Almanya	Hayatta	0.016	0.282	0.391	0.211	0.098
3	Erkek	Almanya	Öldü	0.2	0.6	0.2	0	0
4	Erkek	ABD	Hayatta	0.049	0.289	0.357	0.276	0.026
5	Erkek	ABD	Öldü	0	0.228	0.228	0.473	0.070
6	Erkek	Andora	Öldü	1	0	0	0	0
7	Erkek	Angola	Hayatta	0	1	0	0	0
8	Erkek	Arjantin	Hayatta	0	0.15	0.55	0.3	0
9	Erkek	Avustralya	Hayatta	0.064	0.273	0.319	0.326	0.015
10	Erkek	Avustralya	Öldü	0.12	0.08	0	0.8	0
11	Erkek	Bahamalar	Hayatta	0	0.185	0.518	0.296	0
12	Erkek	Belçika	Hayatta	0.010	0.149	0.279	0.304	0.255
13	Erkek	Benin	Hayatta	0.333	0.333	0.333	0	0
14	Erkek	BAE	Hayatta	0	0	0	1	0
15	Erkek	Bolivya	Hayatta	0	0.227	0.5	0.227	0.045

Hastanın yaşlarına ait koşullu olasılık tablosuna bakıldığında, hastanın cinsiyetinin erkek, ülkesinin Bahamalar ve koronavirüs sonrası hayatta kaldığı bilindiğine göre bu kişinin 42,6 ile 63,4 yaşları arasında olması olasılığı %51,8'dir. Hastanın cinsiyetinin "Erkek", ülkesinin "Avustralya" ve koronavirüs sonrası öldüğü bilindiğine göre bu kişinin 63,4 ile 84,2 yaşları arasında olması olasılığı %80'dir.

Tablo 8
Hastanın cinsiyete ait koşullu olasılık tablosu

	Aile	**Olasılık**	
Sıra	**Ülke**	**Erkek**	**Kadın**
1	Burkina Faso	0.8	0.2
2	Butan	1	0
3	Cezayir	0.590	0.409
4	Ekvator Ginesi	0.454	0.545
5	Ermenistan	1	0
6	Estonya	0.441	0.558
7	Esvatini	0.6	0.4
8	Etiyopya	0.692	0.307
9	Fildişi Sahili	0.666	0.333
10	Filipinler	0.558	0.441
11	Finlandiya	0.2	0.8
12	Fransa	0.857	0.142
13	Gabon	0.6	0.4
14	Gambiya	0.666	0.333
15	Gana	0.615	0.384

Hastanın cinsiyetine ait koşullu olasılık tablosuna bakıldığında, Burkina Faso'da koronavirüs hastalarının %80'i erkek ve %20'si kadındır. Finlandiya'da koranavirüs hastalarının %80'i kadın ve %20'si erkektir.

Tablo 9
Hastanın seyahat geçmişine ait koşullu olasılık tablosu

		Aile			**Olasılık**	
Sıra	**Cinsiyet**	**Ülke**	**Kronik**	**Sonuç**	**Var**	**Yok**
1	Erkek	Afganistan	Yok	Hayatta	1	0
2	Erkek	Almanya	Var	Hayatta	0	1
3	Erkek	Almanya	Yok	Hayatta	0.001	0.998
4	Erkek	Almanya	Yok	Öldü	1	0
5	Erkek	ABD	Var	Hayatta	0.333	0.666
6	Erkek	ABD	Yok	Hayatta	0.130	0.869
7	Erkek	ABD	Yok	Öldü	0.807	0.192
8	Erkek	Andora	Yok	Öldü	0	1
9	Erkek	Angola	Yok	Hayatta	0	1
10	Erkek	Arjantin	Yok	Hayatta	0.75	0.25
11	Erkek	Avustralya	Yok	Hayatta	0.543	0.456

12	Erkek	Avustralya	Yok	Öldü	1	0
13	Erkek	Bahamalar	Yok	Hayatta	1	0
14	Erkek	Belçika	Yok	Hayatta	0	1
15	Erkek	Benin	Yok	Hayatta	0	1
16	Erkek	BAE	Yok	Hayatta	1	0
17	Erkek	Bolivya	Var	Hayatta	0	1
18	Erkek	Bolivya	Yok	Hayatta	0	1
19	Erkek	Bolivya	Yok	Öldü	0.5	0.5
20	Erkek	Brezilya	Var	Hayatta	0	1
21	Erkek	Brezilya	Yok	Hayatta	0.152	0.847
22	Erkek	Brezilya	Yok	Öldü	0.444	0.555
23	Erkek	Bulgaristan	Yok	Hayatta	0	1
24	Erkek	Burkina Faso	Yok	Hayatta	0.5	0.5
25	Erkek	Butan	Yok	Hayatta	0.5	0.5
26	Erkek	Cezayir	Yok	Hayatta	0.4	0.6
27	Erkek	Cezayir	Yok	Öldü	0	1
28	Erkek	Ekvator Gi-nesi	Yok	Hayatta	0.4	0.6
29	Erkek	Ermenistan	Yok	Hayatta	0.5	0.5
30	Erkek	Estonya	Yok	Hayatta	0.001	0.998
31	Erkek	Esvatini	Yok	Hayatta	0.666	0.333
32	Erkek	Etiyopya	Yok	Hayatta	0.441	0.558
33	Erkek	Etiyopya	Yok	Öldü	0	1
34	Erkek	Fildişi Sahili	Yok	Hayatta	0.666	0.333
35	Erkek	Filipinler	Var	Hayatta	0.9	0.1

Hastanın seyahat geçmişine ait koşullu olasılık tablosuna bakıldığında, hastanın cinsiyetinin erkek, Brezilya'da yaşadığı, kronik rahatsızlığının olmadığı ve koronavirüs sonucu hayatta kaldığı bilindiğinde bu kişinin son üç ay içinde seyahat geçmişinin olmama olasılığı %84,7'dir.

Hastanın cinsiyetinin erkek, Amerika Birleşik Devletleri'nde yaşadığı, kronik rahatsızlığı olmadığı ve koronavirüs sonucu öldüğü bilindiğinde bu kişinin son üç ay içinde seyahat geçmişinin olma olasılığı %80,7'dir.

Tablo 10
Sonuç değişkenine ait koşullu olasılık tablosu

	Aile		Olasılık	
Sıra	**Ülke**	**Semptom**	**Hayatta**	**Öldü**
1	Afganistan	Yok	1	0
2	Almanya	Var	1	0
3	Almanya	Yok	0.999	0
4	ABD	Var	0.75	0.25
5	ABD	Yok	0.980	0.019
6	Andora	Var	0	1
7	Angola	Yok	1	0
8	Arjantin	Var	1	0
9	Arjantin	Yok	1	0
10	Avustralya	Var	1	0
11	Avustralya	Yok	0.929	0.070
12	Bahamalar	Var	0.5	0.5
13	Bahamalar	Yok	1	0
14	Belçika	Yok	1	0
15	Benin	Var	1	0
16	BAE	Yok	1	0
17	Birleşik Krallık	Yok	1	0
18	Bolivya	Var	0.666	0.333
19	Bolivya	Yok	0.957	0.042
20	Brezilya	Var	0.844	0.155
21	Brezilya	Yok	0.972	0.027

Sonuç değişkenine ait koşullu olasılık tablosuna bakıldığında, hastanın ülkesinin Avustralya olduğu ve semptomunun olmadığı bilindiğinde bu hastanın hayatta kalma olasılığı %92,9'dur.Hastanın ülkesinin Amerika Birleşik Devletleri olduğu ve semptomu olduğu bilindiğinde bu hastanın koranavirüs hastalığından ölme olasılığı %25'tir. Hastanın ülkesinin Bolivya olduğu ve herhangi bir semptomunun olmadığı bilindiğinde bu hastanın koronavirüs hastalığından sonra hayatta kalma olasılığı %95,7'dir. Hastanın ülkesinin Brezilya olduğu ve herhangi bir semptomunun olmadığı bilindiğinde bu hastanın koronavirüs hastalığından sonra hayatta kalma olasılığı %97,2'dir. Hastanın ülkesinin Bahamalar olduğu ve herhangi bir semptomunun olmadığı bilindiğinde bu hastanın koronavirüs hastalığından sonra hayatta kalıp kalamama olasılığı birbirine eşittir.

Tablo 11
Tan modeline göre verilerin sınıflandırılması

SIRA	YAS	CINSIYET	ULKE	KRONIK	SONUC	SEYAHAT	HASTALIK TARIHI	SEMPTOM	HASTALIK AYI	TAN-SONUC	TAN-P-SONUC
1	35	Erkek	Afganistan	Yok	Hayatta	Var	24.02.2020	Yok	Şubat	Hayatta	1,00
2	53	Kadın	Cezayir	Yok	Hayatta	Var	2.03.2020	Yok	Mart	Hayatta	1,00
3	24	Kadın	Cezayir	Yok	Hayatta	Var	2.03.2020	Yok	Mart	Hayatta	1,00
4	53	Kadın	Cezayir	Yok	Hayatta	Yok	2.03.2020	Yok	Mart	Hayatta	0,76
5	24	Kadın	Cezayir	Yok	Hayatta	Yok	2.03.2020	Yok	Mart	Hayatta	0,81
6	78	Kadın	Cezayir	Yok	Hayatta	Yok	5.03.2020	Yok	Mart	Hayatta	0,54
7	62	Erkek	Cezayir	Yok	Öldü	Yok	5.03.2020	Yok	Mart	Hayatta	0,66
8	54	Kadın	Cezayir	Yok	Hayatta	Yok	5.03.2020	Yok	Mart	Hayatta	0,76
9	84	Kadın	Cezayir	Yok	Öldü	Yok	15.03.2020	Yok	Mart	Hayatta	0,54
10	77	Kadın	Cezayir	Yok	Öldü	Yok	16.03.2020	Yok	Mart	Hayatta	0,54
11	50	Erkek	Cezayir	Yok	Hayatta	Yok	17.03.2020	Yok	Mart	Hayatta	0,66
12	42	Erkek	Cezayir	Yok	Öldü	Yok	17.03.2020	Yok	Mart	Hayatta	0,80
13	83	Erkek	Cezayir	Yok	Hayatta	Var	19.03.2020	Yok	Mart	Hayatta	1,00
14	75	Erkek	Cezayir	Yok	Hayatta	Var	19.03.2020	Yok	Mart	Hayatta	1,00
15	78	Erkek	Cezayir	Yok	Hayatta	Var	20.03.2020	Yok	Mart	Hayatta	1,00
16	49	Erkek	Cezayir	Yok	Hayatta	Var	20.03.2020	Yok	Mart	Hayatta	1,00
17	21	Erkek	Cezayir	Yok	Hayatta	Yok	20.03.2020	Yok	Mart	Hayatta	0,55
18	85	Erkek	Cezayir	Yok	Öldü	Yok	21.03.2020	Yok	Mart	Hayatta	0,60
19	64	Erkek	Cezayir	Yok	Hayatta	Yok	25.03.2020	Yok	Mart	Öldü	0,55
20	84	Kadın	Cezayir	Yok	Hayatta	Yok	1.04.2020	Yok	Nisan	Hayatta	1,00
21	64	Erkek	Cezayir	Yok	Hayatta	Yok	1.04.2020	Yok	Nisan	Hayatta	1,00
22	51	Erkek	Cezayir	Yok	Hayatta	Yok	1.04.2020	Yok	Nisan	Hayatta	1,00
23	49	Erkek	Cezayir	Yok	Hayatta	Yok	1.04.2020	Yok	Nisan	Hayatta	1,00
24	20	Erkek	Andora	Yok	Öldü	Yok	2.03.2020	Var	Mart	Öldü	1,00
25	38	Erkek	Angola	Yok	Hayatta	Yok	19.03.2020	Yok	Mart	Hayatta	1,00

Tablo 11'de verilen Tan modelinin sınıflandırması ve sınıflandırma olasılıklarına bakıldığında, tan modelinde aşağıdaki tabloda görüldüğü üzere ilk 25 hastaya baktığımızda 19 hastanın hayatta kalıp kalamayacağını doğru sınıflanmış, geri kalan 6 hastayı yanlış sınıflamıştır. Örneğin 18. satırdaki gözleme baktığımızda 85 yaşındaki Cezayir'de yaşayan, kronik rahatsızlığı olmayan erkek hastanın sonucu koronavirüs hastalığından sonra öleceği yönünde olmasına rağmen, tan modeli bu hastanın %60 olasılıkla hastalıktan sonra hayatta kalacağını yanlış olarak sınıflandırmıştır.

Tablo 12
Markov modeline göre verilerin sınıflandırılması

SIRA	YAŞ	CINSIYET	ULKE	KRONIK	SONUC	SEYAHAT	HASTALIK TARIHI	SEMPTOM	HASTALIK AYI	$MARKOV-SONUC	$MARKOV-P-SONUC
1	35	Erkek	Afganistan	Yok	Hayatta	Var	24.02.2020	Yok	Şubat	Hayatta	1,00
2	53	Kadın	Cezayir	Yok	Hayatta	Var	2.03.2020	Yok	Mart	Hayatta	1,00
3	24	Kadın	Cezayir	Yok	Hayatta	Var	2.03.2020	Yok	Mart	Hayatta	1,00
4	53	Kadın	Cezayir	Yok	Hayatta	Yok	2.03.2020	Yok	Mart	Hayatta	1,00
5	24	Kadın	Cezayir	Yok	Hayatta	Yok	2.03.2020	Yok	Mart	Hayatta	1,00
6	78	Kadın	Cezayir	Yok	Hayatta	Yok	5.03.2020	Yok	Mart	Öldü	0,63
7	62	Erkek	Cezayir	Yok	Öldü	Yok	5.03.2020	Yok	Mart	Hayatta	0,63
8	54	Kadın	Cezayir	Yok	Hayatta	Yok	5.03.2020	Yok	Mart	Hayatta	1,00
9	84	Kadın	Cezayir	Yok	Öldü	Yok	15.03.2020	Yok	Mart	Öldü	0,63
10	77	Kadın	Cezayir	Yok	Öldü	Yok	16.03.2020	Yok	Mart	Öldü	0,63
11	50	Erkek	Cezayir	Yok	Hayatta	Yok	17.03.2020	Yok	Mart	Hayatta	0,63
12	42	Erkek	Cezayir	Yok	Öldü	Yok	17.03.2020	Yok	Mart	Öldü	1,00
13	83	Erkek	Cezayir	Yok	Hayatta	Var	19.03.2020	Yok	Mart	Hayatta	1,00
14	75	Erkek	Cezayir	Yok	Hayatta	Var	19.03.2020	Yok	Mart	Hayatta	1,00
15	78	Erkek	Cezayir	Yok	Hayatta	Var	20.03.2020	Yok	Mart	Hayatta	1,00
16	49	Erkek	Cezayir	Yok	Hayatta	Var	20.03.2020	Yok	Mart	Hayatta	1,00
17	21	Erkek	Cezayir	Yok	Hayatta	Yok	20.03.2020	Yok	Mart	Hayatta	1,00
18	85	Erkek	Cezayir	Yok	Öldü	Yok	21.03.2020	Yok	Mart	Öldü	1,00
19	64	Erkek	Cezayir	Yok	Hayatta	Yok	25.03.2020	Yok	Mart	Hayatta	1,00
20	84	Kadın	Cezayir	Yok	Hayatta	Yok	1.04.2020	Yok	Nisan	Hayatta	1,00
21	64	Erkek	Cezayir	Yok	Hayatta	Yok	1.04.2020	Yok	Nisan	Hayatta	1,00
22	51	Erkek	Cezayir	Yok	Hayatta	Yok	1.04.2020	Yok	Nisan	Hayatta	1,00
23	49	Erkek	Cezayir	Yok	Hayatta	Yok	1.04.2020	Yok	Nisan	Hayatta	1,00
24	20	Erkek	Andora	Yok	Öldü	Yok	2.03.2020	Var	Mart	Öldü	1,00
25	38	Erkek	Angola	Yok	Hayatta	Yok	19.03.2020	Yok	Mart	Hayatta	1,00

Tablo 12'de verilen Markov modelinin sınıflandırması ve sınıflandırma olasılıklarına bakıldığında, Markov modelinde aşağıdaki tabloda görüldüğü üzere ilk 25 hastaya baktığımızda 23 hastanın hayatta kalıp kalamayacağını doğru sınıflanmış, geri kalan 2 hastayı yanlış sınıflamıştır. Örneğin, 84 yaşındaki Cezayir'de yaşayan, kronik rahatsızlığı olmayan kadın hastanın koranavirüs hastalığından sonra hayatını kaybeden kadını, markov modeli %63 olasılıkla hastalıktan sonra öleceği yönünde doğru bir sınıflama yapmıştır.

Tablo 13
Test ve deneme modeline göre verilerin sınıflandırılması

SIRA	YAŞ	CINSIYET	ULKE	KRONIK	SONUC	SEYAHAT	HASTALIK TARIHI	SEMPTOM	HASTALIK AYI	TEST KÜMESİ	TAN-SONUC	TAN-P-SONUC	MARKOV-SONUC	MARKOV-P-SONUC
1	57	Kadın	Avustralya	Yok	Hayatta	Yok	24.02.2020	Yok	Şubat	Training	Hayatta	0,99	Hayatta	1,00
2	49	Erkek	Avustralya	Yok	Hayatta	Yok	24.02.2020	Yok	Şubat	Training	Hayatta	0,99	Hayatta	1,00
3	24	Kadın	Avustralya	Yok	Hayatta	Yok	24.02.2020	Yok	Şubat	Training	Hayatta	0,99	Hayatta	0,82
4	20	Erkek	Avustralya	Yok	Öldü	Var	25.02.2020	Yok	Şubat	Training	Hayatta	0,83	Öldü	0,64
5	20	Erkek	Avustralya	Yok	Öldü	Var	25.02.2020	Yok	Şubat	Training	Hayatta	0,83	Öldü	0,64
6	79	Erkek	Avustralya	Yok	Hayatta	Var	27.02.2020	Yok	Şubat	Training	Hayatta	0,70	Hayatta	1,00
7	79	Erkek	Avustralya	Yok	Hayatta	Var	27.02.2020	Yok	Şubat	Training	Hayatta	0,70	Hayatta	1,00
8	69	Kadın	Avustralya	Yok	Hayatta	Var	28.02.2020	Yok	Şubat	Testing	Hayatta	0,77	Hayatta	1,00
9	59	Erkek	Avustralya	Yok	Hayatta	Var	28.02.2020	Yok	Şubat	Training	Hayatta	0,75	Hayatta	1,00
10	69	Kadın	Avustralya	Yok	Hayatta	Yok	28.02.2020	Yok	Şubat	Training	Hayatta	0,99	Hayatta	1,00
11	59	Erkek	Avustralya	Yok	Hayatta	Yok	28.02.2020	Yok	Şubat	Testing	Hayatta	0,99	Hayatta	1,00
12	59	Kadın	Avustralya	Yok	Hayatta	Var	29.02.2020	Yok	Şubat	Training	Hayatta	0,83	Hayatta	1,00
13	59	Kadın	Avustralya	Yok	Hayatta	Var	29.02.2020	Yok	Şubat	Training	Hayatta	0,83	Hayatta	1,00
14	63	Kadın	Avustralya	Yok	Hayatta	Var	29.02.2020	Yok	Şubat	Training	Hayatta	0,83	Hayatta	1,00
15	63	Kadın	Avustralya	Yok	Hayatta	Yok	29.02.2020	Yok	Şubat	Training	Hayatta	0,99	Hayatta	1,00
16	29	Kadın	Avustralya	Yok	Hayatta	Yok	29.02.2020	Yok	Şubat	Testing	Hayatta	0,99	Hayatta	0,82
17	29	Kadın	Avustralya	Yok	Hayatta	Yok	29.02.2020	Yok	Şubat	Training	Hayatta	0,99	Hayatta	0,82

Veri kümesinin %80'i ile deneme yapılıp %20'si ile test yapılmıştır. Test ve deneme modeline göre rastgele 17 hastanın tan ve markov modellerinin sınıflandırması ve sınıflandırma olasılıkları Tablo 13'te verilmiştir. Tan modeli bu 17 hastanın 15'ini doğru sınıflandırırken 2 hastayı yanlış sınıflandırmıştır. Markov modeli bu 17 hastanın tümünü doğru sınıflandırmıştır.

Tablo 14
Test ve deneme modelleri için karşılaştırma oranları

Modelleri	**Test**				**Deneme**			
Oransal Karşı-laştırma	**Doğru**	**Oran**	**Yanlış**	**Oran**	**Doğru**	**Oran**	**Yanlış**	**Oran**
Tan Modeli	43.008	%99,97	446	%1,03	170.741	%98,97	1.773	%1,03
Toplam		**43.454**				**172.514**		
Markov Modeli	43.039	%99,04	415	%0,96	171.043	%99,04	1.471	%0,85
Toplam		**43.454**				**172.514**		
Tan-Markov Modeli Birlikte	43.261	%99,56	193	%0,44	171.926	%99,66	588	%0,34
Toplam		**43.454**				**172.514**		
Modelin Aynı Tahmin Ettiği	42.939	%99,26	322	%0,74	170.598	%99,23	1.328	%0,77
Toplam		**43.261**				**171.926**		

Yapılan analiz sonucunda Tablo 14'te görüldüğü üzere Tan Modeli test verilerinin %98,97'sini doğru sınıflarken, %1,03'ünü yanlış sınıflamıştır. Markov Modeli test verinin %99,04'ünü doğru sınıflarken, %0,96'sını yanlış sınıflamıştır. Her iki modelin test verilerinde aynı sonucu verdiği oran %99,56'dır. İki model de birbiri ile uyumludur denilebilir. Her iki modelin test verilerinde aynı sonucu verdiği 43.261 hastadan 42.939 tanesi ham verideki sonuçla aynı iken 322 tanesi farklı sonuç vermiştir. Bu olasılıklar dikkate alındığında test verisi için Markov modeli seçilmiş ve analizler yapılmıştır.

Tablo 15
Yeni hastanın özelliklerine göre Markov modelinde sınıflanması

SIRA	YAS	CINSIYET	ULKE	KRONIK	SONUC	SEYAHAT	HASTA-LIK TA-RIHI	SEMP-TOM	HASTA-LIK AYI	MARKOV-SONUC	MARKOV-P-SONUC
1	59	Kadın	Avustralya	Yok	Hayatta	Var	29.02.2020	Yok	Şubat	Hayatta	1,00
2	63	Kadın	Avustralya	Yok	Hayatta	Var	29.02.2020	Yok	Şubat	Hayatta	1,00
3	63	Kadın	Avustralya	Yok	Hayatta	Yok	29.02.2020	Yok	Şubat	Hayatta	1,00
4	29	Kadın	Avustralya	Yok	Hayatta	Yok	29.02.2020	Yok	Şubat	Hayatta	0,82
5	29	Kadın	Avustralya	Yok	Hayatta	Yok	29.02.2020	Yok	Şubat	Hayatta	0,82
6	79	Erkek	Avustralya	Yok		Var	1.03.2020	Yok	Mart	Hayatta	0,68

Tablo 15'te görüldüğü gibi yeni girilen hastanın hayatta kalıp kalamayacağı tahminine göre Markov modeli, 79 yaşında, Avustralya'da yaşayan, kronik rahatsızlığı olmayan, son üç ayda seyahat geçmişi olan ve mart ayında ilk hastalığa yakalanmış olan erkek bir hastanın %68,3 olasılıkla hayatta kalacağı olasılığını vermektedir.

Sonuç ve Tartışma

Bu çalışmanın amacı, diğer ülkeler için elde edilmiş verilerden yararlanarak bir ön çalışma yaparak Türkiye verisi içinde bir hazırlık yapmak ve altyapı oluşturmaktır. Bu çalışmada Bayes Ağları ile bazı değişkenler kullanılarak hastaların hayatta kalıp kalmayacakları tahmin edilmiştir. Türkiye verisi elde edildiğinde Bayes Ağları kullanılarak Covid-19 geçiren hastalar için hayatta kalma ile ilgili bir risk hesaplaması yapıldığında, bu hem sağlık ile ilgili plan ve programların oluşturulması; ölüm riski yüksek hastalar için ek tedbirler elde edilerek bu hastaların ölüm oranlarının düşürülmesi mümkün olacaktır. Salgının başından beri 12 Mayıs 2022 itibarı ile Türkiye'de Covid-19'dan 98.870 kişinin vefat ettiği düşünülürse bu tür modellerin önemi daha da ortaya çıkmaktadır. Koronavirüse karşı yapılacak analizler ve veri izlemeye ilişkin, salgınla etkin mücadele için ileriye dönük bir planla veriler hayata geçirilmeli, salgının zamanı, seyri ve coğrafi/idari ilgililer açısından izlenmesi gerekmektedir. Çözümleme sürecinin etkin bir şekilde ilerleyebilmesi ve konu ile ilgili eksik bilgi birikimlerinin giderilmesi açısından veri kümesinin tüm alanlardan uzman kişilerle paylaşılması çözümleme sürecine katkı sağlayacaktır. Koronavirüsün ekonomiye olası etkilerine bakılırsa, küresel pandemiden kaynaklı kısa dönem artan ekonomik faaliyetlerin %12 azalacağını düşünürsek, bir ayda neredeyse 31,76 milyar TL'lik bir gayri safi yurt içi hâsıla (GSYH) eksiği oluşabilir. Başka bir kısa dönem elektrik kullanımındaki düşüşü temel alan bir çalışmaya göre, GSMH'de %3,20'lik bir azalma meydana gelebilir. Salgının uzun dönemli izleri göz önünde bulundurulduğunda, ekonomik kayıp tahminlere göre çok daha fazla çıkabilir. COVID 19'dan kaynaklı olarak büyüme oranında düşüş, işsizlik oranlarında artış, enflasyon oranında artış, dış finansmanda zorluklar ve bütçe ve ödemeler dengesinde bozulma gerçekleşebilecektir. Salgının küresel çapta uzun dönem etkileri dikkate alındığında bu tür kötü etkileri teğet geçebilmek adına ekonomiye ihracatlar yoluyla gelir aktarımı yapılmalı ve parasal kolaylaştırmaya gidilmelidir. Borç ertelemeleri, doğrudan fonlama, vergi/kredi kolaylıkları gibi tedbirlerin iyice artırılması gerektiği görülmektedir. Şehir hastaneleri, tecrübeli ve özverili sağlık çalışanları, tarım/gıda ve imalat sektörü, organize sağlık idaresi gibi önemli kuruluşların ve kişilerin ülkemizde yaşanan Covid-19 ile savaşta ayrıca desteklenmelidir. Çalışılan veri kümesi Covid-19'un farklı yaş aralıklarını farklı etkilemekte olduğunu göstermektedir. Bu saptamadan yola çıkarak halkı yaşa göre sınıflandırarak sağlık politikaları hem maliyetleri azaltacak hem de tıbbi müdahalenin daha doğru uygulamasını sağlayacaktır.

Bu çalışmaya ek olarak, daha çok veriye ulaşılıp çalışma detaylandırılabilir. Türkiye verisine ulaşıp daha çok değişken ekleyerek daha verimli sonuçlara ulaşılabilir. Bu çalışmayı herkes tarafından kolayca ulaşılabilecek

bir uygulama haline dönüştürüp insanların olası bir hastalık durumunda riski ölçülebilir. Koronavirüs hayatımızda ne kadar zaman daha kalacağı belirli değilken bu çalışmada hastalıkla karşılaşan bireylerin hastalık sonucu hayatta kalıp kalamayacağı ile ilgili Türkiye verileri ile çalışılabilir. Bayes Ağlarının sağlık alanında kullanımı yaygındır. Bir kişide ortaya çıkan semptomlara bakılarak bu kişinin herhangi bir hastalığa sahip olma olasılığı hesaplanabilir. Benzer şekilde aralarında neden-sonuç ilişkisi olan birçok olayın olasılığı bu modelleme ile ortaya çıkarılabilir. Covid-19 ile ilgili verilere de Bayes Ağları uygulaması yapılmaktadır. Bayes Ağları ile riskli hastalar belirlenir ve tanı testleri ilk etapta riskli hastalar üzerinde yapılabilir. Buradan elde edilen model sonuçları ile kişi kendi verilerini girerek olası bir hastalık durumunda kendinin hayatta kalıp kalamayacağını hesaplayabilir ve bu sayede ek önlemler alabilir.

Bu çalışmada "https://github.com/beoutbreakprepared/nCoV2019/blob-/master/latest_data/latestdata.tar.gz" adresinden elde edilen 19 ülkeye ait 10.309.980 Covid-19 hastası içinden seçilen 215.968 hastadan oluşan 9 değişkenli veri kümesi kullanılmıştır. Bağımlı değişken ise hastanın koronavirüs'e yakalandıktan sonra hayatta kalıp kalmadığı alınmıştır. Ek olarak hastanın kronik rahatsızlığı olup olmaması, son üç ay içinde yurtdışı seyahatinde bulunup bulunmadığı, cinsiyeti ve hangi ayda hastalığa yakalandığı bilgileride kullanılmıştır. Bu değişkenlere için Markov ve Tan modelleri uygulanmış; Tan Modeli test verilerinin %98,97'sini doğru sınıflarken, Markov Modeli test verinin %99,04'ünü doğru sınıflamıştır. Buradan elde edilen sonuçlar ile sisteme yeni giren bir hastanın hayatta kalma olasılıkları hesaplanmıştır.

Türkiye için benzer veriler elde edildiği taktirde bu gibi çalışmalarla gelecekte meydana gelebilecek pandemilerde de ölüm oranlarında ve artan vaka sayılarında önemli bir azalma gözlemlenebilir ve buna ilişkin önlemler alınabilir. Gelecek çalışmalarda Bayes Ağları yönteminin bu veri kümesi üzerinden diğer Makine Öğrenmesi algoritmaları ile karşılaştırılması yapılabilir. Türkiye verileri yayınlandığı taktirde de uygulaması yapılarak elde edilen sonuçlar karar vericiler için yararlı bilgi niteliğinde olacaktır (Yılmaz, 2022).

Yazar Katkıları

Hüseyin Can Yılmaz: Konunun saptanması, Çalışmada kullanılan verileri toplama, analiz etme ve sonuçları yorumlama.

Serpil Aktaş Altunay: Çalışmanın planlanması, Analiz sonuçlarının yorumlanması ve makale yazımı.

Çıkar Çatışması

Yazarlar çıkar çatışması bildirmemişlerdir.

Kaynaklar

Adiga, A., Dubhashi, D., Lewis, B. et al (2020). *Mathematical Models for COVID-19 Pandemic: A Compara tive Analysis*. J Indian Inst Sci 100, 793–807. Doi:https://doi.org/10.1007/s41745-020-00200-6

Atılgan K.Y. & Ersel D., (2017). *Bayesci ağ yapısının öğrenilmesinde grafiksel bir yaklaşım*, Journal of Statisticians: Statistics and Actuarial Sciences, 1, 1-10.

Chen, J. M. (2022). *Novel statistics predict the COVID-19 pandemic could terminate in 2022*. Journal of Medical Virology, 94(6), 2845-2848.

Heckerman, D. (2008). A Tutorial on learning with Bayesian networks. Innovations in Bayesian networks, 33-82. Doi:https://doi.org/10.1007/978-3-540-85066-3_3

Gemela J. (2001). *Financial analysis using Bayesian Networks, Applied Stochastic Models in Business and Industry*, 17(1), 57-67. Doi:https://doi.org/10.1002/asmb.422

Hui D.S. Azhar E.I., Madani, T.A., Ntoumi F., Kock R. Dar O. et al (2020). *The continuing COVID-19 epidemic threat of novel coronavirusesto global health — The latest 2019 novel coronavirus outbreak inWuhan, China*. International Journal of Infectious Diseases, 91; 264-266. Doi:https://doi.org/10.1016/j.ijid.2020.01.009

IBM Corp (2016). *IBM SPSS Statistics for Windows*, Version 23.0. Armonk, New York, U.S.A. Jensen, V. & Nielsen T.D. (2007). Bayesian networks and decision graphs. Vol. 2. New York: Springer. Doi:https://doi.org/10.1007/978-3-540-85066-3_3

Karacan, H. & Eryılmaz, F. (2021). *Covid-19 Detection from Chest X-Ray Images and Hybrid Model*

Recommendation with Convolutional Neural Networks . Journal of Advanced Research in Natural and Applied Sciences , 7 (4) , 486-503. Doi:https://doi.org/10.28979/jarnas.952700

Korb, K.B.& Nicholson, A. E. (2011). *Bayesian artificial intelligence* (Computer science and data analysis series) CRC press. Doi:https://doi.org/10.1201/9780203491294

Laurìa, E. J. M. & Duchessi, P. J.(2006*). A Bayesian Belief Network for IT Implementation Decision Support, Decision Support Systems*, 42(3), 738-742, Doi:https://doi.org/10.1016/j.dss.2006.01.003

Masum, M., Masud, M. A., Adnan, M. I., Shahriar, H., & Kim, S. (2022). *Comparative study of a mathematicalepidemic model, statistical modeling, and deep learning for COVID-19 forecasting and management*. SocioEconomic Planning Sciences, 80, 101249.

Maleki, M., Mahmoudi, M. R., Wraith, D., & Pho, K. H. (2020). *Time series modelling to forecast the confirmed and recovered cases of COVID-19*. Travel medicine and infectious disease, 37, 101742.

Olmuş, H., & Erbaş, S. (2012). *Bayes Ağlarda Kümeleme Metotunu Kullanarak Meme Kanseri Tanısının Modellenmesi*. Turkiye Klinikleri Journal of Biostatistics, 4(1),10-19.

Pearl, J. & Verma, T.S. (1990) *Equivalence and Synthesis of Causal Models*. Proceedings of the 6th Conference on Uncertainty in Artificial Intelligence, Cambridge, 27-29 July, 220-227.

Perone, G. (2020) *An ARIMA model to forecast the spread and the final size of Covid-2019 epidemic in Italy (first version on SSRN 31 march).* SSRN Electron J. Doi:https://doi.org/10.2139/ssrn.3564865

Spiegelhalter, D.J., Dawid, A.P., Lauritzen, S.L. & Cowell R. G. (1993). *Bayesian analysis in expert systems*, Statistical Science, 8(3), 219-247. Doi:https://doi.org/10.1214/ss/1177010888

Scutari, M. (2011). *Measures of Variability for Graphical Models*. (Yayımlanmamış doktora tezi), Universita degli Studi di Padova, Dipartimento di Scienze Statistiche.

Şencan, Ş. N. , Şencan, B. , Borazan Çelikbıçak, M. , Arslan, D. , Özkan, E. S. , Gökçen, A. Ş. , Çiftçi, R. B. , Arıkan, İ. , Uğur, B. , Şahin, H. , Coşkun, A. E. , Konşuk Ünlü, H. & Aktaş, S. (2020). *Lojistik Büyüme ve Üstel Büyüme Modelleri ile Türkiye'de Covid-19 Modellemesi* . Nicel Bilimler Dergisi , 2 (1) , 1-18 . https://dergipark.org.tr/tr/pub/nicel/issue/55149/748068

Tang, S., Wang, C., Nie, J., Kumar, N., Zhang, Y., Xiong, Z. & Barnawi, A. (2021). *EDL-COVID: Ensemble Deep Learning for COVID-19 Case Detection From Chest X-Ray Images. IEEE Transactions on Industrial Informatics*, 17, 6539-6549. doi: 10.1109/TII.2021.3057683

Wendler, T. & Sören G. (2016). *Data Mining with SPSS Modeler Theory, Exercises and Solutions*, Cham Springer International Publishing, Springer. Doi:https://doi.org/10.1007/978-3-319-28709-6

Yılmaz, H. C. (2022). *Covid-19 Verileri İçin Bayes Ağları İle Makine Öğrenmesi*, (Yayınlanmamış yüksek lisans tezi), Hacettepe Üniversitesi, Fen Bilimleri Enstitüsü, Ankara, Türkiye.

Zhou Y, Yang Y, Huang J, Jiang S. & Du L (2019). *Advances in MERS-CoV Vaccines and Therapeutics Based on the Receptor-Binding Domain. Viruses*. 11(1), 60. https://doi.org/10.3390/v11010060

Zeroual A., Harrou F., Dairi A. & Sun Y. (2020). *Deep Learning Methods for Forecasting Covid-19 Time-Series Data: A comparative study. Chaos, Solit Fractals,* 140:110121. Doi:https://doi.org/10.1016/j.chaos.2020.110121

e-ISSN 2757-5195

Çanakkale Onsekiz Mart University
Journal of Advanced Research in Natural andAppliedSciences
Open Access

doi.org/10.28979/jarnas.1166311 2023, Cilt 9, Sayı 1, Sayfa:145-157 dergipark.org.tr/tr/pub/jarnas

Kloramfenikol Aptameri Fonksiyonlandırılmış DNA Hidrojellerinin Sentez Koşullarının Optimizasyonu

Gülnur Camızcı Aran[1], Ceren Bayraç[2,*]

[1,2]Biyomühendislik Bölümü, Mühendislik Fakültesi, Karamanoğlu Mehmetbey Üniversitesi, Karaman, Türkiye

Makale Tarihçesi
Gönderim: 07.09.2022
Kabul: 20.10.2022
Yayım: 05.03.2023

Araştırma Makalesi

Öz − Aptamer fonksiyonlandırılmış DNA hidrojelleri yüksek özgünlük, stabilite ve esneklik gibi özellikleri nedeniyle birçok alanda kullanılmaktadır. Bu çalışma kapsamında kloramfenikole özgü aptamer dizisi fonksiyonlandırılmış DNA hidrojeli sentezi gerçekleştirilmiş ve hidrojel stabilitesi için önemli parametreler optimize edilmiştir. Sentez için 5' uçları akridit modifiyeli kloramfenikole özgü aptamer ile ona kısmen eşlenik DNA ipliği polimer yapıya yan dal olarak katılmış ve eşlenik bölgelerin hibridizasyonu ile bir arada tutularak hidrojel sentezi gerçekleştirilmiştir. Optimize edilmiş parametreler akridit modifiyeli DNA dizilerinin konsantrasyonları, akrilamid yüzdesi, kloramfenikol aptameri ve DNA iplik 1 içeren lineer polimer çözeltilerin molar oranlarıdır. Ayrıca, reaksiyon sıcaklığı ve eşlenik bölgenin uzunluğunun jel stabilitesine etkisi değerlendirilmiştir. Sonuç olarak, DNA hidrojel stabilitesi için %60'lık lineer poliakrilamid-DNA konjugasyonundan, %40 akrilamid stok çözeltisi kullanılarak 1:1 molar oranda karıştırılan aptamer ve DNA iplik çözeltileri ile 25°C'de aptamer fonksiyonlandırılmış DNA hidrojeli sentezi tamamlanmıştır. Bunlara ek olarak, aptamer dizisi ile DNA iplik arasındaki eşlenik bölgenin uzunluğunun stabiliteyi artırdığı sonucuna varılmıştır.

Anahtar Kelimeler − *Aptamer, DNA hidrojel, kloramfenikol*

Optimization of Synthesis Conditions of Chloramphenicol Aptamer-Functionalized DNA Hydrogels

[1]Department of Bioengineering, Faculty of Engineering, Karamanoğlu Mehmetbey University, Karaman, Turkey

Article History
Received: 07.09.2022
Accepted: 20.10.2022
Published: 05.03.2023

Research Article

Abstract − Aptamer-functionalized DNA hydrogels are used in many fields due to their high specificity, stability and flexibility. In this study, the synthesis of chloramphenicol-specific aptamer sequence functionalized DNA hydrogel was performed and certain parameters for hydrogel stability were optimized. For the synthesis, the 5' ends of the acrydite modified chloramphenicol-specific aptamer and the partially conjugated DNA strand were attached to the polymer structure as a side branch and held together by hybridization of the complementary regions, hydrogel synthesis was carried out. The optimized parameters were the concentrations of acrydite-modified DNA sequences, the percentage of acrylamide, the molar ratios of linear polymer solutions containing chloramphenicol aptamer and DNA strand 1. In addition, the effects of reaction temperature and the length of the complementary region on gel stability were evaluated. As a result, aptamer-functionalized DNA hydrogel synthesis was completed at 25°C with aptamer and DNA strand solutions mixed in 1:1 molar ratio using 40% acrylamide stock solution from 60% linear polyacrylamide-DNA conjugation for DNA hydrogel stability. In addition, it was concluded that the length of the conjugate region between the aptamer sequence and the DNA strand increases stability.

Keywords − *Aptamer, DNA hydrogel, chloramphenicol*

[1] camizci.gulnur@gmail.com
[2] cerenbayrac@gmail.com
*Sorumlu Yazar

1. Giriş

Aptamerler çok çeşitli hedeflere yüksek bağlanma etkinliği ve özgünlüğü gösteren DNA ve RNA molekülleridir (Bayrac vd., 2011). Latince kökenli olan bu kelime 'uygun olmak' anlamına gelmektedir (Famulok, 1994). Küçük organik veya inorganik moleküller (Bruno, Carrillo, ve Philips, 2008), büyük protein kompleksleri (Tuerk ve Gold, 1990; Takahashi, 2018), bakteri ya da insan hücreleri ((Bayrac vd., 2011; Bayraç, Eyidoğan, ve Öktem, 2017), ilaçlar (Ferguson vd., 2013) aptamer seçilimi için hedef molekül olabilirler. İlk olarak 1990'lı yıllarda birbirlerinden bağımsız 3 farklı çalışma grubu tarafından geliştirilen aptamerler (Robetson ve Joyce, 1990, Tuerk ve Gold, 1990, Ellington ve Szostak, 1990) bir in vitro seçme ve çoğaltma tekniği olan SELEX (üssel zenginleştirme ile ligandların sistematik evrimi- Systematic Evolution of Ligands by Exponential Enrichment) yöntemi ile üretilirler (Tuerk ve Gold, 1990). Bu yöntemde primer bağlanma bölgeleri arasında rastgele nükleotid dağılımı ile tasarlanmış oligonükleotid kütüphanesi içinden birbirini takip eden eleme ve seçme basamakları aracılığıyla hedef moleküle yüksek bağlanma afinitesi gösteren diziler belirlenir. Sahip olduğu üç boyutlu yapıları nedeniyle hedef moleküle karşı yüksek seçicilik gösterme özellikleri, sentetik olarak kolay üretilmeleri, çeşitli ortam şartlarına karşı stabil olmaları ve modifikasyona açık olmaları nedeniyle aptamerler günümüzde bakteri parazit ve mantarların neden olduğu hastalıkların ya da kanserin teşhisinde, gıdalarda patojen, toksin, ağır metal gibi bulaşanların tespitinde, moleküler görüntülemede, ilaç taşınımında ve biyosensörlerin tanıma ajanı olarak tespit yöntemlerinde kullanılmaktadır (Bayraç vd., 2017). Aptamerlerin mevcut biyosensör sistemlerine adaptasyonları ve yeni tanı sistemlerinin geliştirilmesi 2000'li yıllarla birlikte gıda alanında oldukça hız kazanmıştır. *Escherichia coli* O111 (Luo vd., 2012), *Salmonella* Enteritidis (Bayraç vd., 2017), *Salmonella* Typhimurium (Ma vd., 2014) gibi gıda patojenlerine, lizozim (Ocaña vd., 2015), glüten (Amaya-González, de-Los-Santos-Álvarez, Miranda-Ordieres, ve Lobo-Castañón, 2015), ara h1 fıstık proteini (Trashin, de Jong, Breugelmans, Pilehvar, ve De Wael, 2015) gibi gıda alerjenlere, okratoksin A (Mishra, Hayat, Catanante, Ocaña, ve Marty, 2015), aflatoksin B1 (Castillo vd., 2015) aflatoksin M1 (Istamboulié vd., 2016) gibi mikotoksinlere, tetrasiklin (Guo, Wang, ve Sun, 2015), ve kanamisin (Sun, Li, Shen, Huang, ve Wang, 2014) gibi antibiyotiklere karşı aptamer tabanlı biyosensör geliştirme çalışmaları literatürde mevcuttur.

Hidrojeller yüksek su tutma kapasiteleri, sentetik ya da doğal polimerlerden sentezlenebilmeleri özellikleriyle hidrofilik polimer yapılardır (Abune, Davis, ve Wang, 2021). Çeşitli modifikasyonlarla hedef molekülleri yüksek özgünlükte tanıyabilen polimer haline çevrilebilir ve böylece moleküler tanımlama, ilaç taşıma, hücre yakalama ve doku tedavisinde kullanım alanı bulmuşlardır (Zhu vd., 2010; Zhang, Chen, Li, Battig, ve Wang, 2012; Zhang, Lei, Liu, Li, ve Ju, 2013; Kim, Shon, Miao, Lee, ve Oh, 2016). Örneğin, 2003 yılında yapılan bir çalışmada büyüme hormonu ile fonksiyonlandırılmış hidrojeller ekstraselüler matriks gibi davranarak hücre migrasyonunda görev aldığı gösterilmiştir (Gobin ve West, 2003). Deforest ve arkadaşlarının yaptığı başka bir çalışmada (2010) ise peptit ile fonksiyonlandırılmış hidrojeller kullanılarak üç boyutlu hücre kültürü çalışması gerçekleştirilmiştir. Her ne kadar antikorlar, büyüme faktörleri, polisakkaritler ve peptitler kullanımıyla hidrojellere moleküler tanıma özelliği kazandırılmış olsa da, bu moleküllerin düşük bağlanma afiniteleri, çeşitli ortam şartlarında stabilitelerinin az olması ve kovalent bağlanma yerine çoğu zaman elektrostatik etkileşimlerle hedef moleküle bağlanmaları nedeniyle, bu moleküllere alternatif ligandlara ihtiyaç duyulmaktadır (Belair, Le, ve Murphy, 2014; Mitchell, Briquez, Hubbell, ve Cochran, 2016; He vd., 2019). Bu anlamda nükleik asit aptamerleri yüksek afinite ile hedefe bağlanabilme, yüksek stabilite ve sentetik olarak temin edilebilme özellikleri nedeniyle hidrojel fonksiyonlandırma çalışmalarında günümüzde sıklıkla tercih edilen molekül haline gelmişlerdir (Abune vd., 2021).

Aptamer fonksiyonlandırılmış DNA hidrojellere ilk örnek Yang ve arkadaşları tarafından 2008 yılında adenozin aptameri ile sentezlenen hidrojeldir. Sentez esnasında jele hapsedilen altın nanoparçacıklar hedef molekül olan adenozin varlığında jel yapının bozularak sıvı hale geçmesiyle serbest kalmış ve adenozin tespiti sağlamıştır (Yang, Liu, Kang, ve Tan 2008). Aptamerler fonksiyonlandırılmış hidrojeller kokain (Yin, Ye, Wang, Zhu, ve Tan, 2012), şeker (Yan vd., 2013) ve virüs MT32 proteini (Bai ve Spivak, 2014) tespiti için de oluşturulmuştur. DNA hidrojelleri enzim ya da çeşitli motifler varlığında kendi kendine çapraz bağlar kurarak sentezlenebildiği gibi hidrofobik polimerlere yan dalların oluşumuna sebep olacak DNA moleküllerinin eklenmesi ile de sentezlenebilir (Li vd., 2016). İlk olarak 1996 yılında Nagahara ve Matsuda'nın yayınladığı çalışmada görülen ve sonrasında birçok çalışmada belirtilen sentez yönteminde 5' uçları akridit mofidiyeli iki tek sarmal DNA molekülleri akrilamid, APS ve TEMED ile polimerleşerek lineer polimer zinciri oluşturmuşlardır. Bu lineer polimerler ya birbirlerine eşlenik bölgelerinden bağlanarak bir araya gelir ya da bu iki diziye de eşlenik çapraz bağlayıcı bir oligonüleotid ile bir araya getirilerek hidrojel sentezi gerçekleştirilir. DNA

hidrojellerinin sentez yolları farklılık gösterse de yüksek stabilite ve esneklik özellikleri bu jellerin tespit, çevresel analizler, kontrollü ilaç salınımı, hücre tutunması ve kanser terapisinde kullanımını sağlamıştır (Morya, Walia, Mandal, Ghoroi, ve Bhatia, 2020). Bu çalışmada kloramfenikole özgü aptamer dizisi ile ona kısmen eşlenik DNA dizisi ile lineer polimerler oluşturularak eşlenik bölgelerinde oluşan hibridizasyon ile bir araya getirilmiş ve aptamer fonksiyonlandırılmış DNA hidrojeli sentezlenmiştir.

Kloramfenikol (2,2-dichloro-N-[1,3-dihydroxy-1-(4-nitrophenyl)propan-2-yl]acetamide) gram pozitif ve gram negatif bakterilere karşı etkili geniş spektrumlu bir antibiyotiktir (Dasgupta, 2012). Antibiyotiğin etki mekanizması; bakterilerde 50 S ribozomal alt birime bağlanarak peptidil transferaz enzim aktivitesinin engellenmesi ve translasyon basamağında uzayan peptit zincire amino asidin eklenememesi sonucu protein sentezinin durmasıdır (Van Bambeke, Mingeot-Leclercq, Glupczynski, Tulkens, 2017). Kloramfenikol ucuz ve kolay üretimi nedeniyle hem insan hem de hayvan sağlığı için kullanılan antibiyotikler arasındadır. Bununla beraber, yapılan çalışmalar sonucunda gri bebek sendromu, lösemi, aplastik anemi ve kemik iliği baskılanması gibi birçok hastalıkta etken olduğu belirtilmiştir (Wilson ve Cockerill, 1987; Liu, Yan, Okoth, ve Zhang, 2015). Bu nedenle, kloramfenikol Avrupa Birliği ülkelerinde hayvansal kaynaklı gıdalarda (et, süt, yumurta ve bal) bulunması sınırlandırılmış (maksimum kalıntı limitini 0,3 ng/g) (Karaseva ve Ermolaeva, 2012), ülkemizde ise "Türk Gıda Kodeksi Hayvansal Gıdalarda Bulunabilecek Farmakolojik Aktif Maddelerin Sınıflandırılması ve Maksimum Kalıntı Limitleri Yönetmeliği"nde yasaklı madde olarak belirtilmiş (T.C. Gıda, Tarım ve Hayvancılık Bakanlığı, 2017). Kloramfenikol tespitinde yaygın olarak kullanılan yöntemler gaz kromatografi (GC), yüksek basınçlı sıvı kromatografisi (HPLC) ve sıvı kromatografisi-kütle spektroskopisi (LC-MS) gibi analitik yöntemlerdir (Pfening vd., 2000; Neuhaus, Hurlbut, ve Hammack, 2002; Mottier, Parisod, Gremaud, Guy, ve Stadler, 2003; Dumont, Huet, Traynor, Elliot, ve Delahaut, 2006; Park ve Kim, 2006; Rodziewucz vd., 2007; Yuan, Oliver, Aguilar, ve Wu, 2008; Dong vd., 2009; Mamani, Reyes, ve Ratha, 2009; Zhao ve Ball, 2009; Tajik vd., 2010; Karaseva ve Ermolaeva, 2012). Bununla beraber, hızlı sonuç veren, düşük maliyetli, ön numune hazırlıklarına ihtiyaç duymayan ve kolay uygulanabilen alternatif yöntemlerin geliştirilmesine ihtiyaç duyulmaktadır.

Bu çalışma kloramfenikol tespiti için aptamer fonksiyonlaştırılmış DNA hidrojel tabanlı biyosensör sisteminin geliştirilmesi için hidrojel sentez basamağında yapılan optimizasyon basamaklarını açıklamaktadır. DNA hidrojel yapısının formu ve stabilitesi için akridit modifiyeli DNA dizilerinin konsantrasyonları, akrilamid yüzdesi, kloramfenikol aptameri ve DNA iplik içeren lineer polimer çözeltilerin molar oranları optimize edilmiş, reaksiyon sıcaklığı ve eşlenik bölgenin uzunluğunun jel stabilitesine etkisi değerlendirilmiştir.

2. Materyal ve Yöntem

2.1. Materyaller

Çalışmada kullanılan oligonükelotidler Integrated DNA Technologies (Coralville, ABD) firmasından temin edilmiştir. 5'ucu akridit modifiyeli 40 baz uzunluğunda kloramfenikol aptameri (Mehta vd., 2011) ile ona kısmen eşlenik ve 5'ucu akridit modifiyeli 21 baz uzunluğunda DNA iplik dizisi son konsantrasyonu 300 µM olacak şekilde çözülerek -20°C'de saklanmıştır. Bu oligonükleotidlere ait sentez sonrası bilgiler Tablo 1'de sunulmuştur. Kloramfenikol, akrilamid (%99), amonyum persülfat (APS), N,N,N,N'- tetrametiletilendiamin (TEMED) (%99) Sigma-Aldrich firmasından temin edilmiştir (St. Louis, ABD) ve uygun şartlarda saklanmıştır.

2.2. DNA Hidrojel Sentezi

Deneyde 5' uçları akridit modifiyeli kloramfenikol aptameri ve ona kısmen eşlenik DNA ipliği Tris-EDTA (TE) tampon çözeltisinde çözülmüş ve ayrı stok çözeltiler olarak 4°C' de muhafaza edilmiştir. Aptamer ve DNA iplik çözeltileri, lineer polimer çözeltisi ve hidrojelin hazırlanması için gereken malzemeler ve yüzde içerik değerleri aşağıda sırasıyla belirtilmiştir. Bu değerler çalışmanın ilerleyen basamaklarında optimize edilmiştir.

Aptamer ve DNA iplik çözeltileri;

- %60 aptamer veya DNA ipliği stok çözeltisi (her bir oligonükleotid için ayrı hazırlanacak),
- %10 akrilamid çözeltisi (%40 akrilamid çözeltisinden),
- %10 TE tampon çözelti (pH 8),
- %20 steril distile su

karıştırılarak içerisinde kalabilecek havayı uzaklaştırmak için desikatörde 5 dakika vakuma maruz bırakılmıştır.

Lineer polimer çözeltileri;

- Aptamer ve DNA iplik çözeltisi (her biri için ayrı hazırlanmıştır),
- %1.4 polimerizasyon başlatıcı ve hızlandırıcı çözelti (taze hazırlanmış %10 (a/h) APS ve %10 (h/h) TEMED karışımından)

karıştırılarak tekrar desikatörde polimerizasyon işleminin gerçekleşmesi için 20 dakika kadar bekletilmiştir. Hidrojel sentezi için 1:1 molar oranda aptamer lineer polimer çözeltisi ve DNA ipliği lineer polimer çözeltisi karıştırılarak 25°C sıcaklıkta 120 dakika inkübasyona bırakılmıştır. Bu basamakta; hidrojeli oluşturan lineer polimer çözeltilerinin molar içeriği optimize edilmiştir. Bunun için; farklı konsantrasyonlarda hazırlanan lineer polimer çözeltiler farklı molar oranlarda karıştırılarak hidrojelin oluşması için optimum konsantrasyonlar belirlenmiştir. Ayrıca, sıcaklık optimizasyonu için 25, 45, 55 ve 65°C'de hidrojel sentezi gerçekleştirilmiştir.

3. Bulgular ve Tartışma

3.1. Oligonükleotid Tasarımı

DNA hidrojeli sentezlemek için kullanılan aptamer dizisi Mehta ve ark. tarafından 2011 yılında yayınlanan çalışmadan alınan kloramfenikole özgü seçilmiş DNA aptamer dizisidir. Bu dizi 40 baz uzunluğunda rastgele bölgeye sahip bir DNA kütüphanesinden 8 turluk bir zenginleşme sonucu elde edilen, 0.77 μM Kd değerine sahip ve yüksek özgünlükle kloramfenikole bağlanan bir dizidir (Mehta vd., 2011). Literatürde kloramfenikol için iki aptamer geliştirme çalışması bulunmasına rağmen (Duan vd., 2016; Mehta vd., 2011), kloramfenikol tespiti için geliştirilen biyosensör çalışmalarında sıklıkla bu dizi kullanıldığından bu çalışmada da bu dizi kullanılmıştır (Yadav, Agrawal, Chandra, ve Goyal, 2014; Miao vd., 2015; Liu vd., 2015; Miao vd., 2016). Aptamer fonksiyonlandırılmış DNA hidrojelin sentezlenebilmesi için gerekli olan diğer dizi bu çalışma kapsamında kloramfenikol aptamer dizisine kısmen eşlenik olarak tasarlanmıştır. DNA iplik 1 olarak isimlendirilen bu dizi 21 baz uzunluğunda ve aptamere 15 baz uzunluğunda eşlenik bir bölgeye sahip DNA molekülüdür. Bu iki DNA molekülüne ait bilgiler Tablo 1'de belirtilmiştir. Her iki dizinin 5' uçlarında bulunan akridit modifikasyonu sayesinde her iki DNA dizisi lineer polimer hale getirilmiş ve daha sonra eşlenik bölgelerin bir araya gelmesiyle polimer sentezi tamamlanmıştır.

Tablo 1
Oligonükleotidlerin özellikleri

	Kloramfenikol aptameri*	DNA iplik-1*
Dizisi	5'-acryd-TTTT-T**ACTTCAGTGAGTT-GTCCCACGGTCGG-CGAGTCGGTGGTAG**-3'	5'-acryd-TTTTTTGGGA-CAACTCACTG-3'
Moleküler ağırlık	14,168.2 g/mol	6,345.2 g/mol
GC içeriği	%53.3	%40.0
Erime sıcaklığı (Tm)	69.4 °C	51.0 °C
En düşük katlanma serbest enerji (25°C'de)	-2.21 kcal/mol	-0.83 kcal/mol
En güçlü katlanmanın erime sıcaklığı	40.4°C	41.2°C

*Dizilerdeki altı çizili bölgeler kloramfenikol aptameri ile DNA iplik 1 arasındaki eşlenik bölgeleri, koyu olarak gösterilen bölge ise aptamer dizisini belirtmektedir.

3.2. DNA Hidrojel Sentezi

Bu çalışmada hidrojel sentezi; Şekil 1'de özetlendi gibi (i) 5' uçları akridit modifiyeli kloramfenikol aptameri ve DNA iplik-1 dizisinin ortama eklenen APS ve TEMED ile lineer polimer DNA ipliklerine dönüştürülmesi, (ii) ve elde edilen bu iki lineer polimerin eşlenik bölgelerinin hibridizasyonuyla polimer sentezinin tamamlanmasını içermektedir. DNA molekülünün 5'ucunda bulunan akridit modifikasyonu serbest akrilamid monomeri gibi davranarak DNA molekülünü lineer polimer yapıya yüksek verimde ekleme özelliğine sahiptir (Liu, 2011). Bu aşamalarla sentezlenen DNA hidrojelin sentez esnasında aptamer ve DNA ipliği çözeltilerinde yüzde DNA içerikleri, yüzde akrilamid içeriği, lineer polimer çözeltilerin molar oranları ayrı ayrı optimize edilmiş, sıcaklığın ve eşlenik bölge uzunluğunun jelleşmeye etkisi değerlendirilmiştir.

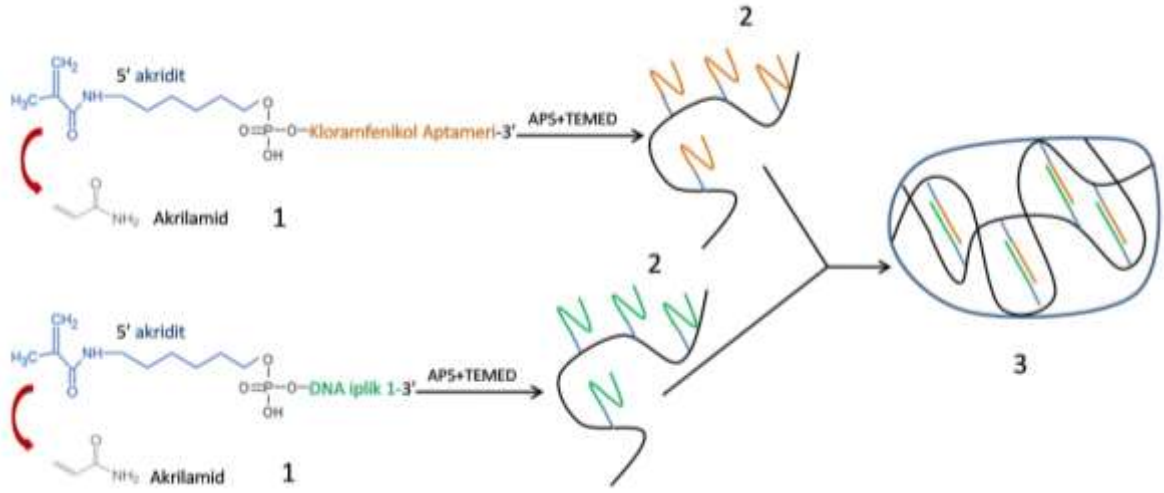

Şekil 1. Aptamer fonksiyonlandırılmış DNA hidrojellerinin sentezi; 1) 5' ucu akridit modifiyeli ve kloramfenikol aptamerine kısmen eşlenik DNA ipliği 1 ile yine 5' ucu akridit modifiyeli kloramfenikol aptameri akrilamid, APS ve TEMED varlığında lineer polimer DNA ipliklerine dönüştürülür. 2) Bu iki lineer polimer, aptamer ve DNA ipliğinin eşlenik bölgelerinin hibridizasyonuyla bir araya getirilerek polimer sentezi gerçekleştirilmiş olur. 3) Sonuç olarak; aptamer bağlayıcılı DNA hidrojelinin sentezi tamamlanmış olur.

İlk olarak akridit modifiyeli DNA dizilerinin konsantrasyonları optimize edilmiştir. Lineer polimer hale getirilmiş DNA molekülünün konsantrasyonu doğrudan DNA hidrojelinin oluşumunu etkilediği için DNA konsantrasyon etkisi değerlendirilmiştir. DNA içeriği %40 ile %60 arasında değişen çözeltiler hazırlanmış, %20'lik akrilamid çözeltisi, APS ve TEMED'in ortama eklenmesiyle lineer polimer çözeltiler oluşturulmuştur. Oluşturulan lineer çözeltiler 1:1 molar oranda karıştırılarak 25°C'de reaksiyona bırakılmıştır. Reaksiyon süresi sonunda elde edilen jelleşme durumları tüplerin resimleri çekilerek değerlendirilmiştir. Şekil 2A'da görüldüğü gibi 1 saatin sonunda aptamer ve DNA iplik içerikleri %60 olan çözeltilerin 1:1 molar oranda karıştırılması ile

oluşturulan örnekte jelleşmenin başladığı ve 2. saatin sonunda diğer örneklere göre daha katı bir jel oluşumu gözlenmiştir. Literatürde bakıldığında, lineer çözeltide DNA yüzdesinin artırılmasıyla birbirine daha yakın ve daha sıkı bir ağ yapının elde edilmesi beklenmektedir (Liu, Han, Pei, ve Du, 2018). Bu çalışmadan alınan sonuçlara bakıldığında %60'lık DNA çözeltileri ile oluşturulan jellerde jelleşme daha fazla elde edildiğinden ilerleyen çalışmalarda DNA çözeltilerinin içeriği %60 olarak hazırlanmıştır. DNA içeriği %60'dan fazla lineer çözeltiler ile daha katı jelleşmenin elde edilmesi olası bir sonuç olarak değerlendirilmiştir, fakat DNA içeriğinin artmasıyla jel sentez maliyetinde de artış olacağından en yüksek %60 DNA içeriği denenmiş ve uygun değer olarak belirlenmiştir.

Akrilamid çözeltisinin yüzde konsantrasyon değişiminin jel oluşumuna etkisini görmek amacıyla akrilamid yüzdesi %20 ve %40 olarak hazırlanmış ve %60'lık DNA içerikleriyle DNA hidrojel sentezi tekrarlanmıştır. Reaksiyon süresi sonunda elde edilen jel görüntüleri Şekil 2B'de sunulmuştur. Akrilamid yüzdesinin %20'den daha düşük yüzdelere indirilmesiyle yumuşak ve kolaylıkla parçalanan jeller elde edilmiş ve bu nedenle deneyde en düşük akrilamid yüzdesi %20 olarak belirlenmiştir. Görüntülerden anlaşıldığı üzere %40 akrilamid çözeltisinden hazırlanan jel daha katı hale görülmüştür. Bunun nedeni olarak; akrilamid konsantrasyonunun artmasıyla jelin daha küçük gözenekli yapı kazanması ve dolayısıyla daha katı olması durumu düşünülmektedir. Dolayısıyla, bu çalışmadan sonra yapılan tüm deneylerde jel sentezi için %40 akrilamid çözeltisi kullanılmıştır.

DNA ve akrilamid yüzde içeriklerine ek olarak, kloramfenikol aptameri ve DNA iplik 1 içeren lineer polimer çözeltilerin karıştırılmasında molar oranların jelleşmeye etkisi değerlendirilmiştir. Bu amaçla aptamer çözeltisi:DNA iplik çözeltisi 2:1, 1.5:1, 1:1, 1:1.5 ve 1:2 molar oranlarında hazırlanmıştır ve reaksiyon sonunda jellere ait görüntüler elde edilmiştir. Bu çalışmada tasarlanan DNA hidrojeli aptamer dizisi ile DNA iplik 1 dizisinin hibridizasyonu sonucu oluştuğundan 1:1 molar oranda hazırlanan jelin diğerlerine göre daha sıkı olacağı beklenilmiştir. Şekil 2C'de görüldüğü üzere 1:1 molar oran dışında hazırlanan diğer jel örneklerinde hem jelleşme daha yavaş olmuş hem de 2 saatin sonunda daha yumuşak jeller elde edilmiştir. Eşit molar oranda hazırlanan jelde ise daha hızlı ve daha katı jel oluşumu gözlenmiştir. Bunun nedeni olarak 1:1 molar oranda karıştırıldıklarında oluşan hidrojelin hibridizasyon doygunluğuna ve dengesine ulaştığı ve bu nedenle daha sıkı ya da katı bir jel elde edildiği düşünülmüştür. Elde edilen sonuçlar literatürdeki bazı çalışmalarla uyum göstermiştir. Örneğin; 2016 yılında yayınlanan bir çalışmada monomerler arası düşük molar oranda sentezlenen jellerin çapraz bağlanma verimindeki azalma nedeniyle sertliklerinde azalma görülmüş ve bu durum ortamda yüksek miktarda bulunan hibridize olmamış tek sarmal DNA'dan kaynaklandığı belirtilmiştir (Jiang, Pan, Vivek, Weeks, ve Ke, 2016).

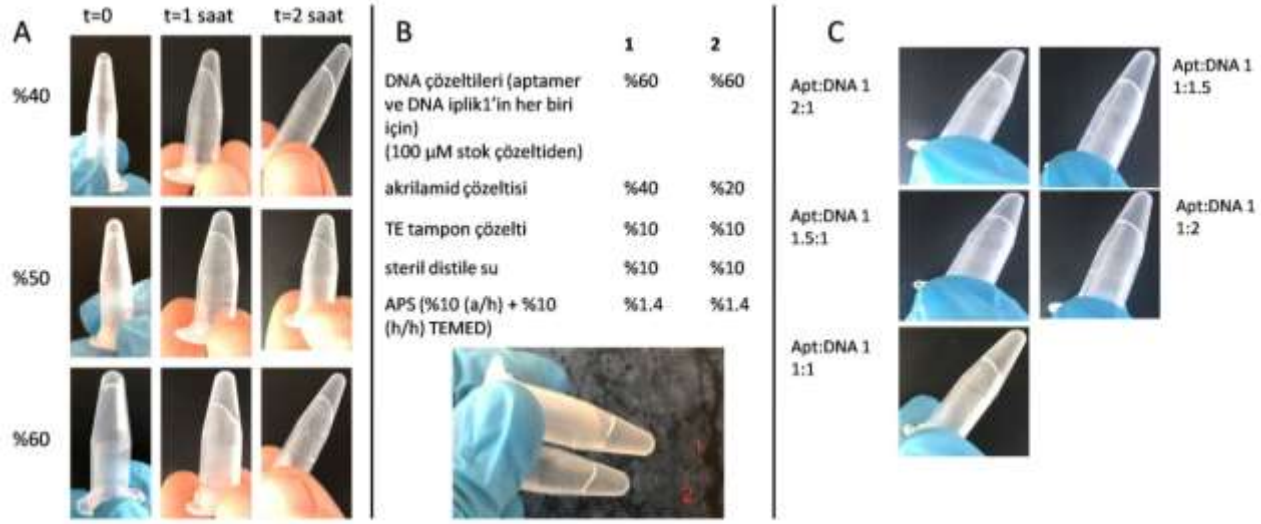

Şekil 2. Aptamer fonksiyonlandırılmış DNA hidrojel sentez koşullarının optimizasyonu; A) akridit modifiyeli DNA dizilerinin yüzde içeriklerinin, B) akrilamid ana çözelti yüzdesinin, C) aptamer ve DNA iplik ile hazırlanmış lineer polimer çözeltilerin molar oranlarının optimizasyonuna ait resimler.

DNA hidrojellerinin stabilitesinde sıcaklık etkeni önemli rol oynamaktadır. Sıcaklığın polimer yapı içerisinde farklı oranlarda bulunan hidrofilik ve hidrofobik kısımların arasındaki ilişkiyi değiştirdiği ve böylece çapraz bağlı ağ yapının çözünürlüğünde değişimin meydana geldiği ve katı-jel form değişiminin yaşandığı bilinmektedir (Bajpai, Shukla, Bhanu, ve Kankane, 2008; Huang vd., 2019). DNA molekülünün çapraz bağlayıcı olarak görev aldığı hidrojellerde sıcaklık faktörünün etkili olmasının sebebi bazlar arası eşleşme stabilitesinin sıcaklıkla beraber değişmesidir. Sentezde kullanılacak DNA moleküllerinin %GC içeriklerinin ve uzunluğunun değiştirilmesiyle hidrojel için istenilen erime sıcaklığı (Tm) elde edilebilir. Erime sıcaklığından daha yüksek sıcaklıklarda DNA molekülleri arasındaki hidrojen bağları kırılır ve DNA molekülleri birbirinden ayrılır. Bu denatürasyon basamağı tersinir bir reaksiyon olduğundan sıcaklık yavaşça düşürüldüğünde hidrojen bağları iki dizi arasında tekrar oluşarak jel oluşumu tekrar gözlenir. Literatürde bu tersinir özellikten yararlanarak tasarlanmış DNA hidrojel çalışmaları bulunmaktadır. 2011 yılında yayınlanan bir çalışmada içerisine kanser ilacı yüklenerek DNA ve poliakrilamitten sentezlenmiş hidrojel ilgili hedef bölgeye yönlendirilerek sıcaklığın artırılmasıyla ilacın salınımı sağlanmıştır (Kang vd., 2011). Çalışmada erime sıcaklığından daha yüksek bir sıcaklıkta hidrojelin yapısında bulunan DNA molekülleri arasındaki hidrojen bağlarının ayrılmaları ve böylece bozulan jel yapıdan ilacın serbest hale gelmesi sağlanmıştır.

Bu çalışmada kloramfenikol aptameri ve DNA iplik 1 arasındaki eşlenik bölgeden çift sarmal yapı oluşarak amin bazlarının istiflenmesi ve aralarındaki hidrojen bağı nedeniyle kararlı bir yapıya sahip olması sağlanmıştır. Farklı sıcaklıkların bu yapıya etkisini değerlendirmek amacıyla DNA hidrojelin sentezi farklı sıcaklıklarda gerçekleştirilmiştir. Tablo 1'de belirtildiği üzere kloramfenikol aptamerinin hem uzunluğu hem de % GC içeriği DNA iplik 1'den fazla olduğu için Tm değeri de DNA ipliğine göre daha yüksektir. Bu dizilerin en güçlü ikincil yapılarının erime sıcaklıklarına bakıldığında ise kloramfenikol aptameri ve DNA iplik 1 için sırasıyla 40.4°C ve 41.2 °C olarak hesaplanmıştır. Bu değerlerden yola çıkarak 25°C, 45°C, 55°C ve 65°C sıcaklıklar deney koşulları olarak belirlenmiş ve optimize edilen koşullarda jeller hazırlanarak bu sıcaklıklarda iki saatlik inkübasyona bırakılmıştır. Şekil 3'de belirlenen koşullarda sentezlenen DNA hidrojellerine ait resimler sunulmuştur. Görsellerin yanı sıra dört farklı sıcaklıkta kloramfenikol aptameri ve DNA iplik-1'in NUPACK yazılımı (www.nupack.org; Zadeh vd., 2011) ile çizilen ikincil yapıları ve bu yapıların serbest enerjileri gösterilmiştir.

Bu sonuçlardan 25°C ve 45°C sentezlenen jellerin diğer jellere göre daha katı forma sahip olduğu görülmüştür. Her iki sıcaklıkta da katı formda jel elde edilse de, 45°C'de örnek hacmi buharlaşma nedeniyle azalmıştır. Yüksek sıcaklıklarda kloramfenikol aptamer dizisi ile DNA iplik 1 dizisi arasındaki 15 bazlık eşleşen bölgedeki hidrojen bağlarının stabil olmaması nedeniyle yumuşak formda, tam jelleşmeyen örnekler elde edilmiştir. Ayrıca serbest enerjilerine bakıldığında en yüksek serbest enerjisiyle 65°C'deki DNA'ların ikincil yapı oluşturma durumları en az olarak değerlendirilmiştir. Bu nedenle DNA hidrojel sentezi için uygun ortam sıcaklığı 25°C olarak belirlenmiştir. Sentez için kullanılan kloramfenikol aptamer ve DNA iplik 1 dizilerinin tek iplik olarak reaksiyona girmelerini sağlamak adına DNA çözeltileri 50°C'de 5 dakika bekletilmiş ve 1:1 molar oranda lineer çözeltiler karıştırıldıktan sonra inkübasyon sıcaklığı 25°C olarak ayarlanmıştır.

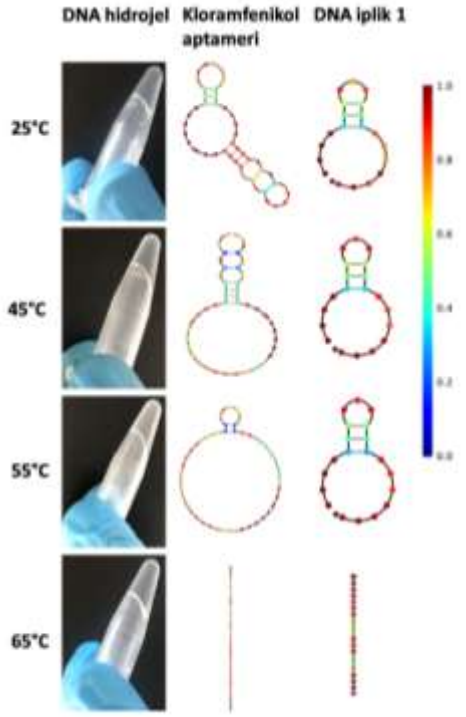

	Kloramfenikol aptameri	DNA iplik 1
Sıcaklık (°C)	Serbest enerji (kcal/mol)	Serbest enerji (kcal/mol)
25	-5,64	-1,15
45	-1,34	-0,44
55	-0,44	-0,08
65	0	0

Şekil 3. Aptamer fonksiyonlandırılmış DNA hidrojel stabilitesinde sıcaklık etkisi (dizilere ait farklı sıcaklıklardaki iki boyutlu yapılar NUPACK yazılımı ile oluşturulmuştur. Renkli gösterge 0-1 arasında denge olasılığını göstermektedir).

Son olarak, kloramfenikol aptamer dizisi ve DNA iplik 1 arasındaki eşlenik bölgenin uzunluğunun jel stabilitesine etkisi değerlendirilmiştir. Bu aşamaya kadar yapılan tüm optimizasyon çalışmalarında iki dizi arasındaki eşlenik bölgesi 15 baz uzunluğunda olan DNA ipliği kullanılmıştır. Bu aşamada ise, kloramfenikol aptamerine farklı uzunlukta eşlenik bölgeye sahip iki adet DNA ipliği daha tasarlanmıştır ve yukarıda belirtilen optimum koşullarda DNA hidrojeli sentezi gerçekleştirilmiştir. Toplam 21 baz uzunluğunda olan DNA iplikleri aptamer dizisine sırasıyla 15, 12 ve 9 baz uzunluğunda eşlenik bölgeye sahip olarak tasarlanmıştır (Şekil 4A). Sentez reaksiyonunun 2. saatinde 15 bazlık eşlenik bölgeye sahip DNA iplik 1(15) dizisi ile sentezlenen jelin 12 ve 9 bazlık eşlenik bölgeye sahip DNA dizileri ile sentezlenen jellerden daha katı olduğu görülmüştür (Şekil 4B). Aptamer ve DNA ipliklerinin lineer polimer haline getirilmesi ve bu iki lineer yapının eşlenik bölgelerinden birbirilerine bağlanması sonucu oluşan DNA hidrojel için baz eşleşme bölgesinin uzun olması daha stabil bir hidrojel sentezine yol açtığı düşünülmüştür. Eşlenik bölgenin kısaltılması iki dizi arasında oluşacak hidrojen bağlarının azlığı nedeniyle daha gevşek jeller oluşmasına neden olduğu sonucuna varılmıştır. Dolayısıyla, eşlenik bölgenin kısaltılması jelin katılaşmasını ve stabilitesinin azalttığından 15 baz eşlenik bölgeye sahip DNA iplik-1'in sentezde kullanılmasına karar verilmiştir.

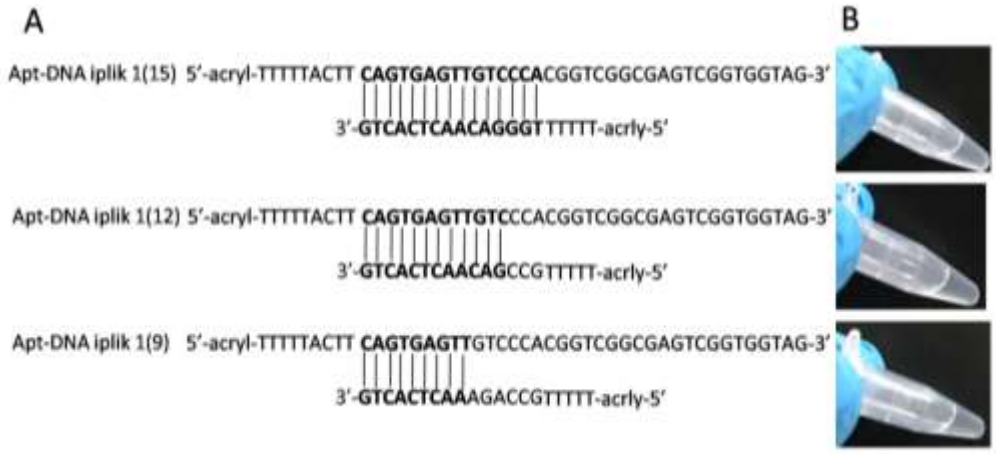

Şekil 4. Aptamer fonksiyonlandırılmış DNA hidrojel stabilitesinde eşlenik bölge uzunluğunun etkisi; A) iki dizi arasındaki eşlenik bölgelerin gösterimi, B) farklı eşlenik bölgeye sahip DNA iplik ile sentezlenen DNA hidrojel görüntüleri

4. Sonuçlar

Bu çalışma aptamer fonksiyonlandırılmış DNA hidrojel sentezi için gerekli optimizasyon basamaklarını belirten ve sıcaklık ve eşlenik bölge uzunluğu gibi parametrelerin hidrojel stabilitesi üzerindeki etkisini açıklayan bir çalışmadır. Temel olarak; kloramfenikol antibiyotiğine özgü belirlenmiş aptamer dizisi ile ona kısmen eşlenik DNA iplik dizisinin kullanıldığı DNA hidrojel sentezi gerçekleştirilmiştir. 5'uçlarından akridit modifiyeli aptamer ve DNA ipliğin akrilamid, APS ve TEMED ile önce polimer yapıya katılması sağlanmış daha sonra birbirlerine eşlenik bölgeden bağlanarak hidrojel sentezi tamamlanmıştır. Daha katı ve stabil jel sentezi için DNA içeriği, akrilamid içeriği ve molar oranlarını belirlemeye yönelik optimizasyon çalışmaları yapılmıştır. Belirlenen optimum koşullar altında yüksek stabiliteli DNA hidrojel sentezi tamamlanmış ve ilerleyen çalışmalarda kloramfenikol tespiti için biyosensör uygulamasına yönelik ön veriler elde edilmiştir.

Teşekkür

Bu çalışma Türkiye Bilimsel ve Teknolojik Araştırma Kurumu (TÜBİTAK) tarafından desteklenmiştir. (Proje No: 218Z125).

Yazar Katkıları

Gülnur Camızcı Aran: Analizi planlamış, tasarlamış ve analizi yapmıştır.

Ceren Bayraç: Çalışmanın sonuçlarını değerlendirmiş ve makaleyi yazmıştır.

Çıkar Çatışması

Yazarlar çıkar çatışması bildirmemişlerdir.

Kaynaklar

Abune, L., Davis, B., ve Wang, Y. (2021). Aptamer-functionalized hydrogels: An emerging class of biomaterials for protein delivery, cell capture, regenerative medicine, and molecular biosensing. *Wires Nanomedicine and nanobiotechnology. 13, 6, e1731.* Doi:https://doi.org/10.1002/wnan.1731

Amaya-González, S., de-Los-Santos-Álvarez, N., Miranda-Ordieres, A.J., ve Lobo-Castañón, M.J. (2015). Sensitive gluten determination in gluten-free foods by an electrochemical aptamer-based assay. *Anal Bioanal Chem., 407, 20, 6021-9.* Doi:https://doi.org/10.1007/s00216-015-8771-6

Bai, W., ve Spivak, D. A. (2014). A Double-Imprinted Diffraction-Grating Sensor Based on a Virus Responsive Super Aptamer Hydrogel Derived from an Impure Extract. Angew. Chem., Int. Ed., 53, 2095–2098. https://doi.org/10.1002/ange.201309462

Bajpai, A.K., Shukla, S.K., Bhanu, S., ve Kankane, S. (2008). Responsive polymers in controlled drug delivery Prog. Polym. Sci., 33, 1088-1118. https://doi.org/10.1016/j.progpolymsci.2008.07.005

Bayrac, A.T., Sefah, K., Parekh, P., Bayrac, C., Gulbakan, B., Oktem, H.A., ve Tan, W. (2011). In Vitro Selection of DNA Aptamers to Glioblastoma Multiforme. ACS Chem. Neurosci., 2, 3, 175–181. https://doi.org/10.1021/cn100114k

Bayraç, C., Eyidoğan, F., ve Avni Öktem, H. (2017). DNA aptamer-based colorimetric detection platform for Salmonella Enteritidis, Biosensors and Bioelectronics, 98, 22-28. https://doi.org/10.1016/j.bios.2017.06.029

Belair, D. G., Le, N. N., ve Murphy, W. L. (2014). Design of growth factor sequestering biomaterials. Chemical Communications, 50, 99, 15651–15668. https://doi.org/10.1039/c4cc04317k

Bruno, J.G., Carrillo, M.P., ve Philips, T. (2008). In vitro antibacterial effects of antilipopolysaccharide DNA aptamer-C1qrs complexes. Folia Microbiol (Praha), 53, 4, 295-302. https://doi.org/10.1007/s12223-008-0046-6

Castillo, G., Spinella, K., Poturnayová, A., Šnejdárková, M., Mosiello, L., ve Hianik, T. (2015). Detection of aflatoxin B1 by aptamer-based biosensor using PAMAM dendrimers as immobilization platform. Food Control, 52, 9-18. https://doi.org/10.1016/j.foodcont.2014.12.008

Dasgupta, A. (2012). Chapter 3 - Advances in antibiotic measurement. Advances in Clinical Chemistry, Editör:. Makowski, G.S. 56, 75-104, Elsevier. https://doi.org/10.1016/b978-0-12-394317-0.00013-3

DeForest, C. A., Sims, E. A., ve Anseth, K.S. (2010). Peptide-functionalized click hydrogels with independently tunable mechanics and chemical functionality for 3D cell culture. Chemistry of Materials, 22, 16, 4783–4790. https://doi.org/10.1021/cm101391y

Dong, Z., Huang, G., Xu, S., Deng, C., Zhu, J, Chen, S., Yang, X., ve Zhao, S. (2009). Real-time and label-free detection of chloramphenicol residues with specific molecular interaction, J. Microsc., 234, 255–261. https://doi.org/10.1111/j.1365-2818.2009.03175.x

Duan Y, Gao Z, Wang L, Wang H, Zhang H, ve Li H. (2016). Selection and Identification of Chloramphenicol-Specific DNA Aptamers by Mag-SELEX. Appl Biochem Biotechnol. 180, 8, 1644-1656. https://doi.org/10.1007/s12010-016-2193-6

Dumont, V., Huet, A. C., Traynor, I., Elliot, C., ve Delahaut, P. (2006). A surface plasmon resonance biosensor assay for the simultaneous determination of thiamphenicol, florfenicol, florfenicol amine and chloramphenicol residues in shrimps, Anal. Chim. Acta. 567, 2, 179–183. https://doi.org/10.1016/j.aca.2006.03.028

Ellington, A.D., ve Szostak, J.W. (1990). In vitro selection of RNA molecules that bind specific ligands. Nature, 346, 818–822. https://doi.org/10.1038/346818a0

Famulok, M. (1994). Molecular recognition of amino acids by RNA aptamers: an L-citrulline RNA motif and its evolution into an L-arginine binder, Journal of the American Chemical Society, 116, 1698–1706. https://doi.org/10.1021/ja00084a010

Ferguson, B. S., Hoggarth, D. A., Maliniak, D., Ploense, K., White, R. J., Woodward, N., Hsieh, K., Bonham, A.J., Eisenstein, M., Kippin T.E., Plaxco, K.W., ve Soh, H. T. (2013). Real-time, aptamer-based tracking of circulating therapeutic agents in living animals. Sci. Transl. Med. 5, 213ra165. https://doi.org/10.1126/scitranslmed.3007095

Gobin, A. S., ve West, J. L. (2003). Effects of epidermal growth factor on fibroblast migration through biomimetic hydrogels. Biotechnology Progress, 19, 6, 1781–1785. https://doi.org/10.1021/bp0341390

Guo, Y., Wang, X., ve Sun, X. (2015). A label-free Electrochemical Aptasensor Based on Electrodeposited Gold Nanoparticles and Methylene Blue for Tetracycline Detection, Int. J. Electrochem. Sci., 10, 4, 3668-3679.

He, C., Ji, H., Qian, Y., Wang, Q., Liu, X., Zhao, W., ve Zhao, C. (2019). Heparin-based and heparin-inspired hydrogels: Size-effect, gelation and biomedical applications. Journal of Materials Chemistry B, 7,8, 1186–1208. https://doi.org/10.1039/c8tb02671h

Huang, H., Qi, X., Chen, Y., ve Wu Z. (2019). Thermo-sensitive hydrogels for delivering biotherapeutic molecules: A review, Saudi Pharmaceutical Journal, 27, 7, 990-999 https://doi.org/10.1016/j.jsps.2019.08.001

Istamboulié, G., Paniel, N., Zara, L., Reguillo Granados, L., Barthelmebs, L., ve Noguer, T. (2016). Development of an impedimetric aptasensor for the determination of aflatoxin M1 in milk. Talanta, 146, 464-9. Doi: https://doi.org/10.1016/j.talanta.2015.09.012

Jiang, H., Pan, V., Vivek, S., Weeks, E.R., ve Ke, Y. (2016). Programmable DNA HydrogelsAssembledfromMultidomain DNA Strands. ChemBioChem, 17, 1156 – 1162. Doi:https://doi.org/10.1002/cbic.201500686

Kang, H., Trondoli, A.C., Zhu, G., Chen, Y., Chang, Y.J., Liu, H., Huang, Y.F., Zhang, X., ve Tan, W. (2011). Near-infrared light-responsive core-shell nanogels for targeted drug delivery, AcsNano., 5, 5094-5099. Doi:https://doi.org/10.1021/nn201171r

Karaseva, N. A., ve Ermolaeva, T. N. (2012). A piezoelectric immunosensor for chloramphenicol detection in food. Talanta, 93, 44–48. Doi:https://doi.org/10.1016/j.talanta.2011.12.047

Kim, M.G., Shon, Y., Miao, W., Lee, J., ve Oh, Y.K. (2016). Biodegradable graphene oxide and polyaptamer DNA hybrid hydrogels for implantable drug deliver. Carbon, 105, 14-22. Doi:https://doi.org/10.1016/j.carbon.2016.04.014

Li, J., Mo, L., Lu., C.H., Fu, T., Yang, H.H., ve Tan, W. (2016). Functional nucleic acid-based hydrogels for bioanalytical and biomedical applications. Chem Soc Rev., 45, 5, 1410–1431. https://doi.org/10.1039/C5CS00586H

Liu, J. (2011). Oligonucleotide-functionalized hydrogels as stimuli responsive materials and biosensors. Soft Matter, 7, 6757.

Liu, Y., Yan, K., Okoth, O. K., ve Zhang, J. (2015). A label-free photoelectrochemical aptasensor based on nitrogen-doped graphene quantum dots for chloramphenicol determination. Biosensors and Bioelectronics, 74, 1016-1021. Doi:https://doi.org/10.1016/j.bios.2015.07.067

Liu , C., Han, J., Pei ,Y., ve Du, J. (2018). Aptamer Functionalized DNA Hydrogel for Wise-Stage Controlled Protein Release, Appl. Sci., 8, 1941. Doi:https://doi.org/10.3390/app8101941

Luo, C., Lei, Y., Yan , L., Yu, T., Li, Q., Zhang, D., Ding, S., ve Ju, H. (2012). A Rapid and Sensitive Aptamer Based Electrochemical Biosensor for Direct Detection of Escherichia Coli O111. Electroanalysis, 24, 5, 1186-1191. Doi:https://doi.org/10.1002/elan.201100700

Ma, X., Jiang, Y., Jia, F., Yu, Y., Chen, J., ve Wang, Z. (2014). An aptamer-based electrochemical biosensor for the detection of Salmonella. J Microbiol Methods, 98, 94-8. Doi:https://doi.org/10.1016/j.mimet.2014.01.003

Mamani, M. C. V., Reyes, F. G. R., ve Ratha, S. (2009). Multiresidue determination of tetracyclines, sulphonamides and chloramphenicol in bovine milk using HPLC-DAD. Food Chem., 117, 3, 545–552. Doi:https://doi.org/10.1016/j.foodchem.2009.04.032

Mehta, J., Van Dorst, B., Rouah-Martin, E., Herrebout, W., Scippo, M. L., Blust, R., ve Robbens, J. (2011). In vitro selection and characterization of DNA aptamers recognizing chloramphenicol, J. Biotechnol., 155, 361–369. https://doi.org/10.1016/j.jbiotec.2011.06.043

Miao, Y., Gan, N., Li, T., Zhang, H., Cao, Y., ve Jiang, Q. (2015). A colorimetric aptasensor for chloramphenicol in fish based on double-stranded DNA antibody labeled enzyme-linked polymer nanotracers for signal amplification. Sensors and Actuators, B: Chemical, 220, 679-687. Doi:https://doi.org/10.1016/j.snb.2015.05.106

Miao, Y., Gan, N., Li, T., Cao, Y., Hu, F., ve Chen, Y. (2016). An ultrasensitive fluorescence aptasensor for chloramphenicol based on FRET between quantum dots as donor and the magnetic SiO2@Au NPs probe as acceptor with exonuclease-assisted target recycling. Sens. Actuators B: Chem., 222, 1066-1072. Doi:https://doi.org/10.1016/j.snb.2015.09.049

Mishra, R.K., Hayat, A., Catanante, G., Ocaña, C., ve Marty, J.L. (2015). A label free aptasensor for Ochratoxin A detection in cocoa beans: An application to chocolate industries. Anal Chim Acta., 889,106-12. https://doi.org/10.1016/j.aca.2015.06.052

Mitchell, A. C., Briquez, P. S., Hubbell, J. A., ve Cochran, J. R. (2016). Engineering growth factors for regenerative medicine applications. Acta Biomaterialia, 30, 1–12. Doi:https://doi.org/10.1016/j.actbio.2015.11.007

Morya, V., Walia, S., Mandal, B.B., Ghoroi, C., ve Bhatia, D. (2020). Functional DNA Based Hydrogels: Development, Properties and Biological Applications. ACS Biomater. Sci. Eng., 6, 11, 6021–6035. Doi:https://doi.org/10.1021/acsbiomaterials.0c01125

Mottier, P., Parisod, V., Gremaud, E., Guy, P. A., ve Stadler, R. H. (2003). Determination of the antibiotic chloramphenicol in meat and seafood products by liquid chromatography – electrospray ionization tandem mass spectrometry. J. Chromatogr. A., 994, 1–2, 75–84. Doi:https://doi.org/10.1016/s0021-9673(03)00484-9

Nagahara, S., ve Matsuda, T. (1996). Hydrogel formation via hybridization of oligonucleotides derivatized in water-soluble vinyl polymers. Polym. Gels Networks, 4, 111–127. Doi:https://doi.org/10.1016/0966-7822(96)00001-9

Neuhaus, B. K., Hurlbut, J. A., Hammack, W. (2002). LC/MS/MS analysis of chloramphenicol in shrimp. USFDA, 18, 20–31.

Ocaña, C., Hayat, A., Mishra, R., Vasilescu, A., del Valle, M., ve Marty, J.L. (2015). A novel electrochemical aptamer-antibody sandwich assay for lysozyme detection. Analyst, 140, 12, 4148-53. Doi:https://doi.org/10.1039/C5AN00243E

Park, I., ve Kim D. (2006). Development of a chemiluminescent immunosensor for chloramphenicol. Anal. Chim. Acta, 578,19–24. Doi:https://doi.org/10.1016/j.aca.2006.07.015

Pfenning, A. P., Roybal, J. E., Rupp, H. S., Turnipseed, S. B., Gonzales, S. A., ve Hurlbut, J. A. (2000). Simultaneous determination of residues of chloramphenicol, florfenicol, florfenicol amine and thiamphenicol in shrimp tissue by gas chromatography with electron capture detection. J. AOAC Int., 83, 1, 26–30. Doi:https://doi.org/10.1093/jaoac/83.1.26

Robertson, D.L., ve Joyce, G.F. (1990). Selection in vitro of an RNA enzyme that specifically cleaves singl stranded DNA. Nature,344, 6265, 467–468. Doi:https://doi.org/10.1038/344467A0

Rodziewicz, L., ve Zawadzka, I. (2007). Rapid determination of chloramphenicol residues in honey by liquid chromatography tandem mass spectrometry and the validation of method based on 2002/657/EC. APIACTA, 42, 25–30.

Sun, X., Li, F., Shen, G., Huang, J., ve Wang, X. (2014). Aptasensor based on the synergistic contributions of chitosan-gold nanoparticles, graphene-gold nanoparticles and multi-walled carbon nanotubes-cobalt phthalocyanine nanocomposites for kanamycin detection. Analyst, 139, 1, 299-308. Doi:https://doi.org/10.1039/c3an01840g

Tuerk, C., ve Gold, L. (1990). Systematic evolution of ligands by exponential enrichment: RNA ligands to bacteriophage T4 DNApolymerase. Science, 249, 505–510. Doi:https://doi.org/10.1126/science.2200121

Tajik, H., Malekinejad, H., Razavi-Rouhani, S.M., Pajouhi, M.R., Mahmoudi, R., ve Haghnazari, A. (2010). Chloramphenicol residues in chicken liver, kidney and muscle: A comparison among the antibacterial residues monitoring methods of four plate test, ELISA, and HPLC. Food & Chemical Toxicology, 48, 2464-2468. Doi:https://doi.org/10.1016/j.fct.2010.06.014

Takahashi, M. (2018). Aptamers targeting cell surface proteins. Biochimie, 145, 63-72. Doi:https://doi.org/10.1016/j.biochi.2017.11.019

Trashin, S., de Jong, M., Breugelmans, T., Pilehvar, S., ve De Wael, K. (2015). Label-Free Impedance Aptasensor for Major Peanut Allergen Ara h 1. Electroanalysis, 27, 1, 32-37. Doi:https://doi.org/10.1002/elan.201400365

Van Bambeke, F., Mingeot-Leclercq, MP., Glupczynski, Y., ve Tulkens, P.M. 2017. 137 – Mechanisms of Action. Infectious Diseases, 4th edition. Editörler: Cohen, J., Powderly, W.G, Opal, S.M., 1162–1180.

Yadav, S.K., Agrawal, B., Chandra, P., ve Goyal, R.N. (2014). In vitro chloramphenicol detection in a Haemophilus influenza model using an aptamer-polymer based electrochemical biosensor. Biosensors and Bioelectronics, 55, 337-342. Doi:https://doi.org/10.1016/j.bios.2013.12.031

Yan, L., Zhu, Z., Zou, Y., Huang, Y., Liu, D., Jia, S., Xu, D., Wu, M., Zhou, Y., Zhou, S., ve Yang C. J. (2013). Target-Responsive "Sweet" Hydrogel with Glucometer Readout for Portable and Quantitative Detection of Non-Glucose Targets. J. Am. Chem. Soc., 135, 3748–3751. Doi:https://doi.org/10.1021/ja3114714

Yang, H., Liu, H., Kang, H., ve Tan W. (2008). Engineering Target-Responsive Hydrogels Based on Aptamer−Target Interactions. J. Am. Chem. Soc., 130, 6320–6321. https://doi.org/10.1021/ja801339w

Yin, B.C., Ye, B.C., Wang, H., Zhu, Z., ve Tan, W. (2012). Colorimetric logic gates based on aptamer-crosslinked hydrogels. Chem Commun. 48, 1248–50. Doi:https://doi.org/10.1039/C1CC15639J

Yuan, J., Oliver, R., Aguilar, M. I., ve Wu, Y. (2008). Surface plasmon resonance assay for chloramphenicol. Anal. Chem., 80, 8329–8333. Doi:https://doi.org/10.1021/ac801301p

Zadeh ,J. N., Steenberg, C. D., Bois, J. S., Wolfe, B. R., Pierce, M. B., Khan, A. R., Dirks, R. M., ve Pierce N. A. (2011). NUPACK: analysis and design of nucleic acid systems. J Comput Chem, 32:170–173. Doi:https://doi.org/10.1002/jcc.21596

Zhang, Z., Chen, N., Li, S., Battig, M. R., ve Wang, Y. (2012). Programmable hydrogels for controlled cell catch and release using hybridized aptamers and complementary sequences. Journal of the American Chemical Society, 134(38), 15716–15719. Doi:https://doi.org/10.1021/ja307717w

Zhang, L., Lei, J., Liu, L., Li, C., ve Ju, H. (2013). Self-assembled DNA hydrogel as switchable material for aptamer-based fluorescent detection of protein. Analytical Chemistry, 85(22), 11077–11082. Doi:https://doi.org/10.1021/ac4027725

Zhao, L., ve Ball, C. H. (2009). Determination of Chloramphenicol, Florfenicol, and Thiamphenicol in Honey Using Agilent SampliQ OPT Solid-Phase Extraction Cartridges and Liquid Chromatography-Tandem Mass Spectrometry. Agilent LC/MS Newsletter.

Zhu, Z., Wu, C., Liu, H., Zou, Y., Zhang, X., Kang, H., Yang, C. J., ve Tan, W. (2010). An aptamer cross-linked hydrogel as a colorimetric platform for visual detection. Angewandte Chemie – International Edition, 49, 1052–1056. Doi:https://doi.org/10.1002/anie.200905570

Wilson, W.R., ve Cockerill, F.R. (1987). Tetracyclines, chloramphenicol, erythromycin, and clindamycin. Mayo Clin Proc., 62, 10, 906-15. Doi: https://doi.org/10.1016/s0025-6196(12)65047-2

e-ISSN 2757-5195

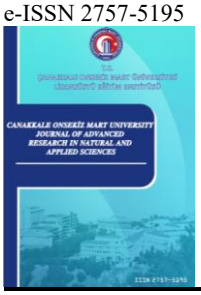

Çanakkale Onsekiz Mart University

Journal of Advanced Research in Natural and Applied Sciences

Open Access

doi.org/10.28979/jarnas.1168028 2023, Vol. 9, Issue 1, Pages: 158-166 dergipark.org.tr/tr/pub/jarnas

Fabrication of Self-Cleaning Perfluoroacrylate Blend Films by Spray Coating Method

Özge Ünzal[1], Sema Nur Belen[2], Uğur Cengiz[3*]

[1]Department of *Bioengineering & Materials Science Engineering*, Faculty of Engineering, Çanakkale Onsekiz Mart University, Çanakkale, Türkiye
[2]Department of Energy Resources and Management, Faculty of Engineering, Çanakkale Onsekiz Mart University, Çanakkale, Türkiye
[3]Department of Chemical Engineering, Faculty of Engineering, Çanakkale Onsekiz Mart University, Çanakkale, Türkiye

Article History

Received: 02.09.2022

Accepted: 28.10.2022

Published: 05.03.2023

Research Article

Abstract − The superhydrophobic surfaces are contained two essential principles. First, low surface energy polymers, such as fluoropolymers pushing the liquid onto the surface are necessary. The surface roughness is the second necessity to obtain superhydrophobicity, providing air packets between the roughness and reducing surface interaction with the liquid. This study fabricated the superhydrophobic blend coating using a spray coating method. The flat surface of PFMA homopolymer synthesized in $scCO_2$ medium was fabricated free meniscus coating method due to the lack of solubility in the conventional solvent. To overcome the solubility problems of the PFMA, the p(Perfluoromethacrylate-ran-Styrene) copolymer was fabricated in a $scCO_2$ medium. Blend solutions are prepared to reduce costs and provide high hydrophobicity by using p(Perfluoromethacrylate-ran-Styrene) copolymer and PS homopolymers. The surface roughness of the blend films was altered using silica nanoparticles coated on a glass slide by a spray coating. The surface morphology was characterized by SEM analyses indicating that double-scale surface morphology was obtained by increasing the SNp of the composite solution. The water contact angle indicated that the superhydrophobic rough surface was obtained with TMS_{70} and PS blend formation having 33.0 % PS and 12.5% silica nanoparticles.

Keywords − *Blend, fluoropolymer, self-cleaning, spray coating, superhydrophobic*

1. Introduction

The control of wettability is curial in many industrial applications such as self-cleaning surfaces (Topcu, Erdogan, & Cengiz, 2018), antifogging (Wang, Yao, Ren, & He, 2019), oil-water separation (Li et al., 2018), anti-icing (Ozbay, Yuceel, & Erbil, 2015). The superhydrophobic surface is expressed as the water contact angle (WCA) higher than 150º and tilt angle or contact angle hysteresis (CAH) values lower than 10º (Erbil, Demirel, Avci, & Mert, 2003). The artificial superhydrophobic surface was fabricated using alkyl ketene dimer wax for the first time in 1996 (Erbil et al., 2003). After that, the superhydrophobic surfaces were fabricated using different techniques such as phase separation (Gengec, Cengiz, & Erbil, 2016), electrospinning (Han & Steckl, 2009), sol-gel (Latthe, Imai, Ganesan, & Rao, 2010), chemical vapor deposition (Meng & Park, 2012), etching (Lee et al., 2011), and spray coating method (Bayer, Brown, Steele, & Loth, 2009). These studies reported that the fabrication of the superhydrophobic surfaces needs to provide two critical conditions: a necessity of low surface energy polymers such as fluoropolymer and surface roughness. However, not only the high expense of the flora polymers or monomers but also the environmental causes pushed researchers to non-fluorinated surface fabrication by obtaining a double-scale surface in the nano- and micron scales roughness (Lee et al., 2011; Topcu et al., 2018; Wang et al., 2019). The double-scale surface is caused a higher surface

[1] ozgeunzal@hotmail.com
[2] semanurbelenn@gmail.com
[3] ucengiz@ comu.edu.tr
*Corresponding Author

roughness. The air pocket is penetrated in this roughness, so the adhesion between water and surface decreases due to the reduction of the solid water contact line. In addition, some researchers reduced the cost by fabricating a copolymer between fluorinated monomers with non-fluorinated low-cost monomers (Gengec et al., 2016) or blending with cheap polymers (Gengec et al., 2016; Huang, Goh, Lai, Huan, & Wee, 2004). A blend formation ensures an essential benefit to combining the advantages of the individual polymers besides the economic (Huang et al., 2004). For example, fluorinated polymer is provided liquid repellency, while polystyrene has dimensional stability. However, a blend formation depends on the miscibility of the individual polymers (Kraus, 1978). The solubility parameter is important in providing a blend formation. Because it is undesirable the agglomeration of the polymer chains in the bad solvent. Phase separation occurred when one of the polymer chains started to agglomerate (Kraus, 1978). Generally, phase separation caused the heterogenous rough surfaces. This event can sometimes occur under control by adding the bad solvent into the polymer solution (Gengec et al., 2016). The controlled surface roughness by adding the nonsolvent in the polymer solution is provided to coat with the phase separation instant. However, this can also cause undesirable problems such as lower mechanical film durability or lower light transmittance due to the increasing roughness. When the well-dispersed blend solution was provided, it is obtained not only good-arranged surface roughness but also higher mechanical behavior of the film surface due to the combination of individual polymer behavior.

This study fabricated the perfluroethylalkyl methacrylate (PFMA) homopolymer in $scCO_2$ medium at 200 bar, 65 ^oC. The cloud point data were collected in a $scCO_2$ medium depending on temperature and pressure at constant polymer content of 1.55 wt. When the pressure decreased, the polymer chains agglomerated, and a cloudy form was obtained. The TMS_{70} statistical copolymer was synthesized in a CO_2-expanded styrene phase at 150 bar and 65^oC using styrene and PFMA monomers. The WCA of the TMS_{70} is reported as 115^o, which is lower than the p(PFMA) homopolymer, about 5^o. The smooth WCA is critical to obtaining a superhydrophobic surface with increasing roughness. The blend formation was formed using PS homopolymer with TMS_{70} copolymers. The smooth surface was prepared with PFMA and TMS_{70} polymers. The PFMA surfaces were coated with free meniscus coating (FMC) due to being soluble in only $scCO_2$, while TMS_{70} surfaces were spray coated. The rough superhydrophobic blend surface was formed using TMS_{70} and PS with silica nanoparticles (SNp). An increasing the SNp content of the blend solution caused rising WCA due to the higher surface roughness. The smooth PFMA and TMS_{70} film contact angles were found as 120^o and 115^o, respectively. The rough blend surface reached 166^o of WCA depending on spray time and distance.

2. Materials and Methods

2.1 Materials

Perfluoroethyl alkyl methacrylate (Zonyl-TM) was purchased from Dupont-Turkey. The CO_2 (99.9%) was obtained from Edremit Gases, A.S., Türkiye. Styrene (99.8%), toluene (99.8%), tetrahydrofuran (THF) (99.8%), polystyrene (PS), and Azobisisobutyronitrile (AIBN) were purchased from Aldrich. In addition, Wacker Silicones-Türkiye supplied pyrogenic silica (HDK-H18) with 99.8 % SiO_2 and a surface area of 170-230 m^2/g.

2.2. Polymer Synthesis and Characterization

2.2.1. Polyperfluoroalmethacrylate homopolymer (PFMA) synthesis:

The p(PFMA) homopolymer was synthesized in a $scCO_2$ medium similar to the literature (Ozbay, Cengiz, & Erbil, 2019) at 24 hours, 200 bar, and 65°C in a high-pressure 100 mL reactor (Bena Lab). The cloud point determination of PFMA homopolymer was determined in the reactor equipped with two sapphire windows.

2.2.2. The styrene-ran-perfluoro methacrylate (TMS_{70}) random copolymer synthesis:

TMS_{70} having 70 wt % styrene and 30 wt % PFMA was fabricated in a CO_2-expanded styrene phase medium according to the literature, in which the polymerization details were given in previous studies (Cengiz & Erbil, 2014; Gengec et al., 2016). The free radical random copolymerization reaction was carried out at 150 bar and 65°C in the high-pressure 100 mL reactor (Bena Lab). The styrene, PFMA, and AIBN were weighed and added to the high-pressure reactor. The CO_2 introduced the monomer mixture, the monomer phase expanded, and a new phase occurred. The reaction started as homogenous but lasted heterogeneous due to the agglomeration

of the higher molecular weight polymer chains. The polymerization finished heterogeneous and called precipitation polymerization. The molecular weight of the copolymers of TMS_{70} was characterized by using GPC**.**

2.3. Fabrication of the flat and rough films

The thin films of p(PFMA) were fabricated by using a free meniscus coating system (Novick, DeSimone, & Carbonell, 2004) (Ozbay et al., 2019). The TMS_{70} and TMS_{70}-PS blend surfaces were prepared by spray coating dissolving in toluene (50 mg/mL). Pen spray apparatus was used to coat glass slides 20 and 30 cm in length under a 5 bar N_2 atmosphere (Figure 1).

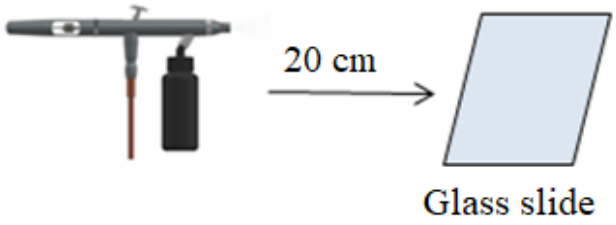

Figure 1. The schematic illustration of Pen spray coating systems

The blend solution of PS and TMS_{70} copolymer was prepared by mixing these polymer solutions and stirred mechanically for 2 h at room temperature. Firstly, the TMS_{70} copolymer solution was prepared as 50 mg/mL in toluene. Next, PS homopolymers were prepared in toluene at 50 mg/mL. Both of the polymer solutions were mixed and stirred. The opaque and the rough blend films were prepared by spray coating. A rough blend solution was prepared by adding silica nanoparticles of 2.5 to 12.5 % wt., which was kept in an oven at 105 ^oC for 2 hours due to moisture removal before use. The WCA of the flat and rough films was measured using the Attention Theta contact angle. All CA values were measured 3 times, having $\pm 1^o$ of standard deviation.

3. Results and Discussion

3.1 Polymer synthesis and characterization

The p(PFMA) homopolymer is soluble in $scCO_2$ due to its CO_2-philic character. The solubility of p(PFMA) homopolymer depends on pressure and temperature. The cloud point data were collected depending on pressure and temperature variation at a constant polymer amount, as shown in figure 2. This study kept the P(PFMA) polymer amount constant at 1.55 wt. due to comparing the literature data(Mawson, Johnston, Combes, & DeSimone, 1995; Ozbay et al., 2019). The rate of cloud point pressures of P(PFMA) with temperature change was defined as $\left(\frac{\partial P}{\partial T}\right)_X$ determined to be 2.15±0.23 bar/°C (Figure 2). In the literature, the similar polymer $\left(\frac{\partial P}{\partial T}\right)_X$ results was reported at 3.0±0.1 bar/°C (Mawson et al., 1995) and 2.4±0.2 bar/°C (Ozbay et al., 2019). The slight differences in the slopes are due to the minor molecular weight of p(PFMA) homopolymers.

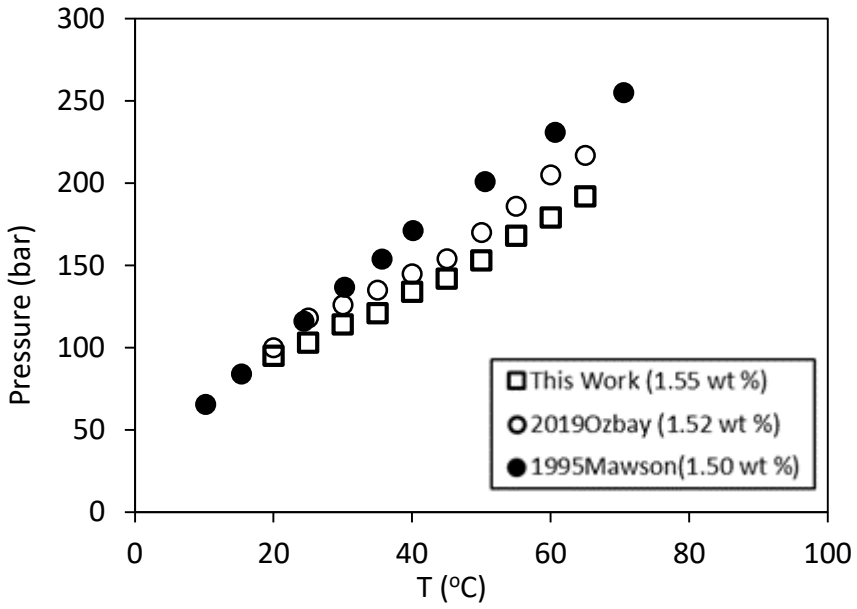

Figure 2. P(PFA) homopolymer Cloud point pressures with temperature in comparison with the Mawson and Ozbay data

The random copolymer of the TMS_{70} was synthesized in $scCO_2$ medium at 80 °C, 250 bar for 8 hours (Cengiz & Erbil, 2014). The polymerization started the homogeneous radical polymerization in CO_2 expanded styrene phase (Cengiz & Erbil, 2014). The monomer phase expands rapidly when CO_2 gas is introduced to the monomer mixtures. Thus, a new phase was obtained called the CO_2-expanded phase (Cengiz & Erbil, 2014). This phase is a stronger solvent than the liquid CO_2 or $scCO_2$ in the presence of the CO_2 -phobic monomers such as styrene or methyl methacrylate. However, the p(PFMA) homopolymer was synthesized homogenous medium in the $scCO_2$ phase due to the CO_2-philic monomer of PFMA. In TMS_{70} copolymerization, the homogenous reaction medium depended on the monomer amount acting like a co-solvent (Cengiz & Erbil, 2014). Thus, the co-monomer amount in the CO-expanded phase increased in the homogenous reaction time (Cengiz & Erbil, 2014). The GPC result of the TMS_{70} was measured, and the molecular weights were found as 15000 (Mn) and 45000 (Mw). The PDI values are determined as Mw/Mn=3. The Intrinsic viscosity values were also measured in chloroform solution as 0.245 dl/g comparisons with literature values (Cengiz & Erbil, 2014).

3.2 Wettability properties of Flat and rough films

The flat P(PFMA) thin films were prepared by the free meniscus coating (FMC) method in $scCO_2$, depending on P(PFMA) concentration. (Table 1).

Tablo 1.
The WCA of P(PFMA) thin films depending on the PFMA amount

Code	M_{PFA} (g)	P (bar)- Reaction Reactor	P (bar)-Coating Reactor	WCA (°)
PFMA-1	0.2	125	60	115
PFMA-2	0.5	125	60	114
PFMA-3	0.7	125	60	116
PFMA-4	1.0	125	60	118
PFMA-5	1.5	125	60	117
PFMA-6	2.0	125	60	120

The P(PFAM) homopolymer was coated in a glass slide in FMC due to the lower solubility of the homopolymer in a conventional solvent such as THF, toluene, or chloroform. As a result, the WCA of the PFMA thin films increased from 115° to 120° depending on the PFMA concentration in the $ScCO_2$ solution (Table 1). The WCA of PFMA-6 was found as 120°, which is the maximum value for a smooth surface (Nishino, Meguro, Nakamae, Matsushita, & Ueda, 1999). The WCA values of PS homopolar surface prepared for 0.5 g/mL in

toluene concentration were found between 60º to 85º depending on spray time and length by the spray coating method (Table 2).

Table 2.
The water CA values of spray-coated PS homopolymer dissolved in toluene solution

Code	Spray time (s)	Spray length (cm)	CA (º)
T_S1	5	20	75
T_S2	10	20	78
T_S3	15	20	80
T_S4	5	30	80
T_S5	10	30	60
T_S6	15	30	86

This table showed a linear correlation between CA values and spray times at 20 cm of spray distance. Thus, the 20 cm distance was chosen for the spray-coated experiment. The WCA of TMS_{70} smooth copolymer surfaces containing % 30 wt PFMA is measured as 115º, which was a sufficient WCA value to obtain a superhydrophobic surface by increasing surface roughness. The blend surface was prepared to reduce the structure's fluorine content due to its lower mechanical properties and cost. Thus, the blend solution was prepared by increasing the PS content, and the solutions were coated by the spray coating method for 20 cm of distance and 20 s of spray time. The changing of WCA values depending on PS content on the blend solution is given in figure 3.

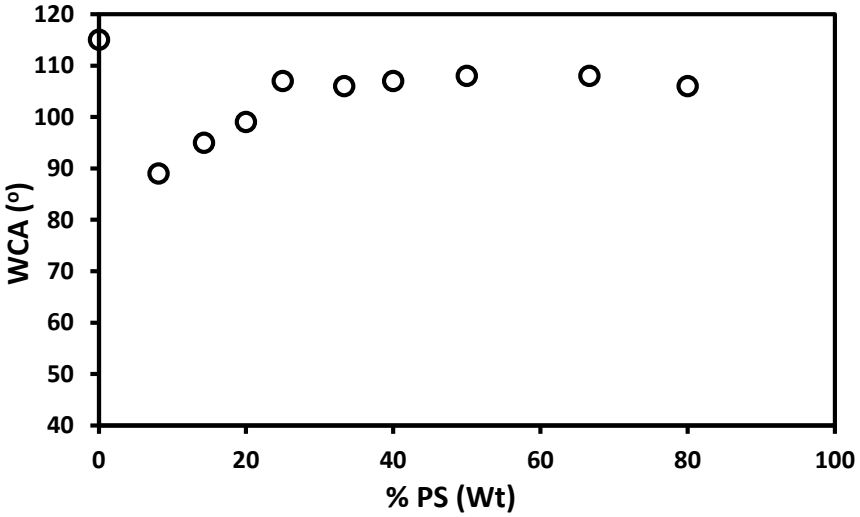

Figure 3. The WCA values of the blend solution depend on the PS content

An increase in the PS content of the blend solution firstly decreases the water contact angle from 115º to 90º compared to the TMS_{70} copolymer surfaces due to the decreasing flor content. Then, however, the WA values increased from 90º to 110º linearly up to % 40 wt. of PS. However, after this content, the contact angle values stayed steady despite the increasing PS content (figure 3). Therefore, the mechanical performance of the blend films decreases with increasing the PS content after % 50 wt. For example, the water drop penetrated the film's coating at the TMS_{70}-PS_{70} surface, having 70 wt PS content. Thus, the maximum PS content of the blend formation was arranged as 50 wt %. In addition, the blend solution's contact angle values indicate that the optimum spray coating experimental condition is 20 cm of spray distance, 10 s of spray time, and % 22 to 50 of PS content in the blend solution.

The superhydrophobic surfaces occurred by increasing the surface roughness using SNp. The rough blend surfaces were prepared using TMS_{70}, PS, and silica nanoparticles using optimized spray coating experimental conditions, as given in Table 3. The "NP" code in the TMS_{70}-PS blend is implied by adding silica nanoparticles.

The maximum SNp percentages are arranged up to 12.5 wt %. Higher SNP content in the composite solution results in lower light transmittance. Therefore, the subscript of the codes is related to the amount added. For example, the spray coating code of "TMS_{70}-$PS_{22}NP_{2.5}$" is indicated the blending of TMS_{70} and PS (22 %) and NP (2.5 %).

Table 3.
The CA values of the rough blend films (Spray coating conditions: 20 cm distance and 10 s of spray coating times)

Code	PS (wt, %)	Silika (wt. %)	WCA (º) (±1º)
TMS_{70}-$PS_{22}NP_{2,5}$	22.5	2.5	110
TMS_{70}-$PS_{22}NP_{5,0}$	22.5	5.0	110
TMS_{70}-$PS_{22}NP_{7,5}$	22.5	7.5	115
TMS_{70}-$PS_{22}NP_{10}$	22.5	10.0	117
TMS_{70}-$PS_{22}NP_{12,5}$	22.5	12.5	148
TMS_{70}-$PS_{33}NP_{2,5}$	33.0	2.5	103
TMS_{70}-$PS_{33}NP_{5,0}$	33.0	5.0	109
TMS_{70}-$PS_{33}NP_{7,5}$	33.0	7.5	115
TMS_{70}-$PS_{33}NP_{10}$	33.0	10.0	125
TMS_{70}-$PS_{33}NP_{12,5}$	33.0	12.5	154
TMS_{70}-$PS_{50}NP_{2,5}$	50.0	2.5	106
TMS_{70}-$PS_{50}NP_{5,0}$	50.0	5.0	107
TMS_{70}-$PS_{50}NP_{7,5}$	50.0	7.5	110
TMS_{70}-$PS_{50}NP_{10}$	50.0	10.0	112
TMS_{70}-$PS_{50}NP_{12,5}$	50.0	12.5	161

The WCA of the TMS_{70}-$PS_{22}NP$ series indicated that increasing the SNp content of the blend solution resulted in an increase in the WCA from 110 to 148º (figure 4). While the PS content of the blend surface was 33 (wt, %), the superhydrophobic surface was obtained at the 12.5 % wt. of the silica nanoparticles due to the phase separation by adding PS (Gengec et al., 2016) (figure 5). The higher WCA angle of 161º was obtained when the PS content of the blend solution was 50 % wt. (figure 4).

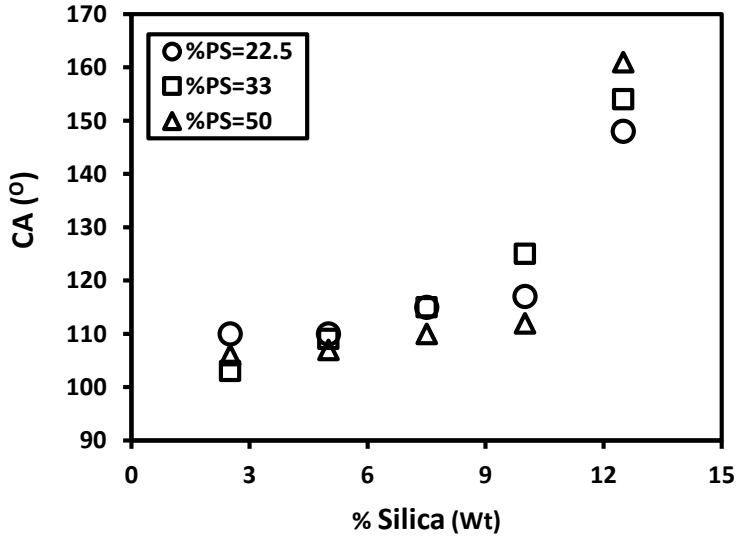

Figure 4. Change of CA (º) results in the change in silica wt % of blend surface

An increase in the PS content at the same nanoparticle content (12.5) increased the CA values of the rough surface. The SEM images also supported the WCA values (Figures 5 and 6). Especially higher magnification SEM images (20000X) indicated that a homogenous coating was obtained with higher PS content of the blend solution (Figure 6) due to the surface covering.

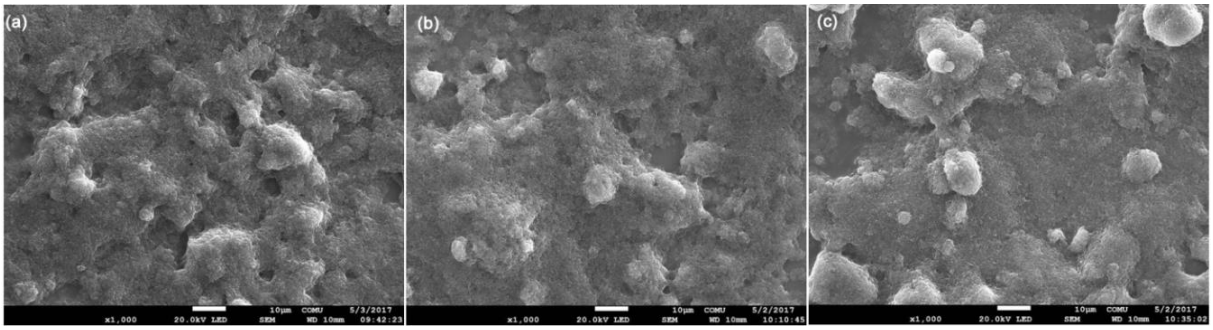

Figure 5. The SEM (1000X) images of spray coating of TMS_{70}-$PS_xNP_{12,5}$ blend coating with increasing the PS content a) TMS_{70}-$PS_{22}NP_{12,5}$ b) TMS_{70}-$PS_{33}NP_{12,5}$ c) TMS_{70}-$PS_{50}NP_{12,5}$ (20 cm distance for 10 s spray coating time)

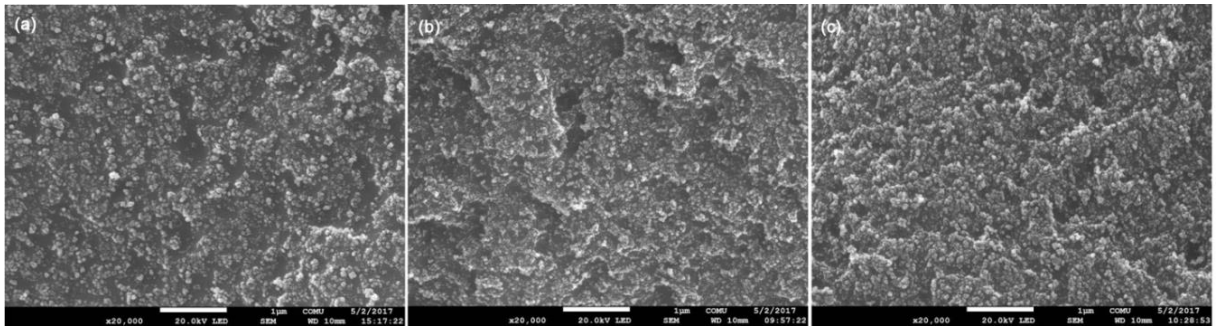

Figure 6. The SEM (20000X) images of spray coating of TMS_{70}-$PS_xNP_{12,5}$ blend coating with increasing the PS content a) TMS_{70}-$PS_{22}NP_{12,5}$ b) TMS_{70}-$PS_{33}NP_{12,5}$ c) TMS_{70}-$PS_{50}NP_{12,5}$ (20 cm distance for 10 s spray coating time)

The spray coating time effect was also investigated at the constant blend composition of TMS_{70}-$PS_{33,}$ as given in figure 7. The superhydrophobic surface of about 170º of contact angle is obtained when increasing the silica content at 15 seconds of spray time. On this surface, the water drop moved rapidly, and the CA value was measured hardly due to the water drop's rapid movement. This phenomenon is due to the lower adhesion attraction between liquid and solid surfaces. However, no correlation is observed between spray time and contact angle. Generally, the CA value is increased depending on surface roughness due to the introduction of the air pockets onto the surfaces, and it is expected that the surface roughness increases depending on spray time due to the accumulation on the surface. Therefore, the best CA values were obtained at 15 s spray time. However, 10 s of spray time is almost close the 15 s.

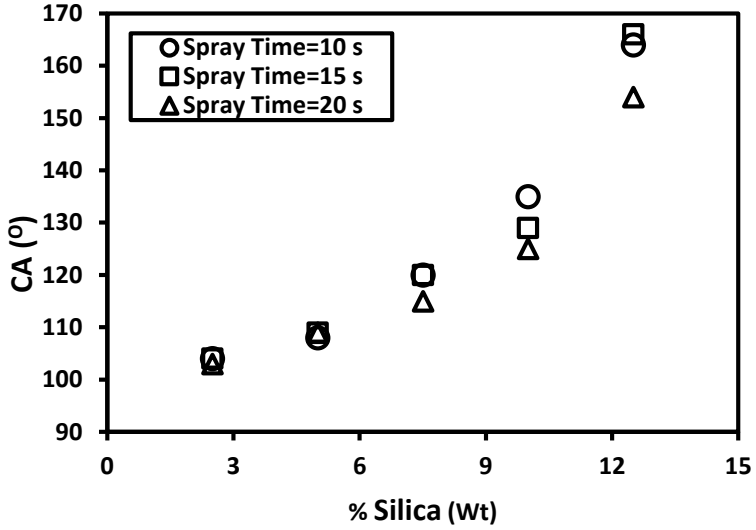

Figure 7 Change of CA (°) results with the change in silica wt % and spray time of blend surface

The spray coating experiment results showed that the flat and rough TMS70-PS blend surface was fabricated by the spray coating method at 20 cm of distance, 10 s of the spray time. In addition, the superhydrophobic surface was obtained at 12.5 % wt silica content. Therefore, the best spray coating formulation is found as TMS_{70}-$PS_{50}NP_{12,5}$.

4. Conclusion

In this study, the $scCO_2$ medium polymerizations of PFMA homopolymers and TMS_{70} statistical copolymers were fabricated by free-radical polymerization technic as AIBN is an initiator. The cloud points data were collected at 1.55 wt. of PFMA homopolymer in $scCO_2$ medium. This experiment indicated that the p(PFMA) homopolymer molecular weight is partly close to the literature on similar polymers. The TMS_{70} copolymer was also fabricated in the CO_2-expanded styrene phase. The TMS_{70} polymerization started as a homogenous phase and lasted heterogeneous due to the agglomeration of the polymer chains. The copolymerization terminated as a precipitation polymerization. The flat copolymer of the TMS_{70} is coated by spray coating, and the WCA is found as 115°. The WCA of the TMS_{70}-PS blend surfaces increased depending on PS content, reaching a plateau of around 40% of PS. The rough blend surface was prepared by adding silica nanoparticles to the TMS_{70}-PS blend solution. Increasing the silica nanoparticles increased the WCA of the rough blend surface. As a result of the spray experiments, the superhydrophobic surfaces were obtained by coating glass slides TMS_{70}-$PS_{50}NP_{12.5}$ blend composition at a 20 cm distance for 10 s of spray time. As a result of the WCA result of the everyday pollutant such as water, milk, tea, coffee, and juice showed the rough blend surface was fabricated successfully. However, the mechanical performance of the surface should have been improved.

Acknowledgment

This work was supported by Çanakkale Onsekiz Mart University, The Scientific Research Coordination Unit, Project number: FHD-2021-3581.

Author Contributions

Özge Ünzal: Experimental, Investigation, Software,

Sema Nur Belen: Methodology, Writing – original draft.

Uğur Cengiz: Conceptualization, Writing – review & editing, Supervision.

Conflicts of Interest

The authors declare no conflict of interest.

References

Bayer, I. S., Brown, A., Steele, A., & Loth, E. (2009). Transforming Anaerobic Adhesives into Highly Durable

and Abrasion Resistant Superhydrophobic Organoclay Nanocomposite Films: A New Hybrid Spray Adhesive for Tough Superhydrophobicity. *Applied Physics Express, 2*(12). doi:10.1143/APEX.2.125003

Cengiz, U., & Erbil, H. Y. (2014). Perfluoromethacrylate-styrene statistical copolymers synthesized in CO2-expanded monomers. *Colloid and Polymer Science, 292*(9), 2207-2215. doi:10.1007/s00396-014-3250-8

Erbil, H. Y., Demirel, A. L., Avci, Y., & Mert, O. (2003). Transformation of a simple plastic into a superhydrophobic surface. *Science, 299*(5611), 1377-1380. doi:DOI 10.1126/science.1078365

Gengec, N. A., Cengiz, U., & Erbil, H. Y. (2016). Superhydrophobic perfluoropolymer/polystyrene blend films induced by nonsolvent. *Applied Surface Science, 383*, 33-41. doi:10.1016/j.apsusc.2016.04.160

Han, D. W., & Steckl, A. J. (2009). Superhydrophobic and Oleophobic Fibers by Coaxial Electrospinning. *Langmuir, 25*(16), 9454-9462.

Huang, H. L., Goh, S. H., Lai, D. M. Y., Huan, C. H. A., & Wee, A. T. S. (2004). Surface Properties of Miscible Poly(1,1,1,3,3,3-hexafluoroisopropyl methacrylate)/Phenoxy Blends. *Journal of Applied Polymer Science, 91*, 1798-1805.

Kraus, G. (1978). Block Copolymers in Blends with Other Polymers In D. R. Paul & S. Newman (Eds.), *Polymer Blends* (Vol. 2, pp. 243-261): Academic Press.

Latthe, S. S., Imai, H., Ganesan, V., & Rao, A. V. (2010). Porous superhydrophobic silica films by sol-gel process. *Microporous and Mesoporous Materials, 130*(1-3), 115-121. doi:10.1016/j.micromeso.2009.10.020

Lee, E. J., Jung, C. H., Hwang, I. T., Choi, J. H., Cho, S. O., & Nhos, Y. C. (2011). Surface Morphology Control of Polymer Films by Electron Irradiation and Its Application to Superhydrophobic Surfaces. *Acs Applied Materials & Interfaces, 3*(8), 2988-2993. doi:10.1021/am200464a

Li, B. G., Lian, Z. X., Yu, H. D., Xu, J. K., Shi, G. F., Yu, Z. J., & Wang, Z. B. (2018). Underwater superoleophobic stainless steel mesh fabricated by laser cladding a copper foil for oil-water separation. *Materials Research Express, 5*(7). doi:ARTN 075014

10.1088/2053-1591/aac200

Mawson, S., Johnston, K. P., Combes, J. R., & DeSimone, J. M. (1995). Formation of Poly(1,1,2,2-Tetrahydroperfluorodecyl Acrylate) Submicron Fibers and Particles from Supercritical Carbon Dioxide Solutions. *Macromolecules, 28*, 3182–3191.

Meng, L. Y., & Park, S. J. (2012). Effect of growth of graphite nanofibers on superhydrophobic and electrochemical properties of carbon fibers. *Materials Chemistry and Physics, 132*(2-3), 324-329. doi:10.1016/j.matchemphys.2011.11.024

Nishino, T., Meguro, M., Nakamae, K., Matsushita, M., & Ueda, Y. (1999). The Lowest Surface Free Energy Based on -CF3 Alignment. *Langmuir, 15*, 4121-4123.

Novick, B. J., DeSimone, J. M., & Carbonell, R. G. (2004). Deposition of Thin Polymeric Films from Liquid Carbon Dioxide Using a High-Pressure Free-Meniscus Coating Process *Industrial and Engineering Chemical Research, 43*, 515–524.

Ozbay, S., Cengiz, U., & Erbil, H. Y. (2019). Solvent-Free Synthesis of a Superamphiphobic Surface by Green Chemistry. *Acs Applied Polymer Materials, 1*(8), 2033-2043. doi:10.1021/acsapm.9b00322

Ozbay, S., Yuceel, C., & Erbil, H. Y. (2015). Improved Icephobic Properties on Surfaces with a Hydrophilic Lubricating Liquid. *Acs Applied Materials & Interfaces, 7*(39), 22067-22077. doi:10.1021/acsami.5b07265

Topcu, A. S. K., Erdogan, E., & Cengiz, U. (2018). Preparation of stable, transparent superhydrophobic film via one step one pot sol-gel method. *Colloid and Polymer Science, 296*(9), 1523-1532. doi:10.1007/s00396-018-4377-9

Wang, Y., Yao, L., Ren, T. T., & He, J. H. (2019). Robust yet self-healing antifogging/antibacterial dual-functional composite films by a simple one-pot strategy. *Journal of Colloid and Interface Science, 540*, 107-114. doi:10.1016/j.jcis.2019.01.008

e-ISSN 2757-5195

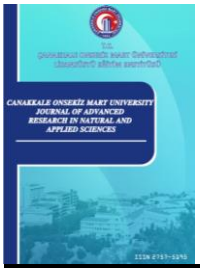

Çanakkale Onsekiz Mart University
Journal of Advanced Research in Natural and Applied Sciences
Open Access

doi.org/10.28979/jarnas.1147638 2023, Cilt 9, Sayı 1, Sayfa: 167-182 dergipark.org.tr/tr/pub/jarnas

Çok Katlı Betonarme Bir Binanın Altsistem Yaklaşımı İle Analizi

Hüseyin Taştan[1,*], Mehmet Özgür[2]

[1]Çanakkale Savaşları Gelibolu Tarihi Alan Başkanlığı, Çanakkale, Türkiye
[2]İnşaat Mühendisliği Bölümü, Mühendislik Fakültesi, Çanakkale Onsekiz Mart Üniversitesi, Çanakkale, Türkiye

Makale Tarihçesi
Gönderim: 01.08.2022
Kabul: 22.10.2022
Yayım: 05.03.2023

Araştırma Makalesi

Öz – Türkiye, bulunduğu coğrafyada ki aktif faylar sebebiyle sıklıkla büyük depremler ile yüzleşmekte, can kayıpları yaşanmakta ve maddi hasarlar oluşmaktadır. Bu bakımdan yapı tasarımında, deprem kuvvetini etkileyebilecek tüm parametrelerin göz önünde bulundurulması ve hesaplamalara dahil edilmesi oldukça önemlidir. Bu çalışmada, kazıklı temel sistemine sahip betonarme bir yapı ile temel zemini arasındaki etkileşim incelenmiştir. Zemin-kazık-yapı etkileşimi, altsistem yaklaşımı "Yöntem I" ile hesaplamalara yansıtılmış olup üstyapı, temel ve kazıklarda iç kuvvet, yer değiştirme ve şekil değiştirme talepleri elde edilmiştir. Sonuçları mukayese edebilmek için aynı yapı, kazıklara tanımlanan yatay yatak katsayısı yayları ile tasarım spektrumu etkisinde analiz edilmiş ve son olarak ise etkileşimsiz durumda ki sonuçlar için yine aynı yapı zemine ankastre mesnetli şekilde modellenerek hesaplama yapılmıştır. Her üç yöntemden elde edilen sonuçlar mukayese edilerek zemin-kazık-yapı etkileşimi irdelenmiştir.

Anahtar Kelimeler *– Altsistem yaklaşımı, yöntem I, zemin-kazık-yapı etkileşimi*

Analysis of a Multi-Storey Reinforced Concrete Building with Substructure Approach

[1]Çanakkale Wars Gallipoli Historical Site Presidency, Çanakkale, Türkiye
[2]Departman of Civil Engineering, Faculty of Engineering, Çanakkale Onsekiz Mart University, Çanakkale, Türkiye

Article History
Received: 01.08.2022
Accepted: 22.10.2022
Published: 05.03.2023

Research Article

Abstract – Due to the active faults in its geography, Turkey is frequently faced with major earthquakes, loss of life and material damage occur. In this respect, it is very important to consider all the parameters that can affect the earthquake force in the building design and to include them in the calculations. In this study, the interaction between a reinforced concrete structure with a pile foundation system and the foundation soil was investigated. The soil-pile-structure interaction has been reflected in the calculations with the subsystem approach "Method I" and the internal force, displacement and deformation demands of the superstructure, foundation and piles have been obtained. In order to compare the results, the same structure was analyzed under the influence of the design spectrum with the horizontal bearing coefficient springs defined for the piles, and finally, the same structure was modeled with a fixed support on the ground for the results in the non-interacting condition. The results obtained from all three methods were compared and the soil-pile-structure interaction was examined.

Keywords *– Substructure method, method I, soil-pile-structure interaction*

[1] hsyn-tastan@hotmail.com
[2] mehmetozgur@comu.edu.tr
*Sorumlu Yazar

1. Giriş

Türkiye Bina Deprem Yönetmeliği 2018 (TBDY 2018) ile zemin-kazık-yapı etkileşimi analiz yöntemleri resmi olarak yönetmelikte yerini almış ve uygulamaya girmiş durumdadır. Yapısal analizlerin zemin etkisinden bağımsız olarak gerçekleştirilmesi eksik/hatalı bir yaklaşımdır. Nitekim TBDY 2018 Bölüm 16'da, zemin-kazık-yapı etkileşimi hesaplamalarının uygulama esasları ve hangi şartlar altında zorunlu olduğu açıklanmıştır. Her ne kadar TBDY 2018'de teorik olarak zemin-kazık-yapı etkileşimi ile ilgili hususlara yer verilmiş olsa da uygulamaya yönelik örnekler (özellikle Yöntem I) ve bu alandaki araştırma sayısı oldukça azdır. Zemin-kazık-yapı etkileşimi hesap yöntemleri, diğer yapısal analiz yöntemleri ile karşılaştırıldığında, tamamlanan araştırma ve uygulama sayısı açısından oldukça bakir bir alan olup bu alandaki bilimsel çalışmaların artırılması, zemin-kazık-yapı etkileşimi hesap yöntemlerinin doğru uygulanması açısından büyük önem arz etmektedir. Türkiye'de yüksek yapı stoğunun büyük bir kısmının aktif fay güzergâhlarında kalıyor olması, zemin-kazık-yapı etkileşiminin yapısal davranış parametreleri üzerindeki etkisinin doğru belirlenmesini hayati bir ihtiyaç kılmaktadır (Öcal ve İnce, 2012).

Keshishian (2001), Doktora tez çalışmasında, büyük açıklıklı sistemler için (köprü vb.), yapı-zemin etkileşiminin analiz sonuçları üzerinde ki etkilerini incelemiştir. Yapı-zemin etkileşimini dikkate alarak yaptığı hesaplamalar neticesinde, zemin ortamının deprem yer hareketinin ivme genliklerinde artırıcı ya da azaltıcı etkileri olabileceği, bu sebeple yapı-zemin etkileşiminin sisteme etkiyecek dinamik yükleri doğrudan etkileyeceği ve hesaplamalarda dikkate alınması gerektiği hususlarını belirtmiştir.

Mamuk (2010), Yüksek Lisans tez çalışmasında, üstyapı ile temel zemini arasındaki etkileşimi incelemiştir. Çalışmaları neticesinde, zemin-yapı etkileşimi modelinin, zemini rijit kabul eden yaklaşımdan farklı olduğunu, etkileşimli modelde periyotların, gerilmelerin, iç kuvvetlerin zemin özelliklerine göre değiştiğini, yapı periyodunun rijit zeminli modele göre daha yüksek olduğunu ve etkileşimin yapıya etkiyen deprem kuvvetini değiştirdiğini ifade etmiştir.

Anderson, Carey ve Amin (2011), büyük ölçekli ağır sanayi yapılarının varlığının yapı-zemin etkileşimi kapsamında yakın civardaki diğer binalar üzerinde oluşturacağı etkileri incelemişlerdir. Çalışmaları sonucu, yapı-zemin etkileşiminin varlığına bağlı olarak çevre yapıların bazılarının yapısal tepkilerinde artış meydana geldiğini belirtmişlerdir.

Aydınoğlu (2011), zayıf zeminlerde inşa edilecek kazık temelli binalarda, zemin özellikleri ve kazıkların etkisi ile deprem dalgalarında meydana gelebilecek değişimi ve bu değişimin etkilerini belirleyebilmek için çalışmalar yapmıştır. Çalışmasında, zemin-yapı etkileşiminin kazık tasarımı bakımından çok önemli bir işlevinin olduğu, kazıkların zayıf zemine oranla çok daha rijit oldukları için büyük etkilere maruz kaldıkları ve dinamik etkiler altında kazıkların doğru tasarlanabilmesi için kinematik etkileşim hesaplamasının zorunlu olması gerektiği hususlarını ifade etmiştir.

Siyahi, Çetin ve Bilge (2013), zemin ortamı ile üstyapı arasındaki etkileşimin hesaplanmasında altsistem yaklaşımının kullanılabileceğini ifade etmişlerdir. Ayrıca sistemin davranışının kinematik etkileşim hesabı ile belirleneceği ve deprem yer hareketinin, kazıklı temel sisteminin rijitliğine göre artma ya da azalma gösterebileceğini belirtmişlerdir.

Pulikanti ve Ramancharla (2013), kazık temellerle desteklenen çerçeve sistemleri incelemişler ve kazıklarda meydana gelebilecek yanal yer değiştirmeleri tespit edebilmek için analitik yöntemler kullanmışlardır. Çalışmaları neticesinde, yapı tepkisinin doğru tayin edilebilmesi için statik ve dinamik durumlar için zemin etkisinin değerlendirilmesi gerektiği, bu etkileri hesaplama noktasında zemin ortamının doğrusal olmayan davranışına dikkat edilmesi gerektiği ve sonlu elemanlar yönteminin oldukça verimli olduğu, zemin ortamını Winkler yayı olarak temsil etmenin doğru sonuçlar verebildiği fakat zeminin pasif direncinin de etkisinin önemli olduğu hususlarını vurgulamışlardır.

Kavitha, P. E., Beena, K. S. ve Narayanan K. P. (2016), yanal yüklü kazıklar için zemin-yapı etkileşimi problemini incelemişlerdir. Yükleme türü ve analiz yöntemlerinin, zemin davranışını tahmin etmede önemli rol oynadığı, yanal yükleme altında zemin yüzeyinin eğiminin zemin-kazık etkileşimini etkilediğini belirtmişlerdir. Ayrıca zemin-kazık sisteminin dinamik yükler etkisi altında analizinde, sistemin doğal frekansının zemin ortamının özelliklerinde ki varyasyonların incelenerek hesaplanması gerektiğini vurgulamışlardır.

Sarıoğlu (2020), Yüksek Lisans tez çalışmasında, zemin-yapı etkileşimli ve etkileşimsiz durumlar için, düşük ve orta yükseklikteki betonarme binalarda, statik ve dinamik analiz yöntemlerini incelemiştir. Çalışmaları sonucunda, görece rijit zeminlerde etkileşimsiz ve etkileşimli modellerdeki deplasman değerlerinin birbirine yakın olduğunu, zemin-yapı etkileşimli durumda, zemin rijitliği düştükçe eksenel yük oranlarının arttığı ve buna bağlı olarak kolon moment kapasitelerinde artış meydana geldiğini belirtmiştir.

Kara, Bozdoğan ve Keskin (2020), düzlem çerçeve sistemlerde zemin-yapı etkileşiminin 4 farklı model üzerinden periyotlar üzerinde ki etkilerini incelemişlerdir. Modelleme de zemin ortamı ve üstyapının birlikte ele alındığı ortak sistem yaklaşımını kullanmışlarıdr. Zemin ortamının yeterli büyüklükte modellenmesi gerektiği aksi halde zemin etkisinin sisteme yeterince yansıtılamayacağı ve zemin ile yapının doğrusal olmayan davranışının hesaplamalarda dikkate alınması gerektiğini belirtmişlerdir.

Yiğit, M. A., Onur, M. İ. ve Balaban, E. (2022), yer altı suyu etkisinde kum ve kil tabakalı zeminlerde teşkil edilmiş tekil/grup kazıklar için Yöntem III kapsamında yapı-kazık-zemin etkileşimini incelemişlerdir. Kazıkların rijitliği arttıkça, kazık-zemin arası rijitlik farkı arttığı için moment değerlerinin arttığını, kazıkların deprem etkisi altında davranışının statik yükler etkisinde ki davranışından farklı olduğu ve bu sebeplerle deprem bölgelerinde yapı-kazık-zemin etkileşiminin hesaplamalara dahil edilmesi gerektiğini belirtmişlerdir.

Bu çalışmada ise altsistem yaklaşımıyla zemin-kazık-yapı etkileşiminin, yapıların zaman tanım alanında doğrusal olmayan yöntem ile deprem hesabını ne ölçüde değiştirdiği ortaya konulmaya çalışılmıştır. Karşılaştırma yapabilmek için TBDY 2018 Bölüm 16'da açıklanan Yöntem I ve yatak katsayısı yöntemi ile deprem hesabı yapılarak sonuçlar mukayese edilmiştir. Ayrıca sistem zemine ankastre şekilde mesnetlenerek etkileşimsiz duruma ait sonuçlar da elde edilmiştir. Böylelikle zemin-kazık-yapı etkileşiminin üstyapıda daha elverişli bir durum oluşturup oluşturmadığı hususu ve her koşulda üstyapı performansına olumlu etkisi olduğu önyargısı sorgulanmış ve açığa çıkarılmaya çalışılmıştır.

1.1. Zemin-Kazık-Yapı Etkileşimi Analiz Yöntemleri

TBDY 2018 Bölüm 16'da zemin-kazık-yapı etkileşimi ile ilgili esaslara yer verilmekte olup burada ortak sistem yaklaşımı ve altsistem yaklaşımı olmak üzere iki hesap yöntemi sunulmaktadır. Bu iki yöntemin uygulama koşulları ise Tablo 1'de yer almaktadır.

Tablo 1
Analiz yöntemlerinin uygulama koşulları (TBDY, 2018)

Analiz Yöntemi	Deprem Tasarım Sınıfı (DTS)	Bina Yükseklik Sınfı (BYS)	Yerel Zemin Sınıfı
Yöntem I	DTS = 1, 1a, 2, 2a	BYS = 1	ZD, ZE, ZF
Yöntem II	DTS = 1a, 2a DTS = 3, 3a, 4, 4a	BYS = 2, 3 BYS = 1	ZD, ZE, ZF
Yöntem III	DTS = 1a, 2a DTS = 1, 2, 3, 3a	BYS $\geq$ 4 BYS $\geq$ 2	ZD, ZE, ZF

1.1.1. Ortak Sistem Yaklaşımı ile Zemin-Kazık-Yapı Etkileşimi

Ortak sistem yaklaşımında, zemin ortamı, kazıklar, bodrum kutusu (varsa), temel ve üstyapı, 3 boyutlu olarak Şekil 1'de gösterildiği gibi birlikte modellenir (Siyahi, Çetin, ve Bilge, 2013). Zemin ile üstyapının birlikte modellendiği bu yaklaşımda, zemin geometrisindeki doğrusal olmayan formlar, zemine ait mekanik özelliklerin tabakalı zemin ortamı şartlarında ki değişimi ve üstyapı temelinin zemin ortamına gömülü olması durumları 3 boyutlu modellere rahatlıkla yansıtılabilir. Gerek ortak sistem yaklaşımında, gerekse de altsistem yaklaşımında, sisteme tabanda x, y ve z yönlerinde tutulu olacak şekilde, yan kısımlarda ise deprem dalgalarının zemin sınırlarından yansıyarak tekrar yapıya dönmemesi için özel geçirgen sınırlar tanımlanarak zemin sınır koşulları idealize edilir (Kausel, 1988).

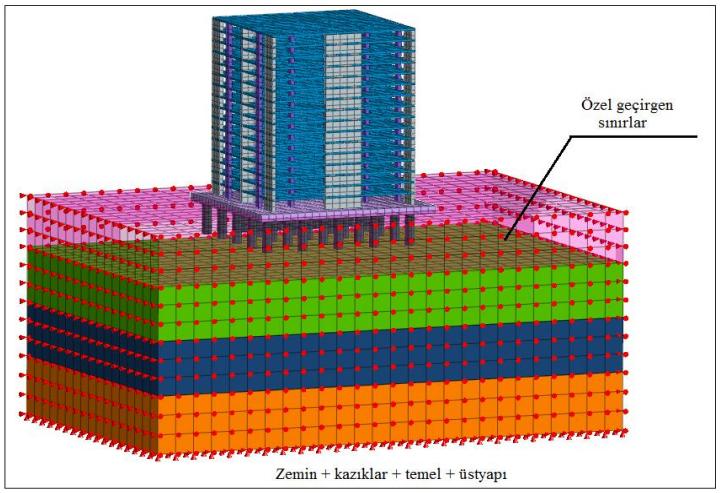

Şekil 1. Ortak sistem yaklaşımı hesap modeli

Ortak sistem yaklaşımında, zemin ortamında ki girdi hareketleri modelin tabanında ve yan kısımlarında tanımlanır, bu hareketten etkilenen sistemin harekete karşı gösterdiği tepki, Denklem 1.1'e göre hesaplanır (Karabörk, Deneme, ve Bilgehan, 2010).

$$[M] \cdot \{\ddot{u}\} + [k] \cdot \{u\} = -|[M] \cdot \{\ddot{u}ff(t)\}| \quad (1.1)$$

1.1.2. Altsistem Yaklaşımı ile Zemin-Kazık-Yapı Etkileşimi

Altsistem yaklaşımında, genel sistem, "zemin ortamı+kazıklar+kütlesiz temel" altsistemi (kinematik etkileşim) ve "kütleli temel+üstyapı" (eylemsizlik etkileşimi) altsistemi olarak iki aşamada ele alınır (TBDY, 2018). Bu hesap yönteminde, yapı temeli geçiş elemanı olup kinematik etkileşim aşamasında hesaplanan parametreler yapı temeli aracılığıyla üstyapıya yani eylemsizlik etkileşimi aşamasına aktarılmaktadır.

a) Altsistem Yaklaşımında Kinematik Etkileşim:

Altsistem yaklaşımı kapsamında iki ana hesap aşamasından ilki olan kinematik etkileşim, üstyapının atalet etkilerinin göz önüne alınmadığı "zemin+kazık+kütlesiz temel" altsistemini temsil etmektedir. Kinematik etkileşim kapsamında en az 11 çift deprem kaydı ile yatay eksenler (x,y) doğrultusunda "zemin+kazık+kütlesiz temel" altsistemine taban kayasından etki ettirilerek yapılacak analizler neticesinde;

- Temel seviyesi deprem kayıtları,
- Kazıklarda ki iç kuvvetler ve şekil değiştirme talepleri (her bir kazıkta 22 analiz ile hesaplanan sonuçların en büyük mutlak değerlerinin ortalaması),

elde edilir (TBDY, 2018). "Zemin+kazık+kütlesiz temel" altsistemini temsil eden örnek bir kinematik etkileşim hesap modeli Şekil 2'de yer almaktadır.

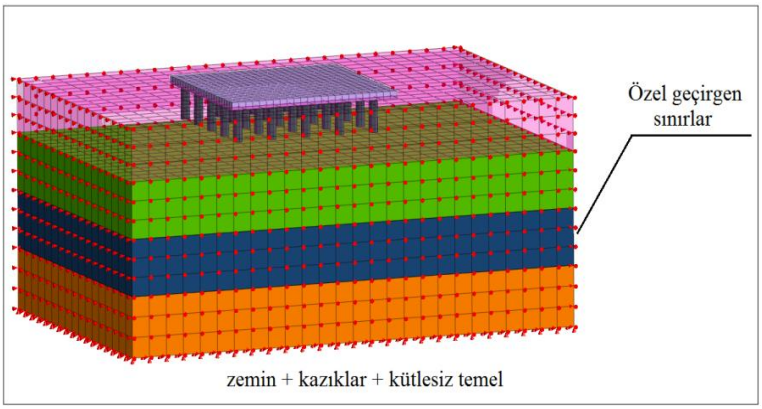

Şekil 2. Kinematik etkileşim sistem hesap modeli

a1) Zemin Ortamı Geometrik Ölçülerinin Belirlenmesi:

Zemin-kazık-yapı etkileşimi analizlerinde, zeminin deprem kaydı üzerinde ki etkisinin hesaplamalara doğru şekilde yansıtılabilmesi için zemin ortamının yeterli büyüklükte modele dahil edilmesi gerekmektedir. Zemin ortamı sonsuz olarak kabul edilmektedir fakat pratikte bu şekilde modelleme yapmak mümkün değildir. Bu sebeple özel geçirgen sınırlara ihtiyaç duyulmaktadır. Dinamik analizlerde zemin etkisinin hesaplara dahil edilebilmesi için TBDY 2018'de zemin ortamının ölçüleri ile ilgili olarak;

- Düşeyde en büyük bina genişliğinin üç katı ve en uzun kazık boyundan,
- Yatayda ise, her iki doğrultuda temel genişliğinin 7 katından daha az olmayacaktır,

denilmekte olup zemin ortamına ait asgari geometrik ölçüler Şekil 3'te yer almaktadır.

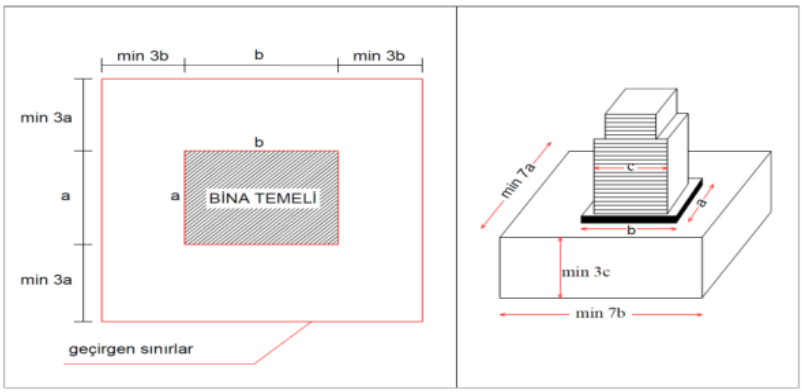

Şekil 3. Zemin ortamı için ihtiyaç duyulan asgari geometrik ölçüler

a2) Kazıkların Modellenmesi ve Arayüz Elemanlarının Tanımlanması:

Zemin-kazık-yapı etkileşimli hesaplamalarda, kazıklar çubuk eleman olarak modellenmeli ve kazık ile zemin arasına uygun arayüz elemanlarının tanımlanması gerekmektedir. Bilgisayar destekli sayısal çözümlemelerde, kullanılan yazılımların birçoğu kazıkların modellenmesi ile ilgili olarak üç seçenek sunmaktadırlar. Bunlar;

- Dolu gövdeli katı eleman modeli,
- Kiriş-katı eleman bağlantı modeli,
- Çizgisel eleman modeli

şeklindedir. Dolu gövdeli katı eleman modelinde ve kiriş-katı eleman bağlantı modelinde, sonlu eleman ağı oluşturma işlemleri her kazık için detaylı olarak yapılmak zorundadır. Bu durumda kazık sayısının fazla olduğu büyük modellerde, sonlu eleman ağı çok büyük boyutlarda olacağı için analiz süreleri çok fazla uzamaktadır.

Çizgisel eleman modelinde ise, Şekil 4'te gösterildiği şekliyle zemin ortamı yine 3 boyutlu katı eleman olarak, kazıklar ise 1 boyutlu çizgisel eleman olarak modellenir. Bu yöntemde 3 boyutlu sonlu eleman yoğunluğu azalacağı için analiz süreleri de diğer iki yönteme kıyasla daha kısa olacaktır. Doğrusal olmayan sürtünme-kayma özellikleri, kazık-zemin arayüz elemanlarına tanımlanabilmektedir.

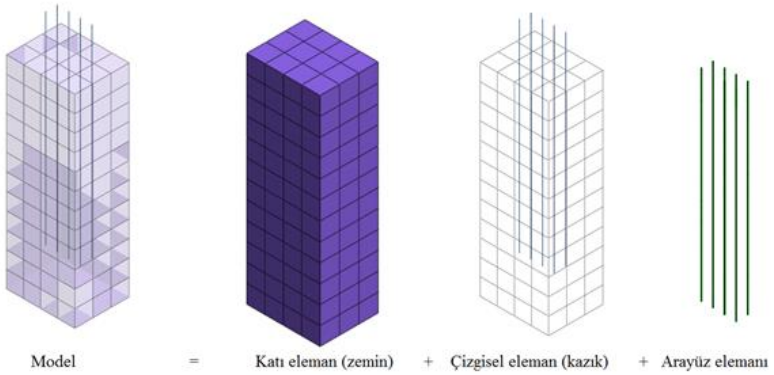

Şekil 4. Çizgisel eleman kazık model

Kazık yüzeyi ile zemin ortamı arasında sürtünme kaynaklı bir kuvvet söz konusudur. Bu sürtünme etkisi, kazıklar ile zemin ortamına ait malzeme rijitliklerine, birim alan ve yüzeye dik yönde etki eden kuvvete bağlıdır. Yay parametreleri; normal direnç modülü (K_n, K_t), kohezyon (c_s, c_n), içsel sürtünme açısı (φ_s, φ_n), çevre uzunluğu, normal yöndeki kuvvet için boşluğa, g (gap) ve efektif gerilmeye bağlı olup referans bağıntılar Tablo 5'te yer almaktadır (Bilal, Fahjan, ve Önen, 2014). Dayanım azaltma faktörü R katsayısı ise, zemin ortamının ve kazık elemanların malzeme özelliğine göre farklı değerler alır. Bu kapsamda R katsayısı;

- Kum zemin - çelik kazık durumu; R = 0,6 - 0,7
- Kil zemin - çelik kazık durumu; R = 0,5
- Kum zemin - betonarme kazık durumu; R = 0,8 - 1
- Kil zemin - betonarme kazık durumu; R = 0,7 - 1

arasında değerler almaktadır (Ünsal, 2017).

a3) Uygun Deprem Kayıtlarının Seçilmesi ve Ölçeklendirilmesi:

Zemin-kazık-yapı etkileşimi hesaplamalarında, Türkiye Deprem Tehlike Haritası (TDTH) aracılığıyla yapının konumuna, yerel zemin sınıfına ve deprem düzeyine bağlı olarak elde edilen tasarım spektrumları kullanılamaz. Bu şekilde üretilen spektrumlar etkileşimin yansıtılmasında yetersiz kalmaktadır. Bunun yerine en az 11 çift (x ve y yönlerinde olmak üzere 22 kayıt) deprem kaydı takımı seçilerek sisteme ayrı ayrı etkitilmelidir.

Deprem kayıtlarının seçimi ve ölçeklendirilmesi ile ilgili hususlar, TBDY 2018 Bölüm 2.5.'te yer almaktadır. 2.5'te, proje alanının depremsellik özelliklerinin araştırılarak ilgili parametrelerin elde edilmesi (fay tipi, büyüklük, fay yırtılma derinliği vb.) ve bu parametreler kullanılarak deprem kayıtlarının seçilmesi istenmektedir. Seçilen kayıtların ölçeklendirilmesi işlemi ise, yine Bölüm 2.5.3'te belirtildiği üzere, TDTH'den elde edilecek proje alanına özgü tasarım spektrumuna uyuşum sağlayacak şekilde yapılmalıdır.

Bu çalışmada deprem kayıtları, TBDY 2018' de belirtilen hususlar çerçevesinde Pasific Earthquake Research Center (PEER) veri tabanından temin edilerek ölçeklendirilmiştir.

a4) Özdeğer Analizi ve Sönüm Sabitleri:

Zaman tanım alanında doğrusal olmayan dinamik analizlerde kullanılacak sönüm değerlerini belirleyebilmek için öncelikle özdeğer (eigenvalue) analizi yapılarak sistemin kritik titreşim modlarının belirlenmesi gerekmektedir. Böylelikle yüksek kütle katılımının sağlandığı kritik titreşim modlarına karşılık gelen periyotlar elde edilir. Özdeğer analizi sonucunda, yüksek kütle katılım faktörü olan birinci ve ikinci mod kontrol edilip bu modlar arasında ki sönüm oranlarına göre dinamik analizlerin yapılması gerekmektedir. Burada kullanılacak sönüm sabitleri, genel kabul olarak 0,05 (%5) seçilerek hesaplamalar yapılıyor olsa da, daha doğru bir çözüm yapabilmek için sönüm sabitleri de hesaplanarak çözüme dahil edilebilir. Sönüm sabitleri, hacimsel modül (λ), kesme modülü (G), elastisite modülü (E), poisson oranı (v) ve yüzey alanına bağlı olarak Denklem 1.2, 1.3 ve 1.4'de yer alan bağıntılar kullanılarak hesaplanabilmektedir.

Birincil dalga; $$Cp = \rho \cdot A \cdot \sqrt{\frac{\lambda + 2G}{\rho}} = W \cdot A \cdot \sqrt{\frac{\lambda + 2G}{W \cdot 9{,}81}} = Cp \cdot A \tag{1.2}$$

İkincil dalga; $$Cs = \rho \cdot A \cdot \sqrt{\frac{G}{\rho}} = W \cdot A \cdot \sqrt{\frac{G}{W \cdot 9{,}81}} = Cs \cdot A \tag{1.3}$$

Konum; $$\lambda = \frac{v \cdot E}{(1+v) \cdot (1-2 \cdot v)} \qquad G = \frac{E}{2 \cdot (1+v)} \tag{1.4}$$

b) Altsistem Yaklaşımında Eylemsizlik Etkileşimi:

Eylemsizlik etkileşimi üstyapı ve üstyapı temelinde zamana bağlı doğrusal olmayan davranış ile ilgilenir. Doğrusal olmayan kazık-zemin etkileşim yayları üstyapı temeline tanımlanır ve kinematik etkileşimden elde edilen temel seviyesi deprem kayıtları etkisinde zaman tanım alanında doğrusal olmayan analizler yapılarak

üstyapı ve üstyapı temelinde iç kuvvetler, şekil değiştirme ve yer değiştirme taleplerinin zamana bağlı değişimleri elde edilir. Nihai kazık iç kuvvetleri, kinematik etkileşim ve eylemsizlik etkileşiminden elde edilen sonuçların mutlak değerce toplamı şeklinde belirlenir. Kinematik etkileşim ve eylemsizlik etkileşimi hesap modelleri ve bu modellerin süperpozisyonu Şekil 5'te yer almaktadır.

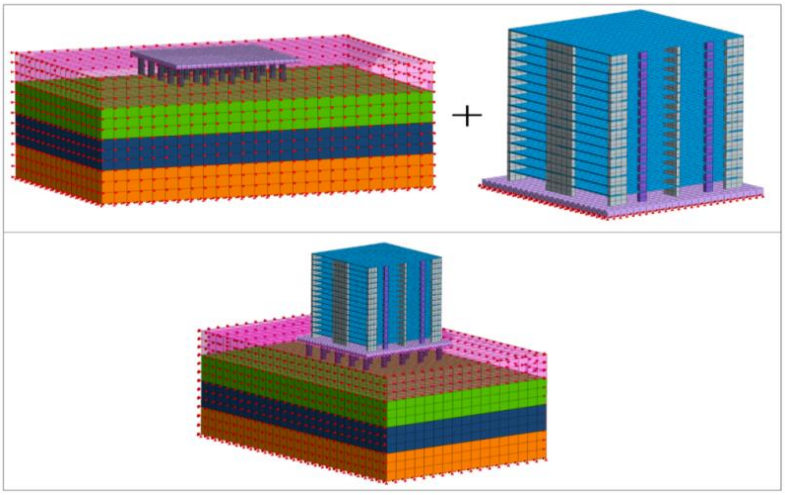

Şekil 5. Kinematik etkileşim - eylemsizlik etkileşimi - genel sistem hesap modelleri

b1) Doğrusal Olmayan Kazık-Zemin İlişkisinin Tanımlanması

TBDY 2018'de zemin-kazık-yapı etkileşimli hesaplamalarda, kazık davranışı ve kazık-zemin etkileşim elemanlarının temsilinde *p-y, t-z* ve *Q-Z* yaylarının kullanılması gerektiği belirtilmektedir. *P-y* yöntemi, zeminin plastik özelliklerinin hesaba katıldığı ve şekil değiştirmelerin bunların bir fonksiyonu olarak tanımlandığı yöntemdir (Öztürk ve Işık, 2015). *P-y* yayları, kazık boyunca belirli aralıklarla her bir kazık için kazık yüzeyine tanımlanmalıdır. Burada *y*; kazıkta meydana gelen yatay yönlü yer değiştirmeyi, *p* ise; zeminin kazık birim uzunluğuna uygulamış olduğu kuvveti ifade etmektedir.

P-y eğrilerinin elde edilmesinde bilgisayar destekli yazılımlar kullanılabileceği gibi literatürde yer alan referans eğriler kullanılarak da hesaplama yapılabilir. TBDY 2018 Bölüm 16C.6.2'de *p-y* yayları için, Bölüm 16C.6.3'de ise, *t-z* ve *Q-Z* yayları için kaynaklar yer almaktadır.

b2) Doğrusal Olmayan Üstyapı Analizleri

Eylemsizlik etkileşiminde sistem; kütlesi tanımlanmış temel (varsa bodrum kutusu) ve üstyapı şeklinde modellenir. Bu altsistemde, temel tabanına doğrusal olmayan *p-y* yayları etkitilerek temel-zemin ilişkisi tanımlanır. Aynı altsisteme kinematik etkileşimde elde edilen temel seviyesi deprem kayıtları tanımlanarak zaman-tanım alanında doğrusal olmayan analizler yapılır. Üstyapı ve üstyapı temelinde iç kuvvetler ile zamana bağlı kuvvet-deplasman değişimleri elde edilir. Temel tabanında tanımlanmış olan *p-y* yaylarından yararlanılarak kazıklar için iç kuvvetler elde edilir. Bu kuvvetler kinematik ekileşimden elde edilen kazık iç kuvvetleri ile toplanarak nihai kuvvetler elde edilmiş olur.

2. Materyal ve Yöntem

2.1. Saha Çalışmaları Ve Mühendislik Verilerinin Temini

Bu çalışmada, analizlerde kullanılan zemin ortamına ait dinamik-elastik mühendislik parametreleri, proje alanında yapılan arazi çalışmaları ve laboratuvar deneyleri neticesinde hazırlanan Veri ve Geoteknik Raporundan temin edilmiştir.

Proje alanına ait spektral ivme katsayıları, TDTH kullanılarak, proje alanının koordinatları, yerel zemin sınıfı ve deprem düzeyi parametreleri aracılığıyla elde edilmiştir.

Analizlerde kullanılan 11 çift deprem kaydı, PEER veri tabanı üzerinden, alana özgü spektral ivme katsayıları referans alınarak hesaplanan ölçek katsayıları ile birlikte elde edilmiştir.

2.2. Uygulanan Yöntem

Zemin-kazık-yapı etkileşiminin yapısal davranış parametreleri üzerindeki etkisi, aynı binanın, altsistem yaklaşımı (Yöntem I) ile ve yatak katsayısı yöntemiyle ayrı ayrı analiz edilerek sonuçların mukayese edilmesi şeklinde incelenmiştir. Ayrıca etkileşimsiz duruma ait sonuçları görebilmek için sistemin zemine ankastre şekilde mesnetlendiği rijit modelin de analizi yapılarak sonuçlar elde edilmiştir. Sonuçları mukayese ederken sistemde ki 36 adet kazıktan, sistemi temsil etmek üzere orta bölgeden ve yan kısımlardan birer adet olmak üzere toplamda 3 adet pilot kazık belirlenerek karşılaştırmalar bu kazıklar üzerinden yapılmıştır.

2.2.1. Üstyapı Geometri Bilgileri

Üstyapı, her bir katı 3 m yüksekliğinde 23 kattan oluşup, bina toplam yüksekliği (H_N) 69 m'dir. Katlara ait kalıp planı, temel kesitleri ve pilot kazıkları da gösterir aplikasyon planı Şekil 6'da yer almaktadır. Temel sistemi, 2 m yüksekliğinde radye temel ve radye temelin tabanında 80 cm çapına sahip 18 m boyunda betonarme kazıklar (fore kazık) şeklindedir. Kazıklar düşey taşıyıcı sistem elemanlarının düğüm noktaları ve grup etkisi dikkate alınarak (min 3D mesafe) aplike edilmiştir.

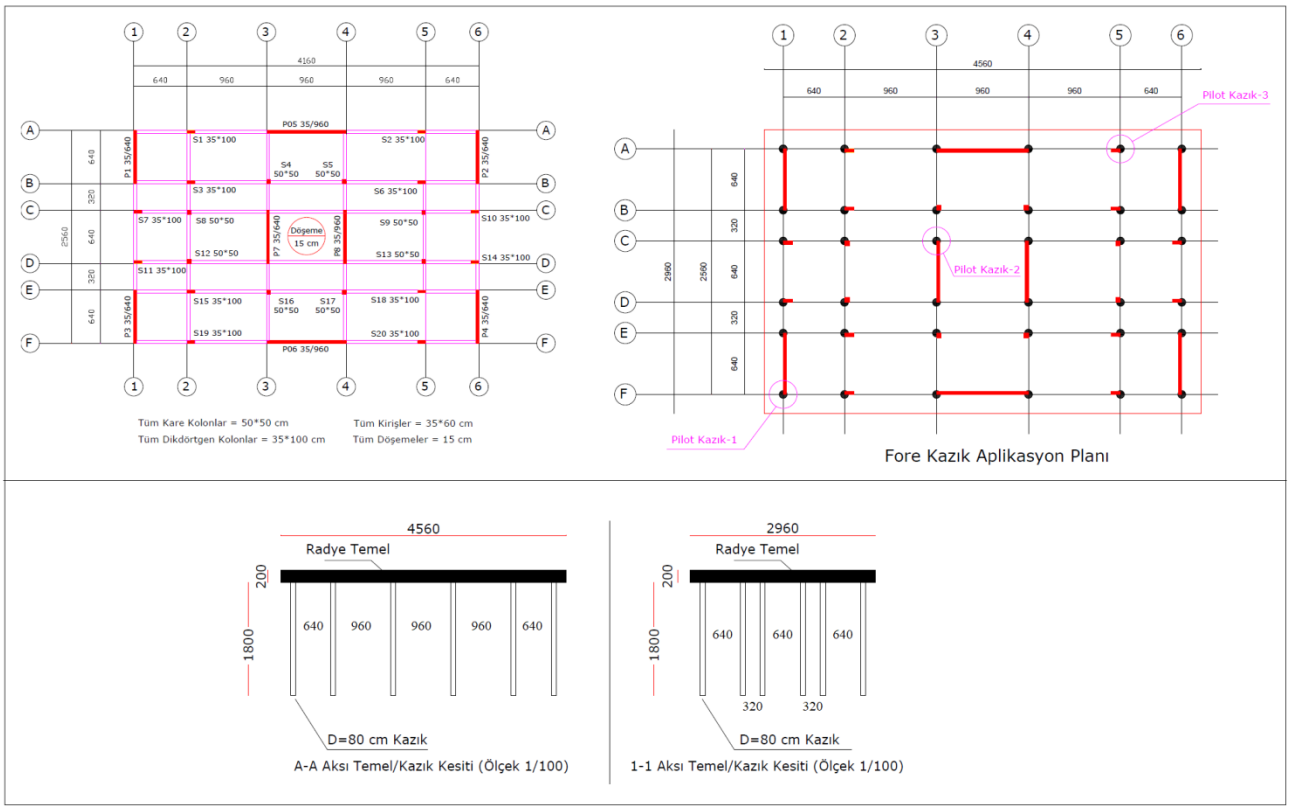

Şekil 6. Kalıp planı ve temel kesitleri

2.2.2. Zemin Ortamı ve Malzeme Parametreleri

Proje alanında 10 adet çok kanallı yüzey dalgası analizi, 5 adet mikrotremör ve 5 adet düşey elektrik sondaj ölçümlerini içeren jeofizik araştırmalar yapılarak dinamik-elastik mühendislik parametreleri elde edilmiştir. Aynı zamanda 35 m derinlikte olmak üzere 3 ayrı lokasyonda zemin araştırma sondajı yapılarak jeolojik zemin kesiti elde edilmiştir (Şekil 7). Her kuyuda standart penetrasyon deneyi, presiyometre deneyleri, yeraltı su seviyesi ölçümleri ve laboratuvar deneyleri yapılmıştır. 30 metre derinlik için hesaplanan ortalama kayma dalgası hızı ($V_{(S)30}$) değeri 452-553 m/sn arasında olup TBDY 2018 Bölüm 16.4.1'e göre yerel zemin sınıfı ZC olarak belirlenmiştir. Zemin ortamına ait tasarım parametreleri Tablo 2'de, tabakalara ait dinamik-elastik mühendislik parametreleri Tablo 3'de ve a1'de belirtilen hususlara göre belirlenen zemin geometrisi ise Şekil 8'de yer almaktadır.

Tablo 2
Zemin ortamı tasarım parametreleri

Zemin Tabakaları	Kumtaşı	Kireçtaşı	Kiltaşı	Marn	Taban Kayası
Bünye modeli	Mohr Coloumb	Mohr Coloumb	Mohr Coloumb	Mohr Coloumb	Mohr Coloumb
K_0	0,809	0,794	0,794	0,809	0,794
Termal katsayı	1,00E-06	1,00E-06	1,00E-06	1,00E-06	1,00E-06
E (kN/m^2)	250.000	250.000	250.000	250.000	250.000
υ	0,25	0,25	0,25	0,25	0,25
γ (kN/m^3)	26	21,8	21,3	21,3	21,4
C (kN/m^2)	550	570	570	550	590
Ø (°C)	11	11,88	11,88	11	12,2

Tablo 3
Tabakalara ait dinamik-elastik mühendislik parametreleri

Sismik Hızlar ve Elastik Parametreler

Ölçü No	Tbk. No	Vp	Vs	Hız Oranı	Ka-lınlık	De-rin-lik	Yoğun-luk (γ)	Pois-son Oranı (υ)	Kes.Mod. (Gsec)	Els. Mod. (E)	Blk. Mod. (K)	V(S)30	TA	T0	TB
		m/sn	m/sn	Vp/Vs	m	m	gr/cm3		kg/cm2	kg/cm2	kg/cm2	m/sn	sn	sn	sn
1	1	815	399	2,0	3,5	3,5	1,66	0,34	2637	7080	7486	479	0,16	0,24	0,36
	2	1395	435	3,2	18,5	22	1,89	0,45	3585	10369	32088				
	3	1940	701	2,8			2,06	0,42	10110	28812	63951				
2	1	838	526	1,6	2,1	2,1	1,67	0,17	4615	10844	5560	524	0,15	0,22	0,33
	2	1100	458	2,4	19,7	21,8	1,79	0,40	3745	10449	16609				
	3	1833	799	2,3			2,03	0,38	12949	35810	50886				
3	1	880	447	2,0	5,4	5,4	1,69	0,33	3374	8948	8577	500	0,14	0,21	0,31
	2	1135	527	2,2	8,2	13,6	1,80	0,36	4997	13618	16516				
	3	950	435	2,2	10,7	24,3	1,72	0,37	3257	8906	11190				
	4	1750	729	2,4			2,01	0,40	10656	29729	47197				
4	1	820	434	1,9	6,5	6,5	1,66	0,31	3125	8158	6988	488	0,16	0,24	0,36
	2	950	449	2,1	16,3	22,8	1,72	0,36	3470	9411	10906				
	3	1764	702	2,5			2,01	0,41	9901	27839	49314				
5	1	767	359	2,1	5,5	5,5	1,63	0,36	2103	5718	6794	452	0,16	0,24	0,35
	2	1000	465	2,2	11	16,5	1,74	0,36	3769	10268	12407				
	3	800	381	2,1	6,5	23	1,65	0,35	2393	6478	7361				
	4	1833	677	2,7			2,03	0,42	9297	26422	55756				
6	1	815	518	1,6	2,4	2,4	1,66	0,16	4444	10321	5076	537	0,15	0,22	0,33
	2	1503	448	3,4	16	18,4	1,93	0,45	3874	11244	38438				
	3	1750	746	2,3			2,01	0,39	11158	30997	46526				
7	1	905	495	1,8	5,7	5,7	1,70	0,29	4166	10720	8371	536	0,13	0,2	0,3
	2	1966	542	3,6	7,3	13	2,06	0,46	6064	17693	71700				
	3	950	485	2,0	11,4	24,4	1,72	0,32	4048	10718	10135				
	4	1850	746	2,5			2,03	0,40	11314	31746	54496				
8	1	950	462	2,1	24,5	24,5	1,72	0,35	3673	9883	10634	492	0,16	0,24	0,36
	2	1700	685	2,5			1,99	0,40	9340	26210	45073				
9	1	850	400	2,1	6,2	6,2	1,67	0,36	2678	7273	8523	461	0,18	0,26	0,4
	2	950	423	2,2	13,6	19,8	1,72	0,38	3079	8477	11427				
	3	1400	585	2,4			1,90	0,39	6489	18095	28514				
10	1	579	372	1,6	9,8	9,8	1,52	0,15	2104	4834	2292	553	0,14	0,21	0,31
	2	1390	691	2,0	15,6	25,4	1,89	0,34	9038	24147	24521				
	3	1900	861	2,2			2,05	0,37	15172	41597	53655				

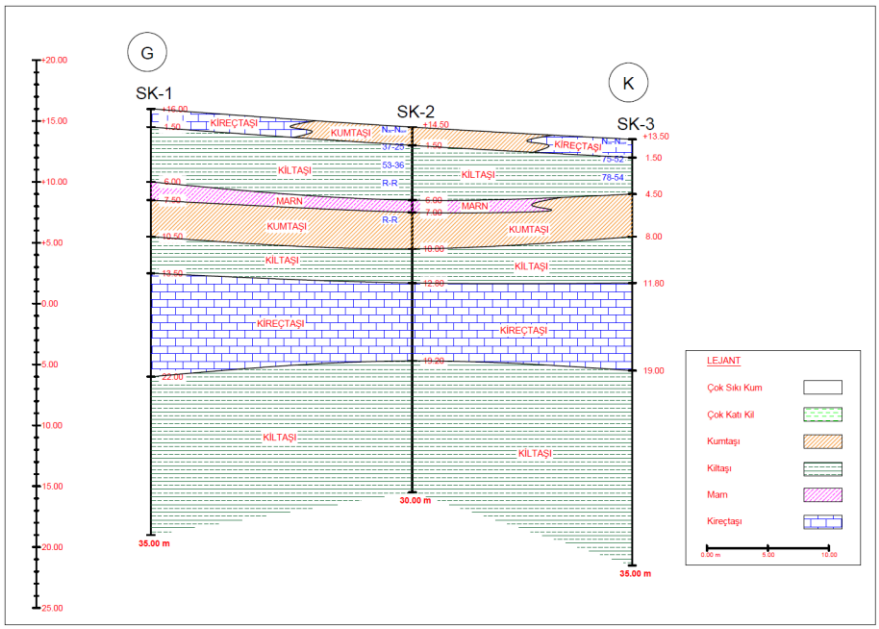

Şekil 7. Sondaja dayalı jeolojik zemin kesiti

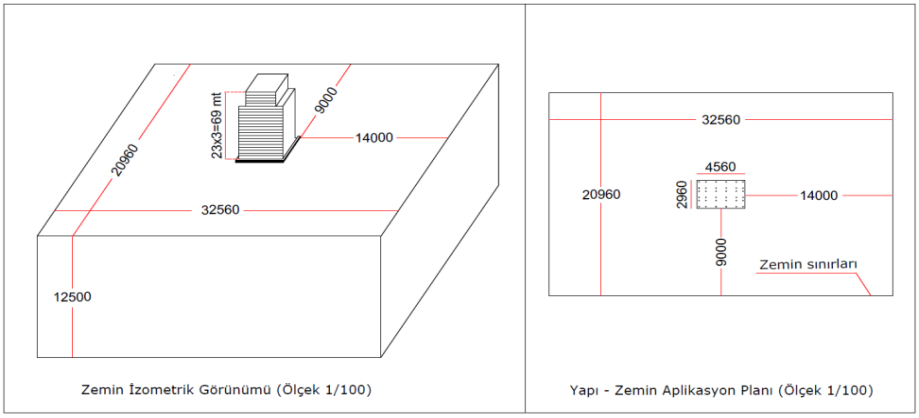

Şekil 8. Modellemeye esas zemin ortamı geometrik ölçüleri

2.2.3. Deprem Kayıtları Ve Ölçek Katsayıları

Sahaya özel uygun deprem kayıtlarının doğru seçilebilmesi için öncelikle proje alanının depremselliği araştırılmış ve bölgede meydana gelen depremlere ait veriler elde edilmiştir. Bu kapsamda Boğaziçi Üniversitesi Kandilli Rasathanesi Deprem Sorgulama Sistemi kullanılarak proje alanını kapsayacak şekilde 100 km yarıçaplı dairesel bir alan taranarak 1990-2021 yılları arasında 3 ila 9 büyüklüğünde olan depremler araştırılmıştır. Aynı zamanda Marmara Bölgesinde 1912 ile 1999 yılları arasında büyüklüğü 6,0 ile 7,4 arasında değişen 15 adet yıkıcı deprem ve Biga Yarım Adası ile Ganos fayı yakın çevresinde 2003-2010 yılları arasında 3,5'ten büyük olan depremler araştırılmıştır. Sahanın deprem özellikleri (fay tipi, büyüklük, fay yırtılma mesafesi, V_S) tespit edildikten sonra, bu özellikler ve proje alanına ait deprem düzeyi-1 (DD-1) için spektral veriler (S_{DS}, S_{D1}, T_L) PEER arama motoruna girilerek proje alanı ile uyumlu deprem kayıtları ve bu kayıtlara ait ölçek katsayıları elde edilmiştir. Ölçek katsayıları Denklem 2.1'e göre hesaplanmıştır. Elde edilen deprem kayıtları ve ölçek katsayıları Tablo 4'te, 11 çift kayda ait ölçeklenmiş ivme spektrumları ise Şekil 9'da yer almaktadır.

Tablo 4
Seçilen deprem kayıtlarına ait parametreler (PEER, 2020)

Kayıt Çifti	Kayıt Adı	YÖN	PGA (g)	PGV (m/sn)	PGD (m)	$V_{(S)30}$ (m/sn)	Büyüklük	Ölçek Katsayısı
1	IMPVALL.H_H-CPE147.AT2	x	0,17	0,12	0,052	471,53	6,53	2,3195
	IMPVALL.H_H-CPE237.AT2	y	0,16	0,19	0,079			
2	IMPVALL.H_H-PTS225.AT2	x	0,11	0,18	0,140	348,69	6,53	2,7492
	IMPVALL.H_H-PTS315.AT2	y	0,21	0,18	0,120			
3	SUPER.B_B-SUP045.AT2	x	0,58	0,24	0,023	362,38	6,54	1,9502
	SUPER.B_B-SUP135.AT2	y	0,84	0,44	0,052			
4	LANDERS_DSP000.AT2	x	0,17	0,19	0,082	359,00	7,28	2,6067
	LANDERS_DSP090.AT2	y	0,15	0,21	0,078			
5	LANDERS_MVH045.AT2	x	0,22	0,30	0,050	396,41	7,28	2,3153
	LANDERS_MVH135.AT2	y	0,16	0,22	0,100			
6	KOBE_KAK000.AT2	x	0,24	0,21	0,064	312,00	6,90	1,7733
	KOBE_KAK090.AT2	y	0,32	0,27	0,088			
7	DUZCE_1062-N.AT2	x	0,12	0,10	0,090	338,00	7,14	2,7612
	DUZCE_1062-E.AT2	y	0,26	0,18	0,089			
8	DUZCE_375-N.AT2	x	0,89	0,37	0,053	454,20	7,14	1,7713
	DUZCE_375-E.AT2	y	0,51	0,20	0,074			
9	HECTOR_HEC000.AT2	x	0,27	0,26	0,200	726,00	7,13	1,4445
	HECTOR_HEC090.AT2	y	0,33	0,45	0,110			
10	TOTTARI_SMN001NS.AT2	x	0,24	0,13	0,054	331,00	6,61	2,5217
	TOTTARI_SMN001EW.AT2	y	0,25	0,19	0,100			
11	DUZCE_498-NS.AT2	x	0,40	0,24	0,180	425,00	7,14	1,6114
	DUZCE_498-EW.AT2	y	0,35	0,25	0,180			

$$lnf = \frac{\sum_i w(Ti) \ln\left(\frac{Sa^{referans}(Ti)}{Sa^{kayıt}(Ti)}\right)}{\sum_i w(Ti)} \quad (2.1)$$

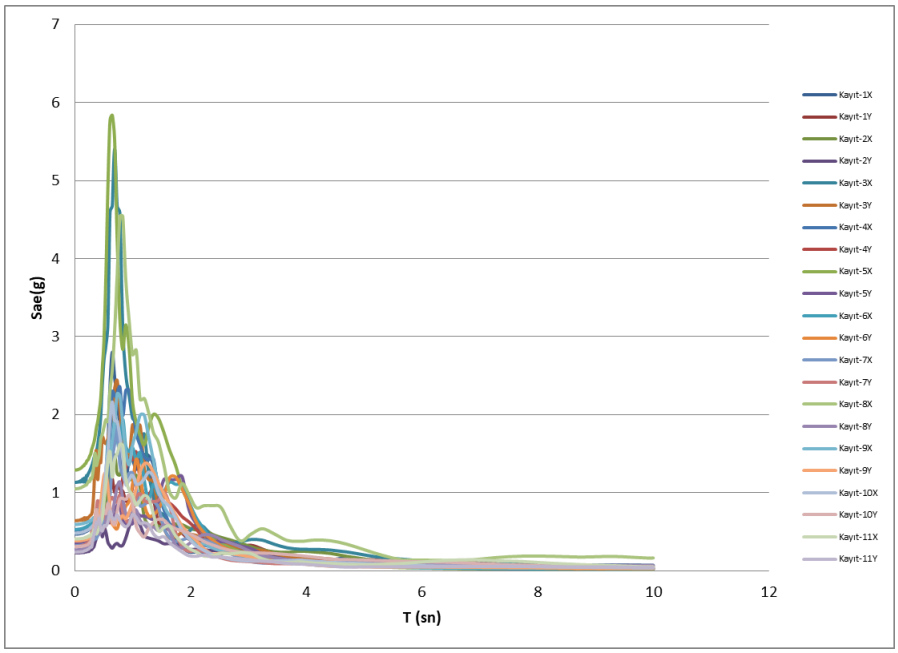

Şekil 9. 11 çift kayda ait ivme spektrum grafiği

2.2.4. Kinematik Etkileşim Hesap Modeli ve Doğrusal Olmayan Analizler

Kinematik etkileşim hesap modeli Şekil 10'da yer almaktadır. Tablo 4'te yer alan 11 çift deprem kaydı ölçeklenerek bu sistemin tabanından etkitilmiştir. Yapılan zaman tanım alanında doğrusal olmayan dinamik analizler sonucu temel seviyesi deprem kayıtları ve kazıklarda meydana gelen iç kuvvetler elde edilmiştir.

Kazık-zemin arayüz parametrelerinin hesaplanmasında kullanılan referans bağıntılar ile K_n ve K_t değerleri, Tablo 5'te yer almaktadır.

Tablo 5
Kazık-zemin arayüz parametreleri

Parametre	Birim	Referans	Değer
$E_{oed,i}$	kN/m²	E*(1-ν) / (1+ν)*(1-2ν)	300.000
L	m	-	18
t_v	Boyutsuz	0,01 - 0,1	0,10
R	Boyutsuz	0,7 - 1	0,70
E	kN/m²	-	250.000
v_{soil}	Boyutsuz	-	0,25
G_{soil}	kN/m²	E/2*(1+ν)	100.000
G_i	kN/m²	R* G_{soil}	70.000
K_n	kN/m³	E_{oed}/(L*t_v)	166.667
K_t	kN/m³	G_i /(L*t_v)	38.889

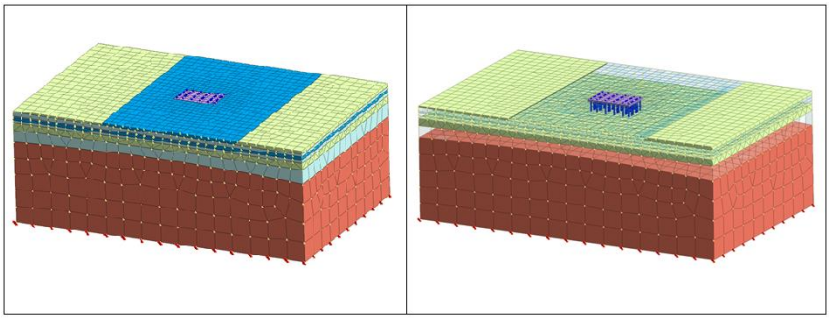

Şekil 10. Kinematik etkileşim hesap modeli

2.2.5. Eylemsizlik Etkileşimi Hesap Modeli ve Üstyapı Analizleri

Eylemsizlik etkileşiminde, temel tabanına tanımlanan doğrusal olmayan *p-y* yayları ve kinematik etkileşimde elde edilen temel seviyesi deprem kayıtları etkisinde dinamik üstyapı analizleri yapılmış ve kinematik etkileşimden elde edilen sonuçlarla birleştirilmek üzere kazıklar için iç kuvvetler elde edilmiştir. Modellemede; radye temel, perdeler ve döşemeler kabuk eleman olarak, kolonlar ve kirişler ise çubuk eleman olarak modellenmiştir (Şekil 11). Kabuk elemanlar 50x50 cm ölçülerinde sonlu elemanlara ayrılmıştır. Temelde ki sonlu elemanların düğüm noktalarına *p-y* yayları tanımlanarak etkileşim modele aktarılmıştır. *P-y* yayları, Sap2000 yazılımında, "Link/Support Property Data" penceresinde "Multilineer Plastic" ve "Nonlineer" seçenekleri seçilerek, *p-y* değerlerinin yazılıma girilmesi ile tanımlanmıştır.

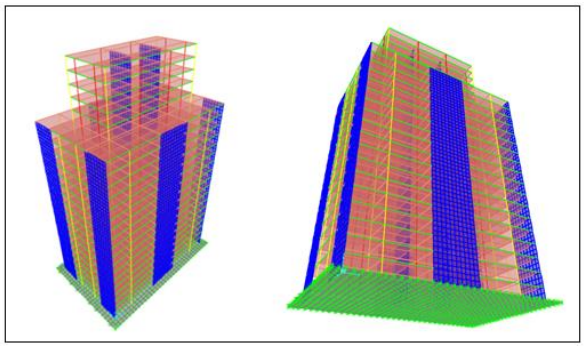

Şekil 11. Eylemsizlik etkileşimi sistem hesap modeli

2.2.6. Yatak Katsayısı Yöntemi Hesap Modeli ve Doğrusal Dinamik Analiz

"Kazık+temel+üstyapı" modelinin, TBDY 2018'de belirtilen hususlar kapsamında TDTH ile yapının konumu, yerel zemin sınıfı ve deprem düzeyine (DD-2) bağlı olarak elde edilen tasarım spektrumu ve çalışma

sahasına ait veri ve geoteknik raporundan alınan yatay yatak katsayısı kullanılarak TBDY 2018'e uygun şekilde doğrusal analiz yapılmış, elde edilen sonuçlar, altsistem yaklaşımından elde edilen sonuçlar karşılaştırılmıştır. Analizde kullanılan proje alanına özel tasarım spektrumları Şekil 12'de, hesap modeli ise Şekil 13'de yer almaktadır.

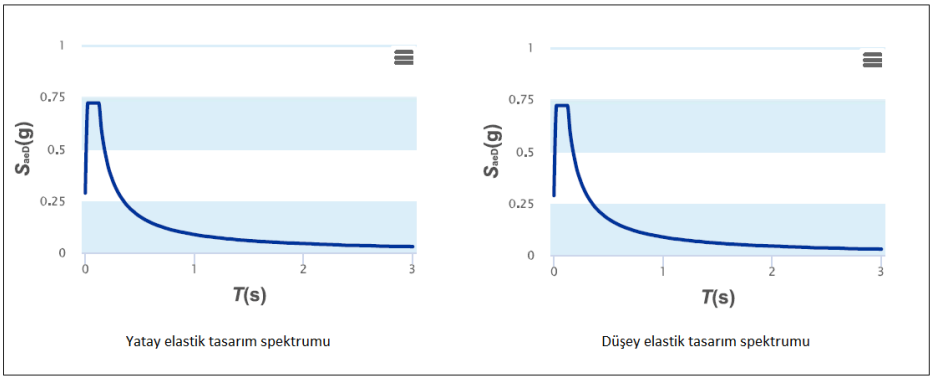

Şekil 12. DD-2 elastik tasarım spektrumları (TDTH İnteraktif Web Uygulaması, 2021)

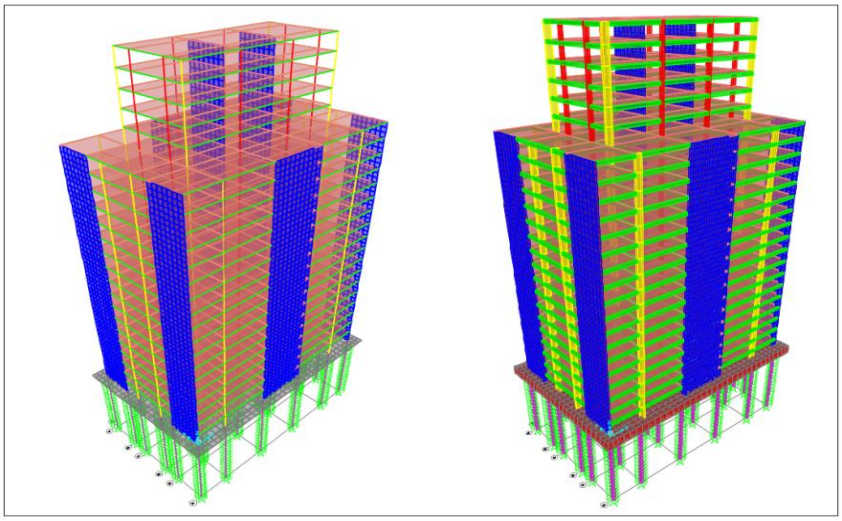

Şekil 13. Yatak katsayısı yöntemi hesap modeli

3. Bulgular ve Tartışma

Farklı hesap yöntemlerine göre elde edilen taban kesme kuvvetleri, doğal titreşim periyotları ve deplasman değerleri arasındaki ilişki Şekil 14'de, kazık iç kuvvetleri arasındaki ilişki ise Şekil 15'te yer almaktadır.

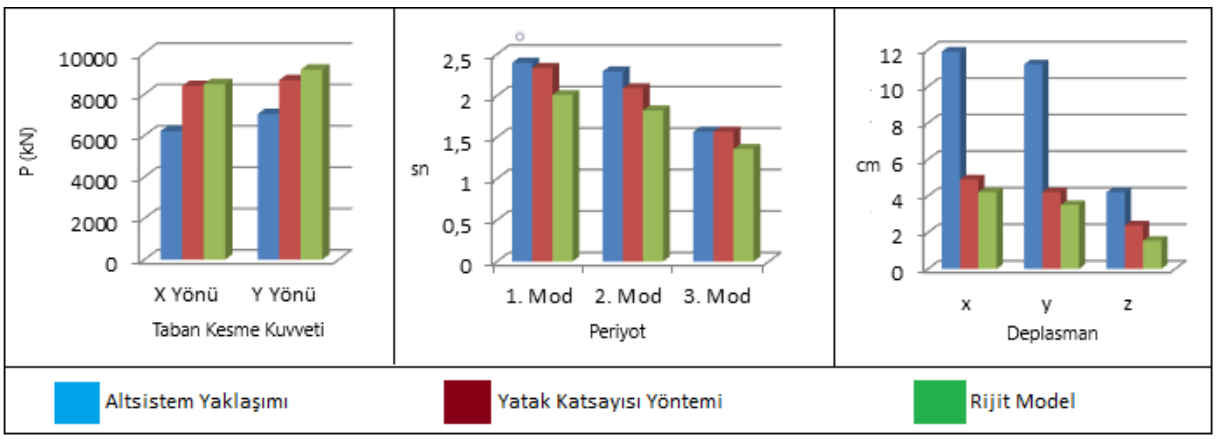

Şekil 14. Hesap yöntemine bağlı elde edilen sonuçlar arasındaki ilişki

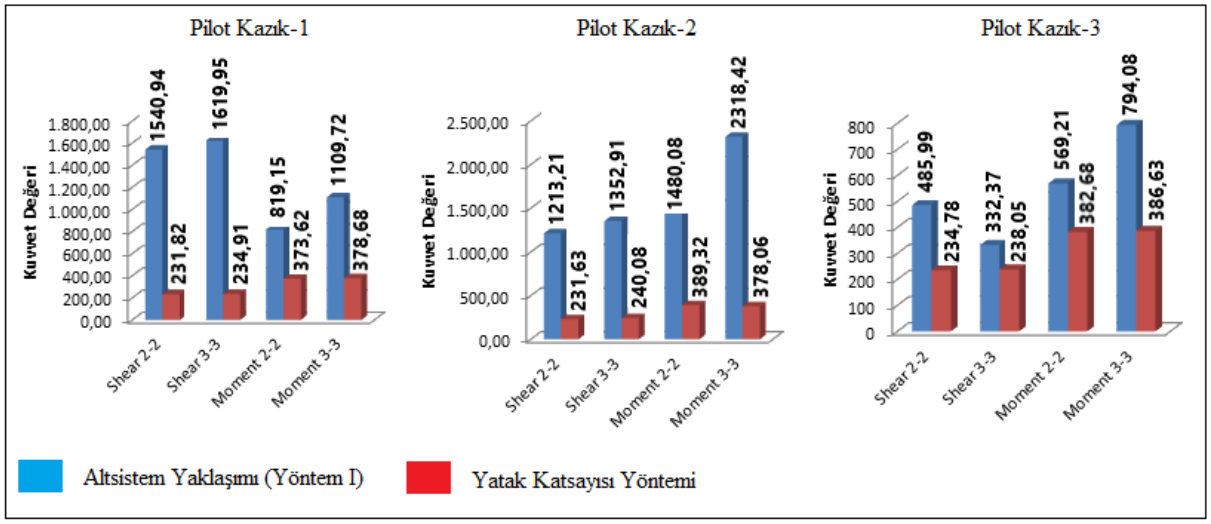

Şekil 15. Hesap yöntemine bağlı kazık iç kuvvetlerindeki değişim

Elde edilen sonuçlara bakıldığında, taban kesme kuvveti bakımından yatak katsayısı ve rijit model sonuçlarının birbirine yakın olduğu, altsistem yaklaşımı sonuçlarının ise her iki yön içinde diğer iki yönteme kıyasla yaklaşık %25 oranında daha düşük olduğu,

Doğal titreşim periyotları bakımından, ilk 3 mod için altsistem yaklaşımı ve yatak katsayısı yöntemi sonuçlarının birbirine yakın olduğu, rijit modelde ise periyot değerlerinin diğer iki yönteme kıyasla yaklaşık %15 oranında daha düşük olduğu,

Sistem deplasmanlarına bakıldığında ise, yatak katsayısı ve rijit model değerlerinin birbirine yakın olduğu, altsistem yaklaşımı sonuçlarının ise özellikle x ve y yönleri için yaklaşık %110 oranında daha fazla olduğu görülmüştür.

Kazık iç kuvvetleri bakımından, altsistem yaklaşımında elde edilen sonuçların diğer iki yönteme kıyasla her bir kazıkta farklı olmakla beraber ortalama %600 oranında daha fazla olduğu tespit edilmiştir

4. Sonuçlar

Bu çalışma sonucunda, altsistem yaklaşımı ile elde edilen kazık iç kuvvetlerinin, yatak katsayısı yöntemi ile elde edilen değerlere göre oldukça büyük olduğu tespit edilmiştir. Bu durum, kazıkların rijitliklerinin zemin ortamına kıyasla çok daha büyük olması sebebiyle, kazıkların deprem etkisiyle zeminde meydana gelen şekil değiştirmelere uyum sağlayamaması sonucu, zemin tabakalarının kazıklara yüklenerek kazıklarda büyük iç kuvvetler oluşturduğu tezini destekler niteliktedir.

Altsistem yaklaşımı ve yatak katsayısı yöntemlerinden elde edilen periyot değerlerinin rijit modele (etkileşimsiz) kıyasla daha yüksek olduğu görülmüştür. Yapı ile zemin arasında ki ilişkinin ankastre mesnetlerle temsil edildiği rijit sistemlerde yapı periyodunun, zemin-yapı ilişkisinin yatak katsayısı ya da kuvvet-yer değiştirme yaylarıyla temsil edilen etkileşimli sistemlere kıyasla daha yüksek olması beklenilen bir durumdur. Periyot uzamasına bağlı olarak beklenildiği üzere etkileşimli modellere etkiyen taban kesme kuvvetinde azalma meydana gelmiştir. Benzer şekilde periyot değerlerinde ki artışa paralel olarak, etkileşimli modellerde ki deplasman değerlerinin de rijit modele göre daha büyük olduğu tespit edilmiştir.

TBDY 2018'de eylemsizlik etkileşimi hesaplamalarının etkileşimli ve etkileşimsiz olarak 2 şekilde yapılarak elverişsiz olan duruma göre üstyapı dizaynının yapılması gerektiği belirtilmektedir. Bu çalışma özelinde, üstyapıya etkiyen taban kesme kuvvetinin rijit modelde daha yüksek olduğu ve üstyapı dizaynında rijit modelden hesaplanan iç kuvetlerin dikkate alınması gerektiği görülmektedir. Kazık dizaynında ise kinematik etkileşim ve eylemsizlik etkileşiminden elde edilen sonuçlar birleştirilmelidir. Bu şekliyle TBDY 2018'in, gerek kazık iç kuvettleri, gerekse de üstyapı yönünden sistemi en güvenli tarafta tutmaya çalıştığı görülmektedir.

Elde edilen sonuçlar, görece iyi zeminlerde, etkileşimli durumda, etkileşimsiz duruma kıyasla üstyapıya etkiyecek deprem kuvvetinde azalma olacağı görüşü ile örtüşmektedir. Fakat belirtilmelidir ki, özellikle kazık

temelli yapılarda, dinamik yükler altında kazık iç kuvvetlerinin doğru tespit edilerek kazık dizaynının yapılabilmesi için zemin-kazık-yapı etkileşimin hesaplamalara dahil edilmesi en doğru yaklaşım olacaktır.

Yazar Katkıları

Hüseyin Taştan: Modellemelerin ve analizlerin yapılması, sonuç çıktılarının raporlanması ve yazım.

Mehmet Özgür: Çalışma iş planı ve organizasyonu, literatür taraması ve raporlamaların değerlendirilmesi.

Çıkar Çatışması

Yazarlar çıkar çatışması bildirmemişlerdir.

Kaynaklar

Anderson, L., Carey, S. ve Amin, J. (2011). Effect of Structure, Soil and Ground Motion Parameters on Structure-Soil-Structure Interaction of Large Scale Nuclear Structures. *Structures Congress*, Las Vegas, USA. https://doi.org/10.1061/41171(401)249

Aydınoğlu, M. N. (2011). Zayıf Zeminlerde Yapılan Binalarda Dinamik Zemin-Kazık-Yapı Etkileşimi İçin Uygulamaya Yönelik Bir Hesap Yöntemi. Erişim adresi: http://www.koeri.boun.edu.tr/depremmuh/raporlar/Aydinoglu_Etkilesim_Rapor.pdf.

Bilal, O., Fahjan, Y. ve Önen, Y. H. (2014). Kazık-Zemin Arayüzeyi Parametrelerinin Dinamik Deprem Analizi Açısından Değerlendirmesi. http://dx.doi.org/10.13140/2.1.3778.1281

Kara, D., Bozdoğan, K.B. ve Keskin, E. (2020). Çerçeve Sistemlerin Yapı Zemin Etkileşimli Serbest Titreşim Analizi. *Politeknik Dergisi*, 23(4), 1347-1355. https://doi.org/10.2339/politeknik.598627

Karabörk, T., Deneme, İ. ve Bilgehan, R. (2010). Temeli İzole Edilen Yapılarda Dinamik Zemin-Yapı Etkileşimi. *Erciyes Üniversitesi Fen Bilimleri Enstitüsü Dergisi*, 26(1): 77-87. Erişim adresi: https://dergipark.org.tr/tr/download/article-file/236264

Kausel, E. (1988). Local Transmtiting Boundaries. *J. Eng. Mech. Div. ASCE*, Vol 114, pp. 1011-1027. https://doi.org/10.1061/%28ASCE%290733-9399%281988%29114%3A6%281011%29

Kavitha, P. E., Beena, K. S. ve Narayanan K. P.(2016). A Review On Soil-Structure Interaction Analysis Of Laterally Loaded Piles. *Innov. Infrastruct. Solut. 1:14.* https://link.springer.com/article/10.1007/s41062-016-0015-x

Keshian, P. G. (2001). *Analysis of Interconnected Systems Accounting for Spatial Variability of Ground Motions and Soil-Structure Interaction.* (Doktora Tezi), Universty of California, Berkeley.

Mamuk, F. (2010). *Üç Boyutlu Dinamik Zemin-Yapı Etkileşimi* (Yüksek Lisans Tezi). Erişim adresi: https://tez.yok.gov.tr/UlusalTezMerkezi

Öcal, C., İnce, H. H. (2012). Türkiye'de Mevcut Yapı Stoğu ve Kentsel Dönüşüm. *SDU International Technologic Science*, Vol.4, No 2, pp. 89-95. Erişim adresi: https://dergipark.org.tr/tr/download/article-file/254810

Öztürk, P. S. ve Işık, N. S. (2015). Sıvılaşan Zeminlerde Kazık Davranışının P-Y Yöntemi ile İncelenmesi. *International Sustainable Buildings Symposium (2 nd)*. Erişim adresi: http://www.isbs2015.gazi.edu.tr/belgeler/bildiriler/349-354.pdf.

PEER, (2020). Pacific Earthquake Engineering Research Center Ground Motion Database. (2021, 21 Mart). Erişim adresi: https://ngawest2.berkeley.edu/site.

Pulikanti, S. ve Ramancharla, P. K. (2013). SSI Analysis Of Framed Structures Supported On Pile Foundations: A Review. *Frontier in Geotechnical Engineering (FGE)*, Vol.2, Issue 2. Erişim adresi: https://www.academia.edu/24683081/SSI_Analysis_of_Framed_Structures_Supported_on_Pile_Foundations_A_Review.

Sarıoğlu, İ. (2020). *Statik İtme Ve Zaman Tanım Alanında Dinamik Analiz Yöntemlerinin Zemin Yapı etkileşimi Dikkate Alınarak İncelenmesi* (Yüksek Lisans Tezi). Erişim adresi: https://tez.yok.gov.tr/UlusalTezMerkezi

Siyahi, B., Çetin, K. Ö. ve Bilge, H. T. (2013). Geoteknik Deprem Mühendisliği Açısından Zemin-Temel-Yapı Etkileşimine Kritik Bakış. *ZMGM (Zemin Mekaniği ve Geoteknik Mühendisliği Derneği) Geoteknik Sempozyumu,* (5), Çukurova Üniversitesi, Adana. Erişim adresi: https://www.researchgate.net/publication/259936494_C71_Geoteknik_deprem_muhendisiligi_acisin

dan_zemin-temel-yapi_etkilesimine_kritik_bakis_Critical_glance_at_soil-foundation-structure_interaction_from_a_geotechnical_earthquake_engineering_perspective

TDTH İnteraktif Web Uygulaması, (2021). Afet ve Acil Durum Yönetimi Başkanlığı. Erişim adresi : https://www.turkiye.gov.tr/afad-turkiye-deprem-tehlike-haritalari

Türkiye Bina Deprem Yönetmeliği, (2018). Afet ve Acil Durum Daire Başkanlığı. Erişim adresi : https://www.resmigazete.gov.tr/eskiler/2018/03/20180318M1-2-1.pdf

Ünsal, S. (2017). GTS NX ile Kolay 3D Fore Kazıklı Köprü Temeli Analizi (2021, 19 Şubat). Erişim adresi: https://www.youtube.com/watch?v=bX50Dz4m198.

Yiğit, M. A., Onur, M. İ., Balaban E. (2022). Kazıklı temellerde zemin kazık etkileşimi parametrelerinin incelenmesi. *Gazi Üniversitesi Mühendislik Mimarlık Fakültesi Dergisi*, 37(2), 625-640. https://doi.org/10.17341/gazimmfd.825224.

e-ISSN 2757-5195

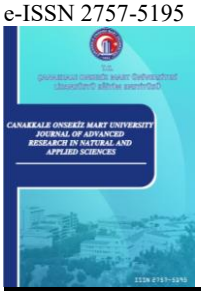

Çanakkale Onsekiz Mart University

Journal of Advanced Research in Natural and Applied Sciences

Open Access

doi.org/10.28979/jarnas.1110421 2023, Vol. 9, Issue 1, Pages: 183-189 dergipark.org.tr/tr/pub/jarnas

Gaussian-bihyperbolic Numbers Containing Pell and Pell-Lucas Numbers

Hasan Gökbaş[1*]

[1]Department of Mathematics, Faculty of Science and Arts, Bitlis Eren University, Bitlis, Türkiye

Article History

Received: 28.04.2022

Accepted: 28.10.2022

Published: 05.03.2023

Research Article

Abstract − In this study, we define a new type of Pell and Pell-Lucas numbers which are called Gaussian-bihyperbolic Pell and Pell-Lucas numbers. We also define negaGaussian-bihyperbolic Pell and Pell-Lucas numbers. Moreover, we obtain Binet's formulas, generating function formulas, d'Ocagne's identities, Catalan's identities, Cassini's identities and some sum formulas for these new type numbers and we investigate some algebraic properties of these. Furthermore, we give the matrix representation of Gaussian-bihyperbolic Pell and Pell-Lucas numbers.

Keywords − *biHyperbolic, Gaussian-bihyperbolic, Gaussian-bihyperbolic Pell, Gaussian-bihyperbolic Pell-Lucas*

1. Introduction

Complex numbers, Dual numbers and Hyperbolic numbers arise in many areas such as coordinate transformation, dynamic analysis, displacement analysis, static analysis, velocity analysis, rigid body dynamics, matrix modeling, geometry, mechanics, mathematics, physics, kinematics and transformation. Horadam (Horadam, 1963) introduced the concept, the complex Fibonacci numbers, called the Gaussian Fibonacci numbers $GF_n = F_n + iF_{n-1}$ where $F_n \in \mathbb{R}, i^2 = -1$ and F_n, nth Fibonacci numbers. Fjelstad and Gal (Fjelstad and Gal, 1998) defined the hyperbolic numbers $H = h + jh^*$ where $h, h^* \in \mathbb{R}, j^2 = 1$ and $j \neq \pm 1$. Clifford (Clifford, 1871) described the dual numbers $D = d + \varepsilon d^*$ where $d, d^* \in \mathbb{R}, \varepsilon^2 = 0$ and $\varepsilon \neq 0$. Messelmi (Messelmi, 2022) expressed the dual-complex numbers $Z = z + \varepsilon z^*$ where $z, z^* \in \mathbb{C}, \varepsilon^2 = 0$ and $\varepsilon \neq 0$. There are a number of studies in the literature concerned with these numbers (Catarino, 2019; Gül, 2020; Soykan, 2021; Vajda, 1989; Gürses, Şentürk and Yüce, 2021). Fjelstad and Gal (Fjelstad and Gal, 1998) inspected the extensions of the hyperbolic complex numbers to *n*-dimensions and they gave *n*-dimensional dual complex numbers in algebra and analysis. Matsuda (Matsuda, Kaji and Ochiai, 2014) et al. inspected the two-dimensional rigid transformation which is more concise and efficient than the standart matrix presentation, by modifying the ordinary dual number construction for the complex numbers. Majernik (Majernik, 1996) gave three types of the four-component number systems which are formed by using the complex, binary and dual two-component numbers. Akar (Akar, Yüce and Şahin, 2018) et al. introduced arithmetical operations on dual-hyperbolic numbers. They investigated dual hyperbolic number and hyperbolic complex number valued functions. Brod (Brod, Szynal-Liana, Wloch, 2020) et al. formulated any bihyperbolic number by $w = x_1 + jx_2 + j_1x_3 + j_2x_4$. Addition, substraction and multiplication of bihyperbolic numbers and was defined as

[1] hgokbas@beu.edu.tr

[*]Corresponding Author

$$w_1 \pm w_2 = (x_1 + y_1) \pm j(x_2 + y_2) \pm j_1(x_3 \pm y_3) + j_2(x_4 \pm y_4)$$
$$w_1 \times w_2 = (x_1y_1 + x_2y_2 + x_3y_3 + x_4y_4) + j(x_1y_2 + x_2y_1 + x_3y_4 + x_4y_3)$$
$$+j_1(x_1y_3 + x_2y_4 + x_3y_1 + x_4y_2) + j_2(x_1y_4 + x_2y_3 + x_3y_2 + x_4y_1).$$

Table 1

Multiplication scheme of bihyperbolic numbers.

$\times$	1	j	j_1	j_2
1	1	j	j_1	j_2
j	j	1	j_2	j_1
j_1	j_1	j_2	1	j
j_2	j_2	j_1	j	1

For $n \in \mathbb{N}_0$, Pell and Pell-Lucas numbers are defined by the recurrence relations, respectively, in the following way: $P_{n+2} = 2P_{n+1} + P_n$, $P_0 = 0$, $P_1 = 1$ and $Q_{n+2} = 2Q_{n+1} + Q_n$, $Q_0 = 2$, $Q_1 = 2$. The nth Pell and Pell-Lucas number are also formulized as $P_n = \frac{\alpha^n - \beta^n}{\alpha - \beta}$ and $Q_n = \alpha^n + \beta^n$, where $\alpha = 1 + \sqrt{2}$, $\beta = 1 - \sqrt{2}$. These formulas are called as their Binet's formulas (Koshy, 2014).

Many researchers have studied several areas of these number sequences. Brod (Brod, Szynal-Liana, Wloch, 2021) et al. examined a new one-parameter of bihyperbolic Pell numbers. They also gave some important features of these newly defined numbers. Soykan and Göcen (Soykan and Göcen, 2020) introduced the generalized hyperbolic Pell numbers over the bidimensional Clifford algebra of hyperbolic numbers. Azak and Güngör (Azak and Güngör, 2017) defined the dual complex Fibonacci and Lucas numbers and gave the well-known properties for these numbers. Aydın (Aydın, 2019) investigated the hyperbolic Fibonacci sequence and the hyperbolic Fibonacci numbers and also gave some algebraic properties of them. Dikmen (Dikmen, 2019) introduced the hyperbolic Jacobsthal numbers and presented recurrence relations, Binet's formula, generating function and the summation formulas for these numbers. Petoukhov (Petoukhov, 2019) desribed the applications of two-dimensional hyperbolic numbers and their algebraic two-dimensional extensions in modeling some genetic phenomena. He also gave the properties of hyperbolic numbers and their matrix representations. Bilgin and Ersoy (Bilgin and Ersoy, 2020) studied the four-dimensional real algebra of bihyperbolic numbers. They also showed conjugates, three hyperbolic valued moduli, real moduli and multiplicative inverse of this numbers.

2. Gaussian-bihyperbolic Pell and Pell-Lucas Numbers

In this sections, the Gaussian-bihyperbolic Pell and Pell-Lucas numbers will be defined. A variety of algebraic properties of Gaussian-bihyperbolic Pell and Pell-Lucas numbers are presented in a unified manner. Some identities will be given for Gaussian-bihyperbolic Pell and Pell-Lucas numbers such as Binet's formulas, generating function formulas, d'Ocagne's identities, Catalan's identities, Cassini's identities and some sum formulas. The properties of Gaussian-bihyperbolic Pell and the Pell-Lucas numbers will also be obtained using their matrix representation.

Horadam (Horadam, 1963) introduced the concept, the complex Fibonacci numbers, called the Gaussian Fibonacci numbers $GF_n = F_n + iF_{n-1}$ where $F_n \in \mathbb{R}, i^2 = -1$ and F_n, the nth Fibonacci numbers. In view of this definition, we will call Gaussian numbers as the numbers whose components are formed by ordering the consecutive terms of a number sequence from largest to smallest. After these explanations, we can give the following definition.

Definition 2.1. For $n \in \mathbb{N}_0$, the Gaussian-bihyperbolic Pell and Pell-Lucas numbers are defined by

$$GP_{n+3} = P_{n+3} + jP_{n+2} + j_1P_{n+1} + j_2P_n$$

$$GQ_{n+3} = Q_{n+3} + jQ_{n+2} + j_1Q_{n+1} + j_2Q_n$$

where P_n and Q_n, are the *nth* Pell and Pell-Lucas numbers. j, j_1 and j_2 denotes ($j^2 = j_1^2 = j_2^2 = 1; j, j_1, j_2 \neq \mp 1$).

$$GP_0 = j - 2j_1 + 5j_2,\ GP_1 = 1 + j_1 - 2j_2,\ GP_2 = 2 + j + j_2,\ \ldots$$

$$GQ_0 = 2 - 2j + 6j_1 - 14j_2,\ GQ_1 = 2 + 2j - 2j_1 + 6j_2,\ GQ_2 = 6 + 2j + 2j_1 - 2j_2,\ \ldots$$

$GP_n = 2GP_{n-1} + GP_{n-2}$ and $GQ_n = 2GQ_{n-1} + GQ_{n-2}$ are a recurrence relationship between Gaussian-bihyperbolic Pell and Gaussian-bihyperbolic Pell-Lucas numbers.

Let GP_{a+3} and GP_{b+3} be two Gaussian-bihyperbolic Pell numbers. The addition, substraction and multiplication of the Gaussian-bihyperbolic Pell numbers are given by

$$GP_{a+3} \pm GP_{b+3} = (P_{a+3} \pm P_{b+3}) + j(P_{a+2} \pm P_{b+2}) + j_1(P_{a+1} \pm P_{b+1}) + j_2(P_a \pm P_b)$$

$$\begin{aligned} GP_{a+3} \times GP_{b+3} &= (P_{a+3}P_{b+3} + P_{a+2}P_{b+2} + P_{a+1}P_{b+1} + P_aP_b) \\ &+ j(P_{a+3}P_{b+2} + P_{a+2}P_{b+3} + P_{a+1}P_b + P_aP_{b+1}) + j_1(P_{a+3}P_{b+1} + P_{a+2}P_b + P_{a+1}P_{b+3} + P_aP_{b+2}) \\ &+ j_2(P_{a+3}P_b + P_{a+2}P_{b+1} + P_{a+1}P_{b+2} + P_aP_{b+3}). \end{aligned}$$

Lemma 2.2. Let P_n and Q_n be the Pell and the Pell-Lucas numbers, respectively. The following relations are satisfied (Koshy, 2014)

i. $P_mP_{n+r} - P_{m+r}P_n = (-1)^nP_{m-n}P_r$
ii. $P_mP_{n+r} + P_{m+r}P_n = \frac{2Q_{m+n+r} - (-1)^nQ_{m-n}Q_r}{8}$
iii. $\sum_{k=1}^{n} P_k = \frac{Q_{n+1}-1}{2}$
iv. $\sum_{k=1}^{n} P_{2k-1} = \frac{P_{2n}}{2}$
v. $\sum_{k=1}^{n} P_{2k} = \frac{P_{2n+1}-1}{2}$.

Similar equations for Pell-Lucas numbers is obtained.

Definition 2.3. The negaGaussian-bihyperbolic Pell and the negaGaussian-bihyperbolic Pell-Lucas numbers are defined by

$$GP_{-n} = (-1)^{n+1}[P_n - jP_{n+1} + j_1P_{n+2} - j_2P_{n+3}]$$

$$GQ_{-n} = (-1)^{n-3}[-Q_n + jQ_{n+1} - j_1Q_{n+2} + j_2Q_{n+3}]$$

where P_n and Q_n, are the *nth* Pell and Pell-Lucas numbers.

Corollary 2.4. Let GP_n and GQ_n be the Gaussian-bihyperbolic Pell and the Gaussian-bihyperbolic Pell-Lucas numbers, respectively. The following relations are satisfied

i. $2(GP_{n+1} + GP_n) = GQ_{n+1}$
ii. $2(GP_{n+1} - GP_n) = GQ_n$
iii. $GP_{n+1} + GP_{n-1} = GQ_n$
iv. $GP_{n+1} - GP_{n-1} = 2GP_n$
v. $GP_{n+2} + GP_{n-2} = 6GP_n$
vi. $GP_{n+2} - GP_{n-2} = 2GQ_n$
vii. $GQ_{n+1} + GQ_n = 4GP_{n+1}$
viii. $GQ_{n+1} - GQ_n = 4GP_n$
ix. $GQ_{n+1} + GQ_{n-1} = 4GP_{n+1}$
x. $GQ_{n+1} - GQ_{n-1} = 2GQ_n$
xi. $GQ_{n+2} + GQ_{n-2} = 6GQ_n$
xii. $GQ_{n+2} - GQ_{n-2} = 16GP_n$

Proof.

i. $$\begin{aligned} 2(GP_{n+1} + GP_n) &= 2(P_{n+1} + jP_n + j_1P_{n-1} + j_2P_{n-2} + P_n + jP_{n-1} + j_1P_{n-2} + j_2P_{n-3}) \\ &= 2(P_{n+1} + P_n) + 2j(P_n + P_{n-1}) + 2j_1(P_{n-1} + P_{n-2}) + 2j_2(P_{n-2} + P_{n-3}) \\ &= Q_{n+1} + jQ_n + j_1Q_{n-1} + j_2Q_{n-2} = GQ_{n+1}. \end{aligned}$$

The remaining equations can be proven by the same method.

Theorem 2.5. (Generating Function Formula) Let GP_n be the Gaussian-bihyperbolic Pell numbers. Generating function formula for these numbers is as follows

$$h(t) = \frac{(j - 2j_1 + 5j_2) + t(1 - 2j + 5j_1 - 12j_2)}{1 - 2t - t^2}.$$

Proof.

Let $h(t)$ be the generating function for Gaussian-bihyperbolic Pell numbers as $h(t) = \sum_{n=0}^{\infty} GP_n t^n$. Using $h(t)$, $2th(t)$ and $t^2h(t)$, we get the following equations, $th(t) = \sum_{n=0}^{\infty} GP_n t^{n+1}$, $t^2h(t) = \sum_{n=0}^{\infty} GP_n t^{n+2}$. After the needed calculations, the generating function for Gaussian-bihyperbolic Pell numbers is obtained as

$$h(t) = \frac{GP_0 + GP_1 t - 2GP_0 t}{1 - 2t - t^2}$$

$$h(t) = \frac{(j - 2j_1 + 5j_2) + t(1 - 2j + 5j_1 - 12j_2)}{1 - 2t - t^2}.$$

Similarly, the generating function formula for Gaussian-bihyperbolic Pell-Lucas numbers is obtained.

Theorem 2.6. (Binet's Formula) Let GP_n be the Gaussian-bihyperbolic Pell numbers. Binet's formula for this numbers is as follows

$$GP_n = \frac{\hat{\alpha}\alpha^{n-3} + \hat{\beta}\beta^{n-3}}{\alpha - \beta}$$

where $\hat{\alpha} = \alpha^3 + j\alpha^2 + j_1\alpha^1 + j_2$, $\alpha = 1 + \sqrt{2}$ and $\hat{\beta} = \beta^3 + j\beta^2 + j_1\beta^1 + j_2$, $\beta = 1 - \sqrt{2}$.

Proof.

$$\begin{aligned} GP_n &= P_n + jP_{n-1} + j_1P_{n-2} + j_2P_{n-3} \\ &= \left(\frac{\alpha^n+\beta^n}{\alpha-\beta}\right) + j\left(\frac{\alpha^{n-1}+\beta^{n-1}}{\alpha-\beta}\right) + j_1\left(\frac{\alpha^{n-2}+\beta^{n-2}}{\alpha-\beta}\right) + j_2\left(\frac{\alpha^{n-3}+\beta^{n-3}}{\alpha-\beta}\right) \\ &= \frac{\alpha^{n-3}(\alpha^3+j\alpha^2+j_1\alpha^1+j_2)}{\alpha-\beta} + \frac{\beta^{n-3}(\beta^3+j\beta^2+j_1\beta^1+j_2)}{\alpha-\beta} \\ GP_n &= \frac{\hat{\alpha}\alpha^{n-3} + \hat{\beta}\beta^{n-3}}{\alpha - \beta}. \end{aligned}$$

Similarly, Binet's formula for Gaussian-bihyperbolic Pell-Lucas numbers is obtained.

Theorem 2.7. (d'Ocagne's Identity) Let GP_n be the Gaussian-bihyperbolic Pell numbers. d'Ocagne's identity for this numbers is as follows

$$\begin{aligned} &GP_mGP_{n+1} - GP_{m+1}GP_n \\ &\quad = j[(-1)^n(P_{m-n-1} - P_{m-n+1})] + j_2(-1)^n[P_{m-n-3} - P_{m-n-1} + P_{m-n+1} - P_{m-n+3}]. \end{aligned}$$

Proof.

$$\begin{aligned} GP_mGP_{n+1} - GP_{m+1}GP_n &= (P_m + jP_{m-1} + j_1P_{m-2} + j_2P_{m-3})(P_{n+1} + jP_n + j_1P_{n-1} + j_2P_{n-2}) \\ &\quad -(P_{m+1} + jP_m + j_1P_{m-1} + j_2P_{m-2})(P_n + jP_{n-1} + j_1P_{n-2} + j_2P_{n-3}) \\ &= j[(-1)^n(P_{m-n-1} - P_{m-n+1})] + j_2(-1)^n[P_{m-n-3} - P_{m-n-1} + P_{m-n+1} - P_{m-n+3}]. \end{aligned}$$

Similarly, d'Ocagne's identity for Gaussian-bihyperbolic Pell-Lucas numbers is obtained.

Theorem 2.8. (Catalan's Identity) Let GP_n be the Gaussian-bihyperbolic Pell numbers. Catalan's identity for this numbers is as follows

$$GP_n^2 - GP_{n+r}GP_{n-r} = 2j(-1)^{n-r}P_r[P_{r-1} - P_{r+1}] + j_2(-1)^{n-r}P_r[P_{r-3} - P_{r-1} + P_{r+1} - P_{r+3}].$$

Proof.

$$\begin{aligned} GP_n^2 - GP_{n+r}GP_{n-r} &= (P_n + jP_{n-1} + j_1P_{n-2} + j_2P_{n-3})(P_n + jP_{n-1} + j_1P_{n-2} + j_2P_{n-3}) \\ &\quad -(P + jP_{n+r-1} + j_1P_{n+r-2} + j_2P_{n+r-3})(P_{n-r} + jP_{n-r-1} + j_1P_{n-r-2} + j_2P_{n-r-3}) \\ &= 2j(-1)^{n-r}P_r[P_{r-1} - P_{r+1}] + j_2(-1)^{n-r}P_r[P_{r-3} - P_{r-1} + P_{r+1} - P_{r+3}]. \end{aligned}$$

Similarly, Catalan's identity for Gaussian-bihyperbolic Pell-Lucas numbers is obtained.

Theorem 2.9. (Cassini's Identity) Let GP_n be the Gaussian-bihyperbolic Pell numbers. Cassini's identity for this numbers is as follows

$$GP_n^2 - GP_{n+1}GP_{n-1} = -4j(-1)^{n-1} - 12j_2(-1)^{n-1}.$$

Proof. If $r = 1$ is taken in the Catalan's identity, Cassini's identity is obtained. Similarly, Cassini's identity for Gaussian-bihyperbolic Pell-Lucas numbers is obtained.

Theorem 2.10. Let GP_n be the Gaussian-bihyperbolic Pell numbers. In this case

i. $\sum_{k=1}^{n} GP_k = \left(\frac{Q_{n+1}-1}{2}\right) + j\left(\frac{Q_n-1}{2}\right) + j_1\left(\frac{Q_{n-1}+1}{2}\right) + j_2\left(\frac{Q_{n-2}-3}{2}\right)$

ii. $\sum_{k=1}^{n} GP_{2k-1} = \left(\frac{P_{2n}}{2}\right) + j\left(\frac{P_{2n-1}-1}{2}\right) + j_1\left(\frac{P_{2n-2}+2}{2}\right) + j_2\left(\frac{P_{2n-3}-5}{2}\right)$

iii. $\sum_{k=1}^{n} GP_{2k} = \left(\frac{P_{2n+1}-1}{2}\right) + j\left(\frac{P_{2n}}{2}\right) + j_1\left(\frac{P_{2n-1}-1}{2}\right) + j_2\left(\frac{P_{2n-2}+2}{2}\right)$.

Proof.

i. $\sum_{k=1}^{n} GP_k = \sum_{k=1}^{n}(P_k + jP_{k-1} + j_1P_{k-2} + j_2P_{k-3})$

$\sum_{k=1}^{n} GP_k = \sum_{k=1}^{n} P_k + j\sum_{k=0}^{n-1} P_k + j_1\sum_{k=-1}^{n-2} P_k + j_2\sum_{k=-2}^{n-3} P_k$

$\sum_{k=1}^{n} GP_k = \left(\frac{Q_{n+1}-1}{2}\right) + j\left(\frac{Q_n-1}{2}\right) + j_1\left(\frac{Q_{n-1}+1}{2}\right) + j_2\left(\frac{Q_{n-2}-3}{2}\right)$.

The remaining sums can be proven by the same method.

Theorem 2.11. Let GP_n be the Gaussian-bihyperbolic Pell numbers. For any positive integer n, we have the matrix representations of these sequences with both negative and positive indices are as follows

i. $\begin{bmatrix}2 & 1\\ 1 & 0\end{bmatrix}^n \begin{bmatrix}GP_2 & GP_1\\ GP_1 & GP_0\end{bmatrix} = \begin{bmatrix}GP_{n+2} & GP_{n+1}\\ GP_{n+1} & GP_n\end{bmatrix}$

ii. $\begin{bmatrix}0 & 1\\ 1 & 2\end{bmatrix}^n \begin{bmatrix}GP_0\\ GP_1\end{bmatrix} = \begin{bmatrix}GP_n\\ GP_{n+1}\end{bmatrix}$

iii. $\begin{bmatrix}0 & 1\\ 1 & -2\end{bmatrix}^n \begin{bmatrix}GP_2 & GP_1\\ GP_1 & GP_0\end{bmatrix} = \begin{bmatrix}GP_{-n+2} & GP_{-n+1}\\ GP_{-n+1} & GP_{-n}\end{bmatrix}$

iv. $\begin{bmatrix}-2 & 1\\ 1 & 0\end{bmatrix}^n \begin{bmatrix}GP_0\\ GP_1\end{bmatrix} = \begin{bmatrix}GP_{-n}\\ GP_{-n+1}\end{bmatrix}$

Proof.

i. For the prove, we utilize induction princible on *n*. The equality hold for $n = 1$. Now assume that the equality is true for $n > 1$. Then, we can verify for $n + 1$ as follows

$$\begin{bmatrix}2 & 1\\ 1 & 0\end{bmatrix}^{n+1} \begin{bmatrix}GP_2 & GP_1\\ GP_1 & GP_0\end{bmatrix} = \begin{bmatrix}2 & 1\\ 1 & 0\end{bmatrix}\begin{bmatrix}2 & 1\\ 1 & 0\end{bmatrix}^n \begin{bmatrix}GP_2 & GP_1\\ GP_1 & GP_0\end{bmatrix}$$

$$= \begin{bmatrix}2 & 1\\ 1 & 0\end{bmatrix}\begin{bmatrix}GP_{n+2} & GP_{n+1}\\ GP_{n+1} & GP_n\end{bmatrix} = \begin{bmatrix}GP_{n+3} & GP_{n+2}\\ GP_{n+2} & GP_{n+1}\end{bmatrix}.$$

Thus, the first step of the theorem can be proved easily. Similarly, the other steps of the proof are concluded by induction on *n*. Matrix representations for Gaussian-bihyperbolic Pell-Lucas numbers are obtained analogously.

3. Conclusion

This study presents the Gaussian-bihyperbolic Pell and Pell-Lucas numbers. We hope that these newly defined number sequences may be used in many areas such as quantum physics, applied mathematics, kinematic, differential equations and cryptology. Since this study includes some new results, it contributes to literature by providing essential information concerning these new numbers. Therefore, we hope that this new number system and its properties that we have found will offer a new perspective to the researchers.

Acknowledgement

The author expresses his sincere thanks to the anonymous referees and the associate editor for their careful reading, suggestions and comments, which improved the presentation of results.

Conflicts of Interest

As the author of this study, we declare that we do not have any conflict of interest statement.

References

Akar, M., Yüce, S., Şahin, S. (2018). On the Dual Hyperbolic Numbers and the Complex Hyperbolic numbers, *Journal of Computer Science & Computational Mathematics,* 8, 1-6.

Aydın, F. T. (2019). Hyperbolic Fibonacci Sequence, *Universal Journal of Mathematics and Applications,* 2(2), 59-64.

Azak, Z., Güngör, M. A. (2017). Investigation of Dual-complex Fibonacci, Dual-complex Lucas Numbers and Their Properties, *Adv. Appl. Clifford Algebras,* 27, 3083-3096.

Bilgin, M., Ersoy, S. (2020). Algebraic Properties of Bihyperbolic Numbers, *Adv. Appl. Clifford Algebras,* DOI: https://doi.org/10.1007/s00006-019-1036-2

Brod, D., Szynal-Liana, A., Wloch, I. (2020). On some combinatorial properties of bihyperbolic numbers of the Fibonacci type, *Wiley,* DOI: https://doi.org/10.1002/mma.7054

Brod, D., Szynal-Liana, A., Wloch, I. (2021). On a new generalization of bihyperbolic Pell numbers, *An. Ştiint. Univ. Al. I. Cuza Iaşi. Mat.,* DOI: https://doi.org/10.47743/anstim.2021.00018

Catarino, P. (2019). Bicomplex k-Pell Quaternions, *Computational Methods and Function Theory,* 19, 65-76.

Clifford, W. K. (1871). A Preliminary Sketch of Biquaternions, *London Mathematical Society.* DOI: https://doi.org/10.1112/plms/s1-4.1.381

Dikmen, C. M. (2019). Hyperbolic Jacobsthal Numbers, *Asian Research Journal of Mathematics,* 15(4), 1-9.

Fjelstad, P., Gal, S. G. (1998). n-dimensional Dual Complex Numbers, *Advances in Applied Clifford Algebras,* 8(2), 309-322.

Gül, K. (2020). Dual Bicomplex Horadam Quaternions, *Notes on Numbers Theory and Discrete Mathematics,* 26, 187-205.

Gürses, N., Şentürk, G. Y., Yüce, S. (2021). A Study on the Dual-Generalized Complex and Hyperbolic-Generalized Complex Numbers, *Journal of Science*, 34(1), 180-194.

Horadam, A. F. (1963). Complex Fibonacci Numbers and Fibonacci Quaternions, *American Math. Monthly,* 70, 289-291.

Koshy, T. (2014). *Pell and Pell-Lucas Numbers with Applications,* Springer New York Heidelberg Dordrecht, London.

Majernik, V. (1996). Multicomponent Number Systems, *Acta Physica Polonica A.,* 90(3), 491-498.

Matsuda, G., Kaji, S., Ochiai, H. (2014). Anti-commutative Dual Complex Numbers and 2 Rigid Transformation, Mathematical Progress in Expressive Inage Synthesis I. Springer.

Messelmi, F. (2022). Dual Complex Numbers and Their Holomorphic Functions. Retrieved from: https://hal.archives-ouvertes.fr/hal-01114178

Petoukhov, S. V. (2019). Hyperbolic Numbers in Modeling Genetic Phenomena, Preprint, DOI: https://doi.org/10.20944/preprints201908.0284.v2

Soykan, Y., Göcen, M. (2020). Properties of hyperbolic generalized Pell numbers, *Notes on Number Theory and Discrete Mathematics,* 26, 136-153.

Soykan, Y. (2021). On Dual Hyperbolic Generalized Fibonacci Numbers, *Indian Journal of Pure and Applied*

Mathematics, 52, 62-78.

Vajda, S. (1989). *Fibonacci and Lucas Numbers and the Golden Section*, Ellis Horwood Limited Publ., England.

e-ISSN 2757-5195

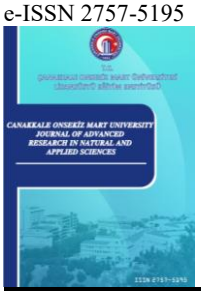

Çanakkale Onsekiz Mart University

Journal of Advanced Research in Natural and Applied Sciences

Open Access

doi.org/10.28979/jarnas.1137363 2023, Vol. 9, Issue 1, Pages: 190-204 dergipark.org.tr/tr/pub/jarnas

Flexibility in Power Systems of Integrating Variable Renewable Energy Sources

Hasan Huseyin Coban[1*], Wojciech Lewicki[2]

[1]Department of Electrical Engineering, Ardahan University, Ardahan, 75002, Türkiye
[2]West Pomeranian University of Technology Szczecin, Faculty of Economics. Zołnierska 47, Szczecin 71-210, Poland

Article History

Received: 29.06.2022

Accepted: 08.12.2022

Published: 05.03.2023

Research Article

Abstract –The issue of energy security is addressed in many publications and by specialists in many fields. None of the researchers has any doubts that renewable sources have an impact on the functioning of the power system, in particular on its reliability. The intermittent nature of renewable energy sources introduces a new type of uncertainty to the operation of power systems. The aim of the article is to present an important research problem in the relationship of a smart power grid - network flexibility - optimization models. This study focuses on the analysis of the short-term (operational) and long-term (investment) aspects of providing flexibility with sources of fossil fuel generation, storage, and demand response. The authors discussed the role of power system flexibility at the stage of generation and planning. Paying special attention to the simplified optimization and load profile effect. The proposed optimization model was implemented using the MATLAB optimization engine. The research results indicate the key role of both the identification of energy flexibility and the factors affecting it in terms of renewable development and in terms of savings in investment and operating costs. The recipients of the research may be public and local government units that plan to increase the share of renewable energy in their energy systems in the future. To ensure energy stability and reduce energy production costs.

Keywords *– Flexibility, investment, optimization models, power system, profitability, renewable energy*

1. Introduction

In recent years, much attention has been paid to energy security in the available literature on the subject (Bird et al., 2013; Deng & Lv, 2020; Sinsel et al., 2020). This topic appeared in many legal acts, reports, studies, and conference materials. Considering the enormity of investments related to the need to modernize the energy sector, i.e. the need to increase the production capacity of electricity, as well as the introduction of a significant share of renewable energy sources in electricity generation, it can be concluded that the demand for energy investment funds will be a big challenge (Impram et al., 2020). Thus, it can be concluded that electricity prices will continue to increase in the coming years, as the energy sector will be forced to seek funds for the necessary investments (Schaber et al., 2012). Simultaneously with the energy efficiency improvement program, opinions appear that the energy and climate policy, i.e. the fight against global warming, and the growing share of - unfortunately - unstable sources of renewable energy mean that the effect of these measures is likely to increase energy prices. And this leads to negative consequences both for industry and residents. Questions arise as to whether the flexibility of the electricity system is appropriate as a result of the increase in the share of energy generation from renewable sources (Papaefthymiou & Dragoon, 2016).

Already at the beginning of the considerations, it should be noted that in the last decade, the traditional structure of energy systems has entered a process of change due to the increasing share of renewable energy sources in the total installed power of countries (Kapitonov & Voloshin, 2017). To cope with the volatility and uncertainty

[1] huseyincoban@ardahan.edu.tr
[2] Wojciech.Lewicki@zut.edu.pl
*Corresponding Author

that renewable energy production brings to the system, prevent energy constraints caused by renewable energy, and provide consumers with the desired energy at all times reliably; it becomes possible by using all kinds of flexible resources in the network.

For an energy system to be considered flexible (Langevin et al., 2021; Schulze et al., 2019):

- It should have the capacity to meet peak loads and net peak loads.
- It should always maintain the balance of supply and demand, ensure that sufficient capacity is available during increasing or decreasing load changes, offer working capacity even in case of low net load, and be able to respond quickly to changes.
- It should have the sufficient storage capacity to fulfill its balancing service during high renewable energy generation or low renewable energy generation in the face of high demand.
- It must be able to manage the demand side to respond to periods of supply shortage or overproduction.
- It must be able to maintain its ability to mitigate potential events that could destabilize the energy system by ensuring that ancillary services are always adequately supplied.
- It should operate in a well-designed market environment where the available flexibility is not hampered by market inefficiencies.

In this article, the authors made an attempt to explain the links between intelligent energy grid - grid flexibility - optimization models. The authors then outlined the need for balance and flexibility in a renewable energy system, using the definition of flexibility on an operating time scale in an hour or a day. Emphasize the importance of flexibility with regard to planning time.

Therefore, the article below has many important political, economic, and practical implications. Considering that the aim of the research is to gain extensive knowledge on a significant research problem in the relation between intelligent energy grid - grid flexibility - optimization models. At the same time, it is a new opening to research the said relationship in relation to renewable sources. This study examines the short-term (operational) and long-term (investment) aspects of providing flexibility using fossil fuel generation sources, storage, and demand response.

The article is organized as follows. Chapter 1 gives information about the author's view of smart grids and what it's all about the reliability and integrity of the power system. Chapter 2 describes keeping the power system in balance and the need for flexibility at the operational time scale. Chapter 3 describes power system flexibility at the planning stage. Chapter 4 describes flexibility and how it is deployed flexibility with the resources. Also, the section explains flexibility in the planning time scale when it has the opportunity to build more resources. Chapter 5 presents the final conclusions of the research, indicating their limitations, practical application, and future directions of research in this field.

1.1. Reliability and integrity of the power system

A grid-tied mini-grid using renewable power sources offers customers benefits that increase overall system flexibility (Tsai et al., 2020). The grid connection strengthens the use of solar PV and wind energy throughout the system. Integrated energy infrastructure based on distributed power generation creates local mini-grids. Although normally autonomous, they can also be connected to the main grid. Installing the system in the desired region increases flexibility by reducing transmission losses (Duran & Sahinyazan, 2021).

The first thing to worry about in a power system is to provide a reliable supply; but there's something else running a power system, it's incredibly expensive (see Figure 2). The running of a traditional power system kind of balances greed and fear. The greed is the grid operator doesn't want to spend more money on operation and management; the fear is consumers can have a blackout. Over many years public services learn how to do such operations. There are monopolies with vertically integrated utility; they have satisfactory reliability and can do so at a very low cost. The technology is also relatively mature; there were not a whole lot of big changes happening there. No real need for innovation therefore in the situation for quite a number of years not much was happening in this field.

But then in a recent year, something else happened. The share of energy consumed from renewable sources in the EU and the world in 2020 was 22.1% and 12.55%, respectively (Mehedintu et al., 2021). Despite the high level of dependence on fossil fuels in the current situation, the use of renewable energy has been increasing over the years. People and governments want to be green, which means integrating renewable energy sources like wind and solar in this context. Therefore, instead of dealing with the fear that has just been decided, it is now necessary to deal with a third aspect, namely, that everything is desired to be green, to have renewable energy sources (see Figure 1).

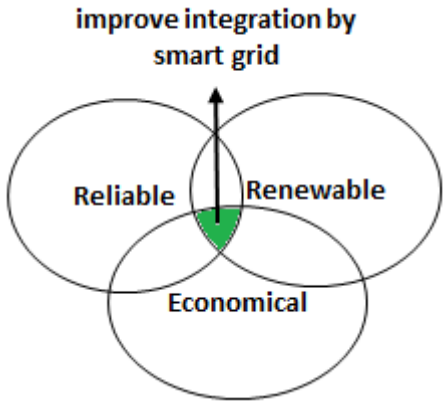

Figure 1. The relationship between the flexible development of energy and the reliability, renewable and economical.

As shown in Figure 1 the three goals should all be taken into account and are commendable, but they go in different directions. Namely, it's easy to be reliable and cheap but it won't be green. It may be environmentally friendly and reliable, but it will not be economical, or it may be cheap and green but not reliable. This is the conundrum about the power system operation trying to satisfy these three goals.

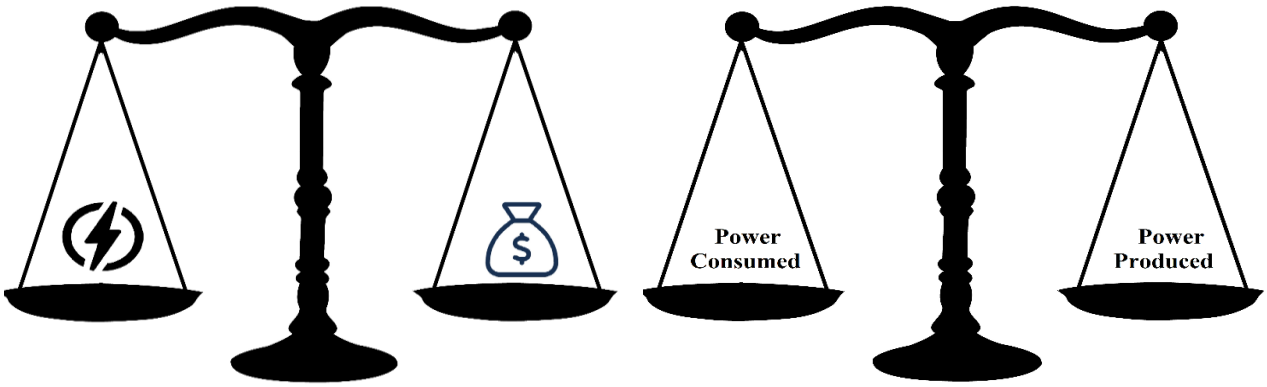

Figure 2. Energy economy and energy balance

There must be a physical balance between the power produced and the power consumed (see Figure 2). These two need to be kept equal, essentially on a second-by-second basis. This balance has to be maintained in the face of fluctuations in the load.

1.2. The Role of Smart Grid

The smart grid is about trying to use new technologies like communication technologies, computing technologies, and control technologies which are a lot cheaper than traditional power technologies; because it doesn't involve a lot of copper steel and concretes (Bouffard, 2010; Gungor et al., 2011). These new technologies must be used to better achieve these three goals simultaneously. There have lots of different definitions of the smart grid (Ardito et al., 2013; Colak et al., 2014; Jenkins et al., 2015; Shabanzadeh, M. Moghaddam, 2013); mainly it is the use of communication control and computer technologies to enhance the operation of the grid. One thing to know about the power system is that the power generation must always be increased to

the power consumed and this balance must be maintained. In the old days, this meant having to adjust the generation as low changes throughout the day. A typical load curve and load duration are shown in Figure 3 and Figure 4 respectively. The data shown in Figure 3 represent the average aggregate U.S. hourly load by day of the week indicated between 2018 and 2021 (U.S. Energy Information Administration, 2022). There are very slow variations in demand, and also quite predictable unless the weather changes drastically.

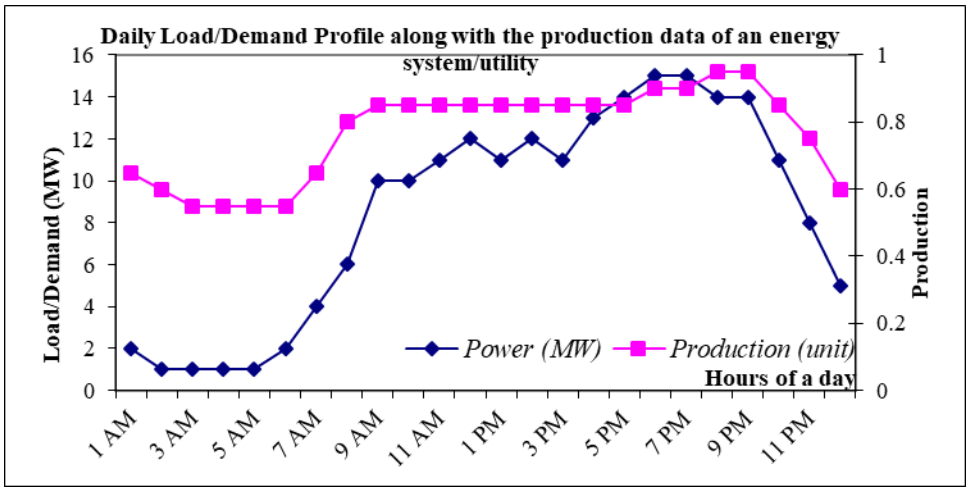

Figure 3. Typical load curve

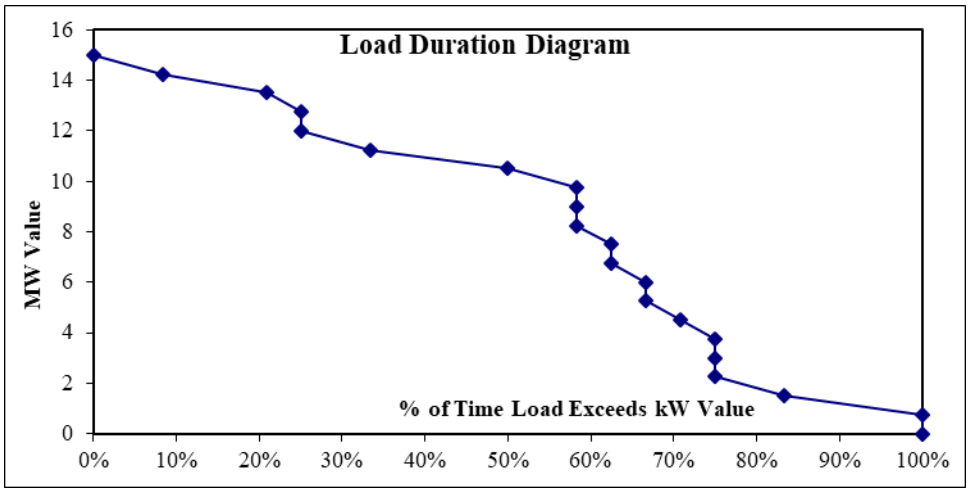

Figure 4. Load duration diagram

When the data set is examined closely, the changes in the hourly consumption values are clearly seen. There may be a remarkable difference between the consumption values and type on weekdays and weekends (see Figure 8). While the peak consumption during the day is in the afternoon on weekends, this is in the morning hours during the weekdays (Bissey et al., 2017). This is because people engage in different activities on weekdays and weekends. While consumption during the week is affected by activities such as lunch breaks, shift changes, and working hours, many different reasons can be considered for the weekend. When the weekly consumption changes are examined closely, seasonal effects can also be noticed (see Figure 8). Different consumption levels caused by the effect of temperature lead to the conclusion that seasonal changes directly affect consumption. Likewise, the difference in consumption values for weekdays and weekends, and the consumption curve corresponding to a day, day and night, give rough information about how different household consumption and industrial consumption are. Therefore, the consumption values for the holiday period are used to calculate the household consumption value. As a result of the seasonal effect, both the difference between day and night and the difference between general consumption amounts increase. One of the important points that make modeling difficult is these changes.

Also in a conventional power system, the low change is relatively slow and they're predictable with good accuracy; conventional generators can be programmed to balance this load. Thus, coal-fired, gas-fired conventional production facilities can be planned to balance this load. But when renewable energy sources are added to the system and here are a few graphs showing the output of a photovoltaic system installed on the university campus that the authors used in their project work on different days. In addition, data were collected with a device called SM206 Solar Power Meter. The curve obtained in solar radiation as a function of time during a day in the Ardahan University campus is shown in Figure 5. As demonstrated in the study of (Bou-Rabee et al., 2015); if it's a clear day, it can get a pretty, smooth curve that's pretty predictable, just as the astronomer tells us when the Sun rises, sets, and rise high. But as it is known, we get the sun under the clouds and as the clouds pass in front of the solar panel, the fluctuations occur in the output and occasionally there may even be a major storm that brings the brightness to near zero. The movement of the clouds and the thickness of the clouds are unknown parameters. Therefore, this brings with it a lot of uncertainty.

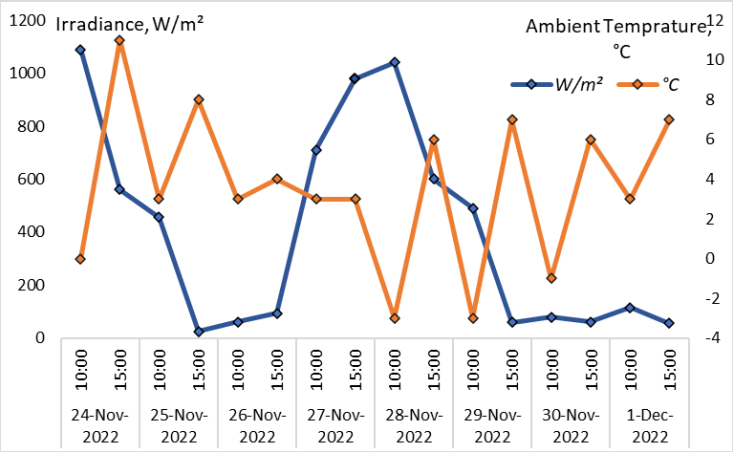

Figure 5. Typical solar irradiance and its fluctuations

In wind energy; the wind speed curve on June 27 (*Turkish State Meteorological Service*, 2022) is shown in Figure 6 and it can be seen there are quite a few fluctuations. Statistically the fluctuation of wind power they quite different from the fluctuations in solar irradiance and therefore PV power. In the wind it may not be so dramatic; wind fluctuations are a bit slower but still, there are significant changes here.

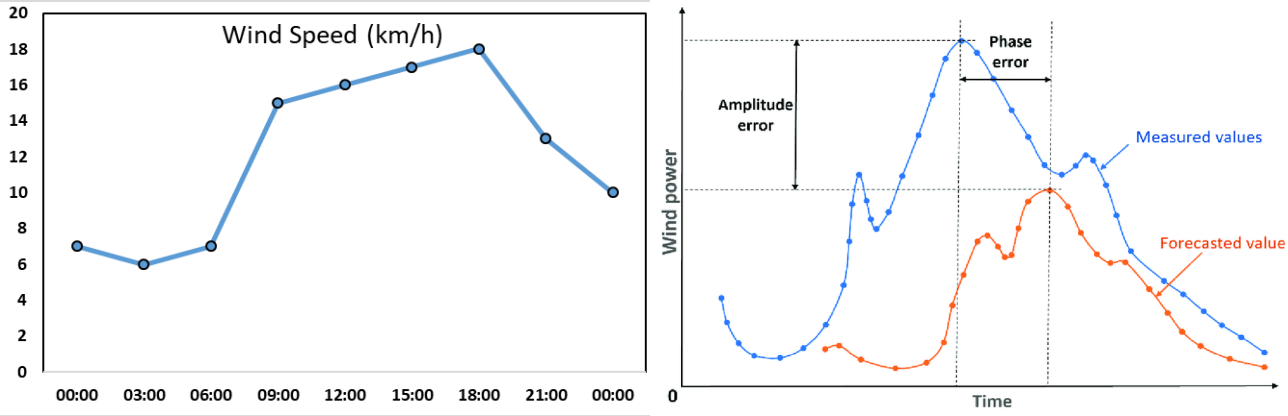

Figure 6. Wind speed for Ankara city and wind power prediction error (Hanifi et al., 2020)

In both cases, however, the fluctuations are quite large and difficult to predict. Another thing is wind strength and direction can be predicted, but the error increases. It can be observed that wind generation and energy demand are in the reverse phase. In many parts of the world, there are places where the wind blows at night and not much energy is used, and consumption peaks during the day. There is good wind around 3:00 AM along the Columbia Gorge (Windfinder, 2022), where most of the wind farms are located.

From a flexibility perspective, hydro is a controllable resource, so it's a traditional manufacturing facility (Gjorgievski et al., 2021). As viewed by power systems, electric vehicles (EVs) can be both a very good thing

and a very bad thing (Zhang & Kezunovic, 2016). The bad side is if a lot of people buy EVs and plug them in at 9:30 pm when they get home, it goes to fluctuate very fast. Therefore, great flexibility is needed to prevent the wind from falling. The good side is EVs are a godsend; users can meet their electricity needs when and where it is needed. That is if they can control the charging of EVs that provides resource flexibility. But in order to do this, the owners need to be persuaded with the incentive of EVs. In terms of batteries, storage is known to be very expensive. Thus, free storage space is obtained when the electric vehicle is purchased. Intelligent charging of electric vehicles adapts the charging cycle to events in the power system, allowing vehicles to be integrated into the power system in a grid and user-friendly manner. Vehicle-to-grid (V2G) technologies can bring even more flexibility to the system by providing power to the grid as needed (Clement-Nyns et al., 2011; Noel et al., 2019).

Large storage systems based on batteries can help integrate high shares of solar and wind power, providing the flexibility needed to manage resource variability. Small-scale, localized battery capacity helps integrate solar and wind power from multiple locations around the power grid. Home-level battery storage, with the right incentives, could unlock demand-side flexibility and facilitate system integration for electricity from these variable renewable energy sources.

In an energy system with a large number of renewable energies, only the load is not considered. The so-called net load should be taken into account, that is, the production of renewable energy sources is subtracted from the load (Equation 1.1). The net load needs to be balanced by the conventional generators which are the hydro generators that are controllable. Because typically the wind and the PV generators are not controllable. Therefore, the net load is subject to much bigger fluctuations than the actual load. As renewables are introduced into the system, the amplitude and uncertainty of these fluctuations will change considerably and are likely to increase significantly. These fluctuations can be much higher than predicted fluctuations in net load.

$$NL = L - RG \tag{1.1}$$

Where;

NL – net load;

L – load;

RG – renewable generation.

To respond to these uncertainties and fluctuations, it is necessary to make the energy system more flexible, but providing the flexibility is costly. Where generators are desired to be more flexible, they must be built to have this flexibility or use smaller and less efficient generators that can be started and stopped more frequently and quickly. Also, how much flexibility is needed should be defined.

What is the best mix of flexible resources? Because it can be obtained this flexibility in generation either through conventional generators possibly and operators provide flexibility or it might be able to get some flexibility from the demand essentially convincing consumers to adapt their demand to the availability of renewable energy sources.

Several utilities and pilot programs implemented to try to solve that. In some cases, flexible storage is used where store renewable energy when we have too much of it and then discharge it from the storage when it is needed. Finally, it can be created virtual flexibility which is simply at that thing the rules according to operating the power system, or the rules of the electricity market, and the market itself provides this flexibility.

But how to optimize the capability in the existing power system to have the necessary flexibility is the main objective of this article. Then, if 40% or more of production is from renewable energy sources over the next 20 years, it must be decided how much flexibility will be needed and what needs to be built to meet them.

Pump-hydro is still the most common economical way of storing energy. The problem with pump storage is that the required investments are huge and the environmental impact is significant. Naturally, there should be two lakes; and there's not a lot of room to put pumps and pipes. But it's a matter of technology at a reasonable cost. Also, since the efficiency is around 70%, there is a cost every time it is pumped, it costs a lot of money.

2. Power system flexibility at the generation stage

How to balance a system using renewable energy sources is to say that the rest of the system will need to be more flexible. But providing flexibility costs money (Figure 2), which is a very important thing to keep in mind because that flexibility will have to come from traditional power plants. To keep these conventional power plants operational, fossil fuels must be burned. If it is necessary to operate more of these traditional production facilities, it will be less efficient. If it could predict what would happen, then it would have to have this reserve to go up and down as the sun and wind change.

Essentially the operational timescale has to be taken into account. The power system operators think about what is going to happen the next day that they want to be ready, they don't want to improvise. But they have to improvise, inefficient and coal-fired power plants can take several hours to get started. Therefore, it cannot be decided at the last moment how big is the demand. How much uncertainty will be faced the next day, and therefore production should be planned for the next day so that you can have the right amount of flexibility when needed. It is a problem of balancing startup costs and variable costs. When a large production is planned, a certain amount of fuel must be used to start it, and then once started, it needs to use more fuel to generate a certain amount of power. Thus, some units may have a low initial cost and a high variable cost, while other units may have the opposite; therefore, both need to be balanced in order to reach the optimal solution.

Estimate how much flexibility will be needed the next day on the operational time scale. We do this based on some statistical analysis we have done using some real data from Ankara city. It was known hourly how much renewable energy is produced in the city and the net load. In Figure 7 it is depicted that there are times when it needs energy. That's why they are called resilience events and a resilience event is characterized by three things. The first is the capacity needed to meet this resilience event, and how high a ramp goes. The next characteristic is the ramp rate of how fast it goes from zero to maximum and the third one is the time; how long has this ramp lasted.

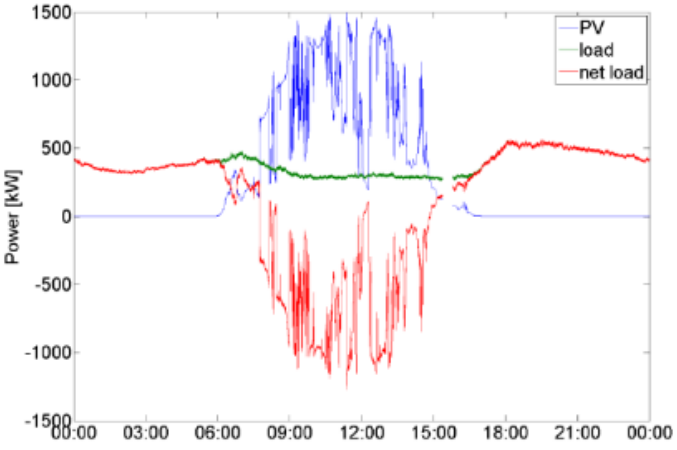

Figure 7. PV generation, load, and net load (Stein et al., 2011)

Since a standard parametric probability distribution function does not work, a non-parametric approach was applied to this problem to represent events, and flexibility requirements can be figured out. What is going to be needed tomorrow in terms of capacity ramp rate and ability to sustain these ramps. The goal is to put a frame around enough of these flexibility events to run a power system or the system operator can be confident that they will have the flexibility they need to meet these expected flexibility times the next day. Therefore, all one has to do without playing with the system is to find the reasonable one.

If it is known how much flexibility is needed; where does this flexibility come from? Typically, it will be from conventional fuel generators, it can ramp them up and down. In addition, consumers can be asked to adjust their consumption according to their needs. If the wind is blowing hard, users can guess and the laundry can be washed; if the wind is not blowing, the dishes can be washed later.

2.1. Refining the requirements: season and day

Some improvements have to be made first, one thing the operators do is define the frame's boundaries. The second improvement is to observe the need for flexibility will vary with the season and day of the week. The day of the week is due to the fact that the electricity demand changes differently on weekends as well as on weekdays. The extent to which the wind speed changes seasonally is important, so it is not necessary to have the same amount of flexibility every time of the year and every day of the week. The third improvement is that it doesn't need the same amount of flexibility of the same type around the time of the day. It can be predicted when the load increases, thus the demand can compensate. There are also times of the day when the wind tends to change very quickly, the wind is a little more stable, or there is no wind at all, as everything else is relatively stable. Thus, the requirements can be adjusted according to the time of day. These flexibility requirements are then used by the optimization solver to determine which conventional generation operators will use the next day.

3. Power system flexibility at the planning stage

The question of how big flexibility will be needed to deliver the expected rate of renewable energy in the coming year should also be taken into account at the planning stage. The idea is to minimize the overall cost of providing this flexibility which has an operating component and an investment component. The following Equation (3.1) shows the form of the modified objective function that minimizes generation costs and investment costs:

$$min\left(\sum_{n=1}^{N} C_{inv}(n) + \sum_{n=1}^{N}\sum_{t=1}^{T} C_{OM}(n,t)\right) \tag{3.1}$$

Where;

C_{inv} - the investment cost;

C_{OM} - the operating and management cost;

N - the number of power plants;

T - the time period.

There can be a lower operating cost if more investment is made in flexibility, but increases the investment cost. If no investment is made, the investment cost is saved, but then the cost is paid daily because it no longer has to provide this flexibility in a more complex and inefficient way. It's a very difficult and huge optimization problem for the operational time scale; following simplifying assumptions needs to be made.

- Centrally planned system: It is assumed a centrally planned system; many parts of the country operate electricity markets where you don't decide that but it's the first step.
- Compare the different types of power plants: The investor decides whether to invest in the more flexible and more expensive option or the opposite.
- Flexibility provided by generating units only: In this case, it is assumed that flexibility is provided only with units of production, and is not sufficient for any flexibility on the demand side or storage.

4. Optimization Model

The objection function of the optimization model is designed to schedule power plants for one or a few days the minimize the total costs (Equation 3.1). It considers a fixed set of available generation units; a set of production units is entered into the program that it can work with to optimize and achieve this minimum cost.

The model enforces dynamic constraints on the scheduling of units because some of the constraints are related to flexibility. For example, each generating unit has an up-ramp rate and down-ramp rate which indicates how quickly the system can get it to increase or decrease its output. Also, each unit has a minimum uptime and a minimum downside which affect the flexibility.

These constraints can be more easily met in this optimization problem when more flexible production units are in place. Therefore, it can achieve a lower operating cost. But this is an operational tool, this is not a planning or investment tool because it ignores the investment cost. This generation schedule is realized by mixed-integer linear programming.

To answer or plan flexibility the optimization tool is developed. The idea of this tool considers not just the operating cost but also the investment costs and it also considers a variable set to optimize not just for a week but at least a set of years where it has a different amount of renewable generation and different fluctuations in wind and solar generation. In Figure 8, the load profiles used for various seasons are shown.

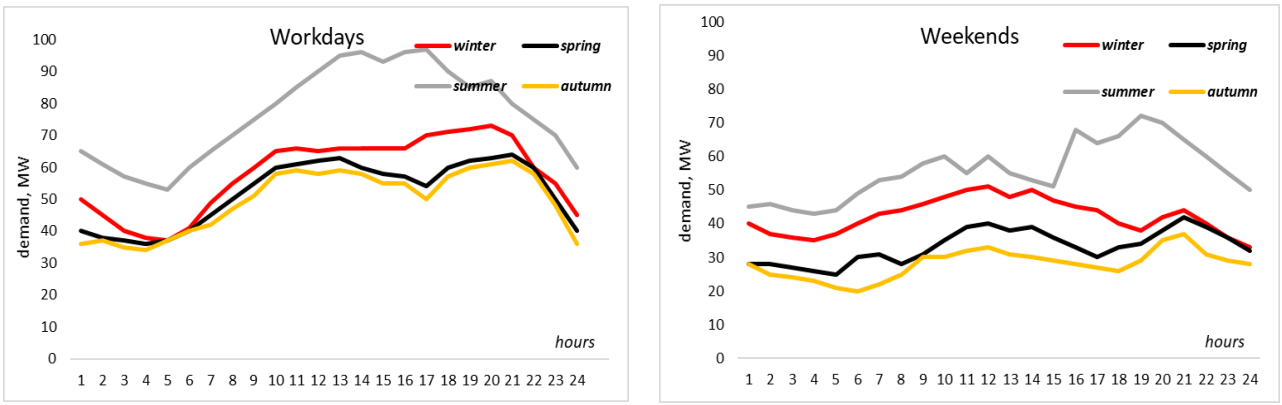

Figure 8. Hourly load profiles of four seasons

Therefore, the seasonal variations have to take into account. The main decision variable in the optimization program was to have the information for each generating unit whether this generating unit is active at this time and how to connect to the network. There is a binary decision variable every hour for every generating unit and it is a very challenging mixed integer linear programming problem. Because much more decision variables can be obtained and optimization takes into account a long time.

In the objective function, the number of days in the season is used to calculate each month's operational expense. Based on this, the solutions to the optimization issue show how many power plants are required to reduce overall costs over the year. It must be taken into account that there can be days with severe changes in load and intermittent renewable generation every few years. It's possible that the ideal level of flexibility determined using typical sample months won't be enough to deal with the cases successfully. The optimization can be performed using a composite load profile of 7 days per year reflecting exceptional circumstances to account for this possibility.

After all, data is entered into the system, only the representative weeks, namely winter, spring, summer, and autumn weeks, are optimized. It also introduced an extreme weather week because those are typically the ones to apply the largest amount of flexibility. Some clustering techniques are used to identify these most representative extreme weeks in each season.

4.1. Simplifying optimization and the load profile effect

It's a very difficult optimization problem, so a way must be found to limit the amount of CPU time. The Monte Carlo method is used to reduce the number of decision variables. The Monte Carlo method is a large class of computational algorithms that rely on repeated random sampling to produce numerical results (Coban & Sauhats, 2022). The underlying concept is to use randomness to solve problems that might be deterministic in principle. The system should not be presented with too many choices, because the more choices it is given, the longer it takes to find the best solution. This priority ordering considerably reduces the amount of time required. Therefore, in order to test a program, firstly, the generation power plants to be ideally created for different load profiles are summarized in Table 1. Investment costs were initially obtained from the Energy Information Administration (EIA) (*Annual Energy Outlook*, 2022), and it is assumed that the lifetime of each power plant is 30 years. The second thing is to reduce the number of decision variables. It is assumed that some of the power plants are already built. The third thing should be built from a reasonably adapted system.

If the peak load is known, it is unnecessary to have three times as many facilities as this peak load, as this provides a lot of flexibility. Therefore, one should get a rough idea of how much capacity should be considered before starting the optimization. Another thing; in power systems, there are many units with essentially the same characteristics, and treating them all as stand-alone units will turn into many combinations that are the same. Therefore, instead of trying all possible combinations, basically, the same units were used in the same order.

Table 1.

Cost and performance characteristics of power plants used in the optimization

Power Plant	**Fuel type**	**Power min (MW)**	**Power max (MW)**	**Investment ($/kW)**	**No-load cost ($/MW)**	**Start-up cost ($/MW)**	**O&M cost ($/kW-yr)**
1	Natural Gas	10	20	971	264	9	7.34
2	Natural Gas	30	50		251	9	
3	Natural Gas	60	100		225	9	
4	Natural Gas	50	150		210	10	
5	Coal	20	40	2925	280	30	31.18
6	Coal	40	70		340	300	
7	Coal	50	100		300	400	
8	Coal	80	200		260	900	
9	Nuclear	100	500	5501	590	0	93.28
10	Oil	20	75	915	340	710	13.17

A system with 10 power plants was created for the analyses. Some of these units are called peak units very flexible but rather inefficient ones. Some units are called big coal, and nuclear units, they are very efficient but very inflexible. Finally, there are some units that are somewhere between the two.

This resulted in a base load profile, a softer load profile, and a sharper load profile. With the basic load profile, it can be concluded that the 2nd power plant should be out of these 10 power plants, when there is a soft load profile, the best way to do it is to have all 10 power plants, when there is a sharper load for 6th and 7th power plant should be out. Table 2 demonstrates the model outcomes that are in line with these predictions. While only 8 power plants are required to handle the softer valley efficiently, the profile with a sharper valley necessitates the availability of all 10 power plants.

Table 2.

Results for various generation profiles

Scenario	**Total Cost**	**Investment Decision**
Soft	266 M.$	Power plants 7 and 8 are not needed.
Sharp	354 M.$	All power plants are needed.

4.2. Wind generation and flexibility

To see the impact of wind generation on flexibility in more detail, there are 4 different things to look at:

1. Thanks to wind turbines, the need for traditional fossil fuel production units is reduced (Equation 4.1). It is relocated producing units and that will be an effect.

$$\sum_{i=1}^{I} P_i(t) = P_{dmnd}(t) - P_w(t) \quad (4.1)$$

Where;

P – the amount of generated power;

P_{dmnd} – total power demand;

P_w - predicted wind power;

i – power plant index;

t – time period.

2. Because renewable resources are less predictable (stochastic nature of renewable energy sources), more reserves are needed and it needs to be taken into account and modeled in the program. Through the demand for spinning reserves, the uncertainty resulting from the wind forecast errors (see Table 2) is taken into account in this study. Here, it is assumed that wind energy is generated by a large number of various wind turbines. To be able to handle both the unexpected loss of the biggest generating unit and a concurrent error in the wind power, the spinning reserve requirement, *sr(t)*, must be increased. This reserve must be large enough to cover the majority of the wind prediction error (Equation 4.2), therefore an extra reserve equal to 3.5 times the wind forecast error's standard deviation is chosen (Black & Strbac, 2007).

$$sr(t) \geq \max(P_i(\max)(t)) + 3.5\sigma_w(t) \quad (4.2)$$

Where; $\sigma_w(t)$ is the standard deviation of wind forecast error.

3. The fact that even if fluctuations in wind speed are predicted correctly, it will require more ramps up and down and turning units on and off.

4. Each generating unit should be operated at the minimum stable production and maximum capacity (Equation 4.3).

$$P_i(max) \geq P_i(t) \geq P_i(min) \quad (4.3)$$

4.3. Test cases

The objective function is to improve this unit commitment by considering both the operating cost and the investment cost. The idea is that not only will a fixed set of power plants available be considered, but a variable set of power plants will be considered. Therefore, the decision variables will decide not only whether this unit will generate at a given hour, but also whether this facility will exist (deciding whether to invest in the generating unit).

The proposed optimization model is implemented using the function "*intlinprog*" in the MATLAB optimization engine. Excluding renewable power plants, tests were conducted for scenarios consisting of 10 conventional power plants. The characteristics of test cases are summarized in Table 3. In the first case, there is no wind power and no forecast error. In the second case, there is 10% wind but no fluctuation, so it just needs to be unloaded and doesn't need much reserve. Case-3 has wind power and no fluctuation, there are some forecast errors to see the effect of this. In the last case, there is wind power and volatility but predictability.

Table 3.

The test cases and investment decisions

	Case-1	**Case-2**	**Case-3**	**Case-4**
Renewable forecast	No renewable	10% wind, without fluctuations	10% wind, without fluctuations	10% wind, with fluctuations
Forecast error	No error	8%	15%	8%
Investment decision	Power plants 3, 8, and 10 are out	Power plants 7, 8, and 10 are out	Power plants 7, and 10 are out	Power plants 7, and 8 are out
Total cost	251 M€	227 M€	246 M€	241 M€

The first scenario offers greater flexibility and generating capacity than the base scenario which consists of all 10 power plants. The overall cost is decreased by forgoing the build of some power plants. Case-2 demonstrates part of the base-producing units is replaced with wind generation, which further lowers the overall cost. However, in Scenario-3, it is decided to construct power plant 8, demonstrating that variations in wind power improve the ideal level of flexibility. Case-4 demonstrates more flexible generating power facilities are required to have the lowest overall cost and the reserve need is raised for larger uncertainty in the wind prediction.

These test findings demonstrate that the linear programming algorithm can maximize the flexibility of the generating mix for various wind penetrations. More power plants are needed to give greater flexibility due to fluctuations in wind power and wind forecast errors. Constant wind integration (as in Scenario 2) can be treated as a negative demand, which reduces the need for conventional fueled power generation facilities.

4.4. Effect of the renewable generation

The results for comparing these various scenarios are shown in Table 3. According to these results, in the basic case, three power plants are not needed. When wind turbines are added to the system, and although there is a forecast error, it becomes clear that even fewer units are needed because fossil fuel-generating units have been replaced by wind-generating units. In another scenario, when the wind is added and there are some fluctuations, the 7th and 10th power plants will not be needed. However, some of the other production units will be needed to provide the necessary flexibility. In the other scenario, when fluctuations and estimation errors are added to the system, the results change; it turns out that the 10th power plant should be used instead of the 8th one.

5. Conclusions, discussion, and future study

None of the contemporary researchers (Göransson et al., 2014; Syranidou et al., 2020; Zappa & van den Broek, 2018) dealing with the research issues mentioned by the authors have any doubts that energy efficiency is an important aspect taken into account when it comes to energy security. Improving the efficiency of energy use can significantly reduce the need to build new energy sources. Therefore, additional challenges need to be prepared in the coming years; The reason for this is the projected increase in demand for electricity with the simultaneous shutdown of older generating units. That is why, for several years now, attempts have been made to define a new model of the energy mix which, on the one hand, would take into account the needs of consumers, and on the other hand, would respond to the challenges posed by environmental protection. The answer to these needs, as emphasized by other researchers (Syranidis et al., 2018; Zsiborács et al., 2019), may be renewable energy sources. A case has been presented that requires a precise quantification of the flexibility needed by the power system and likely to be required as the share of renewable energy generation increases is a sure answer. The authors will confirm with other researchers that these requirements depend on the type and amount of renewable energy (Niekurzak et al., 2022; Ryberg et al., 2019). What it needs for wind will not be exactly the same as for solar energy. It also depends on the system. Renewable energy sources behave differently depending on the location of the source. In addition, studies have confirmed the thesis of other researchers (Chakraborty et al., 2019) that the amount of flexibility needed also depends on the time of day, day of the week, and season of the year. By adapting these requirements, significant savings can be made. At

the same time, if the flexibility you need is invented; it can be optimized for savings in investment and operating costs.

Like other research, these also have their limitation in the form of imprecise definitions and integration of optimization with the planning of electricity production over a longer period of time. The aim of future research is to create a model of integrated optimization with production planning covering all determinants that affect both the efficiency of the system and its reliability. As the amount of renewable energy production increases, it will be possible to measure how these requirements will change and what they will be. Their effects on the energy system. In the opinion of the authors, the problems and planning should be combined, and the functioning of the power system must be better represented in planning models. Another important issue requiring a solution will be the integration of flexibility and generation units in the smart grid system.

Summing up the presentation of the research on flexibility in power systems of the integration of variable renewable energy sources, the authors are aware that they do not fully exhaust the essence of the presented considerations. This topic certainly requires further analysis and research in an interdisciplinary approach, which will certainly be conducted by the authors along with the increasing importance of renewable energy in energy systems and the role of individual factors in this process.

Author Contributions

Hasan Huseyin Coban: Methodology, Data curation, Software, Writing-original draft, Writing – Review & Editing, Visualization, Investigation, Validation, Supervision, Conceptualization.

Wojciech Lewicki: Writing-original draft, Writing – Review & Editing, Visualization, Investigation, Conceptualization.

Conflicts of Interest

The authors declare no conflict of interest.

References

Annual Energy Outlook. (2022). U.S. Energy Information Administration (EIA). https://www.eia.gov/outlooks/aeo/assumptions/pdf/table8_2_2014er.pdf

Ardito, L., Procaccianti, G., Menga, G., & Morisio, M. (2013). Smart Grid Technologies in Europe: An Overview. *Energies*, *6*(1), 251–281. https://doi.org/10.3390/en6010251

Bird, L., Milligan, M., & Lew, D. (2013). *Integrating Variable Renewable Energy: Challenges and Solutions*. https://doi.org/10.2172/1097911

Bissey, S., Jacques, S., & Le Bunetel, J.-C. (2017). The Fuzzy Logic Method to Efficiently Optimize Electricity Consumption in Individual Housing. *Energies*, *10*(11), 1701. https://doi.org/10.3390/en10111701

Black, M., & Strbac, G. (2007). Value of Bulk Energy Storage for Managing Wind Power Fluctuations. *IEEE Transactions on Energy Conversion*, *22*(1), 197–205. https://doi.org/10.1109/TEC.2006.889619

Bou-Rabee, M. A., Sulaiman, S. A., Choe, G., Han, D., Saeed, T., & Marafie, S. (2015). Characteristics of solar energy radiation on typical summer and winter days in Kuwait. International Journal of Automotive and Mechanical Engineering, 12, 2944–2953. https://doi.org/10.15282/ijame.12.2015.11.0246

Bouffard, F. (2010). The challenge with building a business case for smart grids. *IEEE PES General Meeting*, 1–3. https://doi.org/10.1109/PES.2010.5589906

Chakraborty, P., Baeyens, E., Khargonekar, P. P., Poolla, K., & Varaiya, P. (2019). Analysis of Solar Energy Aggregation Under Various Billing Mechanisms. *IEEE Transactions on Smart Grid*, *10*(4), 4175–4187. https://doi.org/10.1109/TSG.2018.2851512

Clement-Nyns, K., Haesen, E., & Driesen, J. (2011). The impact of vehicle-to-grid on the distribution grid. *Electric Power Systems Research*, *81*(1), 185–192. https://doi.org/10.1016/j.epsr.2010.08.007

Coban, H. H., & Sauhats, A. (2022). Optimization tool for small hydropower plant resource planning and development: A case study. *Journal of Advanced Research in Natural and Applied Sciences*. https://doi.org/10.28979/jarnas.1083208

Colak, I., Bayindir, R., Fulli, G., Tekin, I., Demirtas, K., & Covrig, C.-F. (2014). Smart grid opportunities and

applications in Turkey. *Renewable and Sustainable Energy Reviews*, *33*, 344–352. https://doi.org/10.1016/j.rser.2014.02.009

Deng, X., & Lv, T. (2020). Power system planning with increasing variable renewable energy: A review of optimization models. *Journal of Cleaner Production*, *246*, 118962. https://doi.org/10.1016/j.jclepro.2019.118962

Duran, A. S., & Sahinyazan, F. G. (2021). An analysis of renewable mini-grid projects for rural electrification. *Socio-Economic Planning Sciences*, *77*, 100999. https://doi.org/10.1016/j.seps.2020.100999

Gjorgievski, V. Z., Markovska, N., Abazi, A., & Duić, N. (2021). The potential of power-to-heat demand response to improve the flexibility of the energy system: An empirical review. *Renewable and Sustainable Energy Reviews*, *138*, 110489. https://doi.org/10.1016/j.rser.2020.110489

Göransson, L., Goop, J., Unger, T., Odenberger, M., & Johnsson, F. (2014). Linkages between demand-side management and congestion in the European electricity transmission system. *Energy*, *69*, 860–872. https://doi.org/10.1016/j.energy.2014.03.083

Gungor, V. C., Sahin, D., Kocak, T., Ergut, S., Buccella, C., Cecati, C., & Hancke, G. P. (2011). Smart Grid Technologies: Communication Technologies and Standards. *IEEE Transactions on Industrial Informatics*, *7*(4), 529–539. https://doi.org/10.1109/TII.2011.2166794

Hanifi, S., Liu, X., Lin, Z., & Lotfian, S. (2020). A Critical Review of Wind Power Forecasting Methods—Past, Present and Future. *Energies*, *13*(15), 3764. https://doi.org/10.3390/en13153764

Impram, S., Varbak Nese, S., & Oral, B. (2020). Challenges of renewable energy penetration on power system flexibility: A survey. *Energy Strategy Reviews*, *31*, 100539. https://doi.org/10.1016/j.esr.2020.100539

Jenkins, N., Long, C., & Wu, J. (2015). An Overview of the Smart Grid in Great Britain. *Engineering*, *1*(4), 413–421. https://doi.org/10.15302/J-ENG-2015112

Kapitonov, I. A., & Voloshin, V. I. (2017). Strategic Directions for Increasing the Share of Renewable Energy Sources in the Structure of Energy Consumption. *International Journal of Energy Economics and Policy*, *7*(4), 90–98.

Langevin, J., Harris, C. B., Satre-Meloy, A., Chandra-Putra, H., Speake, A., Present, E., Adhikari, R., Wilson, E. J. H., & Satchwell, A. J. (2021). US building energy efficiency and flexibility as an electric grid resource. *Joule*, *5*(8), 2102–2128. https://doi.org/10.1016/j.joule.2021.06.002

Mehedintu, A., Soava, G., Sterpu, M., & Grecu, E. (2021). Evolution and Forecasting of the Renewable Energy Consumption in the Frame of Sustainable Development: EU vs. Romania. *Sustainability*, *13*(18), 10327. https://doi.org/10.3390/su131810327

Niekurzak, M., Lewicki, W., Drożdż, W., & Miązek, P. (2022). Measures for Assessing the Effectiveness of Investments for Electricity and Heat Generation from the Hybrid Cooperation of a Photovoltaic Installation with a Heat Pump on the Example of a Household. *Energies*, *15*(16), 6089. https://doi.org/10.3390/en15166089

Noel, L., Rubens, G. Z. de, Kester, J., & Sovacool, B. K. (2019). *Vehicle-to-Grid*. Palgrave Macmillan: London, UK.

Papaefthymiou, G., & Dragoon, K. (2016). Towards 100% renewable energy systems: Uncapping power system flexibility. *Energy Policy*, *92*, 69–82. https://doi.org/10.1016/j.enpol.2016.01.025

Ryberg, D. S., Caglayan, D. G., Schmitt, S., Linßen, J., Stolten, D., & Robinius, M. (2019). The future of European onshore wind energy potential: Detailed distribution and simulation of advanced turbine designs. *Energy*, *182*, 1222–1238. https://doi.org/10.1016/j.energy.2019.06.052

Schaber, K., Steinke, F., Mühlich, P., & Hamacher, T. (2012). Parametric study of variable renewable energy integration in Europe: Advantages and costs of transmission grid extensions. *Energy Policy*, *42*, 498–508. https://doi.org/10.1016/j.enpol.2011.12.016

Schulze, C., Blume, S., Siemon, L., Herrmann, C., & Thiede, S. (2019). Towards energy flexible and energy self-sufficient manufacturing systems. *Procedia CIRP*, *81*, 683–688. https://doi.org/10.1016/j.procir.2019.03.176

Shabanzadeh, M. Moghaddam, M. P. (2013). What is the smart grid? Definitions, perspectives, and ultimate goals. *28th International Power System Conference (PSC)*, 1–10.

Sinsel, S. R., Riemke, R. L., & Hoffmann, V. H. (2020). Challenges and solution technologies for the integration of variable renewable energy sources—a review. *Renewable Energy*, *145*, 2271–2285. https://doi.org/10.1016/j.renene.2019.06.147

Stein, J., Miyamoto, Y., Nakashima, E., & Lave, M. (2011). *Ota City : characterizing output variability from 553 homes with residential PV systems on a distribution feeder*. https://doi.org/10.2172/1035324

Syranidis, K., Markowitz, P., Linssen, J., Robinius, M., & Stoltcn, D. (2018). Flexible Demand for Higher Integration of Renewables into the European Power System. *2018 15th International Conference on the European Energy Market (EEM)*, 1–6. https://doi.org/10.1109/EEM.2018.8469962

Syranidou, C., Linssen, J., Stolten, D., & Robinius, M. (2020). Integration of Large-Scale Variable Renewable Energy Sources into the Future European Power System: On the Curtailment Challenge. *Energies*, *13*(20), 5490. https://doi.org/10.3390/en13205490

Tsai, C.-T., Beza, T. M., Molla, E. M., & Kuo, C.-C. (2020). Analysis and Sizing of Mini-Grid Hybrid Renewable Energy System for Islands. *IEEE Access*, *8*, 70013–70029. https://doi.org/10.1109/ACCESS.2020.2983172

Turkish State Meteorological Service. (2022). https://www.mgm.gov.tr/eng/forecast-cities.aspx?m=Ankara

U.S. Energy Information Administration. (2022). *Hourly Electric Grid Monitor*. https://www.eia.gov/electricity/gridmonitor/dashboard/electric_overview/regional/REG-NE

Windfinder. (2022). *Meno/Columbia River Gorge*. https://www.windfinder.com/forecast/meno_columbia_river_gorge

Zappa, W., & van den Broek, M. (2018). Analysing the potential of integrating wind and solar power in Europe using spatial optimisation under various scenarios. *Renewable and Sustainable Energy Reviews*, *94*, 1192–1216. https://doi.org/10.1016/j.rser.2018.05.071

Zhang, B., & Kezunovic, M. (2016). Impact on Power System Flexibility by Electric Vehicle Participation in Ramp Market. *IEEE Transactions on Smart Grid*, *7*(3), 1285–1294. https://doi.org/10.1109/TSG.2015.2437911

Zsiborács, H., Baranyai, N. H., Vincze, A., Zentkó, L., Birkner, Z., Máté, K., & Pintér, G. (2019). Intermittent Renewable Energy Sources: The Role of Energy Storage in the European Power System of 2040. *Electronics*, *8*(7), 729. https://doi.org/10.3390/electronics8070729

e-ISSN 2757-5195

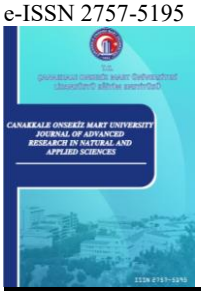

Çanakkale Onsekiz Mart University

Journal of Advanced Research in Natural and Applied Sciences

Open Access

doi.org/10.28979/jarnas.1119957 2023, Vol. 9, Issue 1, Pages: 205-217 dergipark.org.tr/tr/pub/jarnas

A Modified Dijkstra Algorithm for ROS Based Autonomous Mobile Robots

Orkan Murat Çelik[1], Murat Köseoğlu[2,*]

[1]Havelsan A.Ş., Ankara, Türkiye
[2]Department of Electrical-Electronics Engineering, Faculty of Engineering, Inonu University, Malatya, Türkiye

Article History

Received: 23.05.2022

Accepted: 08.12.2022

Published: 05.03.2023

Research Article

Abstract − Autonomous Mobile Robots (AMRs) are frequently used in many fields of technology. In this study, an AMR was designed to execute different path planning algorithms. Firstly, working principle, system architecture and motion planning of AMR are presented. Then, a map for the current environment is produced by a Robot Operating System (ROS) powered AMR which was designed for this study. The AMR locates itself on the produced map with the aid of an integrated Light Detection and Ranging sensor (LIDAR). The locomotion of AMR to a user-defined target on the produced map is performed by an optimal path based on AMR's own navigation plan. Two different path planning algorithms, which are Dijkstra's algorithm and a modified version of Dijkstra's algorithm, are executed on a cost-effective AMR platform, which has the capability of Simultaneous Localization and Mapping (SLAM). The reason why Dijkstra algorithm is handled in this study rather than A*, D* and RRT algorithms is that this algorithm is a basic and widely used algorithm. Dijkstra's algorithm is modified, and pros and cons of the modified algorithm are analysed compared to Dijkstra algorithm. The proposed algorithm and navigation of AMR are tested both in real time in real world and as a simulation in Gazebo. Two algorithms were compared according to the results obtained from the robot locomotion both in real application and simulation environment. It is observed that the modified version of the Dijkstra's algorithm comparatively yielded a bit more satisfactory results in the aspect of path planning.

Keywords − *AMR, dijkstra algorithm, path planning, robot navigation, ROS*

1. Introduction

Different robotic technologies and production methods based on the robots, which have been increasingly involved in production in recent years, have rapidly developed and evolved to high levels, especially after the 3rd Industrial Revolution. When the robots were first used in the industry, it was aimed to perform a predefined task at a certain time and with a certain quality in the production process. Since the main purpose of most of the industrial robots produced until today is to perform a defined task, it was sufficient to simply program and use the robots in accordance with the requirements of the production line. However, as the production of different items have become more complex in several industrial fields, it has become a necessity to evolve production techniques to adapt to the resulting complexity. Depending on the technological developments and requirements, some major improvements have been made in robot designs, and the robots have been technologically updated in accordance with the requirements. In this way, it has been possible for robots to adapt to the developing industry. As a result of the complexity brought by the developing technology, it has become inefficient to use industrial robots only for a specific job. Accordingly, Autonomous Guided Vehicles (AGV), which were widely used in the industry, have led up the development of AMRs (Autonomous Mobile Robot). Since the AMRs have a considerable locomotion capability, they can perform complex tasks under

[1] orkanmcelik@gmail.com
[2] murat.koseoglu@inonu.edu.tr
[*]Corresponding Author

different working conditions and environments, such as disaster relief operations, factories and restaurants. Depending on their interacting environment, they can be classified as aquatic, terrestrial and airborne (Ben-Ari Mordechai and Mondada, 2018). Arkin and Murphy emphasized the importance of autonomous navigation and AMRs in the industrial plants and flexible production systems in future. They also gave comparative basic information on autonomous robot architecture and explained the disadvantages of AGVs (Arkin & Murphy, 1990). Efficient navigation is one of the most important capabilities of autonomous mobile robots (AMRs) to successfully perform industrial tasks, especially in irregular environments with moving obstacles (Nguyen et al., 2022).

An AMR is capable of navigating in an unpredictable environment. AMRs can sense the environment, create a model based on the environmental properties and locate itself in this model. This capability enables AMR to make a navigation plan and optimize this plan by a special planning algorithm. This is known as simultaneous localization and mapping (SLAM) (Köseoğlu et al., 2017). As the environmental flexibility increases, the AMRs have been used for different scenarios in a wide range of industrial applications. (Pagani et al., 2018).

When a task is assigned to an AMR, it plans how to perform this task, then it performs this task according to this plan. The AMR makes this plan by using several algorithms, which work on itself and include flexible steps defining how to this task will be performed. This process is called autonomy.

In this study, an AMR, which performs the movement task by using Dijkstra's Shortest Path Algorithm and Modified Dijkstra's Shortest Path Algorithm, is developed. Then, the performance of the AMR is analyzed for these algorithms, comparatively. In the locomotion process, the AMR localizes itself in the current environment by using SLAM algorithm and completes its movement from an initial point to a target point which is defined by the user.

2. Materials and Methods

In this section, some basic concepts, methods and tools, which are used in the movement and path planning of the AMRs, are presented.

2.1. Design of the AMR

The AMR used in this study was designed cost-effectively by using off-the-shelf commercial products. Details of hardware is explained below:

- A Raspberry Pi 2 Model B was used as single board computer (SBC) for the Operating System (Ubuntu 14.04) and ROS (Indigo). All of the robotic algorithms were executed on the SBC.
- An STM32F4 Discovery was used as the peripheral controller which is gathering data from the sensor and driving the motors for locomotion. The software developed for the peripheral controller uses FreeRTOS to keep all tasks running in real time.
- An RpLidar A1 that collects point cloud data for SLAM algorithms was used to create a map describing the perimeter of the AMR.
- As actuator two 12V 76 RPM gear motors were used. Each motor has a 64 CPR quadrature encoder at the motor shaft for the odometry calculation with the direction information. The motor was driven by PID signals which generated by the peripheral controller based on the velocity signal which calculated by the ROS algorithms.
- A 9 DOF RazorIMU was used for the odometry correction based on Extended Kalman Filter.

2.2. Localization

For a mobile robot, localization means that the robot positions itself on the environment in which it will move. In robotics, localization is an important problem. Since all the movement of the mobile robot is estimated based on an initial point, its position must be determined accurately for the movement planning to take place as intended. Position of an autonomous robot can be described as a vector given in Equation 2.1 in the Cartesian coordinate system as seen in Figure 1. In this figure, x is the position component on the X axis,

y is the position component on the Y axis, and θ is the heading angle. v(t) is the velocity, and w(t) is the rotation speed of the robot.

$$p = \begin{bmatrix} x \\ y \\ \theta \end{bmatrix} \tag{2.1}$$

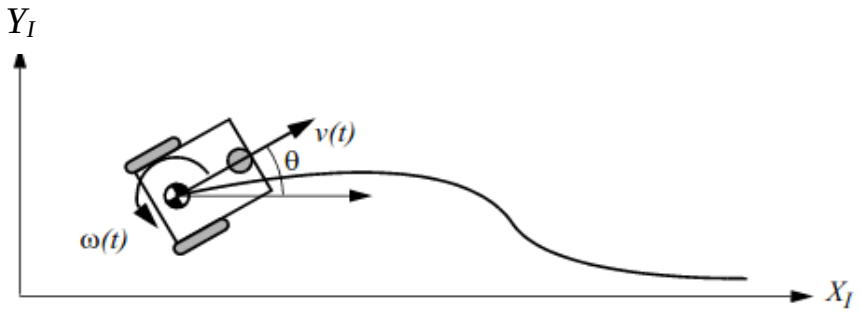

Figure 1**.** Position and Movement of a differential-drive robot (Siegwart et al., 2011).

2.3. Dead Reckoning

Dead reckoning means that the next position of a moving object is estimated based on its previous position. In addition to being an important position estimation method especially in aerial and nautical vehicles, it is also frequently used in mobile robotics. Making an estimation based on the latest velocity and obtained direction data is an important issue for dead reckoning (Tsai, 1998). It should be noted that the difference between the estimated location and the actual location can increase by the use of former velocity and direction data.

2.4. Mapping

2.4.1. Map Based Localization

The environment can be expressed in a Cartesian coordinate system, and the position of the robot can be shown on the coordinate plane for a robot moving on a flat surface. In addition, a map can be created with the help of SLAM algorithms and a sensor (Lidar, Stereo Camera, etc.) placed on the robot. The map which is created by the robot used in this study is given in Figure 2.

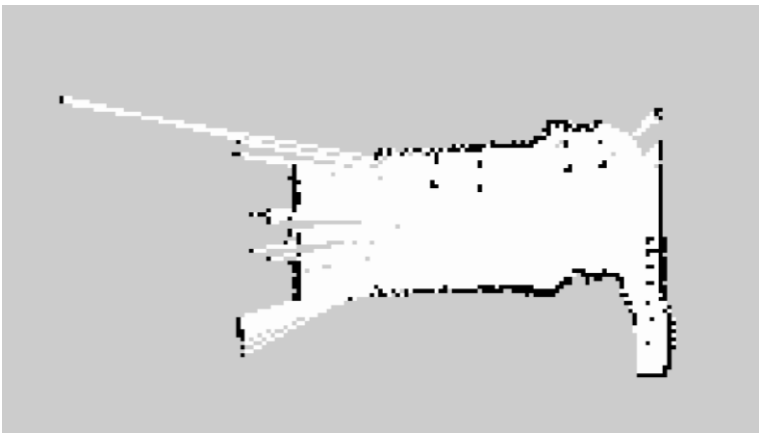

Figure 2. A map example that was created by the designed robot for this study.

2.4.2. Simultaneous Localization and Mapping (SLAM)

SLAM is the building of an environmental model of the environment in which a mobile robot is located, positioning itself in the model it creates and mapping its surroundings according to the created environmental model (Wolf & Sukhatme, 2005). Various sensors have been developed for SLAM to solve the fundamental problem of finding robot position in a global representation (Merzlyakov & Macenski, 2021).

For most of the SLAM algorithms, the robot continually updates and expands the environmental model while it is in motion (Durrant-Whyte & Bailey, 2006). In other words, the map created by SLAM is a dynamic map. In Figure 3, the position of the robot is shown on the map based on SLAM.

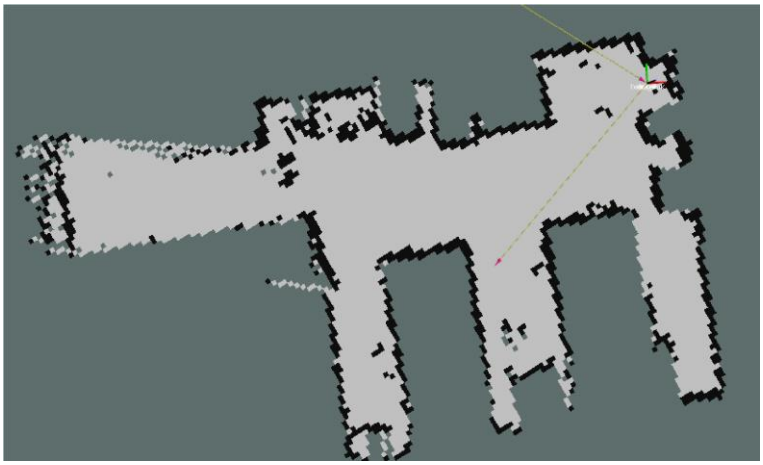

Figure 3. SLAM example which was created by the designed robot for this study.

The SLAM can be explained mathematically by following steps:

Position of the robot (X_T) at each sample time T can be expressed as

$$X_T = \{x_0, x_1, x_2, \dots, x_T\} \tag{2.2}$$

If the motion of the robot in the time interval of $T-1$ and T is expressed as U_T, and it is assumed that the motion data is obtained from encoder readings or control inputs to the motor, the time dependent motion of the robot can be written as:

$$U_T = \{u_0, u_1, u_2, \dots, u_T\} \tag{2.3}$$

Accordingly, if it is assumed that the value of m_i represents the objects around the robot, M is expressed as:

$$M_T = \{m_0, m_1, m_2, \dots, m_{n-1},\} \tag{2.4}$$

Assuming that each sensor on the robot takes only one measurement at a time, we can express the entire measurement for one sensor as follows:

$$Z_T = \{z_0, z_1, z_2, \dots, z_T,\} \tag{2.5}$$

According to the stated terminology, we can accept SLAM as a structure that improves the map model (M) and the path of the robot according to the data obtained from position (X_T), odometry (U_T) and observations (Z_T). There are two different algorithms as full SLAM and online SLAM that are used by AMRs. AMR can follow many different paths composed of consecutive joints on the map to reach the target point. The probability of the next joint to be followed by AMR along the full SLAM $X_{T,}$ depends on different parameters, and this relationship is represented by the following equation:

$$p\{X_T, M \vee Z_T, U_T\} \tag{2.6}$$

A difference between the full SLAM and online SLAM can be explained as follows: In online SLAM, x_t shows the next common probability along M for the next joint to be followed. As seen, full SLAM tries to estimate the entire path (X_T) of the robot, while online SLAM only shows the current position (x_t).

2.5. Navigation and Motion

Autonomous navigation is the autonomous movement of the robot from its current location to a target point, which is located on the map defined by the SLAM algorithm previously. Navigation generally works based on odometry data which is provided by the encoders. Velocity and steering commands, which are calculated by using sensor data, are transmitted to the robot's controllers. In the current study, steering commands are also transmitted to the controllers as velocity information, since the designed robot is a specific robot that moves with a differential driving system. However, there are some important concepts that should be known in the navigation process. These concepts can be explained as:

***TF*:** TF is a package that lets the user keep track of multiple coordinate frames over time. TF maintains the relationship between coordinate frames in a tree structure buffered in time, and lets the user transform points, vectors, etc. between any two coordinate frames at any desired point in time (*Http://Wiki.Ros.Org/Tf*, 2021).

***Odometry*:** A mobile robot uses odometry data to track its movement as it navigates a familiar environment. However, any uncertainty in the odometry data confuses the robot about its current position. (Panigrahi & Bisoy, 2021). Odometry can be defined as the relative position determination of a robot according to the surrounding objects with the help of integrated sensors such as IMU, encoder, etc. For example, if the circumference and the number of rotations of the wheels of a mobile robot are known, the path length and displacement of the robot can be calculated according to its initial position. Because odometry calculations are generally based on the result of the sensor data, the result of erroneous readings from the sensors makes the calculations increasingly inaccurate.

In this study, as primary sensor readings for odometry calculations, 2 channel quadrature encoders are used. In addition to the velocity information, the direction of the rotation of the motor can be obtained by quadrature encoders due to 90 degrees phase shift between 2 channels of encoders. However, in case of misreading from the encoder, the Navigation system uses an IMU (Inertial Measurement Unit) to make more accurate odometry calculations. For more accurate odometry calculations, sensor readings are combined by EKF (Extended Kalman filter) which is one of the sensor fusion algorithms.

***EKF (Extended Kalman Filter)*:** Almost all sensors, which are used in robotics, generate some noise associated with the measured signals during the measurement process. This noise quite affects the system and navigation performance negatively. If there is a Gaussian noise, which may cause a deterioration in the system, the Kalman filter significantly reduces the average measurement error in a gradual way. Thus, the Kalman filter used in the system is a causal filter, which operates by considering the former measurements.

An EKF generally reduces a nonlinear system model to a linear system for each sample time. For a system, which includes a single variable, this process uses the current value of the variable and the derivative of that variable at each sample time. However, in a system with several variables, Jacobian matrices are used to analyze and obtain an approximate linear model of the system. The general expression of EKF can be written as below:

$$x_k = Ax_{(k-1)} + Bu_k + w_{(k-1)} \quad (2.7)$$

$$z_k = Hx_k + v_k \quad (2.8)$$

In Equations 2.7 and 2.8, k describes the measurement number (for each separate measurement), x_k is the instant signal value, $x_{(k-1)}$ is the previous instant signal value, u_k is the control signal, $w_{(k-1)}$ describes the disturbances, z_k is the sensor measurement, v_k is the sensor disturbance, A is the state matrix, B is the input matrix and H is the observation matrix. When Equations 2.7 and 2.8 are considered, it can be clearly seen that EKF cannot predict the position of the robot for the non-gaussian values of the $w_{(k-1)}$ and v_k.

EKF is implemented in 2 stages. First stage is the prediction phase and can be written as:

$$\hat{x}_k^- = A\hat{x}_{k-1} + Bu_k \quad (2.9)$$

$$\hat{P}_k^- = AP_{k-1}.A^T \quad (2.10)$$

In Equations 2.9 and 2.10, k is the index term for the measurement, $\hat{x}_k^-$ is the predicted value, $\hat{x}_{k-1}$ is the previous predicted value, u_k is the control signal applied to the system, $\hat{P}_k^-$ is the error covariance and P_{k-1} is the former error covariance. When the prediction equations are inspected, these equations show that $\hat{x}_k^-$ element expresses a general prediction for the first loop of the filter due to the update process after prediction phase. The same methodology is valid for the calculation of $\hat{P}_k^-$. The main duty of the prediction phase is to stabilize the filter output with calculation of variables at the update phase.

Second stage of EKF is the update phase and can be expressed with three equations which are written below:

Calculation of the Kalman filter gain:

$$K_k = P_k^- H^T (HP_k^- H^T + R)^{-1} \quad (2.11)$$

- Prediction Update by Sensor Measurements:

$$\hat{x}_k = \hat{x}_k^- + K_k(Z_k - H\hat{x}_k^-) \quad (2.12)$$

- Updating of Error Covariance:

$$P_k = (1 - K_k H)P_k^- \quad (2.13)$$

When Equations 2.11, 2.12 and 2.13 are examined, it's clearly shown that these equations have analogies with the standard Kalman Filter equations. In each cycle of the filter, the prediction and update phases work recursively. It can be seen that each sensor measurement should be defined with an independent and different Z variable in Equation 2.12. Thus, sensor fusion must be set according to the weight of each different Z variable.

***Navigation Methodology*:** Navigation planning for an autonomous mobile robot could be basically described as motion planning from a specific initial point to a target point which is defined by the user. Basically, the

success of navigation planning is measured by whether it is heuristic or not. A heuristic navigation algorithm should create the shortest path to the target point.

Based on the data acquired from the environment, there are two types of motion planning approaches, namely global path planning and local path planning. If the environment is well known, it is identified as global path planning, and the motion planning serving in unknown environment is identified as local path planning (Tang SH & Zulkifli N, 2015).

In this study Dijkstra's Algorithm was used as a global path planning algorithm. Dijkstra's algorithm is an algorithm for finding the shortest paths between the nodes in a graph (*Dijkstra's Algorithm*, 2021; Iscan & Tuncel, 2022). Dijkstra is a breadth-first-search (BFS) algorithm for finding the shortest paths from a single source vertex to all other vertices, and it is able to produce the shortest route (Fadzli et al., 2015; Kumar & Gao, 2021).

Dijkstra's algorithm is a simple but powerful method (Guo, 2013). When the robot is located on a well-defined and mapped environment, the algorithm can calculate the heuristic path swiftly. According to the algorithm, the initial point of the robot could be described as the first node, and the desired point could be described as the last node. Dijkstra's method is a method that can determine the shortest route from the boarding point to the arrival point by the smallest weight (Hartomo et al., 2019).

The algorithm used in this study is given below:

Step 1: To calculate the shortest path from an initial node to a target node, an empty array/list is created to keep vertices which generate the path tree.

Step 2: All the nodes except the initial node are defined as unvisited nodes, and the initial distances of all unvisited nodes are set as infinite. The distance of the initial node is set to zero.

Step 3: Each distance value is calculated from initial node (Current node) to neighbor nodes. The shortest distance value is appended to the shortest path list as an element. Along the path finding process, this step is applied between each current node and neighboring node. After the end of calculation step for each node, the current node is removed from the unvisited nodes list and appended to the visited nodes list. Third step is applied until the target node is found.

Step 4: When the robot arrives to the target node, the algorithm ends.

When Dijkstra's Algorithm is compared with the other weighted algorithms, it can be seen that it is one of the simplest implementable algorithms (Kumar & Gao, 2021). Also, it has a flexible structure and can be modified conveniently to find the most available path on the map. Calculation cost of the algorithm is very low since the algorithm is based on the basic mathematical calculations. To calculate the most available path, the robot can try a few of the existing modified algorithms. In this study, the original Dijkstra's algorithm and modified Dijkstra's algorithm are tested on an AMR comparatively. The evaluations are presented in the next section.

3. Results and Discussion

ROS is a widely used platform for robot's implementation (Ochiai et al., 2014; Zaman et al., 2011). ROS official packages are adequate in common robotics tasks. Furthermore, ROS provides API to build custom packages or communicate with external systems or equipment e.g. interfaces and planner (Ochiai et al., 2014).

In this study, a ROS based differential drive AMR was designed for the implementation of Dijkstra's algorithm (Figure 4). The AMR is a custom design, and it has own lidar sensor to identify environment and generates a map by Hector SLAM package, and the ROS software version preferred in this study is the ROS indigo. The nodes in the Dijkstra's algorithm were determined as the vertices of grids on the map. By this way, each corner on the map could be described as a node.

The nodes were clearly shown on the map in Figure 5. This figure shows a navigation plan which is denoted by a thin red line. The navigation plan was prepared based on Dijkstra's original algorithm. The green dot shows the initial node, and the purple one shows the target node. The thick red arrow shows the motion of the robot. Along the study, robot actuators have been driven by the Proportional-Integral-Derivative (PID)

algorithm, which is designed for this study. Although there are different tuning methods such as Ziegler–Nichols and Tyreus Luyben, the PID coefficients in this study were tuned by try and error method due to the ease of application. The same PID parameters were used in all of navigation plans. The simplicity and fast computation of the PID controller made it the most popular low-level control strategy, and it is currently implemented in several mobile robots' control systems (Carlucho et al., 2019). For this reason, PID controller is selected as a motion control method. As seen in Figure 5, the robot has reached the target point by using its own navigation plan. When Figure 5 is inspected, the entire navigation plan passes through the nodes on the map until it reaches the target point. So, the robot has applied almost the same plan toward to the target point, but there is a little deviation from the plan due to physical reasons such as the features of the motors, PID algorithm tolerance and encoder counts. However, the heading angle of the robot, which is described with a thick arrow cone, is directed to the target node. For these reasons, there is a particularly small deviation according to the navigation plan. When the same algorithm is applied for a different target as shown in Figure 6, the observed deviation is more than the deviation shown in Figure 5.

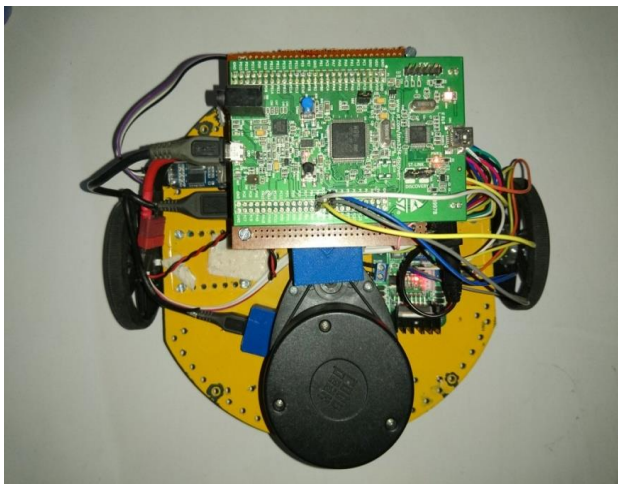

Figure 4. The designed AMR for this study

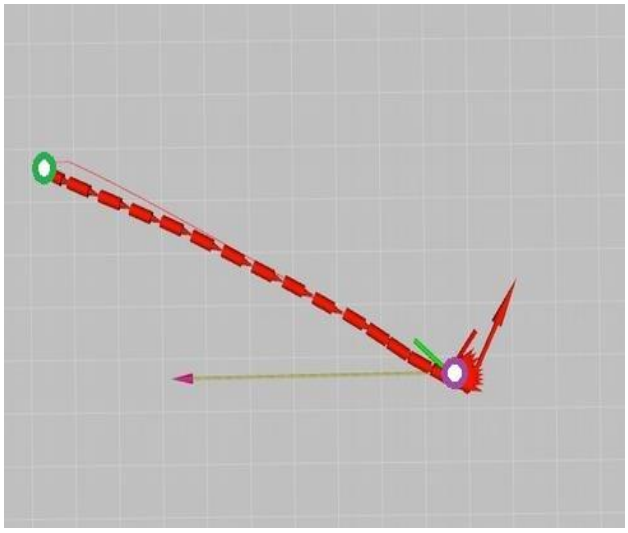

Figure 5. Nodes and navigation plan on the map

When the motion, which is shown in Figure 6, is compared with the motion shown in Figure 5, it is seen that the main difference in the beginning of the motions is the initial head angle of the robot. The target is defined almost 90 degrees on the left side of the initial heading of the robot. According to the illustration in Figure 6, the navigation plan is almost the same as the plan that is shown in Figure 5. In the implementation of the navigation plan, which is shown in Figure 6, the robot has started its motion by rotating heading angle. The linear motion of the robot does not start until the error between the navigation plan and the robot's head angle decreases. Along all motion tracks from start point to target point, a little deviation can be seen on the motion. The deviation is thought to arise from the non-ideal PID algorithm.

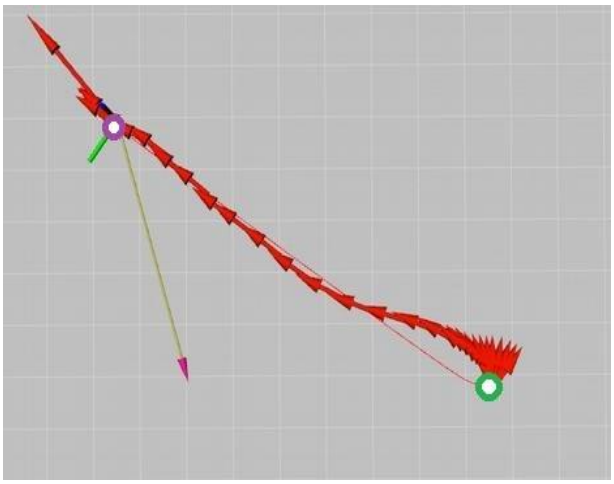

Figure 6. Dijkstra's algorithm-based navigation plan and motion trail on the map

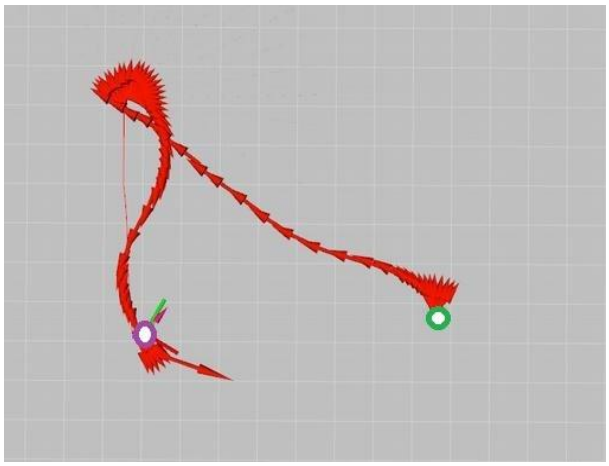

Figure 7. Modified Dijkstra's algorithm-based navigation plan and motion trail on the map

Figure 7 shows the application of a navigation plan, which is shown by a thin red line, based on the Modified Dijkstra's algorithm. The modified Dijkstra's algorithm predicts the path by using the basic estimation principles of conventional Dijkstra's algorithm except the third step of the algorithm. According to the original algorithm's third step, the algorithm just calculates the distances between the neighbour nodes. The modified algorithm uses the same calculation methodology of the classic Dijkstra's algorithm, but as a difference, the modified algorithm also calculates the further neighbours' successive node distances after the existing node while the neighbour's node distances are calculated. Main aim of the modified algorithm is to search the possible shorter navigation paths as well as possible.

When Figure 7 is inspected, the robot navigation could be described in two stages. The first stages of both two navigation algorithms are similar as seen in Figure 5 and Figure 6. In the second stage of the navigation algorithm, the target point has been defined at 135 degrees left from the robot's heading. The motion of the

robot is illustrated with a red thick curved line in Figure 7. The curve results from the calculation of the third step of the modified algorithm. According to the modified algorithm, the navigation plan is shown to be more optimistic than the conventional algorithm due to the soft direction changes which are predicted. It is thought that the unexpected slight deviations arise from the non-ideal tuning of PID algorithms, and some problems encountered in practice due to the component tolerances.

As mentioned above, at first, a real ROS Indigo based AMR was developed in the study. The proposed algorithm and the classical Dijkstra algorithm were practically executed and compared by using this robot. Then, the same algorithms were executed and compared in Gazebo simulation environment which includes obstacles. This simulation environment was constructed by using ROS Humble-based Turtlebot3, and the comparison was made by considering both two path plans in this environment. These two path plans are presented in Figure 8 and Figure 9. In both path plans, it has been observed that the modified Dijkstra algorithm produces approximately 1% to 3% shorter paths than the classical Dijkstra algorithm.

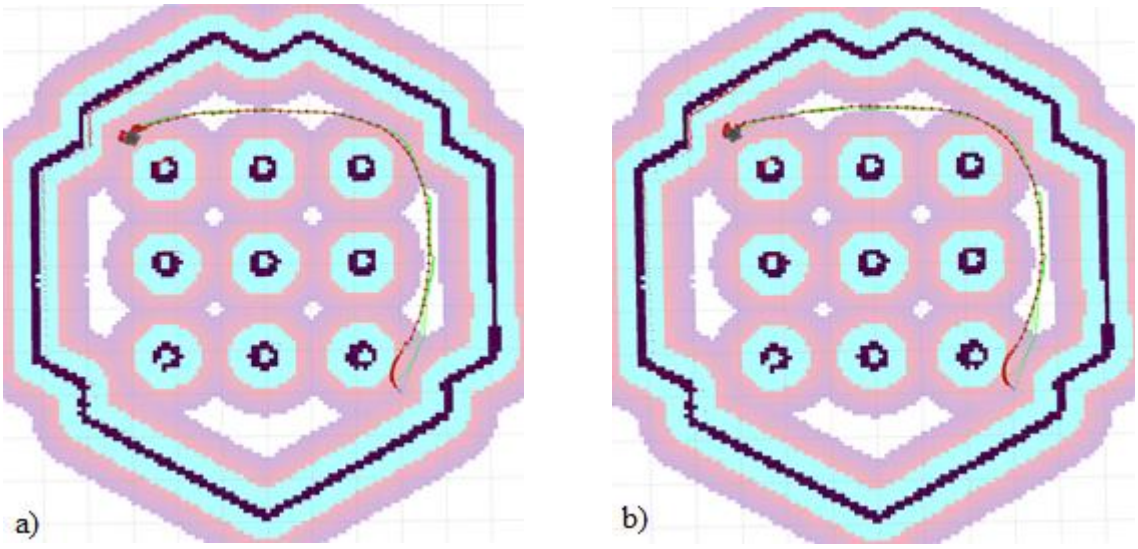

Figure 8. The movement of AMR by considering the Classical Dijkstra (a) and Modified Dijkstra (b) algorithms for path planning in Gazebo TurtleBot World environment.

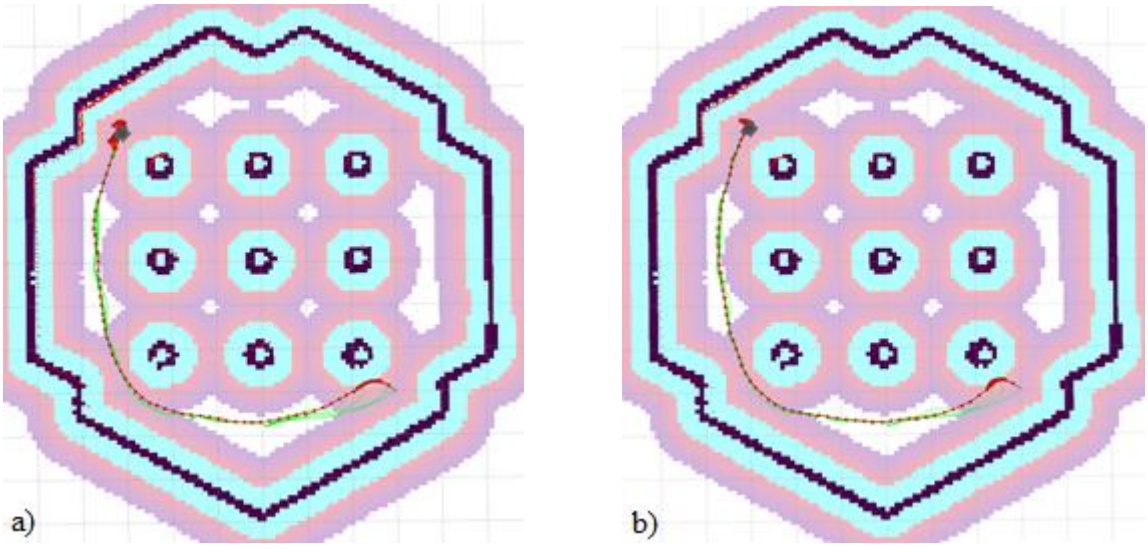

Figure 9. The movement of AMR by considering the Classical Dijkstra (a) and Modified Dijkstra (b) algorithms for path planning in Gazebo TurtleBot World environment.

In Figure 8a, the path, which is obtained by the classical Dijkstra algorithm, and the movement of the robot on this path planning are presented. This algorithm is simulated on ROS Humble using Gazebo and Rviz with a plugin written on the Navigation2 stack. The Navigation2 stack was designed for a high-degree of

configurability and future expansion (Macenski et al., 2020). In Figure 8b, the path planning obtained by the modified Dijkstra algorithm and the movement of the robot, which is simulated as in Figure 8a, are shown. The red line indicates the odometry data of the robot's movement on the plan, while the green lines indicate the dynamic path plan produced by the algorithm. The navigation2 stack has its own distance measuring tool. All distance measurements of the path plans used in this study were obtained by using the Distance Remaining data on the Navigation2 panel on Rviz.

The reason why the green lines are constantly changing throughout the robot's movement is that the Navigation2 stack dynamically updates the movement plan by making a cost-based planning. As seen in Figures 8a and 8b, the path length between the starting point and final point of the movement was measured as 651 cm for classical Dijkstra algorithm, while it was measured as 631 cm for the proposed algorithm. In the same way for the other path planning, the path length between the starting point and final point of the movement was measured as 640 cm for classical Dijkstra algorithm (see Figure 9a), while it was measured as 633 cm for the proposed algorithm (see Figure 9b).

As seen in Figure 8 and Figure 9, there are cylindrical obstacles in the environment. The path planning and the simulation are realized by considering the cost values based on Navigation2 stack around these obstacles. The cost values are determined according to the risk factor around each obstacle. The risk factor is a quantitative value and expresses the crash risk of the robot in the environment during the movement.

Both the classic Dijkstra algorithm and the modified Dijkstra algorithm try to achieve small cumulative cost value for the planned route by trying to minimize the cost value for each step while planning the navigation. In this context, the magenta-colored regions on the images represent high-cost zones, the blue-colored regions represent the zones with medium-cost values, and the white-colored regions represent low-risk zones.

4. Conclusion

The Dijkstra's Shortest Path Algorithm is one of the common path planning algorithms in mobile robotics. Due to the current pace of mobile robotics, the algorithm should be upgraded to different variations to improve the task completion performance. In this study, Dijkstra's Shortest Path Algorithm is modified by continuously estimating the node distances for two successive steps between two successive neighbors in addition to the estimation of different neighbor node distances for only one step. Thus, to find the other optimal paths for the robot, the AMR does not only consider the next shortest node distance, but it also estimates the total shortest path for successive two steps by summing two distances between subsequent nodes. The proposed algorithm gives promising results in terms of total estimation time as well as optimal path planning. When the experimental and simulation results based on the conventional Dijkstra's algorithm and proposed modified algorithm are compared, it is observed that the proposed Modified Dijkstra's algorithm has exhibited a little bit better performance in terms of navigation path planning and estimation time. Also, when the tests made in Gazebo environment are considered, it was seen that the proposed algorithm has yielded 1% to 3% shorter path distances compared to Dijkstra's Shortest Path Algorithm. It is certain that more experiments should be done, considering many more scenarios, to obtain a generalized statement about the efficiency of the proposed method. However, since the path planning capability and the velocity of decision-making process have increased, the hardware components such as sensors and actuators, which have more accurate responses in shorter reaction times, are recommended to be provided. In the future works, it is aimed to implement the fractional order control methods or model predictive control methods in order to improve the navigation path planning of the AMR for the robots which have fast decision-making processes. Also, it is planned to carry out a new study regarding the development of the proposed algorithm and its comparison with the A* and D* algorithms on a more advanced robot.

Acknowledgement

This work was supported by Inonu University, Scientific Research Projects Coordination Unit (BAP) [Grant number FDK-2022-2777].

Author Contributions

Orkan Murat Çelik: Prepared the experimental environment, conducted the experiments and simulations, analysed the received data and contributed to all stages of the article.

Murat Köseoğlu: Designed the study, performed analyses, contributed to all stages of the article as the supervisor.

Conflicts of Interest

The authors declare no conflict of interest.

References

Arkin, R. C., & Murphy, R. R. (1990). Autonomous navigation in a manufacturing environment. *IEEE Transactions on Robotics and Automation*, *6*(4), 445–454. https://doi.org/10.1109/70.59355

Ben-Ari Mordechaiand Mondada, F. (2018). Robots and Their Applications . In *Elements of Robotics* (pp. 1–20). Springer International Publishing. https://doi.org/10.1007/978-3-319-62533-1_1

Carlucho, I., De Paula, M., & Acosta, G. G. (2019). Double Q-PID algorithm for mobile robot control. *Expert Systems with Applications*, *137*, 292–307. https://doi.org/https://doi.org/10.1016/j.eswa.2019.06.066

Dijkstra's algorithm. (2021). https://en.wikipedia.org/wiki/Dijkstra%27s_algorithm

Durrant-Whyte, H., & Bailey, T. (2006). Simultaneous localization and mapping: part I. *IEEE Robotics Automation Magazine*, *13*(2), 99–110. https://doi.org/10.1109/MRA.2006.1638022

Fadzli, S. A., Abdulkadir, S. I., Makhtar, M., & Jamal, A. A. (2015). Robotic Indoor Path Planning Using Dijkstra's Algorithm with Multi-Layer Dictionaries. *2015 2nd International Conference on Information Science and Security (ICISS)*, 1–4. https://doi.org/10.1109/ICISSEC.2015.7371031

Guo, C. (2013). A Solution to Best Itinerary Problem Based on Strategy Set under Dijkstra Algorithm. *Applied Mechanics and Materials*, *333–335*, 1442–1445. https://doi.org/10.4028/www.scientific.net/AMM.333-335.1442

Hartomo, K., Ismanto, B., Nugraha, A., Yulianto, S., & Laksono, B. (2019). Searching the shortest route to distribute disaster's logistical assistance using Dijkstra method. *Journal of Physics: Conference Series*, *1402*(7), 77014. https://doi.org/10.1088/1742-6596/1402/7/077014

http://wiki.ros.org/tf. (2021).

Iscan, H., & Tuncel, E. (2022). TurtleBot 3 İle Ros Tabanlı Yol Planlama Uygulaması. European Journal of Science and Technology. https://doi.org/10.31590/ejosat.1081097

Köseoğlu, M., Çelik, O. M., & Pektaş, Ö. (2017). Design of an autonomous mobile robot based on ROS. *2017 International Artificial Intelligence and Data Processing Symposium (IDAP)*, 1–5. https://doi.org/10.1109/IDAP.2017.8090199

Kumar, A., & Gao, N. (2021). *Optimization of Distributıon Route Using Dijkstra's Based Greedy Algorithm : Case of Retaıl Chain*. *6*(8), 186–190.

Macenski, S., Martin, F., White, R., & Clavero, J. G. (2020). The Marathon 2: A Navigation System. 2020 IEEE/RSJ International Conference on Intelligent Robots and Systems (IROS), 2718–2725. https://doi.org/10.1109/IROS45743.2020.9341207

Merzlyakov, A., & Macenski, S. (2021). A Comparison of Modern General-Purpose Visual SLAM Approaches. 2021 IEEE/RSJ International Conference on Intelligent Robots and Systems (IROS).

Nguyen, T. Van, Do, M. H., & Jo, J. (2022). MoDeT: a low-cost obstacle tracker for self-driving mobile robot navigation using 2D-laser scan. Industrial Robot, ahead-of-p(ahead-of-print). https://doi.org/10.1108/IR-12-2021-0289/FULL/PDF

Ochiai, Y., Takemura, K., Ikeda, A., Takamatsu, J., & Ogasawara, T. (2014). Remote control system for multiple mobile robots using touch panel interface and autonomous mobility. *2014 IEEE/RSJ International Conference on Intelligent Robots and Systems*, 3272–3277. https://doi.org/10.1109/IROS.2014.6943017

Pagani, P., Colling, D., & Furmans, K. (2018). A Neural Network-Based Algorithm with Genetic Training for a Combined Job and Energy Management for AGVs. Logistics Journal : Proceedings, 2018(01). https://doi.org/10.2195/lj_Proc_pagani_en_201811_01

Panigrahi, P. K., & Bisoy, S. K. (2021). Localization strategies for autonomous mobile robots: A review. *Journal of King Saud University - Computer and Information Sciences*.

https://doi.org/https://doi.org/10.1016/j.jksuci.2021.02.015

Siegwart, R., Nourbakhsh, I. R., & Scaramuzza, D. (2011). *Introduction to Autonomous Mobile Robots* (Second Edi, Vol. 5). The MIT Press.

Tang SH, K. F., & Zulkifli N, K. W. (2015). A Review on Motion Planning and Obstacle Avoidance Approaches in Dynamic Environments. Advances in Robotics & Automation, 04(02). https://doi.org/10.4172/2168-9695.1000134

Tsai, C.-C. (1998). A localization system of a mobile robot by fusing dead-reckoning and ultrasonic measurements. *IEEE Transactions on Instrumentation and Measurement*, *47*(5), 1399–1404. https://doi.org/10.1109/19.746618

Wolf, D. F., & Sukhatme, G. S. (2005). Mobile Robot Simultaneous Localization and Mapping in Dynamic Environments. *Autonomous Robots*, *19*(1), 53–65. https://doi.org/10.1007/s10514-005-0606-4

Zaman, S., Slany, W., & Steinbauer, G. (2011). ROS-based mapping, localization and autonomous navigation using a Pioneer 3-DX robot and their relevant issues. *2011 Saudi International Electronics, Communications and Photonics Conference (SIECPC)*, 1–5. https://doi.org/10.1109/SIECPC.2011.5876943

e-ISSN 2757-5195

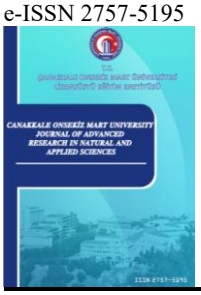

Çanakkale Onsekiz Mart University

Journal of Advanced Research in Natural and Applied Sciences

Open Access

doi.org/10.28979/jarnas.1180443 2023, Vol. 9, Issue 1, Pages: 218-227 dergipark.org.tr/tr/pub/jarnas

Evaluating of Bean (*Phaseolus vulgaris* L.) Cultivars for Boron Efficient and Tolerant

Fatma Gökmen Yılmaz[1,*], Ayşegül Korkmaz[2], Sait Gezgin[3]

[1,2,3]Department of Soil and Plant Nutrition, Faculty of Agriculture, Selçuk University, Konya, Türkiye

Article History

Received: 26.09.2022

Accepted: 22.11.2022

Published: 05.03.2023

Research Article

Abstract – This study was carried out in a greenhouse in 2021 to determine the boron response of some bean cultivars at increasing levels of boron doses. The experiment established according to the complete randomized design with three replications was applied to 15 registered bean cultivars at 0, 5, and 10 mg B/kg doses using $Na_2B_8O_{13}.4H_2O$ (20.8% B) fertilizer. The above-ground organs were harvested during the blooming period, and the cultivars of B-efficient and B-tolerant were determined in the investigation of their dry weight, B content, and concentrations. Dry weights increased by 1% (Doruk, 10 mg B/kg) and 38% (Kantar-05, 5 mg B/kg) under B conditions, compared with the non-treatment group. Furthermore, insufficient B levels in the soil conditions were evaluated as B-efficient bean cultivars having a dry weight above the average, but cultivars having a dry weight below the average were named B-tolerant cultivars. As a result of the study, it was determined changing depends on the boron application of boron efficient (B-effect) and boron tolerant (B-tolerant) bean cultivars. Cihan, Güngör, Berrak, Elkoca-05, Özdemir, Kantar-05 and Arslan cultivars were confirmed as B-efficient, although Zülbiye, Sururbey, Doruk, Göksun, Karacabey, Özmen, Battallı and Zirve cultivars were determined as B-tolerant cultivars. As a result of the study, it was determined that the efficient boron cultivars were Zülbiye, Zirve and Battallı, while the boron tolerant cultivars Cihan and Arslan.

Keywords *– Bean, B-efficient, boron activity, boron content, B-tolerant*

1. Introduction

Boron (B) is a micronutrient element that affects vegetative and generative growth in plants and, is necessary for plant development. Although the effect of boron on plant growth is still discussed in the literature, it is known that deficiency or excess B intake damages plant growth. (Dhaliwal et al., 2021). Boron deficiency and toxicity prevent the metabolic function of plants and cause damage. Determining the response of plants to boron is important as it affects yield and quality when boron deficiency and toxicity levels are narrow to each other. (Brdar-Jokanovic, 2020). These responses show variation between cultivars and even within-cultivar genotypes (Schnurbusch et al., 2010). It has been determined in the studies that some of the plants develop well in soils that do not contain enough boron and give quality products, while some show average growth in soils with rich boron (Punchana et al., 2012). B efficient plants show optimum plant development by taking enough B to meet their needs in soils that do not contain enough boron and provide optimum yield. Still, B-resistant or tolerant plants are growing at optimum growth by reducing B uptake as much as possible in soils having rich boron (Torun et al., 2006). Harmankaya et al. (2008) reported that wide genetic variation in the study investigated efficiencies of boron utilization in different bean genotypes. Because plants give different morphological and physiological responses to boron deficiency or toxicity, for this reason, this study aimed to determine the B-efficient and B-tolerant cultivars by considering the boron efficiencies of bean cultivars, which have the main legume plant.

[1] fgokmen@selcuk.edu.tr

[2] aysegul.korkmaz22@gmail.com

[3] sgezgin@selcuk.edu.tr

[*]Corresponding Author

2. Materials and Methods

2.1. Plant Material

This research used 15 registered cultivars of the bean (*Phaseolus vulgaris* L) as plant material (Table 1). The seed of recorded cultivars, being different properties in terms of physiological, morphological characteristics, and resistance to disease and pests, were obtained from the research institutes where they were registered.

Table 1
Proprietary bean cultivars, sources, and some properties

No	Cultivars	Growth Form	Seed Color	Hundred Seed Weight,g	Registrant Institution
1	Zülbiye	Dwarf	White	49.5-51.5	Black Sea Agricultural Research Institute
2	Arslan	Dwarf	White	27.6-62.1	Mersin Commodity Exchange Seed Research Industry and Trade Joint Stock Company
3	Battallı	Dwarf	beige	26.5-34.7	Mersin Commodity Exchange Seed Research Industry and Trade Joint Stock Company
4	Berrak	Dwarf	Beige	25.7-33.7	Field Crops Central Research Institute
5	Cihan	Dwarf	White	42.1-46.0	Aegean Agricultural Research Institute
6	Doruk	Semi dwarf	White	37.0-39.0	Safgen Seed Agricultural Products Industry and Trade Limited Company
7	Elkoca-05	Dwarf	White	42.4-46.0	Atatürk University, Faculty of Agriculture, Department of Field Crops
8	Güngör	Semi dwarf	White	60.0-65.3	East Mediterranean Transitional Zone Agrıcultural Research of Institute
9	Göksun	Dwarf	White	53.5-55	East Mediterranean Transitional Zone Agrıcultural Research of Institute
10	Kantar-05	Dwarf	Dark red	32.434.3	Atatürk University, Faculty of Agriculture, Department of Field Crops
11	Özmen	Dwarf	White	24.4-34.4	Avesa Agriculture Food and Livestock Limited Company
12	Sururbey	Semi dwarf	White	42.2-54.5	Mersin Commodity Exchange Seed Research Industry and Trade Joint Stock Company
13	Zirve	Drawf	White	37.3-39.7	Taşpınar Agriculture Food and Livestock Limited Company
14	Özdemir	Semi dwarf	Dark red	42.9-51.3	Mersin Commodity Exchange Seed Research Industry and Trade Joint Stock Company
15	Karacabey	Dwarf	White	38.6-42.0	Transitional Zone Agrıcultural Research of Institute

2.2. Soil Material Used in the Experiment

The soil used in the experiment had a slightly alkaline pH, no salinity problem, high lime content, and low organic matter content. In the soil, Ca (1150-3500 mg/kg), Mg (160-780 mg/kg), K (109-289 mg/kg), Cu (0.2-0.25 mg/kg) and Mn (1-5 mg/kg) were at sufficient level although P (<15 mg/kg), Fe (<2.5 mg/kg), Zn (<0.5 mg/kg) and B (<0.5 mg/kg) were at insufficient level (Gezgin et al., 2002) (Table 2).

Table 2
Some physical and chemical properties of soil tested in greenhouse

Parameters	Results
pH (1:2.5 soil: water)	7.58
EC (1:5 soil: water) (µS/cm)	52
%	
$CaCO_3$	36.6
Organic matter	1.64
Clay	37.60
Silt	20.66
Sand	41.74
Texture class	Clay Loam
Field capacity	22.5
1N NH_4AOC Extractable, mg/kg	
Ca	1622
Mg	231
K	222
Na	9
mg/kg	
P	16.4
İnorganic N (NH_4+NO_3-N)	12.0
Fe	0.70
Zn	0.16
Mn	2.20
Cu	0.80
B	**0.36**

2.3. Setting up and carried out the trial

The trial was carried out in the Computer Controlled Research Greenhouse Department of Soil Science and Plant Nutrition, Faculty of Agriculture, Selcuk University. We provided the greenhouses climate, 25±3 ºC temperature, 1750±50 kcal/m^2 of solar radiation, and 60±10% relative humidity during the experiment. In the greenhouse experiment conducted according to the complete randomized design with three replications, the pots were put through a 4 mm sieve, and 2000 g of soil was added based on the kiln dry weight of the pots.

Essential fertilization was made to ensure the plant's normal development due to nutrient deficiencies in the soil material. As basic fertilization, 200 mg N/kg (Ca $(NO_3)_2$.$4H_2O$) in solution, 80 mg P/kg (TSP), 300 mg K/kg (K_2SO_4), 10 mg Fe/kg (Sequestrene), 2.5 mg of Zn/kg ($ZnSO_4.7H_2O$) was applied.

B doses applied in the trial were given in below.

Control (B_0) = 0 mg/kg (Control)

B_5 = 5 mg B/kg

B_{10} = 10 mg B/kg

It was made by using $Na_2B_8O_{13}.4H_2O$ (20.8% B) fertilizer.

In the experiment, which consisted of 135 pots with 15 bean cultivars x 3 boron doses x 3 replications used, each pot was sown with eight seeds, and thinning was made so that four plants after germination. During the experiment, we irrigated the plants with deionized water at the field capacity and changed the pots in the greenhouse every 4-5 days. This trial was harvested separately according to the flowering time of each variety. Harvesting was done by cutting the above-ground parts.

2.3 Taking plant samples and preparing them for analysis

After the samples brought to the laboratory were washed with tap water, they were washed with pure water 0.2 N HCl solution, distilled water, deionized water, and dried with coarse filter papers. Then the plant sample was placed in a paper bag. The samples were dried in a circulating air-drying cabinet at 70 ºC until they reached

a constant weight, and after their dry weight was determined, they were ground in an agate mill. Then, we weighed about 0.2 g of the dried samples. After adding 5 ml of concentrated HNO_3 and 2 ml of H_2O_2 (30 % w/v), the transferred microwave device (Cem MARSXpress; CEM Corp; Matthews. NC. USA) under high pressure (200 PSI) was dissolved. A blank and certified reference materials were added to the 40-cell microwave set to ensure the reliability of the analysis. The volumes of the dissolved samples were made up of 20 ml of deionized water. The obtained percolates were filtered through blue-banded filter paper. The B concentrations in the percolator were determined in the ICP-OES (Inductively Coupled Plasma-Optical Emission Spectrometer). These values were controlled using reference plant material from the National Institute of Standards and Technology (NIST, Gaithersburg, MD, USA). B contents were calculated by multiplying the dry weights of the cultivars with the B concentrations. Since the sufficiency limit values (20-75 mg B/kg) specified by Jones et al. (1991) are taken into account in the calculation of boron efficiency, it is sufficient for all varieties in B_5 application according to control and B10 application. For this reason, B_5 application was used instead of B_{10} to calculate boron efficiency. In addition, the following equation [(1.1)] was used to determine efficient B (Graham, 1984).

$$\text{B efficient}, \% = (100)\text{x dry weight (B0)} \ / \ \text{dry weight (B5)} \quad (1.1)$$

2.4. Statistical Evaluation

The data obtained within the scope of the experiment were subjected to statistical evaluation with the JMP 7 statistical package program by the complete randomized design. The variance analysis was performed to determine the differences between the dry weight, boron contents, and concentrations of the samples belonging to each application group. The average values of the applications determined the differences and were grouped according to the "Student's t-test" of significance.

3. Results and Discussion

3.1. B Concentration of Bean Cultivars

The average values of boron concentration of bean cultivars under B treatments are given in Table 3. In addition, according to the studies of variance analysis performed to determine the effects of applications on boron concentration, cultivars (C), boron treatments (BAD) and interactions (C x BAD int.) were found to be statistically significant ($p< 0.01$) (Table1). The C x BAD interaction was found to be a change in the response of boron concentrations of bean cultivars of above-ground organs to the treatment of boron.- (Figure 1). Although the reactions during the flowering period of the cultivars used in the study varied depending on the cultivar and boron doses, we determined that the toxicity symptoms were more apparent at 10 mg B/kg. (Figure 1).

Table 3

Analysis of variance on dry weight, B content, B concentration of cultivars

Sources of Variance	**Mean of Squares**		
	Dry Weight	B Content	B Concentration
Total	330.9	1764185	5366714
Cultivar (C)	105.3**	52142**	592528**
Boron Application Doses (BAD)	114.2**	1644200**	107064421**
C X BAD int.	68.6**	64921**	489685**
Error	42.8	2921	4.84

** $p< 0.01$

The B concentration of dry bean cultivars increased from 4 (Zülbiye) to 8 (Güngör) times at 5 mg B/kg and between 14 (Özmen) and 15 (Battallı) times at 10 mg B/kg when compared to the control group (Table 3).

Figure 1. The responses of different bean cultivars (a: Battallı, b: Battallı c: Battallı d: Doruk, e: Doruk, f: Doruk, g: Arslan, h: Arslan, j: Arslan, k: Berrak, m: Berrak, n: Berrak cultivars) to boron doses (0 mg B/kg dose, 5 mg B/kg dose, 10 mg B/kg dose)

As shown in Table 4, the highest B concentration was obtained at 10 mg B/kg dose with 291.43 mg /kg depending on the average boron dose. In addition to, it was followed by decreasing concentration of 5 mg B/kg (135.78 mg/kg) and 0 mg B/kg (22.20 mg/kg). Jones et al. (1991) reported that the B concentration required to be adequate in bean leaves during the blooming period was about 20-75 mg B/kg. Then, above boron amounts of this level caused toxicity symptoms, which is in line with our study. In research; the non-treatment group was shown that insufficient B in Özmen, Sururbey, and Karacabey bean cultivars. Treatments of 5 and 10 mg B/kg caused B toxicity in all cultivars. Although the B concentration of the above-ground organs for bean cultivars was higher at approximately >75 mg B/kg in 5 mg B/kg, toxicity symptoms were less than 10 mg B/kg. (Figure 1). This situation could be derived from being B-efficient or B-tolerant cultivars. Akoğlu (2013) investigated the effects of increasing doses of B (0, 8, 16, and 24 mg B/kg) applications on boron concentrations of bean cultivars (Eyri Oturak, Ferasetsiz, Şeker bean, and Local genotype) in the greenhouse. Subsequently, increasing boron treatment caused B toxicity symptoms in cultivars.

Table 4

Effects of B treatments on B concentration (mg B/kg) of registered dry bean cultivars

	B concentration (mg B/kg)			
Cultivars	Control (B_0)	B_5	B_{10}	Average
Zülbiye	29.11 q	102.19 p	330.58 c	153.96 de
Arslan	21.40 qr	140.71 jkl	289.98 d	150.70 e
Battallı	24.97 qr	146.79 ıj	373.98 b	181.91 b
Berrak	22.69 qr	145.79 ıjk	323.54 c	164.00 c
Cihan	21.91 qr	133.96 klm	288.32 d	148.06 e
Doruk	25.35 qr	153.14 hı	295.67 d	158.05 cd
Elkoca – 05	21.15 qr	145.37 ıjk	235.08 fg	133.87 f
Güngör	21.42 qr	164.75 h	391.59 a	192.59 a
Göksun	21.25 qr	146.08 ıjk	326.14 c	164.49 c
Kantar – 05	23.25 qr	117.99 no	231.19 g	124.14 g
Özmen	16.64 r	113.20 op	230.61 g	120.15 g
Sururbey	18.50 qr	132.62 lm	259.25 e	136.79 f
Zirve	24.57 qr	130.21 lmn	244.77 f	133.18 f
Özdemir	21.06 qr	121.88 mno	265.35 e	136.10 f
Karacabey	19.67 qr	142.07 ı-l	285.38 d	149.04 e
Average	22.20 C	135.78 B	291.43 A	--

In variance analysis was determined to be statistically significant in the differences between the responses of the cultivars to boron. Therefore, we obtained the maximum B concentration from Güngör cultivar with 192.59 mg/kg and established the minimum concentration from Özdemir (136.10 mg/kg), Elkoca-05 (133.87 mg/kg), Zirve (133.18 mg/kg), Kantar-05 (124.14 mg/kg) and Özmen (120.15 mg/kg) cultivars (Table 3). However, previous study reported that boron concentrations varied between cultivars and species in all legumes and bean cultivars (Harmankaya, 2008).

3.2. B Content in Registered Bean Cultivars

Boron treatment on bean cultivars was changed of B content and it was determined significant statistically at the 1% level cultivars, boron doses, and their interaction (Table 5). The boron content increased along with increasing in boron doses applied to the cultivars, and we determined the maximum content at the highest B_{10} dose. The significant interaction could prove that boron treatments influenced the development of cultivars and plant dry weight, which showed this effect difference between boron application dose and cultivars. The B contents of the cultivars increased from 4 (Zülbiye) to 10 (Güngör) times at the B_5 dose and from 12 (Elkoca-05) to 14 (Zülbiye) times at the B_{10} dose when compared to the control group (Table 5).

Table 5

Effect of B treatments on B content (µg B/pot) of registered dry bean cultivars

	B Content (µg B/pot)			
Cultivars	Control (B_0)	B_5	B_{10}	Average
Zülbiye	163.08 p	581.02 o	2354.40 a	1032.84 ab
Arslan	114.60 p	1083.31 fgh	1686.93 c	961.62 bc
Battallı	112.51 p	780.63 lmn	1746.01 c	879.72 de
Berrak	107.78 p	914.71 ı-l	2027. 23 b	1016.58 b
Cihan	111.55 p	832.93 j-m	1498.17 d	814.22 efg
Doruk	147.84 p	1001.09 ghı	1733.13 c	960.67 bc
Elkoca – 05	98.62 r	916.91 ı-l	1136.36 fg	717.30 hı
Güngör	111.89 p	1102.35 fgh	2121.71 b	1111.99 a
Göksun	108.52 p	835.98 j-m	1723.26 c	889.25 cde
Kantar – 05	116.30 p	810.54 klm	1313.92 e	746.92 gh
Özmen	84.03 s	661.17 no	1222.07 ef	655.76 ı
Sururbey	99.73 r	757.90 mn	1521.72 d	793.12 fgh
Zirve	148.09 p	921.53 ıjk	1528.89 d	866.17 ef
Özdemir	94.45 r	737.28 mn	1502.63 d	778.12 gh
Karacabey	116.30 p	968.78 hıj	1774.35 c	953.30 bcd
Average	115.72 C	860.41 B	1659.39 A	

As seen in Table 5, the maximum B concentration was obtained at 1659.39 µgB/pot from the B_{10} dose within an treatment of boron doses. Then, it was followed by decreasing amounts of B_5 (860.41 µgB/pot) and 0 mg B/kg (115.72 µg B/pot) doses. The highest B content was determined in Güngör (1111.99 µg/pot), and the lowest B content was determined in Özmen (655 µg/pot) within cultivars means. However, Ceyhan et al. (2006) stated that using six dry bean cultivars in their field trial, the B contents of the types were diverse due to the difference in B concentrations and the cultivar yield variance. In particular, he reported that cereals have a wide content of B levels on plant species and cultivars of the same species (Topal et al., 2002). Therefore, the genetic diversity of plants could cause this difference.

3.3. Dry Weight and Efficiency B in Registered Bean Cultivars

As seen in Table 6, boron treatments on bean cultivars impact dry weight and boron efficiency (%). It was determined that the effects of variety, B application doses and interactions on the dry weight of boron applications of variance analysis were statistically significant at the 1% level. This critical interaction confirms that the effect of boron applications on the dry weight of plants varies depending on the cultivars. For example, the dry weight of the cultivars increased from 2% (Zülbiye) to 37% (Kantar-05) at 5 mg B/kg dose and between 1% (Doruk) and 38% (Zülbiye) at 10 mg B/kg dose when compared to the control group (Table 6).

The maximum dry weight was obtained from the Zirve cultivar with 12.92 g, while the minimum value was determined from the Battallı (9.66 g) cultivar among the averages of the cultivars. When considering boron application doses, boron applied increased in dry weight according to the control group, except at 10 mgB/kg, which was a high boron dose. Some research reported that the yield in wheat (Taban and Erdal, 2000), chickpeas (Hakkoymaz et al., 2006; Ceyhan et al., 2007), and bean (Sadiq and Mohammed, 2022) increased with boron applications when compared to the control group. However, high-dose B applications decreased the yields of plants. It is thought that the decrease in the dry weight of plants may result from the reduction of biomass production due to photosynthetic pigment loss or inhibition of photosynthesis due to damage to photosynthetic membranes (Gunes et al., 2006; Sahin, 2009).

Table 6

The effects of B application on dry weight and B activity of registered dry bean cultivars

	Dry weight (g/pot)				B Efficient (%)
Cultivars	Control (B_0)	B_5	B_{10}	Average	B_0/B_5*100
Zülbiye	11.19 f-k	11.39 f-k	15.39 ab	12.27 ab	98
Arslan	10.71 g-n	14.22 a	11.64 e-j	12.58 a	75
Battallı	9.01 o	10.64 g-n	9.34 mno	9.66 g	85
Berrak	9.49 l-o	12.55 c-f	12.53 c-f	11.52 b-e	76
Cihan	10.18 j-o	12.44 c-f	10.39 ı-o	11.03 def	82
Doruk	11.62 e-j	13.07 b-e	11.72 e-ı	12.14 abc	89
Elkoca – 05	9.33 no	12.62 c-f	9.66 l-o	10.54 f	74
Güngör	10.45 ı-o	13.38 bcd	10.84 g-l	12.56 b-e	78
Göksun	10.19 j-o	11.45 f-k	10.57 j-o	10.73 ef	89
Kantar – 05	10.01 k-o	13.76 bc	11.38 f-k	11.72 bcd	73
Özmen	10.09 k-o	11.68 e-ı	10.59 h-n	10.79 ef	86
Sururbey	10.82 g-m	11.43 f-k	11.74 e-ı	11.33 c-f	95
Zirve	12.06 d-h	14.20 ab	12.49 c-f	12.92 a	85
Özdemir	8.98 o	12.10 d-g	11.33 f-k	10.80 ef	74
Karacabey	11.87 e-ı	13.64 bc	12.44 c-f	12.65 a	87
Average	10.40 C	12.65 A	11.39 B		83

Boron-efficient (B-efficient) plants are identified as the plants that show the optimum growth and produce the yield at a decent level in the soil, having boron content insufficient by uptaking as B their needs. However, boron-tolerant (B-tolerant) plants are the plants that show the optimum growth in the soil with boron at sufficient or excess levels by decreasing B uptake (Punchana et al., 2012). Wang et al., (2005) reported that the efficiency of plants at low and high boron concentrations was calculated. In the same study, the researcher determined B-efficient, above 85% boron efficiency, while B-tolerant, below this value. Güneş et al., (2006) reported other boron efficiency evaluation methods. In this method, B activity was made by considering the average of the cultivars. Then, the types below the average were evaluated as B-tolerant cultivar and had above the average as B-efficient cultivar. Therefore, we selected the latter method to determine boron efficiency because the average B efficiency of the cultivars was 83%. Thus, our study considered that B-tolerant cultivars were below the average while B-efficient cultivars were above the mean.

Boron efficiency on cultivars showed varies from 70% (Arslan) to 98% (Zülbiye) (Table 5). It was determined that B-tolerant cultivars were Cihan, Güngör, Berrak, Elkoca-05, Özdemir, Kantar-05 and Arslan cultivars having below 83%. However, B-efficient cultivars were Zülbiye, Sururbey, Doruk, Göksun, Karacabey, Özmen, Battallı and Zirve cultivars above the mean. B-efficient cultivars produced more dry weight than other cultivars under low boron conditions. Also, B-tolerant types showed optimum growth than different cultivars in high or excess boron conditions. Some previous studies reported that B-efficient was a criterion for determining significant cultivars of bean (Harmankaya et al., 2008), wheat (Taban and Erdal, 2000; Hamurcu and Gezgin, 2007), barley (Atalay et al., 2003), and maize (Güneş and Alpaslan, 2000). It was determined that B efficiency varied depending on the increasing dry weight of the plant with boron treatment (0, 5, and 10 mgB/kg) to the soil. There are notable variations in response to boron of cultivars in the studies on beans (Paul et al., 1988; Huang and Graham, 1990; Nable and Paull, 1991; Ceyhan et al., 2006; Hamurcu and Gezgin, 2007). Also, it has been stated that other cultivated plants, except for beans, show wide genetic variation in response to boron (Taban and Erdal, 2000; Topal et al., 2002; Torun et al., 2021). According to their findings, the primary reason for this could be caused that plants show various responses as physiological and morphological to B toxicity and deficiency (Dordas et al., 2000; Dordas and Brown, 2001).

4. Conclusion

The limit range between B deficiency and toxicity in plants is very narrow. However, it is observed that yield and quality decrease significantly in case of B deficiency and toxicity. We applied increasing doses of boron (0, 5, and 10 mgB/kg) to B-efficient and B-tolerant registered dry bean cultivars to increase yield and quality. As a result, we comprehended a wide variation among cultivars against B activity. We could state that the cultivars determined as B-efficient had dry weight values above average in soil conditions at toxic boron levels. In contrast, the cultivars with low B-activity occurred with less dry weight. We determined that the most critical difference between the cultivars having low and high B activity was the dry weight values and B contents at the low B application. We determined among the cultivars used in the study that Zülbiye, Sururbey, Doruk, Göksun, Karacabey, Özmen, Battallı, and Zirve cultivars had the highest B activity, in other words, the B-efficient cultivars. However, Cihan, Güngör, Berrak, Elkoca-05, Özdemir, Kantar-05, and Arslan cultivars showed the lowest B efficiency. In other words, we stated a B-tolerant cultivar for these cultivars. In bean agriculture under soils conditions having sufficient or excess boron content, using Zülbiye, Sururbey, Doruk, Göksun, Karacabey, Özmen, Battallı, and Zirve cultivars could provide more yield per unit area by reducing the yield losses due to excess B in the soil. In addition, there is extremely important regarding both economy and using less labor to use B-efficient plant cultivars in agricultural production.

Acknowledgement
This study was financed by Selçuk University Scientific Research Projects Coordinatorship (Project No: 20401074). We would like to thank Selçuk University Scientific Research Projects Coordinatorship for their support.

Author Contributions

Fatma Gökmen Yılmaz: Designed the experiments and performed the statistical analysis and wrote the manuscript.

Ayşegül Korkmaz: Applied the experiment, analyzed the plant sample, and wrote the manuscript.

Sait Gezgin: Designed the experiment and investigation.

Conflicts of Interest

The authors declare no conflict of interest.

References

Akoğlu, A. (2013). *The response of some common bean (Phaseolus vulgaris L.) genotypes to boron applications (In Turkish)* (Master's thesis). Eskişehir Osman Gazi Üniversitesi, Eskişehir, Turkey.

Atalay, E., Gezgin, S., & Babaoğlu, M. (2003). Boron uptake of in vitro seedlings of wheat (Triticum durum Desf.) and barley (Hordeum vulgare L.) as determined by ICP-AES. *Selcuk Journal of Agriculture and Food Sciences*, *17*(32), 47-52.

Brdar-Jokanović, M. (2020). Boron toxicity and deficiency in agricultural plants. *International journal of molecular sciences*, *21*(4), 1424. https://doi.org/10.3390/ijms21041424

Ceyhan, E., Önder, M., Hamurcu, M., Harmankaya, M., Gökmen, F., & Gezgin, S. (2006). Response of dry bean (Phaseolus vulgaris L) cultivars to foliar and soil applied in boron defficient calcareous soils. *Plant and Soil*.

Ceyhan, E., Önder, M., Harmankaya, M., Hamurcu, M., & Gezgin, S. (2007). Response of chickpea cultivars to application of boron in boron-deficient calcareous soils. *Communications in soil science and plant analysis*, *38*(17-18), 2381-2399. https://doi.org/10.1080/00103620701588734

Dhaliwal, S. S., Sharma, V., Shukla, A. K., Verma, V., Behera, S. K., Sandhu, P. S., Kaur, K., Gaber, A., Althobaiti, Y. S., Abdelhadi, A. A. & Hossain, A. (2021). Assessment of agroeconomic indicators of Sesamum indicum L. as influenced by application of boron at different levels and plant growth stages. *Molecules*, *26*(21), 6699. https://doi.org/10.3390/molecules26216699

Dordas, C., Chrispeels, M. J., & Brown, P. H. (2000). Permeability and channel-mediated transport of boric acid across membrane vesicles isolated from squash roots. *Plant physiology*, *124*(3), 1349-1362. https://doi.org/10.1104/pp.124.3.1349

Dordas, C., & Brown, P. H. (2001). Permeability and channel-mediated transport of boric acid across plant membranes. An explanation for differential B uptake in plants. *In Plant Nutrition* (pp. 190-191). Springer, Dordrecht. https://doi.org/10.1104/pp.124.3.1349

Gezgin, S., Dursun, N., Hamurcu, M., Harmankaya, M., Önder, M., Sade, B., Akgün, N., Yorgancılar, M., Ceyhan, E., Çiftçi, N., Acar, B., Gültekin, İ., Işık, Y., Şeker, C., & Babaoglu, M. (2002). Boron content of cultivated soils in Central-Southern Anatolia and its relationship with soil properties and irrigation water quality. In Boron in Plant and Animal Nutrition (pp. 391-400). Springer, Boston, MA.

Graham, R. D. (1984). Breeding for nutritional characterstics in cereals. *Advances in plant nutrition, 1*, 57-102. https://doi.org/10.3759/tropics.12.295

Güneş, A., & Alpaslan, M. (2000). Boron uptake and toxicity in maize genotypes in relation to boron and phosphorus supply. *Journal of Plant Nutrition, 23*(4), 541-550. https://doi.org/10.1080/01904160009382038

Güneş, A., Inal, A., Alpaslan, M., & Çakmak, İ. (2006). Genotypic variation in phosphorus efficiency between wheat cultivars grown under greenhouse and field conditions. *Soil Science & Plant Nutrition*, 52(4), 470-478. https://doi.org/10.1111/j.1747-0765.2006.00068.x

Hakkoymaz, O., Önder, M., & Gezgin, S. (2006). The adaptatıon of the summer lentıl varıetıes and determınıng the effect to boron toxıc ın konya ecologıcal condıtıons. *Selcuk Journal of Agriculture and Food Sciences, 20*(38), 98-107.

Hamurcu, M., & Gezgin, S. (2007). Effect of boron and zınc applıcatıons on bıomass values of bean (phaseolus vulgaris l.) genotypes. *Selcuk Journal of Agriculture and Food Sciences, 21*(41), 11-22.

Harmankaya, M., Hamurcu, M., Ceyhan, E., & Gezgin, S. (2008). Response of common bean (Phaseolus vulgaris L.) cultivars to foliar and soil applied boron in borondeficient calcareous soils. *African Journal of Biotechnology*, *7*(18).

Huang, C., & Graham, R. D. (1990). Resistance of wheat genotypes to boron toxicity is expressed at the cellular level. *Plant and Soil, 126*(2), 295-300.

Jones Jr, J. B., Wolf, B., & Mills, H. A. (1991). *Plant analysis handbook. A practical sampling, preparation, analysis, and interpretation guide*. Micro-Macro Publishing, Inc.

Nable, R. O., & Paull, J. G. (1991). Mechanism and genetics of tolerance to boron toxicity in plants. *In Current topics in plant biochemistry and physiology: Proceedings of the... Plant Biochemistry and Physiology Symposium held at the University of Missouri, Columbia (USA)*.

Punchana, S., Cakir, M., Rerkasem, B., & Jamjod, S. (2012). Mapping the Bod2 gene associated with boron efficiency in wheat. *ScienceAsia, 38*(3), 235-243. http://dx.doi.org/10.2306/scienceasia1513-1874.201...

Sadiq, S. M. S. M., & Mohammed, A. A. M. A. (2022). Response of faba bean to plantıng dıstance between plants and sprayıng wıth nano and tradıtıonal boron: response of faba bean to plantıng dıstance between plants and sprayıng wıth nano and tradıtıonal boron. *Iraqi Journal of Market Research and Consumer Protection, 14*(1)), 84-93. http://dx.doi.org/10.28936/jmracpc

Schnurbusch, T., Hayes, J., Hrmova, M., Baumann, U., Ramesh, S. A., Tyerman, S. D., & Sutton, T. (2010). Boron toxicity tolerance in barley through reduced expression of the multifunctional aquaporin HvNIP2; 1. *Plant Physiology*, *153*(4), 1706-1715. https://doi.org/10.1104/pp.110.158832

Taban, S., & Erdal, İ. (2000). Effects of boron on growth of various wheat varieties and distribution of boron in aerial part. *Turkish Journal of Agriculture and Forestry*, *24*(2), 255-262.

Topal, A., Gezgin, S., Akgün, N., Dursun, N., & Babaoglu, M. (2002). Yield and yield attributes of durum wheat (Triticum durum Desf.) as affected by boron application. *In Boron in Plant and Animal Nutrition* (pp. 401-406). Springer, Boston, MA. https://doi.org/10.1007/978-1-4615-0607-2_42

Torun, A. A., Yazici, A., Erdem, H., & Çakmak, İ. (2006). Genotypic variation in tolerance to boron toxicity in 70 durum wheat genotypes. *Turkish Journal of Agriculture and Forestry*, *30*(1), 49-58.

Torun, A. A., Bozgeyik, S., & Duymuş, E. (2021). The Effect of Boron Application in Increasing Doses on Shoot Boron Concentration and Uptake of Other Nutrients of Pistachio (Pistacia vera L.). *Turkish Journal of Agriculture-Food Science and Technology*, *9*(5), 855-862. https://doi.org/10.24925/turjaf.v9i5.855-862.4044

Wang, Q., Li, J., Li, Z., & Christie, P. (2005). Screening Chinese wheat germplasm for phosphorus efficiency in calcareous soils. *Journal of Plant Nutrition, 28*(3), 489-505. https://doi.org/10.1081/PLN-200049186

e-ISSN 2757-5195

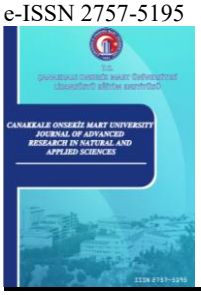

Çanakkale Onsekiz Mart University

Journal of Advanced Research in Natural and Applied Sciences

Open Access

doi.org/10.28979/jarnas.1134363 2023, Vol. 9, Issue 1, Pages: 228-236 dergipark.org.tr/tr/pub/jarnas

The role of Anatolia between Asia and Europe: A case study of oak gall wasp species, *Cynips quercus (Hymenoptera, Cynipidae)*

Serap Mutun[1,*], Serdar Dinç[2]

[1,2]Department of Biology, Faculty of Art and Science, Bolu Abant İzzet Baysal University, Bolu, Türkiye

Article History

Received: 22.06.2022

Accepted: 04.10.2022

Published: 05.03.2023

Research Article

Abstract – In this study, we used DNA sequence data of a western Palearctic oak gall wasp species, *Cynips quercus*, showing distribution from Europe to Iran to answer the following questions: i) Do the eastern *C. quercus* populations have higher genetic diversity than the European populations?, ii) Are the eastern populations source for the European populations?, iii) What is the possible date of divergence between the Asian and European populations? For these purposes, we analysed 88 cytochrome b sequences representing Iran, Türkiye, Hungary, and Spain. Our analyses revealed that the highest genetic diversity was in Türkiye followed by Iran, Hungary, and Spain, respectively. Iranian samples were most divergent from the Spain and Hungary sequences. Pairwise comparisons showed that the highest gene flow was between Türkiye and Hungary, and between Türkiye and Iran, respectively. Phylogenetic analysis grouped the Turkish haplotypes with the Iranian sequences, and Spain was grouped with Hungary. Network analysis revealed that the western Turkish samples were separated from eastern sequences, and all of the eastern Turkish sequences were clustered with the Iranian samples meanwhile a western Turkish lineage provided a source to Hungary and then to Spain. Times of divergence analysis estimated that the Turkish lineage split from the Iranian lineage around 4,67 million years ago, and Hungarian and Spanish lineages diverged from each other about 3 million years ago. Correspondingly, our analyses suggested that Anatolia played a key role as a bridge between the Asian and European populations of *C. quercus*.

Keywords – *Asia, Cynips quercus, cyt b, Europe, Oak gall wasp*

1.Introduction

Anatolia as a natural bridge connecting the three continents was formed around the late Oligocene and middle Miocene because of the collision of the Arabian and African plates (Şengör & Yılmaz, 1981). After the collision, the eastern Anatolia uplifted while the western part was still lowland. By the end of the subsequent Pliocene epoch, Anatolian geomorphology was almost completed generating the current topological structure of the Turkish landmass (Erol, 1983). Associated palaeogeologic and palaeotectonic events accompanied by paleoclimatic fluctuations during the Tertiary and the Pleistocene epoch of the Quaternary have had a profound effect on the Anatolian biodiversity (Demirsoy, 2002). In many instances, these ongoing changes have either promoted speciation events or caused substantial range shifts in many plant and animal species that already inhabited Anatolia (Bilgin, 2011). The Anatolian Peninsula is located at the junction of three phytogeographic regions as the Irano-Turanian, the Mediterranean and the Euro-Siberian, and Asian, Mediterranean, Caucasian, and African faunistic elements are currently the inhabitants of Anatolia (Şekercioğlu et al., 2011). With over 10.000 plant and 80.000 animal species/subspecies constituting one of the 35 biodiversity hotspots Anatolia

[1] smutun@ibu.edu.tr

[2] dinc_s@ibu.edu.tr

[*]Corresponding Author

has been reported as a biodiversity corridor between Asia and Europe (Stone et al., 2007; Ansell et al., 2011; Bilgin, 2011). In particular, during the recurring changes of Pleistocene most of the northern latitudes of Asia and Europe were inhabitable for many taxa, thus populations of those species retreated to southern latitudes (Hewitt, 1999). In recent years, there is an increasing number of studies addressing Iran and Anatolia as the eastern, and the Balkans, Spain, and Italy as the southern source populations for post-Pleistocene colonization of Europe (Ansell et al., 2011; Koch et al., 2017). Specifically, in oak gall wasps Iranian and Anatolian populations have been proposed as the origin for the European populations (Rokas et al., 2003).

Oak gall wasps from the family Cynipidae are obligate parasites of the oak taxa, and nearly 150 species have been recorded from Türkiye (Bayrak & Avcı, 2019). *Cynips quercus* Fourcroy, 1785 (Hymenoptera, Cynipidae, Cynipini) is an oak gall wasp species with alternation of generation between sexual and asexual generations and shows widespread distribution in the western Palearctic (Melika, 2006). The species forms its asexual generation galls under the leaves of white oak taxa from the Quercus section of the family Fagaceae. In this study, we used 88 sequences of the mitochondrial DNA cytochrome b gene (cyt b) covering a 433 base pairs of *C. quercus* downloaded from NCBI GenBank representing Iran, Türkiye, Hungary, and Spain to answer the following questions: i) Do the eastern *C. quercus* populations have higher genetic diversity than the European populations?, ii) Are the eastern populations source for the European populations?, iii) What is the possible date of divergence between the Asian and European populations?

2.Materials and Methods

Eighty-eight cyt b sequences of *C. quercus* currently present in GenBank were downloaded and used in this study to estimate genetic diversity among the Turkish, Iranian, Hungarian, and Spanish populations (Table 1). We used Arlequin 3.5.2.2 (Excoffier & Lischer, 2010) and DnaSP 5.10.1 programs (Librado & Rozas, 2009) to determine the number of polymorphic sites (S), nucleotide (π) and haplotype/allele (h) diversity (Nei, 1987), gene flow (N_m) and population differentiation (F_{ST}). Demographic analyses and any deviations from neutrality were analysed by calculating the raggedness index (Hri) (Harpending, 1994), the sum of squared deviations (SDD) (Schneider & Excoffier, 1999), Tajima's *D* (Tajima, 1989) and Fu's F_S (Fu, 1997) using Arlequin 3.5.2.2 (Excoffier & Lischer, 2010).

For revealing phylogenetic relationships among haplotypes, we performed maximum parsimony (MP) and maximum likelihood (ML) analyses using PAUP*4.0b10 (Swofford, 2002). In all tree reconstruction analyses, we used equivalent sequences for the cyt b gene of *C. divisa*, *C. disticha*, and *C. korsakovi* as outgroups (GenBank Accession numbers are given in Figure 1). For the MP analysis, the TBR branch-swapping algorithm with 1000 replicates of random addition of taxa under the heuristic search options and 1000 bootstrap replicates were employed to assess support for branches (Swofford, 2002). We used JModeltest 2 (Darriba et al., 2012) to determine the best fit model for our dataset and detected the GTR+G model (ln= -198.5792), and we applied this model in ML and other analyses. To estimate divergence times of the *C. quercus* lineages we performed Bayesian Inference (BI) using the software package BEAST version 1.5.2 (Drummond et al., 2012) by applying 1.19% sequence divergence per lineage (2.39% pairwise) per million years of mutation rate for the age calibration (Papadopoulou et al., 2010). Both MRCAs (most recent common ancestors) and MACAs (most ancient common ancestors) calculations and operator optimizations (Hayward & Stone, 2006) were performed with BEAUti ver. 1.8.0. The BEAST analysis was run for 100 million generations sampling every 1000 and we controlled the convergence to stationary and the effective sample size (ESS) of model parameters using Tracer ver. 1.6.0. The maximum clade credibility tree was built with Treeannotator ver. 1.8.4. through discarding the initial 25% samples as burn-in. For visualization of the results, we used Fig-Tree ver. 1.3.1 (http://tree.bio.ed.ac.uk/software/figtree/). Further, an unrooted parsimony haplotype network with 95% probability levels was constructed using HapStar Version 0.5 (C) to better understand the evolutionary relationships of haplotypes (Teacher & Griffiths, 2011).

3.Results and Discussion

A 433 base-pair of the mitochondrial cyt b gene of 88 sequences representing 52 Turkish, 17 Hungarian, 10 Iranian, and 9 Spanish haplotypes possessed 325 constant and 108 polymorphic characters (Table 1, GenBank Accession Number for each haplotype is shown on the phylogenetic tree in Figure 1). Among polymorphic sites, only 78 characters were parsimony informative. There were no shared haplotypes among Türkiye, Iran, Hungary, and Spain, thus haplotype diversity was calculated as 1.000 for each of these localities. Nucleotide diversity was highest in Türkiye (π= 0.0258) followed by Iran (π= 0.0233), Hungary (π= 0.0166), and Spain (π= 0.0083) (Table 1). A recent study conducted on only the Turkish populations of *C. quercus* revealed the presence of high genetic variation in the species particularly in the eastern/southeastern Anatolian populations (Mutun & Dinç, 2019). In this current study, the presence of high genetic diversity in each of the *C. quercus* populations is not unexpected since the Iberian Peninsula and the Balkans have been used as shelter areas by many taxa during the harsh environmental conditions of the last few ice ages, thus constituting the two important diversity centres for Europe (Hewitt, 2004). Nonetheless, Iran and Anatolia are also well-proven refugia and eastern centres of diversity for the western Palearctic which are known to combine Caucasian and Asian diversity (Bilgin, 2011). Sequences used in this study representing four of the diversity centres harboured diversity in oak gall wasps were generated congruent results with other oak gall wasp species (Rokas et al., 2003; Stone et al., 2007). For instance, in *Andricus kollari* the nucleotide diversity was greatest in the Anatolian populations, it was intermediate in Hungary, and the lowest diversity was determined in Spain (Stone et al., 2007). Further, in *Andricus quercustozae* Anatolia was with the highest genetic richness as compared to Morocco, Spain, France, Italy, Hungary, and Greece (Rokas et al., 2003). In another oak gall wasp species with similar geographic distribution, *Andricus coriarius*, the Turkish populations had the highest genetic variation when compared to the Iranian and Lebanon populations (Challis et al., 2007). Population studies conducted on gall wasp species revealed a decline in genetic diversity from east to west in the refugia in the Mediterranean Basin (Atkinson, 2007). In the case of *C. quercus*, higher genetic diversity revealed in Anatolia in comparison with the Iranian population may be either due to the unequal number of sequences representing the Turkish and the Iranian localities, or Anatolia, indeed, harbours much higher diversity than Iran. Nevertheless, more samples from Iran are necessary for the clarification of Iran and its role in oak gall wasp species.

Population demographic analysis of *C. quercus* produced negative but non-significant Tajima's *D* values for Türkiye, Iran and Spain while Hungary was with positive and insignificant value (Table 1). However, all four populations generated statistically significant negative Fu's F_S values indicating population expansion expected under neutrality in the population growth model (Ramos-Onsins & Rozas, 2002). We also calculated low and non-significant Hri and SSD values for each locality of *C. quercus* which suggest expanding populations.

Table 1.
C. quercus populations, GenBank Accession numbers of haplotypes, N_{hap}: haplotype number, h: haplotype diversity, π: nucleotide diversity, and resulting values calculated for demographic analyses of each population. (*=P ≤ 0.05).

Pop.	GenBank Acc. No.	N_{hap}	h/π	Tajima's *D*	Fu's *Fs*	Hri	SSD
Türkiye	MH361234-MH361285	52	1.000 +/- 0.0038 / 0.0258 +/- 0.0132	-0.9364	-245.120*	0.021	0.032
Hungary	JQ416460-JQ416478, DQ218011	17	1.000 +/- 0.0202 / 0.0166 +/- 0.0091	0.2281	-117.324*	0.041	0.021
Iran	JQ416448-JQ416459	10	1.000 +/- 0.0447 / 0.0233 +/- 0.0131	-0.5110	-34.451*	0.065	0.042
Spain	JQ416436-JQ416445	9	1.000 +/- 0.0524 / 0.0083 +/- 0.0052	-11.690	-612.711*	0.037	0.005

It is known that higher and non-significant Hri and SSD values are observed in stable and non-expanding populations while lower and non-significant values are predicted under suddenly expanding populations (Rogers & Harpending, 1992). Population expansion has been reported, for instance, for *Andricus kollari* where the European population of the species originated after the expansion of two genetically divergent eastern Mediterranean diversity centres including the Turkish source population in the east (Stone et al., 2007). Although more sequences, in particular, from Iran and three other localities, are necessary for drawing a more general

conclusion on *C. quercus*, it seems that Anatolia as one of the eastern populations provided a genetic source to the European localities, yet each of the European locality implied recent population expansion as well.

Gene flow (N_m) estimates revealed that the highest gene flow was between Türkiye and Hungary (N_m= 0.3486), and between Türkiye and Iran (N_m= 0.2845), respectively. However, the least amount of genetic exchange was between Iran and Spain (N_m= 0.1391) (Table 2). Correspondingly, pairwise genetic differentiation (F_{ST}) analysis revealed that Iran was the most diverged population from Spain (F_{ST}= 0.7823), and Hungary (F_{ST}= 0.7202), respectively, and as expected it was least differentiated from Türkiye (F_{ST}= 0.6374). Thus, genetic differentiation analysis produced supporting evidence for the gene flow between populations of *C. quercus*. Under isolation by distance model of population, gene flow or genetic exchange between geographically distant populations is lower than the geographically proximate populations (Stone et al., 2002). In *C. quercus*, the lowest and statistically significant F_{ST} values between Iran and Spain, and between Türkiye and Spain support the isolation by distance. Expectedly, the lowest F_{ST} calculated for the pairwise comparisons of Türkiye and Hungary may propose that the Turkish lineages might have provided a source to the Hungarian population.

Table 2.
Genetic differentiation and gene flow between populations. The lower diagonal shows F_{ST}, and the upper diagonal indicates gene flow (N_m), where all values are significant, $p \leq 0.001$.

	Türkiye	**Hungary**	**Iran**	**Spain**
Türkiye		0.3486	0.2845	0.2119
Hungary	0.5892		0.1942	0.2567
Iran	0.6374	0.7202		0.1391
Spain	0.7024	0.6608	0.7823	

Maximum parsimony, maximum likelihood, Bayesian inference and Beast analysis were conducted to reveal evolutionary relationships of haplotypes and times of divergence of *C. quercus* lineages. Since all phylogenetic analyses generated a similar topology, we presented here only a single tree (Figure 2). Our ingroup species, *C. quercus*, seems to diverge from the outgroup taxa around 7,85 million years ago (MYA). The sorting of the ingroup haplotypes from the outgroup sequences dates back to the Tortonian age (11.6- 7.2 MYA) of the Late Miocene epoch, which is characterized by important geological, climatic, and environmental changes altering the world and its biodiversity (Pound et al., 2011). After its first divergence, the *C. quercus* lineage split into two distinct haplogroups ~6.34 MYA during the Messinian age (7.2- 5.3 MYA) of the Late Miocene. This first separation generated two main clades where the first was comprised of the Iranian and all of the Turkish sequences, and the second clade was constituted by the Hungarian and the Spanish sequences. Therefore, hereafter we termed the former clade as the Asian and the latter as the European clade. Recent studies have well proved that the Messinian age was characterised by great palaeogeological and temperature changes which are associated very closely with climatic fluctuations, particularly in the Mediterranean Basin (Krijgsman et al., 1999). It seems that at least the ancestral basal lineage of *C. quercus* spread around the Irano-Anatolian landmass was divided into haplogroups which coincides with the Messinian environmental crisis. The Messinian stage appears to have further promoted the diversification of this clade into a Turkish haplogroup of only in the eastern Anatolian sequences and Iran, the other clade including all other sequences from the rest of Türkiye. Subsequent diversification events occurred ~4.67 MYA around the early Pliocene resulting the formation of the Iranian lineages from the Turkish lineage. Similar deep splitting events during the early to mid-Pliocene also ended up with inner clade formation within the Turkish *C. quercus* lineages. Our analysis related to the eastern part of the West Palearctic is strongly supported by the time estimation for the speciation of other gall wasp species including *Andricus coriarius* and its cryptic species formed as a result of ongoing events spanning the same period around Anatolia, Iran, and the Levant region (Challis et al., 2007). In *A. coriarius*, the main lineage formation occurred in Pliocene and further splits have occurred in subsequent periods. In correlation with the ongoing changes, it, most probably, caused a pre-Pleistocene separation of the Hungarian and Spanish

lineages around ~ 3 MYA. Along the recurrent cyclic changes of Pleistocene, a series of intermediate to relatively shallow divergences of *C. quercus* lineages within each of the Anatolian, Iranian, Hungarian, and Spanish subclades seem to generate the current polygenetic lineages of the species. Our current results are overall in agreement with the findings from other western Palearctic species (Hewitt, 2004; Poulakakis et al., 2005).

Past geologic and environmental changes and accompanied climatic oscillations have been shown to correlate with the phylogenetic structuring of species by leaving a profound effect on the organismal groups in the western Palearctic (Nichols & Hewitt, 1994) and these signals can be revealed through network analysis. Our haplotype network analysis revealed the same structuring of the *C. quercus* sequences (Figure 2). A clear separation of four distinct clusters representing the Turkish, Iranian, Hungarian, and Spanish haplotypes is well-defined and the Turkish samples were further divided into the western and eastern Anatolian haplogroups. Moreover, the eastern Turkish haplogroup is directly connected to the Iranian cluster through many hypothetical haplotypes that were not either sampled or are extinct. While all the Turkish sequences related to the Iranian samples a haplotype from a western Turkish lineage connected directly to a Hungarian haplotype implies that Anatolia might have provided a genetic source to Hungary and then to Spain. Eventually, both Spain and Hungary sequences formed separate haplogroups. It is important to note here that Spain haplotypes are directly connected to the Hungary haplotypes via several hypothetical haplotypes. All phylogenetic inferences in addition to the network analysis signal the great effect of the relatively ancient to intermediate splits being well-correlated with the past changes spanning from 8 MY to the last few more recent glaciation periods. Thus, our current analysis of *C. quercus* representing the two Asian and two European glacial refugia produced congruent results with other animal groups from the western Palearctic (Rokas et al., 2003; Challis et al., 2007).

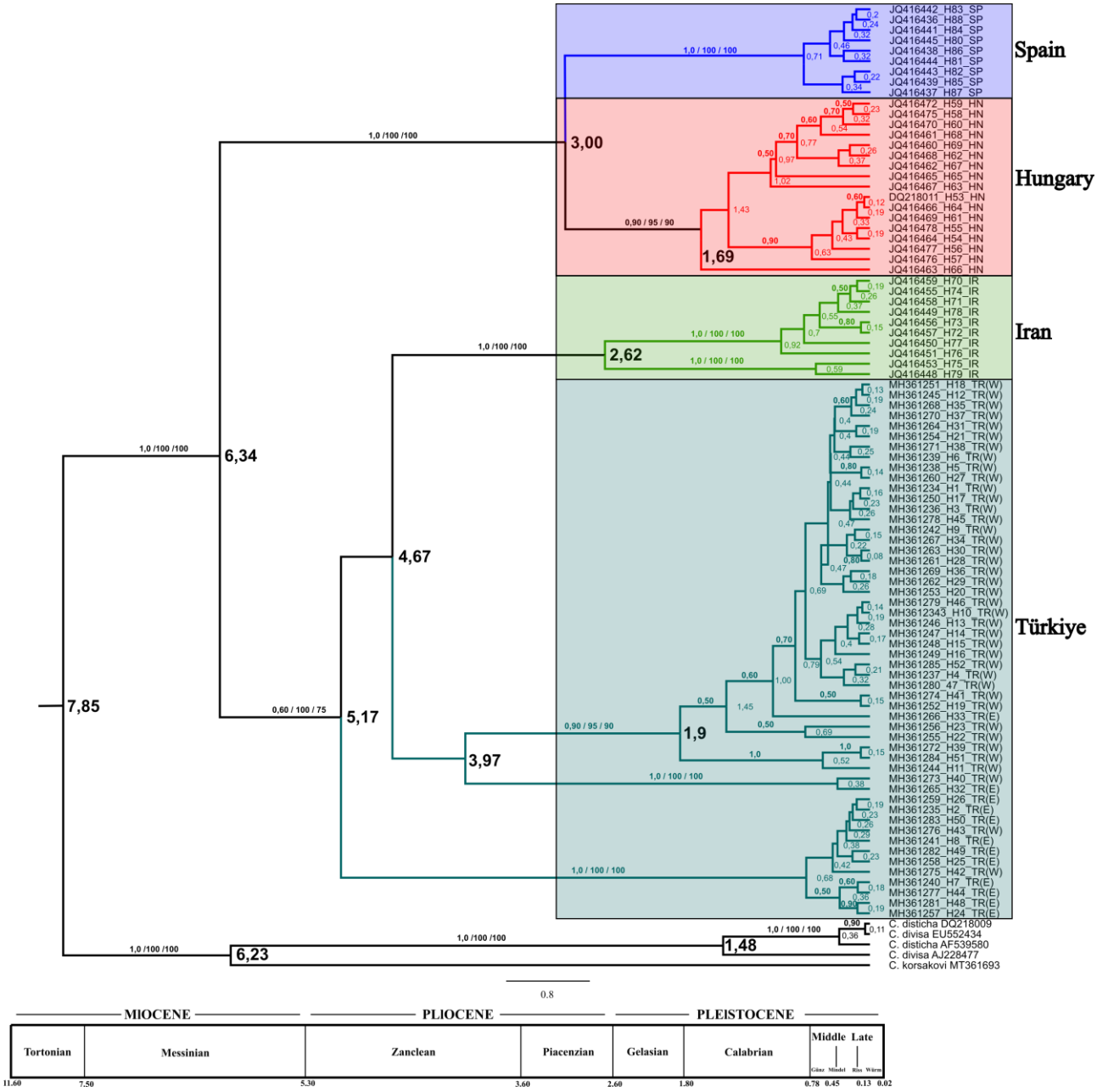

Figure 1. The resulting Beast tree of *C. quercus*. Values at each node represent times of divergence, and numbers on the branches show bootstrap values for the BI posterior probability, and MP/ML, respectively. (E= the east side and W= the west side of Türkiye in reference to major physical barriers in Anatolia).

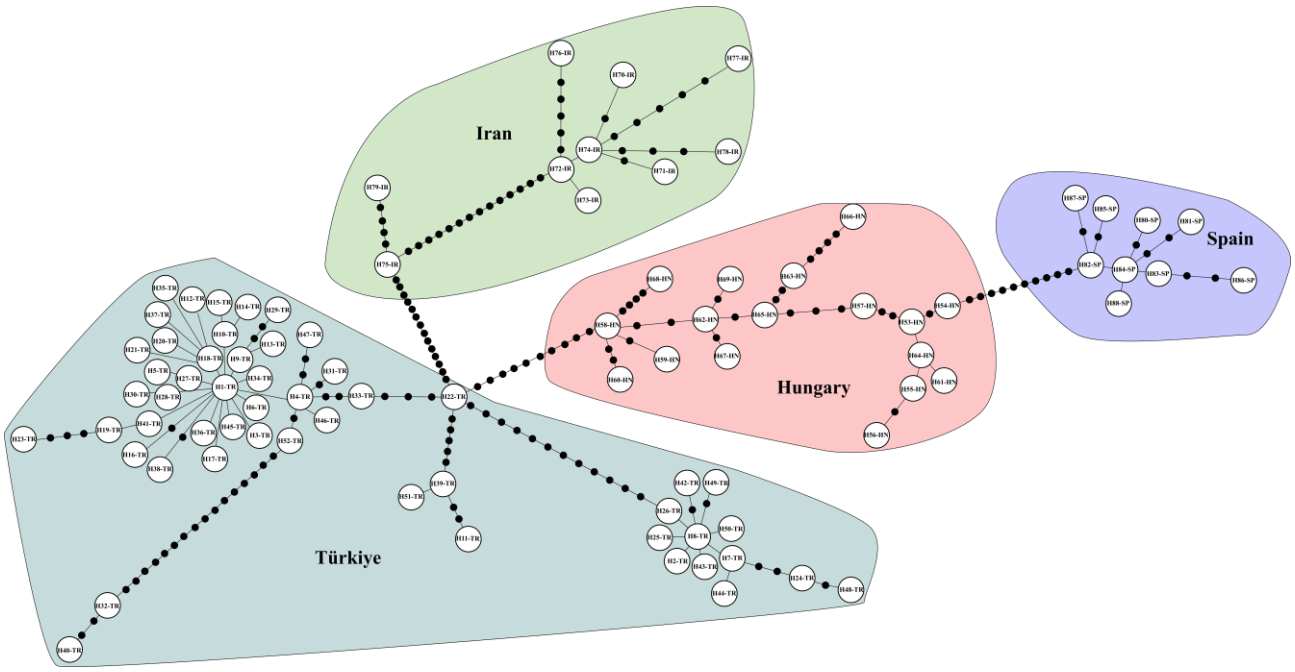

Figure 2. Haplotype network of *C. quercus* sequences. Each circle represents a haplotype which is shown by numbers within the relevant circle. Hypothetical haplotypes are represented by black circles.

4.Conclusion

Genetic diversity analysis revealed that Türkiye harboured the highest level of genetic diversity. Iran, Spain, and Hungary localities also harbour relatively high diversity which is not unexpected since each played a significant role as a distinct glacial refugium in the past. Our phylogenetic tree proposed that the Turkish samples were separated from the eastern sequences, and all the eastern Turkish sequences were clustered with the Iranian samples. Further, a western Turkish lineage provided a source to Hungary and then to Spain eventually these two European localities formed separate haplogroups. Gene flow and genetic differentiation estimates supported an east-to-west dispersal of the species. Moreover, times of divergence analysis implied that past drastic paleogeologic and paleoclimatic changes have been the main drivers of the species phylogenetic structuring since the late Miocene. Our overall analysis indicates that *C. quercus* is currently represented by two Asian and two European major lineages and Anatolia played a key role as a natural bridge between Asia and Europe.

Author Contributions

Serap Mutun: Conceptualization, Methodology, Data Curation, Writing - Original Draft, Writing - Review & Editing.

Serdar Dinç: Formal analysis, Data Curation, Writing - Review & Editing.

Conflicts of Interest

The authors declare no conflict of interest.

References

Ansell, S. W., Stenoien, H. K., Grundmann M., Russell S.J., Koch MA, Schneider H & Vogel, J.C. (2011) The importance of Anatolian Mountains as the cradle of global diversity in *Arabis alpina*, a key Arctic-Alpine species. *Annals of Botany*, 108: 241-252. DOI: https://doi.org/10.1093/aob/mcr134

Atkinson, R. J., Rokas, A. & Stone, G. N. (2007). Longitudinal patterns in species richness and genetic diversity in European oaks and oak gallwasps. In Weiss, S. & Ferrand, N. (Ed.), *Phylogeography of Southern European Refugia* (pp. 127-151). Springer, Dordrecht. DOI: https://doi.org/10.1007/1-4020-4904-8_4

Bayrak, S., & Avcı, M. (2019). Gall forming Cynipini (Hymenoptera: Cynipidae) species in Isparta oak forests. *Munis Entomology & Zoology*, 14(2), 552-564. Retrieved from: https://www.munisentzool.org/yayin/vol14/issue2/vol14issue2-2076075.pdf

Bilgin, R. (2011). Back to the Suture: The distribution of intraspecific genetic diversity in and around Anatolia. *International Journal of Molecular Sciences*, 12(6): 4080-4103. DOI: https://doi.org/10.3390/ijms12064080

Challis, R. J., Mutun, S., Nieves-Aldrey, J. L., Preuss, S., Rokas, A., Aebi, A., Sadeghi, E., Tavakoli, M. & Stone, G. N. (2007). Longitudinal range expansion and cryptic eastern species in the western Palaearctic oak gallwasp *Andricus coriarius*. *Molecular Ecology*, 16 (10): 2103-2114. DOI: https://doi.org/10.1111/j.1365-294X.2006.03210.x

Darriba, D., Taboada, G. L., Doallo, R. & Posada, D. (2012). Jmodeltest 2: More models. New Heuristics and Parallel Computing. *Nature Methods*, 9(8): 772. DOI: https://doi.org/10.1038/nmeth.2109

Demirsoy, A. (2002). *Genel ve Türkiye zoocoğrafyası, "Hayvan Coğrafyası*. Meteksan Basımevi, Ankara.

Drummond, A. J., Suchard, M. A., Xie, D. & Rambaut, A. (2012). Bayesian phylogenetics with BEAUti and the BEAST 1.7. *Molecular Biology and Evolution*, 29(8): 1969–1973. DOI: https://doi.org/10.1093/molbev/mss075

Erol, O. (1983). Türkiye'nin genç tektonik ve jeomorfolojik gelişimi. *Jeomorfoloji Dergisi* 11: 1-22.

Excoffier, L. & Lischer, H. E. L. (2010). Arlequin Suite Ver 3.5: A new series of programs to perform population genetics analyses under Linux and Windows. *Molecular Ecology Resources*, 10: 564-567. DOI: https://doi.org/10.1111/j.1755-0998.2010.02847.x

Fu, Y. X. (1997). Statistical tests of neutrality against population growth, hitchhiking and background selection. *Genetics* 147: 915–925. DOI: https://doi.org/10.1093/genetics/147.2.915

Harpending, H. C. (1994). Signature of ancient population growth in a low-resolution mitochondrial DNA mismatch distribution. *Human Biology*, 66(4): 591-600. Retrieved from: https://www.jstor.org/stable/41465371?seq=1

Hayward, A. & Stone, G. N. (2006). Comparative phylogeography across two trophic levels: The oak gallwasp *Andricus kollari* and its chalcid parasitoid *Megastismus stigmatizans*. *Molecular Ecology*, 15: 479-489. https://DOI: https://doi.org/10.1111/j.1365-294X.2005.02811.x

Hewitt, G. M. (1999). Post-Glacial re-colonization of European biota. *Biological Journal of the Linnean Society*, 68: 87-112. DOI: https://doi.org/10.1006/bijl.1999.0332

Hewitt, G. M. (2004). Genetic consequences of climatic oscillations in the Quaternary. *Philosophical transactions of the Royal Society of London. Series B, Biological sciences*, 359(1442), 183–195. DOI: https://doi.org/10.1098/rstb.2003.1388

Krijgsman, W., Hilgen, F., Raffi, I., Sierrro, F. J. & Wilson, D. S. (1999). Chronology, causes and progression of the Messinian salinity crisis. *Nature* 400, 652–655. DOI: https://doi.org/10.1038/23231

Koch, M. A., Bani, B., German, D. A. & Huang, X. (2017). Phylogenetics, phylogeography and vicariance of polyphyletic Grammosciadium (Apiaceae: Careae) in Anatolia. *Botanical Journal of the Linnean Society*, 185, 168-188. DOI: https://doi.org/10.1093/botlinnean/box051

Librado, P. & Rozas, J. (2009). DnaSP v5: A software for comprehensive analysis of DNA polymorphism data. *Bioinformatics*, 25: 1451-1452. DOI: https://doi.org/10.1093/bioinformatics/btp187

Melika, G. (2006). *Gallwasps of Ukraine: Cynipidae*. Schmalhausen Institute of Zoology, National Academy of Sciences, 646, Ukraine. Retrieved from: http://mail.izan.kiev.ua/vz-pdf/suppl/Supplement%202006-21-1.pdf

Mutun, S., and Dinç, S. (2019). The Anatolian diagonal and paleoclimatic changes shaped the phylogeography of *Cynips quercus* (Hymenoptera, Cynipidae). *Annales Zoologici Fennici*. 56, 65–83. DOI: https://doi.org/10.5735/086.056.0107

Nei, M. (1987). *Molecular Evolutionary Genetics*. Columbia University Press, New York. DOI: https://doi.org/10.7312/nei-92038

Nichols, R. A., Hewitt, G. M. (1994). The genetic consequences of long-distance dispersal during colonization. *Heredity* 72: 312–317. DOI: https://doi.org/10.1038/hdy.1994.41

Papadopoulou, A., Anastasiou, I. & Vogler, A. P. (2010). Revisiting the insect mitochondrial molecular clock: the Mid-Aegean trench calibration. *Molecular Biology and Evolution*, 27(7): 1659-72. DOI: https://doi.org/10.1093/molbev/msq051

Poulakakis, N., Lymberakis, P., Valakos, E., Pafilis, P., Zouros, E. & Mylonas, M. (2005). Phylogeography of Balkan wall lizard (*Podarcis taurica*) and its relatives inferred from mitochondrial DNA sequences. *Molecular Ecology*, 14: 2433-2443. DOI: https://doi.org/10.1111/j.1365-294X.2005.02588.x

Pound, M. J., Haywood, A. M., Salzmann, U., Riding, J. B., Lunt, D. J., & Hunter, S.J. (2011). A Tortonian (Late Miocene, 11.61–7.25 Ma) global vegetation reconstruction. *Palaeogeography, Palaeoclimatology, Palaeoecology*, 300, 29-45. DOI: https://doi.org/10.1016/j.palaeo.2010.11.029

Ramos-Onsins, S. E. & Rozas, J. (2002). Statistical properties of new neutrality tests against population growth. *Molecular Biology and Evolution*, 19: 2092-2100. DOI: https://doi.org/10.1093/oxfordjournals.molbev.a004034

Rogers, A. & Harpending, H. (1992). Population growth makes waves in the distribution of pairwise differences. *Molecular Biology and Evolution*, 9: 552 -569. DOI: https://doi.org/10.1093/oxfordjournals.molbev.a040727

Rokas, A., Atkinson, R. J., Webster, L. M. I., Csöka, G. & Stone, G. N. (2003). Out of Anatolia: Longitudinal gradients in genetic diversity support an eastern origin for a circum-Mediterranean oak gallwasp *Andricus quercustozae*. *Molecular Ecology*, 12: 2153-2174. DOI: https://doi.org/10.1046/j.1365-294x.2003.01894.x

Schneider, S. & Excoffier, L. (1999). Estimation of past demographic parameters from the distribution of pairwise differences when the mutation rates vary among sites: application to human mitochondrial DNA. *Genetics*, 152: 1079–1089. DOI: https://doi.org/10.1093/genetics/152.3.1079

Stone, G. N., Atkinson, R. J., Brown, G. & Rokas, A. (2002). The population genetic consequences of range expansion: a review of pattern and process, and the value of oak gallwasps as a model system. *Biodiversity Sciences*, 10 (1): 80-97. Retrieved from: https://www.biodiversity-science.net/EN/article/downloadArticleFile.do?attachType=PDF&id=7155

Stone, G. N., Challis, R. J., Atkinson, R. J., Csoka, G., Hayward, A., Melika, G., Mutun, S., Preuss, S., Rokas, A., Sadeghi, E. & Schönrogge, K. (2007). The phylogeographical clade trade: Tracing the impact of human-mediated dispersal on the colonization of northern Europe by the oak gallwasp *Andricus kollari*. *Molecular Ecology*, 16 (13): 2768-2781. DOI: https://doi.org/10.1111/j.1365-294X.2007.03348.x

Swofford, D. L. (2002). *PAUP: Phylogenetic analysis using parsimony ver. 4.0b10*. Sinauer Associates, Sunderland, Massachusetts. Retrieved from: https://paup.phylosolutions.com/

Şekercioğlu, Ç. H., Anderson, S., Akçay, E., Bilgin, R., Can, Ö. E., Semiz, G., Tavşanoğlu, Ç., Yokeş, M. B., Soyumert, A., İpekdal, K., Sağlam, İ. K., Yücel, M. & Dalfes, H. N. (2011). Turkey's globally important biodiversity in crisis. *Biological Conservation*, 144: 2752-2769. DOI: https://doi.org/10.1016/j.biocon.2011.06.025

Şengör, A. M. C. & Yılmaz, Y. (1981). Tethyan evolution of Turkey: A plate tectonic approach. *Tectonophysics*, 75:181-241. DOI: https://doi.org/10.1016/0040-1951(81)90275-4

Tajima, F. (1989). The effect of change in population size on DNA polymorphism. *Genetics*, 23(3): 597-601. DOI: https://doi.org/10.1093/genetics/123.3.597

Teacher, A. G. F. & Griffiths, D. J. (2011). HapStar: Automated haplotype network layout and visualisation. *Molecular Ecology Resources*, 11(1): 151-153. DOI: https://doi.org/10.1111/j.1755-0998.2010.02890.x

e-ISSN 2757-5195

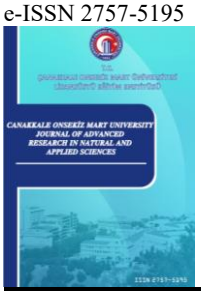

Çanakkale Onsekiz Mart University

Journal of Advanced Research in Natural and Applied Sciences

Open Access

doi.org/10.28979/jarnas.1117590 2023, Vol. 9, Issue 1, Pages: 237-250 dergipark.org.tr/tr/pub/jarnas

Investigation of Current, Temperature, and Concentration Distribution of a Solid Oxide Fuel Cell with Mathematical Modelling Approach

S.Mehdi Rezvan[1], Mohammad Ahangari[1], Nagihan Delibaş[2*], Soudabeh Bahrami[1], Asgar Moradi[1], Aligholi Niaei[1,2]

[1]Department of Chemical & Petroleum Engineering, University of Tabriz, Tabriz, Iran
[2]Department of Physics, Faculty of Science, University of Sakarya, 54050 Serdivan, Sakarya, Türkiye

Article History

Received: 21.05.2022

Accepted: 06.09.2022

Published: 05.03.2023

Research Article

Abstract − The usage of environment-friendly energy converter devices is getting more and more attention as a result of environmental crises and regulations. SOFCs are among the highly efficient chemical to electrical energy converters. Thus, their effectiveness is a significant issue to improve. To increase the efficiency of SOFCs, their properties should be investigated. However, it is costly and time-consuming to test all the important characteristics of a solid oxide fuel cell by experimental methods. Computational methods can contribute to evaluate the influence of each parameter on the performance of the fuel cell. In this paper, a 3D mathematical model of a SOFC is presented. The model can describe the fuel cell's temperature, the concentration of material, and current distribution inside the cell. Also, the influence of the flow pattern (co-current and counter-current) on the distribution plots and performance of the solid oxide fuel cell is investigated. The results demonstrate that the distribution of the current, concentration, and temperature is firmly related and wherever the concentration of reactants is higher, the temperature and current increase too. Also, the plots of power density and cell potential versus current were consistent with the results of the literature. Moreover, the comparison between two types of flow patterns shows that there is no significant variation when the type of current changes from counter to co-current. However, the performance of the SOFC is mildly better with a co-current flow pattern.

Keywords − *Flow pattern, fuel cell, mathematical modeling, SOFC,*

1. Introduction

Fuel cells are one of the most important electrical energy sources since they convert chemical energy to electrical energy directly. The direct conversion of energies decreases the energy losses that occur in conventional conversion of fuel energies to electricity which is through heat (Ferriday & Middleton, 2021; Shaari, et. al., 2021; Singh, et. al.,2021).

Among different types of fuel cells, solid oxide fuel cells attract a lot of attention because of their advantages like being safer than fuel cells with liquid electrolytes and higher efficiency at high temperatures. Not only SOFCs have high-energy efficiency and power density, but also they emit low or zero amounts of pollutants and, because they work at high temperatures (600-1000 ^{o}C) they can use various materials as fuel (hydrocarbons, hydrogen or ammonia) (Delibaş et al., 2022; Hussain & Yangping, 2020; Kurahashi et al., 2022; Laosiripojana et al., 2009).

[1] rezvan.amir80@gmail.com
[2] m.ahangare95@gmail.com
[3] caylak@sakarya.edu.tr
[4] sudabehbahrami68@yahoo.com
[5] asgharmoradi1374@gmail.com
[6] ali.niaei@gmail.com
[*] Corresponding Author

SOFCs have different operating parts. However, the most significant parts are two electrodes and the electrolyte between them. Anode and cathode electrodes should be porous, ion conductor, electron conductor, thermally compatible with the electrolyte and stable at high temperatures. The electrolyte which locates between two electrodes should possess some special properties, like being dense, ion conductor, thermally compatible with electrodes, stable in both reduction and oxidation environments and a weak electron conductor, or not being electron conductor at all (Ahmad et al., 2021; Burnwal, et. al., 2016). In the cathode, the oxygen reduction reaction (ORR) happens, as (1.1), and then the oxygen transfers to the anode through the electrolyte and in the anode, where the hydrogen turn to the proton, oxygen ions and protons react and turn to water, as (2.1) (Aydın, Matsumoto, & Shiratori, 2021; Kurahashi, Murase, & Santander, 2022; Stambouli & Traversa, 2002).

$$\tfrac{1}{2}O_2 + 2e^- \rightarrow O^{2-} \tag{1.1}$$

$$O^{2-} + H_2 \rightarrow H_2O + 2e^- \tag{1.2}$$

In this reaction, electrons are released and move to the cathode and in this way electricity required for transport or electronic devices can be produced. Figure 1 (Shu et al., 2019). demonstrates the operation of SOFC with H_2 as fuel.

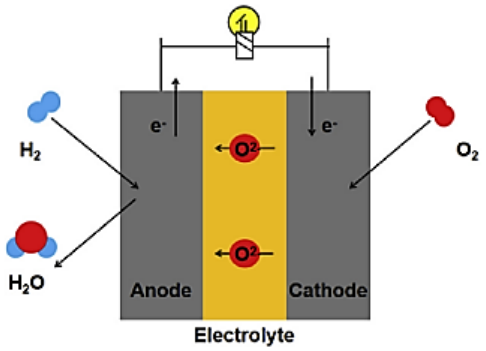

Figure 1. Schematic diagram of operation of a SOFC (Shu et al., 2019)

Numerous parameters such as geometrical properties, type of fuel, electrode and electrolyte material, type of flow etc. affect the performance and efficiency of SOFCs. Since investigating all of these parameters in labs and through experimental work is costly and can be a waste of time, researchers suggest computational work to avoid these problems and study the influence of each parameter in shorter time with much lower cost. In other words, numerical study can contribute to investigating the influence of different geometrical characteristics of the cell without producing different cells, which are expensive, measuring the effect of different materials like anode, cathode and electrolyte, which is difficult to test, studying the distribution of materials' concentration, temperature and charge inside each part of the cell which is impossible to be done experimentally (Abdalla et al., 2018).

There are numerous studies regarding mathematical modeling and simulation of SOFCs and researchers have utilized different approaches to model SOFCs and investigate their properties. For instance, COMSOL Multiphysics software is one of the practical and user-friendly software that can be utilized for studying various aspects of the problem since it contains numerous physics related to mass, heat and charge transform. It also provides various kinds of modeling and simulation such 1D, 2D, and 3D. Moreover, the results can be shown as plots or in the geometry of the problem itself, which is very important in understanding the performance of the fuel cells (Kakac et al., 2007).

Ranasinghe et al, studied the modeling of a single solid oxide fuel cell with COMSOL and reported that the performance of the fuel cell is better when the gas flow pattern is radial rather than a counter flow pattern (Ranasinghe & Middleton, 2017).

Yakabe et al, investigated a three-dimensional mathematical modeling of a planar SOFC and studied the temperature, potential, and chemical species distribution and calculated current density with a finite volume method (Yakabe et al., 2001).

Li et al proposed a quasi 2D model of a tublar SOFC and studied the performance of the cell under the operating condition. The results demonstrated that the quasi approximations used in the model can work well (Li & Suzuki, 2004).

Andersson et al, investigated the material structure grading of a solid oxide fuel cell in the direction normal to the electrode/electrolyte interface and claimed that grading the electron tortuosity and the pore tortuosity in the direction normal to the electrode/electrolyte interface increases performance, but grading the porosity has negative effect on the performance (Xia et al., 2002).

Parametric and transient analysis of non-isothermal, planar Solid oxide fuel cells with COMSOL modeling was studied by Tseronis et al, and they reported the temperature, species composition, electronic and ionic voltage, and current density distributions in a single cell. They also studied the dynamics of SOFC as a result of altering the operation condition of the fuel cell (Tseronis et al., 2012).

The results of the study of Akkaya, which worked on a turbular solid oxide fuel cell, showed that operating conditions play an important role in order to have a fuel cell with optimal performance. Therefore, the change in the operating conditions directly affects the performance of the solid oxide fuel cell. In addition, concentration of polarization is also an important key in limiting the current density (Akkaya, 2007).

Ebrahimi et al, found the optimized fuel cell operation condition using a 3D modeling of transport phenomena in a planar anode-supported solid oxide fuel cell (Chiu et al., 2012).

In this work, we focused on the 3D modeling of a planar solid oxide fuel cell with Yttria-Stabilized Zirconia (YSZ) as electrolyte of the cell, NiO/YSZ (wt.%: 60/40) and $La_{0.6}Sr_{0.4}MnO_3$ were used as anode and cathode materials, respectively. Oxygen flows into the cathode electrode and hydrogen is considered as the fuel of the cell in the anode electrode. The distribution of the concentration of O_2 and H_2, charge, temperature distribution inside the cell and current distribution are investigated and the plots of the potential and power densities versus current density are demonstrated. All of this data is obtained for both conditions of the current. In other words, the study was done for both co-current and counter current flow pattern inside the fuel cell when the inlet temperature of currents was considered to be 1000 ^{o}C (Tseronis et al., 2012, Ranasinghe & Middleton, 2017).

2. SOFC Modeling

First we draw a cross section of our desired SOFC in 2D, it is turned into a three-dimensional model. (Figure 2, Figure 3)

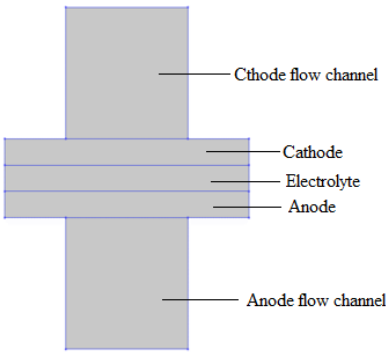

Figure 2. 2D model of SOFC

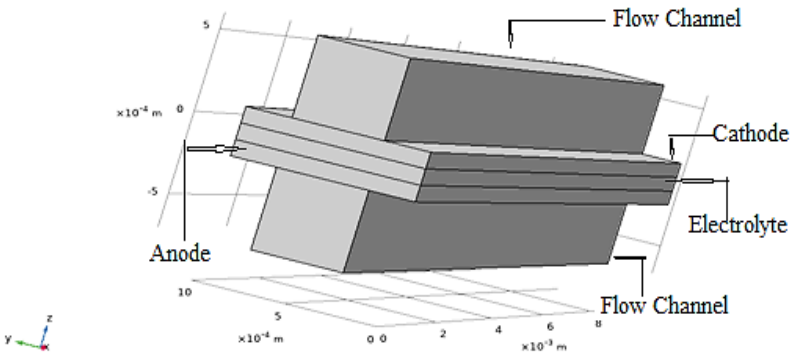

Figure 3. 3D model of SOFC

The physics used for this model are as follows:

- Secondary Current Distribution
- Equations of gas diffusion in porous media and flow channels
- Transport of Concentrated Species
- Heat Transfer in Solids and Fluids

The values of input electrochemical and geometric parameters used in SOFC modeling are given in Table 1 (Ilbas & Kumuk, 2019; Ranasinghe & Middleton, 2017; Suzuki, Shikazono, Fukagata, & Kasagi, 2008; Wang, Yang, Zhang, & Xia, 2007). The OCV in this study is very close to the Nernst value (1.097 V) (Caliandro, Diethelm, & Nakajo, 2015).

Table 1
Parameters used in SOFC model

Value	Parameter	Value	Parameter
Atmospheric pressure	1 [atm]	Air mixture thermal conductivity	0.58 [$W.m^{-1}.K^{-1}$]
Temperature	800-1000 [℃]	Inlet weight fraction H_2 at anode	0.4
Viscosity, air	$3e^{-5}$ [Pa.s]	Inlet weight fraction O_2 at cathode	0.15
Pressure drop, anode	2 [Pa]	Electrolyte conductivity	5 [$S.m^{-1}$]
Pressure drop, cathode	6 [Pa]	Molecular weight H_2	2 [$g.mol^{-1}$]
Exchange current density, anode	0.1 [$A.m^{-2}$]	Molecular weight O_2	32 [$g.mol^{-1}$]
Exchange current density, cathode	0.01 [$A.m^{-2}$]	Molecular weight N_2	28 [$g.mol^{-1}$]
Active specific surface area, cathode	$1e^{9}$ [$1.m^{-1}$]	Molecular weight H_2O	18 [$g.mol^{-1}$]
Initial cell polarization	0.05 [V]	Gas flow channel width	
Anode permeability	$1e^{-10}$ [m^2]	Rib width	$0.5e^{-3}$ [m]
Cathode permeability	$1e^{-10}$ [m^2]	Gas diffusion electrode thickness	$0.5e^{-3}$ [m]
Equilibrium voltage, anode	0 [V]	Electrolyte thickness	$1e^{-4}$ [m]
Equilibrium voltage, cathode	1 [V]	Gas flow channel height	$1e^{-4}$ [m]
Ionic effective conductivity, anode	1 [$S.m^{-1}$]	Flow channel length	$0.5e^{-3}$ [m]
Electrical effective conductivity, anode	1000 [$S.m^{-1}$]	Gas flow channel width	$10e^{-3}$ [m]
Fuel mixture thermal conductivity	0.32 [$W.m^{-1}.K^{-1}$]	Flow channel length	$0.5e^{-3}$ [m]

2.1. Secondary Current Distribution

By using this physics, the relationship between charge transfer and over potential can be described using the Butler-Volmer and Tafel equations. Since the current from the solid oxide fuel cell is generated during an electrochemical reaction at the electrode/electrolyte material interface, it is necessary to correctly determine the kinetics of this reaction. The Butler-Volmer equation is an important equation in electrochemistry that can be used to balance the charge between current and overvoltage η. The general form of the Butler-Volmer equation, which was also used in this simulation, is as follows (Ilbas & Kumuk, 2019):

$$i = i_0 \left[\left(\frac{C_o}{C_o^*}\right) \exp\left(\frac{\alpha_a F\eta}{RT}\right) - \left(\frac{C_r}{C_r^*}\right) \exp\left(\frac{-\alpha_c F\eta}{RT}\right) \right] \quad (2.1)$$

where i is the electrode current density, i_0 exchange current density, C_o and C_r refer to the concentration of the species to be oxidized and to be reduced, respectively, F is the Faraday's constant, R is the gas constant, T is the temperature, η is the overvoltage, α_c cathodic charge transfer coefficient and α_a anodic charge transfer coefficient. Since the current distribution is dependent on the electrochemical reaction and any reaction is also dependent on the concentration of the species participating in the reaction, therefore, the use of this form of the Butler-Volmer equation, which shows the dependence of the current distribution to the concentration of oxidant and reducer species, will be required.

The overvoltage is defined by (Ranasinghe & Middleton, 2017; Yaoxuan, Cheng, & Kening, 2021):

$$\eta = \phi_{electronic} - \phi_{ionic} - \Delta\phi_{eq} \quad (2.2)$$

where $\Delta\phi_{eq}$ is the equilibrium potential difference.
The cathode and anode charge transfer kinetics is given by (2.3) and (2.4) equations respectively:

$$i = i_{0.c} \left[\exp\left(\frac{3.5F\eta}{RT}\right) - x_{o2} \left(\frac{C_t}{C_{o2.ref}}\right) \exp\left(\frac{-0.5F\eta}{RT}\right) \right] \quad (2.3)$$

$$i_{a,ct} = i_{0.a} \left[\left(\frac{C_{h2}}{C_{h2.ref}}\right) \exp\left(\frac{0.5F\eta}{RT}\right) - \left(\frac{C_{h2o}}{C_{h2o.ref}}\right) \exp\left(\frac{-1.5F\eta}{RT}\right) \right] \quad (2.4)$$

where $i_{0.c}$ and $i_{0,a}$ refer to the cathode exchange current density and anode exchange current density respectively, x_{o2} is the molar fraction of O_2, ch_2 is the molar concentration of H_2, ch_2o is the molar concentration of H_2O, ct is the total concentration of species, ch_2,ref and ch_2o,ref is the reference molar concentrations.
We used the anode inlet voltage as a fixed reference voltage which is equal to zero. Also the cathode inlet voltage (V_{cell}) is given by:

$$V_{cell} = \Delta\phi_{eq.a} - \Delta\phi_{eq.c} - V_{pol} \quad (2.5)$$

In this model, $\Delta\phi_{eq.a} = 0$ V, $\Delta\phi_{eq.c} = 1$ V and 0.05 V $< V_{pol} <$ 0.8 V was considered. In addition to the above boundary conditions, the initial condition $\phi_{electronic} = 0$ and $\phi_{ionic} = 0$ was considered for the anode and electrolyte, while according to the selected boundary conditions, the initial condition $\phi_{electronic} = V_{cell}$ and $\phi_{ionic} = 0$ was applied to the cathode. We have applied the insulating boundary conditions for all the external boundaries for the ionic charge balance equations of the model.

2.2. Equations of gas diffusion in porous media and flow channel

In the solid oxide fuel cell, there are two fluids, one is the air fluid, which reaches the surface of the cathode material through the channel on the cathode side, so that the oxygen inside it performs the electrochemical reaction of the cathode half-cell. The other fluid is the fuel, which reaches the surface of the anode material through a channel on the anode side. Both air and fuel fluids, when they reach the surface of the porous

electrode material, diffuse and transfer in this porous electrode. Therefore, it is necessary to model fluid transport in both gas flow channel and porous media through appropriate equations
Gas flows in open channels are modelled by using the weakly compressible Navier-Stokes equation as given below (Ilbas & Kumuk, 2019).

$$\rho(\frac{\partial u}{\partial t} + u.\nabla u) = -\nabla p + \nabla(\mu(\nabla u) + (\nabla u)^T) - \frac{2}{3}\mu(\nabla u) I) + F \quad (2.6)$$

where u is the fluid velocity, F is volume force vector, p is the fluid pressure, ρ is the fluid density, I is identity tensor and μ is the fluid dynamic viscosity.
Also, the Brinkman equations are used for gas diffusion in porous electrodes. This equation is given by (Ranasinghe & Middleton, 2017):

$$\nabla p = -\frac{\mu}{\kappa}v + \mu_e \nabla^2(v) \quad (2.7)$$

where v is fluid velocity, μ is fluid dynamic viscosity, μ_e is the effective viscosity parameter. At the inlet of the cathode and anode flow channel, the pressure was considered 6 and 4 Pa, respectively. Also, the outlet of the cathode and anode flow channel, the pressure was applied 0 Pa as boundary conditions.

2.3. Transport of Concentrated Species

For each electrode flow compartment (anode and cathode flow channels), the material transport is modelled by the Maxwell-Stefan's diffusion and convection equations. The Maxwell-Stefan diffusion and convection equation given by:

$$\frac{\partial \rho \omega_i}{\partial t} + \nabla.(j_i + \rho \omega_i u) = R_i \quad (2.8)$$

where ρ denotes the density, ω_i the mass fraction, j_i is the molecular flux and R_i is the reaction rate of the i^{th} species, u is the velocity.
The boundaries at the walls of the gas channels and the electrodes are considered as zero mass flux (insulation condition). We considered the outlet conditions as convective flux. This means that the component transport is perpendicular to the boundary. Furthermore, it is assumed that there is continuity in all the transport compositions. At the inlet of the air and fuel flow channel, the mass fraction of O_2 and H_2 was considered to be 0.15 and 0.4, respectively.

2.4. Heat Transfer in Solids and Fluids

The general equation of heat transfer intended for the model is given below. In this model, we used steady state heat transfer and considered the convection heat transfer only for gas channels. In addition, we ignored radiation heat transfer (Tseronis, Bonis, Kookos, & Theodoropoulos, 2012).

$$\rho . c_p . u . \nabla T = \nabla . (k \nabla T) + Q \quad (2.9)$$

Here Q is the heat generation or consumption, k the effective thermal conductivity, T the temperature and c_p the specific heat capacity. Heat generated by electrochemical suction, ohmic polarization and etc. given by (Mohammad Ebrahimi, 2017; Tseronis et al., 2012):

$$Q = i.(\frac{T.\ \Delta S_r}{n_e.\ F} + \eta) + \sum \frac{i^2}{\sigma} + \sum(r_{ref}.\ \Delta H_{ref}) \quad (2.10)$$

where ΔS_r is entropy change of the reaction, r_{ref} the reforming reaction rates (mol/m^3s) and ΔH_{ref} the enthalpy of the reactions.

The heat exchange at the interface between the electrode material and the gas flow (fuel or air) is conductive in the electrode material and convection in the gas flow. Therefore, the following boundary condition can be considered for the interface between the electrode material and the air or fuel flow (Grondin et al., 2013):

$$n.(-k\nabla T) = h.(T_w - T_f) \quad (2.11)$$

where T_w is the channel wall temperature and T_f is the fluid temperature. h is the heat transfer coefficient in gas flow channels is calculated using the Nusselt number (Nu ≈ 3.09) (Grondin et al., 2013) according to the following equation:

$$h = \frac{Nu\, k_{gas}}{D_h} \quad (2.12)$$

D_h is hydraulic diameter for the channel is also given by:

$$D_h = \frac{2\, W_{CH} H_{CH}}{W_{CH} + H_{CH}} \quad (2.13)$$

Where W_{CH} and H_{CH}, the length and height of gas channels are respectively.
After choosing the suitable physics and boundary conditions, the mesh of the fuel cell is adjusted (Figure 4) and the results of the model obtained by computing and solving the model with FEM. As it is shown in Figure 4 Mesh is finer in electrodes and electrolyte in comparison with flow channels.

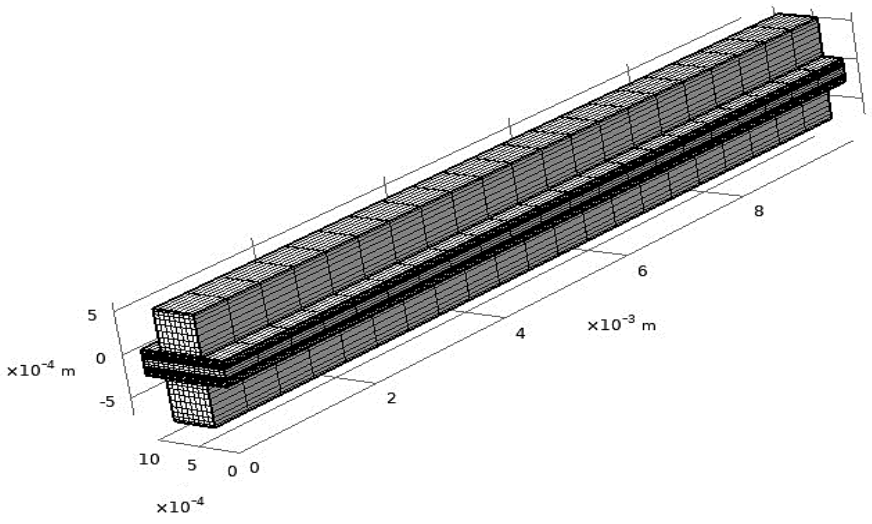

Figure 4. Mesh of the solid oxide fuel cell

3. Results and Discussion

The results of the study were achieved by considering the flow pattern co-current and counter current inside the cell. When the flow pattern was co-current, both the cathode and anode currents enter from the back of the fuel cell and exit from the front part of the cell. For counter current flow pattern, the inlet of the cathode flow channel is at the back of the cell while the inlet of the anode flow channel is in front of the fuel cell.

The graph in Figure 5 shows the average power density versus current density for both co-current and counter current flow patterns. As it is obvious from the plots, the potential of the cell decreases as the current density increases and the power density enhances at lower current densities, but it decreases when the current density passes a certain amount (about 1500 $A.m^{-2}$). In addition, it can be seen that around the current density of 1500 $A.m^{-2}$, the two curves are slightly separated from each other, and this point also indicates the maximum power

density for the two current patterns. The value of the maximum power density for the co-current and counter current flow pattern was obtained as 1073 $W.m^{-2}$ and 1050 $W.m^{-2}$, respectively.

Figure 6 also shows the trend of cell voltage changes versus current density. There is little difference between the voltages in the two current patterns. However, from the two graphs related to Figures 5 and 6, it is clear that the co-current flow has a more suitable performance in terms of power density and voltage.

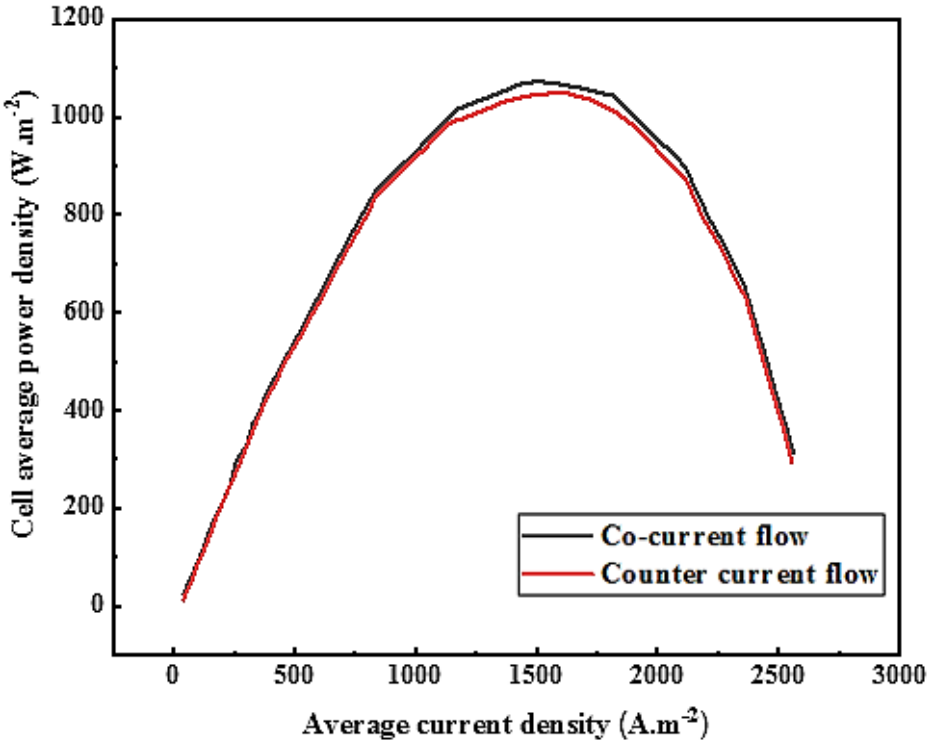

Figure 5. Power density- current density plot for co-current and counter-current flow pattern

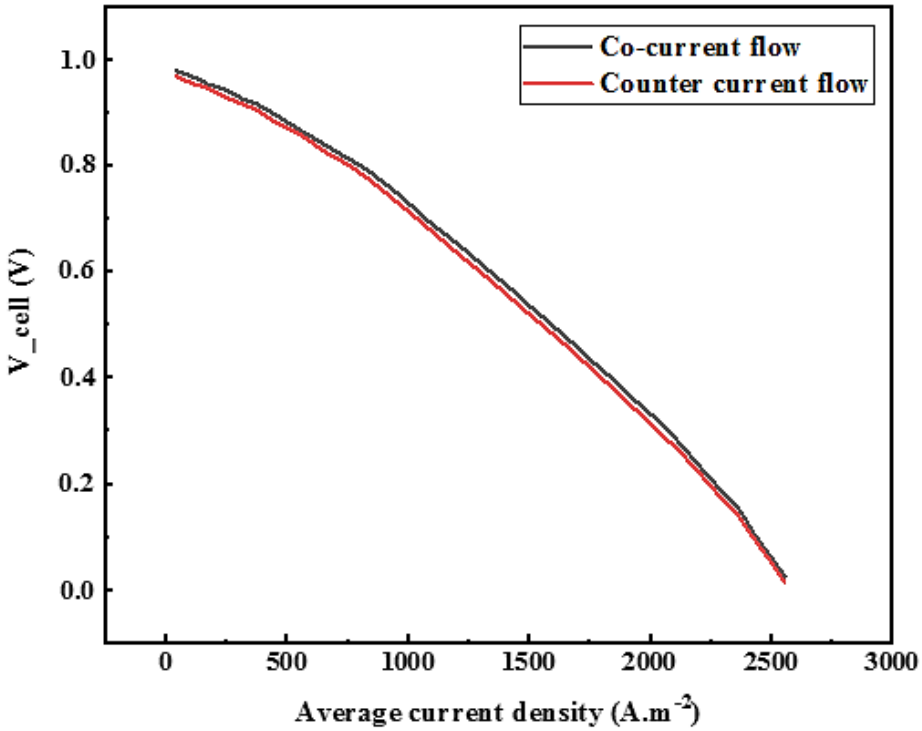

Figure 6. Cell voltage- current density plot for co-current and counter-current flow pattern

The distribution of the temperature, current, and concentration of chemical species are demonstrated in Figure 7 to Figure 14. Distributions of these parameters are connected to each other. In other words, when the concentration of hydrogen and oxygen is high, the reactions inside the cell occur faster and better and this way the produced heat and electrical current enhance and when the concentration of chemical species decreases the amount of generated heat and electricity reduce.

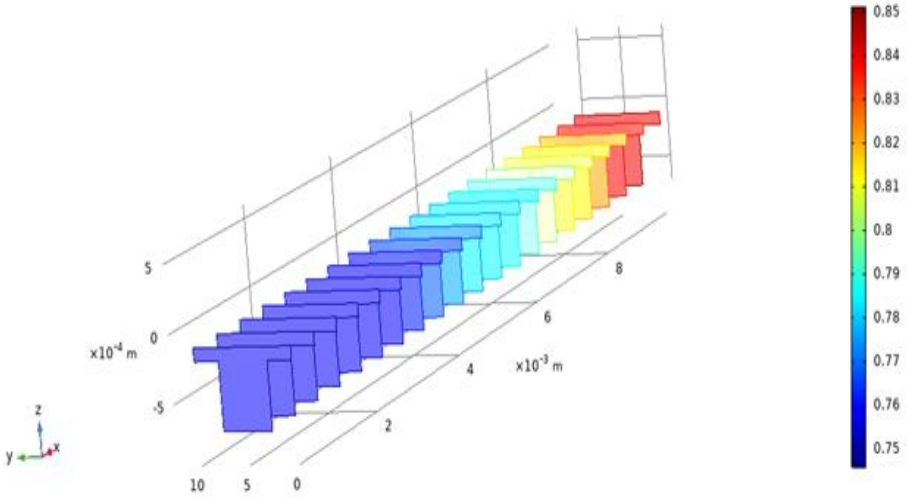

Figure 7. Distribution of molar fraction of H_2 inside the cell for co-current flow pattern

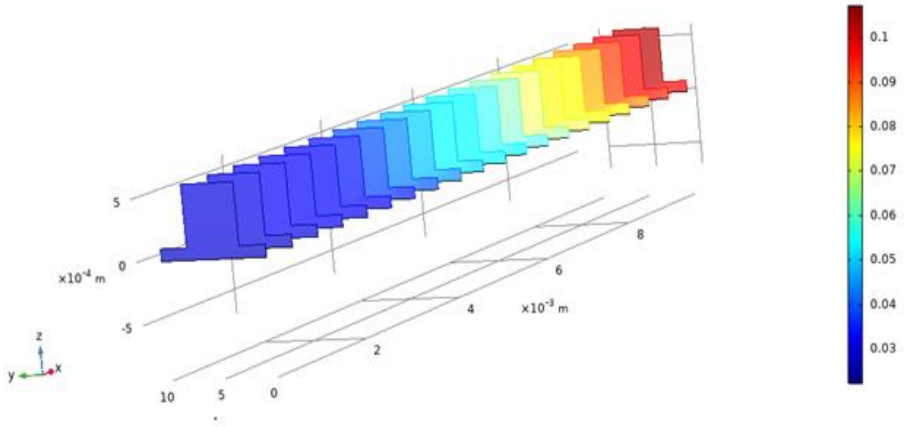

Figure 8. Distribution of molar fraction of O2 inside the cell for co-current flow pattern

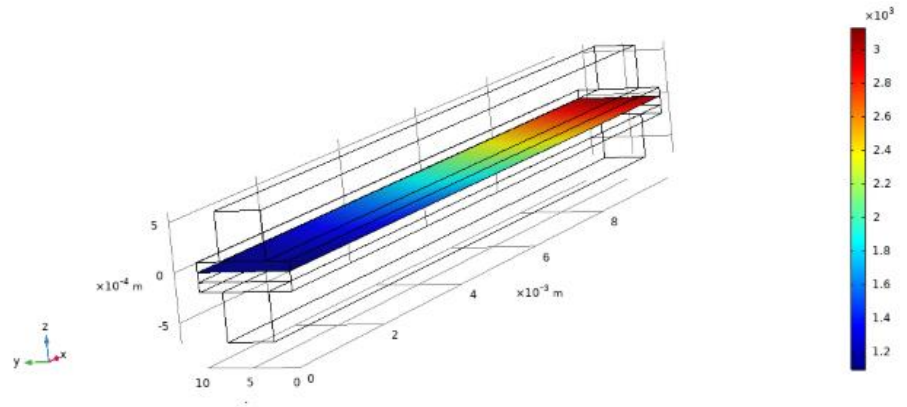

Figure 9. Distribution of current inside the cell for co-current flow pattern

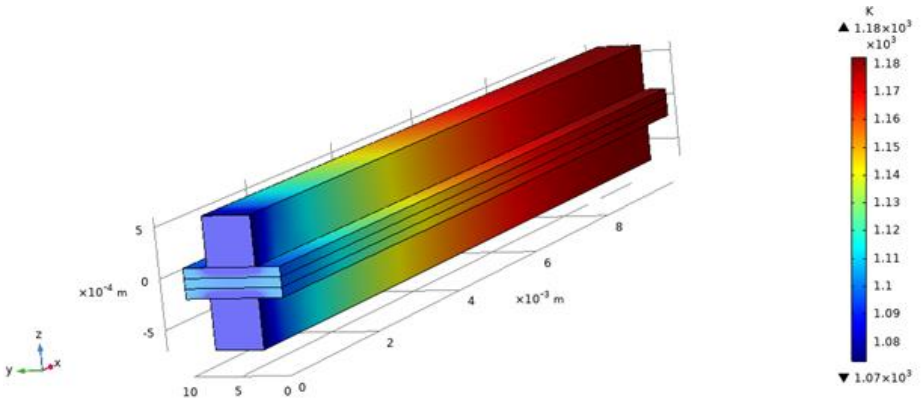

Figure 10. Distribution of temperature inside the cell for co-current flow pattern

For co-current flow pattern, the "3D temperature distribution" diagram (Figure 10) provides a 3D view of the temperature distribution throughout the fuel cell. According to this Figure 10, the maximum temperature is at the inlet of the fuel channel (anode side) and close to it. By analyzing the figure of the "molar hydrogen fraction (Figure 7)"at the inlet of the fuel channel, it is understood that the molar hydrogen fraction is also maximum and in the continuation of the channel with the reaction of hydrogen, its concentration decreases and reaction in anode side occurs and electricity is produced. In fact, at the beginning of the channel, where the hydrogen concentration is high, the electrochemical reaction of the fuel cell also takes place optimally, and at the end of the channel, this reaction and the hydrogen concentration are minimized. In general, the heat released by the half-cell reaction of the cathode is greater than the heat released by the half-cell reaction of the anode. That is, the electrochemical reaction of the fuel cell is exothermic (Mohammad Ebrahimi, 2017). Therefore, as can be seen, at the entrance of the channels, where the concentration is high, the current and temperature are also high.The heat released along the Z axis is transmitted mainly through convection to the gas channels (air and fuel), and then this heat exits from the flow channel with gas flow. As a result, the temperature inside the cell decreases.

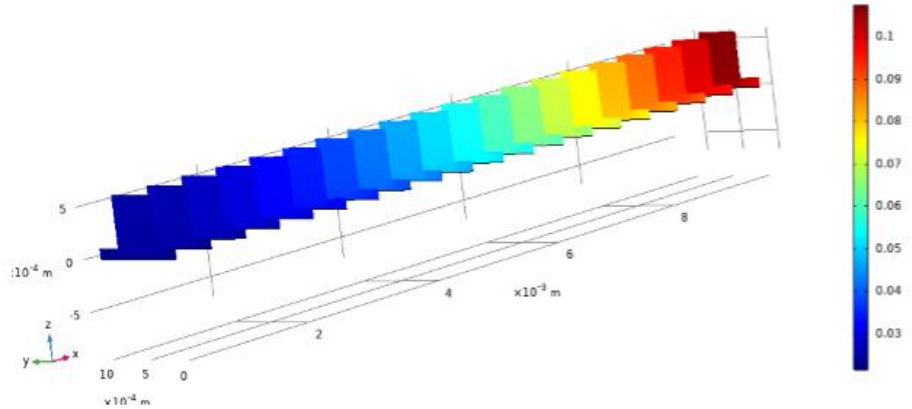

Figure 11. Distribution of molar fraction of O_2 inside the cell for counter-current flow pattern

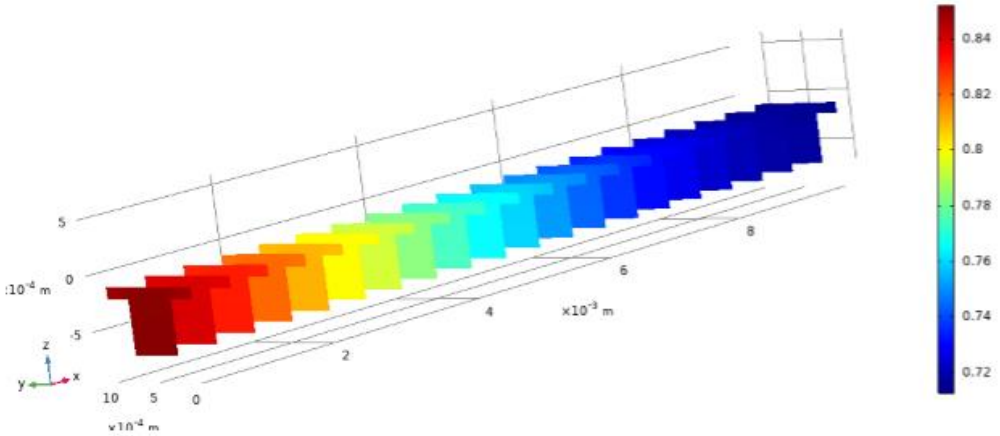

Figure 12. Distribution of molar fraction of H_2 inside the cell for counter-current flow pattern

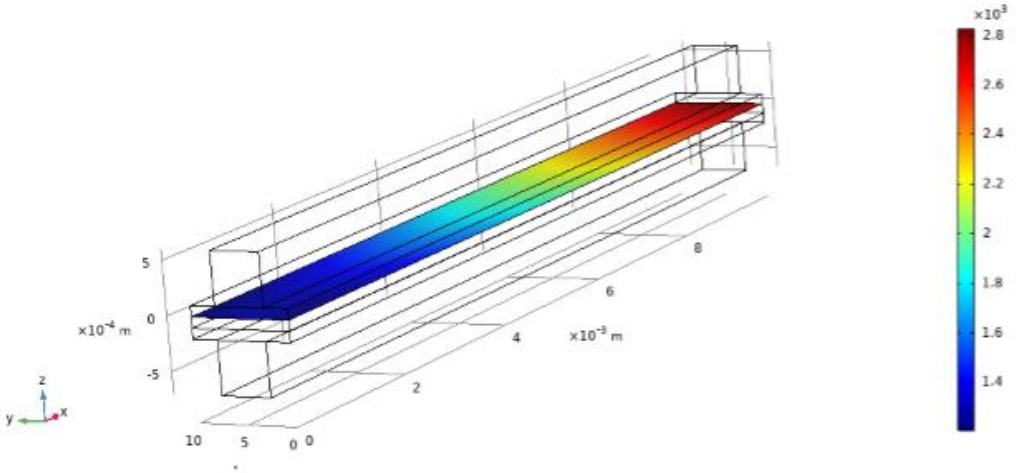

Figure 13. Distribution of current inside the cell for counter-current flow pattern

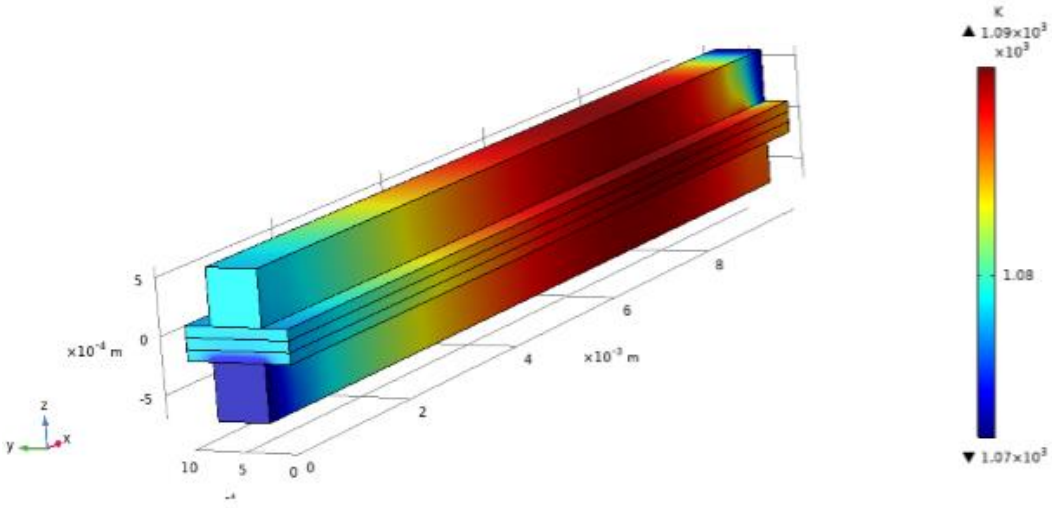

Figure 14. Distribution of temperature inside the cell for counter-current flow pattern

In counter-current flow pattern (Figure 11-14) , the inlet gas of each channel from the other side of the fuel cell is in contact with the outlet of the other channel, so initially the temperature of the inlet gas to the channels drops. Then the temperature rises by performing the exothermic electrochemical reactions inside the cell. The temperature drops at the outlets of the channels again (Figure 14). Despite the fact that the concentration at the inlet is high (Figure 11, Figure 12) , the temperature has its lowest value, and then even with the decrease in the concentration of the reaction material, followed by a decrease in the rate of reaction, the temperature increases and, also, the produced electricity enhances.That is because of the enhancement of the transforming of the chemical substances and reactions that occur in three-phase boundaries of the cell. According to the molar fraction diagrams, in the center of the cell, the maximum concentrations of both reactants (oxygen and hydrogen) are present at the reaction site. Only in the center of the fuel cell, the concentrations of these two substances are in the right amount to perform good reactions. Therefore, the electrochemical reactions in the center of the fuel cell are performed optimally, and the temperature in this area is high.

4. Conclusion

In this study, a 3D mathematical model of a SOFC is rendered which can demonstrate the temperature, concentration and current distributions inside the cell and the performance of the solid oxide fuel cell. In addition, the design parameter (flow pattern) of the inlet and outlet currents' influence on the performance of the cell was evaluated. In other words, the performance of the cell is calculated when the flow pattern changes from counter-current to co-current. The results stated that the distribution of temperature, current and concentration of reactants (O_2 and H_2) are related and wherever the concentration of materials is higher, the performance of the cell and the amount of the temperature and produced current enhance. Furthermore, changing the flow pattern from counter–current to co-current does not affect the efficiency of the cell significantly. However, the performance of the solid oxide fuel cell is better when the flow pattern is co-current.

Acknowledgements

The researchers extend their thanks and appreciation to the collaboration and support of the University of Tabriz, the Department of Physics at the University of Sakarya and the Scientific and Technological Research Council of Turkey (TUBİTAK).

Author Contributions

S.Mehdi Rezvan: Simulate the mathematical modelling prepared by M.Ahangari.

Mohammad Ahangari: Prepared the requirements for mathematical modelling (parameters, equations, etc.)

Nagihan Delibas: Contributed to the formation of idea and provided scientific and financial support.

Soudabeh Bahrami: Prepared theoretical information about SOFCs and mathematical modelling.

Asgar Moradi: Contributed to debugging the computational works.

Aligholi Niaei: Contributed to the formation of idea and provided scientific and financial support.

Conflicts of Interest

The authors declared no potential conflicts of interest with respect to the research, authorship and publication of this article.

References

Abdalla, A. M., Hossain, S., Azad, A. T., Petra, P. M. I., Begum, F., Eriksson, S. G., & Azad, A. K. (2018). Nanomaterials for solid oxide fuel cells: A review. *Renewable and sustainable energy reviews, 82*, 353-368. DOI: https://doi.org/10.1016/j.rser.2017.09.046

Ahmad, M. Z., Ahmad, S. H., Chen, R. S., Ismail, A. F., Hazan, R., & Baharuddin, N. A. (2021). Review on recent advancement in cathode material for lower and intermediate temperature solid oxide fuel cells application. *International Journal of Hydrogen Energy*. DOI: https://doi.org/10.1016/j.ijhydene.2021.10.094

Akkaya, A. V. (2007). Electrochemical model for performance analysis of a tubular SOFC. *International Journal of Energy Research, 31*(1), 79-98. DOI: https://doi.org/10.1002/er.1238

Aydin, Ö., Matsumoto, G., & Shiratori, Y. (2021). Thermal stresses in SOFC stacks: the role of mismatch among thermalconductivity of adjacent components. *Turkish Journal of Chemistry, 45*(3), 719-736. DOI: https://doi.org/10.3906/kim-2011-48

Aygün, B., Sariboğa, V., & Öksüzömer, M. A. F. (2021). Effect of fuel choice on conductivity and morphological properties of samarium doped ceria electrolytes for IT-SOFC. *Turkish Journal of Chemistry, 45*(5), 1408-1421. DOI: https://doi.org/10.3906/kim-2104-56

Burnwal, S. K., Bharadwaj, S., & Kistaiah, P. (2016). Review on MIEC cathode materials for solid oxide fuel cells. *Journal of Molecular and Engineering Materials, 4*(02), 1630001. DOI: https://doi.org/10.1142/S2251237316300011

Caliandro, P., Diethelm, S., & Nakajo, A. (2015). Electrochemical model of a triode solid oxide fuel cell. *ECS Transactions, 68*(1), 2387. DOI: https://doi.org/10.1149/06801.2387ecst

Chiu, H.-C., Jang, J.-H., Yan, W.-M., Li, H.-Y., & Liao, C.-C. (2012). A three-dimensional modeling of transport phenomena of proton exchange membrane fuel cells with various flow fields. *Applied energy, 96*, 359-370. DOI: https://doi.org/10.1016/j.apenergy.2012.02.060

Delibaş, N., Gharamaleki, S. B., Mansouri, M., & Niaei, A., Reduction of operation temperature in SOFCs utilizing perovskites. *International Advanced Researches and Engineering Journal, 6*(1), 56-67. DOI: https://doi.org/10.35860/iarej.972864

Ferriday, T. B., & Middleton, P. H. (2021). Alkaline fuel cell technology-A review. *International Journal of Hydrogen Energy, 46*(35), 18489-18510. DOI: https://doi.org/10.1016/j.ijhydene.2021.02.203

Grondin, D., Deseure, J., Ozil, P., Chabriat, J.-P., Grondin-Perez, B., & Brisse, A. (2013). Solid oxide electrolysis cell 3d simulation using artificial neural network for cathodic process description. *Chemical Engineering Research and Design, 91*(1), 134-140. DOI: https://doi.org/10.1016/j.cherd.2012.06.003 https://doi.org/10.1002/er.6353

Hussain, S., & Yangping, L. (2020). Review of solid oxide fuel cell materials: Cathode, anode, and electrolyte. *Energy Transitions, 4*(2), 113-126. DOI: https://doi.org/10.1007/s41825-020-00029-8

Ilbas, M., & Kumuk, B. (2019). Numerical modelling of a cathode-supported solid oxide fuel cell (SOFC) in comparison with an electrolyte-supported model. *Journal of the Energy Institute, 92*(3), 682-692. DOI: https://doi.org/10.1016/j.joei.2018.03.004

Kakac, S., Pramuanjaroenkij, A., & Zhou, X. Y. (2007). A review of numerical modeling of solid oxide fuel cells. *International Journal of Hydrogen Energy, 32*(7), 761-786. DOI: https://doi.org/10.1016/j.ijhydene.2006.11.028

Kurahashi, N., Murase, K., & Santander, M. (2022). High-Energy Extragalactic Neutrino Astrophysics. *arXiv preprint arXiv:2203.11936*. DOI: https://doi.org/10.48550/arXiv.2203.11936

Laosiripojana, N., Wiyaratn, W., Kiatkittipong, W., Arpornwichanop, A., Soottitantawat, A., & Assabumrungrat, S. (2009). Reviews on solid oxide fuel cell technology. *Engineering Journal, 13*(1), 65-84. DOI: https://doi.org/10.4186/ej.2009.13.1.65

Li, P.-W., & Suzuki, K. (2004). Numerical modeling and performance study of a tubular SOFC. *Journal of the Electrochemical Society, 151*(4), A548. DOI: https://doi.org/10.1149/1.1647569

Mohammad Ebrahimi, I. (2017). Three-dimensional modeling of transport phenomena in a planar anode-supported solid oxide fuel cell. *Iranian Journal of Hydrogen & Fuel Cell, 4*(1), 37-52. DOI: http://doi.org/ 10.22104/IJHFC.2017.2342.1144

Ranasinghe, S. N., & Middleton, P. H. (2017). *Modelling of single cell solid oxide fuel cells using COMSOL multiphysics.* Paper presented at the 2017 IEEE International Conference on Environment and Electrical Engineering and 2017 IEEE Industrial and Commercial Power Systems Europe (EEEIC/I&CPS Europe). DOI: https://doi.org/ 10.1109/EEEIC.2017.7977790

Shaari, N., Kamarudin, S. K., Bahru, R., Osman, S. H., & Md Ishak, N. A. I. (2021). Progress and challenges: Review for direct liquid fuel cell. *International Journal of Energy Research, 45*(5), 6644-6688. DOI:

Shu, L., Sunarso, J., Hashim, S. S., Mao, J., Zhou, W., & Liang, F. (2019). Advanced perovskite anodes for solid oxide fuel cells: A review. *International Journal of Hydrogen Energy, 44*(59), 31275-31304. DOI: https://doi.org/10.1016/j.ijhydene.2019.09.220

Singh, M., Zappa, D., & Comini, E. (2021). Solid oxide fuel cell: Decade of progress, future perspectives and challenges. *International Journal of Hydrogen Energy, 46*(54), 27643-27674. DOI: https://doi.org/10.1016/j.ijhydene.2021.06.020

Stambouli, A. B., & Traversa, E. (2002). Solid oxide fuel cells (SOFCs): a review of an environmentally clean and efficient source of energy. *Renewable and sustainable energy reviews, 6*(5), 433-455. DOI: https://doi.org/10.1016/S1364-0321(02)00014-X

Suzuki, M., Shikazono, N., Fukagata, K., & Kasagi, N. (2008). Numerical analysis of coupled transport and reaction phenomena in an anode-supported flat-tube solid oxide fuel cell. *Journal of power sources, 180*(1), 29-40. DOI: https://doi.org/10.1016/j.jpowsour.2008.02.039

Tseronis, K., Bonis, I., Kookos, I., & Theodoropoulos, C. (2012). Parametric and transient analysis of non-isothermal, planar solid oxide fuel cells. *International Journal of Hydrogen Energy, 37*(1), 530-547. DOI: https://doi.org/10.1016/j.ijhydene.2011.09.062

Tseronis, K., Bonis, I., Kookos, I., & Theodoropoulos, C. (2012). Parametric and transient analysis of non-isothermal, planar solid oxide fuel cells. *International Journal of Hydrogen Energy, 37*(1), 530-547. DOI: https://doi.org/10.1016/j.ijhydene.2011.09.062

Wang, G., Yang, Y., Zhang, H., & Xia, W. (2007). 3-D model of thermo-fluid and electrochemical for planar SOFC. *Journal of power sources, 167*(2), 398-405. DOI: https://doi.org/10.1016/j.jpowsour.2007.02.019

Xia, C., Rauch, W., Wellborn, W., & Liu, M. (2002). Functionally graded cathodes for honeycomb solid oxide fuel cells. *Electrochemical and solid-state letters, 5*(10), A217. DOI: https://doi.org/10.1149/1.1503203

Yakabe, H., Ogiwara, T., Hishinuma, M., & Yasuda, I. (2001). 3-D model calculation for planar SOFC. *Journal of power sources, 102*(1-2), 144-154. DOI: https://doi.org/10.1016/S0378-7753(01)00792-3

Yaoxuan, Q., Cheng, F., & Kening, S. (2021). *Multiphysics simulation of a solid oxide fuel cell based on COMSOL method.* Paper presented at the E3S Web of Conferences. DOI: https://doi.org/10.1051/e3sconf/202124501005

e-ISSN 2757-5195

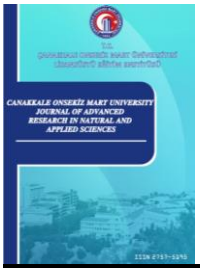

Çanakkale Onsekiz Mart University
Journal of Advanced Research in Natural and Applied Sciences
Open Access

doi.org/10.28979/jarnas.1139883 2023, Cilt 9, Sayı 1, Sayfa: 251-267 dergipark.org.tr/tr/pub/jarnas

Sürdürülebilir ve Yeni Bir "Gıda" Alternatifi Olarak Yenilebilir Böcekler

Ali Emre Andaç[1], Neşe Yılmaz Tuncel[2,*]

[1]Gıda Mühendisliği Bölümü, Mühendislik Fakültesi, Çanakkale Onsekiz Mart Üniversitesi, Çanakkale, Türkiye
[2]Gıda Teknolojisi Bölümü, Uygulamalı Bilimler Fakültesi, Çanakkale Onsekiz Mart Üniversitesi, Çanakkale, Türkiye

Makale Tarihçesi

Gönderim: 03.07.2022
Kabul: 12.10.2022
Yayım: 05.03.2023

Derleme Makale

Öz − Bazı böcek türlerinin insanlar tarafından tüketilmesi yeni bir konu olmamakla birlikte, son yıllarda özellikle nüfusun ve hayvansal protein talebinin artışı ile birlikte yeniden ele alınan bir konudur. Böceklerin hâlihazırda en az 2 milyar insan tarafından tüketildiği tahmin edilmektedir. Diğer pek çok hayvansal kaynağa göre daha az yem ile daha fazla vücut ağırlığı kazanımı ve küresel ısınmada çok önemli rol oynayan sera gazı salınımındaki payının oransal olarak çok daha az olması, yenilebilir böceklerin gelecek senaryolarında hem insan gıdası hem de hayvan yemi olarak potansiyelinin değerlendirilmesini önemli kılmaktadır. Besinsel açıdan değerlendirildiğinde yenilebilir böceklerin protein, yağ, diyet lif ve mineral bakımından oldukça zengin kaynaklar olduğu görülmektedir. Bu besin öğeleri içerisinde özellikle protein miktar ve kalitesi dikkat çekmektedir. Diğer yandan, yenilebilir böcekler geleneksel hayvansal kaynaklara kıyasla daha az yem ve su kullanılarak, daha küçük alanlarda yetiştirilebilmekte olup, atık miktarları da oldukça düşüktür. Bununla birlikte, yenilebilir kabul edilen bu böcek türlerinin yetiştirilmesi oldukça yeni bir konu olup hem gıda güvenliği hem de doğal denge bakımından bazı riskler taşımaktadır. Konuya ilişkin yasal mevzuatlarda da ciddi bir boşluk söz konusudur. Yenilebilir böceklere olan ilgi ve bu konudaki bilimsel araştırmaların sayısı son yıllarda dikkate değer bir artış göstermiştir. Bu çalışmada; yenilebilir böceklerin besleyicilik değeri, üretimi, işlenmesi, depolanması, ekonomisi, sağlık ve çevre üzerine etkileri, tüketici kabulü ve yasal düzenlemeler gibi başlıklar ele alınarak konu çok boyutlu bir yaklaşımla ve güncel literatürler taranarak derlenmiştir.

Anahtar Kelimeler − *Alternatif protein kaynakları, küresel ısınma, sürdürülebilirlik, yeni gıdalar, yenilebilir böcekler*

Edible Insects as a Sustainable and Novel "Food" Alternative

[1]Department of Food Engineering, Faculty of Engineering, Çanakkale Onsekiz Mart University, Çanakkale, Türkiye
[2]Department of Food Technology, Faculty of Applied Sciences, Çanakkale Onsekiz Mart University, Çanakkale, Türkiye

Article History

Received: 03.07.2022
Accepted: 12.10.2022
Published: 05.03.2023

Review Article

Abstract − Although the consumption of some insect species by humans is not a novel issue, it has been a topic that has been reconsidered in recent years, especially with the increase in population and demand for animal protein. It is estimated that insects are currently consumed by at least 2 billion people. Compared to many other animal sources, gaining more body weight with less feed and the proportionally lower share of greenhouse gas emissions, which play a very important role in global warming, makes it important to evaluate the potential of edible insects as both human food and animal feed in future scenarios. From a nutritional point of view, it is indicated that edible insects are rich sources of protein, fat, dietary fiber, and minerals. Among these nutrients, especially the amount and quality of the protein draws attention. On the other hand, edible insects can be grown in smaller areas using less feed and water when compared to traditional animal sources, and the amount of waste is quite low. However, breeding of edible insects is a fairly new issue and involve some risks in terms of both food safety and natural balance. There is also a serious gap in the legal regulations on the subject. Interest in edible insects and the number of scientific researches on this subject have considerably increased in recent years. In this study, topics such as nutritional value, production, processing, storage, economy, health and environmental effects of edible insects, consumer acceptance and legal regulations have been discussed and the subject has been compiled with a multidimensional approach by reviewing the most up-to-date literature.

Keywords − *Alternative protein source, edible insects, global warming, novel foods, sustainability*

[1] aliemreandaciletisim@gmail.com
[2] neseyilmaz@comu.edu.tr
*Sorumlu Yazar

1. Giriş

Son yıllarda gıda konusundaki en büyük endişelerden biri hızlı bir şekilde büyüyen dünya nüfusunun sürdürülebilir biçimde beslenmesini sağlamaktır. 2050 yılında dünya nüfusunun 9 milyar olacağı tahmin edilmekte ve bu nüfusu beslemek için bugün ürettiğimiz gıda miktarını neredeyse iki katına çıkarmamız gerekmektedir (FAO, 2022; Van Huis vd., 2013). Tüm dünyada ve özellikle gelişmemiş ve gelişmekte olan ülkelerde yetersiz beslenme ve gıda güvenliğinin sağlanamaması gibi sorunlar halen önemli küresel sorunlardandır. 800 milyondan fazla birey sağlıklı ve aktif bir yaşam sürdürmek için gerekli gıdaya sahip değil iken, özellikle Güney Asya ve Afrika ülkeleri en yüksek açlık oranlarına sahiptir (Tao ve Li., 2018). Bunun yanında, Dünya Sağlık Örgütü'nün tahminlerine göre küresel olarak 2 milyar insandan fazlası mikro besin öğesi eksikliğinden etkilenmektedir (WHO, 2021).
Kaynakların sınırlı olması, daha fazla üretimin karbon ve su ayak izlerini arttırması dolayısıyla sürdürülebilirlik bakımından bazı sakıncaları beraberinde getirmesi ve küresel ısınmanın getireceği kısıtlamalar düşünüldüğünde gıda üretiminin yeniden ve daha farklı bir perspektifle ele alınması gerektiği aşikârdır. Bu bağlamda geliştirilen stratejileri temel olarak 2 kategoriye ayırmak yanlış olmaz: Gıda kayıp ve atıklarının azaltılması ve yeni gıda kaynakları ile üretim stratejileri geliştirilmesi.

Bu bağlamda "yeni" bir gıda kaynağı olarak yenilebilir böcekler dikkat çekmektedir. Hayvansal proteinin her bakımdan maliyetinin artması, gıda ve yem konusundaki güvenlik endişeleri, çevresel etkiler, nüfus artışı gibi pek çok sebep 21. yüzyılda böceklerin bir gıda kaynağı olarak yeniden ele alınmasına neden olmuştur. Yunanca kökenli bir kelime olan "entomofaji" kavramı (ἔντομον éntomon, "böcek" ve φᾰγεῖν phagein, "yemek") böceklerin insanlar tarafından tüketilmesini ifade etmektedir ve bu, insanlar için yeni bir olgu değildir (Evans vd., 2015). Bulunan arkeolojik kanıtlar, insanların evrimsel tarihinde böceklerin köklü bir geçmişe sahip olduğuna işaret etmektedir (Peniche, 2021). Böcekleri içeren beslenmenin ilk kayıtları Altamira'da (Kuzey İspanya) keşfedilen, petek ve arıları temsil eden mağara resimlerinde gözlenmekte ve milattan önce yaklaşık 30.000-9.000 yıllarına dayanmaktadır (Baiano, 2020).

Böcekler bugüne kadar bilinen bir milyondan fazla türü ve keşfedilmeyi bekleyen daha milyonlarcası ile hayvanlar arasında sayıca en fazla bulunan özel bir gruptur. Yenilebilir böceklere olan ilgi ve bu konudaki bilimsel yayınların sayısı özellikle 2010'lu yıllardan beri her geçen yıl artmaktadır (Del Mastro, 2021; Meyer-Rochow ve Jung, 2020; Van Huis, 2021b).Küresel olarak en yaygın tüketilen böcekler sırasıyla; kın kanatlılar (*Coleoptera*, %31), pul kanatlılar (tırtıllar) (*Lepidoptera*, %18), zar kanatlılar (arılar, eşek arıları, karıncalar) (*Hymenoptera*, %14), düz kanatlılar (çekirgeler, cırcır böcekleri) (*Orthoptera*, %13), yarım kanatlılar (ağustos böcekleri, bitki piresi, kabuklu bitler, gerçek böcekler) (*Hemiptera*, %10), termitler (*Isoptera*, %3), kız böcekleri (helikopter böceği) (*Odonata*, %3), çift kanatlılar (sinekler) (*Diptera*, %2) ve diğer (%5) çeşitlerdir (FAO, 2020).

Bu çalışmada, gelecekte insan diyetlerinde önemli bir gıda kaynağı olacağı düşünülen yenilebilir böceklere; besleyicilik özellikleri, sağlık üzerine etkileri, çevresel etkileri, üretimi, işlenmesi ve depolanması, ekonomik etkisi, tüketici kabulü, gıda güvenliği ve yasal düzenlemeler başlıkları altında genel bir inceleme yapılmıştır. Konu hakkında literatür kısıtlı olmakla birlikte, yapılan yayınların sayısı her geçen yıl artmaktadır.

2. Yenilebilir Böceklerin Besleyicilik Değeri ve Sağlık Üzerine Etkileri

Günümüzde geleneksel olarak çeşitli popülasyonlar tarafından tüketilen böceklerin gelecekte insan beslenmesinde daha fazla yer alabileceği öngörülmektedir. Öncelikle, yenilebilir böceklerin besleyicilik değeri göz önünde bulundurulmalıdır. Böcekler proteinler, yağlar ve diyet lifleri bakımından zengindir ve türe bağlı olarak 100 gramda yaklaşık 400-500 kcal enerji sağlamaktadır (Rumpold ve Schlüter, 2015). Yenilebilir böceklerin ortalama besleyicilik değerleri ve sağladıkları enerji Tablo 1'de gösterilmektedir. Tür, yaşam evresi (Şekil 1), beslenme, cinsiyet, gelişme ortamı, inaktivasyon/öldürme şekli ve işleme metotları böceklerin besin öğesi kompozisyonu etki eden faktörler arasındadır (Meyer-Rochow, Gahukar, Ghosh ve Jung, 2021; Oonincx ve Finke, 2021).

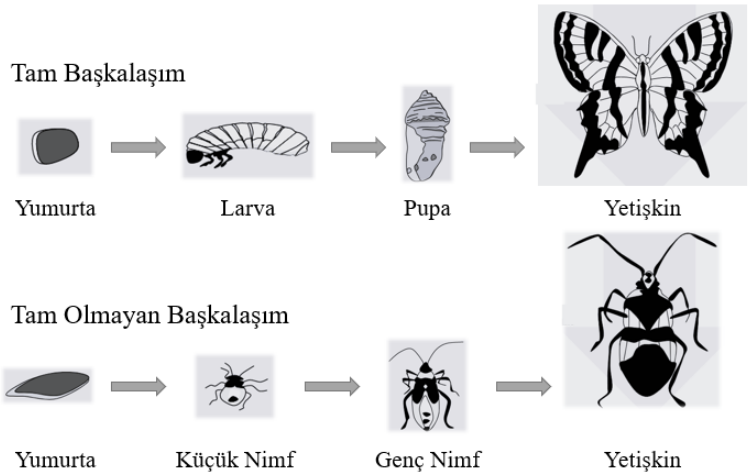

Şekil 1. Böceklerin Yaşam Evreleri (Biology Dictionary, 2022)

Tablo 1

Yenilebilir böceklerin ortalama besleyicilik değerleri (Rumpold ve Schlüter, 2015)

	Protein (%)	Yağ (%)	Diyet Lifi (%)	Kül (%)	Enerji (kcal/100g)
Çekirgeler ve cırcır böcekleri (*Orthoptera*)	61.32	13.41	9.55	3.85	426.25
Hamam böcekleri (*Blattodea*)	57.30	29.90	5.31	2.94	-
Kız böcekleri (*Odonata*)	55.23	19.83	11.79	8.53	431.33
Sinekler (*Diptera*)	49.48	22.75	13.56	10.31	409.78
Yarım kanatlılar (*Hemiptera*)	48.33	30.26	12.40	5.03	478.99
Arılar, eşek arıları ve karıncalar (*Hymenoptera*)	46.47	25.09	5.71	3.51	484.45
Tırtıllar (*Lepidoptera*)	45.38	27.66	6.6	4.51	508.89
Kın kanatlılar (*Coleoptera*)	40.69	33.40	10.74	5.07	490.30
Termitler (*Isoptera*)	35.34	32.74	5.06	5.88	-

Yenilebilir böceklerin önemli bir bileşeni olan proteinler kuru maddede yaklaşık %35-60 arasında değişen miktarlarda bulunmaktadır (Dobermann, Swift ve Field, 2017). Özellikle *Orthoptera* (çekirge, cırcır böceği vb.) grubu böcekler protein içeriği bakımından oldukça zengindir. Bazı çekirge türlerinin protein içeriğinin kuru maddede %77'ye kadar çıktığı rapor edilmektedir (Ayensu, Annan, Edusei ve Lutterodt, 2019). Yaklaşık %36 protein içeriğine sahip olan soya fasulyesi gibi bitkisel kaynaklarla karşılaştırıldığında böceklerin alternatif protein kaynağı olarak önemi ortaya çıkmaktadır (Rumpold ve Schlüter, 2015). Yenilebilir böcek proteinleri esansiyel aminoasitleri yeterince içerdikleri için yüksek kaliteli özellik taşımaktadır. Çoğu böcek türü Dünya Sağlık Örgütü'nün diyetteki amino asit önerilerini karşılamaktadır (Gravel ve Doyen, 2020; Tang vd., 2019). Bunun yanında, yenilebilir böcek proteinlerinin insanlar tarafından yüksek oranda sindirilebildiği belirtilmektedir (Dürr ve Ratompoarison, 2021). Cırcır böceği (*Gryllus assimilis*), güve (*Cirina forda*), çekirge (*Melanoplus foedus*) ve termitin (*Macrotermes nigerensis*) biyolojik değerinin (%85.49-93.02) kazeine göre (%73.45) daha yüksek olduğu belirtilmiştir (Ojha, Bekhit, Grune ve Schlüter, 2021a).

Diğer yandan Boulos, Tännler ve Nyström, (2020) yenilebilir böceklerin protein miktarlarının gerçekte olduğundan daha fazla bulunduğunu, bunun da temel olarak azotun proteine çevirim faktöründen kaynaklandığını belirtmiştir. Bilindiği gibi Kjeldahl gibi pek çok protein tayin metodunda esasen azot tespit edilmekte ve proteinlerdeki azot oranının ortalama %16 olduğu genel varsayımından yola çıkarak "6.25", genel azotu proteine çevirme faktörü olarak kullanılmaktadır. Burada göz ardı edilen temel gerçeklik bulunan azotun tamamının protein kaynaklı olmadığıdır. Güvenilir ve kesin bir sonuç olmak için amino asit analizi yapılmalı veya söz konusu kaynağa özgü daha spesifik bir protein çevrim faktörü hesaplanmalıdır. Bu bağlamda Boulos vd. (2020) un kurdu larvası (*T. molitor*), ev cırcırı (*A. domesticus*) ve göçmen çekirge (*L. migratoria*) örneklerini analiz etmişler ve bu örneklerin oldukça benzer amino asit profillerine sahip olduklarını, gerçek protein miktarlarının da sırasıyla 51, 55 ve 47 g/100 g (kuru maddede) olduğunu tespit etmişlerdir. Araştırmacılar sözü edilen her bir böcek türüne spesifik olarak kullanılması gereken azot protein çevrim faktörünü 5.41 (un kurdu), 5.25 (cırcır böceği) ve 5.33 (çekirge) olarak hesaplamış ve böylece literatürde geleneksel 6.25 azot çevrim faktörünü kullanan çalışmalarda yenilebilir böceklerin protein miktarının gerçekte olduğundan yaklaşık %17 civarında daha fazla hesaplandığını bildirmişlerdir (Boulos vd., 2020). Benzer biçimde Janssen, Vincken, Van Den Broek, Fogliano ve Lakemond vd. (2017) de un kurdu ve cırcır böceklerinin her ikisi için de azot çevrim faktörünü 4.7 olarak hesaplamıştır (Janssen vd., 2017).

Yenilebilir böceklerde proteinden sonra bulunan ana bileşen yağdır ve kuru maddede %7-77 arasında değişen miktarlarda bulunmaktadır (Elhassan, Wendin, Olsson ve Langton, 2019). Yağ asidi profilleri değerlendirildiğinde böceklerin genellikle çoklu doymamış yağ asitleri bakımından zengin olduğu görülmektedir (Kim, Yong, Kim, Kim ve Choi, 2019). Çoklu doymamış yağ asidi içeriği toplam yağ asidi miktarının %75'ine ulaşabilmektedir. Özellikle *Orthoptera* (çekirge, cırcır böceği vb.) ve *Lepidoptera* (tırtıl vb.) grubu bu bakımından zengindir. Un kurtlarının omega-3 çoklu doymamış ve diğer yağ asitleri kompozisyonu balıkta bulunan ile karşılaştırılabilir seviyede iken domuz ve sığırlardan daha yüksektir. Karada yaşayan böceklerin çoklu doymamış yağ asidi içeriği suda yaşayanlara göre daha yüksektir (Lange ve Nakamura, 2021). Bununla birlikte, böceklerin yağ profilleri beslemede kullanılan yemden de oldukça etkilenmektedir. Genellikle larvalar olgun böceklerden daha fazla yağ içeriğine sahip olmaktadır (Da Silva Lucas, De Oliveira, Da Rocha, Prentice, 2020).

Yenilebilir böceklerin karbonhidrat içeriği genellikle düşüktür (%6.71-15.98) ve çoğunlukla kitin formundadır (De Carvalho, Madureira ve Pintado, 2020). Böceklerin ve kabukluların dış iskeletlerinde yer alan ve yapısal olarak poli-beta-1,4-N-asetilglukozamin olan kitin (11.6-137.2 mg/kg), diyet lifi açısından oldukça zengindir (Melgar-Lalanne, Hernández-Álvarez ve Salinas-Castro, 2019). Bütün halde kurutulmuş böcekler en az %10 kitin içermektedir ve insanlar için potansiyel bir prebiyotik kaynağıdır (Imathiu, 2020). Kitin ve kitosan başlıca kabukluların dış iskeletlerinden elde edilmekte iken, böcekler bu iki maddenin alternatif bir kaynağı olma potansiyeline sahiptir (Saadoun vd., 2022).

Yenilebilir böcekler, yüksek kaliteli proteinlerinin yanında yüksek mineral madde içeriği ile de dikkat çekmektedir (Gabaza, Shumoy, Muchuweti, Vandamme ve Raes, 2018; Mwangi, 2018). Yenilebilir böceklerin mikro besin öğesi içeriğinin genellikle beslemede kullanılan yemden etkilendiği düşünülmektedir. Böceklerin mineral madde içeriği türler arasında ve aynı tür içinde oldukça değişkendir. Bununla birlikte, yenilebilir böcek tüketimi önemli miktarlarda bakır, demir, magnezyum, mangan, fosfor, selenyum ve çinko sağlamaktadır. Yenilebilir böcekler aynı zamanda bazı vitaminlerin de kaynağıdır. Genel olarak riboflavin (B_2), pantotenik asit (B_5), folik asit (B_9) ve biyotin (B_7) içerikleri yüksektir. Gıda ve Tarım Örgütü (FAO)'ne göre böcekler, mineral ve vitamin içeriği bakımından günlük önerilen miktarları karşılamaya yardımcı olabilir nitelik taşımaktadır (Ordoñez-Araque ve Egas-Montenegro, 2021).

Yenilebilir böceklerin diyetlere dâhil edilmesiyle insanlara gastrointestinal sağlığın iyileştirilmesi, bağışıklık fonksiyonlarının artırılması ve bakteriyel enfeksiyon riskinin azaltılması gibi birtakım sağlık yararları sağlama potansiyeli olduğu belirtilmektedir. Bu bakımdan özellikle kitin, kısa zincirli ve orta zincirli yağ asitleri ve glikozaminoglikanlar gibi bileşenler öne çıkmaktadır (Nowakowski, Miller, Miller, Xiao ve Wu, 2021). Ayrıca, yenilebilir böcek proteinlerinin antioksidan, antihipertansif, antikarsinojen, antiinflamatuar, antiobezite, antidiyabetik ve antimikrobiyal etkileri de rapor edilmiştir (Borrelli vd., 2021; Lee vd., 2021).

3. Yenilebilir Böceklerin Çevresel Etkisi

Dünya nüfusunun artmasıyla birlikte yükselen gıda talebi küresel olarak sürdürülemez hasat ve üretim uygulamalarını artırmaktadır. Bu uygulamalar da habitat kaybına, ormanların tahrip edilmesine, yüksek düzeyde hayvan yetiştirilmesi ve sera gazlarının artmasına yol açmaktadır. Bu sorunlara çözüm olarak özellikle

kırmızı et tüketiminin azaltılması, tarımsal üretim veriminin artırılması ve üretim için daha az toprak ve su kullanılacak alternatif gıda kaynaklarına yönelim önerilmektedir (Mariutti vd., 2021).

Sürdürülebilirlik, günümüz dünyasının ve gelecek nesillerin ihtiyaçlarını göz önünde bulundurarak kaynakların en verimli şekilde kullanılması şeklinde tanımlanmaktadır (Galanakis, 2019). Gıda üretiminin çevreye olan etkisi bu başlık altında giderek daha fazla öne çıkmaktadır. Gıda üretiminin çevreye olan etkisi tüm süreç boyunca kullanılan kaynakların karbon ayak izi hesaplanarak belirlenmektedir. Karbon ayak izi, bir ürünün üretimi, kullanımı ve nihai bertarafı sırasında yayılan sera gazlarının kg ürün başına ifade edilen toplam miktarıdır (Clune vd., 2017). Kyoto protokolüne göre ölçüt alınan sera gazları karbondioksit, metan, nitröz oksit, hidrofloro karbonlar, perfloro karbonlar ve sülfür heksaflorittir. Karbon ayak izi hesaplanmasında karbondioksit baz alındığından diğer sera gazlarının karbondioksit eşdeğerleri kullanılmaktadır.

Gıda üretiminin çevreye olan etkisi konusunda genellikle göz ardı edilen ancak önemli olan diğer bir husus ise su ve toprak kullanımıdır. Dünyadaki tatlı su kaynakları sınırlıdır ve yaklaşık %70'i tarım ve hayvancılık endüstrileri tarafından kullanılmaktadır. Bunun yanında, yakın gelecekte Dünya nüfusunun üçte ikisinin su kaynakları sınırlı ve tehlikede olan bölgelerde yaşayacağı tahmin edilmektedir. Ayrıca, günümüzde küresel tarıma elverişli alanların %70'i de hayvancılık endüstrisi tarafından kullanmaktadır (Kawabata, Berardo, Mattei ve Pee, 2020; Kemsawasd, Inthachat, Suttisansanee ve Temviriyanukul, 2022).

Mevcut gıda sistemi artan dünya nüfusu için besleyici ve yüksek protein içerikli gıdaları üretme konusunda zorluklar yaşamaktadır. Sınırlı tarım alanları ve su kaynakları ile 9 milyar olması beklenen küresel nüfusun beslenmesi için gerekecek gıda talebi artışını karşılayıp karşılayamayacağı konusunda endişeler bulunmaktadır (Do, Ramudhin, Colicchia, Creazza ve Li, 2021). Bu endişeler insanları sürdürülebilir alternatif gıda (böcekler, mantarlar, algler vb.) ve yem kaynaklarına (böcekler, gıda yan ürünleri vb.) yöneltmektedir. Böceklerin önemli besleyicilik değerinin yanı sıra görece daha sürdürülebilir bir kaynak oluşları (Şekil 2) küresel popülerliklerini artırmaktadır (FAO, 2021).

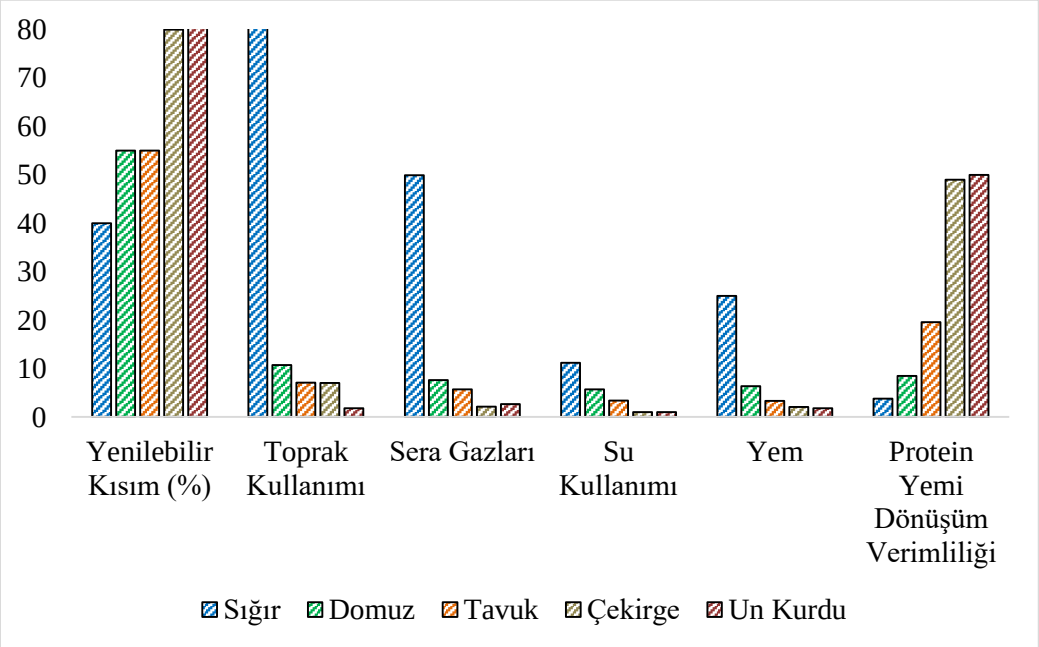

Şekil 2. Geleneksel çiftlik hayvanları ile karşılaştırıldığında çekirge ve un kurdunun çevresel ayak izi (FAO, 2021; Ponce-Reyes ve Lessard, 2021)

*Yenilebilir Kısım: Yüzde (%) (Un Kurdu: %100)

*Toprak Kullanımı: 100 gram protein üretimi için gerekli olan alan (m^2) (Sığır: 163.6 m^2)

*Sera Gazları: 100 gram protein için üretilen miktar (kg CO_2-e)

*Su Kullanımı: 100 gram hayvan ağırlığı için gerekli olan miktar (ton)

*Yem: Her hayvandan 1 kg üretimi için gerekli olan miktar (kg)

*Protein Yem Dönüşüm Verimliliği: Yüzde (%)

Böcekler, yemi gıdaya dönüştürme oranı açısından oldukça verimlidir. Dönüşüm oranı yaklaşık %50'dir, yani 1 kg protein üretimi için 2 kg yem kullanılması yeterlidir. Böceklerin yaklaşık %80'i yenilebilirdir ve daha düşük miktarlarda gıda ve su ihtiyacına sahiptir. Böylelikle, böceklerle ilişkili atık miktarı daha azdır. Un kurtları ile kıyaslandığında, tavuklar üç kat daha fazla alana ihtiyaç duymakta ve iki kat daha fazla sera gazı salınımına neden olmakta iken; sığırlar on kat daha fazla alana ihtiyaç duymakta ve 18 kat daha fazla sera gazı salınımına neden olmaktadır. Çekirge ve un kurtları aynı miktarda protein üretmek için sığır yetiştiriciliği için gereken yemin onda birinden daha azına ihtiyaç duymaktadır (Ponce-Reyes ve Lessard, 2021). Böcek üretiminin düşük çevresel ayak izi, onları sürdürülebilir ve ekonomik alternatif protein kaynağı olma potansiyeli bakımından çekici kılmaktadır (Delvendahl, Rumpold ve Langen, 2022; La Barbera, Verneau, Videbæk, Amato ve Grunert, 2020).

Günümüzde, üretilen ürünlerin çevreye olan etkisinin değerlendirilmesinde genellikle karbon ayak izi ve yaşam döngüsü analizi kavramları öne çıkmaktadır. Bir ürünün üretim, kullanım ve bertaraf edilmesi sürecinde çevreye yaydığı sera gazının kilogram ürün başına toplam miktarı karbon ayak izi ile ifade edilmektedir. Kısaca, insan faaliyetleri ile üretilen bir ürünün doğrudan veya dolaylı olarak neden olduğu sera gazı salınımı anlamına gelmektedir. Şekil 2'den görülebildiği gibi çekirge ve un kurdunun karbon ayak izleri sığır, domuz ve tavuğa göre oldukça düşüktür. Yapılan yaşam döngüsü analizlerine (bir ürünün yaşam döngüsü sürecince girdilerinin, çıktılarının ve potansiyel çevresel etkisinin değerlendirilmesi) göre yenilebilir böceklerin insan gıdası veya hayvan yemi olarak üretimlerinin çevresel etkisinin diğer hayvancılık ürünlerine göre oldukça düşük olduğu ve sürdürülebilir sistemler konusunda önemli bir potansiyele sahip olduğu ortaya çıkmaktadır (Dreyer vd., 2021; Halloran, Roos, Eilenberg, Cerutti ve Bruun, 2016; Nikkhah vd., 2021; Smetana, Spykman ve Heinz, 2021). Diğer yandan konu daha derin araştırmalara muhtaç olmakla beraber, böceklerin, memelilere ve kuşlara göre zoonoz hastalıkların insana, diğer hayvanlara ve vahşi yaşama geçişleri bakımından daha az riskli oldukları bildirilmektedir (Dicke vd., 2020; Doi, Gałęcki ve Mulia, 2021; FAO, 2020; Kemsawasd, Inthachat, Suttisansanee ve Temviriyanukul, 2022; Lange ve Nakamura, 2021; Van Huis vd., 2013).

4. Yenilebilir Böceklerin Üretimi, İşlenmesi ve Depolanması

Yenilebilir böceklerin gıda veya yem olarak kullanımının artırılması için böcek tarımının desteklenmesi gerekmektedir. Dünya genelinde yenilebilir böceklerin büyük bir çoğunluğu yabani ortamdan (ormanlar, çöller, su yolları ve tarımsal alanlar) hasat edilmekte ve sadece küçük bir kısmı özel olarak yetiştirilmektedir (Guiné, Correia, Coelho ve Costa, 2021). Bunun sonucunda bazı önemli dezavantajlar ortaya çıkmaktadır. Örneğin, yabani ortamdan elde edilen böceklerin kalitesi ve güvenliği garanti edilememektedir. Bunun yanında, kontrolsüz hasat ve aşırı kullanım bazı türlerin soyunun tükenmesine neden olabilmekte ve her böcek tipi tamamen yapay ortamlarda yetiştirilememektedir (Gahukar, 2020; Van Huis ve Oonincx, 2017). İnsan gıdası olarak böcek yetiştiriciliği oldukça yeni bir konu olmakla birlikte tropik bölgelerde, Tayland ve Vietnam'da özellikle cırcır böceği (crickets) üretim tesislerinin örnekleri bulunmaktadır. Daha ılıman bölgelerde böcek yetiştiriciliği daha ziyade küçük aile şirketleri tarafından yürütülmekte ve esasen evcil hayvan veya hayvanat bahçelerine yönelik olarak üretim yapılmaktadır. Endüstriyel ölçekte böcek üretimi yapan birkaç işletme mevcut olsa da insan tüketimine yönelik ticarileşmiş böcek üretimi hala düşük düzeydedir. Bunun temel sebebi mevcut böcek üretim sistemlerinin yüksek maliyetli olması ve otomasyona geçilmemiş olmasıdır. Ancak, konuya ilişkin çok sayıda patent başvurusu söz konusu olup değerlendirilmektedir (Van Huis vd., 2013).

Yenilebilir böcek tarımının şüphesiz bazı avantajları da bulunmaktadır. Örneğin, tarım ürünlerine zarar veren böcek türlerinin pestisit ve insektisit gibi çeşitli kimyasallar ile kontrol edilmesinin yerine bu böceklerin kontrollü ortamlarda yetiştirilmesi hem tarım ürünlerini hem de çevreyi koruyacaktır (FAO, 2021; Patel, Suleria ve Rauf, 2019). Bu konudaki ilginç durumlardan birisi de, örneğin %14'ten fazla olmayan bitkisel protein içeren kaynakların kurtarılması için her yıl milyarlarca dolar harcanarak %75'e kadar yüksek kaliteli hayvansal protein içeren bir kaynağın (böcekler) öldürülmesidir (Sosa ve Fogliano, 2017).

Yenilebilir böcek üretiminin artması için öncelikle ideal böcek türlerinin belirlenmesi gerekmektedir. İdeal bir böceğin sahip olması gereken özellikler arasında yüksek yumurta üretimi ve yumurtadan çıkma oranı, kısa larva dönemi, yüksek ağırlıklı larva ve pupa, yüksek verim, uygun yem maliyeti, düşük hassasiyet ve yüksek

kaliteli protein içeriği bulunmaktadır. Örneğin, siyah asker sineği (*Hermetica illucens*), yukarıda sıralanan kriterleri sağlamaktadır ancak yetiştirme tekniğinin optimize edilmesi gerekmektedir (Dobermann vd., 2017).

Günümüz böcek yetiştiriciliği uygulamalarında 3 farklı çiftlik türü bulunmaktadır: (1) tedarikçiden yumurtalar veya küçük larvalar alıp onları hasat edilebilir aşamaya kadar yetiştiren çiftlikler; (2) yumurtadan kurutulmuş böceklere kadar bütün üretim sürecini kapsayan çiftlikler; ve (3) hem üretimi hem de işlemeyi (larvalardan protein, yağ veya kitin eldesi) kapsayan çiftlikler (Niyonsaba, Höhler, Kooistra, Van Der Fels-Klerx ve Meuwissen, 2021). Yenilebilir böcek üretiminde genellikle hasat ve ön işlemler (böceklerin substrat kalıntılarından ayrılması, böceğin inaktivasyonu/öldürülmesi, kanatların/bacakların ayrılması ve yıkama), dekontaminasyon (haşlama, pişirme/kaynatma, buharda pişirme, marinasyon, kurutma, dumanlama, kızartma ve bunların kombinasyonları), ambalajlama (vakum, modifiye atmosfer) ve depolama aşamaları kullanılmaktadır. Üretilen böcekler bütün (kurutulmuş, dondurulmuş, ön pişirilmiş), işlenmiş (toz veya macun) ve ekstrakt (protein, yağ, kitin) şeklinde pazarlanabilmektedir (Ojha, Bußler, Psarianos, Rossi ve Schlüter, 2021b).

Hayvancılık ve tarım üretim sistemleri belirli seviyelerde otomasyona sahiptir ve bu da el işçiliği maliyetlerini azaltmaktadır. Ancak besleme, temizleme ve işlemenin el işçiliği ile yapıldığı çoğu böcek çiftliğinde bu durum geçerli değildir. Bu çiftliklerde, yem maliyetleri düşük olsa bile çiftlikte yetiştirilen böcekler pahalı olmaktadır. Bu nedenle, böceklerin sığır eti ya da kanatlılar için alternatif protein kaynağı olabilmesi için otomasyon tekniklerinin geliştirilmesi ve son ürün fiyatının düşürülmesi gerekmektedir. Bunun yanında, yetiştirme tesislerindeki sıcaklık, ışık, nem, havalandırma, yetiştirme kapları, popülasyon yoğunluğu, yumurtlama alanları, yem ve su mevcudiyeti, yemin bileşimi ve kalitesi gibi koşulların optimum seviyede kontrol edilmesi gerekmektedir (Dobermann vd., 2017).

Tablo 2'de küçük ve büyük ölçekli yenilebilir böcek üretimi yapan işletmelerin durumlarına değinilmektedir. Küçük ölçekli üretim yapan işletmeler daha çok güneydoğu Asya ve Afrika'da gelişmekte olan ülkelerde bulunurken büyük (endüstriyel) ölçekli üretim yapan işletmeler daha çok Avrupa ve Asya'da gelişmiş ülkelerde bulunmaktadır (Berggren, Jansson ve Low, 2018). Avrupa'da en çok yetiştirilen böcek türleri arasında un kurdu larvası (*Tenebrio molitor*) ve ev cırcırı (*Acheta domesticus*) bulunmaktadır (Francis vd., 2019). Un kurdunun dünyada en fazla yetiştirilen böcek türlerinden biri olduğu kabul edilmektedir (Gkinali, Matsakidou, Vasileiou ve Paraskevopoulou, 2022).

Tablo 2.

Yenilebilir böcek üretimi yapan küçük ve büyük ölçekli işletmelerdeki durum (Berggren vd., 2018)

Konu	Küçük Ölçekli İşletmeler	Büyük Ölçekli İşletmeler
Üretim hedefi	İnsan tüketimi	Tıbbi amaçlar, evcil hayvan gıdaları
Besleme, temizleme ve işleme	El işçiliği	Otomatik
Sağlık açısından kontrol	Görsel değerlendirme	Patojenler için geniş izleme programları
Üretim stoku	Damızlık ve yetiştirme hayvanları karışabilir, Yeniden stoklama için yabani ortamdan yararlanabilme	Damızlık ve yetiştirme hayvanları ayrılmalı, Yeniden stoklama için titiz kalite ve güvenlik değerlendirmesi
Potansiyel patojen etkisi	Sınırlı popülasyonu etkileme	Yüksek sayıda popülasyonu etkileme
Ortam şartları kontrolü	Sınırlı, dış ortamlarda kontrol zorlukları	Gelişmiş ortam kontrol sistemleri gerekli
Yem kaynakları	Daha esnek ve değişken kaynaklar	Aynı tip yemden büyük miktarda ihtiyaç
Genel özellikler	Düşük kapasite; esnek yönetim; düşük miktarda atık	Büyük depolama, üretim ve ambalajlama kapasitesi; büyük miktarda atık

Hayvancılık sistemlerinde olduğu gibi, tarımı yapılan böceklerin gıda ve yem olarak kullanılabilmesi için genellikle işlenmesi gerekmektedir. Çiftlik hayvanlarının işlenmesini içeren sayısız standart bulunmasına karşın yenilebilir böceklerin işlenmesi için uygun standartlar yaygın değildir. Verimli bir sistemin sağlanması için bir dizi standart ve üretim prosedürlerine ihtiyaç bulunmaktadır. Bu konuda örnek bir üretim sistemi Şekil 3'te verilmiştir (Dobermann vd., 2017).

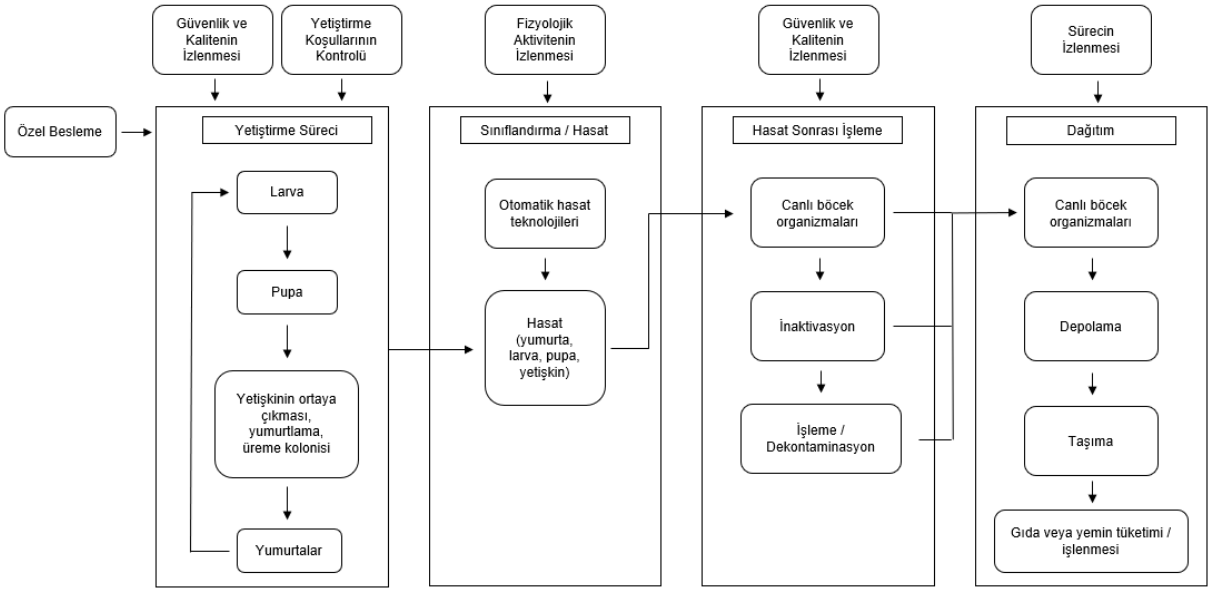

Şekil 3. Yenilebilir böceklerden gıda ve yem üretim süreci (Rumpold ve Schlüter, 2013)

Yenilebilir böceklerin işlenmesi konusunda ideal yemin seçimi önem taşımaktadır. Günümüzde mevcut olan böcek çiftliklerinin çoğunda kümes hayvanı yemleri kullanılmaktadır. Bu çiftliklerde biyoatık kaynaklarının, özellikle gıda atığının kullanımının araştırılması birçok çalışmada önerilmektedir. Küresel olarak her yıl üretilen gıdanın yaklaşık üçte birlik kısmının (~1 milyar ton) atık olduğu ve bunların büyük bir kısmının da sera gazı salan çöplüklere doldurulduğu göz önüne alındığında, gıda atıklarının yenilebilir böcek üretiminde kullanılması sürdürülebilir bir yaklaşım olarak düşünülmektedir. Gıda yan ürünleri bazlı yapılandırılmış diyetlerin siyah asker sineği, kara sinek, un kurdu ve cırcır böceği yetiştirilmesinde kullanılabileceği belirtilmektedir (UNEP, 2021; Varelas, 2019).

Geleneksel kültürlerde böcekler duyusal ve besinsel kaliteyi iyileştirmek ve raf ömrünü artırmak amacıyla güneşte kurutma, buharda pişirme, kavurma, dumanlama, kızartma ve kürleme gibi çeşitli şekillerde işlenmektedir. Bu işlemlerden önce mikrobiyal yükü azaltmak ve enzimleri inhibe etmek amacıyla haşlama işlemi uygulanmaktadır (Matiza Ruzengwe vd., 2022). Batı kültürlerinde ise genellikle tüketici ilgisinin artırılması amacıyla böcekler bazı teknolojilerle toz veya un gibi tanınmayacak forma dönüştürülmekte ve bu şekilde kullanılmaktadır (Ayieko, Onyango, Ngadze ve Ayieko, 2021). Bu teknolojiler arasında kurutma (dondurarak kurutma, fırın kurutma, vakum kurutma, akışkan yatak kurutucu ve mikrodalga kurutma) ve esas olarak protein, yağ ve/veya kitin ekstraksiyonu için tasarlanmış yeni metotlar (ultrases destekli ekstraksiyon, süper kritik CO_2 ekstraksiyonu, soğuk atmosferik basınç plazma ve kuru fraksiyonlama) bulunmaktadır (Meshulam-Pascoviche, David-Birman, Refael ve Lesmes, 2022).

Böcek unlarında bulunan proteinlerin teknofonksiyonel özellikleri (çözünürlük, köpürme, su ve yağ tutma, emülsifikasyon, jel özellikleri vb.) ürün formülasyonlarında kullanımları açısından önem taşımaktadır (Liceaga, 2021; Mishyna, Keppler ve Chen, 2021). Bu özellikler genellikle böcek türüne, gelişim evresine ve kullanılan işleme yöntemine bağlı olarak değişmektedir (Sosa ve Fogliano, 2017).

Dünyanın pek çok yerinde "tüketime hazır böcekler" güneşte kurutulduktan veya kızartıldıktan sonra yetersiz hijyen koşullarında yerel pazarlarda satılmaktadır. Bu böceklere daha önceden bir ısıl işlem uygulanmadığı takdirde böcekler mikrobiyal yük içerebilmektedir ve yeniden kontaminasyon ve/veya çapraz kontaminasyon riski bulunmaktadır. Bu nedenle, bakteriyel yükün en aza indirilmesi için böceklerin uygun bir şekilde işlenmesi, ambalajlanması ve depolanması gerekmektedir. Genellikle, yenilebilir böceklerin depolama

koşulları ve raf ömrü böcek türüne ve ürün tipine (bütün, toz veya tüketime hazır böcekler) bağlı olmaktadır. Taze böceklerde kalitenin korunması için soğukta muhafaza (5-7°C) yerine dondurarak depolama (-20°C) önerilmektedir (Melgar-Lalanne vd. 2019). Kurutulmuş ve toz haline getirilmiş böceklerde ise oksidatif ve mikrobiyal bozulmanın önlenmesi için soğukta muhafaza iyi bir yöntemdir (Baiano, 2020). Modifiye atmosfer veya vakum ambalajlama soğukta muhafaza ile kombine edildiğinde ürünlerin raf ömrü önemli derecede artmaktadır (Melgar-Lalanne vd. 2019).

5. Yenilebilir Böcek Ekonomisi

Yenilebilir böceklerin toplanması veya yetiştirilerek hasat edilmesi hem küçük hem de daha büyük, endüstriyel boyuttaki uygulamalar için para ve istihdam kaynağı yaratabilir. Güney ve Orta Afrika ile Güneydoğu Asya'da gelişmekte olan ülkelerde yenilebilir böceklere hâlihazırda talep mevcuttur ve bu bölgelerde bir sokak lezzeti olarak ya da tavuk ve balık yemi olarak küçük çaplı işletmelerde satılması söz konusu olabilmektedir. Birkaç istisna dışında yenilebilir böceklerin uluslararası ticareti oldukça önemsiz düzeydedir. Gelişmiş ülkelere yapılan ticaret daha ziyade göçmen topluluklardan gelen talep veya egzotik gıdalar satan niş marketlerin gelişmesi nedeniyledir. Yenilebilir böcekler üzerinden yapılan sınır ticareti ise özellikle Güneydoğu Asya ve Orta Afrika arasında önemlidir (Van Huis vd., 2013).

Dünyada en hızlı büyüyen alternatif protein pazarı olan yenilebilir böceklerin pazar büyüklüğünün 2030 yılı itibariyle yaklaşık 8 milyar dolar olacağı öngörülmektedir (Van Huis, Rumpold, Van Der Fels-Klerx ve Tomberlin, 2021a). Avrupa (özellikle İngiltere, Almanya ve Belçika) ve Amerika faaliyet gösteren 400'den fazla yenilebilir böcek işletmesi ile Batı dünyasında önde gelen pazarlardır (Pippinato, Gasco, Di Vita ve Mancuso, 2020). Güneydoğu Asya (özellikle Tayland) ve Afrika'da (özellikle Kenya, Tanzanya ve Uganda) yenilebilir böceklerin ihracatı ve ithalatı ekonomik açıdan önem taşımaktadır (Tanga vd., 2021). Dünya çapında 1 milyondan fazla böcek türü bulunmasına rağmen, insan tüketimi için özellikle çekirgeler ve un kurtları başarılı bir şekilde ticarileştirilmiştir (FAO, 2021; Ponce-Reyes ve Lessard, 2021).

AgriProtein (Güney Afrika), Ynsect (Fransa), Protifarm (Hollanda) ve Flying Spark (İsrail) gibi insan ve hayvan tüketimi amaçlı siyah asker sineği, un kurdu, cırcır böceği, çekirge, sinek ve diğer böcek türlerini üreten girişimlerin sayısı her geçen yıl artmaktadır (Mishyna, Chen ve Benjamin, 2020; Wade ve Hoelle, 2020). Ülkemizde de Antalya Çekirge (https://www.antalyacekirge.net/) adıyla hayvan yemi amaçlı farklı türlerde çekirgeler, kurtlar ve hamam böcekleri üreten bir işletme bulunmaktadır.

Yenilebilir böcekler geleneksel olarak kurutulmuş ve/veya öğütülmüş olarak satılırken, bazen de unlar, kurutulmuş larvalar, pupalar ve bütün şekilde satılmaktadır. Günümüzde yenilebilir böcekler çeşitli gıdalar (protein barları, ekmekler, krakerler, cipsler, unlar, et alternatifleri, makarnalar vb.), içecekler (alkolsüz içecekler, biralar, sütler vb.) ve şekerler (çikolatalar, dondurmalar, kurabiyeler vb.) gibi farklı şekillerde pazarlanmaktadır (Ponce-Reyes ve Lessard, 2021). Son 10 yılda başlıca Avrupa, Güney Asya ve Kuzey Amerika olmak üzere dünya genelinde yüzlerce şirket yenilebilir böcek esaslı gıda ürünleri ticareti amacıyla kurulmuştur. İşletmeler genellikle ticari formda aromalı atıştırmalıklar, enerji barları ve tozlar (sporcu takviyesi) satmaktadır ve en fazla satılan böcek türleri cırcır böcekleri, çekirgeler ve un kurtlarıdır (Melgar-Lalanne vd., 2019; Placentino, Sogari, Viscecchia, De Devitiis ve Monacis, 2021).

6. Tüketici Kabulü

Entomofaji, elbette kültürel ve dini pratiklerden etkilenen bir olgudur. Böcekler başlıca Asya, Afrika ve Güney Amerika ülkeleri olmak üzere yaklaşık 130 ülkede hâlihazırda geleneksel gıda olarak tüketilmektedir. Bu ülkeler arasında tüketim ve çeşitlilik açısından Meksika, Çin, Tayland ve Hindistan öne çıkmaktadır (Ordoñez-Araque ve Egas-Montenegro, 2021; Liceaga, 2021). Diğer yandan pek çok batı Avrupa ülkesinde böcek tüketimi tiksinme ve ilkel davranış tipi ilişkilendirilmekte ve kabul görmemektedir (Van Huis vd., 2013). Yine de entomofaji kavramı son yıllarda küresel olarak ilgi çekmeye başlayan bir konudur.

Yenilebilir böcek tüketiminin coğrafi olarak farklı bölgelerde yoğunlaşmasının en önemli nedenlerinden birisi de çevresel koşullarının bu böcek türlerinin üretimine elverişli olup olmamasıdır. Bu konuda tropik koşullar en fazla biyoçeşitliliği sunduğu için bu bölgelerde böcek tüketimi daha yaygındır. Tropik koşullardan uzaklaştıkça böcek tüketimi azalmaktadır (Lesnik, 2017). Günümüzde, entomofaji 2000'den fazla böcek türünü ilgilendirmektedir ve bu sayı giderek artmaktadır (Berggren, Jansson ve Low, 2019; Jongema, 2017). Pek çok kaynakta yenilebilir böcekleri tüketen insan sayısı yaklaşık 2 milyar olarak tahmin edilmiştir. Bazı kaynaklarda ise bu tahminin biraz yüksek olduğu, böcek tüketen insan sayısının yüz milyonlar seviyesinde olduğu belirtilmektedir (Van Huis, Halloran, Van Itterbeeck, Klunder ve Vantomme, 2022).

Yenilebilir böcek tüketiminin coğrafi dağılımı düşünüldüğünde, tüketimin başlıca kültürel özelliklerden etkilendiği ileri sürülebilir (Grabowski vd., 2022). Özellikle gelişmekte olan ülkelerde yenilebilir böceklerin "yoksul gıdası" olarak sosyal bir statüye bağlanması tüketim üzerinde olumsuz bir algıya neden olmaktadır (Murefu, Macheka, Musundire ve Manditsera, 2019). Böcekleri gıda olarak değerlendirmenin bireyler üzerinde başlıca iki farklı tepkisi vardır. Böceklerin geleneksel olarak tüketildiği ülkelerde böcekler değerli bir protein kaynağı olarak kabul edilmekte iken, Batı kültürlerinde böcekler kirli, iğrenç ve tehlikeli olarak kabul edilmektedir (Jensen ve Lieberoth, 2019). Bunun yanında, tüketicilerin sağlık ve çevresel yararları hakkında bilgilendirildikleri takdirde entomofaji hakkındaki fikirlerini değiştirmeye istekli oldukları da belirtilmiştir (Mancini vd., 2019).

Yenilebilir böceklerin kabul edilebilirliği üzerine tüketim formu ve duyusal özellikleri etkili olmaktadır. Böceklerin duyusal özellikleri; yaşadığı ortam, beslenme şekli ve pişirme metodundan etkilenmektedir. Yenilebilir böcekler çeşitli yaşam dönemlerinde ve çiğ, kızartılmış, kaynatılmış, kavrulmuş veya öğütülmüş formlarda tüketime sunulabilmektedir (Baiano, 2020). Kabul edilebilirliği artırmak amacıyla yenilebilir böcekler işlenerek tanınmayacak formda ve çeşitli ürünlerin içerisinde (ekmek, bisküvi, çikolata vb.) bir katkı bileşeni olarak da tüketilebilmektedir (Dagevos, 2021; Mancini vd., 2022; Meyer-Rochow ve Hakko, 2018; Orsi, Voege ve Stranieri, 2019).

Yenilebilir böceklerin lezzet karakteristikleri değerlendirildiğinde gündelik olarak tüketilen birçok gıdaya benzer tatlara sahip oldukları görülmektedir. Örneğin karıncalar ve termitlerin fındığa benzer tat, hamamböceklerinin mantara benzer tat ve siyah böcek larvalarının da kepekli ekmeğe benzer tat özelliklerine sahip olduğu bildirilmektedir. Tablo 3'te başlıca böcek gruplarının tat ve aroma özellikleri verilmektedir (Muslu, 2020).

Tablo 3.
Farklı Yöntemler ile İşlenmiş Yenilebilir Böceklerin Aroma Tanımları (Mishyna vd., 2020; Kouřimská ve Adámková, 2016)

Yenilebilir Böcek	Gelişim Evresi	Aroma
Agave kurtları	Larva	Börülcemsi, kızarmış domuz jambonu, baharat
Karıncalar	Yetişkin	Tatlı, fındığımsı, karbonize limon
Kara cadı güvesi	Larva	Ringa balığı
Cırcır böcekleri ve çekirgeler	Yetişkin	Yavan, balığımsı
Helikopter böceği	Larva	Balık
Bal arısı	Yavru	Tereyağımsı, sütümsü, bitkisel, fındığımsı, etsi, karaciğer, mantar, ceviz
Un kurdu	Larva	Fındığımsı
Süne	Yetişkin	Elma, acı kırmızı biber
Termitler	Yetişkin	Fındığımsı
Ağaç kurtları	-	Kızarmış domuz derisi
Ağustos böceği	-	Avokado, kızarmış kabak
Eşek arısı	-	Çamfıstığı
Hamam böcekleri	-	Mantar
Sandal böceği	Yetişkin	Balık, karides
Su böceği	Yetişkin	Özgün
Pamuklu bitler	-	Patates kızartması
Sarı un kurdu böceği	Larva	Tam buğday ekmeği

7. Gıda Güvenliği ve Yasal Düzenlemeler

Böceklerin insan diyetlerine dâhil edilmesi güvenlik endişelerini de beraberinde getirmektedir. Gıda güvenliği açısından böcek ve ürünlerinin de diğer gıda ürünleri ile aynı sağlık ve sanitasyon düzenlemelerine tabi olması gerekmektedir. Yenilebilir böcekler söz konusu olduğunda, mikrobiyolojik güvenlik, toksisite, lezzet ve inorganik maddelerin varlığı gibi konular göz önünde bulundurulmalıdır. Ayrıca, özellikle gübre

veya mezbaha atıkları gibi kaynaklar ile yetiştirilen böceklerde belirli sağlık etkileri de dikkate alınmalıdır (Van Huis vd., 2013).

Yenilebilir böcekler yetiştirme ortamına ve kullanılan yemlere bağlı olarak mikotoksinlere, pestisitlere ve ağır metallere (kadmiyum, civa, kurşun ve arsenik) maruz kalabilmektedir (Schrögel ve Wätjen, 2019). Bu kontaminantların insan gıdası ve hayvan yemi olarak kullanılan böceklere potansiyel transferi ve birikimi, gelişmekte olan bu sektörde dikkate alınması gereken önemli konular arasındadır (Dobermann vd., 2017; Imathiu, 2020).

Mikrobiyal açıdan bakıldığında, yenilebilir böcekler patojen mikroorganizmaların ve bazı cinslerin sporlarının (özellikle *Bacillus*) mekanik veya biyolojik vektörleri olabilmektedir (Osimani ve Aquilanti, 2021). Bunun yanında, yenilebilir böcekler ve ürünleri ile ilişkili mikrobiyal riskler yetiştirme, hasat, işleme, depolama ve taşıma sırasında uygulanacak iyi hijyen uygulamaları ile büyük ölçüde kontrol altına alınabilmektedir. Hem çiftliklerde yetiştirilen hem de yabani ortamdan hasat edilen böcekler birkaç bakteri türü ile ilişkilendirilmektedir. Bunlar arasında *Staphylococcus, Streptococcus, Bacillus, Pseudomonas, Micrococcus, Lactobacillus, Erwinia, Clostridium* ve *Acinetobacter* cinslerinden bazı türlerin yanı sıra *Enterobacteriaceae* familyasınının bazı üyeleri yer almaktadır. Bu bakterilerden bazıları patojenik ve fırsatçı bakteri olmasının yanı sıra yenilebilir böceklerin raf ömrünün azalmasından da sorumlu olabilmektedir. Çiftlik hayvanlarıyla yakın temas halinde olan veya karton yumurta kutularında yetiştirilen böceklerde *Campylobacter* ve *Salmonella* cinslerine ait türlerin kontaminasyon riski bulunmaktadır. Gıda kaynaklı virüslerin yenilebilir böcek tüketimi ile oluşturabileceği riskler kısıtlıdır ancak yemler yoluyla virüs kontaminasyonu riskine dikkat edilmelidir. Gıda kaynaklı mantarlar hem gıda bozulması yoluyla kalite ve gıda kaybına neden olmakta hem de bazı patojenik türler mikotoksin oluşturabilmektedir. Yenilebilir böceklerle ilişkilendirilmiş mayalar arasında *Tetrapisispora, Candida, Pichia* ve *Debaromyces* cinslerine ait bazı türler yer alırken, küfler arasında ise *Aspergillus, Alternaria, Cladosporium, Fusarium, Penicillium, Phycomycetes* ve *Wallemia* cinslerine ait bazı türler bulunmaktadır (FAO, 2021).

Böcek tüketimine bağlı alerji vakaları oldukça nadir olmakla birlikte yok değildir. Özellikle eklembacaklılarla ilgili alerji vakaları rapor edilmiştir (Van Huis vd., 2013). Kabuklular (karides vb.) ve böcekleri de içeren pek çok eklembacaklının duyarlı bireylerde tropomiyozin, α-amilaz, arjinin kinaz ve hemosiyanin varlığından kaynaklanan alerjik reaksiyonlara neden olduğu bilinmektedir. Kabuklu alerjisi olan bireylerin bağışıklık sistemi, kabuklulardan gelen bazı proteinlere karşı duyarlıdır. Böcek tüketimi ile benzer proteinlerin tanınması sonucunda alerjik reaksiyonlar tetiklenebilmektedir (FAO, 2021). Dahası, bu alerjenler arasında çapraz reaksiyonlar da mümkündür (De Gier ve Verhoeckx, 2018). Eklembacaklı alerjisine sahip olan bireylerin böceklere karşı da alerjik reaksiyonlar / hassasiyet gösterdiği birden fazla çalışmada belirtilmiştir (Ribeiro, Cunha, Sousa-Pinto ve Fonseca, 2018).

Gelişmiş ülkelerde böceklerin gıda ve yem olarak kullanılmasına rehberlik edecek net bir yasal düzenlemenin bulunmaması, bu ürünlerin endüstriyel olarak geliştirilmesinin önündeki en büyük engeldir. Gelişmekte olan ülkelerde ise böceklerin gıda veya yem olarak kullanılması yasal düzenlemeden bağımsız olarak daha fazla tolere edilmektedir. Yem sektörü, böceklere ilişkin yasal düzenleme normlarının oluşmasını en fazla teşvik eden sektördür. "Novel food"/ "Yeni ürün" konseptinin böceklerin insan gıdası olarak kullanılmasının önünü açabileceği düşünülmektedir (Van Huis vd., 2013).

Avrupa Birliği'nde insan tüketimi için üretilmiş böcek esaslı ürünler (bütün, parça veya ekstrakt), Ocak 2018'den beri "EU 2015/2283" yeni gıda yönetmeliği kapsamına alınmıştır. Bunun anlamı, bu ürünlerin pazarda yerini almasından önce Avrupa Gıda Güvenliği Otoritesi (European Food Safety Authority, EFSA) tarafından yapılacak bilimsel değerlendirme ile Avrupa Komisyonu'na (EC) başvurmanın gerekli olduğudur (FAO, 2021). Günümüzde, EFSA tarafından insan tüketimi için güvenli olarak onaylanmış iki yenilebilir böcek türü bulunmaktadır: Kurutulmuş un kurdu (*Tenebrio molitor*) (EFSA, 2021a) ve göçmen çekirge (*Locust migratoria*) (EFSA, 2021b). Avrupa Birliği, üçüncül ülkelerden gelen ve uzun sürelerce (25 yıl boyunca kesintisiz) güvenli olarak tüketilen yenilebilir böcek ürünlerini "yeni gıda" olarak nitelendirebilmektedir. Bu tip ürünler, gerekli koşulları sağladığı takdirde 4 ay gibi kısa bir sürede Avrupa Birliği pazarlarında yerlerini alabilmektedir (FAO, 2021).

Amerika Birleşik Devletleri'nde, yenilebilir böceklerin (bütün, parça veya türev) gıda olarak kullanımları Gıda ve İlaç Dairesi'nin (FDA) denetimi altındadır. Bu bakımdan, yenilebilir böcek ürünlerinin "Federal Gıda, İlaç ve Kozmetik (FD&C)" yasasına ve yükümlülüklerine uyması gerekmektedir. Kanada'da ise ipek böcekleri,

cırcır böcekleri ve un kurtları Health Canada tarafından belirlenen "Gıda ve Gıda Bileşenleri için Yeni Olmayan Belirleyiciler Listesi" içerisinde bulunmaktadır. Kanadalı tüketiciler için üretilen yenilebilir böcekler, ülkedeki diğer gıdalarla aynı hijyen ve güvenlik standartlarını karşılamak durumundadır (FAO, 2021). Afrika ve Asya gibi kıtalarda ve Meksika'da yenilebilir böcekler geleneksel olarak insanlar tarafından rahatça tüketilmektedir ancak konuyla ilgili düzenlemeler ve yönetmelikler oldukça nadirdir veya hiç bulunmamaktadır (Raheem vd., 2019).

8. Sonuçlar

Mevcut durumda küresel olarak hayvansal protein ihtiyacı büyük oranda sığır, domuz ve kanatlılar gibi geleneksel olarak yetiştirilen hayvanlardan sağlanmaktadır. Ancak, nüfus, refah ve talep artışı nedeniyle gelecekte hayvansal ürünlere olan talebin ikiye katlanması beklenmektedir. Geleneksel hayvansal proteinin üretimi hem oldukça verimsiz bir yem/protein çevrim oranına, hem de oldukça yüksek bir çevre maliyetine neden olmaktadır. Hayvancılık sektörü tek başına, küresel sera gazı salınımının %14'ünden, önemli miktarda toprak ve su kullanımından sorumludur. Hayvansal gıdalar, gıda kaynaklı proteinin yalnızca %37'sini sağlamalarına rağmen, orantısız olarak tarımsal alan işgalinin %83'ünden ve gıda ile ilişkili sera gazı emisyonlarının %58'inden sorumludur (Poore ve Nemecek, 2018; Tamburino, Bravo, Clough ve Nicholas, 2020). Dolayısıyla giderek artan protein ihtiyacına yönelik daha sürdürülebilir çözümler bulmak gerektiği tartışmasız biçimde açıktır. Yenilebilir böcekler dikey tarıma elverişli olması, düşük su gereksinimi, yüksek yem/protein çevrim verimi ve düşük sera gazı salınımı gibi avantajları ile bu konuda sürdürülebilir bir alternatif olarak öne çıkmaktadır. Bununla birlikte, bu alternatifin pratikte daha geniş bir popülasyon tarafından yaygın olarak tüketilebilmesi için yenilebilir böcek üretiminin belli bir yasal düzenleme çerçevesinde ele alınması ve gıda güvenliğine ilişkin endişelerinin giderilmesi birincil ihtiyaç olarak öne çıkmaktadır. Ayrıca, özellikle bazı coğrafyalarda böceklerin gıda olarak tüketilmesine ilişkin kültürel ve etik kısıtlamaların dikkate alınması gerektiği de vurgulanmalıdır.

Yazar Katkıları

Ali Emre Andaç: Literatür taraması yapılması, derlemenin kaleme alınması ve düzenlenmesinde katkı sağlamıştır.
Neşe Yılmaz Tuncel: Konunun ve konseptin dizaynı, derlemenin kaleme alınması ve gözden geçirilmesinde katkı sağlamıştır.

Çıkar Çatışması

Yazarlar herhangi bir çıkar çatışması bulunmadığını beyan eder.

Kaynaklar

Ayensu, J., Annan, R. A., Edusei, A., Lutterodt, H. (2019). Beyond nutrients, health effects of entomophagy: a systematic review. *Nutrition and Food Science*, *49*(1), 2-17, https://doi.org/10.1108/NFS-02-2018-0046.

Ayieko, I. A., Onyango, M., Ngadze, R. T., Ayieko, M. A. (2021). Edible Insects as New Food Frontier in the Hospitality Industry. *Frontiers in Sustainable Food Systems*, *325*, https://doi.org/10.3389/fsufs.2021.693990.

Baiano, A. (2020). Edible insects: an overview on nutritional characteristics, safety, farming, production technologies, regulatory framework, and socio-economic and ethical implications. *Trends in Food Science and Technology*, *100*, 35-50, https://doi.org/10.1016/j.tifs.2020.03.040.

Berggren, Å., Jansson, A., Low, M. (2019). Approaching ecological sustainability in the emerging insects-as-food industry. *Trends in Ecology and Evolution*, *34*(2), 132-138, https://doi.org/10.1016/j.tree.2018.11.005.

Berggren, Å., Jansson, A., Low, M. (2018). Using current systems to ınform rearing facility design in the insect-as-food industry. *Journal of Insects as Food and Feed*, *4*(3), 167-170, https://doi.org/10.3920/JIFF2017.0076.

Biology Dictionary, (2022). Böceklerin Yaşam Evreleri, Erişim Tarihi: 26.03.2022, Erişim: https://biologydictionary.net/complete-metamorphosis/.

Borrelli, L., Varriale, L., Dipineto, L., Pace, A., Menna, L. F., Fioretti, A. (2021). Insect derived lauric acid as promising alternative strategy to antibiotics in the antimicrobial resistance scenario. *Frontiers in Microbiology, 12*, 330, https://doi.org/10.3389/fmicb.2021.620798.

Boulos, S., Tännler, A., Nyström, L. (2020). Nitrogen-to-Protein Conversion Factors for Edible Insects on the Swiss Market: *T. molitor, A. domesticus,* and *L. migratoria*. *Frontiers in nutrition, 7*, 89, https://doi.org/10.3389/fnut.2020.00089.

Clune, S., Crossin, E., Verghese, K. (2017). Systematic review of greenhouse gas emissions for different fresh food categories. *Journal of Cleaner Production*, 140, 766–783. https://doi.org/10.1016/j.jclepro.2016.04.082.

Dagevos, H. (2021). A literature review of consumer research on edible insects: recent evidence and new vistas from 2019 studies. *Journal of Insects as Food and Feed*, 7(3), 249-259, https://doi.org/10.3920/JIFF2020.0052.

Da Silva Lucas, A. J., De Oliveira, L. M., Da Rocha, M., Prentice, C. (2020). Edible insects: an alternative of nutritional, functional and bioactive compounds. *Food Chemistry*, *311*, 126022, https://doi.org/10.1016/j.foodchem.2019.126022.

De Carvalho, N. M., Madureira, A. R., Pintado, M. E. (2020). The potential of insects as food sources–a review. *Critical Reviews in Food Science and Nutrition*, *60*(21), 3642-3652, https://doi.org/10.1080/10408398.2019.1703170.

Del Mastro, N. L. (2021). Evolution of the Interest on Edible Insects. *American Journal of Biological and Environmental Statistics*, *7*(2), 52-56, https://doi.org/10.11648/j.ajbes.20210702.13.

Delvendahl, N., Rumpold, B. A., Langen, N. (2022). Edible Insects as Food–Insect Welfare and Ethical Aspects from a Consumer Perspective. *Insects*, *13*(2), 121, https://doi.org/10.3390/insects13020121.

De Gier, S., Verhoeckx, K. (2018). Insect (food) allergy and allergens. *Molecular Immunology*, *100*, 82-106, https://doi.org/10.1016/j.molimm.2018.03.015.

Dicke, M., Ellenberg, J., Salles, J.F., Jensen, A.B., Lecocq, A., Pijlman, G.P., van Loon, J.J.A., van Oers, M.M. (2020). Edible insects unlikely to contribute to transmission of coronavirus SARS-CoV-2. *Journal of Insects as Food and Feed*, *6*(4), 333–339, https://doi.org/10.3920/JIFF2020.0039.

Do, Q., Ramudhin, A., Colicchia, C., Creazza, A., Li, D. (2021). A systematic review of research on food loss and waste prevention and management for the circular economy. *International Journal of Production Economics*, *239*, 108209, https://doi.org/10.1016/j.ijpe.2021.108209.

Doi, H., Gałęcki, R., Mulia, R. N. (2021). The merits of entomophagy in the post COVID-19 world. *Trends in Food Science & Technology*, 110, 849-854., https://doi.org/10.1016/j.tifs.2021.01.067.

Dobermann, D., Swift, J. A., Field, L. M. (2017). Opportunities and hurdles of edible insects for food and feed. *Nutrition Bulletin*, *42*(4), 293-308, https://doi.org/10.1111/nbu.12291.

Dreyer, M., Hörtenhuber, S., Zollitsch, W., Jäger, H., Schaden, L. M., Gronauer, A., Kral, I. (2021). Environmental life cycle assessment of yellow mealworm (*Tenebrio molitor*) production for human consumption in Austria–a comparison of mealworm and broiler as protein source. *The International Journal of Life Cycle Assessment*, *26*(11), 2232-2247, https://doi.org/10.1007/s11367-021-01980-4.

Dürr, J., Ratompoarison, C. (2021). Nature's "Free Lunch": The Contribution of Edible Insects to Food and Nutrition Security in the Central Highlands of Madagascar. *Foods*, *10*(12): 2978 p., https://doi.org/10.3390/foods10122978.

EFSA Panel on Nutrition, Novel Foods and Food Allergens (NDA)., Turck, D., Castenmiller, J., De Henauw, S., Hirsch-Ernst, K. I., Kearney, J., Maciuk, A., Mangelsdorf, I., McArdle, H. J., Naska, A., Pelaez, C., Pentieva, K., Siani, A., Thies, F., Tsabouri, S., Vinceti, M., Cubadda, F., Frenzel, T., Heinonen, M., Marchelli, R., Neuhauser-Berthold, M., Poulsen, M., Maradona, M. P., Schlatter, J. R., van Loveren, H., Ververis, E. Knutsen, H. K. (2021). Safety of dried yellow mealworm (*Tenebrio molitor* larva) as a novel food pursuant to Regulation (EU) 2015/2283. *EFSA Journal*, *19*(1), Article e06343, https://doi.org/10.2903/j.efsa.2021.6343.

EFSA Panel on Nutrition, Novel Foods and Food Allergens (NDA)., Turck, D., Castenmiller, J., De Henauw, S., Hirsch-Ernst, K. I., Kearney, J., Maciuk, A., Mangelsdorf, I., McArdle, H. J., Naska, A., Pelaez, C., Pentieva, K., Siani, A., Thies, F., Tsabouri, S., Vinceti, M., Cubadda, F., Frenzel, T., Heinonen, M., Marchelli, R., Neuhauser-Berthold, M., Poulsen, M., Maradona, M. P., Schlatter, J. R., van Loveren, H., Azzollini, D., Knutsen, H. K. (2021b). Safety of frozen and dried formulations from migratory locust (*Locusta migratoria*) as a novel food pursuant to Regulation (EU) 2015/2283. *EFSA Journal*, *19*(7), Article e06667, https://doi.org/10.2903/j.efsa.2021.6667.

Elhassan, M., Wendin, K., Olsson, V., Langton, M. (2019). Quality aspects of insects as food—nutritional, sensory, and related concepts. *Foods*, *8*(3), 95, https://doi.org/10.3390/foods8030095.

Evans, J., Alemu, M. H., Flore, R., Frøst, M. B., Halloran, A., Jensen, A. B., Maciel-Vergara, G., Meyer-Rochow, V. B., Münke-Svendsen, C., Olsen, S. B., Payne, C., Roos, N., Rozin, P., Tan, H. S. G., Van Huis, A., Vantomme, P., Eilenberg, J. (2015). 'Entomophagy': an evolving terminology in need of review. *Journal of Insects as Food and Feed*, *1*(4), 293-305, https://doi.org/10.3920/JIFF2015.0074.

FAO, (2022), *How to feed the world in 2050.*, https://www.fao.org/fileadmin/templates/wsfs/docs/expert_paper/How_to_Feed_the_World_in_2050.pdf.

FAO, (2021), *Looking at edible insects from a food safety perspective. challenges and opportunities for the sector.* Rome., https://doi.org/10.4060/cb4094en.

FAO, (2020). Insects for food and feed. the contribution of insects to food security, livelihoods and the environment, Erişim Tarihi: 05.04.2022, Erişim: https://www.fao.org/edible-insects/en/.

Francis, F., Doyen, V., Debaugnies, F., Mazzucchelli, G., Caparros, R., Alabi, T., Blecker, C., Haubruge, E., Corazza, F. (2019). Limited cross reactivity among arginine kinase allergens from mealworm and cricket edible insects. *Food Chemistry*, *276*, 714-718, https://doi.org/10.1016/j.foodchem.2018.10.082.

Gabaza, M., Shumoy, H., Muchuweti, M., Vandamme, P., Raes, K. (2018). Baobab fruit pulp and mopane worm as potential functional ingredients to improve the iron and zinc content and bioaccessibility of fermented cereals. *Innovative Food Science and Emerging Technologies*, *47*, 390-398 p., https://doi.org/10.1016/j.ifset.2018.04.005.

Gahukar, R. T. (2020). Edible insects collected from forests for family livelihood and wellness of rural communities: A review. *Global Food Security*, *25*, 100348, https://doi.org/10.1016/j.gfs.2020.100348.

Galanakis, C. M. (ed.), (2019). Sustainable Meat Production and Processing. *Academic Press*, The UK, 259, https://doi.org/10.1016/C2017-0-02230-9.

Gkinali, A. A., Matsakidou, A., Vasileiou, E., Paraskevopoulou, A. (2022). Potentiality of *Tenebrio molitor* larva-based ingredients for the food industry: A review. *Trends in Food Science and Technology*, *119*, 495-507, https://doi.org/10.1016/j.tifs.2021.11.024.

Grabowski N. T., Abdulmawjood A., Acheuk F., Barragán Fonseca K., Chhay T., Costa Neto Eraldo M., Ferri M., Franco Olivas J., González Aguilar Delia G., Keo S., Lertpatarakomol R., Miech P., Piofczyk T., Proscia F., Mitchaothai J., Guerfali Meriem M., Sayed Waheed, Tchibozo S., Plötz M. (2022) Insects-a source of safe and sustainable food?–yes and no. *Frontiers in Sustainable Food Systems*, *5*, 701797, https://doi.org/10.3389/fsufs.2021.701797.

Gravel, A., Doyen, A. (2020). The use of edible insect proteins in food: Challenges and issues related to their functional properties. *Innovative Food Science and Emerging Technologies*, *59*, 102272, https://doi.org/10.1016/j.ifset.2019.102272.

Guiné, R. P., Correia, P., Coelho, C., Costa, C. A. (2021). The role of edible insects to mitigate challenges for sustainability. *Open Agriculture*, *6*(1), 24-36, https://doi.org/10.1515/opag-2020-0206.

Halloran, A., Roos, N., Eilenberg, J., Cerutti, A., Bruun, S. (2016). Life cycle assessment of edible insects for food protein: a review. *Agronomy for Sustainable Development*, *36*(4), 1-13, https://doi.org/10.1007/s13593-016-0392-8.

Imathiu, S. (2020). Benefits and food safety concerns associated with consumption of edible insects. *NFS Journal*, *18*, 1-11, https://doi.org/10.1016/j.nfs.2019.11.002.

Janssen, R. H., Vincken, J. P., van den Broek, L. A., Fogliano, V., Lakemond, C. M. (2017). Nitrogen-to-protein conversion factors for three edible insects: *Tenebrio molitor, Alphitobius diaperinus,* and *Hermetia illucens*. *Journal of Agricultural and Food Chemistry*, *65*(11), 2275-2278, https://doi.org/10.1021/acs.jafc.7b00471.

Jensen, N. H., Lieberoth, A. (2019). We will eat disgusting foods together–Evidence of the normative basis of Western entomophagy-disgust from an insect tasting. *Food Quality and Preference*, *72*, 109-115, https://doi.org/10.1016/j.foodqual.2018.08.012.

Jongema, Y. (2017), Dünyadaki yenilebilir böceklerin listesi, Erişim Tarihi: 25.03.2022, Erişim: https://www.wur.nl/en/Research-Results/Chair-groups/Plant-Sciences/Laboratory-of-Entomology/Edible-insects/Worldwide-species-list.htm.

Kawabata, M., Berardo, A., Mattei, P., de Pee, S. (2020). Food security and nutrition challenges in Tajikistan: Opportunities for a systems approach. *Food Policy*, *96*, 101872, https://doi.org/10.1016/j.foodpol.2020.101872.

Kemsawasd, V., Inthachat, W., Suttisansanee, U., Temviriyanukul, P. (2022). Road to The Red Carpet of Edible Crickets through Integration into the Human Food Chain with Biofunctions and Sustainability: A Review. *International Journal of Molecular Sciences*, *23*(3), 1801, https://doi.org/10.3390/ijms23031801.

Kim, T. K., Yong, H. I., Kim, Y. B., Kim, H. W., Choi, Y. S. (2019). Edible insects as a protein source: A review of public perception, processing technology, and research trends. *Food Science of Animal Resources*, *39*(4), 521, https://doi.org/10.5851/kosfa.2019.e53.

Kouřimská, L., Adámková, A. (2016). Nutritional and sensory quality of edible insects. *NFS Journal*, *4*, 22-26, https://doi.org/10.1016/j.nfs.2016.07.001.

La Barbera, F., Verneau, F., Videbæk, P. N., Amato, M., Grunert, K. G. (2020). A self-report measure of attitudes toward the eating of insects: Construction and validation of the Entomophagy Attitude Questionnaire. *Food Quality and Preference*, *79*, 103757, https://doi.org/10.1016/j.foodqual.2019.103757.

Lange, K. W., Nakamura, Y. (2021). Edible insects as future food: chances and challenges. *Journal of Future Foods*, *1*(1), 38-46, https://doi.org/10.1016/j.jfutfo.2021.10.001.

Lee, J. H., Kim, T. K., Jeong, C. H., Yong, H. I., Cha, J. Y., Kim, B. K., Choi, Y. S. (2021). Biological activity and processing technologies of edible insects: a review. *Food Science and Biotechnology*, *30*(8), 1003-1023, https://doi.org/10.1007/s10068-021-00942-8.

Lesnik, J. J. (2017). Not just a fallback food: global patterns of insect consumption related to geography, not agriculture. *American Journal of Human Biology*, *29*(4), e22976, https://doi.org/10.1002/ajhb.22976.

Liceaga, A. M. (2021). Processing insects for use in the food and feed industry. *Current Opinion in Insect Science*, *48*, 32-36, https://doi.org/10.1016/j.cois.2021.08.002.

Mancini, S., Sogari, G., Espinosa Diaz, S., Menozzi, D., Paci, G., Moruzzo, R. (2022). Exploring the Future of Edible Insects in Europe. *Foods*, *11*(3), 455, https://doi.org/10.3390/foods11030455.

Mancini, S., Sogari, G., Menozzi, D., Nuvoloni, R., Torracca, B., Moruzzo, R., Paci, G. (2019). Factors predicting the intention of eating an insect-based product. *Foods*, *8*(7), 270, https://doi.org/10.3390/foods8070270.

Mariutti, L. R. B., Rebelo, K. S., Bisconsin-Junior, A., de Morais, J. S., Magnani, M., Maldonade, I. R., Maderia, N. R., Tiengo, A., Marostica, M. R., Cazarin, C. B. B. (2021). The use of alternative food sources to improve health and guarantee access and food intake. *Food Research International*, *149*, 110709, https://doi.org/10.1016/j.foodres.2021.110709.

Matiza Ruzengwe, F., Nyarugwe, S. P., Manditsera, F. A., Mubaiwa, J., Cottin, S., Matsungo, T. M., Chopera, P., Ranawana, V., Fiore, A., Macheka, L. (2022). Contribution of edible insects to improved food and nutrition security: a review. *International Journal of Food Science and Technology*, 1-13, https://doi.org/10.1111/ijfs.15570.

Melgar-Lalanne, G., Hernández-Álvarez, A. J., Salinas-Castro, A. (2019). Edible insects processing: traditional and innovative technologies. *Comprehensive Reviews in Food Science and Food Safety*, 18(4), 1166-1191, https://doi.org/10.1111/1541-4337.12463.

Meshulam-Pascoviche, D., David-Birman, T., Refael, G., Lesmes, U. (2022). Big opportunities for tiny bugs: Processing effects on the techno-functionality and digestibility of edible insects. *Trends in Food Science and Technology*, *122*, 265-274, https://doi.org/10.1016/j.tifs.2022.02.012.

Meyer-Rochow, V. B., Gahukar, R. T., Ghosh, S., Jung, C. (2021). Chemical composition, nutrient quality and acceptability of edible insects are affected by species, developmental stage, gender, diet, and processing method. *Foods*, *10*(5), 1036, https://doi.org/10.3390/foods10051036.

Meyer-Rochow, V. B., Jung, C. (2020). Insects used as food and feed: isn't that what we all need. *Foods*, *9*(8), 1003, https://doi.org/10.3390/foods9081003.

Meyer-Rochow, V. B., Hakko, H. (2018). Can edible grasshoppers and silkworm pupae be tasted by humans when prevented to see and smell these insects. *Journal of Asia-Pacific Entomology*, *21*(2), 616-619, https://doi.org/10.1016/j.aspen.2018.04.002.

Mishyna, M., Keppler, J. K., Chen, J. (2021). Techno-functional properties of edible insect proteins and effects of processing. *Current Opinion in Colloid and Interface Science*, *56*, 101508, https://doi.org/10.1016/j.cocis.2021.101508.

Mishyna, M., Chen, J., Benjamin, O. (2020). Sensory attributes of edible insects and insect-based foods–future outlooks for enhancing consumer appeal. *Trends in Food Science & Technology*, *95*, 141-148, https://doi.org/10.1016/j.tifs.2019.11.016.

Murefu, T. R., Macheka, L., Musundire, R., Manditsera, F. A. (2019). Safety of wild harvested and reared edible insects: A review. *Food Control*, *101*, 209-224, https://doi.org/10.1016/j.foodcont.2019.03.003.

Muslu, M. (2020). Sağlığın geliştirilmesi ve sürdürülebilir beslenme için alternatif bir kaynak: yenilebilir böcekler. *Gıda*, *45*(5), 1009-1018, https://doi.org/10.15237/gida.GD20071.

Mwangi, M. N., Oonincx, D. G., Stouten, T., Veenenbos, M., Melse-Boonstra, A., Dicke, M., Van Loon, J. J. (2018). Insects as sources of iron and zinc in human nutrition. *Nutrition Research Reviews*, *31*(2), 248-255, https://doi.org/10.1017/S0954422418000094.

Nikkhah, A., Van Haute, S., Jovanovic, V., Jung, H., Dewulf, J., Cirkovic Velickovic, T., Ghnimi, S. (2021). Life cycle assessment of edible insects (*Protaetia brevitarsis seulensis* larvae) as a future protein and fat source. *Scientific Reports*, *11*(1), 1-11, https://doi.org/10.1038/s41598-021-93284-8.

Niyonsaba, H. H., Höhler, J., Kooistra, J., Van Der Fels-Klerx, H. J., Meuwissen, M. P. M. (2021). Profitability of ınsect farms. *Journal of Insects as Food and Feed*, *7*(5), 923-934 , https://doi.org/10.3920/JIFF2020.0087.

Nowakowski, A. C., Miller, A. C., Miller, M. E., Xiao, H., Wu, X. (2021). Potential health benefits of edible insects. *Critical Reviews in Food Science and Nutrition*, *62*(13), 3499-3508, https://doi.org/10.1080/10408398.2020.1867053.

Ojha, S., Bekhit, A. E. D., Grune, T., Schlüter, O. K. (2021a). Bioavailability of nutrients from edible insects. *Current Opinion in Food Science*, *41*, 240-248, https://doi.org/10.1016/j.cofs.2021.08.003.

Ojha, S., Bußler, S., Psarianos, M., Rossi, G., Schlüter, O. K. (2021b). Edible insect processing pathways and implementation of emerging technologies. *Journal of Insects as Food and Feed*, *7*(5), 877-900, https://doi.org/10.3920/JIFF2020.0121.

Ordoñez-Araque, R., Egas-Montenegro, E. (2021). Edible insects: a food alternative for the sustainable development of the planet. *International Journal of Gastronomy and Food Science*, *23*, 100304, https://doi.org/10.1016/j.ijgfs.2021.100304.

Orsi, L., Voege, L. L., Stranieri, S. (2019). Eating edible insects as sustainable food? Exploring the determinants of consumer acceptance in Germany. *Food Research International*, *125*, 108573, https://doi.org/10.1016/j.foodres.2019.108573.

Osimani, A., Aquilanti, L. (2021). Spore-forming bacteria in insect-based foods. *Current Opinion in Food Science*, *37*, 112-117, https://doi.org/10.1016/j.cofs.2020.10.011.

Oonincx, D. G. A. B., Finke, M. D. (2021). Nutritional value of insects and ways to manipulate their composition. *Journal of Insects as Food and Feed*, *7*(5), 639-659, https://doi.org/10.3920/JIFF2020.0050.

Patel, S., Suleria, H. A. R., Rauf, A. (2019). Edible insects as innovative foods: Nutritional and functional assessments. *Trends in Food Science and Technology*, *86*, 352-359, https://doi.org/10.1016/j.tifs.2019.02.033.

Peniche, P.C.Y.C. (2021). Drivers of insect consumption across human populations. *Evolutionary Anthropology*., https://doi.org/10.1002/evan.21926.

Pippinato, L., Gasco, L., Di Vita, G., Mancuso, T. (2020). Current scenario in the European edible-insect industry: a preliminary study. *Journal of Insects as Food and Feed*, *6*(4), 371-381, https://doi.org/10.3920/JIFF2020.0008.

Placentino, U., Sogari, G., Viscecchia, R., De Devitiis, B., Monacis, L. (2021). The New Challenge of Sports Nutrition: Accepting Insect Food as Dietary Supplements in Professional Athletes. *Foods*, *10*(5), 1117, https://doi.org/10.3390/foods10051117.

Ponce-Reyes R., Lessard B. D. (2021). Edible Insects - A roadmap for the strategic growth of an emerging Australian industry. CSIRO, Canberra, https://www.futurefoodsystems.com.au/an-industry-with-legs-csiro-releases-australias-first-edible-insects-roadmap/.

Poore, J., Nemecek, T. (2018). Reducing food's environmental impacts through producers and consumers. *Science*, *360*(6392), 987-992, https://doi.org/10.1126/science.aaq0216.

Raheem, D., Raposo, A., Oluwole, O. B., Nieuwland, M., Saraiva, A., Carrascosa, C. (2019). Entomophagy: nutritional, ecological, safety and legislation aspects. *Food Research International*, *126*, 108672, https://doi.org/10.1016/j.foodres.2019.108672.

Ribeiro, J. C., Cunha, L. M., Sousa-Pinto, B., Fonseca, J. (2018). Allergic risks of consuming edible insects: a systematic review. *Molecular Nutrition and Food Research, 62*(1), 1700030, https://doi.org/10.1002/mnfr.201700030.

Rumpold, B. A., Schlüter, O. (2015). Insect-based protein sources and their potential for human consumption: nutritional composition and processing. *Animal Frontiers, 5*(2), 20-24, https://doi.org/10.2527/af.2015-0015.

Rumpold, B. A., Schlüter, O. K. (2013). Potential and challenges of insects as an innovative source for food and feed production. *Innovative Food Science and Emerging Technologies, 17,* 1-11, https://doi.org/10.1016/j.ifset.2012.11.005.

Saadoun, J. H., Sogari, G., Bernini, V., Camorali, C., Rossi, F., Neviani, E., Lazzi, C. (2022). A critical review of intrinsic and extrinsic antimicrobial properties of insects. *Trends in Food Science and Technology, 122,* 40-48, https://doi.org/10.1016/j.tifs.2022.02.018.

Schrögel, P., Wätjen, W. (2019). Insects for food and feed-safety aspects related to mycotoxins and metals. *Foods, 8*(8), 288, https://doi.org/10.3390/foods8080288.

Smetana, S., Spykman, R., Heinz, V. (2021). Environmental aspects of ınsect mass production. *Journal of Insects as Food and Feed, 7*(5), 553-571, https://doi.org/10.3920/JIFF2020.0116.

Sosa, D. A. T., Fogliano V. (2017). Potential of insect-derived ingredients for food applications. *Insect Physiology and Ecology*, 215-231, http://dx.doi.org/10.5772/67318.

Tamburino, L., Bravo, G., Clough, Y., Nicholas, K. A. (2020). From population to production: 50 years of scientific literature on how to feed the world. *Global Food Security, 24:* 100346 p., https://doi.org/10.1016/j.gfs.2019.100346.

Tanga, C. M., Egonyu, J. P., Beesigamukama, D., Niassy, S., Emily, K., Magara, H. J., Omuse, E. R., Subramanian S., Ekesi, S. (2021). Edible insect farming as an emerging and profitable enterprise in East Africa. *Current Opinion in Insect Science, 48,* 64-71, https://doi.org/10.1016/j.cois.2021.09.007.

Tang, C., Yang, D., Liao, H., Sun, H., Liu, C., Wei, L., Li, F. (2019). Edible insects as a food source: a review. *Food Production, Processing and Nutrition, 1*(1), 1-13, https://doi.org/10.1186/s43014-019-0008-1.

Tao, J., Li, Y. O. (2018). Edible insects as a means to address global malnutrition and food insecurity issues. *Food Quality and Safety, 2*(1), 17-26, https://doi.org/10.1093/fqsafe/fyy001.

UNEP (United Nations Environment Programme) (2021). Food waste index report 2021. Nairobi, ISBN: 978-92-807-3868-1., 100, https://www.unep.org/resources/report/unep-food-waste-index-report-2021.

Van Huis, A., Halloran, A., Van Itterbeeck, J., Klunder, H., Vantomme, P. (2022). How many people on our planet eat insects: 2 billion. *Journal of Insects as Food and Feed, 8*(1), 1-4, https://doi.org/10.3920/JIFF2021.x010.

Van Huis, A., Rumpold, B. A., Van Der Fels-Klerx, H. J., Tomberlin, J. K. (2021a). Advancing edible insects as food and feed in a circular economy. *Journal of Insects as Food and Feed, 7*(5), 935-948, https://doi.org/10.3920/JIFF2021.x005.

Van Huis, A. (2021b). Prospects of insects as food and feed. *Organic Agriculture, 11*(2), 301-308, https://doi.org/10.1007/s13165-020-00290-7.

Van Huis, A., Oonincx, D. G. (2017). The environmental sustainability of insects as food and feed. A review. *Agronomy for Sustainable Development, 37*(5), 1-14, https://doi.org/10.1007/s13593-017-0452-8.

Van Huis, A., Van Itterbeeck, J., Klunder, H., Mertens, E., Halloran, A., Muir, G., Vantomme, P. (2013). Edible insects: future prospects for food and feed security (No. 171). Food and agriculture organization of the United Nations., ISBN: 978-92-5-107596-8, https://research.wur.nl/en/publications/edible-insects-future-prospects-for-food-and-feed-security.

Varelas, V. (2019). Food wastes as a potential new source for edible insect mass production for food and feed: a review. *Fermentation, 5*(3), 81, https://doi.org/10.3390/fermentation5030081.

Wade, M., Hoelle, J. (2020). A review of edible insect industrialization: Scales of production and implications for sustainability. *Environmental Research Letters, 15*(12), 123013, https://doi.org/10.1088/1748-9326/aba1c1.

World Health Organization (WHO), United Nations Children's Fund (UNICEF), International Bank for Reconstruction and Development/The World Bank. (2021). Levels and trends in child malnutrition: key findings of the 2021 edition of the joint child malnutrition estimates. Geneva: World Health Organization. ISBN: 9789240025257, https://www.who.int/publications/i/item/9789240025257.